

Medical University of South Carolina

MEDICA

MUSC Theses and Dissertations

2020

Inhibition of Penicillin-Binding Protein 2: Toward New Therapeutics for Antimicrobial-Resistant Gonorrhea

Jonathan M. Turner

Medical University of South Carolina

Follow this and additional works at: <https://medica-musc.researchcommons.org/theses>

Recommended Citation

Turner, Jonathan M., "Inhibition of Penicillin-Binding Protein 2: Toward New Therapeutics for Antimicrobial-Resistant Gonorrhea" (2020). *MUSC Theses and Dissertations*. 63.

<https://medica-musc.researchcommons.org/theses/63>

This Dissertation is brought to you for free and open access by MEDICA. It has been accepted for inclusion in MUSC Theses and Dissertations by an authorized administrator of MEDICA. For more information, please contact medica@musc.edu.

JONATHAN M. TURNER. Inhibition of Penicillin-Binding Protein 2: Toward New Therapeutics for Antimicrobial-Resistant Gonorrhea (Under the direction of CHRISTOPHER DAVIES and PATRICK WOSTER)

Inhibition of Penicillin-Binding Protein 2: Toward New Therapeutics for Antimicrobial-Resistant Gonorrhea

by

Jonathan M. Turner

A dissertation submitted to the faculty of the Medical University of South Carolina in partial fulfillment of the requirements for the degree of Doctor of Philosophy in the College of Graduate Studies

Department of Biochemistry & Molecular Biology

2020

Approved by:

Chairman, Advisory Committee

Christopher Davies

Patrick Woster

Shaun Olsen

John J. Lemasters

Roger White

TABLE OF CONTENTS

Acknowledgments & Dedication.....	iii
List of Figures.....	iv
List of Tables.....	x
List of Schema.....	xii
List of Appendices.....	xiii
List of Abbreviations.....	xiv
ABSTRACT	xvi
CHAPTER 1: Introduction	1
CHAPTER 2: Materials & Methods	88
CHAPTER 3: Structure-Activity Relationships of Cephalosporins against Penicillin- and Cephalosporin-Resistant <i>Neisseria gonorrhoeae</i> H041	100
CHAPTER 4: Discovery of Novel PBP-Inhibitory Chemotypes as Potential Antigonococcal Agents	153
CHAPTER 5: Derivatization of Identified PBP-Inhibitory chemotypes	187
CHAPTER 6: Conclusion	228
References Cited.....	240
Appendix Materials.....	290

ACKNOWLEDGMENTS & DEDICATION

First, I would like to thank Christopher Davies and Patrick Woster for their mentorship and confidence. This project was an entirely new venture for both of you, and if not for your ambition, patience, and belief in my ability to succeed, none of this would have been possible. There is always more work to be done, but I am very proud of the scientist I have become in my time under your guidance.

I feel privileged to have worked so closely with the members of the Davies and Woster laboratories, past and present. Graduate school can be an isolating experience, but thanks to all of you, I have felt much more inspired and much less alone each day than I would have otherwise. Special thanks to Joy Kirkpatrick for becoming not only a friend but also a collaborator – there is something so exciting and even magical about discovering and publishing with friends.

I would also like to acknowledge my institutional support systems. Thank you to the Medical Scientist Training Program – to Perry Halushka for seeing promise in a quiet boy from Fairmont, West Virginia, to Amy Connolly for ensuring I stay on track, and to Nancy Demore and Donald Menick for your leadership these last few years. Thank you also to the Departments of Biochemistry and Drug Discovery for your kindness, as well as your support in shipping and receiving critical items for this work. Thank you to my committee members for your insightful questions and suggestions that challenge me to think beyond my immediate point of view. And thank you to our collaborators in the Nicholas laboratory at UNC and the Jerse laboratory at USUHS.

Thank you to my family and friends for supporting my desire to pursue this long path, especially to Neal and Benzene for loving me on my worst days.

I dedicate this work to all those suffering from infectious disease without the proper resources to seek and acquire treatment – to the socioeconomically disadvantaged and to the systemically oppressed. I hope to one day use my scientific knowledge and voice to advocate for you and diminish this disparity.

LIST OF FIGURES

Figure 1.1: Epidemiology of gonococcal disease in the United States

Figure 1.2: Timeline of treatment recommendations and resistance development in *Neisseria gonorrhoeae*

Figure 1.3: Structure of Gram negative peptidoglycan

Figure 1.4: Functions of PBPs and the mechanism of action of β -lactam antimicrobials

Figure 1.5: Conserved active site motifs in the PBPs

Figure 1.6: Illustrations of Woodward height and Cohen parameter for several classes of β -lactam antimicrobials

Figure 1.7: Structures of major classes of β -lactams in clinical use

Figure 1.8: Salient features of cephalosporin design by generation

Figure 1.9: Mechanisms of β -lactam resistance in *N. gonorrhoeae*

Figure 1.10: Changes to the PBP2 active site in penicillin-resistant FA6140 as a result of an Asp346a insertion

Figure 1.11: Mosaic *penA* allele and PBP2 structure

Figure 1.12: Mutations identified as critical to β -lactam resistance in PBP2^{H041}

Figure 1.13: The impact of A501P on the structure of the β 3 strand

Figure 1.14: Structures of boronic acid transpeptidase inhibitors

Figure 1.15: Crystal structures of boronic acid transpeptidase inhibitors in complex with their targets, showing their tetrahedral intermediate mimicry

Figure 1.16: Structures of activated carbonyl transpeptidase inhibitors

Figure 1.17: Crystal structures of activated carbonyl transpeptidase inhibitors in complex with their targets, showing their tetrahedral intermediate mimicry

Figure 1.18: Structures of phosph(on)ate transpeptidase inhibitors

Figure 1.19: Crystal structures of phosph(on)ate transpeptidase inhibitors in complex with their targets, showing their tetrahedral intermediate mimicry

Figure 1.20: Structures of γ -lactam and γ -lactam-like transpeptidase inhibitors

Figure 1.21: Structural alignments of γ -lactams with penicillin G

Figure 1.22: Structures of lactivicin and lactivicin-like transpeptidase inhibitors.

Figure 1.23: Crystal structure of lactivicin in complex with *S. pneumoniae* PBP1b

Figure 1.24: Structures of DBO transpeptidase inhibitors

Figure 1.25: Crystal structure of DBO FP1465 in complex with *E. coli* PBP1b

Figure 1.26: Structures of arylalkylidene rhodanine and arylalkylidene iminothiazolidin-4-one transpeptidase inhibitors

Figure 1.27: Proposed mechanism of arylalkylidene rhodanine transpeptidase inhibition

Figure 1.28: Structures of transpeptidase inhibitors discovered through serendipity

Figure 1.29: Structures of PBP inhibitors identified through physical screening methods

Figure 1.30: Structures of PBP inhibitors identified through *in silico* screening methods

Figure 3.1: Protein-ligand interaction fingerprints (PLIFs) for pharmacophore-constrained induced-fit docking of cephalosporins to tPBP2^{H041}

Figure 3.2: Consensus pharmacophore generated from all docked poses of cephalosporins in tPBP2^{H041}, set against a representative pose of ceftriaxone

Figure 3.3: Positioning of the R₁ and R₂ groups of ceftriaxone within the active site of tPBP2^{H041}

Figure 3.4: Statistical analysis of docked poses, showing two distinct predicted binding modes

Figure 3.5: Representative poses of ceftriaxone and cefoperazone docked to tPBP2^{H041}

Figure 3.6: Overlay of docked ceftriaxone poses with tPBP2^{H041}-CRO complex structure

Figure 3.7: Protein-ligand interaction fingerprints (PLIFs) for pharmacophore-constrained induced-fit docking of cephalosporins to *apo* tPBP2^{WT}

Figure 3.8: Protein-ligand interaction fingerprints (PLIFs) for pharmacophore-constrained induced-fit docking of cephalosporins to tPBP2^{WT} with T498 rotated toward the active site, as is seen in the ceftriaxone-bound structure

Figure 3.9: Representative poses of ceftriaxone docked to tPBP2^{WT}

Figure 3.10: Overlay of docked ceftriaxone poses with tPBP2^{WT}-CRO complex structure

Figure 3.11: Second-order rate of acylation of Bocillin-FL against tPBP2^{H041}

Figure 3.12: Partial least squares quantitative structure-activity relationship of cephalosporins against tPBP2^{H041}

Figure 3.13: Classification quantitative structure-activity relationship of cephalosporins against *N. gonorrhoeae* H041

Figure 3.14: Alignment of $\alpha 4$ of class B PBPs showing conservation of a lysine residue in several important Gram negative pathogens

Figure 3.15: Second-order rate of acylation of Bocillin-FL against tPBP2^{H041}-K361E

Figure 3.16: Pharmacophore-constrained induced fit docking of select cephalosporins to tPBP2^{H041}-K361E

Figure 3.17: Overlay of ceftriaxone- and cefoperazone-acylated structures of tPBP2^{H041}

Figure 3.18: Crystal structure of cefoperazone in complex with tPBP2^{H041}

Figure 3.19: Overlay of docked cefoperazone poses with tPBP2^{H041}-CFP complex structure

Figure 3.20: Evaluation of cefoperazone in a murine model of gonococcal infection

Figure 3.21: Energy score analyses for docking of cephalosporins against tPBP2^{H041}

Figure 3.22: Contact of the 2,3-dioxopiperazine moiety of cefoperazone with tPBP2^{H041} in a preliminary complex crystal structure

Figure 3.23: Surface views of ceftriaxone and cefoperazone docked to tPBP2^{H041}

Figure 3.24: Overlay of ceftriaxone docked to *apo* tPBP2^{WT} with the major pose of ceftriaxone docked to tPBP2^{H041}

Figure 3.25: Overlay of ceftriaxone docked to T498-rotated tPBP2^{WT} with the minor pose of ceftriaxone docked to tPBP2^{H041}

Figure 4.1: Structures of compounds reported by Kirkpatrick *et al.* (coded JEK-XX)

Figure 4.2: Inhibition data for JEK compounds against tPBP2^{WT}

Figure 4.3: Activity data for JEK-42

Figure 4.4: Activity data for sulfonamide derivative JMT-1

Figure 4.5: Structural similarities between cepheems and the base scaffolds of JEK-42 and JMT-1

Figure 4.6: Energy and position analyses for molecular dynamics simulations of JEK-42 and JMT-1 in complex with tPBP2^{WT} and tPBP2^{H041}

Figure 4.7: Change in positions of JEK-42 and JMT-1 in the active site of tPBP2^{WT} over the first 500 ps of molecular dynamics simulations

Figure 4.8: Change in positions of JEK-42 and JMT-1 in the active site of tPBP2^{H041} over the first 500 ps of molecular dynamics simulations

Figure 4.9: Molecular dynamics simulations of JEK-42 and JMT-1 in complex with tPBP2^{WT} after stabilization of ligand position

Figure 4.10: Molecular dynamics simulations of JEK-42 and JMT-1 in complex with tPBP2^{H041}

Figure 4.11: Common interactions of JEK-42 and JMT-1 with tPBP2

Figure 4.12: Alignment of $\alpha 8$ of class B PBPs showing conservation of an aromatic residue in several important Gram negative and Gram positive pathogens

Figure 4.13: Pharmacophore model developed from the flexible alignment of JEK-42 and JMT-1 with bicyclic β -lactam scaffolds

Figure 4.14: Pharmacophore search of a virtualized library of molecular fragments

Figure 4.15: Structures of polycyclic fragments resembling β -lactams

Figure 4.16: Structures of unsaturated carbocyclic fragments

Figure 4.17: Structures of fragments possessing amide bioisosteres

Figure 4.18: Structures of fragments possessing combinations of attributes from sets in Figures 4.15-4.17

Figure 4.19: Structures of reported arylamide and arylsulfonamide PBP inhibitors

Figure 4.20: Overlay of ceftriaxone (CRO) acyl structures with JEK-42 and JMT-1

Figure 4.21: 1,2,4-oxadiazole and 2-ureidobenzenesulfonic acid PBP inhibitors

Figure 5.1: Structures of prototype compounds JEK-42 and JMT-1

Figure 5.2: Structures of compounds JMT-2 through JMT-15, which possess substitutions on the anthranilic acid moiety of JMT-1

Figure 5.3: Inhibition data for JMT-2 through JMT-15 against tPBP2^{WT} and tPBP2^{H041} at 100 μ M

Figure 5.4: Inhibition data for selected anthranilic acid-substituted derivatives of JMT-1 against tPBP2^{H041} at 10 μ M

Figure 5.5: Disc diffusion data for potent anthranilic acid-substituted derivatives of JMT-1 against *N. gonorrhoeae* FA19 and H041

Figure 5.6: Structures of compounds JMT-16 through JMT-25, which possess a 1*H*-tetrazol-5-yl moiety at C1 in place of the carboxylic acid seen in JMT-1

Figure 5.7: Inhibition data for JMT-16 through JMT-25 against tPBP2^{WT} and tPBP2^{H041} at 100 μ M

Figure 5.8: Inhibition data for *1H*-tetrazol-5-yl derivatives of JMT-1 against tPBP2^{H041} at 10 μ M

Figure 5.9: Disc diffusion data for potent *1H*-tetrazol-5-yl derivatives of JMT-1 against *N. gonorrhoeae* FA19 and H041

Figure 5.10: Structures of compounds JMT-26 through JMT-30, which possess nitrogen-containing heterocyclic carboxylic acids in place of the anthranilic acid seen in JMT-1

Figure 5.11: Inhibition data for JMT-26 through JMT-30 against tPBP2^{WT} and tPBP2^{H041} at 100 μ M.

Figure 5.12: Structures of compounds JMT-31 through JMT-39, which lack the biphenyl 4'-methyl group seen in JMT-1

Figure 5.13: Inhibition data for JMT-31 through JMT-39 against tPBP2^{WT} and tPBP2^{H041} at 100 μ M

Figure 5.14: Inhibition data for 4'-desmethyl derivatives of JMT-1 against tPBP2^{H041} at 10 μ M

Figure 5.15: Structures of compounds JMT-40 through JMT-58, which possess a 4'-methoxy in place of the 4'-methyl group seen in JMT-1

Figure 5.16: Inhibition data for JMT-40 through JMT-58 against tPBP2^{WT} and tPBP2^{H041} at 100 μ M

Figure 5.17: Inhibition data for 4'-methoxy derivatives of JMT-1 against tPBP2^{H041} at 10 μ M

Figure 5.18: Structures of compounds JMT-59 through JMT-83, which possess a halogen in place of the 4'-methyl group seen in JMT-1

Figure 5.19: Inhibition data for JMT-59 through JMT-83 against tPBP2^{WT} and tPBP2^{H041} at 100 μ M

Figure 5.20: Inhibition data for 4-fluoro and 4-chloro derivatives of JMT-1 against tPBP2^{H041} at 10 μ M

Figure 5.21: Structures of compounds JMT-84 through JMT-100, which possess a 4'-trifluoromethyl group in place of the 4'-methyl group seen in JMT-1

Figure 5.22: Inhibition data for JMT-84 through JMT-100 against tPBP2^{WT} and tPBP2^{H041} at 100 μ M

Figure 5.23: Inhibition data for 4'-trifluoromethyl derivatives of JMT-1 against tPBP2^{H041} at 10 μ M

Figure 5.24: Disc diffusion data for potent 4'-substituted derivatives of JMT-1 against *N. gonorrhoeae* FA19 and H041

Figure 5.25: Structures of compounds JMT-101 through JMT-118, which possess a 4-cyclohexylphenyl group in place of the 1,1'-biphenyl system seen in JMT-1

Figure 5.26: Inhibition data for JMT-101 through JMT-118 against tPBP2^{WT} and tPBP2^{H041} at 100 μ M

Figure 5.27: Inhibition data for 4-cyclohexylphenyl derivatives of JMT-1 against tPBP2^{H041} at 10 μ M

Figure 5.28: Structures of compounds JMT-119 through JMT-128, which possess a bicyclo[4.4.0] ring system in place of the 1,1'-biphenyl system seen in JMT-1

Figure 5.29: Inhibition data for JMT-119 through JMT-128 against tPBP2^{WT} and tPBP2^{H041} at 100 μ M

Figure 5.30: Inhibition data for bicyclo[4.4.0] derivatives of JMT-1 against tPBP2^{H041} at 10 μ M

Figure 5.31: Disc diffusion data for potent cyclohexylphenyl derivatives of JMT-1 against *N. gonorrhoeae* FA19 and H041

Figure 5.32: Docked poses of compounds showing potent tPBP2 inhibition and antigonococcal activity

Figure 5.33: Surface rendering of modeled JMT-1 derivatives in complex with tPBP2^{WT}

Figure 5.34: Surface rendering of modeled JMT-1 derivatives in complex with tPBP2^{H041}

Figure 5.35: Flexible alignment and consensus pharmacophore based on the most potent antigonococcal compounds

Figure 5.36: Overlay of ceftriaxone after leaving group departure and 2-(4'-methyl-[1,1'-biphenyl]-4-amido)-6-fluorobenzoic acid

Figure 5.37: Carboxylic acid bioisosteres

Figure 6.1: Features of cephalosporins enhancing the second-order rate of tPBP2^{H041} acylation, illustrated by cefoperazone

Figure 6.2: Predicted tPBP2 binding mode of antigonococcal prototypes

Figure 6.3: Structures of JMT-1 derivatives

Figure 6.4: Flexible alignment of JMT-84 with published noncovalent PBP inhibitors

Figure 6.5: Model for early antimicrobial discovery

LIST OF TABLES

- Table 1.1:** Summary of non-PBP-mediated β -lactam resistance in *N. gonorrhoeae*
- Table 1.2:** Characteristics of PBP2 from *N. gonorrhoeae* with various resistance profiles
- Table 1.3:** Summary of antigonococcal data for FDA-approved therapies
- Table 1.4:** Summary of antigonococcal data for experimental therapeutics belonging to classes of FDA-approved therapies
- Table 1.5:** Summary of antigonococcal data for experimental therapeutics with mechanisms of action distinct from current FDA-approved therapies
- Table 1.6:** Activity of boronic acid compounds against bacterial transpeptidases
- Table 1.7:** Activity of activated carbonyl compounds against bacterial transpeptidases
- Table 1.8:** Activity of phosphate and phosphonate compounds against bacterial transpeptidases
- Table 1.9:** Activity of γ -lactams against bacterial transpeptidases
- Table 1.10:** Activity of lactivicins against bacterial transpeptidases
- Table 1.11:** Activity of DBOs against bacterial transpeptidases
- Table 1.12:** Activity of arylalkylidene rhodanines and arylalkylidene iminothiazolidin-4-ones against bacterial transpeptidases
- Table 1.13:** Activity of noncovalent inhibitors against bacterial transpeptidases
- Table 3.1:** Second-order acylation rates and minimum inhibitory concentrations for the selected panel of cephalosporins
- Table 3.2:** Pairwise comparisons of cephalosporins with identical R_2
- Table 3.3:** Partial least squares QSAR model of tPBP2^{H041} acylation rate constant data
- Table 3.4:** Application of PLS QSAR to a test set of null cephalosporins
- Table 3.5:** Classification QSAR model of *Neisseria gonorrhoeae* H041 antimicrobial activity data
- Table 3.6:** Superimposition of class B PBPs
- Table 3.7:** Homology model template-target matching parameters for class B PBPs
- Table 3.8:** Homology model quality measures for class B PBPs

Table 3.9: Second-order acylation rates for select cephalosporins against tPBP2^{H041}-K361E

Table 3.10: X-ray diffraction data and model refinement statistics for a preliminary crystal structure of tPBP2^{H041} in complex with cefoperazone

Table 4.1: Summary data for molecular dynamics simulations of JEK-42 and JMT-1 in complex with tPBP2

Table 4.2: Superimposition of class B PBPs

Table 5.1: Summary data for the JMT-1 derivatives showing the most potent anticonococcal activity

Table 5.2: Calibrated dichotomous sensitivity disc diffusion literature values for FDA-approved antimicrobials against *N. gonorrhoeae* with varied susceptibility profiles

LIST OF SCHEMA

Scheme 4.1: Synthesis of JEK-42 from 4'-methyl-[1,1'-biphenyl]-4-carboxylic acid

Scheme 4.2: Synthesis of JMT-1 from 4'-methyl-[1,1'-biphenyl]-4-sulfonyl chloride

Scheme 4.3: Synthetic routes to arylamides

Scheme 4.4: Synthetic routes to arylsulfonamides

Scheme 5.1: Synthesis of JMT-1 derivatives

Scheme 5.2: Proposed synthesis of 4'-methyl-[1,1'-biphenyl]-4-sulfonyl chloride from S-acetyl 4-bromothiophenol

Scheme 5.3: Proposed synthesis of 4'-methyl-[1,1'-biphenyl]-4-carboxylic acid from methyl 4-bromobenzoate

Scheme 6.1: Proposed synthesis of novel cephalosporins from 7-aminocephalosporanic acid

LIST OF APPENDICES

- Appendix A:** Pharmacophore-constrained cephalosporin docking parameters
- Appendix B:** Untransformed activity data (IC_{50}) for cephalosporins against tPBP2^{H041}
- Appendix C:** Quantitative structure-activity relationship descriptors
- Appendix D:** Characterization of synthesized compounds by ESI-MS and ¹HNMR
- Appendix E:** Pharmacophore screening of FDA-approved therapies for putative PBP inhibitors
- Appendix F:** High-throughput virtual screen for inhibitors of *Pseudomonas aeruginosa* PBP3

LIST OF ABBREVIATIONS

ATAO – 2-(2-aminothiazol-4-yl)-2-(alkoxyimino)acetyl

BOC – Bocillin-FL

BPR – ceftobiprole

CAZ – ceftazidime

CDR – cefdinir

CEC – cefaclor

CFM – cefixime

CFP – cefoperazone

CFZ – cefazolin

CMRNG – chromosomally mediated resistant *N. gonorrhoeae*

CMZ – cefmetazole

CPD – cefpodoxime

CPT – ceftaroline

CRO – ceftriaxone

CTB – ceftibuten

CTX – cefotaxime

CXM – cefuroxime

DBO – 1,6-diazabicyclo[3.2.1]octan-7-ones

ESBL – extended-spectrum β -lactamase

ESI-MS – electrospray ionization mass spectrometry

ESKAPE – *Enterococcus spp.*, *Staphylococcus aureus*, *Klebsiella pneumoniae*, *Acinetobacter baumannii*, *Pseudomonas aeruginosa*, *Enterobacter spp.*

ESC – extended-spectrum cephalosporin

EtOAc – ethyl acetate

EUCAST – European Committee on Antimicrobial Susceptibility Testing

FEP – cefepime

FOX – cefoxitin

HIV – human immunodeficiency virus

¹HNMR – proton nuclear magnetic resonance

LOR – cephaloridine

LOT – cephalothin

MIC – minimum inhibitory concentration

MRSA – methicillin-resistant *Staphylococcus aureus*

MSM – men who have sex with men

MSW – men who have sex with women

NMTT – *N*-methyltetrazole

PBP – penicillin-binding protein

PID – pelvic inflammatory disease

PLIF – protein-ligand interaction fingerprint

PLS – partial least squares

PPNG – penicillinase-producing *N. gonorrhoeae*

QSAR – quantitative structure-activity relationship

SAR – structure-activity relationship

STI – sexually transmitted infection

THF – tetrahydrofuran

TLC – thin layer chromatography

TOL – ceftolozane

TTN – thiotriazinone

TTZ – *1H*-tetrazole

VRE – vancomycin-resistant *Enterococcus*

ZOX – ceftizoxime

ABSTRACT

Gonorrhea is the second most common sexually transmitted bacterial infection in the United States, with nearly 600,000 cases reported in 2018 by the Centers for Disease Control. Alarmingly, the causative agent *Neisseria gonorrhoeae* has developed resistance to a number of antimicrobials over the last century. With limited options remaining, the CDC now recommends dual therapy with ceftriaxone and azithromycin to decrease the likelihood of resistance development. However, strains with combined cephalosporin and macrolide resistance have now emerged, raising concerns of a post-antibiotic future in which untreatable gonorrhea would impose enormous human and economic cost. The discovery and development of novel antigonococcal agents is, therefore, necessary to avoid a public health crisis.

The pharmacologic receptors for β -lactams are a group of transpeptidases known as penicillin-binding proteins (PBP), which catalyze the cross-linkage of peptidoglycan, an essential component of the bacterial cell wall that plays major roles in cell growth and division. *N. gonorrhoeae* develops chromosomally mediated β -lactam resistance via alterations of PBPs affecting drug affinity, specifically through the acquisition of mutations in the *penA* gene encoding PBP2. Resistant strains harbor mosaic *penA* alleles encoding PBP2 variants containing around 60 amino acid changes compared to wild-type. In this work, we examine inhibition of a mosaic form of *N. gonorrhoeae* PBP2 from the cephalosporin-resistant strain H041, seeking to understand better which features of ligand structure enhance or diminish PBP2 binding in order to develop more effective PBP2 inhibitors.

First, we report structure-activity relationships (SAR) for the cephalosporin class of β -lactams against PBP2 from *N. gonorrhoeae* H041 with the goal of identifying or designing cephalosporins effective against resistant strains. We find that structural features of the C7 acylamino side chain (R_1) correlate highly with the second-order rate of PBP2^{H041}

acylation, including increased size, modest lipophilicity, and two ring systems separated by a single branch point. The C3 side chain (R_2) makes lesser, but still important, contributions to inhibition, with electronegative elements and planarity enhancing activity. We also found that many of the features enhancing target inhibition (e.g., lipophilicity, aromaticity) diminish antimicrobial activity against the H041 strain, perhaps due to decreased accumulation in the periplasm. Finally, we identify cefoperazone as highly active against PBP2^{H041} and similarly active against *N. gonorrhoeae* H041 both *in vitro* and *in vivo* compared to ceftriaxone. Second, we report the *in silico* discovery of novel noncovalent PBP2 inhibitors possessing a 1,1'-biphenyl system. Arylamide **JEK-42** and its isosteric sulfonamide derivative **JMT-1** are capable of inhibiting PBP2 from both β -lactam-susceptible and -resistant gonococcal strains. Their cross-inhibition of *P. aeruginosa* PBP3, predicted binding modes showing interaction with highly conserved residues, and structural similarities to bicyclic β -lactam scaffolds indicate their potential for broader activity against class B PBPs. Using the structural similarities between **JEK-42**, **JMT-1**, and bicyclic β -lactam scaffolds (*i.e.*, penam, carbapenem, and cephem), a three-point pharmacophore was generated that can be used to identify additional PBP-inhibitory scaffolds. Third, we report the synthesis of 127 derivatives of **JMT-1**, showing specific substitutions that enhance the inhibition of PBP2 derived from both β -lactam-susceptible and -resistant strains. In keeping with the cephalosporin SAR, hydrophobic substitutions enhance PBP2 inhibition, likely through increased van der Waals contact with the active site, but they can also result in diminished antimicrobial activity. Together, our efforts yielded 10 compounds that show near full inhibition of PBP2 from susceptible and resistant strains, as well as large zones of gonococcal growth inhibition in disc diffusion assays. These studies lay the groundwork for the development of several structurally diverse antigonococcal chemotypes, thereby increasing the probability of producing a successful preclinical candidate.

CHAPTER 1: Introduction

1.1 *Neisseria gonorrhoeae*

1.1.a. Epidemiology and clinical features of gonococcal disease

Neisseria gonorrhoeae is a Gram negative diplococcus responsible for the sexually transmitted infection (STI) gonorrhea. Gonorrhea is a global problem and, despite a sound public health infrastructure, a growing issue in the United States. There are nearly 600,000 cases reported annually by the Centers for Disease Control (CDC)¹ and 87 million cases reported annually by the World Health Organization (WHO),² and as with many infectious diseases, the true number of cases is expected to be much higher due to asymptomatic infection and underreporting. In the United States, overall rates of infection showed a substantial decline until 2009, reaching a low of 98.1 cases per 100,000 person years; in the last decade, however, an upward trend in infection rates has begun and persisted, with 179.1 cases per 100,000 person years reported in 2018¹ (**Figure 1.1**). The highest reported rates are seen among the following groups: adolescents and young adults, racial minorities, men who have sex with men (MSM) and persons living in the southeastern states¹ (**Figure 1.1**). Symptomatic disease is generally associated with urethritis in men and cervicitis in women, although rectal and pharyngeal gonorrhea are not uncommon. Untreated, the infection can spread in an ascending pattern, resulting in epididymitis in males and pelvic inflammatory disease (PID) in females. These complications can result in serious sequelae, including infertility and ectopic pregnancy. Disseminated gonococcal infections result most commonly in suppurative arthritis or tenosynovitis but can cause more serious disease, such as endocarditis or meningitis.³⁻⁸ Importantly, gonococcal infection results in mucosal disruption and can therefore increase the risk of both transmitting and contracting human immunodeficiency virus (HIV).^{9,10}

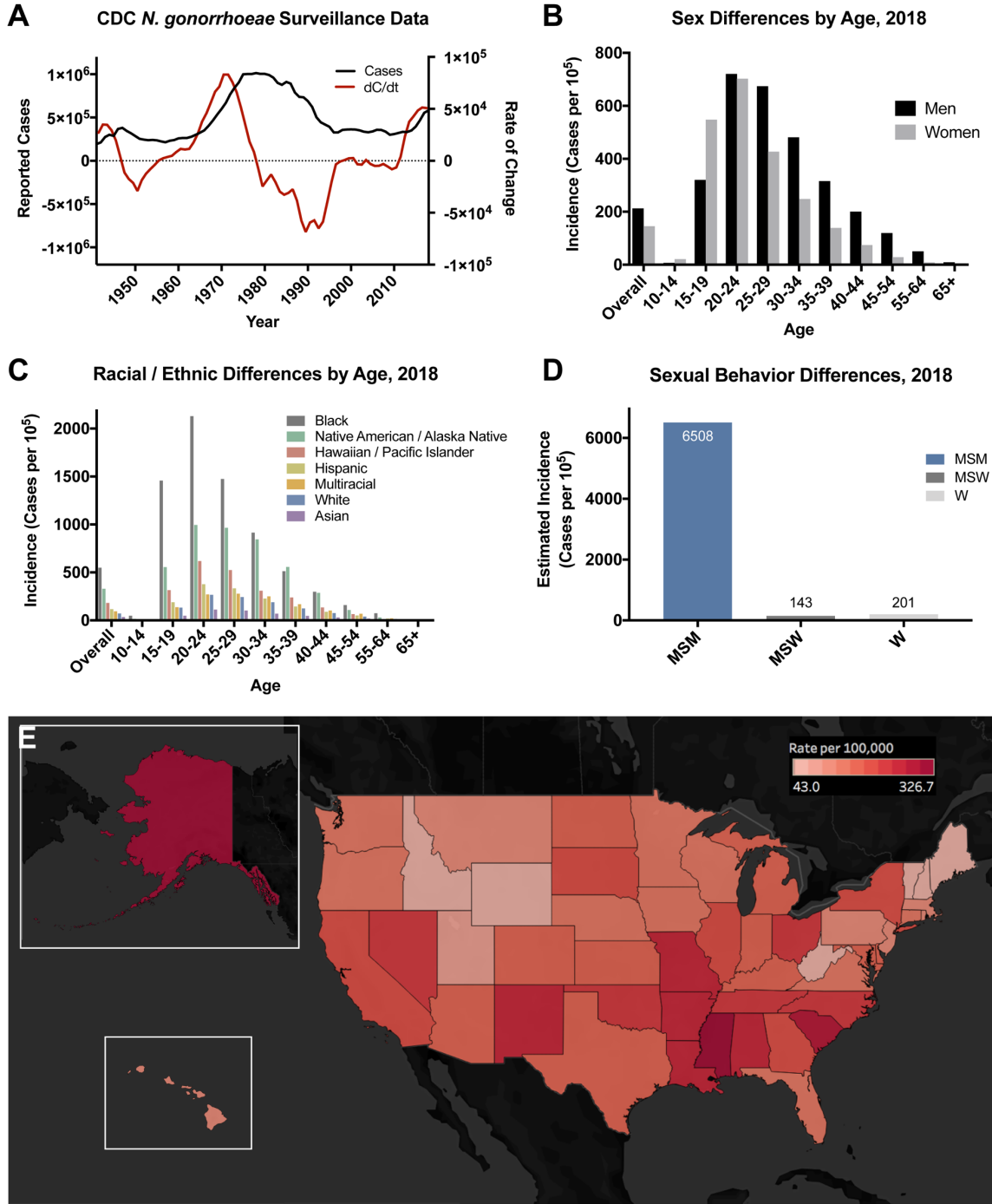


Figure 1.1: Epidemiology of gonococcal disease in the United States. **A.** Reported incidence of gonorrhea in the United States over the last 70 years. The absolute incidence is shown in black, and the rate of change is shown in red. **B.** Incidence of gonorrhea stratified by age and sex. Data are from 2018. **C.** Incidence of gonorrhea stratified by age and ethnicity. Data are from 2018. **D.** Estimated incidence in gonorrhea stratified by sexual behavior. Values are modeled based on interviews of a random sample of reported cases ($n = 6,482$ patients). Key: men who have sex with men (MSM), men who have sex with women (MSW), women (W). **E.** Heat map of gonococcal incidence by state. All data are from CDC infectious disease surveillance.

1.1.b. Emerging antimicrobial resistance

Historically, gonorrhea was treated with sulfanilamide or penicillin, but due to increased prevalence of resistant strains, the Centers for Disease Control & Prevention (CDC) called for their withdrawal as recommended antibiotics for gonococcal infections due to emerging resistance.¹¹⁻²⁰ With the subsequent withdrawal of spectinomycin,²¹⁻²⁵ tetracyclines,²⁶⁻³⁰ and fluoroquinolones³¹⁻³⁸ for the same reason, only third-generation cephalosporins (e.g., ceftriaxone and cefixime) remained as CDC-recommended drugs of choice in the United States^{39,40} (**Figure 1.2**). In the last two decades, strains of *N. gonorrhoeae* with decreased susceptibility to extended-spectrum cephalosporins (ESCs) have emerged, prompting concerns that gonococcal infections may soon become untreatable using monotherapy.⁴¹⁻⁵⁹ For this reason, treatment guidelines now recommend dual therapy with ceftriaxone and azithromycin in the United States and Europe.^{60,61} Alarming, strains exhibiting high-level resistance to ESCs have now been isolated on most continents (Asia, Australia, Europe, North America, and South America),⁶²⁻⁸⁷ and macrolide resistance has become increasingly common.^{48,88-93} While combined ESC and macrolide resistance is exceedingly rare, a few such cases have been reported.⁷⁸⁻⁸⁰ This rapidly changing landscape of antimicrobial resistance indicates that the currently used dual regimen will not provide a long-term solution for antigonococcal chemotherapy.⁹⁴⁻⁹⁸

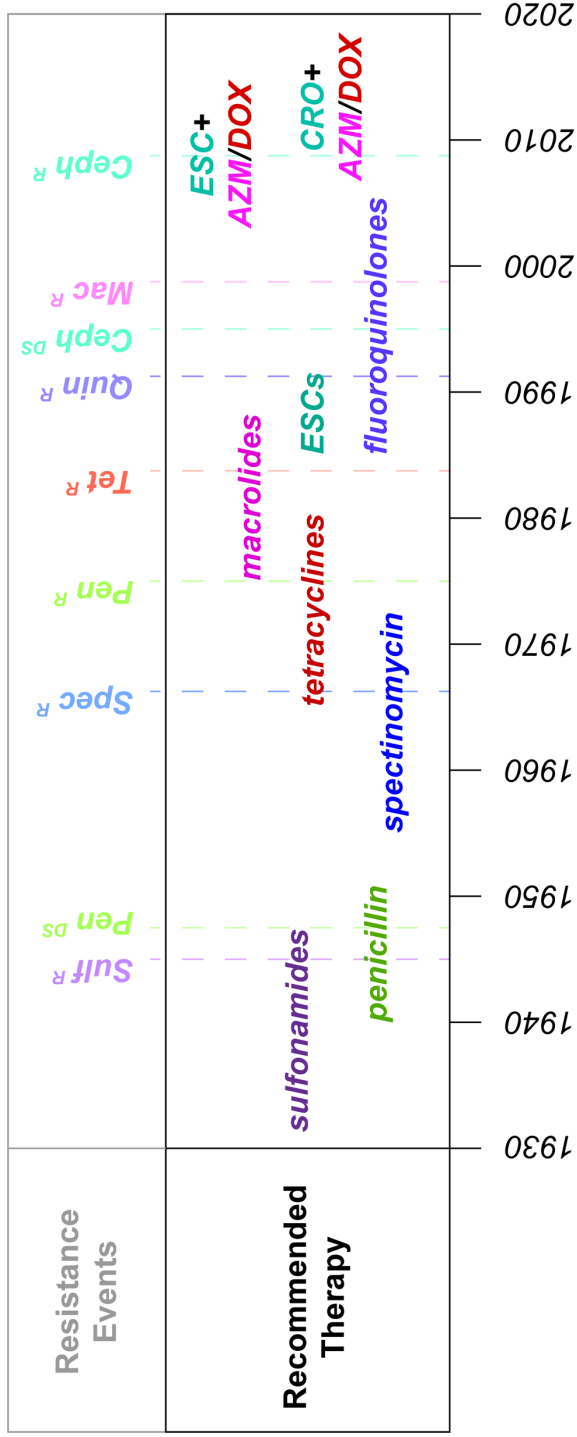


Figure 1.2: Timeline of treatment recommendations and resistance development in *Neisseria gonorrhoeae*. In the immediately pre-antimicrobial era, options for the treatment of gonorrhea included urethral irrigation, potassium permanganate, silver compounds, mercurochrome, and hyperthermia. Key: sulfonamides (Sulf), penicillin (Pen), spectinomycin (Spec), tetracyclines (Tet), fluoroquinolones (Quin), cephalosporins (Ceph), macrolides (Mac), decreased susceptibility (DS), resistance (R).

In addition to the human costs, STIs have a substantial impact on the national and global economies. Diagnosis and treatment alone cost the United States healthcare system \$16B annually, with gonococcal infections contributing an estimated \$162M in direct costs.⁹⁹ With the present surge of multidrug-resistant gonorrhea, disease prevalence and severity are expected to rise due to treatment failure, augmenting the economic burden of gonorrhea and its sequelae. To date, there have been no strains exhibiting high resistance to ESCs isolated in the United States; however, with the recent international transmission of a ESC-resistant clone from Asia to Canada,⁶⁷ the arrival of such a strain to the United States seems imminent. It is predicted that if antimicrobial-resistant *N. gonorrhoeae* were to become established in North America, there will be 5.9 million new cases, an added cost of approximately \$780M, over a seven-year period.¹⁰⁰

1.2 β -Lactams and their biological targets

1.2.a. Penicillin-binding proteins as the molecular targets for β -lactam antibiotics

The pharmacologic receptors for β -lactams are a group of DD-transpeptidases known as penicillin-binding proteins (PBPs), which catalyze the cross-linkage of peptidoglycan via the formation of isopeptide bonds.¹⁰¹⁻¹⁰³ Peptidoglycan is a mesh-like polymeric macromolecule consisting of glycan strands of β -1,4-linked *N*-acetylmuramic acid and *N*-acetylglucosamine covalently linked to L-alanyl- γ -D-glutamyl-L-diaminoacyl-D-alanine peptide chains via amidation of the muramic acid carboxyl group by the L-alanine amino group¹⁰⁴ (**Figure 1.3**). Cross-linkage of peptidoglycan units occurs when a unit of endogenous pentapeptide substrate, L-alanyl- γ -D-glutamyl-L-diaminoacyl-D-alanyl-D-alanine, forms an isopeptide bond between the penultimate D-alanine and the side chain amine of the diaminoacyl residue at the expense of the D-alanyl-D-alanine peptide bond, a process catalyzed by the PBPs (**Figure 1.4**). Peptidoglycan is an essential component of the bacterial cell wall and plays major roles in cell growth and division, as well as protection from osmotic or tensile stress, and it has a natural turnover rate dictated by the

processes of synthesis and autolysis.^{104,105} There are three classes of PBP: class A are bifunctional enzymes, with transpeptidase and transglycosylase functionalities; class B are monofunctional transpeptidases; and class C catalyze either carboxypeptidase or endopeptidase reactions.^{102,103} Whereas PBPs of classes A and B are generally essential for the survival of bacteria, class C can often be genetically deleted without significant effects on cell growth or morphology.

The transpeptidase active site contains three conserved motifs: SxxK, SxN, and KTG (where x denotes a variable residue)¹⁰⁶ (**Figure 1.5**). The catalyzed reaction involves three steps: Michaelis-Menten binding of peptide substrate, acylation, and deacylation. It is proposed that the KTG lysine serves as an electrostatic anchor for the pentapeptide carboxy terminus to allow initial recognition of the substrate.¹⁰⁷⁻¹¹² In *N. gonorrhoeae* PBP2, there is evidence that the KTG threonine then rotates in response to carboxylate binding, acting as a trigger that initiates the acylation reaction by allowing β 3 strand rotation for formation of the oxyanion hole.¹¹³ The SxxK lysine acts as a base, polarizing the hydroxymethylene sidechain of the SxxK serine to form a pseudo-alkoxide nucleophile that attacks the carbonyl carbon of the peptide substrate's penultimate D-Ala.¹⁰⁷⁻¹¹² The resulting substitution reaction goes through a tetrahedral intermediate stabilized by an oxyanion hole made up of the backbone amides of the SxxK serine and a residue following the KTG motif.¹¹⁴⁻¹¹⁷ Upon resolution of the tetrahedral intermediate, the terminal D-alanine is eliminated to form an activated L-alanyl- γ -D-glutamyl-L-diaminoacyl-D-alanyl acyl enzyme, at which time the carbonyl carbon undergoes nucleophilic attack by the diaminoacyl residue of an adjacent peptidoglycan strand.

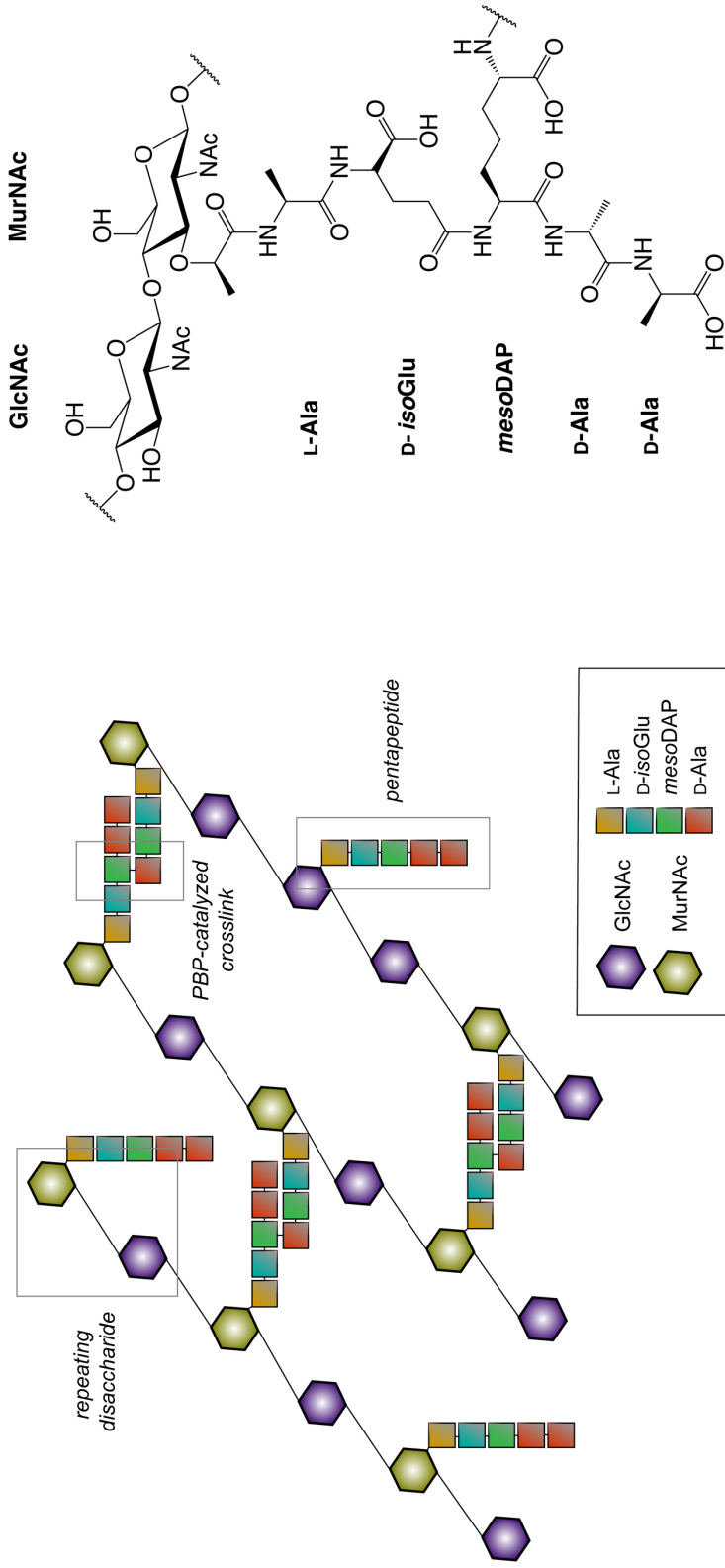


Figure 1.3: Structure of Gram negative peptidoglycan. On the left is a schematic depiction of the overall polymeric structure. On the right is a detailed chemical drawing of a single unit. Key: N-acetylglucosamine (GlcNAC), N-acetylmuramic acid (MurNAC), meso-diaminopimelate (meso-DAP)

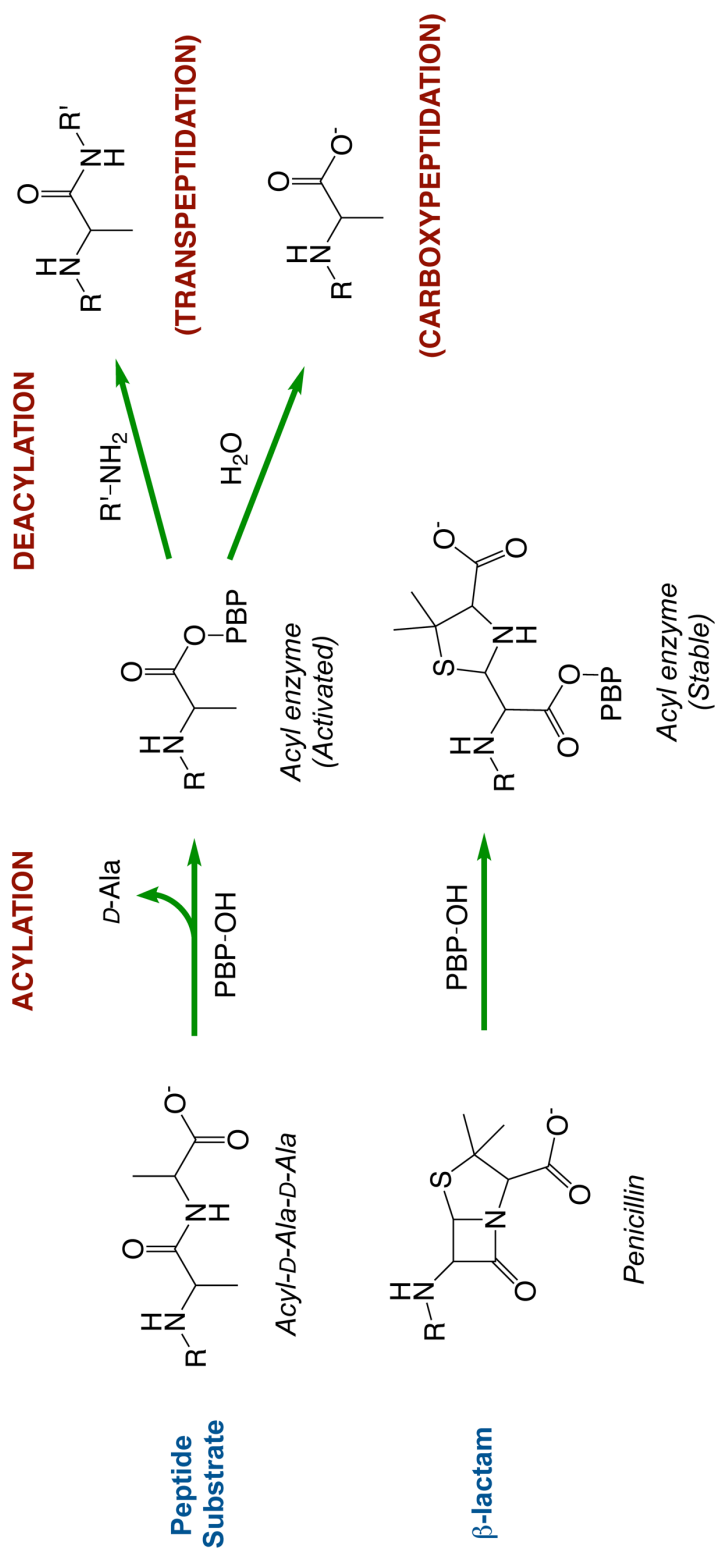


Figure 1.4: Functions of PBPs and the mechanism of action of β -lactam antimicrobials.

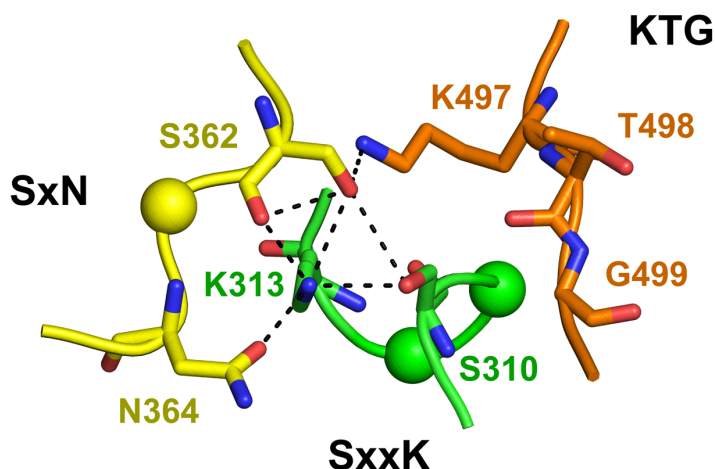
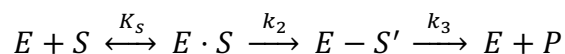


Figure 1.5: Conserved active site motifs in the PBPs. The example shown is PBP2 of *N. gonorrhoeae*.

β -lactam antibiotics mimic the D-Ala-D-Ala terminus of the peptidyl substrate.¹¹⁸⁻¹²⁴ In the presence of a β -lactam, the serine nucleophile instead attacks the carbonyl carbon of the cyclic amide, but upon resolution of the tetrahedral intermediate, the leaving group remains tethered to the acyl-enzyme, blocking deacylation¹²⁵⁻¹²⁷ (**Figure 1.4**). The reaction of β -lactams with PBPs is described by **Equation 1**, where E·S is the noncovalent enzyme-lactam complex, E-S' is the acyl-enzyme complex, and P is the hydrolyzed β -lactam.



The second-order rate constant (k_2/K_s) is a direct measure of the reactivity of a β -lactam with a PBP, and these rate constants can exceed $10^6 \text{ M}^{-1}\text{s}^{-1}$ against PBPs of susceptible strains.¹²⁸ As described above, the rate of deacylation (k_3) is slow, occurring on the order of one reaction per hour.¹²⁹⁻¹³²

Four PBPs are encoded by the genome of *N. gonorrhoeae*.¹³³ PBP1 (class A), and PBP2 (class B) are both essential and are potential targets for bactericidal activity; however, because PBP2 is inhibited at tenfold lower penicillin concentrations than PBP1, it is generally accepted to be the clinical target for susceptible strains. While PBP3 and PBP4 (class C) are nonessential, deletion of both in one strain results in pleiomorphy and slowed growth.¹¹¹

1.2.b. Factors affecting β -lactam acylation of PBPs

As shown in **Equation 1**, there are two component steps to β -lactam acylation of PBPs: formation of the precovalent enzyme-lactam complex (K_s) and reaction of the serine nucleophile with the lactam ring to form the covalent acyl-enzyme (k_2). The first step is determined by factors affecting affinity of the β -lactam for the active site of the PBP, including complementarity of size, shape, and charge; however, very little is known about how these features contribute to the binding of β -lactams. Isothermal titration calorimetry (ITC) and surface plasmon resonance (SPR) are not especially useful to this end, as they can only report an apparent association constant (K_a) due to the overall reaction being covalent. Mutation of the nucleophilic serine to alanine has been performed in our laboratory, however, and in ITC studies of this modified system, we have shown that affinity is important for acylation.¹³⁴ Whereas K_d of ceftriaxone was measured to be 2.3 μM against PBP2 derived from a fully susceptible strain of *N. gonorrhoeae*, no heat exchange was seen upon titration of millimolar ceftriaxone into PBP2 derived from cephalosporin-resistant strains. Previous studies have indicated that the common acylamino side chain of many β -lactams may be an important driver of affinity against PBPs, but more rigorous analyses were not done to determine which characteristics specifically enhance or hinder acylation.¹³⁵⁻¹³⁹ In one instance, a high-affinity penicillin analogue was designed with a specific acylamino group that rendered it orders of magnitude more active than other β -lactams ($k_2/K_s = 1.5 \times 10^7 \text{ M}^{-1} \text{ s}^{-1}$).^{140,141} Finally, complex formation is largely dependent

upon the active site architecture of the specific PBP being studied. Each bacterial species has its own collection of PBPs, and beyond the conserved motifs, there is considerable sequence variation. Resistant mutants arising from target modification complicate this problem further.

In addition to side chains and overall topology of the molecule, another factor, the Cohen parameter c , describes the precovalent complementarity of β -lactams in the PBP active site.^{142,143} The Cohen parameter is defined as the distance between the carboxylate carbon and the amide oxygen in bicyclic β -lactam systems (**Figure 1.6**). Lower Cohen parameters are correlated with higher complementarity, likely due to a physical requirement created by the distance between the carboxylate-binding residues and the oxyanion hole created by the SxxK serine and a β 3 residue following the KTG motif.

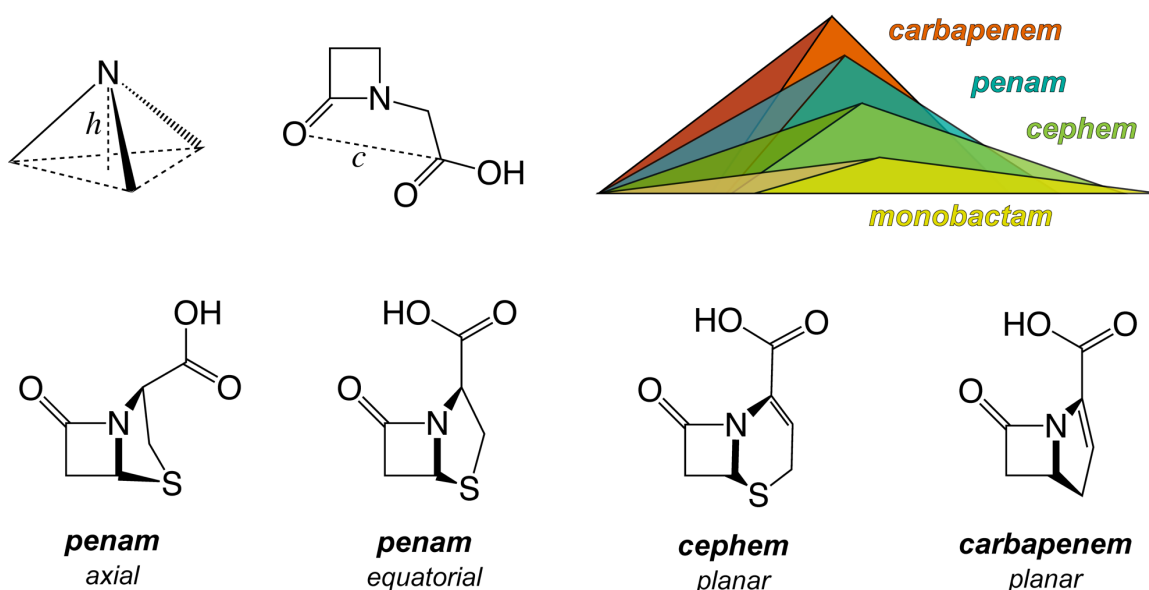


Figure 1.6: Illustrations of Woodward height and Cohen parameter for several classes of β -lactam antimicrobials.

The acylation reaction by β -lactams is determined by factors governing nucleophilic attack of the lactam ring, including both target and ligand factors. Target factors involve the electronic environment of the serine and how this environment affects its ability to act as a nucleophile. From studies of the mechanistically analogous serine protease chymotrypsin, as well as studies assigning protonation states to active site lysines in several PBPs, it is widely accepted that the SxxK motif lysine polarizes the serine hydroxyl group, forming an activated pseudo-alkoxide.¹⁰⁷⁻¹¹² The acid-base chemistry of the SxxK serine and lysine has been shown to be key to this process and is influenced by the local environment of the active site. For a Brønsted-Lowry acid or base to function optimally in a catalytic cycle, its pK_a must be near the effective pH at the reaction site so that its protonation state can be readily restored.¹⁴⁴⁻¹⁴⁷ In the case of the conserved SxxK residues of PBPs, there are three predominating factors influencing protonation states: local electrostatics, the presence of an extensive hydrogen bonding network, and the Born effect.^{148,149} The presence of additional nearby ionizable groups can influence the pK_a of an ionizable residue in accordance with the thermodynamic tendency away from Coulombic repulsion.¹⁵⁰ The presence of the KTG lysine adjacent the SxxK lysine in PBPs will, therefore, decrease the pK_a of both toward surrounding pH. The active site of PBPs also contains an extensive hydrogen bonding network, including a direct SxxK serine-lysine donor-acceptor pair. The favorable energy of this interaction results in an increase in the acidity of the serine hydroxyl group due to the stabilization of its conjugate base.¹⁵¹ Finally, the Born effect prescribes that the ionized state of an acid or base exists more readily in a hydrophilic environment – when buried in a protein, the pK_a is perturbed to favor the neutral species (*i.e.*, the pK_a of the SxxK lysine is decreased).¹⁵² In studies on the pH dependence of *E. coli* PBP5 activity, these general principles have been supported experimentally, with results showing that the SxxK lysine is in its free-base form at optimal catalysis.¹⁰⁸ Further, disruption of the residue's pK_a by substitution with arginine's

guanidine side chain results in a 600-fold decrease in the second order rate constant for penicillin binding.¹⁵³

The preeminent ligand factor affecting β -lactam binding to PBPs is the activation of the lactam ring itself to reaction with nucleophiles, a property determined by the p -orbital character of the lactam nitrogen. In monocyclic 2-azetidinone systems, the amide system is stabilized by resonance, decreasing the electrophilicity of the carbonyl group. In bicyclic systems, however, the amide nitrogen is geometrically constrained to an sp^3 hybridized trigonal pyramidal geometry, decreasing this resonance effect.¹⁵⁴⁻¹⁵⁹ The result is that in bicyclic systems, the lactam ring exhibits much higher intrinsic reactivity to nucleophiles. The amount of nitrogen p -orbital character can be measured by the distance of the nitrogen from the base of the trigonal pyramid defined by its three bond-pair substituents, a parameter known as the Woodward height¹⁶⁰⁻¹⁶² (**Figure 1.6**).

1.2.c. Major classes of β -lactam antimicrobials

Monobactams are the simplest class of β -lactam antimicrobials, possessing a monocyclic 2-azetidinone system with an N -sulfonic acid moiety (**Figure 1.7**) the base structure of which was first isolated from *Chromobacterium violaceum*.¹⁶³⁻¹⁶⁵ Due to their monocyclic structure, they are the least activated of the β -lactam antimicrobials, and their activity is thought to be a consequence predominantly of their ease of entry into PBP active site. However, there is evidence to suggest that the electron-withdrawing inductive effect of the N -sulfonic acid serves to disrupt amide resonance, albeit slightly, lending to partial p -orbital character of the nitrogen's hybrid orbitals.¹⁶⁶ There is currently only one monobactam in clinical use, aztreonam, which exhibits potent inhibition of Gram-negative PBPs.¹⁶⁷⁻¹⁷⁰ It finds limited utility clinically, however, as it has no activity against Gram-positive or anaerobic bacteria.

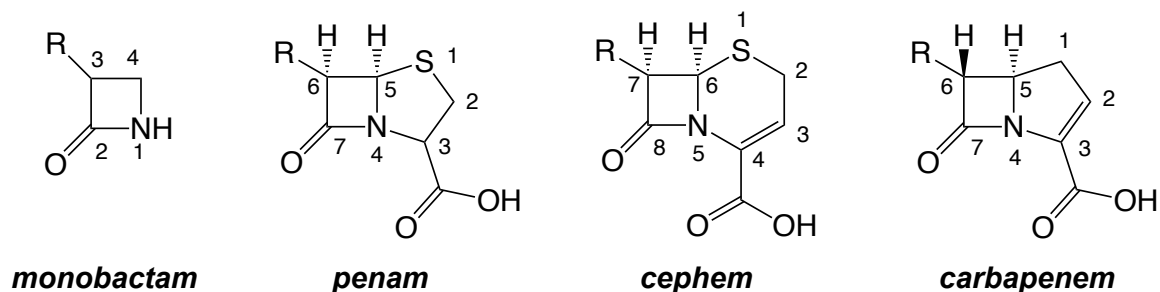


Figure 1.7: Structures of major classes of β -lactams in clinical use.

Penams are a class of β -lactams possessing an azabicyclo[3.2.0]heptane ring system, a carboxylic acid moiety at C3, and a sulfur atom at position one (**Figure 1.7**). They exhibit a large Woodward height ($h \sim 0.4 \text{ \AA}$) due to strain imparted by 5-membered ring fusion, and as such, exhibit good intrinsic reactivity to nucleophiles. Interestingly, molecules of the penam class can exist in two distinct conformational states, one in which the C3 carboxylate is in an equatorial position in relation to the ring system and one in which it is axial¹⁷¹⁻¹⁸⁷ (**Figure 1.6**). In the equatorial position, it contributes to a lower Cohen distance ($c \sim 3.9 \text{ \AA}$) and, thus, a better fit to the geometric requirements of the PBP active site. In the axial position, the structure is considered inactive ($c \sim 4.3 \text{ \AA}$). The existence of two equally populated states related by rotation results in lowered activity compared with lactams possessing constrained carboxylate α -carbons. The prototypic and most well-known penam is penicillin G, or benzylpenicillin, discovered in cultures of *Penicillium chrysogenum* in the 1920s.¹⁸⁸ The other natural product penam is penicillin V, or phenoxymethylpenicillin. In the absence of β -lactamases, the natural penicillins show good Gram-positive activity but fail to inhibit the growth of many Gram-negative organisms.¹⁸⁹⁻¹⁹³ A great deal of medicinal chemistry has been executed on the penam scaffold to modulate the spectrum of this class, resulting in many structural subclasses. The penicillinase-resistant penicillins (e.g., nafcillin, oxacillin, cloxacillin, dicloxacillin), as the name implies, were introduced specifically to combat the acquisition of narrow-

spectrum β -lactamases and do not exhibit improved Gram-negative activity over the natural product compounds;¹⁹⁴⁻²⁰⁴ the aminopenicillins (e.g., ampicillin, amoxicillin) show better Gram-negative activity but are generally outperformed by the natural penicillins against Gram-positive organisms;²⁰⁵⁻²⁰⁷ the carboxypenicillins (e.g., carbenicillin, ticarcillin) exhibit rather potent Gram-negative inhibition while retaining good Gram-positive coverage;²⁰⁸⁻²¹² and the ureidopenicillins (e.g., piperacillin, mezlocillin, azlocillin) show similar spectrum to the carboxypenicillins but generally possess increased potency in comparison.^{208,209,211,213,214}

Cephems are a class of β -lactams possessing an azabicyclo[4.2.0]oct-2-ene ring system, a carboxylic acid moiety at C4, and a sulfur atom at position one (**Figure 1.7**) These systems generally exhibit low Woodward heights ($h \sim 0.3 \text{ \AA}$) due to conformational flexibility afforded by having a 6-membered ring fusion; however, there exists a competitive enamine resonance, resulting from the delocalization of the nitrogen's lone electron pair into the π electron system of the dihydrothiazine ring, that contributes to disrupted amide resonance.^{155,159,215} A unique feature of cephem-based compounds is their chemistry at the C3 position, which can act as a leaving group upon ring opening due to the aforementioned enamine resonance. The departure of a C3 leaving group results in the formation of an exocyclic olefin that may enhance the thermodynamic stability of the acyl enzyme complex, thereby decreasing regeneration of apoenzyme.²¹⁶ Whether or not it is a leaving group, C3 can participate in long range inductive effects with the β -lactam amide moiety, and strongly electron withdrawing groups are postulated to enhance the electrophilicity of the active carbonyl.^{159,217,218} A fixed, low Cohen parameter is characteristic of the class due to sp^2 hybridization of C4 ($c \sim 3.2 \text{ \AA}$) (**Figure 1.6**).

The first identified cephem, cephalosporin C, was isolated from *Acremonium chrysogenum* and showed only marginal antimicrobial activity;²¹⁹⁻²²⁵ however, its many semisynthetic derivatives have enjoyed great success as potent

therapeutics. The cephalosporins are categorized into “generations” based on medicinal chemistry and antimicrobial spectrum (**Figure 1.8**). First generation agents generally possess an aromatic acylamino side chain at C7 and possess potent Gram-positive activity.²²⁶⁻²³² While second generation agents explore other aromatic acylamino groups at C7, much of the variation found in this generation is from the replacement of the acetoxy group with various nucleophiles (*i.e.*, carbamates, heterocyclic mercaptans, and pyridines) (**Figure 1.8**). Second generation agents largely exhibit broader spectrum than their earlier counterparts, with some showing potent inhibition of Gram negatives with high intrinsic resistance.²³³⁻²⁴⁰ Among the key findings of this iteration of cephalosporin design was the alkoxyimino moiety, seen in cefuroxime, which confers resistance to degradation by serine β -lactamases.²⁴¹⁻²⁴³ This functional group became a mainstay in the design of third generation agents, while the aryl group was modified to an aminothiazole, a change found to enhance Gram negative activity (**Figure 1.8**). One notable outlier is cefoperazone, which borrows its C7 acylamino group from the ureidopenicillin piperacillin. This group exhibits not only further expanded spectrum compared to previous generations, but also good stability to serine β -lactamases.²⁴⁴⁻²⁵⁹ In the fourth generation, various quaternary nitrogen-containing C3 were examined to enhance passive transport through the Gram negative outer membrane, decrease affinity for β -lactamases, and promote departure of the leaving group.²⁶⁰⁻²⁶⁶ Fifth generation agents are specifically engineered to combat various resistance problems while attempting to maintain spectrum.²⁶⁷⁻²⁸⁰ In general, these compounds maintain the alkoxyimino group, exchange the aminothiazole for an aminothiadiazole, and exhibit planarity in their C3 substituents.

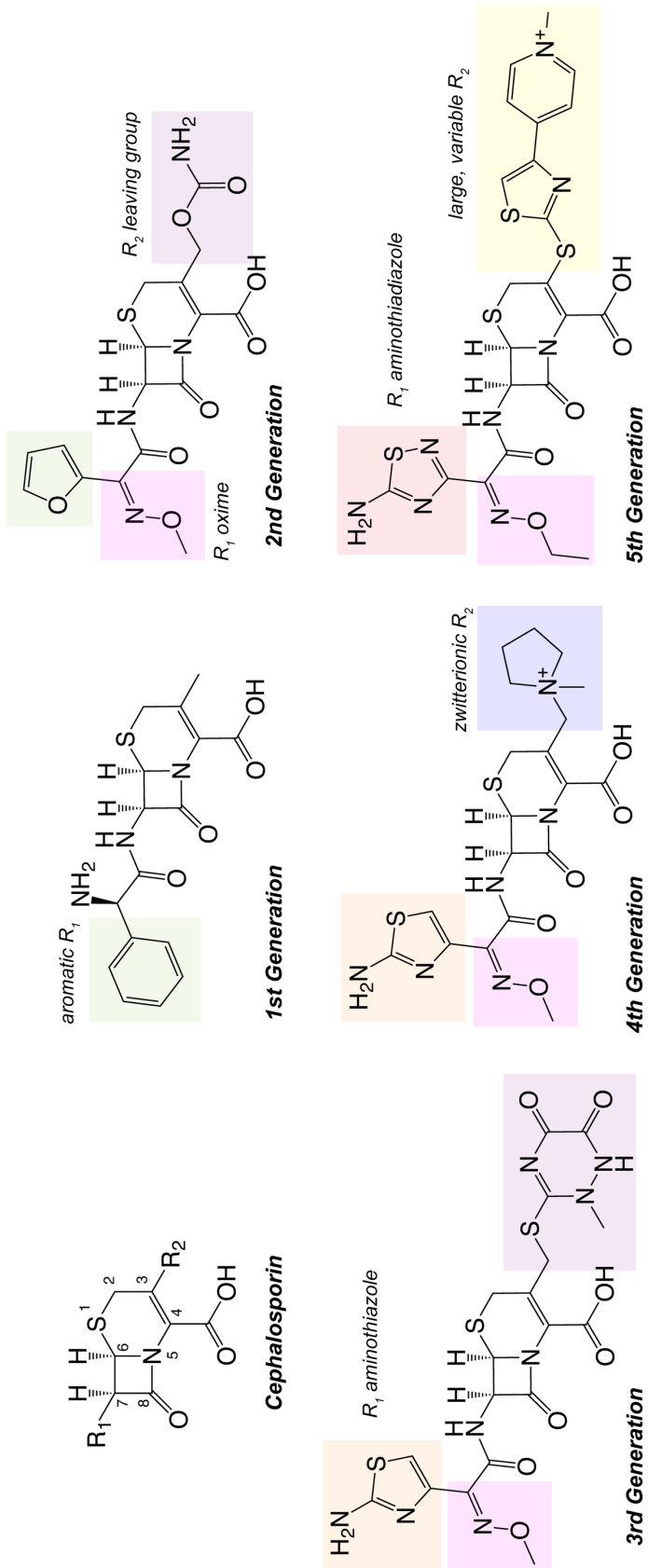


Figure 1.8: Salient features of cephalosporin design by generation.

Carbapenems are a class of bicyclic β -lactams possessing an azabicyclo[3.2.0]hept-2-ene ring system, a carboxylic acid moiety at C3, and a carbon atom at position one (**Figure 1.7**). The carbapenems are thought to be the most intrinsically active of known β -lactams – their rapid acylation of PBPs and potent antimicrobial activity have been ascribed to a highly activated lactam ring system, as shown by experiments examining the kinetics of base hydrolysis.^{156,162} Crystallographic structures reveal a high Woodward coefficient ($h \sim 0.5 \text{ \AA}$) attributable to the geometric constraints introduced by the unsaturation between C2 and C3 and the replacement of sulfur with carbon at position one. Similar to the cepheems, the carbapenems exhibit a fixed Cohen distance due to an sp^2 hybridized C3, but the bond angles imposed by a 5-membered fused ring position the carboxylate slightly further from the lactam ($c \sim 3.5 \text{ \AA}$) (**Figure 1.6**). The C6 *R*-hydroxyethyl side chain possessed by molecules of this class represents a significant departure from penams and cepheems, which generally exhibit large and variable aminoacyl side chains at this position. Differences in activity and spectrum among compounds of this class are, therefore, dictated almost exclusively by the side chain at C2. Since the isolation of thienamycin from *Streptomyces cattleya* in the 1970s,^{281,282} only four carbapenems have been approved for clinical use by the FDA: imipenem, doripenem, meropenem, and ertapenem.²⁸³⁻²⁸⁶ Given their broad spectrum, as well as their stability against β -lactamases afforded by their C6 *R*-hydroxyethyl side chain and *trans* C5-C6 geometry,²⁸⁷⁻²⁸⁹ the carbapenems have found most of their clinical utility as antimicrobials of last resort in infections with multidrug resistant organisms.

1.3. β -lactams in the treatment of *Neisseria gonorrhoeae*

1.3.a. Overview of antimicrobial resistance

The discovery of penicillin and other compounds capable of inhibiting bacterial growth revolutionized modern medicine and continues to shape its practice. These therapies not only provided a means of pharmacologically managing conditions and injuries that in the past killed or impaired many, but also provided avenues to prevent infection post-operatively and in immunosuppressed patients, including those undergoing solid organ transplant, those with advanced stage HIV / AIDS, and those receiving myelotoxic cancer therapies. However, with increased and sometimes improper use of antibiotics, resistance to these and other drugs has emerged in a number of common pathogens, thereby limiting treatment options. Prominent examples include methicillin resistant *Staphylococcus aureus* (MRSA),²⁹⁰ vancomycin resistant enterococcus (VRE),²⁹¹ multidrug resistant nosocomial pathogens (*Pseudomonas aeruginosa*, *Klebsiella pneumonia*, *Stenotrophomonas maltophilia*, etc.),²⁹²⁻²⁹⁴ and sexually transmitted infections (*Neisseria gonorrhoeae*, *Mycoplasma genitalium*).^{295,296} In 2014, the WHO began to warn of a post-antibiotic era, citing antimicrobial resistance as among the most dangerous current threats to public health.²⁹⁷ With the increasing prevalence of strains resistant to the existing armamentarium of antimicrobials, there is a great and manifest need for the development of new drugs to treat these infections.

Antimicrobial resistance is classically ascribed to any combination of the following processes: decreased accumulation at the site of action, drug inactivation by degradative or modifying enzymes, overproduction of endogenous substrates, or target alteration by either chromosomal or enzymatic means (**Figure 1.9**). While *N. gonorrhoeae* employs multiple mechanisms in achieving β -lactam resistance, among its most powerful tools is the modification of the penicillin-binding proteins.

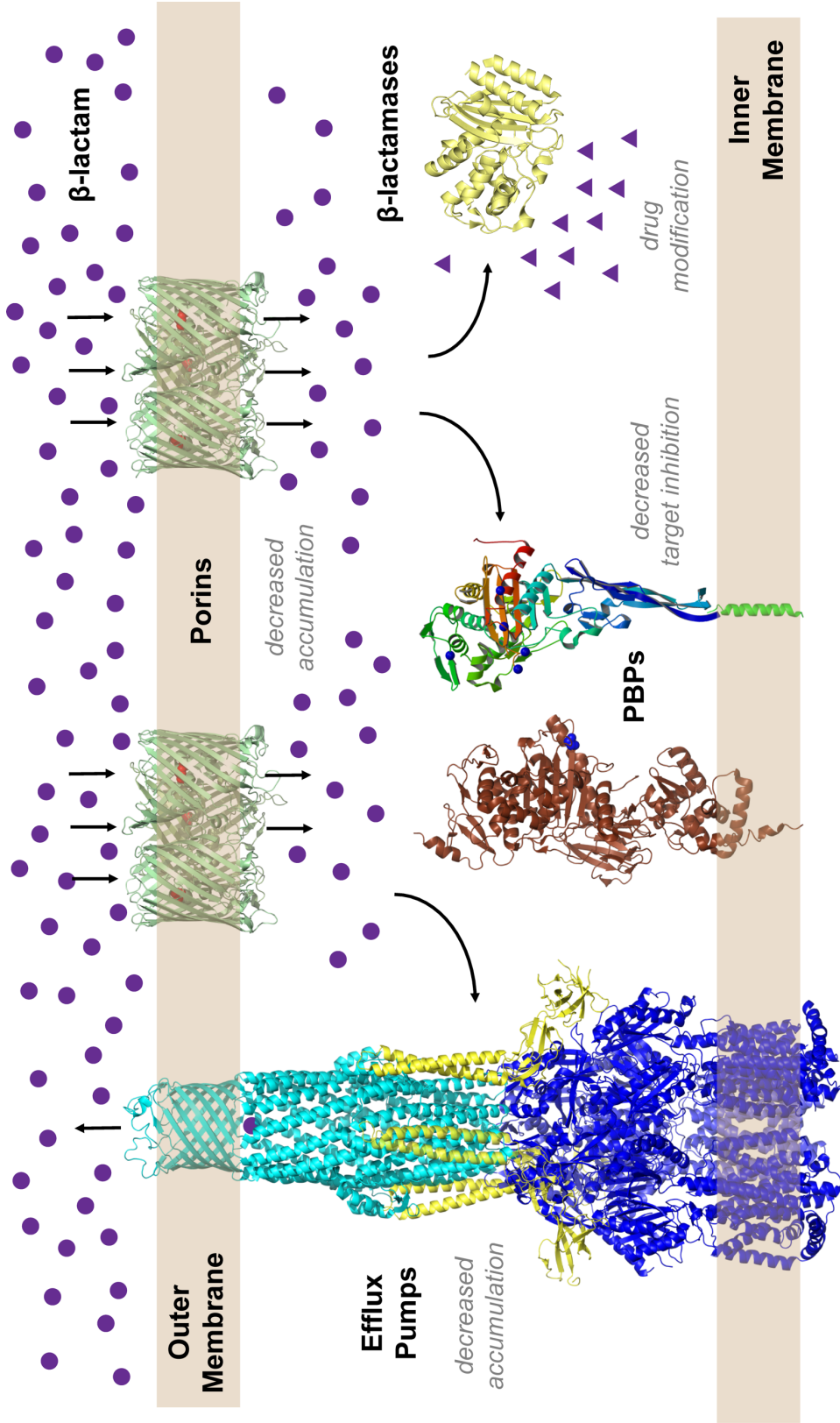


Figure 1.9: Mechanisms of β -lactam resistance in *N. gonorrhoeae*. Figure borrowed from Robert Nicholas, PhD, and adapted.

1.3.b. Gonococcal β -lactam resistance not mediated by PBPs

Because peptidoglycan crosslinking occurs in the periplasmic space, β -lactams must permeate the bacterial outer membrane to exert their cytotoxic effects. Hydrophilic small molecules require aqueous channels known as porins to cross this barrier, and bacteria have developed several mechanisms for restricting entry²⁹⁸ including global decreases in porin expression,²⁹⁹⁻³⁰² shifts in expression from one porin type to another of smaller channel radius,³⁰³ and porin mutations resulting in impaired permeation through the channel.³⁰⁴ In *Neisseria gonorrhoeae*, changes in antimicrobial permeability are mediated in part by mutations in *porB_{1B}* encoding the major outer membrane protein porin B1b, known as the *penB* resistance determinant.³⁰⁵ These mutations are located at positions 120 and 121 on loop 3, which lies within the β -barrel in crystal structures of several porins (including *N. meningitidis* porin B).^{304,305} It is hypothesized that these mutations perturb the structure of the pore constriction, thereby disallowing entry of larger solutes; however, *penB* is phenotypically silent in the absence of efflux overexpression.³⁰⁶ Changes to other pore-forming elements may also diminish the periplasmic accumulation of β -lactams in *N. gonorrhoeae*, such as point mutations to the *pilQ* gene encoding secretin PilQ acquired by laboratory strains.³⁰⁷ This type of mutation, known as the *penC* resistance determinant, decreases β -lactam susceptibility, but its disruption of transformation and piliation make it unlikely to be found in clinical isolates.

As illustrated by mutations to *porB1b* and *pilQ*, changes in outer membrane permeability alone frequently do not alter susceptibility significantly and are often associated with additional resistance mechanisms.³⁰⁸ Another mechanism responsible for diminished intracellular accumulation is the production of multiunit macromolecular machineries that extrude amphipathic xenobiotic compounds, including dyes, detergents, solvents, and antimicrobials. These efflux pump systems can be categorized structurally into the following families: the ATP-binding cassette (ABC) family, the resistance-

nodulation-cell division (RND) family, the multidrug and toxic compound extrusion (MATE) family, and the small multidrug resistance (SMR) family.^{309,310} These families are distinguished from one another by species specificity, macromolecular structure, substrate range, and energy source. While baseline expression of efflux systems can afford survival in the presence of certain classes of antimicrobials (*i.e.*, intrinsic resistance), their overexpression is of key concern in the development of marked or multidrug resistance.³¹¹ *N. gonorrhoeae* possesses a tripartite multiple transferable resistance (Mtr) efflux pump system belonging to the RND family.³¹²⁻³¹⁶ The Mtr system has broad substrate specificity that includes many classes of antimicrobial drugs, cationic antimicrobial peptides, natural antibiotics, and detergents.^{312,317,318} It is encoded by the *mtrCDE* gene complex and regulated by the opposing actions of an activator (*mtrA*) and a repressor (*mtrR*).³¹⁹⁻³²² Several mutations conferring resistance are observed this system, but the most common are single missense mutations to a 13 base-pair inverted repeat in the *mtrR* promoter region.^{320,323-326} Nonconservative mutations in the *mtrR* DNA binding region have also been reported.^{324,326,327} These loss-of-function mutations in *mtrR* result in the derepression of *mtrCDE*, allowing for the overexpression of efflux components and a concomitant increase in their assembly.

A final, less ubiquitous mechanism by which bacteria hinder antimicrobial entry is the formation of biofilms.^{328,329} The biofilm state reduces the overall surface area of antimicrobial exposure, relative to the bacterium's planktonic form. Permeation is also an issue, with thicker biofilms being generally more difficult to fully eliminate. The observed antimicrobial tolerance is likely influenced by more than simple diffusion mechanics, however. Studies of expression programs indicate cells in a biofilm go into a dormant "persister" state that renders them less susceptible to antimicrobial drugs targeting protein synthesis and cellular division.^{330,331} The gonococcus has developed means of hindering antimicrobial access by decreasing exposed bacterial surface area as well. Expression of

surface molecules (*i.e.*, phase variable pili, opacity-associated proteins, and lipooligosaccharide) promotes gonococcal interactions *in vitro*, resulting in microcolony aggregation and, ultimately, in biofilm formation.³³²⁻³³⁵ Gonococcal aggregation has been shown to increase ceftriaxone tolerance *in vitro*, with cultivable bacteria being isolated after 24-hour exposure to 1 µg/mL.³²⁹ In the same set of experiments, residual gonococcal viability was found even in a 10 µg/mL treatment group, as measured by ATP production. This phenomenon is relevant *in vivo* as well, as there is evidence of gonococcal biofilm formation in cervical biopsies of patients with gonococcal cervicitis.³³⁶

Another mechanism of resistance is production of enzymes that inactivate the molecule by addition or removal of chemical moieties or destroy it by hydrolysis.³³⁷ Several classes of modifying enzymes have been identified that catalyze the following reactions: acetylation of aminoglycosides, chloramphenicol, and streptogramins; phosphorylation of aminoglycosides and chloramphenicol; and adenylation of aminoglycosides and lincosamides.³³⁸⁻³⁴³ These reactions alter molecular moieties critical to interaction with antimicrobial targets, thereby diminishing binding. The predominating degradative enzymes are the hydrolytic β-lactamases, which cleave β-lactams at the active amide bond, rendering them incapable of participating in the covalent inhibition process characteristic to the class.³⁴⁴⁻³⁴⁸ High-level gonococcal resistance to penicillin can also be achieved through the acquisition of plasmids containing the *bla*_{TEM-1} gene, which encodes a TEM-1 β-lactamase capable of hydrolyzing penicillins, rendering them inactive.^{18,19,349} Although no extended-spectrum β-lactamases (ESBLs) have yet been reported in gonococcal isolates, another plasmid containing *bla*_{TEM-135} has been identified.³⁵⁰⁻³⁵² From structural and functional comparisons, it is proposed that the encoded TEM-135 penicillinase may be a direct precursor to an ESBL capable of hydrolyzing cephalosporins.³⁵¹

Less studied resistance mechanisms involve the modulation or evolution of pathways that compensate for loss of an essential cellular component or enzyme. Bacteria are capable of making sophisticated global adaptations to metabolism, including shifts between glycolytic and oxidative pathways, alterations in fructose utilization, or changes in fatty acid oxidation.³⁵³⁻³⁵⁷ Many of these changes are postulated to result in modulation of cell wall autolytic activity and other cell surface properties. In gonococcal strains exhibiting mosaic *penA*, whose gene products likely function suboptimally as transpeptidases, compensatory metabolic changes ameliorate fitness defects. It has been shown that introduction of mosaic *penA41* to a wild-type strain results in the development of spontaneous mutations in the *acnB* gene encoding the TCA cycle enzyme aconitase B, as well as in other metabolism-related genes, and that these mutations increase the fitness of strains harboring mosaic *penA* alleles to near-wild-type levels.³⁵³ While the exact effect of these mutations remains unknown, there are large global shifts in the expression of genes involved in energy and carbon metabolism that occur in the presence of a specific *acnB*-G348D mutation, a change that slows the interconversion of citrate and isocitrate by the enzyme.

There are yet additional resistance mechanisms in *N. gonorrhoeae* that have not yet been fully elucidated. Factor X, as it is termed, is a nontransformable determinant of unknown identity that can increase penicillin MICs as much as 6-fold.³⁵⁸

Table 1.1: Summary of non-PBP-mediated β -lactam resistance in *N. gonorrhoeae*. *Only seen in laboratory strains. **Plasmid-mediated. ***Observed in laboratory strains transformed with mosaic *penA*. Have not yet been confirmed in clinical isolates.

Target (<i>gene</i>)	Function	Mutations	Consequence	Mechanism
MtrCDE (<i>mtrR</i>)	Efflux pump system	Single nucleotide deletion in promoter region, G45D	Overexpression	Increased efflux
PorB1b (<i>porB1b</i>)	Porin	G120K, G120D, A121D	Altered constriction pore	Reduced influx
PilQ (<i>pilQ</i>)*	Pore-forming secretin of type IV pilus	E666K	Disruption of pore formation	Reduced influx
Opa, Pil, LgtE	intercellular interactions	None	Aggregation, biofilm formation	Decreased permeability
Factor X	Unknown	Unknown	Unknown	Unknown
TEM-1, TEM-135 (<i>bla_{TEM}</i>)**	Penicillinase	-	Expression from plasmid	Hydrolysis
aconitase B (<i>acnB</i>)***	TCA cycle enzyme (citrate \rightarrow isocitrate)	G348D	Decreased flux through TCA cycle, changes in expression of metabolic genes	Compensatory changes in energy metabolism
MleN (<i>mleN</i>)***	malate-2H ⁺ / lactate-Na ⁺ antiporter	Δ A467	Uncharacterized	Uncharacterized

1.3.c. Target modification involving gonococcal PBP2

Target modification is a common mechanism of antimicrobial resistance in which the target active site is obscured or its topology altered to diminish binding of the antimicrobial. This can be accomplished by mutations to the gene encoding the target,³⁵⁹ enzymatic addition of chemical moieties to critical contact atoms,^{360,361} or conformational changes resulting from interaction with other macromolecules.^{362,363} There exist several examples of pathogens with modified PBPs that exhibit diminished acylation by β -lactams. The MRSA *mecA* determinant is a notable example of target modification; this gene encodes a homolog of the *S. aureus* β -lactam target possessing a closed active site, such that β -lactams cannot gain access for inhibition.³⁶⁴⁻³⁶⁶ *S. pneumoniae* develops chromosomally-mediated high resistance to β -lactams through the acquisition of mutations in any or all of five of its PBPs.³⁶⁷⁻³⁷⁴ While point mutations can contribute to a

resistant phenotype, the hallmark of pneumococcal resistance is horizontal transfer of portions of the *pbpx* gene from resistant commensal streptococci with that of pneumococcus, generating a low-affinity mosaic PBP2x protein. *E. faecium* not only acquires point mutations in *pbp5* under selective pressure, but it also begins to overexpress the low-affinity PBP5 mutant.³⁷⁵⁻³⁷⁷ Point mutations to the *ftsI* gene encoding PBP3 have been shown to commonly contribute to β -lactam resistance in *H. influenzae*,³⁷⁸⁻³⁸¹ and alterations in PBP1 have been reported in penicillin-resistant *C. perfringens*.^{382,383}

Biochemical and molecular studies have shown that a majority of the decrease in susceptibility seen in β -lactam-resistant strains of *N. gonorrhoeae* is due to chromosomal alterations resulting in the modification of PBP2.^{358,384} First, isolated membrane preparations from β -lactamase-negative penicillin-resistant gonococci show marked reduction in acylation of PBP2 by [³H]-penicillin G.^{385,386} These results have been replicated in purified protein assays, showing decreased acylation of PBP2 from penicillin- and cephalosporin-resistant strains by a variety of β -lactams.^{384,387-390} Additionally, when *penA* genes from resistant strains are transformed into the fully susceptible standard FA19 (*i.e.*, in the absence of other resistance determinants), susceptibility to β -lactams plummets.^{128,358,384,385} In early studies of penicillin resistance, transformation of *penA* genes from chromosomally resistant strains isolated in Australia caused a 100- to 400-fold increase in the minimum inhibitory concentrations (MIC) of penicillin. More recently, transformation of the *penA* gene from a Ceph^{DS} strain (*penA35*) into FA19 resulted in 20- and 40-fold increases in the MICs of ceftriaxone and cefixime, respectively, while transformation of the *penA* gene from a Ceph^R strain (*penA41*) resulted in 300- and 500-fold increases. The MICs exceeded the European Committee on Antimicrobial Susceptibility Testing (EUCAST) clinical resistance breakpoint of 0.125 μ g/mL in both cases (0.31 μ g/mL and 1.6 μ g/mL for ceftriaxone and cefixime, respectively). These experiments establish mutations in PBP2 as the primary β -lactam resistance determinant in *N. gonorrhoeae*.

1.3.d. PBP2 modifications resulting in penicillin resistance

The first use of penicillin against gonococcal infection was in a case of gonococcal ophthalmia neonatorum in 1930.³⁹¹ Due to its success in treating the affected infant, and with growing concerns of sulfonamide resistance at the time, penicillin was tested against gonococcal urethritis in the early 1940s. In several studies, therapeutic efficacies of 76-100% were obtained in men after verified sulfonamide failure.^{11,13,393-397} Penicillin thus replaced sulfonamides as first-line treatment for gonococcal infections. Despite early success, the proportion of penicillin-resistant gonococcal strains climbed steadily over the coming years.¹⁵ In a longitudinal study of 5,700 isolates, conducted from 1959 to 1967, a marked temporal increase in resistance was observed.¹⁴ At the outset of the study, 63% of isolates were susceptible to 0.01 µg/mL, and all isolates were susceptible to 0.3 µg/mL. Eight years later, only 13% were susceptible to 0.01 µg/mL, and 83% were susceptible to 0.3 µg/mL, with 9% showing resistance to concentrations greater than 1.0 µg/mL. During this period, prescribed doses were increased to maintain satisfactory cure rates, and an increasing number of treatment failures were reported.³⁹⁸⁻⁴⁰⁵ In 1976, the first gonococcal strains possessing plasmid-borne penicillinases were identified in California,^{17-20,406} but the growing prevalence of chromosomally mediated resistance is what eventually drove reevaluation of treatment guidelines and a search for more efficacious therapies.^{16,385,386,407-412}

Examination of the *penA* sequences of chromosomally mediated penicillin-resistant *N. gonorrhoeae* (CMRNG) revealed that their PBP2 variants generally contain 5 to 8 amino acid changes compared to wild-type enzyme from FA19.^{413,414} A key mutation is the insertion of an Asp (Asp346a) after position 346^{415,416} (**Figure 1.10**). This insertion is positioned in the transpeptidase domain immediately adjacent to another Asp (Asp346), which forms a functionally significant hydrogen bond with Ser363 of the SXN motif.³⁸⁸ The hydrogen bond is maintained in the Asp364a mutant, and the insertion appears to confer

increased flexibility to the β 2c- β 2d loop.^{397,389} Additionally, the side chain of Asp346a projects toward the β -lactam binding site, so while the precise mechanism of resistance is not entirely clear, it has been proposed that the insertion may sterically hinder antibiotic binding during Michaelis-Menten complex formation or electronically hinder breakage of the β -lactam ring during acylation.³⁸⁹ PBP2 variants of Pen^R strains generally possess additional mutations in the carboxy-terminal region, further decreasing the acylation rate and reducing susceptibility.^{387,389} Interestingly, these mutations do not greatly change the structure of the enzyme, even locally, indicating that the mechanism of resistance may be dependent upon protein dynamics.

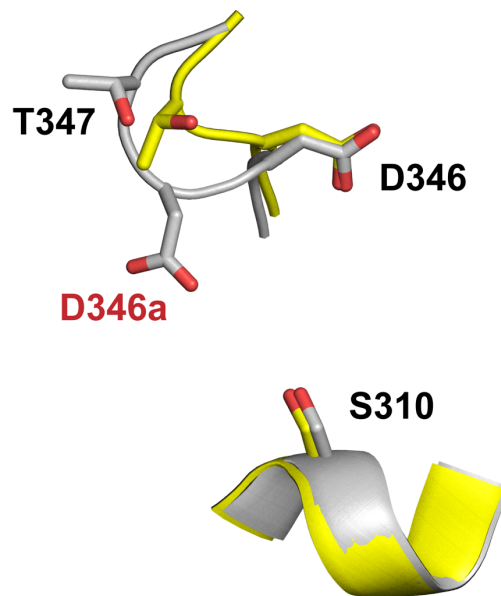


Figure 1.10: Changes to the active site of penicillin-resistant FA6140 as a result of an Asp346a insertion. PBP2^{WT} is shown in yellow. PBP2⁶¹⁴⁰ is shown in grey.

1.3.e. PBP2 modifications resulting in cephalosporin resistance

After the withdrawal of fluoroquinolones in the early-to-mid 2000s, cephalosporins were the only remaining drugs indicated for the treatment of gonococcal infections.³⁹ However, in the last two decades, cephalosporin resistance has emerged as well.⁴¹⁻⁵⁹ Among the first reported cases of reduced susceptibility (Ceph^{DS}) was the Swedish 35/02 strain in 2002.⁴¹⁷ The 35/02 strain exhibits MIC values of 0.38 and 0.094 µg/mL for cefixime and ceftriaxone, respectively, corresponding to 25- and 60-fold increases compared to a wild-type reference strain 119/05. Many additional Ceph^{DS} strains were isolated in Sweden, the UK, and the United States around this time, showing MICs of 0.19-0.38 and 0.094-0.125 µg/mL for cefixime and ceftriaxone, respectively.⁴¹⁷

The primary difference between penicillin-resistant and ESC-resistant strains is the number and types of *penA* mutations present. Whereas Pen^{DS/R} strains contain relatively few mutations in PBP2, Ceph^{DS/R} strains possess *penA* alleles encoding PBP2 variants with around 60 amino acid changes compared to the wild type protein (**Figure 1.11**). It is proposed that these *penA* genes are acquired by horizontal transfer events between *N. gonorrhoeae* and commensal *Neisseria* species (e.g., *N. flavescens*, *N. cinerea*, *N. lactamica*, etc.).^{45,46,418,419} The commensal species, occupying microbiological niches in the urogenital tract and pharynx, develop chromosomal resistance through frequent exposure to antimicrobials and subsequently act as reservoirs for antimicrobial resistance genes.^{420,421} When prolonged gonococcal infection occurs at these sites, these genes are readily acquired by the gonococci by transformation and subsequent homologous recombination, resulting in a “mosaic” allele encoding a PBP2 variant with lowered cephalosporin acylation.^{390,417} Three mutations in mosaic PBP2^{35/02} (encoded by the *penA35* allele), G545S, I312M, and V316T, are significant for decreased ESC susceptibility in 35/02,⁴²² but when incorporated into wild type *penA* and transformed into

the Pen^SCeph^S FA19 strain, resistance to ESC increased only marginally.¹²⁸ However, when these three mutations were reverted to wild-type in the *penA35* background, they were found to have a prominent effect on resistance (**Table 4.2**). This result indicates that these resistance mutations require other mutations present in the *penA35* mosaic to exert their effects, a phenomenon known as epistasis.

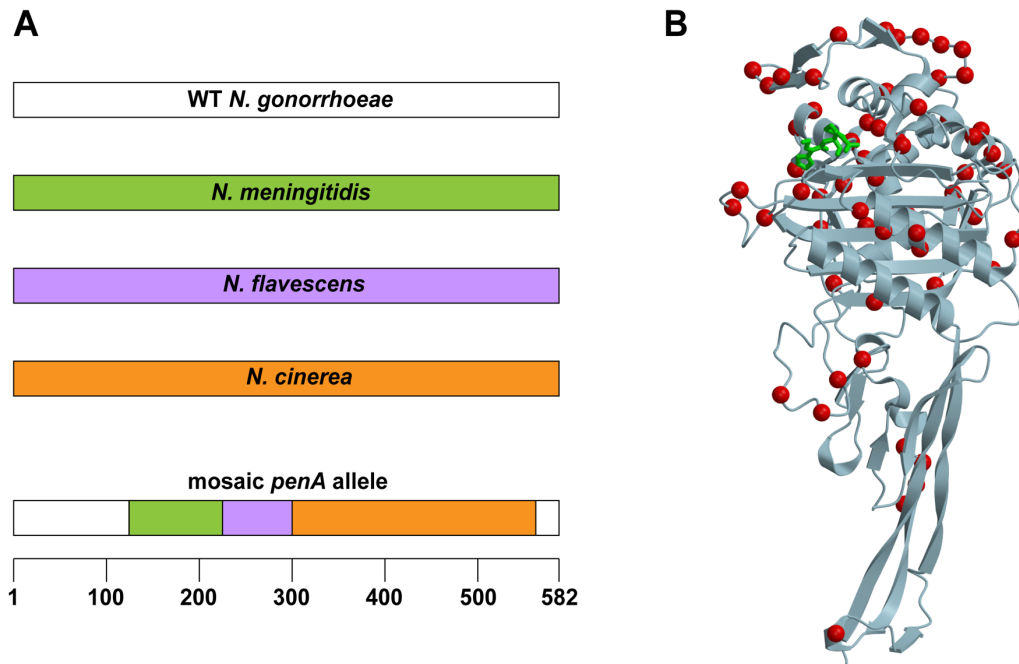


Figure 1.11: Mosaic *penA* allele and PBP2 structure. **A.** Mosaic *penA* alleles are created by *N. gonorrhoeae* through homologous recombination of the *penA* allele of wild-type *N. gonorrhoeae* with those of β -lactam-resistant *Neisseria* commensal species. **B.** The PBP2 variants encoded by mosaic *penA* have around 60 mutations compared to wild-type enzyme (H041 shown, mutations indicated as red spheres).

By generating chimeric *penA* in which segments, or modules, of *penA35* were reverted to the wild-type sequence, information was gained on which mutations in *penA35* contribute to β -lactam resistance. FA19 transformants with wild-type module 4 (comprising residues 489 to 528) on a *penA35* background showed the greatest increase in susceptibility, indicating one or more mutations in this region are critical to resistance.¹²⁸

Subsequent transformation experiments with *penA35* alleles lacking individual module 4 mutations showed that F504L, A510V, and N512Y also contribute to β -lactam resistance in the 35/02 strain, with A510V seeming to specifically affect penicillin susceptibility.

Cephalosporin-resistant gonorrhea was first identified in 2009, as a single case involving a female Japanese sex worker with a pharyngeal infection.^{62,63} Pharyngeal cultures came back positive two weeks after standard therapy with ceftriaxone, and infection clearance was only achieved by a repeat dose upon follow-up. While cultures for the patient's second presentation were not tested (indicating the potential for reinfection, rather than treatment failure), the isolated strain, known as H041, exhibits MIC values of 8 and 2 $\mu\text{g/mL}$ for cefixime and ceftriaxone, respectively, corresponding to 6,000- and 3,000-fold increases compared to Pen^SCeph^S strain FA19. Its notable resistance to many other antibiotics marks H041 as the first identified pan-resistant strain. This sentinel event in the timeline of antibiotic resistance led the WHO to declare *N. gonorrhoeae* a "superbug" in 2012 and the CDC to update its designation to "urgent threat" in 2013.⁴²³

The *penA* gene from the H041 strain (*penA41*) is a mosaic containing 13 additional mutations compared to *penA35*. When transformed into FA19, the *penA41* allele increases the MICs of ceftriaxone and cefixime by 300- and 570-fold, respectively.³⁸⁴ Three mutations, A311V, T316P, and T483S, were identified in the *penA41* allele that, when incorporated into the *penA35* allele, confer a majority of the increased resistance seen in H041 compared to 35/02. A311V and T316P are located near the serine nucleophile (Ser310) and are expected to affect $\alpha 2$ in some yet unconfirmed way. T483 is predicted to recognize the carboxylate moiety of β -lactam antibiotics via its hydroxyl group, and while T483S is a conservative mutation, loss of the methyl group likely alters this interaction. An H541N mutation is present in many nonmosaic and mosaic *penA* from strains with decreased cephalosporin susceptibility as well.^{45,46,417,422,424-426} In all, the work revealed a total of eight mutations that together confer a majority of the ESC resistance seen in H041 (**Table 1.2, Figure 1.12**).

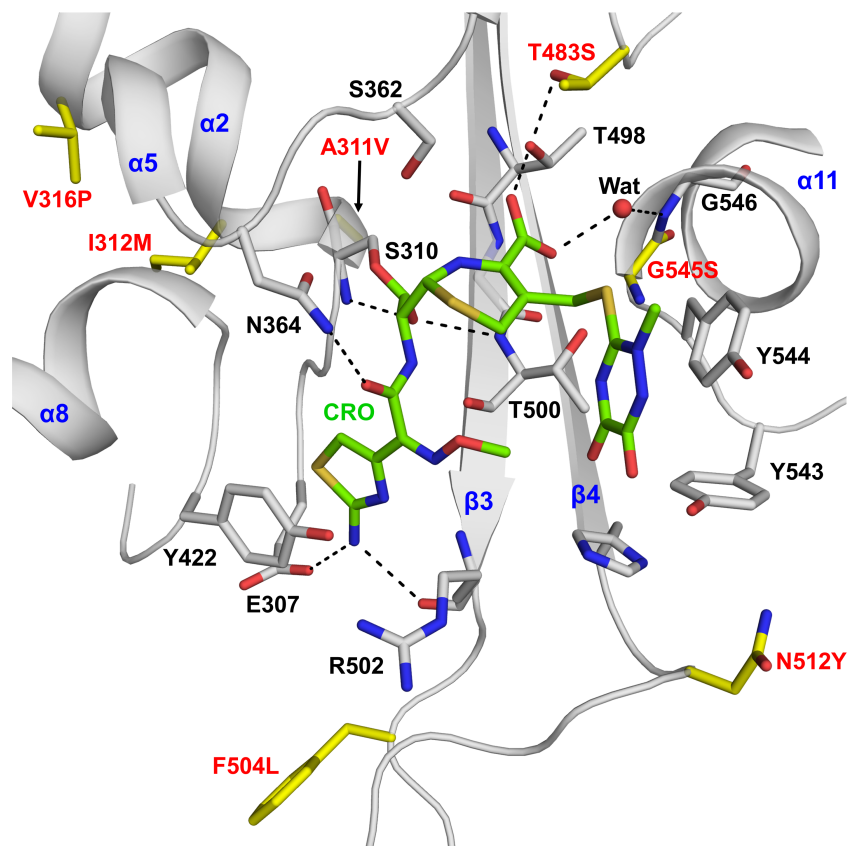


Figure 1.12: Mutations identified as critical to β -lactam resistance in PBP2^{H041}. Resistance mutations (yellow) highlighted within the active site of an acyl-enzyme structure of ceftriaxone (green) in complex with a transpeptidase-only construct of PBP2^{H041}. Polar contacts are shown as black dashed lines. Figure taken from Singh *et al.*, 2020.¹³⁴

Transformation of *N. gonorrhoeae* with a *penA* construct containing these eight mutations alone (8M) was unsuccessful, indicating an insurmountable loss of fitness from a decrease in PBP2 transpeptidase activity [unpublished]. Further experiments revealed that just one mutation, T483S, is responsible for this failure. A construct lacking this mutation (7M) successfully transformed *N. gonorrhoeae*, but to a much lesser level of resistance. It is thus apparent that background epistatic mutations are required for the T483S mutation to contribute to resistance without loss of transpeptidase activity. Transformation experiments have identified these mutations as substitutions within

hydrophobic cores of the protein distant from the active site – A437V, L447V, and F462I [unpublished]. A construct including 8M plus the three epistatics (11M) successfully transformed into *N. gonorrhoeae*, indicating restored transpeptidase activity. Reversal of T483S in 11M reduced MICs of transformed bacteria to the same values as for 7M, confirming the influence of this mutation, and the lack of influence of the epistatic mutations, on ESC resistance.

Structural analysis of PBP2^{H041} reveals that several of these mutations act to restrict protein dynamics required for efficient acylation.¹³⁴ First, the side chain of S545 participates in a hydrogen bonding interaction with the side chain of T498, disallowing its rotation upon recognition of the β -lactam carboxylate. This “locking” of T498 hinders β 3 strand twisting and, thus, oxyanion hole formation. It also affects the final position of the β -lactam by presenting an alternative hydrogen bonding partner for the carboxylate moiety. Second, F504L and N512Y appear to prevent hinging of the β 3- β 4 loop toward the active site, altering key interactions with the β -lactam acylamino side chain. In fact, the β 3- β 4 loop occupies an “outbent” conformation in both *apo* and acyl forms of PBP2^{H041}. Finally, the α 2 mutations A311V, I312M, and T316P cause no obvious structural changes in PBP2^{H041}. However, the A311V and I312M mutations involve increased size of hydrophobic side chains and may increase hydrophobic packing around α 2, decreasing its mobility in the acylation reaction.

Ceph^R *N. gonorrhoeae* has now been reported several times since the emergence of H041. The first case of successful transmission occurred with the French strain F89, isolated in 2010. Initially reported in a man who has sex with men (MSM) with urethritis, the strain came back in a positive repeat urethral culture 3 weeks after cefixime therapy.⁷⁰ Clearance was attained with gentamicin on follow-up. The strain was subsequently reported in Spain in two sexually related MSM.⁶⁴ It exhibits MICs of 4 and 2 μ g/mL for cefixime and ceftriaxone, respectively, and also it possesses resistance to many other antimicrobials. The *penA* gene of F89 possesses only one additional mutation compared

to *penA35*, A501P. Interestingly, alterations at the 501 position had been hypothesized as contributing to cephalosporin resistance only two years prior to F89's isolation. Tomberg *et al.*, while conducting molecular studies of *penA35*, noted the frequency of A501V in nonmosaic *penA* from gonococcal strains with reduced cephalosporin susceptibility^{128,418,424,425} (**Table 1.2**). They found not only that transformation of *penA35*-A501V into FA19 increased its MICs for cefixime and ceftriaxone 2.5-fold compared to *penA35*, but also that cefixime's second order acylation rate against a purified PBP2^{35/02}-A501V construct is half that seen with PBP2^{35/02}. The 501 position continues to be the subject of much investigation due to its differential effects on different classes of β -lactams. Despite further increasing cephalosporin resistance, mutations at this position appear to restore some susceptibility to penams and carbapenems.^{128,427}

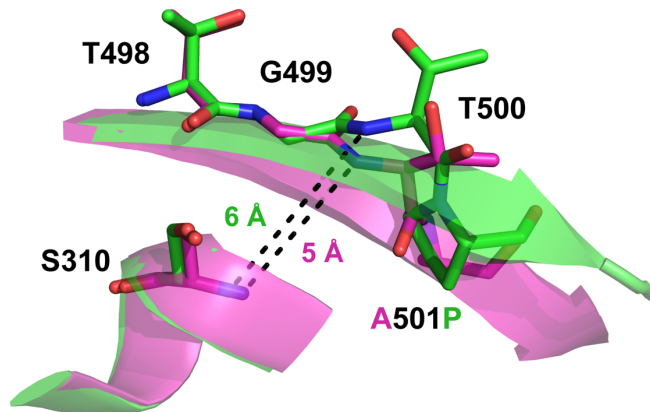


Figure 1.13: *The impact of A501P on the structure of the β 3 strand. P501 causes a displacement of T500, a critical residue involved in oxyanion hole formation.*

Transformation of FA19 with a diverse set of *penA35-A501X* genes revealed that only specific mutations could increase cephalosporin resistance while maintaining essential transpeptidase function.⁴²⁸ Among these, A501P (found in NgF89) and A501R (not yet observed in clinical strains) had the biggest impact, increasing MICs for cefixime and ceftriaxone by 5-fold compared to a *penA35*-transformed control. Consistent with previous data from Bharat *et al.*, every successful *penA35-A501X* transformant had some restoration of penicillin G susceptibility. The differential effect of mutations at the 501 position on the various classes of β -lactams may have to do with perturbation of the oxyanion hole. Kinking of β 3 strand by the introduction of a proline could displace the oxyanion hole more distally from S310. Because the distance between the C4 carboxylate and lactam carbonyl in the cephem framework is typically short, and assuming the SxN, SxxK, and KTG residues act as an electrostatic anchor for the carboxylate, the lactam oxygen may not make the appropriate contacts with both S310 and T500 when in its oxyanionic state, rendering the cephalosporins universally less able to acylate structures with the 501P mutation.

More reports of full cephalosporin resistance are continuing to emerge at an accelerated rate worldwide, including strains from the following countries: China, Japan (GU140106, FC428, FC460, FC498), France (F90), England (G97687/G7944), Denmark (GK124), Australia (A8806, A7536, A7846), Argentina, and Canada (47707). The PBP2 mutants harbored by most of these strains (excluding that reported in Argentina, which is nonmosaic) possess structural similarities, sharing A311V and T483S mutations known to contribute to resistance through studies of H041 (**Table 1.2**). The functional significance of additional mutations in *penA* alleles from these strains has not yet been examined. Interestingly, sufficient genetic relatedness was found in six of these strains to consider them clonal, providing the first evidence of sustained international transmission of cephalosporin-resistant *N. gonorrhoeae*.

Non-mosaic PBP2 can also result in ESC resistance, although so far they have done so to a lesser extent. As mentioned previously, A501V is seen in a variety of non-mosaic *penA* alleles of strains with reduced ESC susceptibility.^{418,424,425} In addition to providing evidence for the role of potential mutations at the 501 position in a mosaic *penA*, Tomberg *et al.* also showed the impact of a variety of these mutations in a non-mosaic *penA4* background.⁴²⁸ The resulting *penA4-A501X* transformants exhibited MICs 2- to 14-fold higher for cephalosporins compared to a *penA4*-transformed control. A statistical approach was used to determine if additional common mutations, G542, P551S, and P551L, have an effect on decreased ESC susceptibility in non-mosaic PBP2 variants. In this study, Whiley *et al.* determined that strains harboring non-mosaic *penA* with any of the three mutations exhibit a significant decrease in ESC susceptibility, with G542-, P551S-, and P551L-harboring strains exhibiting median MICs 7.5-, 3.8-, and 7.5-fold higher than pooled strains lacking the mutations.⁴²⁹ In 2014, a strain possessing a non-mosaic PBP2 variant with P551S was isolated from a young man with purulent urethritis. Its ceftriaxone MIC was 0.5 µg/mL, marking it as the first reported strain of *N. gonorrhoeae* having full resistance to ceftriaxone in the absence of a mosaic PBP2 variant.⁶⁹

Table 1.2: Summary of PBP2 structural changes in key strains of *N. gonorrhoeae* exhibiting a variety of β -lactam susceptibility profiles. ^aAmino acid changes from wild-type characterized as having an effect on β -lactam resistance. ^bMinimum inhibitory concentration.

Strain	Location, Year	Phenotype	Mosaic	Key mutations	PCN (μ g/mL)	CFX (μ g/mL)	CRO (μ g/mL)
FA19	Reference	Pen ^S , Ceph ^S	No	-	0.01	0.001	0.0006
FA6140	USA, 1983	Pen ^R , Ceph ^S	No	D345a, F504L, A510V, A516G, P551S	2	0.05	0.06
35/02	Sweden, 2002	Pen ^R , Ceph ^{DS}	Yes	I312M, V316T, N512Y, G545S	2	0.4	0.1
H041	Japan, 2009	Pen ^R , Ceph ^R	Yes	A311V, I312M, V316P, N512Y, T483S, F504L, H541N, G545S	4	8	2
F89	France, 2010	Pen ^R , Ceph ^R	Yes	35/02 mutations, A501P	1	4	1
A8806	Australia, 2013	Pen ^R , Ceph ^R	Yes	A311V, T483S, V316T	1	-	0.5
GU140106	Japan, 2014	Pen ^R , Ceph ^R	Yes	A311V, T483S, V316T	2	2	0.5
unnamed	Argentina, 2014	Pen ^R , Ceph ^R	No	P551L	8	0.5	0.5
FC428	Japan, 2015 International, 2017-	Pen ^R , Ceph ^R	Yes	A311V, I312M, V316T, N512Y, T483S, F504L, H541N, G545S	>32.0	1	0.5
F460	Japan, 2015	Pen ^R , Ceph ^R	Yes	A311V, T483S	>32.0	1	0.5
FC498	Japan, 2015	Pen ^R , Ceph ^R	Yes	A311V, T483S	-	1	0.5
F90	France, 2017	Pen ^R , Ceph ^R	Yes	A311V, I312M, V316T, T483S, G545S	-	1	0.5

1.3.f. PBP1 modifications contributing to β -lactam resistance

While its primary mechanism of β -lactam resistance is the acquisition of mutations in the *penA* gene encoding PBP2, *N. gonorrhoeae* can also acquire mutations in *ponA*, the gene encoding the other β -lactam target PBP1, that diminish its acylation.⁴³⁰ A specific mutation in *ponA*, L421P (the “*ponA1* determinant”), is common and reduces the rate of PBP1 acylation by a variety of β -lactams by 50-75%. Despite this significant reduction, *ponA1* is not sufficient for clinically significant resistance alone because the *ponA1* gene fails to transform FA19 to a higher level of β -lactam resistance. Moreover, it fails to transform a series of laboratory-generated intermediate-resistant strains to higher levels of resistance. However, reversion of *ponA1* to wild-type in FA6140 reduces its penicillin MIC by two-fold, indicating that this mutation requires the presence of a number of other determinants in order to exert its effect.

1.4. Use of additional antimicrobial classes as antigonococcal therapeutics

1.4.a. FDA-approved therapies

With the fall of β -lactams as useful antigonococcal agents, it may seem attractive to look toward FDA-approved therapies from other antimicrobial classes. However, as aforementioned, *N. gonorrhoeae* has developed marked resistance to a number of other classes of antimicrobials as well, including sulfonamides, spectinomycin, tetracyclines, and fluoroquinolones. Some approved therapies show continued activity against gonococcal isolates, but with each comes a drawback making it a suboptimal candidate for widespread use (**Table 1.3**).

In vitro susceptibility to spectinomycin is currently high globally, with rare cases of resistance, but there is concern that, given rapid resistance development before, resistance is likely to be selected again. In several countries, gentamicin has been used in combination with doxycycline for the syndromic management of urogenital infections, and several studies had shown high microbiological cure rates with the regimen, but no specific data on

pharyngeal and anorectal infection existed until a study of gentamicin in combination with azithromycin showed that microbiological cure was achieved in 100% of subjects, including 10 cases of pharyngeal infection.⁴³¹ Moreover, according to a recent meta-analysis, the cure rate of single dose is 91.5% across 3 studies with 346 total participants.^{432,433} An additional meta-analyses comparing 23 oral and parenteral therapies found gentamicin to rank highly among them,⁴³⁴ but a third found cure rates with high variability.⁴³⁵ While this could be an option for cases of treatment failure with other agents, gentamicin is unfavorable as a first-line agent because of the risk for ototoxicity and nephrotoxicity,^{436,437} and there exists no data on the relationship between gentamicin MIC and pharmacokinetics with clinical outcomes to establish evidence-based microbiological resistance breakpoints. Finally, a randomized control trial comparing 240 mg intramuscular gentamicin and 500 mg intramuscular ceftriaxone failed to demonstrate noninferiority of the regimen.^{438,439} The bacterial cell wall synthesis inhibitor fosfomycin shows good *in vitro* activity as well, exhibiting a median MIC of 8-16 µg/mL in several studies.⁴⁴⁰⁻⁴⁴⁴ Studies of acute and subacute gonococcal urethritis treated with fosfomycin yielded cure rates greater than 90%,^{445,446} but rapid resistance selection *in vitro* raises concern for widespread use.⁴⁴⁷ Nonetheless, a small clinical trial found 3 g oral fosfomycin trometamol (96.8% cure rate) to be noninferior to 250 mg intramuscular ceftriaxone (95.3% cure rate).⁴⁴⁸ Like gentamicin, fosfomycin suffers from a lack of data allowing the establishment of evidence-based microbiological resistance breakpoints. The glycylicycline tigecycline also shows *in vitro* activity against gonococcal isolates,^{444,449,450} but its primary biliary clearance raises concern that the drug will not accumulate sufficiently in the urine to treat gonococcal urethritis.⁴⁵¹

Carbapenems must bind PBPs in the same way as other β-lactams, and their activity is dictated by the ability to undergo the same nucleophilic substitution reaction to form the inactive acyl enzyme. With this mechanistic similarity, known carbapenems expectedly show decreased efficacy in penicillin- and ESC-resistant strains of *N.*

gonorrhoeae due to changes in the PBP2 active site. Due to the aforementioned structural differences between classes, however, carbapenem reactivity with the target is still much higher than that of penams or cepheems, with meropenem and ertapenem exhibiting MICs against H041 of 0.125 and 0.064 µg/mL, respectively.⁶³ In a study examining *in vitro* activity of ertapenem against clinical *N. gonorrhoeae* isolates, the antimicrobial potency of ertapenem was comparable to that of ceftriaxone, with a median MIC of 0.032 µg/mL for both compounds. For isolates with mosaic *penA* alleles conferring ceftriaxone resistance (MIC = 0.5 to 4 µg/mL), however, resistance to ertapenem was much less pronounced (MIC = 0.016 to 0.064 µg/mL).⁴⁵² While elevated MICs can be seen in strains possessing mosaic *penA* alleles,^{427,452,453} the A501P mutation in PBP2 conferring further cephalosporin resistance, as seen in strain F89, restores carbapenem susceptibility to near-wild-type levels.⁴²⁷ In 2018, after reported treatment failures with both ceftriaxone and spectinomycin, the English strain G97687/G7944 was ultimately cleared with a 3-day course of intravenous ertapenem, demonstrating its clinical promise as a treatment of last resort.⁷⁶

In addition to well-established antimicrobials, newly FDA-approved therapies are emerging as promising in the treatment of gonococcal infections. One such drug is the novel fluoroquinolone delafloxacin. In early studies of its *in vitro* activity, it was consistently found to inhibit the growth of *N. gonorrhoeae* clinical isolates more potently than ciprofloxacin.⁴⁵⁴⁻⁴⁵⁶ However, in a Phase 3 randomized control trial of 460 patients, oral administration of 900 mg delafloxacin resulted in only an 85.1% cure rate for urogenital gonorrhea (compared to 91.0% for 250 mg intramuscular ceftriaxone).⁴⁵⁷ Novel fluorocycline eravacycline also shows good activity *in vitro*,⁴⁴⁴ but its similar pharmacokinetic profile to tigecycline raises doubts about its ability to treat gonococcal urethritis.

Table 1.3: Summary of antigonococcal data for FDA-approved therapies.

FDA-approved Therapy	<i>In vitro</i> Data	<i>In vivo</i> Data	Limitations
gentamicin <i>aminoglycoside</i>	<p>MIC₉₀ = 8 µg/mL (333 strains)⁴⁵⁸</p> <p>MIC₉₀ = 8 µg/mL (25 strains)⁴⁵⁹</p> <p>MIC₉₀ = 12 µg/mL (32 strains)⁴⁴²</p> <p>MIC₉₀ = 4 µg/mL (99 strains)⁴⁶⁰</p>	<p>62-98% microbiological cure rates among 5 studies using gentamicin monotherapy⁴³⁵</p> <p>91.5% pooled microbiological cure rate from meta-analysis using gentamicin monotherapy^{432,433}</p> <p>100% microbiological cure rate in combination with azithromycin (202 subjects)⁴³¹</p> <p>Successful noninferiority trial of 240 mg IM in combination with 2 g azithromycin PO (versus 500 mg ceftriaxone IM with 2 g azithromycin PO)⁴⁶¹</p> <p>Found to rank highly in meta-analysis comparing 23 oral and parenteral therapies (<i>p</i> score = 0.83 versus 0.924 for ceftriaxone)⁴³⁴</p>	<p>Failed in non-inferiority trial against ceftriaxone comparator group^{438,439}</p> <p>Adverse effect profile^{436,437}</p> <p>No official evidence-based resistance breakpoints</p>
fosfomycin	<p>MIC₉₀ = 16 µg/mL (89 strains)⁴⁴⁰</p> <p>MIC₉₀ = 16 µg/mL (51 strains)⁴⁴¹</p> <p>MIC₉₀ = 24 µg/mL (32 strains)⁴⁴²</p> <p>MIC range 8-48 µg/mL (15 strains)⁴⁴³</p> <p>MIC₉₀ = 32 µg/mL (112 strains)⁴⁴⁴</p>	<p>0% microbiological cure rate (17 subjects)⁴⁶²</p> <p>90% microbiological cure rate (70 subjects)⁴⁴⁶</p> <p>92% microbiological cure rate (85 subjects)⁴⁴⁵</p> <p>Successful small-scale noninferiority trial versus ceftriaxone (62 subjects)⁴⁴⁸</p>	<p>Rapidly selected resistance <i>in vitro</i>⁴⁴⁷</p> <p>No official evidence-based resistance breakpoints</p>

<p>ertapenem <i>carbapenem</i></p>	<p>MIC = 0.064 µg/mL against H041⁶³</p> <p>MIC₉₀ = 0.25 µg/mL (112 strains)⁴⁴⁴</p> <p>MIC₉₀ = 0.25 µg/mL (52 strains)⁴⁵³</p> <p>MIC₉₀ = 0.008 µg/mL (22 strains)⁴⁶³</p> <p>MIC₉₀ = 0.062 µg/mL (654 strains)⁴⁶⁴</p> <p>MIC₉₀ = 0.064 µg/mL (257 strains)⁴⁵²</p>	<p>Cure of patient infected with international FC428 clone⁷⁶</p>	<p>Elevated MICs in the presence of β- lactam resistance determinants^{453,452}</p>
<p>delafloxacin <i>fluoroquinolone</i></p>	<p>MIC₉₀ ≤ 0.004 µg/mL (10 strains)⁴⁵⁴</p> <p>MIC₉₀ = 0.03 µg/mL (44 strains)⁴⁵⁵</p> <p>MIC₉₀ = 0.125 µg/mL (117 strains)⁴⁵⁶</p>	<p>900 mg PO failed in noninferiority RCT against 250 mg ceftriaxone IM (85.1% cure versus 91.0%)⁴⁵⁷</p>	<p>Modestly elevated MICs seem to result in treatment failure⁴⁵⁷</p>
<p>tigecycline <i>glycylcycline</i></p>	<p>MIC₉₀ = 0.5 µg/mL (54 strains)⁴⁴⁹</p> <p>MIC₉₀ = 0.5 µg/mL (112 strains)⁴⁴⁴</p> <p>MIC₉₀ = 0.25 (120 strains)⁴⁵⁰</p>	<p>NA</p>	<p>Biliary clearance⁴⁵¹</p>
<p>eravacycline <i>fluorocycline</i></p>	<p>MIC₉₀ = 0.25 µg/mL (112 strains)⁴⁴⁴</p>	<p>NA</p>	<p>Biliary clearance⁴⁶⁵</p>

1.4.b. Novel analogues of known antimicrobial classes

In addition to considering existing drugs from diverse antimicrobial classes, the synthesis of novel, potent derivatives of these classes is another potential strategy (**Table 1.4**). New broad-spectrum semisynthetic fluoroquinolones avarofloxacin and sitafloxacin exhibit good *in vitro* activity against gonococcal clinical isolates, with MIC values ranging from ≤ 0.001 to $1 \mu\text{g/mL}$ (compared to ≤ 0.001 to $> 32 \mu\text{g/mL}$ for ciprofloxacin).⁴⁶⁶⁻⁴⁶⁸ Macrolide derivatives known as bicyclolides (*e.g.*, modithromycin, EDP-322) have had promising results *in vitro* as well, including activity against strains with decreased macrolide susceptibility.⁴⁶⁹ The MIC range of modithromycin and EDP-322 against gonococcal strains of varying resistance profiles were found to be 0.004 to $256 \mu\text{g/mL}$ and 0.008 to $16 \mu\text{g/mL}$, respectively. Unfortunately, high level azithromycin resistance (defined as an MIC $\geq 256 \mu\text{g/mL}$) correlates with decreased susceptibility to these agents as well. Two newly developed 2-aryl carbapenems, SM-295291 and SM-369926, have shown variable *in vitro* antigonococcal activity against clinical isolates (MIC₉₀ $\leq 1 \mu\text{g/mL}$).⁴⁷⁰ The design and synthesis of novel carbapenem structures that show specifically enhanced affinity for the PBP2 transpeptidase domain in the presence of Ceph^R mutations thus presents another strategy for the development of effective therapies against highly resistant strains.

Table 1.4: Summary of antigonococcal data for experimental therapeutics belonging to classes of FDA-approved therapies.

Derivative Compound	Derivative Class	Results
avarofloxacin (JNJ-Q2)	fluoroquinolone	MIC ₉₀ = 0.25 µg/mL (75 strains) ⁴⁶⁸
sitafloxacin	fluoroquinolone	MIC ₉₀ = 0.5 µg/mL (47 strains) ⁴⁶⁷ MIC ₉₀ = 0.25 µg/mL (250 strains) ⁴⁶⁶
modithromycin	macrolide (bicyclolide)	MIC ₉₀ = 1 µg/mL (254 strains) ⁴⁶⁹
EDP-322	macrolide (bicyclolide)	MIC ₉₀ = 1 µg/mL (254 strains) ⁴⁶⁹
SM-295291	carbapenem	MIC ₉₀ < 1 µg/mL (16 strains) ⁴⁶⁹
SM-369926	carbapenem	MIC ₉₀ < 1 µg/mL (16 strains) ⁴⁶⁹

1.4.c. Identification of new antimicrobial targets

Several antimicrobial compounds with novel mechanisms of action have been designed or discovered in the last decade, many of which show *in vitro* activity against multi-drug resistant *N. gonorrhoeae* (**Table 1.5**). Some successful compounds utilize known strategies for antimicrobial activity, including novel mechanisms of protein synthesis inhibition (*e.g.*, pleuromutilin BC-3781, fluoroketolide solithromycin, and boronate AN3365) and modes of topoisomerase inhibition (*e.g.*, aminobenzimidazole VXc-486, spiropyrimidinetrione ETX0914, tricyclic 2-quinolone REDX05391, and triazaacenaphthylene gepotidacin). BC-3781, AN3365, VXc-486, and REDX05391 show early promise *in vitro*, with good antimicrobial potency against panels of gonococcal

strains. REDX05391 has been further tested in a murine model of gonococcal infection. In this study, significant reductions in gonococcal colonization load were seen with the oral administration of single 10, 30, or 60 mg/kg doses, and full infection clearance was seen in the group given 60 mg/kg.⁴⁷¹ Solithromycin and ETX0914 have advanced to small clinical trials of urogenital gonococcal infection, with results indicating a 91% cure rate with oral administration of 1 g solithromycin and a 96% cure rate with 2 g ETX0914.^{472,473} Interestingly, in strains exhibiting lowered macrolide susceptibility, solithromycin remains effective *in vitro*; however, similar to the bicyclolides, when tested against isolates with high-level azithromycin resistance, solithromycin begins to fail.

Other compounds in the pipeline exhibit entirely novel mechanisms of antimicrobial action. One such mechanism is the depletion of essential lipids. FabI is an NADPH-dependent *trans*-2-enoyl-acyl carrier protein reductase identified as a key enzyme in bacterial fatty acid synthesis. MUT056399, a specific FabI inhibitor, was originally developed as an anti-staphylococcal agent. Its measured IC₅₀ against *S. aureus* FabI is 12 nM, and its MIC₉₀ against MRSA is 0.12 µg/mL. In studies of spectrum, MUT056399 was shown to have activity against *N. gonorrhoeae*, exhibiting an MIC₉₀ of 0.25 µg/mL.⁴⁷⁴ LpxC is a UDP-3-O-acyl-N-acetylglucosamine deacetylase involved in lipid A biosynthesis. LPC-067, an LpxC inhibitor designed specifically to target *N. gonorrhoeae*, exhibits MICs of 0.1 µg/mL against FA19 and 1.0 µg/mL against 35/02.⁴⁷⁵ Further iterations of design, synthesis, and testing have yielded LPC-067 analogues with MICs of 0.005 µg/mL and 0.05 µg/mL against the two strains, respectively.

Table 1.5: Summary of anticonococcal data for experimental therapeutics with mechanisms of action distinct from current FDA-approved therapies.

Compound	Target	Mechanism	Results
BC-3781 (lefamulin)	23S ribosomal RNA	Inhibited protein synthesis	MIC ₉₀ = 0.5 µg/mL (24 strains) ⁴⁷⁶ MIC ₉₀ = 1 µg/mL (251 strains) ⁴⁷⁷
CEM-101 (solithromycin)	23S ribosomal RNA	Inhibited protein synthesis	MIC ₉₀ = 0.25 µg/mL (246 strains) ⁴⁷⁸
GSK2251052 / AN3365	leucyl-tRNA synthetase	Inhibited protein synthesis	MIC ₉₀ = 0.5 µg/mL (28 strains) ⁴⁷⁹
VXc-486	gyrase B	Dysfunctional transcription, DNA replication	MIC ₉₀ = 0.125 µg/mL (220 strains) ⁴⁸⁰
ETX0914 / AZD0914 (zolidodacin)	gyrase B	Dysfunctional transcription, DNA replication	MIC ₉₀ = 0.25 µg/mL (250 strains) ⁴⁸¹ MIC ₉₀ = 0.125 µg/mL (37 strains) ⁴⁸² MIC ₉₀ = 0.125 µg/mL (873 strains) ⁴⁸³
REDX05391	gyrase B topoisomerase IV	Dysfunctional transcription, DNA replication	MIC(WHO L) = 4 µg/mL ⁴⁸⁴ MIC(ATCC49226) = 0.12 µg/mL ⁴⁸⁴
MUT056399	FabI	Depletion of essential lipids	MIC ₉₀ = 0.25 µg/mL (10 strains) ⁴⁷⁴
LPC-067	LpxC	Diminished lipid A synthesis	MIC(FA19) = 0.1 µg/mL ⁴⁷⁵ MIC(35/02) = 1 µg/mL ⁴⁷⁵
GSK2140944 (gepotidacin)	gyrase A, topoisomerase IV	Dysfunctional transcription, DNA replication	MIC ₉₀ = 0.25 µg/mL (25 strains) ⁴⁸⁵

1.5. Development of non- β -lactam PBP inhibitors

1.5.a. Tetrahedral intermediate mimics

In addition to novel PBP-inhibiting compounds based on active β -lactam frameworks, non- β -lactam compounds can also be explored as antigonococcal agents, including other covalent inhibitors leveraging the nucleophilic serine. Electron-poor boronic acids have been known to inhibit serine proteases for several decades,⁴⁸⁶ and, after early work showing their utility as β -lactamase inhibitors,⁴⁸⁷⁻⁴⁸⁹ have more recently been examined as PBP inhibitors as well (**Figure 1.14**). In 2003, Pechenov *et al.* explored several electrophilic functional groups as potential mimics of the transient tetrahedral oxyanion intermediate generated in the PBP catalytic cycle, and among these, dipeptidic boronate **1** was found active against several low molecular weight PBPs, exhibiting its most potent inhibitory activity against *N. gonorrhoeae* PBP3 ($K_i = 0.370 \mu\text{M}$).⁴⁹⁰ Later, a 1.6 Å crystal structure of tripeptide analogue **2** in complex with *E. coli* PBP5 ($K_i = 13 \mu\text{M}$) revealed a covalent adduct in which the O γ of Ser44 is bonded to the inhibitor boron and one boronic acid oxygen projects into the oxyanion hole comprising the backbone amides of Ser44 and His216, establishing this class of compounds as true tetrahedral intermediate mimics¹¹⁷ (**Figure 1.15A**). Another peptidic boronate **3**, which possesses a diaminopimelic acid as its diaminoacyl group, has been shown to bind with high affinity to *Actinomadura* R39 DD-peptidase ($K_i = 32 \text{ nM}$). In a 2.4 Å crystal structure, **3** was found to bind R39 DD-peptidase in a mode similar to that seen in previous studies of boronates and *E. coli* PBP5, with the boron covalently bound to nucleophilic Ser49, and one boronate oxygen occupying the oxyanion hole⁴⁹¹ (**Figure 1.15B**).

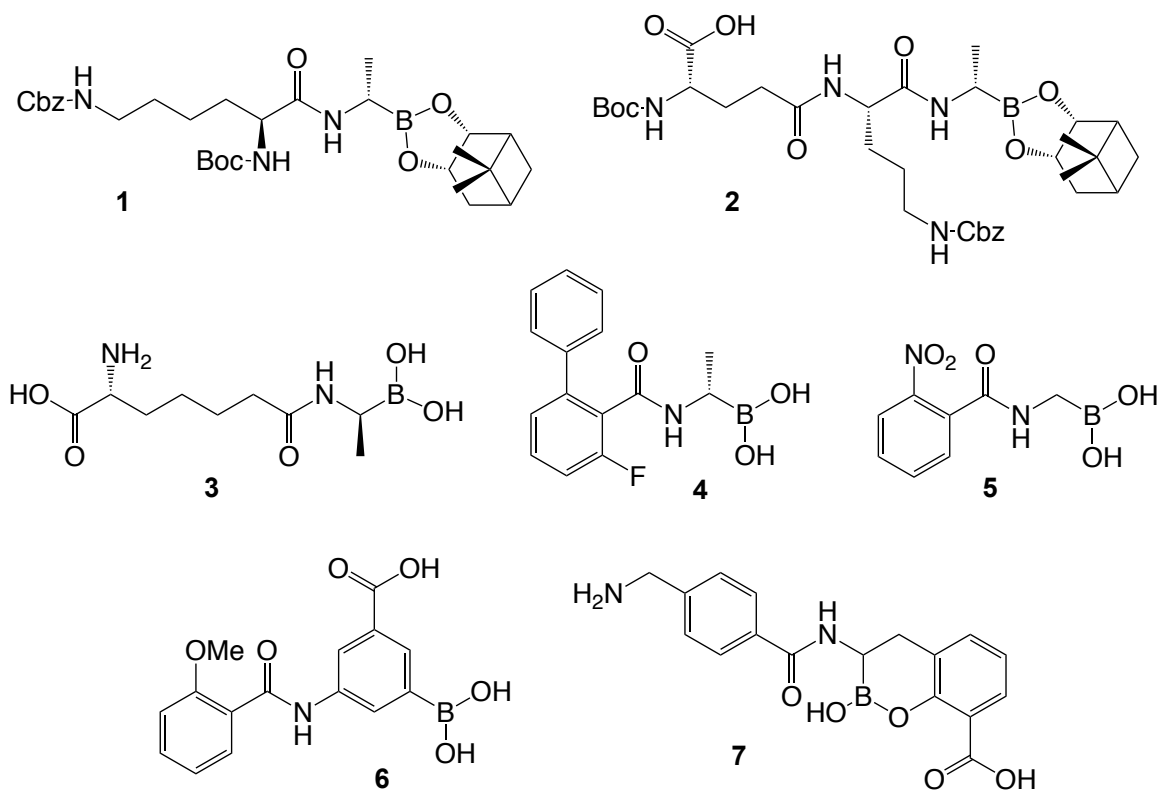


Figure 1.14: Structures of boronic acid transpeptidase inhibitors.

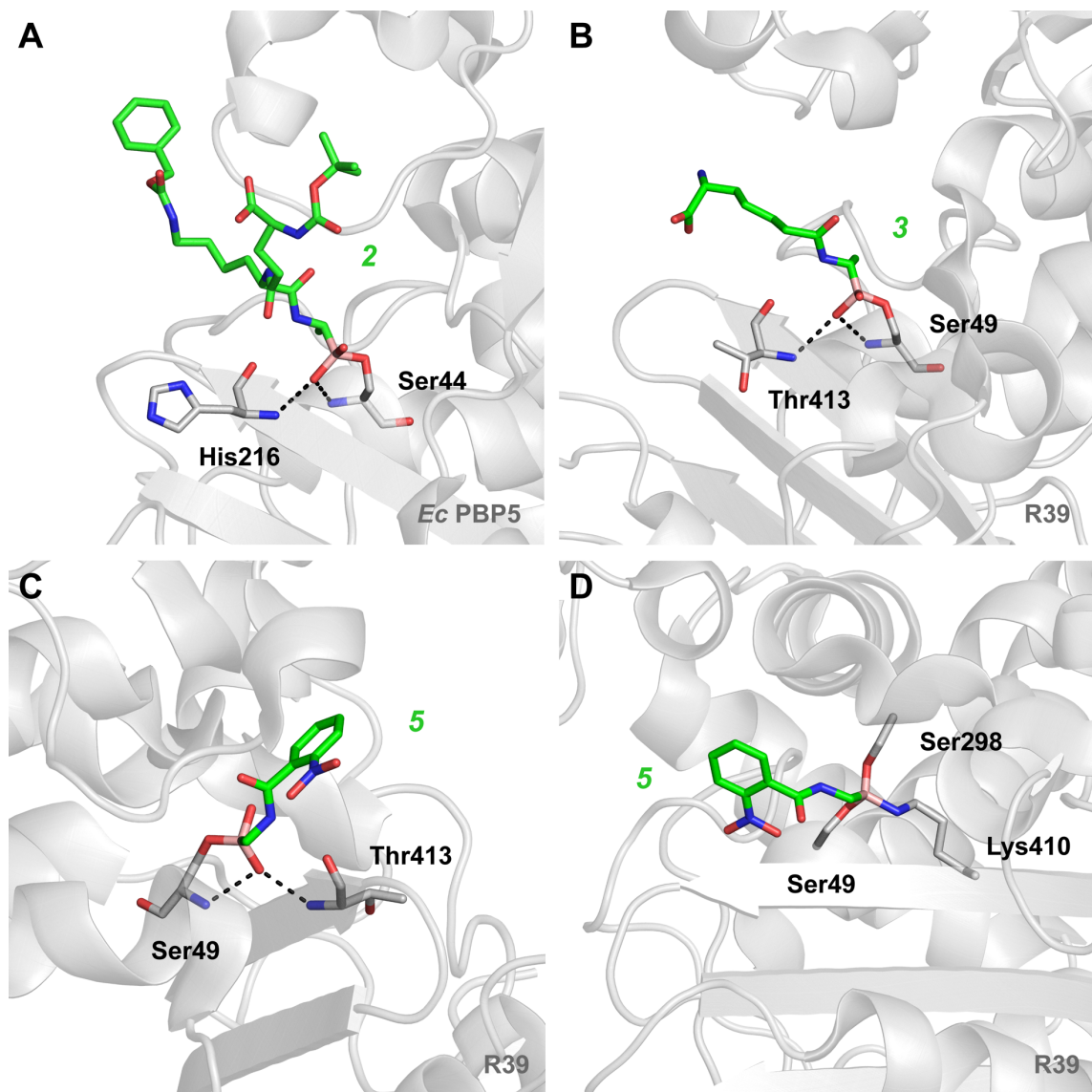


Figure 1.15: Crystal structures of boronic acid transpeptidase inhibitors in complex with their targets, showing their tetrahedral intermediate mimicry. **A.** Compound 2 (green) in complex with *E. coli* PBP5. **B.** Compound 3 (green) in complex with *Actinomadura R39* DD-peptidase. **C.** Compound 5 (green) in complex with *Actinomadura R39* DD-peptidase. **D.** Compound 5 (green) in complex with *Actinomadura R39* DD-peptidase, showing a unique tricovalent binding mode.

Structure-guided design strategies led to the development of acylaminoethylboronic acids such as **4**, which inhibits both *Actinomadura* R39 DD-peptidase ($IC_{50} = 0.27 \mu\text{M}$) and *S. aureus* PBP1b ($IC_{50} = 20 \mu\text{M}$).^{492,493} In further explorations of the class, acylaminomethylboronic acids were found to inhibit *Actinomadura* R39 DD-peptidase as well, and subsequent derivatization of this scaffold yielded **5**, which has been shown to inhibit PBPs of classes A (*S. pneumoniae* PBP1b, $IC_{50} = 26 \mu\text{M}$), B (*S. pneumoniae* PBP2x, $IC_{50} = 138 \mu\text{M}$), and C (*Actinomadura* R39 DD-peptidase, $IC_{50} = 0.6 \mu\text{M}$).⁴⁹⁴ Distinguishing the methylboronic acids, which mimic a C-terminal glycine, from their alanine-like predecessors is the formation of a tricovalent complex within the transpeptidase active site, as shown by crystal structures of **5** and close analogues in complex with R39 DD-peptidase (**Figure 1.15D**).⁴⁹⁵ In these structures, the boronic acid oxygens have been displaced by O_{γ} of nucleophilic Ser49, O_{γ} of SxN Ser298, and N_{ϵ} of KTG Lys410. However, a tetrahedral oxyanion-occupying state similar to prior published structures was seen in some molecules of the asymmetric unit (**Figure 1.15C**), leading the authors to hypothesize that the ligands bind similarly at the outset, but that a lack of bulk at C_{α} allows the ligand to move more freely after initial binding.

A final set of boronic acid-containing scaffolds is the (dihydroxyboranyl)benzoic acids and [(hydroxyboranyloxy)]benzoic acids. Initial studies found that the *m*-(dihydroxyboranyl)benzoic acid fragment inhibits R39 DD-peptidase, and subsequent design of 5-acylamino derivatives yielded mid-micromolar inhibitor **6** ($IC_{50} = 23 \mu\text{M}$).⁴⁹⁶ Recent work presents bicyclic *o*-[(hydroxyboranyl)oxy]benzoic acids as potent inhibitors of *E. coli* PBP5, with **7** exhibiting an IC_{50} of 1.6 nM.⁴⁹⁷ Although these compounds were found to have surprisingly little antimicrobial activity alone, they were able to potentiate meropenem activity against highly resistant *E. coli* and *K. pneumoniae* in a dose-dependent manner due to their potent metallo- β -lactamase inhibition.

Table 1.6: Activity of boronic acid compounds against bacterial transpeptidases. ^aThermodynamic equilibrium constant (K_i). ^bHalf-maximal inhibitory concentration (IC_{50}).

Compound	Species	Target	Activity	Reference
1	<i>N. gonorrhoeae</i>	PBP3	0.37 μM^a	490
	<i>N. gonorrhoeae</i>	PBP4	34 μM^a	
	<i>E. coli</i>	PBP5	16 μM^a	
2	<i>E. coli</i>	PBP5	13 μM^a	117
3	<i>Actinomadura</i> spp.	R39 DD-peptidase	32 nM ^a	491
4	<i>Actinomadura</i> spp.	R39 DD-peptidase	0.27 μM^b	492,493
	<i>S. aureus</i>	PBP1b	20 μM^b	
5	<i>Actinomadura</i> spp.	R39 DD-peptidase	0.36 μM^a	495
	<i>Actinomadura</i> spp.	R39 DD-peptidase	0.6 μM^b	494
	<i>S. pneumoniae</i>	PBP1b	26 μM^b	
	<i>S. pneumoniae</i> R6	PBP2x	138 μM^b	
6	<i>Actinomadura</i> spp.	R39 DD-peptidase	23 μM^b	496
7	<i>E. coli</i>	PBP5	1.6 nM ^b	497

Additional tetrahedral intermediate analogues synthesized by Pechenov *et al.* include peptidic and peptidomimetic aldehydes **8**, α -trifluoromethyl ketones **9**, and α -chloromethyl ketones **10**⁴⁹⁰ (Figure 1.16). However, these analogues are less potent than their boronate parent compound (K_i values of 60 μM for both **8** and **9** against *N. gonorrhoeae* PBP3, no measurable inhibition by **10**), and activated carbonyl analogues of other boronic acid R39 DD-peptidase inhibitors identified by Woon *et al.* were found to be inactive up to 1 mM.⁴⁹³ These data indicate that creation of a potent activated carbonyl inhibitor may prove a futile effort. That said, Dzhekieva *et al.* hypothesized that attachment of a specific peptidoglycan fragment was key to inhibition and synthesized compound **11**, a direct α -trifluoroketone analogue of **3**, with K_i values of 0.37 μM and 13.5 μM against *Actinomadura* R39 DD-peptidase and *B. subtilis* PBP4a, respectively.⁴⁹⁸ A crystal structure of **11** in complex with R39 DD-peptidase reveals a tetrahedral adduct with O γ of Ser49 and the oxygen from the inhibitor ketone positioned in the oxyanion hole formed by Ser49 and Thr413 (Figure 1.17A).

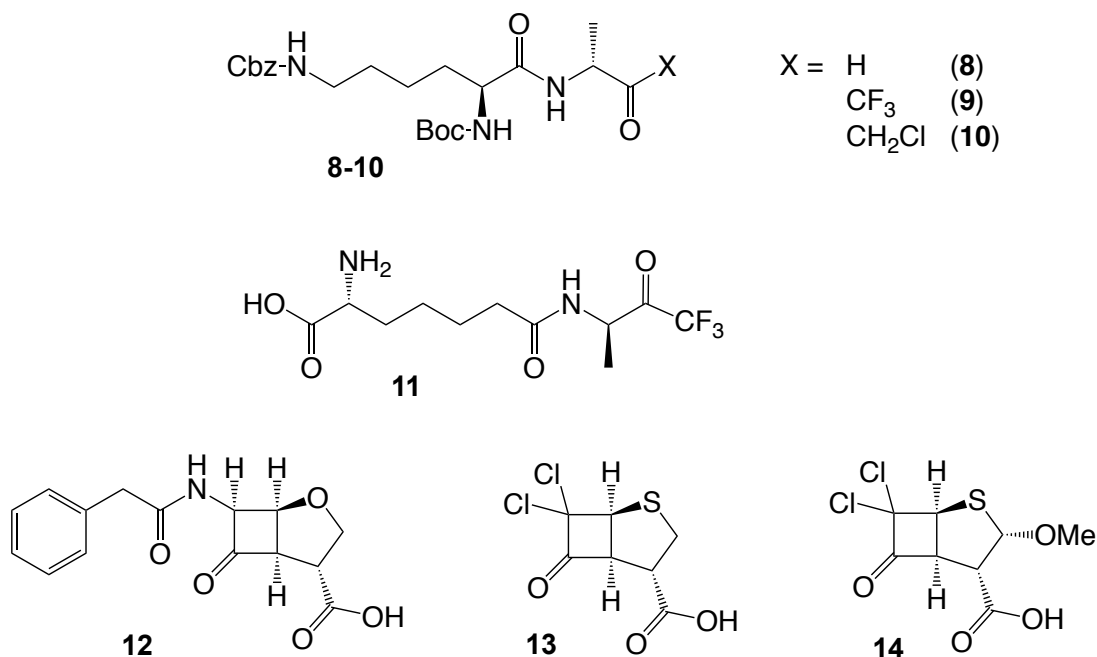


Figure 1.16: Structures of activated carbonyl transpeptidase inhibitors.

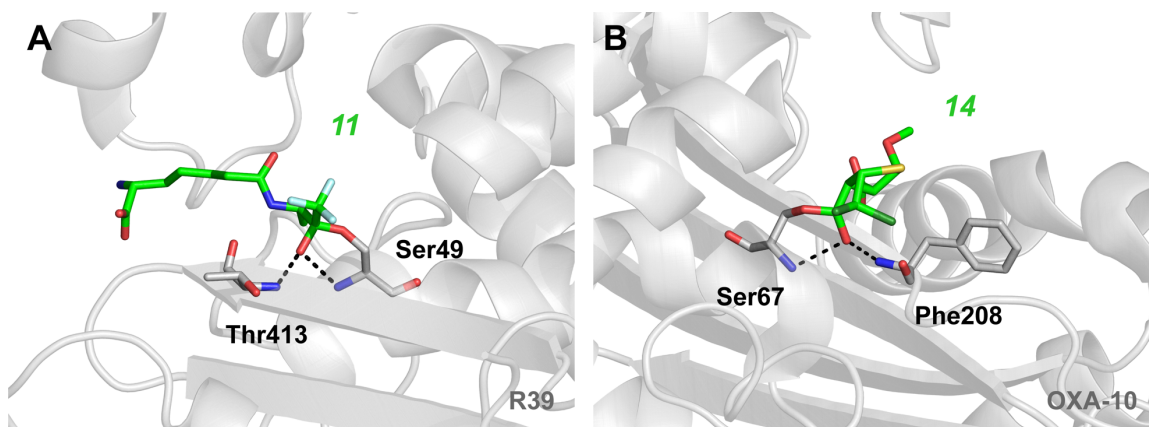


Figure 1.17: Crystal structures of activated carbonyl transpeptidase inhibitors in complex with their targets, showing their tetrahedral intermediate mimicry. **A.** Compound 11 (green) in complex with *Actinomadura R39* DD-peptidase. **B.** Compound 14 (green) in complex with β -lactamase OXA-10.

The chemically similar cyclobutanones were originally synthesized for their potential as β -lactamase or transpeptidase inhibitors, with the rationale that they, like the α -trifluoromethyl and α -chloro ketones, would be able to form a stable enzyme-bound hemiketal. However, several early studies failed to produce agents with any inhibitory activity against either β -lactamases or transpeptidases^{499,500} until Lowe & Swain reported the synthesis of compound **12**, capable of inhibiting both *E. coli* R-TEM and *B. cereus* I, as well as *Streptomyces* R61 DD-peptidase.⁵⁰¹ Later, the 7,7-dichloro compound **13** was also found to inhibit both β -lactamases and R61 DD-peptidase.^{502,503} Structural studies on factors influencing hemiketal formation have led to compound **14**, 98% of which exists in the hemiketal state at equilibrium in methanol.⁵⁰⁴ In addition to structure-activity relationships showing a correlation of methyl hemiketal formation with activity, crystal structures with serine lactamase OXA-10 show their tetrahedral intermediate mimicry, with nucleophilic Ser67 bound covalently to C6 and the hemiketal oxygen occupying the oxyanion hole created by Ser67 and Phe208⁵⁰⁵ (**Figure 1.17B**). With these new insights into the synthesis of more electrophilic cyclobutanone scaffolds, as well as definitive evidence of their hemiketal-based mechanism, perhaps this class can be approached for new attempts at harnessing their PBP-inhibitory potential.

Table 1.7: Activity of activated carbonyl compounds against bacterial transpeptidases. ^aThermodynamic equilibrium constant (K_i) unless indicated otherwise. ^bMeasured K_i divided by two under the assumption that one enantiomer is inactive.

Compound	Species	Target	Activity ^a	Reference
8	<i>N. gonorrhoeae</i>	PBP3	60 μ M	490
	<i>N. gonorrhoeae</i>	PBP4	>1 mM	
	<i>E. coli</i>	PBP5	>1 mM	
9	<i>N. gonorrhoeae</i>	PBP3	60 μ M	490
	<i>N. gonorrhoeae</i>	PBP4	>1 mM	
	<i>E. coli</i>	PBP5	>1 mM	
10	<i>N. gonorrhoeae</i>	PBP3	~1 mM	490
	<i>N. gonorrhoeae</i>	PBP4	>1 mM	
	<i>E. coli</i>	PBP5	>1 mM	
11	<i>Streptomyces</i> spp.	R61 DD-peptidase	~0.9 mM	501
12	<i>Actinomadura</i> spp.	R39 DD-peptidase	0.37 μ M ^b	498
	<i>B. subtilis</i>	PBP4a	13.5 μ M ^b	
13	<i>Streptomyces</i> spp.	R61 DD-peptidase	~1 mM	502, 503

The phosphonates are another structural class initially examined as inhibitors of serine proteases, and later expanded to β -lactamases and PBPs due the enzymes' mechanistic similarities (**Figure 1.18**). Designed with the rationale that a phosphonate should form a tetrahedral adduct with the nucleophilic serine similar to that observed with boronic acids, the acetamidomethylphosphonate **15** was the first of its class to show potent inhibition of a β -lactamase, capable of phosphonylating *Enterobacter cloacae* P99 at a rate of $1,120 \text{ M}^{-1}\text{s}^{-1}$.⁵⁰⁶ Equally impressive was the stability of the complex, which underwent regeneration of the apo-enzyme (k_3) at a rate of $2.32 \times 10^{-6} \text{ s}^{-1}$. However, this molecule failed to inhibit *Streptomyces* R61 DD-peptidase, as did its retro-amide analogue.⁵⁰⁷ Soon after, a *p*-nitro analogue of this compound (**16**) was shown to be a weak inhibitor of R61 DD-peptidase ($k_2/K_i = 0.07 \text{ M}^{-1}\text{s}^{-1}$), giving credence to the idea of phosphonates as transpeptidase inhibitors.⁵⁰⁸

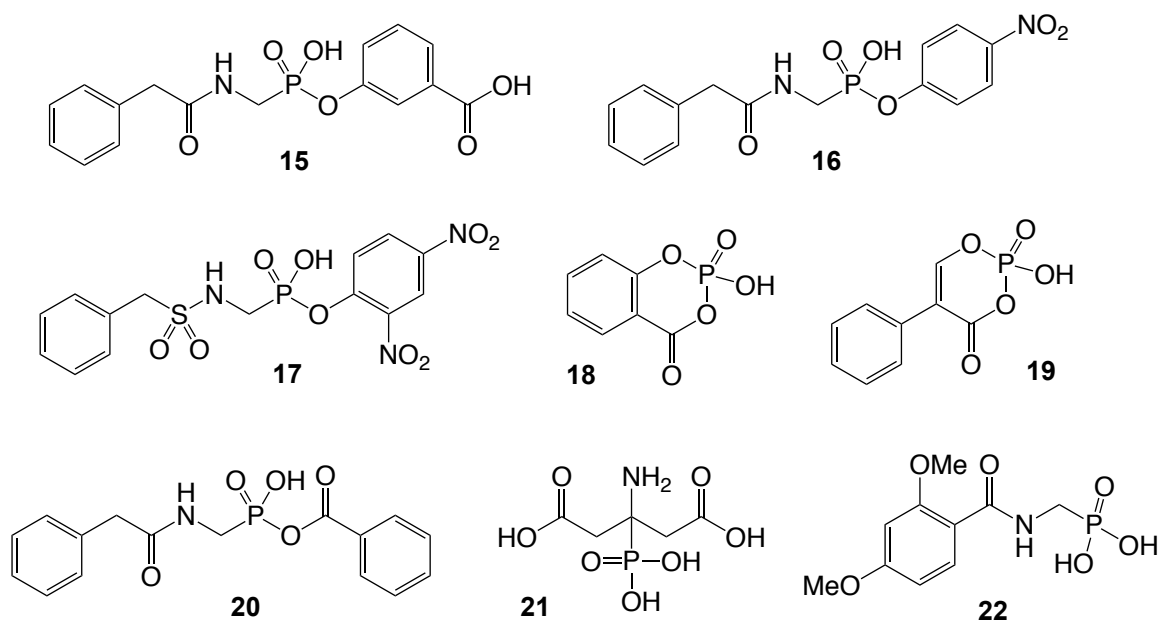


Figure 1.18: Structures of phosph(on)ate transpeptidase inhibitors.

Since then, a great deal of work has been done to elucidate the basic inhibitory mechanisms of this class. First, the phosphoester substituent acts as a leaving group, as evidenced by the formation of stoichiometric quantities of alcohol upon β -lactamase inactivation. Moreover, good leaving group ability is key for the covalent reaction to proceed.⁵⁰⁹ This was further illustrated by experiments with phosphoramidates, which exhibited much slower rates due to the relative instability of deprotonated amines.^{510,511} The rate-determining step for this subclass is the acquisition of a proton, a requirement that may limit their utility in the absence of a general acid catalyst.⁵¹⁰ Proof of covalent adduct formation with β -lactamases was eventually obtained by electrospray mass spectrometry,⁵¹² and later crystal structures showed the formation of covalent complexes mimicking the β -lactam tetrahedral intermediate state.⁵¹³⁻⁵¹⁵ In a 2.0 Å structure of TEM-1 in complex with **16**, the nucleophilic Ser70 is phosphonylated by the inhibitor, the oxyanion hole created by Ser70 and Ala237 is occupied by the unsubstituted phosphonate oxygen,

and the *p*-nitrophenol leaving group has departed⁵¹⁵ (**Figure 1.19A**). Other studies have examined structure-activity relationships of the alkyl side chain, demonstrating that the incorporation of an (acetamido)methyl group increases the rate of β -lactamase inactivation by 10,000-fold.⁵¹¹ Complementarity (in this case, mimicry of the β -lactam R₁ acylamino group) is, therefore, requisite for fast β -lactamase inactivation. Li *et al.* established, however, that a sulfonamidomethyl isostere is suitable.⁵¹⁶ Compound **17** is not only an inhibitor of *E. cloacae* P99 ($1.2 \times 10^3 \text{ M}^{-1}\text{s}^{-1}$), but was also identified as another weakly inhibitory compound against *Streptomyces* R61 DD-peptidase ($k_2/K_i = 0.06 \text{ M}^{-1}\text{s}^{-1}$).

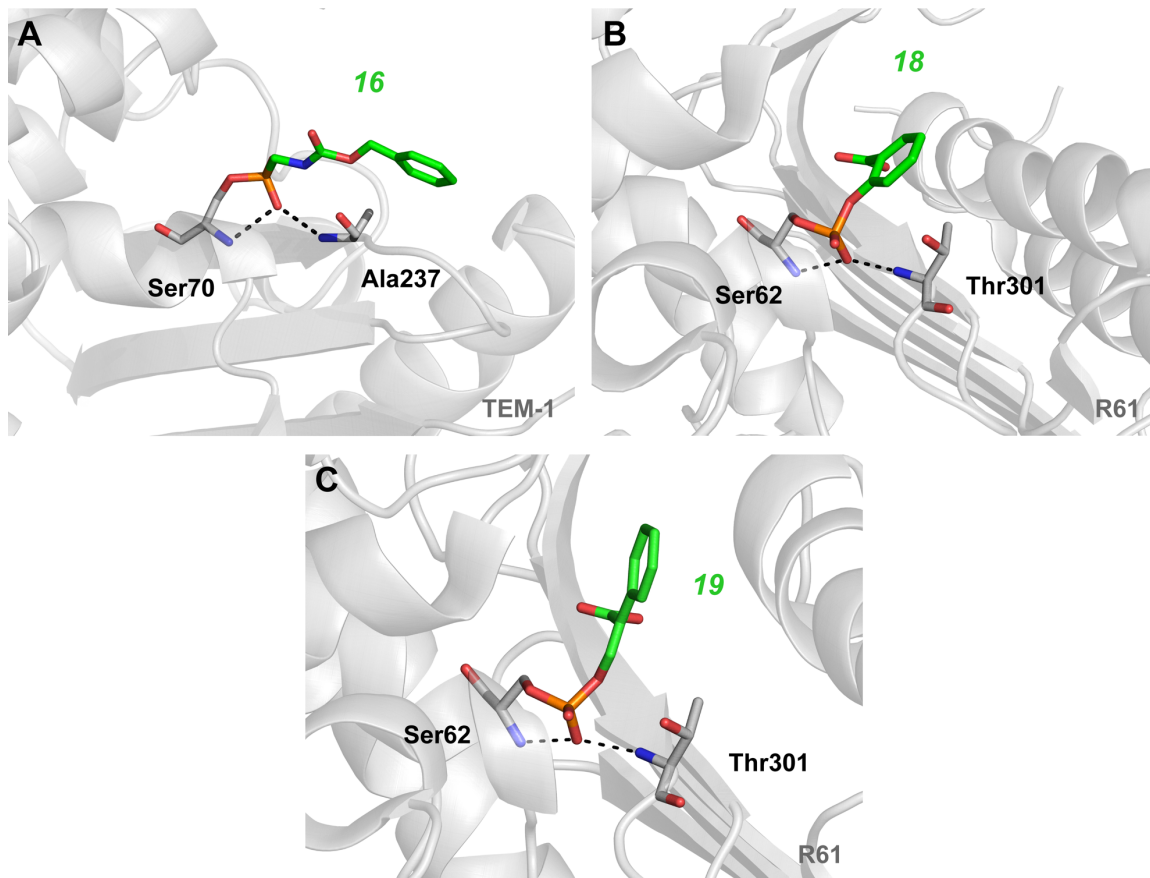


Figure 1.19: Crystal structures of phosph(on)ate transpeptidase inhibitors in complex with their targets, showing their tetrahedral intermediate mimicry. **A.** Compound 16 (green) in complex with β -lactamase TEM-1. **B.** Compound 18 (green) in complex with *Streptomyces* R61 DD-peptidase. **C.** Compound 19 (green) in complex with *Streptomyces* R61 DD-peptidase.

Cyclic phosphonates like **18**,⁵¹⁷ while demonstrating improvement compared to their acyclic analogues (R61 DD-peptidase $k_2/K_i = 0.46 \text{ M}^{-1}\text{s}^{-1}$), still suffer from a lack of potency. However, they offer the benefit of generating a stable ligand-enzyme complex. As with the β -lactams, when the leaving group is ejected upon reaction with the target, it remains tethered to the phosphonate and hinders hydrolysis of the resulting complex (R61 DD-peptidase $k_3 = 3.4 \times 10^{-5} \text{ s}^{-1}$). A phosphonate analogue of **18** was found to inactivate the *E. cloacae* P99 β -lactamase more rapidly ($k_2/K_i = 9.8 \times 10^3 \text{ M}^{-1}\text{s}^{-1}$ versus $6.7 \times 10^3 \text{ M}^{-1}\text{s}^{-1}$), albeit with a faster off-rate ($k_3 = 9.8 \times 10^{-2} \text{ s}^{-1}$ versus $1.1 \times 10^{-3} \text{ s}^{-1}$), but its activity against transpeptidases was never reported.⁵¹⁸ Further derivatization of salicyloyl phosphate and cyclic benzoyl phosphonate led to compounds capable of inactivating P99 at rates of over $10^4 \text{ M}^{-1}\text{s}^{-1}$,⁵¹⁹ but only compound **19** was tested against transpeptidases. Its inactivation rate against *Streptomyces* R61 DD-peptidase was measured to be $24 \text{ M}^{-1}\text{s}^{-1}$ ($k_3 = 8.9 \times 10^{-5} \text{ s}^{-1}$), a 50- to 400-fold improvement over previous phosphonates for which inhibition data is available.⁵²⁰ Crystal structures of **18** and **19** in complex with R61 DD-peptidase confirm tetrahedral intermediate mimicry, showing phosphonylation of nucleophilic Ser62, as well as occupancy of the oxyanion hole created by Ser62 and T301 by the anionic oxygen⁵²⁰ (**Figure 1.19B & C**). The emergence of salicyloyl phosphate and cyclic benzoyl phosphonates led to the pursuit of acyl and diacyl phosph(on)ates as inhibitors of β -lactam-recognizing enzymes.⁵²¹⁻⁵²⁷ In general, these compounds are poor substrates of both β -lactamases and DD-peptidases, with low enough turnover to be considered irreversible inhibitors.^{521,528} Among these, benzoyl phosphonate **20** was identified as a poor inhibitor of transpeptidase activity, exhibiting a rate of inactivation of $0.005 \text{ M}^{-1}\text{s}^{-1}$ against R61 DD-peptidase.⁵²⁸ Additional variations of the phosphonate have been attempted for β -lactamase inhibition, including mercaptophosphonates,^{529,530} 2-aryl-2-(methoxyimino)acetyl amino phosphonates,⁵³¹ but no activity data against transpeptidases is available for these scaffolds.

Other phosphonate and phosphate analogues take advantage of the moiety as an electrostatic anchor rather than an electrophilic center. The potential for acylation by acyl phosphonates was leveraged with the development of electron withdrawn ketophosphonates.^{532,533} While these molecules inhibited β -lactamases, no evidence was found for the formation of a covalent tetrahedral adduct. Moreover, no substantial inhibition of R61 DD-peptidase was seen. Inhibition of β -lactam-recognizing enzymes by citrate and isocitrate and their amino derivatives,^{534,535} as well as high-occupancy crystal structures showing their binding in the active sites of β -lactamases,^{534,536} led to the synthesis and testing of a series of phosphonic acid isosteres.⁵³⁵ One such compound, **21**, is a bioisostere of aminocitrate that exhibits 53% inhibition of *Actinomadura* R39 DD-peptidase at 500 μ M. Naturally occurring phosphates, including guanosine monophosphate and inosine monophosphate, are reported micromolar inhibitors of β -lactamases as well, but no data is available on potential transpeptidase inhibition.⁵³⁷ Phosphate analogues of active boronic acids synthesized by Woon *et al.* have also shown little inhibitory potency, with the most active (**22**) showing 35% inhibition of R39 DD-peptidase at 1 mM.⁴⁹³ Dzhekieva *et al.* have had similar results, with the direct phosphate analogue of boronic acid **3** and α -trifluoroketone **11** showing no inhibition of R39 DD-peptidase up to 2 mM.⁴⁹⁸ Heterocyclic methylphosphates have also shown promise as inhibitors of β -lactamases,^{538,539} but no data on transpeptidase inhibition have been reported.

Overall, while synthesized molecules of this class have shown promise in the inhibition of β -lactamases, all attempts to date have yielded quite poor inhibitors of transpeptidases. Most compounds of these classes suffer from a slow on-rate, a major determinant of covalent inhibitors' potency, and a need for additional derivatization to increase complementarity with the transpeptidase active site. However, their properties as electrophiles allow them to inhibit both serine- and metallo- β -lactamases as well as PBPs, opening possibilities for the development of dual inhibitors.

Table 1.8: Activity of phosphate and phosphonate compounds against bacterial transpeptidases. ^aSecond-order rate of reaction with the target (k_2/K_i). ^bPercent inhibition of target activity at 500 μM . ^cPercent inhibition of target activity at 1 mM.

Compound	Species	Target	Activity	Reference
16	<i>Streptomyces</i> spp.	R61 DD-peptidase	$0.07 \text{ M}^{-1}\text{s}^{-1}$ ^a	508
17	<i>Streptomyces</i> spp.	R61 DD-peptidase	$0.06 \text{ M}^{-1}\text{s}^{-1}$ ^a	511
18	<i>Streptomyces</i> spp.	R61 DD-peptidase	$0.46 \text{ M}^{-1}\text{s}^{-1}$ ^a	517
19	<i>Streptomyces</i> spp.	R61 DD-peptidase	$24 \text{ M}^{-1}\text{s}^{-1}$ ^a	520
20	<i>Streptomyces</i> spp.	R61 DD-peptidase	$0.005 \text{ M}^{-1}\text{s}^{-1}$ ^a	528
21	<i>Actinomadura</i> spp.	R39 DD-peptidase	53% ^b	535
22	<i>Actinomadura</i> spp.	R39 DD-peptidase	35% ^c	493

1.5.b. β -lactam mimics

Other inhibitory chemotypes rely on mimicry of the substrate in a manner similar to the β -lactams, frequently through acylation of the target by an activated carbonyl electrophile (**Figure 1.20**). The first γ -lactam-based PBP inhibitors were attempted shortly after the discovery of penicillin. These molecules were close analogues of penams, such as penicillin G, but showed neither antimicrobial activity nor hydrolysis in aqueous solution.⁵⁴⁰⁻⁵⁴² This lack of success continued with a variety of monobactam, penam, oxapenam, and carbapenam derivatives failing to show any antimicrobial activity.⁵⁴³⁻⁵⁴⁶

It was known at the time that a bicyclic β -lactam's ability to acylate its target is, in part, due to disrupted amide resonance, and that one valuable measurement of this disruption is the pyramidalization of the lactam nitrogen.¹⁵⁴⁻¹⁶² In computational studies, 1-azabicyclo[3.2.0]heptane systems were predicted to have high degrees of *N*-pyramidalization; however, synthesized molecules of this scaffold still failed to exhibit any appreciable antimicrobial activity.^{547,548} It was not until the introduction of the 2-oxo-1-azabicyclo[3.2.0]hept-6-enes (**23**), which combine a high degree of bicyclic strain with a

competing enamine resonance also known to contribute to amide destabilization,^{155,159,215} that the γ -lactam class gained traction as antimicrobials.⁵⁴⁹ Subsequent penem and carbapenem derivatives (**24 & 25**), which incorporate the resonant olefin into less strained systems, also showed marginal antimicrobial activity with limited spectrum, indicating that for the γ -lactam to have utility as a potent PBP-acylating scaffold, additional activation of the ring system would likely be required.⁵⁵⁰⁻⁵⁵³

Much of the work that followed was conducted to determine structure-activity relationships for the class. With the diminished carbonyl electrophilicity seen in γ -lactams compared to β -lactams, affinity for the transpeptidase active site becomes a much more critical aspect of target binding and biological activity. While penems and carbapenems lacking an acylamino group still possess antimicrobial activity, their γ -lactam analogues generally do not.⁵⁵⁴ Further computational studies examined the optimal placement and stereochemistry of the acylamino side chain, determining that 7R-substitution provides the most morphological resemblance to the β -lactams (**Figure 1.21**). These analyses also suggested that, like cephalosporins, the bicyclic olefinic γ -lactams can be activated by long-range electron-withdrawing inductive effects at the C3 position. The relationship between biological activity and the C3-substituent is supported by the increased potency of compounds possessing cyano, carboxylic, and sulfonyl moieties compared to those with methyl and acetoxy groups.^{554,555}

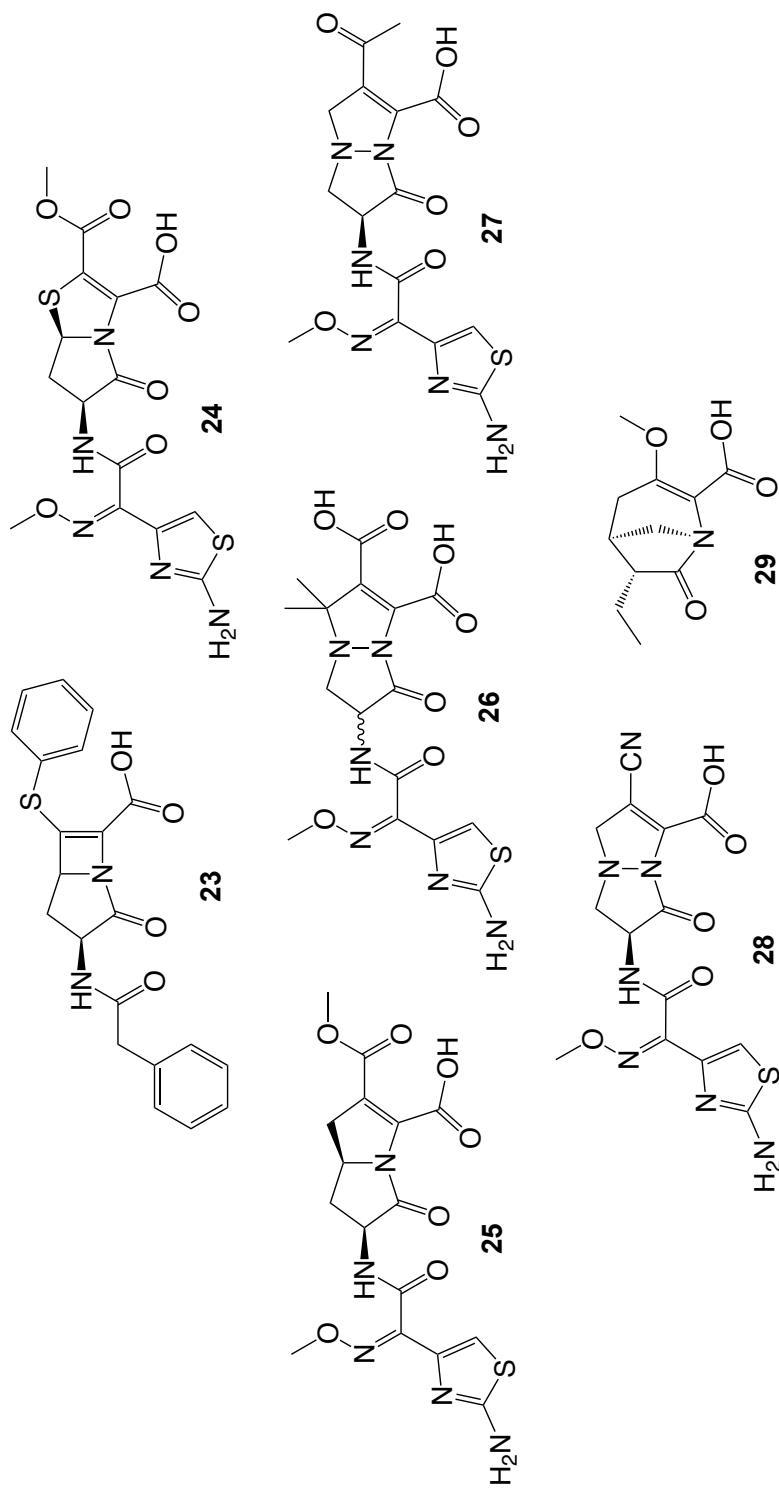


Figure 1.20: Structures of γ -lactam and γ -lactam-like transpeptidase inhibitors.

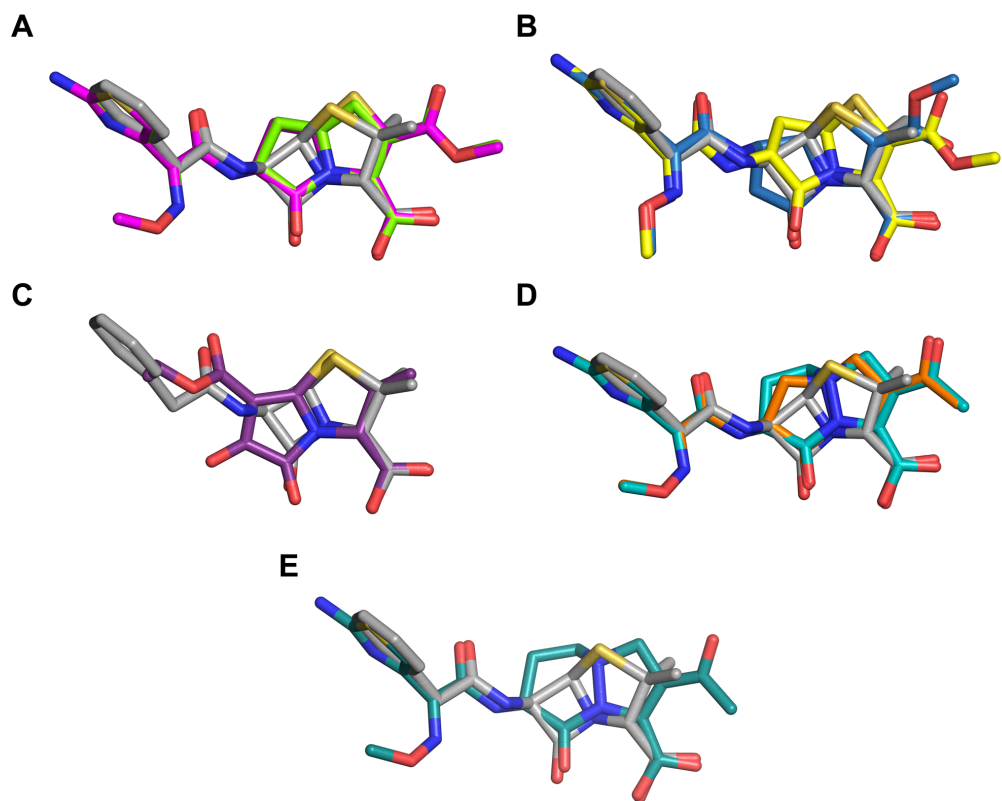


Figure 1.21: Structural alignments of γ -lactams with penicillin G. **A.** Alignment of penicillin G (grey) with γ -lactams 24 (magenta) and 25 (lime), showing good agreement of key features. **B.** Alignment of penicillin G with the 7S stereoisomer γ -lactam 24. There is still good agreement between features, consistent with the activity of both stereoisomers. **C.** Alignment of penicillin G with an inactive 1H-pyrrole-2,3-dione derivative. The inactivity of this scaffold suggests that the 3-oxo group projects into space unfavorable for productive binding to the transpeptidase active site. **D.** Alignment of penicillin G with pyrazolidin-5-one 27, showing retention of feature agreement from 24, but with a more activated ring system. **E.** Alignment of penicillin G with an inactive δ -lactam derivative. The inactivity of this scaffold suggests that the larger, more flexible ring system group presents conformational uncertainty and projects into space unfavorable for productive binding to the transpeptidase active site.

Parallel efforts to increase the reactivity of the β -lactam ring itself led to the syntheses of 1,2-diazetid-3-ones.^{556,557} The resulting scaffolds were too successful, however, because they lacked the stability to be useful in drug-like molecules. Seeing this work, and recognizing a need for more reactivity in the γ -lactam ring system, Jungheim *et al.* designed and synthesized a series of bicyclic pyrazolidin-5-ones (**26**) that, despite a bulky and ill-positioned *gem*-dimethyl group, exhibited good antimicrobial activity.⁵⁵⁸ Development of novel synthetic schema, in combination with the structure-activity

relationship data available for γ -lactam derivatives of penems and carbapenems, allowed derivatization of this class to yield highly biologically active compounds **27** and **28**.⁵⁵⁹⁻⁵⁶⁶ Compound **27** exhibits good spectrum, and decreases cell wall synthesis and crosslinking without effects on the synthesis of other macromolecules. It binds *E. coli* PBP3 at concentrations as low as 0.1 $\mu\text{g}/\text{mL}$.⁵⁶⁷ Compound **28** has antimicrobial activity against a variety of Gram positive and Gram negative species, and exhibits high potency against *E. coli* PBP3 as well ($\text{IC}_{50} = 0.25 \mu\text{g}/\text{mL}$).^{568,569}

Further exploration of structure-activity relationships in this active scaffold has led to very few positive results. Modifications at C7 based on the 6*R*-hydroxyethyl side chain of carbapenems led to a reduction in activity,⁵⁷⁰ as did expansion to a more cephem-like [4.3.0] bicyclic system.^{566,571,572} Notably, removal of the C7 substituent altogether decreases antimicrobial potency but does not abolish it entirely.⁵⁷³ Monocyclic pyrazolidin-5-ones suffer from a similar lack of potency.⁵⁷⁴ That these C7-unsubstituted and monocyclic pyrazolidin-5-ones retain antimicrobial activity while their monoaza analogues do not, indicates the marked activation of this scaffold, and demonstrates its promise in the development of PBP-acylating antimicrobials.

Other attempts have been made to activate γ -lactam ring systems, including the introduction of electron-withdrawing groups to the ring itself. Synthesis of bicyclic 1*H*-pyrrole-2,3-diones showed adduct formation with methanol, indicating successful activation and potential for PBP acylation;⁵⁷⁵ however, these compounds lack antimicrobial activity, and fit poorly into the transpeptidase active site (**Figure 1.21**). Other groups have surveyed additional ring strain through the synthesis of bridged γ -lactams. To this end, the 7-oxo-1-azabicyclo[3.2.1]oct-2-ene **29** was synthesized.⁵⁷⁶ The compound has an IC_{50} of 5 μM against both PBP3 and PBP4 of *P. aeruginosa* and exhibits modest antimicrobial activity against a variety of species.

In kinetics studies to determine which other cyclic amides, if any, hold promise in transpeptidase or serine protease acylation, hydrolysis of monocyclic lactams was measured to determine reactivity with nucleophiles. Surprisingly, δ -valerolactam underwent alkaline hydrolysis at a rate almost equivalent to that of β -propiolactam (second-order rate constants of $1.21 \times 10^{-4} \text{ M}^{-1}\text{s}^{-1}$ and $2.37 \times 10^{-4} \text{ M}^{-1}\text{s}^{-1}$, respectively), while all other ring sizes were 40- to 1,700-fold less reactive.⁵⁷⁷ However, early syntheses of direct δ -lactam penam analogues yielded no biological activity.⁵⁷⁸ Even in the context of the activated diaza scaffold discussed above, δ -lactams failed to show much potency despite high pseudo-first order rates of alkaline hydrolysis ($k = 8.8 \times 10^{-4} \text{ s}^{-1}$).⁵⁶⁹ Through computational modeling and structural alignment of the synthesized compounds with known actives, it was concluded that the disparity between chemical reactivity and biological activity could be explained by three factors unique to the larger ring system that decrease productive binding to the transpeptidase active site: 1) the spatial arrangement of the acylamino side chain, 2) additional steric bulk, and 3) increased conformational freedom (**Figure 1.21**).

Table 1.9: Activity of γ -lactams against bacterial transpeptidases. ^aHalf-maximal inhibitory concentration (IC_{50}). ^bApproximation from PBP-binding shown for isolated membrane proteins.

Compound	Species	Target	Activity ^a	Reference
27	<i>E. coli</i>	PBP3	$\sim 1.5 \mu\text{g/mL}^b$	567
28	<i>E. coli</i>	PBP3	$0.25 \mu\text{g/mL}$	569
29	<i>P. aeruginosa</i>	PBP3	$5 \mu\text{M}$	576
	<i>P. aeruginosa</i>	PBP4	$5 \mu\text{M}$	

Lactivicin (**30**), a cycloserine- and γ -lactone-containing natural product, has also been shown to inhibit a variety of PBPs at micromolar concentrations⁵⁷⁹ (**Figure 1.22**). It is highly active against Gram positive organisms, but its modest Gram negative activity revealed a need for derivatization. Early analogues employing acylamino side chains similar to third-generation cephalosporins (**31**) exhibited improved antimicrobial spectrum, likely due to enhanced outer membrane permeability, as well as improved interactions with the transpeptidase active site.^{580,581} Improved target inhibition by such modifications was later shown by phenoxyacetyl lactivicin **32**, an analogue of penicillin V, which is 6- and 40-fold more potent against two different *S. pneumoniae* PBP2x variants than the parent compound.⁵⁸² Further attempts to extend spectrum involved the use of specific, charged acylamino side chains employed in antipseudomonal cephalosporins. Compound **33**, which shares an acylamino group with ceftazidime, shows both increased potency against Gram negatives and enhanced inhibition of pseudomonal PBPs.⁵⁸³ Conjugation of this molecule to siderophoric 4,5-dihydroxyphthalimide (compound **34**) improves its uptake into Gram negative bacilli without negatively affecting target inhibition, enhancing its antimicrobial activity by as much as 500-fold.^{583,584}

Through mechanistic studies conducted by Macheboeuf *et al.*, it is now known that the lactivicins inhibit PBPs covalently via an acylation reaction distinct from β -lactams.⁵⁸² In a crystal structure of lactivicin in complex with *S. pneumoniae* PBP1b, O γ of nucleophilic Ser460 has formed a covalent bond with the cycloserine carbonyl carbon, causing the cycloserine ring to open and, by resonance, the γ -lactam as well (**Figure 1.23**). The oxygen of the resulting ester carbonyl is located in the oxyanion hole formed by Ser460 and Thr654. The γ -lactone γ -carboxylate group makes polar contacts with the side chains of Thr652 (KTG) and Thr654, and the carbonyl oxygen of the cycloserine *N*-acetyl group contacts Asn518 (SxN). The structure has marked similarities with a PBP1b-cefotaxime acyl-enzyme structure,⁵⁸⁵ indicating a similarity of pre-covalent binding mode that allows

the acylation reactions to proceed. Like β -lactams, lactivicins probably act as C-terminal peptidomimetics, where the γ -lactone γ -carboxylate acts as the C-terminus, an electrostatic anchor that helps to position the electrophilic carbonyl for attack by the serine nucleophile, while the acetylamino group aids in complex formation by mimicking the peptide bond of a third amino acid.

The reactivity of the lactivicin cycloserine (4-aminoisoxazolidin-3-one) moiety has led to the exploration of novel isoxazolidin-5-one compounds. While several of the initial compounds to come out of this work, including **35**, had only marginal antimicrobial activity, they readily formed adducts with methanol, showing that they are reactive to nucleophilic species.⁵⁸⁶ It should be noted that many of these molecules are esterified and would likely be manifold more potent as carboxylic acids. Cao *et al.* subsequently designed and synthesized a series of 3-alkoxyisoxazolidin-5-ones possessing carboxylic acid moieties in accordance with the geometric requirements established for transpeptidase inhibition by β -lactams.⁵⁸⁷ These compounds represent a significant improvement over earlier efforts, with the 3-isopropoxyisoxazolidin-5-one **36** inhibiting *B. subtilis* growth at 0.2 $\mu\text{g/mL}$. Target inhibition was confirmed via spectroscopic PBP labeling with a dansylated version of the 5-methoxy analogue, but no determinations of potency were made.

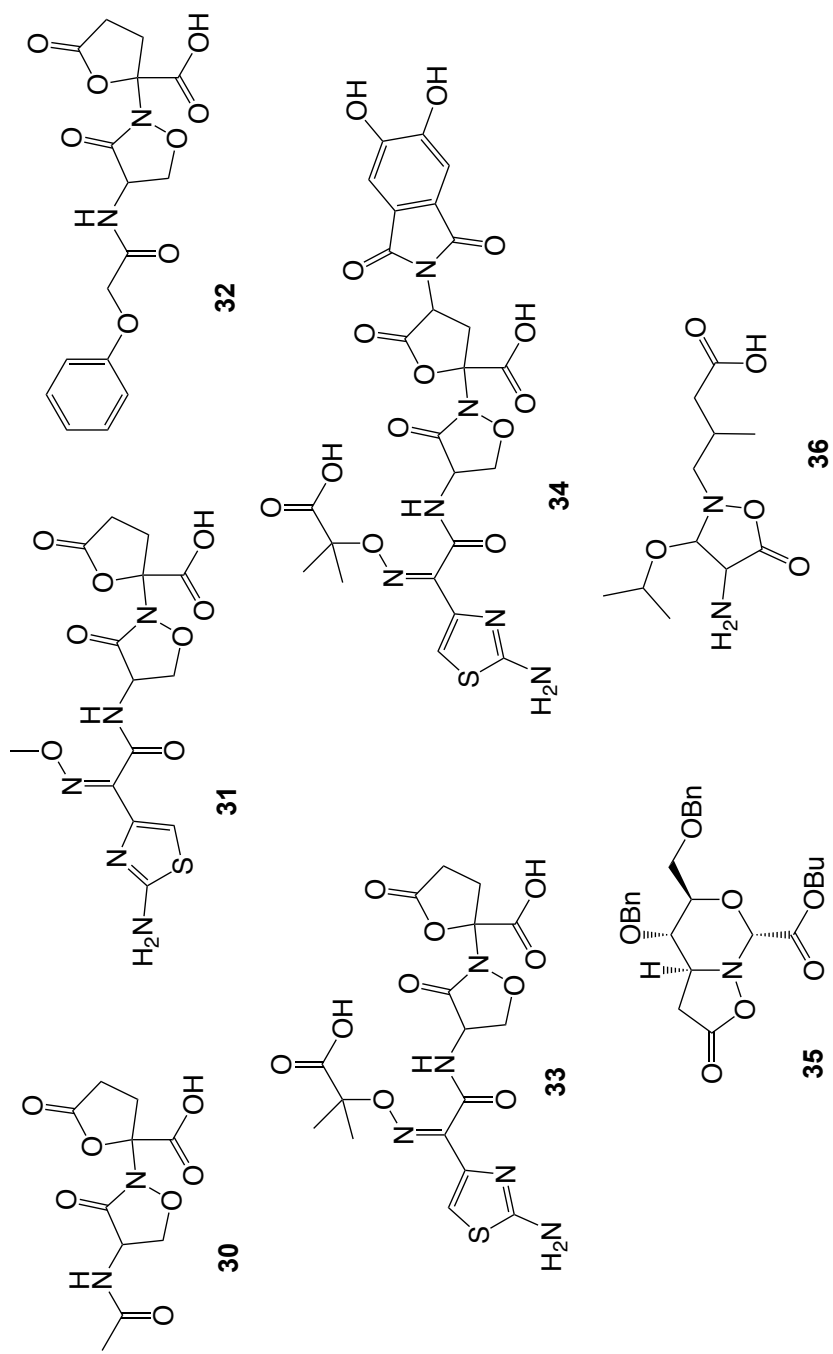


Figure 1.22: Structures of lactivicin and lactivicin-like transpeptidase inhibitors.

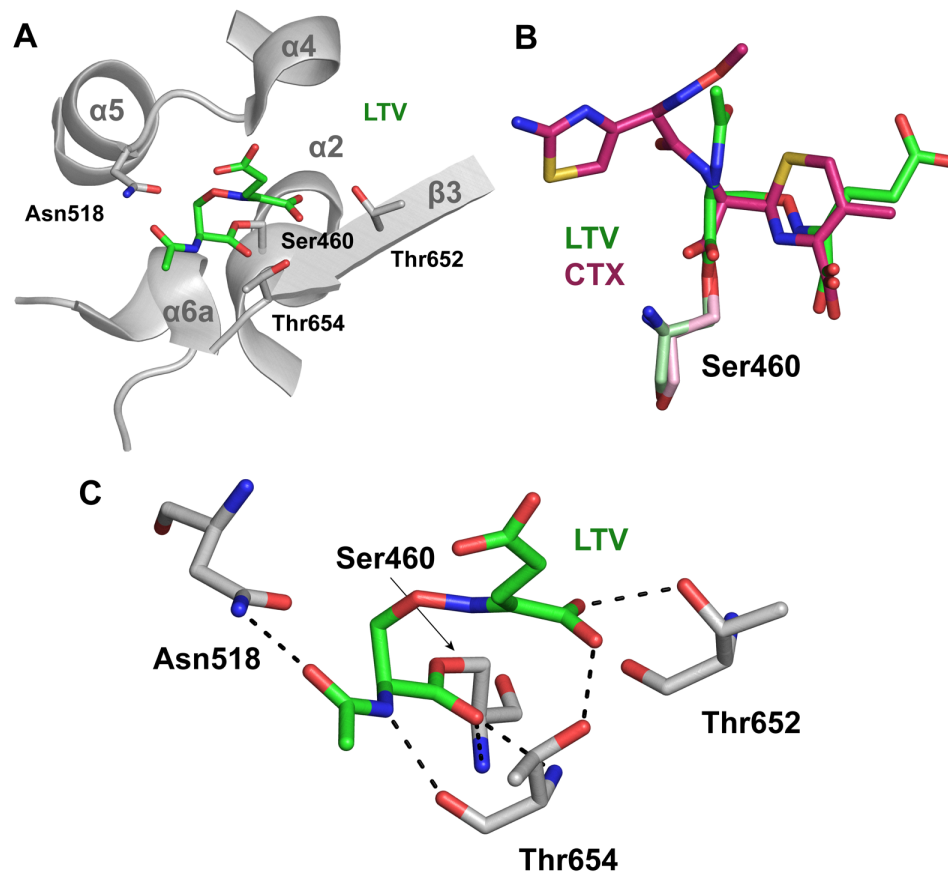


Figure 1.23: Crystal structure of lactivicin in complex with *S. pneumoniae* PBP1b. **A.** Lactivicin (LTV, green) covalently bound in the transpeptidase active site of PBP1b. **B.** Overlay of covalently bound cefotaxime with lactivicin. **C.** Detailed view of lactivicin interactions (polar contacts are shown as black dashed lines).

Table 1.10: Activity of lactivicins against bacterial transpeptidases. ^aHalf-maximal inhibitory concentration (IC₅₀) unless otherwise denoted. ^bSecond-order acylation rate constant (k_2/K_s).

Compound	Species	Target	Activity ^a	Reference
30	<i>B. subtilis</i>	PBP1	0.28 µg/mL	579
	<i>B. subtilis</i>	PBP2	1.0 µg/mL	
	<i>B. subtilis</i>	PBP3	12 µg/mL	
	<i>B. subtilis</i>	PBP4	0.05 µg/mL	
	<i>E. coli</i>	PBP1a	5.0 µg/mL	
	<i>E. coli</i>	PBP1b	14 µg/mL	
	<i>E. coli</i>	PBP2	22 µg/mL	
30	<i>S. pneumoniae</i> R6	PBP2x	380 M ⁻¹ s ⁻¹ ^b	582
	<i>S. pneumoniae</i> 5204	PBP2x	0.6 M ⁻¹ s ⁻¹ ^b	
32	<i>S. pneumoniae</i> R6	PBP2x	2,150 M ⁻¹ s ⁻¹ ^b	582
	<i>S. pneumoniae</i> 5204	PBP2x	25 M ⁻¹ s ⁻¹ ^b	
33	<i>P. aeruginosa</i>	PBP1a	0.046 µM	583
	<i>P. aeruginosa</i>	PBP1b	1.23 µM	
	<i>P. aeruginosa</i>	PBP2	33.3 µM	
	<i>P. aeruginosa</i>	PBP3	0.092 µM	
34	<i>P. aeruginosa</i>	PBP1a	0.03 µM	583
	<i>P. aeruginosa</i>	PBP1b	0.27 µM	
	<i>P. aeruginosa</i>	PBP2	3.7 µM	
	<i>P. aeruginosa</i>	PBP3	0.046 µM	

A more recently identified class of β -lactam-mimicking compounds is the 1,6-diazabicyclo[3.2.1]octan-7-ones (DBO), which possess a 5-membered diazacyclic system resembling that seen in pyrazolidinones **26-28** discussed above, as well as a bridged structure similar to **29** (**Figure 1.24**). The DBO carbonyl is activated by a disruption of urea resonance caused by geometric constraints of the bicyclic system on the bridgehead nitrogen side, and by an electron-withdrawing inductive effect on the *N*-sulfonic acid side, as shown in the prototypical compound NXL104 (avibactam, **35**). Avibactam was originally developed as a covalent β -lactamase inhibitor with a fast on-rate ($k_2/K_i > 10^4 \text{ M}^{-1}\text{s}^{-1}$) against a variety of classes, as well as a slow off-rate ($k_3 < 10^{-3} \text{ s}^{-1}$).⁵⁸⁸⁻⁵⁹¹ Early crystal structures of avibactam with serine β -lactamases show carbamoylation of the serine nucleophile and occupancy of the oxyanion hole by the carbonyl oxygen.^{590,592-594} Unlike other β -lactamase inhibitors, however, avibactam exhibits intrinsic antimicrobial activity.^{595,596} In subsequent investigations of this activity, it was found to bind PBPs with

low- to mid-micromolar affinity, with a notable preference for PBP2 from a variety of species.^{597,598} From these data, the DBO scaffold has become a jumping off point for one of the first successful ventures into dual inhibition.

Many derivatization efforts have focused on modification of the avibactam 2-carbamoyl moiety. Synthesis and testing of direct *N*-alkyl and *N*-aryl derivatives was reported by Blizzard *et al.*, who explored a series of carbocyclic and heterocyclic substitutions.⁵⁹⁹ Interestingly, *N*-(pyridin-2-yl) compounds exhibited nanomolar inhibition of class A, C, and D β -lactamases, but they failed to show much synergy with carbapenems against resistant Gram negative bacilli. The best synergy results were obtained with *N*-(pyrrolidin-3-yl) and *N*-(piperidin-4-yl) analogues, the latter of which has been pursued as MK7655 (relebactam, **36**). While relebactam's carbapenem-potentiating effects are well documented,⁶⁰⁰⁻⁶⁰³ it has relatively weak intrinsic antimicrobial activity,⁶⁰⁴ and its PBP-binding profile has not been characterized. Further investigations of the 2-carbamoyl group led to the *N*-alkoxycarboxamides FPI1459 (nacubactam, **37**) and FPI1465 (**38**). Nacubactam is an *N*-(2-aminoethoxy) derivative with potent β -lactamase inhibition and better intrinsic antimicrobial activity than either avibactam or relebactam against a variety of problematic Gram negative species.⁶⁰⁵ In keeping with its improved intrinsic activity, it also inhibits *E. coli* PBP2 more potently than avibactam, with an IC₅₀ of 0.12 μ g/mL. FPI1465 is a ring-constrained *N*-(pyrrolidin-3-yloxy) analogue of nacubactam with similar antimicrobial activity.⁶⁰⁶ Although its reported IC₅₀ against *E. coli* PBP2 is higher than that reported for nacubactam, the enzymatic assays reported by King *et al.* were done under conditions of simultaneous addition rather than preincubation. Comparing results from similar techniques, both compounds represent an ~5-fold improvement over avibactam. A 2.9 Å crystal structure of FPI1465 in complex with *E. coli* PBP1b reveals marked similarities between the PBP binding modes of DBOs and β -lactams⁶⁰⁶ (**Figure 1.25**). The nucleophilic Ser510 is carbamoylated, and the ligand

carbonyl oxygen occupies the oxyanion hole created by Ser510 and Thr701. The sulfonic acid makes polar contacts with Thr699 (KTG) and Thr701, similar to what is seen in complex structures of aztreonam, ampicillin, and cephalexin, and it is also within hydrogen bonding distance of Ser572 (SxN).⁶⁰⁷ Neither the FPI1465 2-carbamoyl group nor the aztreonam C3 acylamino group contact Asn574 (SxN), a common point of interaction with 6-acylamino and 7-acylamino groups of penams and cepheams, respectively. A final subclass arising from modifications to the 2-carbamoyl group are the diacylhydrazines FPI1523 (**39**), FPI1602 (**40**), WCK5153 (**41**), and WCK5107 (zidebactam, **42**). FPI1523 is a simple acetyl derivative with 20-fold better *E. coli* PBP2 inhibition than avibactam, as well as 8- to 16-fold better antimicrobial activity against *E. coli* transformed with a variety of β -lactamases.⁶⁰⁶ FPI1602, WCK5153, and zidebactam are a series of nitrogen heterocycle-substituted acyl hydrazines of increasing ring size. Of the compounds reported by King *et al.*, FPI1602 is the most potent single agent antimicrobial, with MICs less than 0.5 $\mu\text{g/mL}$ against *E. coli* transformed with a variety of β -lactamases and good activity against NDM-1-producing clinical isolates of *E. coli* and *E. cloacae*.⁶⁰⁶ It exhibits *E. coli* PBP2 inhibition similar to FPI1523. WCK5153 and zidebactam have been characterized largely for their considerable antipseudomonal properties.⁶⁰⁸ They exhibit submicromolar inhibition of *P. aeruginosa* PBP2, as well as antimicrobial activity against even metallo- β -lactamase-producing strains. While they are potent inhibitors of PBP2 from *K. pneumoniae* and *A. baumannii* as well, WCK5153 and zidebactam are only capable of inhibiting growth of non-MBL-producing *K. pneumoniae* and fail against *A. baumannii* entirely.⁶⁰⁹⁻⁶¹¹

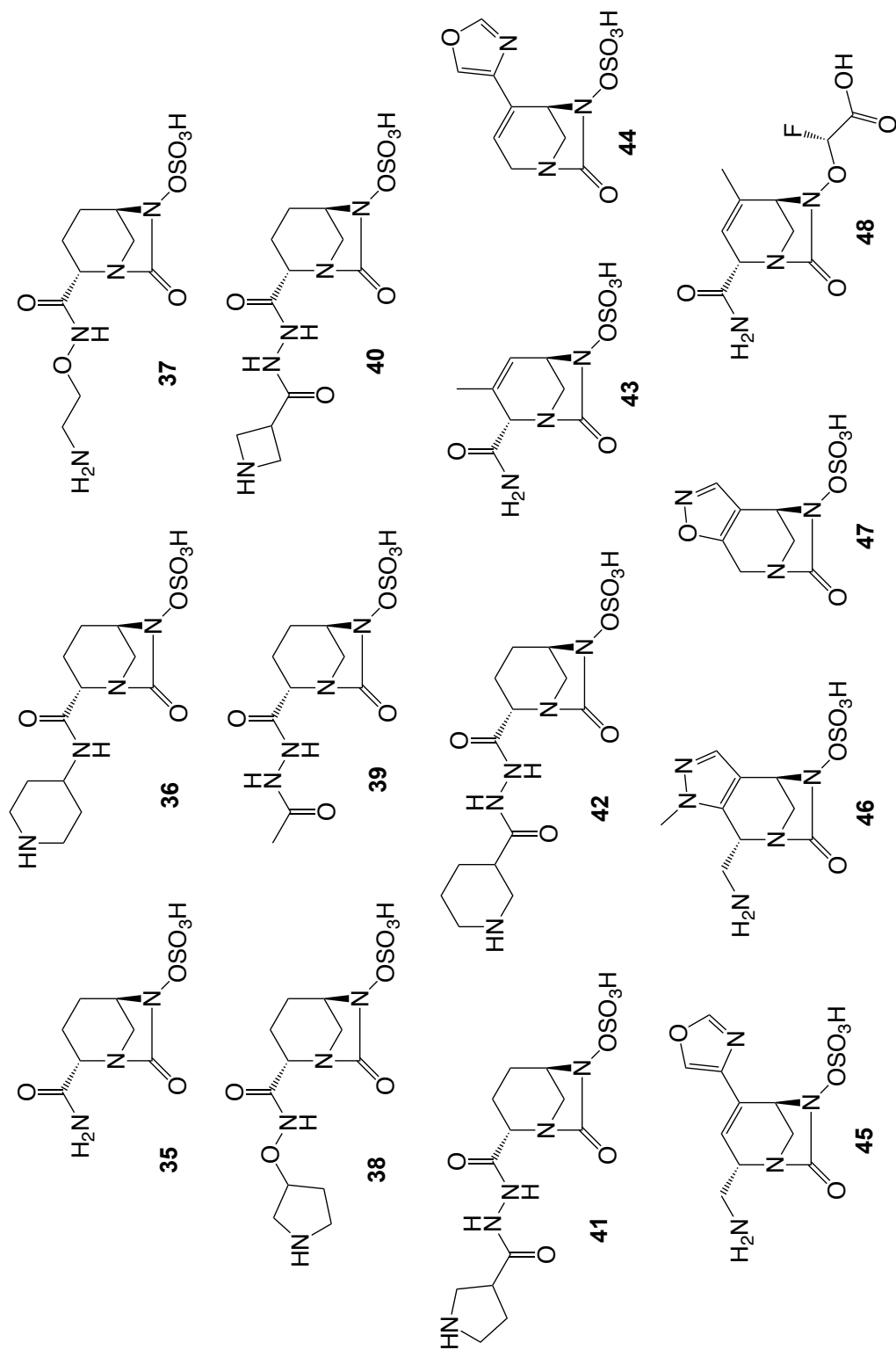


Figure 1.24: Structures of DBO transpeptidase inhibitors.

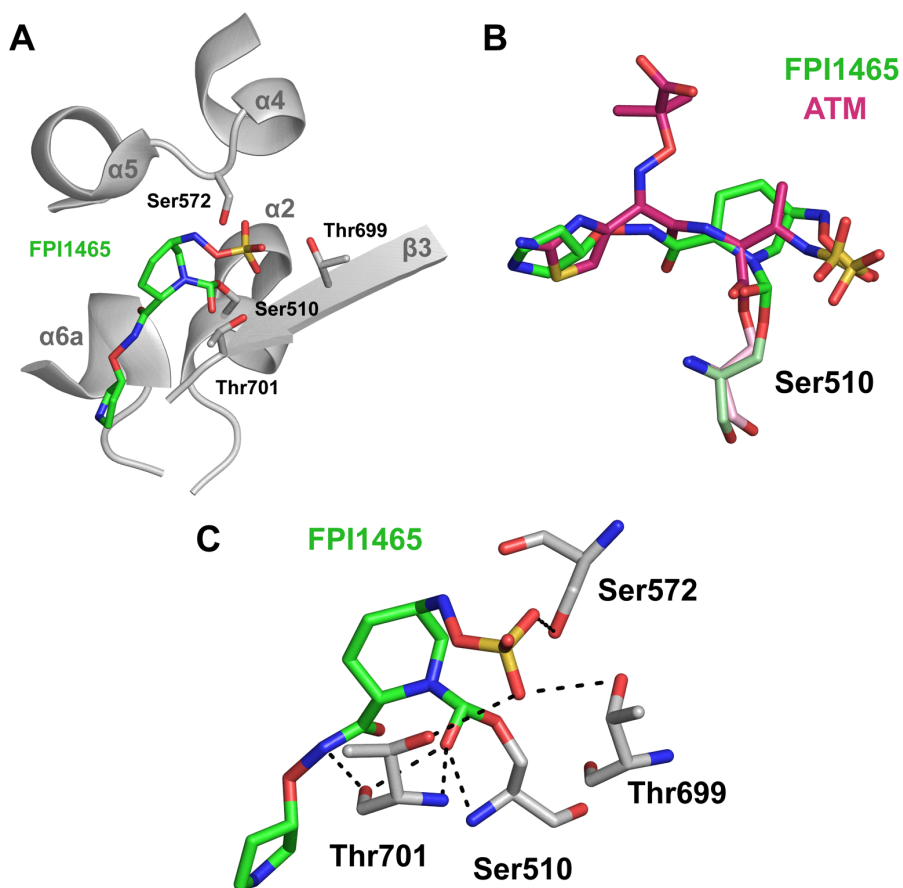


Figure 1.25: Crystal structure of DBO FP1465 in complex with *E. coli* PBP1b. **A.** FPI1465 covalently bound in the transpeptidase active site of PBP1b. **B.** Overlay of covalently bound aztreonam structure.⁶⁰⁷ **C.** Detailed view of FPI1465 interactions (polar contacts shown as black dashed lines).

Other groups have explored the chemistry of the 3- and 4-positions. One such example is ETX2514/durlobactam (**43**), a 3-unsaturated 3-methyl analogue of avibactam. Durlobactam shows good antimicrobial activity against a series of Gram negative bacilli, including *K. pneumoniae* and *S. maltophilia*.⁶¹² However, despite its relatively rapid carbamoylation of *A. baumannii* PBP2 and its marked potentiation of carbapenem and sulbactam activity against metallo- β -lactamase-producing strains, durlobactam does not have significant intrinsic anti-acinetobacter activity itself.^{612,613} Durlobactam is a poor antipseudomonal agent, perhaps due to its poor carbamoylation of *P. aeruginosa* PBPs.

Additional 3-unsaturated DBOs include 2-decarbamoyl 4-(oxazol-4-yl) product CPD3 (**44**) and its 2-aminomethyl analogue CPD4 (**45**). In this work, Levy *et al.* explored a series of 4-substituted analogues and found that, with few exceptions, those with a 4-heterocyclic moiety are more potent than the unsubstituted parent compound.⁶¹⁴ CPD3 and CPD4 are both nanomolar *E. coli* PBP2 inhibitors, but addition of the aminomethyl group seen in CPD4 improves its antimicrobial potency considerably, making it among the most intrinsically active of the DBOs reported to-date (mean MIC values of 0.031 µg/mL and 1 µg/mL against *E. coli* and *P. aeruginosa* clinical isolates, respectively). Fused pyrazolo[3,4-e] (NXL105, **46**) and oxazolo[4,5-e] (**47**) products and derivatives show intrinsic activity against *E. coli* and a series of *P. aeruginosa* strains, but no further reports of spectrum or PBP inhibition could be found.⁶¹⁵⁻⁶¹⁸ However, resistance to these compounds in *E. coli* has been ascribed to mutations in the *mrdA* gene encoding PBP2, indicating significant binding in susceptible strains.⁶¹⁵ ETX1317 (**48**) occupies unique chemical space, with a 2-fluoroacetic acid in place of the sulfonic acid seen in other DBOs. ETX1317 has potent intrinsic antimicrobial activity, with a median MIC of 0.25 µg/mL against a panel of 1,875 clinical isolates of Gram negative enterics, and has been shown to bind *E. coli* PBP2 from membrane preparations.⁶¹⁹

Table 1.11: Activity of DBOs against bacterial transpeptidases. ^aHalf-maximal inhibitory concentration (IC₅₀) unless otherwise denoted. ^bConducted with simultaneous addition of inhibitor and substrate, as opposed to an inhibitor preincubation period usually used for IC₅₀ measurements. ^cSecond-order carbamoylation rate constant (k_2/K_s).

Compound	Species	Target	Activity ^a	Reference	
35	<i>E. coli</i>	PBP2	0.92 µg/mL	597	
	<i>P. aeruginosa</i>	PBP2	1.1 µg/mL		
	<i>P. aeruginosa</i>	PBP3	1.8 µg/mL		
	<i>P. aeruginosa</i>	PBP4	11 µg/mL		
	<i>H. influenza</i>	PBP2	3.0 µg/mL		
	<i>S. pneumoniae</i>	PBP3	8.1 µg/mL		
	<i>S. aureus</i>	PBP2	51 µg/mL		
	<i>S. aureus</i>	PBP3	156 µg/mL		
	<i>E. coli</i>	PBP2	0.59 µM		614
	<i>E. coli</i>	PBP2	63 µM ^b		606
	<i>K. pneumoniae</i>	PBP2	2 µg/mL	598	
37	<i>E. coli</i>	PBP2	0.12 µg/mL	605	
38	<i>E. coli</i>	PBP2	14.8 µM ^b	606	
39	<i>E. coli</i>	PBP2	3.2 µM ^b	606	
40	<i>E. coli</i>	PBP2	3.6 µM ^b	606	
41	<i>P. aeruginosa</i>	PBP2	0.14 µg/mL	608	
	<i>A. baumannii</i>	PBP2	0.01 µg/mL	609	
	<i>K. pneumoniae</i>	PBP2	0.07 µg/mL	610	
42	<i>P. aeruginosa</i>	PBP2	0.26 µg/mL	608	
	<i>A. baumannii</i>	PBP2	0.01 µg/mL	609	
	<i>K. pneumoniae</i>	PBP2	0.08 µg/mL	610	
43	<i>A. baumannii</i>	PBP1a	180 M ⁻¹ s ^{-1 b}	612	
	<i>A. baumannii</i>	PBP2	1,800 M ⁻¹ s ^{-1 b}		
	<i>A. baumannii</i>	PBP3	3.37 M ⁻¹ s ^{-1 b}		
	<i>P. aeruginosa</i>	PBP1a	12 M ⁻¹ s ^{-1 b}		
	<i>P. aeruginosa</i>	PBP2	24.3 M ⁻¹ s ^{-1 b}		
	<i>P. aeruginosa</i>	PBP3	60 M ⁻¹ s ^{-1 b}		
	<i>E. coli</i>	PBP1a	120 M ⁻¹ s ^{-1 b}		
	<i>E. coli</i>	PBP2	17,000 M ⁻¹ s ^{-1 b}		
<i>E. coli</i>	PBP3	2.3 M ⁻¹ s ^{-1 b}			
44	<i>E. coli</i>	PBP2	25 nM	614	
45	<i>E. coli</i>	PBP2	10 nM	614	

1.5.c. Other reactive (presumed covalent) inhibitors

There are several identified PBP inhibitors that possess functional groups reactive to nucleophiles, but which have not been fully characterized as covalent in mechanism. Two such classes are the arylalkylidene rhodanines and arylalkylidene iminothiazolidin-4-ones, identified as inhibitory scaffolds in a high-throughput screen and subsequently derivatized to yield **49** and **50**⁶²⁰ (**Figure 1.26**). These compounds exhibit single-digit micromolar inhibition of *S. aureus* PBP2a and are active against a series of diverse transpeptidases, including *S. pneumoniae* PBP2x, *E. coli* PBP3, *E. coli* PBP5, *Streptomyces* R61 DD-peptidase, and *Actinomadura* R39 DD-peptidase. They were also shown to inhibit growth of several pathogens and confirmed to inhibit cell wall synthesis in [³H]-glycine incorporation assays. Arylalkylidene rhodanine **51** was identified in a high-throughput screen, this time against PBP2 of *N. gonorrhoeae*.⁶²¹ This compound was found to have much more potent antimicrobial activity (2 µg/mL) than expected from its modest target inhibition (153 µM), suggesting potential off-target effects. The arylalkylidene rhodanines and arylalkylidene iminothiazolidin-4-ones contain an electron withdrawing olefin motif that can act as a Michael acceptor, and the former have been shown to bind covalently to cysteine residues through nucleophilic attack by the side chain thiol.⁶²² Moreover, they have been found to inhibit *S. pneumoniae* PBP2x noncompetitively.⁶²⁰ These molecules may, therefore, bind to the activated serine nucleophile of transpeptidases through a similar mechanism (**Figure 1.27**). The arylalkylidene rhodanine structure is considered a pan-assay interference (PAIN) compound substructure, but because derivatization can result in high selectivity for a given target, it is considered a privileged scaffold.⁶¹²

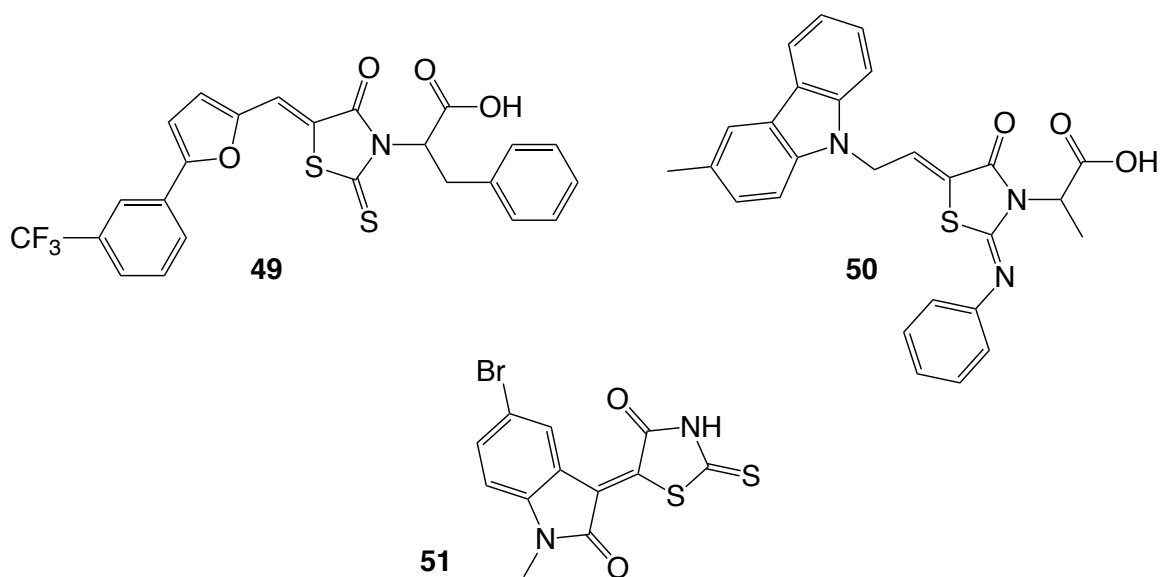


Figure 1.26: Structures of arylalkylidene rhodanine and arylalkylidene iminothiazolidin-4-one transpeptidase inhibitors.

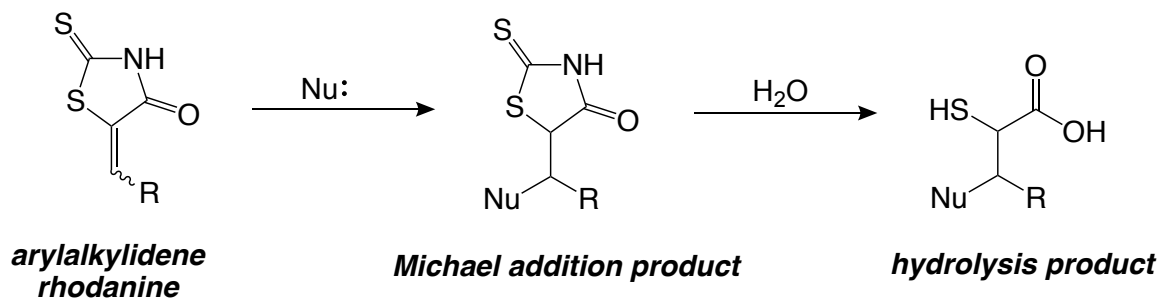


Figure 1.27: Proposed mechanism of arylalkylidene rhodanine PBP inhibition.

Table 1.12: Activity of arylalkylidene rhodanines and arylalkylidene iminothiazolidin-4-ones against bacterial transpeptidases. ^aHalf-maximal inhibitory concentration (IC₅₀). ^bPercent inhibition at 50 μM. ^cPercent inhibition at 100 μM.

Compound	Species	Target	Activity	Reference
49	<i>S. aureus</i>	PBP2a	5 μM ^a	620
	<i>S. pneumoniae</i>	PBP2x, S	96% ^b	
	<i>S. pneumoniae</i>	PBP2x, R	90% ^c	
	<i>E. coli</i>	PBP3	87% ^b	
	<i>E. coli</i>	PBP5	94% ^b	
	<i>Streptomyces spp.</i>	R61 DD-peptidase	75% ^b	
	<i>Actinomadura spp.</i>	R39 DD-peptidase	95% ^b	
50	<i>S. aureus</i>	PBP2a	9 μM ^a	620
	<i>S. pneumoniae</i>	PBP2x, S	31% ^b	
	<i>S. pneumoniae</i>	PBP2x, R	90% ^c	
	<i>E. coli</i>	PBP3	86% ^b	
	<i>E. coli</i>	PBP5	83% ^b	
	<i>Streptomyces spp.</i>	R61 DD-peptidase	44% ^b	
	<i>Actinomadura spp.</i>	R39 DD-peptidase	55% ^b	
51	<i>N. gonorrhoeae</i>	PBP2	153 μM ^a	621

1.5.d. Noncovalent inhibitors

Physical screening of molecules against PBPs has resulted in the discovery and development of many classes of noncovalent inhibitors, but very few have been pursued for optimization and development into preclinical leads. Some initial hits were found serendipitously in the course of other experiments, followed by more purposeful physical screening (**Figure 1.28**). In early studies of *S. aureus* PBP2a, it was noted that chromatographic stationary phase Cibacron blue (**52**) bound the protein tightly, such that it would not elute upon introduction of a salt gradient.⁶²⁴ Subsequent testing of Cibacron blue revealed that it is a mid-micromolar inhibitor of PBP2a, and screening of chemically similar compounds from a Merck collection allowed the identification of the more potent Erie yellow (**53**), which exhibits an IC₅₀ of 13 μM. No antimicrobial data was reported for these hits, however. In another study, a PBP inhibitor was found by testing a hit from screens against a different enzyme. Physical screening of a cyclic heptapeptide

bacteriophage display library revealed **54** to inhibit activity of a synthetic catalytic antibody with β -lactamase-like activity.⁶²⁵ During biochemical characterization, **54** was found to inhibit TEM-1, as well as several high- and low-molecular weight PBPs to varying degrees.⁶²⁶ Although this scaffold was subject to some minor derivatization, the β -lactamases were the primary focus of this work, and none of the analogues were tested against PBPs. No antimicrobial data was reported from these studies.

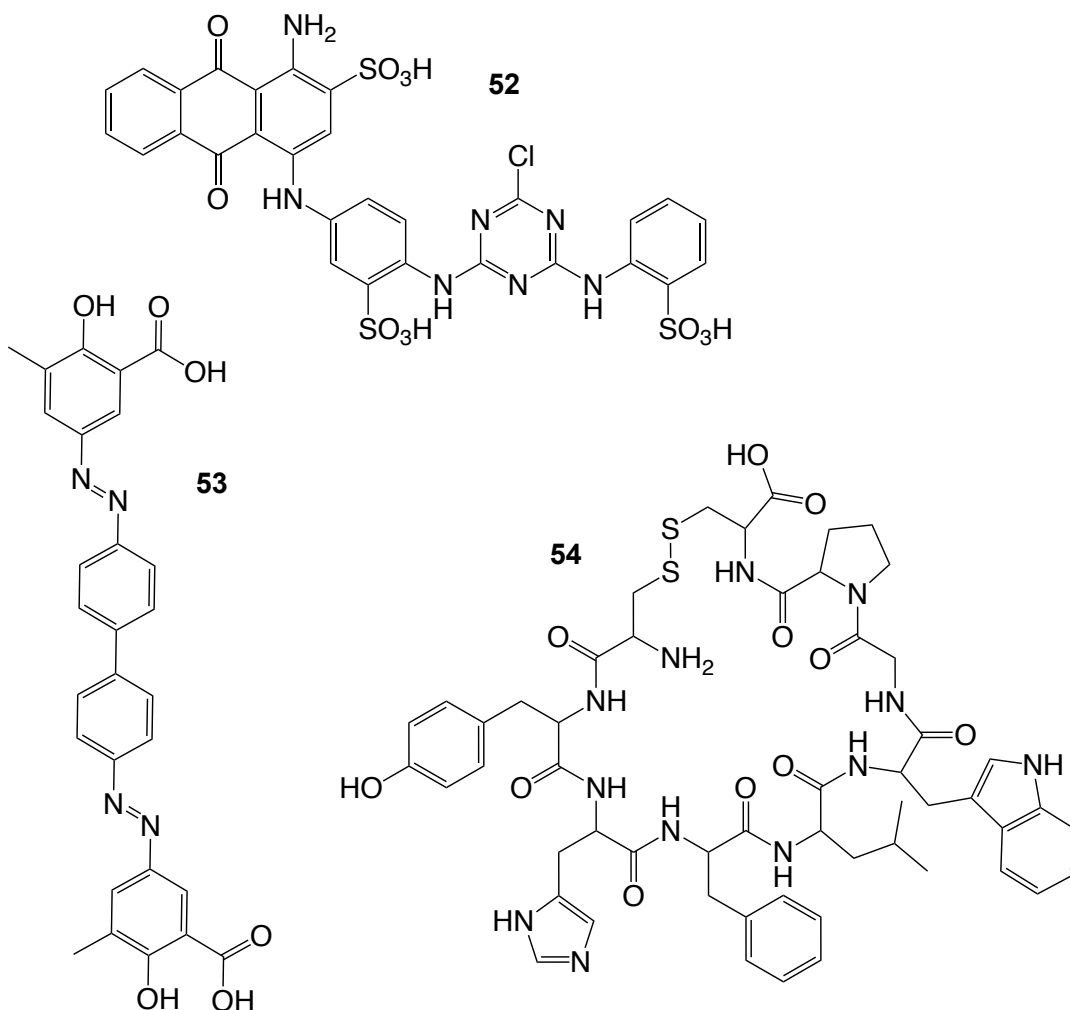


Figure 1.28: Structures of transpeptidase inhibitors discovered through serendipity.

Focused physical screening with the aim of discovering more drug-like small molecule PBP inhibitors followed these initial ventures (**Figure 1.29**). One class of such inhibitors was identified from small parallel physical screens against MRSA PBP2a, *Streptococcus pneumoniae* PBP2x, and *Enterococcus faecium* PBP5.⁶²⁷ The screen and subsequent analogue search, synthesis, and testing identified anthranilic acid-derived arylsulfonamides and their isosteric arylamide derivatives as mid- to high-micromolar inhibitors of the tested PBPs.^{627,628} The most potent inhibitors from each scaffold, **55** and **56**, exhibit half-maximal inhibition of MRSA PBP2a at 80 μM and 210 μM , respectively. Both compounds show only marginal suppression of staphylococcal growth, however. Shortly thereafter, high-throughput screening of a 50,000-compound library from the ChemBridge Corporation identified a number of compounds that exhibit activity against *N. gonorrhoeae* PBP2 in the micromolar range.⁶²¹ While a few of the compounds from this study possess functional groups concerning for nonspecific binding (e.g., arylalkylidene rhodanine **51** above), arylsulfonamides **57** and **58** are promising hits, exhibiting half-maximal inhibition of PBP2 at 50 μM and 56 μM , respectively, as well as comparable activities against penicillin-susceptible and -resistant strains of *N. gonorrhoeae* (MIC = 8-16 $\mu\text{g/mL}$).⁶²¹

Screening for antimicrobial natural products has also successfully identified PBP-inhibitory compounds. The endophytic fungus *Aspergillus* TJ23 was found to inhibit the growth of ATCC43300 (MRSA) *in vitro*.⁶²⁹ Subsequent separation of liquid culture components yielded the active species **59**, a meroterpenoid metabolite with a dioxabicyclo[2.2.1]heptane skeleton. This compound, named aspermerodione, inhibits MRSA growth at 32 $\mu\text{g/mL}$ and PBP2a at 18.4 μM .

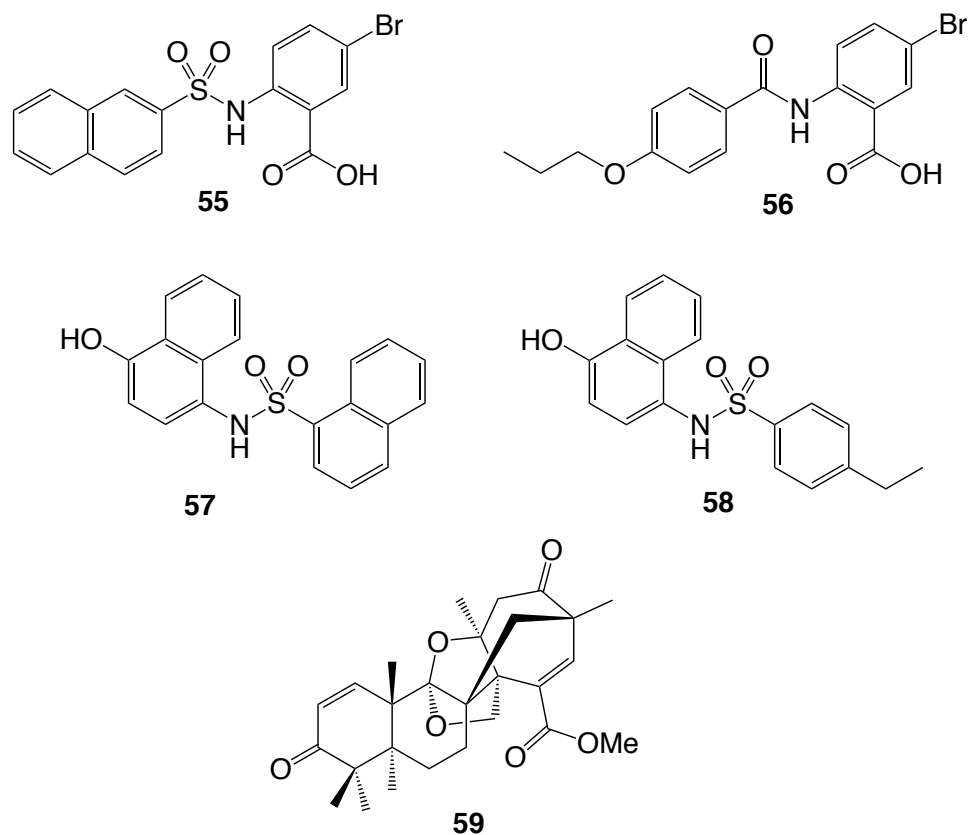


Figure 1.29: Structures of transpeptidase inhibitors identified through physical screening methods.

In addition to physical screening, *in silico* tools have also been utilized for PBP drug discovery because this approach forgoes the need for large physical libraries, a high-throughput transpeptidase assay or liquid handling robot, or large repositories of natural product sources (**Figure 1.30**). One early study employed a four-point pharmacophore model to conduct a high-throughput virtual screen of the NCI database (~260,000 ligands) against *S. pneumoniae* PBP2x.⁶³⁰ The screen successfully identified 2-((1,3,4-thiadiazol-2-yl)amino)benzenesulfonic acid **60** and 2-ureidobenzenesulfonic acids **60** and **61** as inhibitors of PBP2x. While **61** and **62** show similar potency against PBP2x from penicillin-resistant *S. pneumoniae* 5204 ($IC_{50} = 71 \mu\text{M}$ and $72 \mu\text{M}$, respectively), **62** shows significantly better inhibition of PBP1b.

In another study, a fragment-based docking protocol was used against the active site of *E. coli* PBP5.⁶³¹ The computational analysis revealed the 4-quinolone scaffold as a putative binder of the active site, and upon synthesis of derivatized 4-quinolones, several were shown to inhibit high molecular weight PBPs of *E. coli* at mid-micromolar concentrations. While the best inhibitor reported, **63**, demonstrates affinity for every PBP from *E. coli*, this compound showed no suppression of *E. coli* growth up to 1 mM.

Among the most successful noncovalent PBP inhibitors discovered to date are the 1,2,4-oxadiazoles (**Figure 1.30**). The prototype of this class, **64**, was identified from a high-throughput virtual screen of the ZINC database against MRSA PBP2a, with energy scoring performed by four separate algorithms.⁶³² The hydroxyl derivative **65** is a micromolar-range inhibitor of PBP2a with antimicrobial activity against a series of Gram positive organisms (MIC = 1-2 µg/mL against a series of staphylococci and enterococci). The compound was also observed to be on-target, inhibiting [³H]-alanine incorporation into peptidoglycan without effects on the synthesis of protein or polynucleotides. From extensive exploration of the scaffold through medicinal chemistry, **66** has emerged as a promising antimicrobial candidate, exhibiting favorable pharmacokinetic properties as well as efficacy in a murine model of staphylococcal peritonitis.⁶³³⁻⁶³⁵ While the 1,2,4-oxadiazoles have excellent activity against staphylococci and other Gram positives,⁶³⁴⁻⁶³⁶ no antimicrobial data against Gram negative organisms has been published. Additional computational work has been done to determine quantitative structure-activity relationships (QSAR) for the class using comparative molecular field analysis (CoMFA), comparative molecular similarity indices analysis (CoMSIA), and field-based 3D-QSAR, but no compounds designed with the guidance of these models have been reported.⁶³⁷

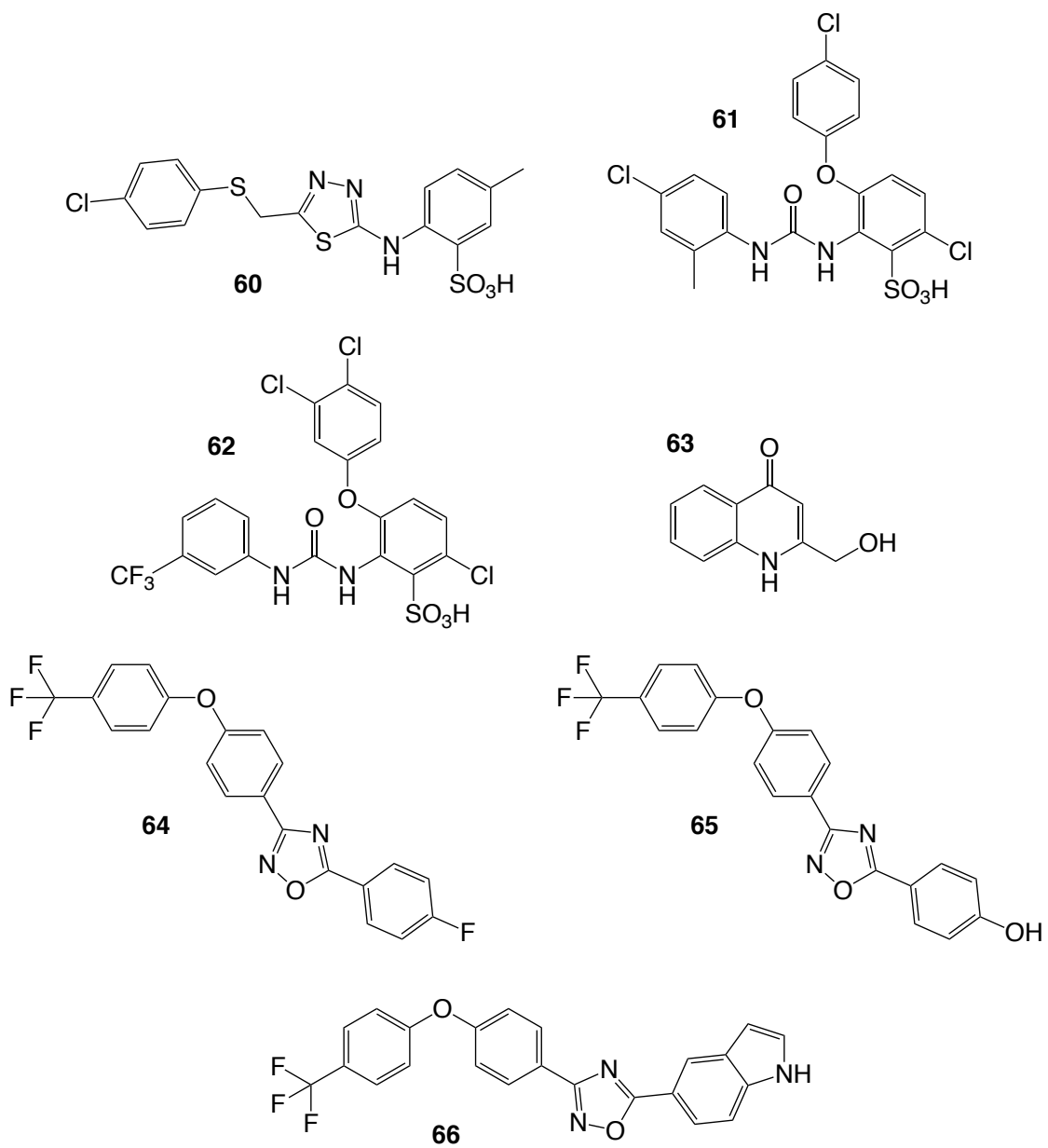


Figure 1.30: Structures of transpeptidase inhibitors identified through *in silico* screening methods.

While many of the noncovalent PBP inhibitors mentioned here are in need of additional testing and medicinal chemistry to achieve standards of potency and selectivity required of a preclinical lead, these studies suggest that novel classes of PBP-targeted drugs may provide a workable route toward antimicrobials that 1) circumvent the changes associated with resistance that affect β -lactam binding, and 2) proactively avoid the potential issue of ESBL acquisition by *N. gonorrhoeae*. Moreover, because there are so few examples of successful compounds from which to draw, this is an area of need in antigenococcal therapeutic discovery.

Table 1.13: Activity of noncovalent inhibitors against bacterial transpeptidases. ^aHalf-maximal inhibitory concentration (IC₅₀) unless otherwise noted. ^bPercent inhibition at 1 mM. ^cThermodynamic equilibrium constant (K_i)

Compound	Species	Target	Activity ^a	Reference
52	<i>S. aureus</i>	PBP2a	24 μM	624
53	<i>S. aureus</i>	PBP2a	13 μM	624
54	<i>E. coli</i>	PBP1b	28.6 μM	626
	<i>E. coli</i>	PBP3	62.5 μM	
	<i>E. coli</i>	PBP5	6.3 μM	
	<i>E. faecium</i>	PBP5	21.6 μM	
	<i>Streptomyces spp.</i>	R61 DD-peptidase	26.8 μM	
55	<i>S. aureus</i>	PBP2a	80 μM	628
	<i>E. faecium</i>	PBP5	0% ^b	
	<i>S. pneumoniae</i>	PBP1b	60% ^b	
56	<i>S. aureus</i>	PBP2a	210 μM	627
	<i>E. faecium</i>	PBP5	32% ^b	
	<i>S. pneumoniae</i> 5204	PBP2x	59% ^b	
57	<i>N. gonorrhoeae</i>	PBP2	50 μM	621
58	<i>N. gonorrhoeae</i>	PBP2	56 μM	621
59	<i>S. aureus</i>	PBP2a	18.4 μM	629
60	<i>S. pneumoniae</i> 5204	PBP2x	219 μM	630
61	<i>S. pneumoniae</i> 5204	PBP2x	71 μM	630
	<i>S. pneumoniae</i> R6	PBP2x	336 μM	
	<i>S. pneumoniae</i>	PBP1b	259 μM	
	<i>S. pneumoniae</i> 5204	PBP2x	72 μM	
62	<i>S. pneumoniae</i> R6	PBP2x	255 μM	630
	<i>S. pneumoniae</i>	PBP1b	88 μM	
	<i>E. coli</i>	PBP1a/1b	27 μM ^c	
63	<i>E. coli</i>	PBP2	26 μM ^c	631
	<i>E. coli</i>	PBP3	27 μM ^c	
	<i>E. coli</i>	PBP4	4.8 μM ^c	
	<i>E. coli</i>	PBP5/6	220 μM ^c	
	<i>E. coli</i>	PBP2a	8 μg/mL	
65	<i>S. aureus</i>	PBP2a	8 μg/mL	632

1.6. Goal and Significance

With the emergence and spread of multi-drug resistant strains, the therapeutic landscape for *Neisseria gonorrhoeae* has become increasingly barren. The bacterium has demonstrated a strong proclivity for development of resistance against each FDA-approved therapy tried in the last 90 years. Furthermore, any existing FDA-approved alternatives suffer from some weakness, and other experimental therapies that show promise are still in the early stages of their development. For this reason, continued efforts to identify antigonococcal compounds using all avenues of drug discovery (e.g., repurposing of FDA-approved therapies, *in silico* tools, physical screening, etc.) are necessary to ensure a future in which disease caused by this pathogen is still treatable.

Much work has been done in our laboratory regarding the structural mechanisms of PBP2-mediated β -lactam resistance in *Neisseria gonorrhoeae*. In the past several years, our efforts have been focused on determining how specific amino acid changes in mosaic PBP2, including that expressed by strain H041, affect its structure, function, and ability to bind various β -lactams. In this project, the focus was reframed toward the ligand to examine what features are shared among active compounds with the goal of designing new compounds, or unearthing existing ones, capable of inhibiting PBP2 variants from both β -lactam-susceptible and -resistant strains. Here, we report data from three studies. The first is an analysis of the structure-activity relationships for inhibition of PBP2^{H041} by cephalosporins, as well as for antimicrobial activity against the strain itself. The second applies the knowledge gained from the structure-activity relationships to discover several novel scaffolds capable of inhibiting PBP2. Finally, the third explores the chemical space surrounding one of the identified scaffolds using medicinal and synthetic chemistry in order to improve potency and begin the process of hit-to-lead optimization.

CHAPTER 2: Materials & Methods

2.1. Materials

Fifth Generation cephalosporins were kindly provided by Basilea (ceftobiprole), Merck (ceftolozane), and Allergan (ceftaroline). Other cephalosporins were purchased from TCI America Inc, Sigma Aldrich Inc, and Alfa Aesar Inc, and Bocillin-FL was purchased from ThermoFisher Scientific Inc. Compounds coded NSC in the text were kindly provided by the Developmental Therapeutics Program at NCI from their Open Chemicals Repository. Compounds coded Z/EN, CB, and STK/STL were purchased from Enamine Ltd, ChemBridge Corp, and Vitas-M Chemicals Ltd, respectively.

2.2. Biochemical and microbiological methods

2.2.a. Cloning, expression, and purification of truncated *N. gonorrhoeae* PBP2 constructs

Truncated constructs comprising only the transpeptidase domain of PBP2 (tPBP2) were generated as previously described.³⁸⁹ The expression construct was transformed into *Escherichia coli* BL21 (DE3) cells; 2 L of cell culture were grown at 37 °C, and protein expression was induced by addition of 0.3 mM isopropyl β -D-thiogalactoside, followed by overnight incubation at 20 °C. Cells were harvested by centrifugation, lysed in 20 mM Tris-HCl (pH 8.0), 500 mM NaCl, and 10% glycerol (TNG), and the MBP-PBP2 fusion protein was purified on a 5 mL HisTrap FF Ni²⁺ affinity column (GE Healthcare, Piscataway, NJ). The fusion protein was pooled, mixed with His₆-tagged TEV protease at a molar ratio of 50:1, and dialyzed overnight at 4 °C against TNG to allow cleavage of the fusion protein and to remove imidazole. The resulting digest was then passed over a 5 mL HisTrap HP column equilibrated with TNG. Purified tPBP2 did not elute in the flow-through but instead was eluted by a TNG/15 mM imidazole step gradient. Uncleaved fusion protein, His₆-TEV, and His₆-maltose-binding protein remained bound to the column and were eluted with a TNG/250 mM imidazole wash step. The purified protein was pooled, dialyzed into 20 mM Tris (pH 8.0), 500 mM NaCl, and 10% glycerol, and concentrated by ultrafiltration.

2.2.b. Site directed mutagenesis of tPBP2^{H041}

A K361E mutation was introduced into tPBP2^{H041} using the QuikChange Lightning Kit (Agilent, Santa Clara, CA). The forward 5'-CATTATGCAAGAATCTTCCAACGTCG-3' and reverse 5'-CCGCGCACATCCAAAGTA-3' primers were used to amplify the plasmid DNA containing *penA41* as per the manufacturer's recommended protocol. The amplified PCR product was treated with Dpn1 enzyme and then used to transform in *E. coli* BL21 (DE3) cells. The mutant was confirmed by sequencing.

2.2.c. Sodium dodecyl sulfate polyacrylamide gel electrophoresis (SDS-PAGE)-based binding assay for Bocillin-FL

The rate of acylation of PBP2 by the fluorescent Bocillin-FL⁶³⁸ was determined by time-course kinetics experiments in which 1 μ M tPBP2 was incubated with Bocillin-FL under pseudo-first order conditions. Aliquots were removed at specified time points between 2 seconds and 1 hour, and the reaction quenched by 4X SDS-PAGE sample buffer. Samples were heated at 95°C for 2 minutes, and acylated protein was separated from free Bocillin-FL using 12% Mini-Protean TGX SDS-PAGE gels. Gels were scanned using a Kodak EDAS 290 UV imaging system, followed by staining with Coomassie R-250 to confirm equal loading. Bocillin-FL-bound PBP2 was quantified by densitometry using ImageJ.⁶³⁹ Data were normalized to the maximum fluorescence intensity and fit to a one-phase association curve to determine pseudo-first order rate constants, which were plotted against Bocillin-FL concentration and fit to a linear regression to give the second-order acylation rate as the slope.

2.2.d. SDS-PAGE-based competition binding assay for β -lactams

Acylation rates for β -lactam compounds were derived by determining the concentration of β -lactam required to inhibit half the binding of a known amount of Bocillin-FL. tPBP2 was co-incubated with a specified concentration of Bocillin-FL (10 or 100 μ M) and increasing concentrations (1 μ M to 1 mM) of β -lactam for 1 hour. Samples were

denatured, separated by SDS-PAGE, and imaged as above. Data were normalized to the maximum fluorescence intensity and fit to a four-parameter inhibitor-response curve to determine half-maximal inhibitory concentrations (IC_{50}), and the acylation rates of the β -lactams were determined by the following relationship:

$$k_2/K_s(BOC) \cdot [BOC] = k_2/K_s(\beta L) \cdot IC_{50}(\beta L)$$

2.2.e. SDS-PAGE-based binding assay for noncovalent inhibitors

Potency of noncovalent inhibitors was measured by determining the concentration of compound required to inhibit half the binding of a known amount of Bocillin-FL. PBP was incubated with 1 μ M to 1 mM test compound for one hour, followed by the addition of 1 μ M Bocillin-FL. The reaction was allowed to proceed for a time period corresponding to the linear phase of Bocillin-FL binding for the PBP used. Samples were denatured, separated by SDS-PAGE, and imaged as above. Data were normalized to the maximum fluorescence intensity to give fractional residual activity. For IC_{50} determinations, data were then fit to a four-parameter inhibitor-response curve.

2.2.f. Crystallization of tPBP2^{H041} in complex with cefoperazone

tPBP2^{H041} was concentrated to 13 mg/mL, and crystallization conditions were set using a Gryphon liquid dispensing system (Art Robbins, Sunnyvale, CA, USA) in a 96-well sitting drop format in which 200 nL protein solution was mixed with 200 nL well solution. Crystals were obtained at 18°C over wells containing 37-40% PEG 600, buffered with 0.1 M CHES at pH 9.1-9.3. Crystals appeared after 3-4 days and exhibited a plate-like morphology.

To generate an acylated complex of tPBP2^{H041}, crystals were soaked in a 60 mM solution of cefoperazone for 30 minutes at room temperature, followed by flash freezing without adding cryo-protectant. Diffraction data were collected at a wavelength of 1.00 Å

on a MX300-HS detector at the SER-CAT 22-BM beamline at the Advanced Photon Source in Argonne, IL, USA. 360° of data were collected in 1° oscillations, with an exposure time of 2 s/frame and a crystal-to-plate distance of 220 mm, and were processed using HKL2000.⁶⁴⁰ The structure was solved by refinement of the tPBP2^{H041} structure. Cefoperazone was modeled using the |Fo|-|Fc| difference electron density map, followed by iterative cycles of model building and refinement using the graphics programs O⁶⁴¹ or COOT⁶⁴², and REFMAC.⁶⁴³ The stereochemistry of models was analyzed with PROCHECK.⁶⁴⁴

2.2.g. Disc diffusion against *Neisseria gonorrhoeae*

N. gonorrhoeae (FA19 and H041) was streaked onto gonococcal medium base (GCB) agar plates and incubated overnight at 37°C under 5% CO₂. The next day, *N. gonorrhoeae* growth was collected from the overnight plates, resuspended in GCB+ (composed of GCB broth, supplements I and II, 20 mM NaHCO₃, and 10 mM MgCl₂), and diluted to a final OD₆₀₀ of 0.18. Aliquots of dilute gonococcal cells (200 µL, ~50,000 CFU) were added to 3 mL GCB top agar (GCB broth + 0.7% agar), and the mixtures were gently poured onto new GCB plates and allowed to set. For each compound tested, 5 µL of a 2 mg/mL solution in DMSO (10 µg total) was pipetted onto a disc, and each disc was placed on a prepared plate. Plates were then incubated at 37°C under 5% CO₂ for 24 hours, at which time the diameter of the zone of inhibition was measured. These experiments were conducted in the laboratory of Robert Nicholas, PhD, at the University of North Carolina Chapel Hill.

2.2.h. Minimum inhibitory concentrations against *Neisseria gonorrhoeae*

Neisseria gonorrhoeae H041 was passaged on GCB plates and resuspended at an OD₆₀₀ of 0.18. GCB plates containing 2-fold changes in concentrations of test compound were poured on the day of the experiment, and agar dilution minimum inhibitory concentrations (MIC) were determined by the spot method. Briefly, aliquots (~50,000

CFU) of each clone were spotted onto the antimicrobial-containing plates, and the plates were incubated overnight. The next morning, the plates were examined, and the MIC was reported as the lowest concentration of antimicrobial suppressing growth (growth is defined as > 5 colonies growing in the spot of inoculation). MIC determinations were repeated a minimum of two times. These experiments were conducted in the laboratory of Robert Nicholas, PhD, at the University of North Carolina Chapel Hill.

2.3. Computational methods

2.3.a. Pharmacophore-constrained docking of β -lactams against tPBP2 variants

Structures used in pharmacophore-constrained docking experiments can be accessed through the Protein Databank. PDB accession codes: 6P53 (tPBP2^{WT} apoenzyme), 6P54 (tPBP2^{WT}-ceftriaxone), 6VBC (tPBP2^{H041} apoenzyme), 6VBD (tPBP2^{H041}-ceftriaxone). tPBP2 coordinates were prepared by protonation at pH 7.4, explicit solvation with water, and minimization under the AMBER12 forcefield.⁶⁴⁵ The minimized structure was then allowed to relax by with a short (1,000 ps) molecular dynamics simulation at 2 fs resolution using the Nosé-Poincaré-Andersen (NPA) algorithm.⁶⁴⁶ A pharmacophore model was then generated to constrain the β -lactam ring to the area surrounding Ser310 of PBP2, including the oxyanion hole formed by Ser310 and Thr500. Selected β -lactams were then docked to the receptor using an induced-fit protocol in which compounds were first placed in the active site using the pharmacophore and scored using the London dG algorithm. The top 50 scored conformers were then refined against the AMBER12 forcefield with flexible rotation of receptor side chains and rescored using GBVI/WSA dG algorithm. All rescored conformers were retained for analysis by energy score amplitude, as well as protein-ligand interaction fingerprint (PLIF). All calculation used Molecular Operating Environment 2018.01.

2.3.b. Quantitative-structure activity relationship (QSAR) for cephalosporins against *N. gonorrhoeae* H041

Partial least squares (PLS) analysis was used to examine the relationship between activity measurements, reported as $\log(k_2/K_s)$, and descriptor variables, including structural and molecular properties of the cephalosporins tested. The generated PLS model was validated using the square of the correlation coefficient obtained by the leave-one-out cross-validation method. The resulting model was also validated using *y*-randomization, as well as application to a small test set of null cephalosporins. All analyses, including descriptor calculations and PLS model generation, were conducted in MOE 2018.01.

To examine the relationship between MICs and molecular descriptors, a classification QSAR model was developed, with an activity cutoff set at median MIC ≤ 4 $\mu\text{g/mL}$. Cefdinir consistently modeled as an outlier, as it exhibits a low rate of PBP2 acylation and yet has high antimicrobial potency, and likely has a different mechanism of action (*e.g.*, rapid PBP1 acylation). For this reason, it was excluded from the model. The generated classification model was validated using the leave-one-out cross-validation method, as well as by *y*-randomization. All analyses, including descriptor calculations and model generation, were conducted in MOE 2018.01.

2.3.c. Homology modeling and rigid alignment of class B PBPs

To generate homology models of class B penicillin-binding proteins, amino acid sequences were obtained from the NCBI Protein database and used as templates in the SWISS-MODEL server.⁶⁴⁷ Template searching and target-template sequence alignment were then performed by BLAST and HHblits analysis of the PDB repository to identify structural models of highly similarity. The best templates were selected according to sequence identity, quality of the available structural data, and the Global Model Quality Estimation (GMQE). Models were exported to the Structural Analysis and Verification

Server (SAVES) v5.0, and their overall stereochemical quality was checked in PROCHECK. Crystal structures of additional class B PBPs were accessed (PDB accession codes can be found in **Table 3.6**), and all models were subjected to sequence alignment and rigid-body superposition to examine conservation of residues.

2.3.d. tPBP2-ceftriaxone structure-guided docking of JEK-42 and JMT-1 to tPBP2 variants

Using tPBP2-ceftriaxone complex coordinates (tPBP2^{WT}-ceftriaxone: 6P54, tPBP2^{H041}-ceftriaxone: 6VBD), pharmacophore constraints were placed around the cephem C4 carboxylate (CO₂⁻ centroid, radius 2.0 Å) and the acyl carbonyl oxygen (hydrogen bond acceptor, radius 1.0 Å). The receptor was prepared for docking by the deletion of ceftriaxone from the active site and subsequent protonation at pH 7.4. Prototype PBP2 inhibitors (amide **JEK-42** and sulfonamide **JMT-1**) were then docked to the receptor using an induced-fit protocol in which ligands were first placed in the active site using the pharmacophore and scored using the London dG algorithm. The top 10 scored conformers were then refined against the AMBER12 forcefield with flexible rotation of receptor side chains and rescored using the GBVI/WSA dG algorithm, and the top rescored conformer was retained. The tPBP2-JMT complex was prepared for molecular dynamics by explicit solvation with water and minimization under AMBER12 forcefield. The minimized structure was then allowed to equilibrate with a short (100 ps) molecular dynamics simulation (NPA algorithm, time step = 2 fs) with constraints placed on bond length. After equilibration, the solvated complex underwent 5 ns of molecular dynamics without constraints, and the overall structure of the complex, energies of ligand-receptor interaction, and trajectories of ligands were analyzed. These experiments were conducted in MOE 2018.01.

2.3.e. Virtual screening of fragments against a three-point pharmacophore

The base structures of **JEK-42** and **JMT-1**, *N*-acetylanthranilic acid and *N*-(methylsulfonyl)anthranilic acid, were flexibly aligned to the bicyclic penam, carbapenem, and cephem systems using a stochastic conformational search. From the alignment, a consensus pharmacophore was generated using a 100% threshold and 1.0 Å tolerance, yielding a model with three features: anionic (radius = 0.7 Å), hydrophobic/aromatic (radius = 0.9 Å), and hydrogen bond accepting (radius = 1.0 Å). This model was used to screen a custom ZINC library of 790,417 molecular fragments, defined as having a molecular weight < 250, for matching structures. This experiment was conducted in MOE 2018.01.

2.3.f. Validation of in silico methods for *Pseudomonas aeruginosa* PBP3

β-lactam antibiotic structures were uploaded to the Database of Useful Decoys: Enhanced (DUD-E) server,⁶⁴⁸ and physicochemically matched decoy structural files were generated. All structures, true ligands and decoys, were combined into a single file for docking. The transpeptidase domain of PBP3 (PDB accession code: 3PBN) was prepared for docking using by protonation at pH 7.4, addition of partial charges, and the identification of potential binding sites by the calculation of alpha spheres. True ligands and decoys were then docked flexibly to the receptor using the rigid-receptor DOCK6.5 protocol with 1,000 orientations.⁶⁴⁹ The compounds were scored against the AMBER forcefield and ranked. Receiver operator and enrichment curves were generated from the docking scores and ranks, and an area under the curve (AUC) was calculated for each.

Using MOE 2018.01, coordinates for the transpeptidase domain of PBP3 prepared by removal of crystallographic waters and ions, correction of structural incompleteness, addition of partial charges, and protonation at physiologic pH. The structure was then energy minimized and allowed to relax with a short (500 ps) molecular dynamics simulation at 2 fs resolution using the NPA algorithm. The active site was defined by the cluster of alpha spheres containing the active serine residue (Ser294), and the database

of β -lactams and decoys was then docked flexibly to the defined site using triangle matching. Top conformers were refined against the AMBER12 forcefield with flexible rotation of receptor side chains, and conformers were ranked via GBVI/WSA dG scoring. Receiver operator and enrichment curves were generated from the docking scores and ranks, and an AUC was calculated for each.

2.3.g. *In silico* virtual screen against *Pseudomonas aeruginosa* PBP3

A custom library of 100,000 ligands derived from the ZINC database⁶⁵⁰ was docked to previously prepared *P. aeruginosa* PBP3 coordinates using the rigid-receptor DOCK6.5 protocol above. Ranked ligands with docking scores two standard deviations below the mean of all docked compounds ($Z < -2$) were selected for consensus analysis via an induced-fit docking protocol in MOE2018.01 as done for the database of β -lactams and decoys above. Molecules were scored according to their overall binding by both protocols (*i.e.*, sum of ranks), as well as agreement between protocols (*i.e.*, difference between ranks).

2.4. Synthetic methods

2.4.a. Synthesis of 5-fluoro-2-(4'-methyl-[1,1'-biphenyl]-4-carboxamido)benzoic acid (JEK-42)

To a solution of 4'-methyl-[1,1'-biphenyl]-4-carboxylic acid (1.0 eq) in DCE were added oxalyl chloride (1.1 eq) and DMF (*cat.*) with stirring. Acyl chloride formation was allowed to proceed for 12 hours at room temperature. Volatiles were removed under reduced pressure to give 4'-methyl-[1,1'-biphenyl]-4-carbonyl chloride, which was used without further workup. A solution of methyl 2-amino-5-fluorobenzoate (1.0 eq) in anhydrous DCM was added, followed by pyridine (1.0 eq) portionwise, and the reaction was allowed to proceed at room temperature for 8 hours. After completion, as determined by TLC, the reaction was acidified to pH 2 with 1 M HCl, and the product was extracted with dichloromethane. The combined organic phases were washed with saturated NaHCO_3 and brine, dried over Na_2SO_4 , and filtered. Solvent was then removed under

reduced pressure, and the crude reaction mixture was purified by trituration using dichloromethane and hexanes.

To a stirred solution of product methyl 5-fluoro-2-(4'-methyl-[1,1'-biphenyl]-4-carboxamido)benzoate in tetrahydrofuran, 1 M aqueous LiOH (2 eq) was added. The reaction was allowed to proceed with stirring at room temperature overnight. Solvent was then evaporated under reduced pressure, and the residue was subsequently diluted with water and acidified to pH 2 using 1 M HCl. The mixture was then extracted using EtOAc, and the combined organic phases were washed with brine, dried over Na₂SO₄, and filtered. Solvent was then removed under reduced pressure to provide 5-fluoro-2-(4'-methyl-[1,1'-biphenyl]-4-carboxamido)benzoic acid as a white solid. The product was purified by normal phase flash chromatography using a dichloromethane / methanol mobile phase. Products needing additional purification were recrystallized from ethyl acetate and hexanes.

2.4.b. General procedure I: Synthesis of 2-(arylsulfonamido)benzoic acids

Arylsulfonyl chloride (1.0 eq) and methyl 2-aminobenzoate (1.0 eq) were dissolved in anhydrous dichloromethane and stirred for 10 minutes, at which time pyridine (1.0 eq) was added dropwise. The reaction was allowed to proceed with stirring at room temperature for 12 h. After completion, as determined by TLC, the reaction was acidified to pH 4 with 1 M HCl, and the product was extracted with dichloromethane. The combined organic phases were washed with brine, dried over Na₂SO₄, and filtered. Solvent was then removed under reduced pressure, and the crude reaction mixture was purified by trituration using dichloromethane and hexanes.

To a stirred solution of product methyl 2-(arylsulfonamido)benzoate in tetrahydrofuran, 1 M aqueous LiOH (2 eq) was added. The reaction was allowed to proceed with stirring at room temperature overnight. Solvent was then evaporated under reduced pressure, and the residue was subsequently diluted with water and acidified to pH 2 using 1 M HCl. The mixture was then extracted using EtOAc, and the combined

organic phases were washed with brine, dried over Na₂SO₄, and filtered. Solvent was then removed under reduced pressure to provide the corresponding 2-(arylsulfonamido)benzoic acid as an off-white solid. The product was purified by normal phase flash chromatography using a dichloromethane / methanol mobile phase. Products needing additional purification were recrystallized from ethyl acetate and hexanes.

2.4.c. General procedure II: Synthesis of N-(2-(1H-tetrazol-5-yl)phenyl)benzenesulfonamides

Arylsulfonyl chloride (1.0 eq) and methyl 2-aminobenzonitrile (1.0 eq) were dissolved in anhydrous dichloromethane and stirred for 10 minutes, at which time pyridine (1.0 eq) was added dropwise. The reaction was allowed to proceed with stirring at room temperature for 12 h. After completion, as determined by TLC, the reaction was acidified to pH 5 with HCl, and the product was extracted with dichloromethane. The combined organic phases were washed with brine, dried over Na₂SO₄, and filtered. Solvent was then removed under reduced pressure, and the crude reaction mixture was purified by trituration using dichloromethane and hexanes.

To a stirred solution of product 2-(arylsulfonamido)benzonitrile (1.0 eq) in DMSO, sodium azide (1.0 eq) and copper(II) sulfate (0.02 eq) were added. The reaction was heated to 150 °C and allowed to proceed with stirring for 1 h. After cooling, the reaction mixture was diluted with water and acidified to pH 2 using 1 M HCl. The mixture was then extracted using EtOAc, and the combined organic phases were washed with brine, dried over Na₂SO₄, and filtered. Solvent was then removed under reduced pressure to provide the corresponding N-(2-(1H-tetrazol-5-yl)phenyl)benzenesulfonamide as an off-white solid. The product was purified by normal phase flash chromatography using a dichloromethane / methanol mobile phase. Products needing additional purification were recrystallized from ethyl acetate and hexanes.

CHAPTER 3: Structure-Activity Relationships of Cephalosporins against Penicillin- and Cephalosporin-Resistant *Neisseria gonorrhoeae* H041

3.1. Introduction

The cephalosporins are a structurally diverse class of antibiotics divided into generations based on their timeline of development, as well as specific medicinal chemical modifications that affect activity and antimicrobial spectrum. While the 3rd generation agents cefixime and ceftriaxone have been the most commonly prescribed cephalosporins for gonorrhea over recent years, few members of this class have been tested against ESC-resistant (ESC^R) strains. This is especially the case for 4th and 5th generation cephalosporins such as ceftaroline and ceftobiprole that have been approved relatively recently. Building structure-activity relationships (SAR) for cephalosporins against their PBP2 target and an ESC^R strain of *N. gonorrhoeae* offers the potential to address ESC^R *N. gonorrhoeae* in two ways: it may reveal existing FDA-approved cephalosporins that exhibit efficacy against such strains, and suggest ways in which the efficacy of specific cephalosporins can be improved by chemical modification.

Here, we report a quantitative structure-activity relationship (QSAR) of 22 cephalosporins for inhibition of PBP2 from H041 and antimicrobial activity against *N. gonorrhoeae*. The data reveal key features of cephalosporins that enhance formation of the precovalent PBP2-cephalosporin complex, as well as those that may independently hinder or enhance antimicrobial activity. The study also reveals that FDA-approved agents cefoperazone (Cefobid, Pfizer), ceftaroline (Teflaro, Allergan), and ceftobiprole (Zevtera, Basilea) acylate mosaic PBP2 at higher rates than ceftriaxone, and that cefoperazone exhibits higher antimicrobial activity against H041. Overall, our data reveal there is considerable potential in adopting and/or adapting these cephalosporins as anti-gonococcal agents to address ESC^R *N. gonorrhoeae*.

3.2. Computational predictions of precovalent cephalosporin-PBP2 interactions

3.2.a. Pharmacophore-constrained docking of cephalosporins against tPBP2^{H041}

In order to identify residues of PBP2 involved in the recognition of cephalosporins in the precovalent complex, cephalosporins were docked to the active site of tPBP2^{H041}. A pharmacophore constraint (shown in **Appendix A**) was used to confine the β -lactam ring system to the area around the Ser310 nucleophile and the oxyanion hole formed by the amide nitrogens of Ser310 and Thr500, and the refined poses for all compounds remained largely within the volume specified. Protein-ligand interaction fingerprints (PLIF) of all poses were generated for each molecule, their interactions with individual residues were analyzed by frequency and type of interaction (**Figure 3.1**), and the predominant interactions were used to generate a consensus pharmacophore (**Figure 3.2**).

For all cephalosporins, S310 and T500 contact the β -lactam carbonyl oxygen with side chain and main chain hydrogen bonding interactions, respectively, while K313 and K497 are predominantly involved in side chain ionic interactions with the cephem C4 carboxylate group. In addition, most of the cephalosporins contact T347, K361, S483, and S545. The C4 carboxylate moiety participates in additional hydrogen bonding interactions with the hydroxyl group of S483, and in most poses, S1 of the cephem dihydrothiazine ring participates in weak hydrogen bonding with the side chain hydroxyl group of T347. Electronegative elements of many of the cephalosporin R₂ groups make side chain and main chain polar contacts with K361, including the thiotriazinone (TTN) moiety of ceftriaxone (**Figure 3.3A**). Finally, the common amide moiety of all R₁ groups makes variable polar contacts within the active site. In some poses, the amide nitrogen participates in hydrogen bonding with S545 and the carbonyl oxygen with N364, while in others, the C7-N bond is rotated such that the carbonyl oxygen interacts with S545. This rotation also affects the position of the R₁ aromatic ring systems of several cephalosporins, leading to two distinct conformational states: one in which the rings reach toward the

hydrophobic pocket formed by Y422 on the α 8- β 2f loop, and one in which they project toward Y544 on the β 5- α 11 loop (**Figure 3.3B**). The aromatic rings do not make substantial formal contacts with the active site in either of these conformations, however.

Closer inspection of the poses reveals two possible binding modes for all cephalosporins examined: a “major pose” is observed for approximately 60% of poses (131/220), and a “minor pose” for 40% (89/220) (**Figure 3.4**). While there appear to be no differences in docked energy scores for the major pose ($-6.39 \pm 0.56 \text{ kcal}\cdot\text{mol}^{-1}$) over the minor pose ($-6.54 \pm 0.79 \text{ kcal}\cdot\text{mol}^{-1}$, $p = 0.17$), compounds with faster acylation rates tend to occupy the minor pose (OR = 0.38, $p = 0.01$). Representative examples of each pose for ceftriaxone and cefoperazone are shown in **Figure 3.5**. In the major pose, the C4 carboxylate of the cephalosporin interacts with O γ of S483, and the β -lactam ring is positioned away from the nucleophile (**Figure 3.5A and C**). In the minor pose, the carboxylate is situated within the hydrogen bonding network created by K313 and S310, bringing the β -lactam ring in closer proximity to S310 (**Figure 3.5B and D**). Interestingly, neither pose overlaps with ceftriaxone observed in the crystal structure of tPBP2^{H041} acylated by this antibiotic¹³⁴ (**Figure 3.6**). Of the two binding modes, the minor pose appears more favorable for initiation of the acylation reaction. The β -lactam carbonyl is well-situated for attack by the O γ of S310 and for subsequent stabilization of the resulting tetrahedral intermediate by the oxyanion hole created by the amides of S310 and T500 (**Figure 3.5B and D**).

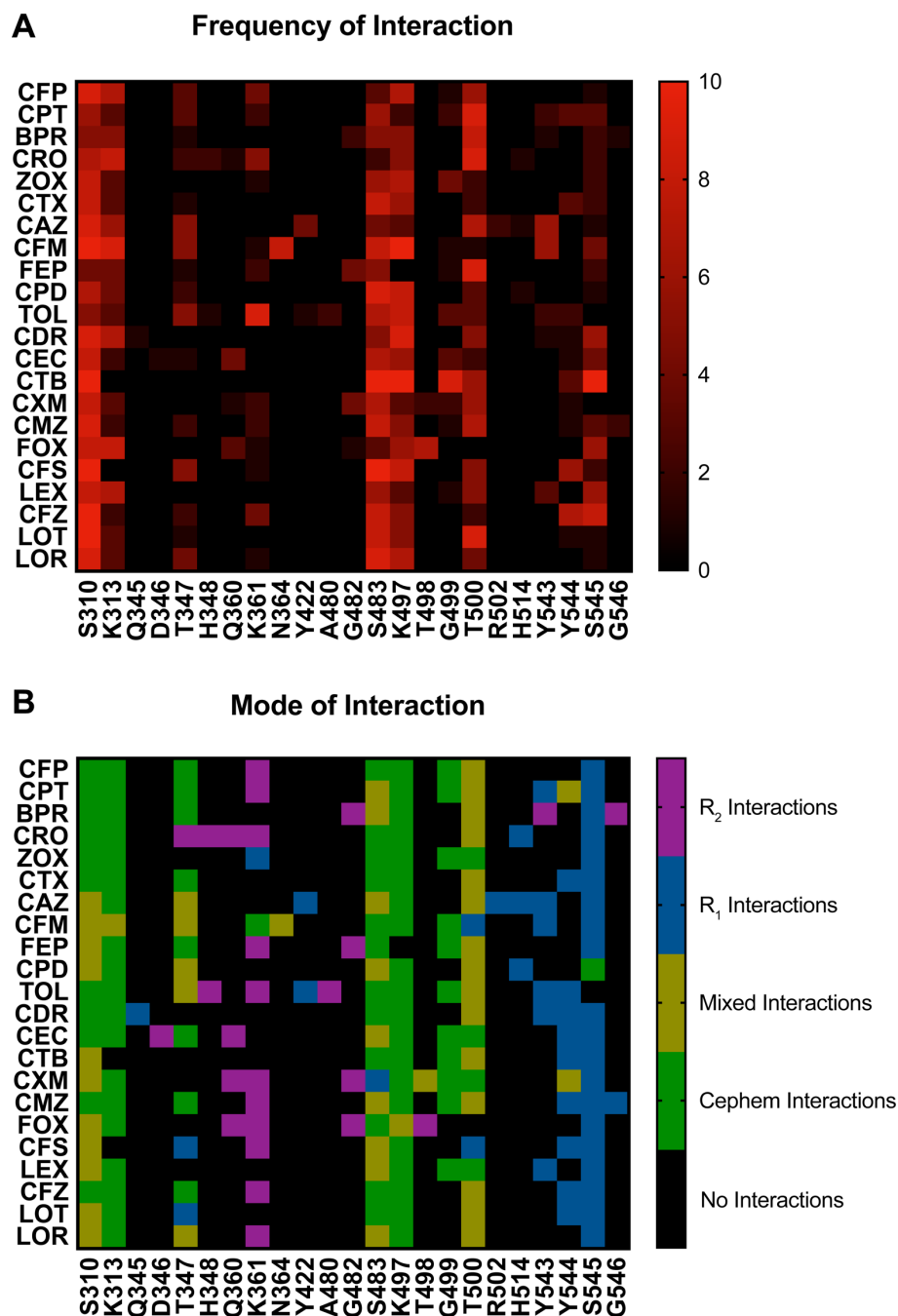


Figure 3.1: Protein-ligand interaction fingerprints (PLIFs) for pharmacophore-constrained induced-fit docking of cephalosporins to $tPBP2^{H041}$. **A.** Heat map of cephalosporin- $tPBP2^{H041}$ interactions colored by number of poses interacting with a given residue. **B.** Heat map of cephalosporin- $tPBP2^{H041}$ interactions, colored by the cephalosporin moiety interacting with a given residue. Key: cefoperazone (CFP), ceftaroline (CPT), ceftobiprole (BPR), ceftriaxone (CRO), ceftizoxime (ZOX), cefotaxime (CTX), ceftazidime (CAZ), cefixime (CFM), cefepime (FEP), cefpodoxime (CPD), ceftolozane (TOL), cefdinir (CDR), cefaclor (CEC), ceftibuten (CTB), cefuroxime (CXM), cefmetazole (CMZ), cefoxitin (FOX), cefsulodin (CFS), cephalixin (LEX), cefazolin (CFZ), cephalothin (LOT), cephaloridine (LOR)

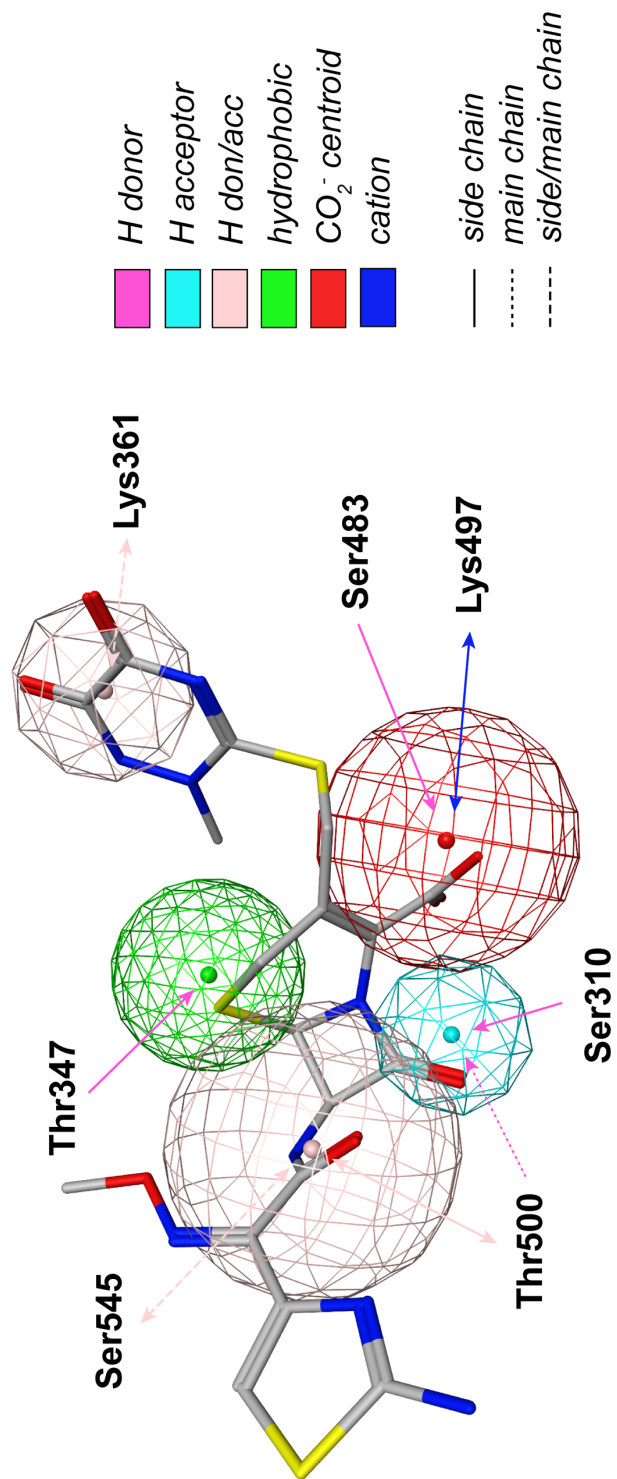


Figure 3.2: Consensus pharmacophore generated from all docked poses of cephalosporins in *tBPB2^{H041}*, set against a representative pose of ceftriaxone. The radius of the sphere indicates the variance of a given feature across all poses.

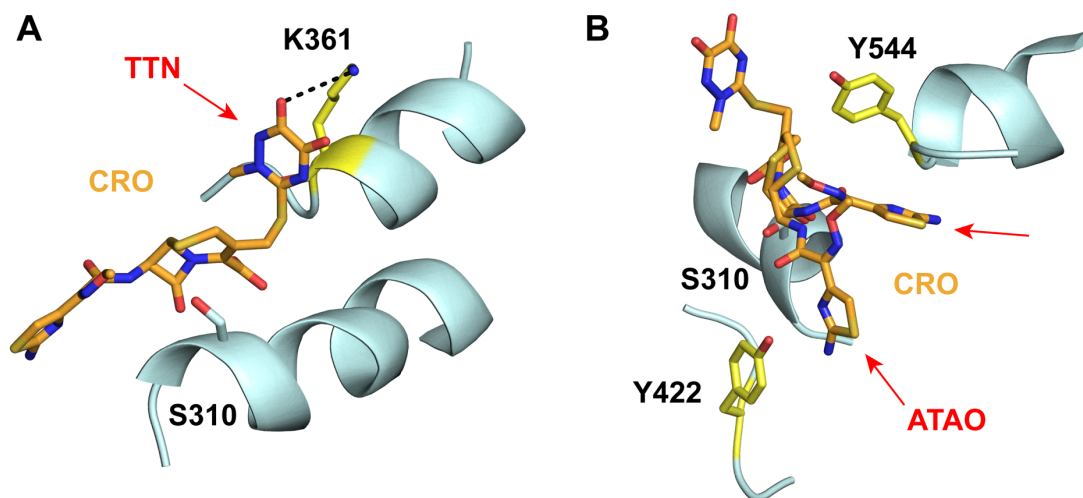


Figure 3.3: Positioning of the R₁ and R₂ groups of ceftriaxone within the active site of tPBP2^{H041}. **A.** The thiotriazinone (TTN) R₂ of ceftriaxone (CRO, orange) makes contact with K361 (yellow) in a majority of docked poses. **B.** The 2-(aminothiazol-4-yl)-2-(alkoxyiminoacetyl) (ATAO) R₁ group of CRO (orange) adopts two conformations in the docked poses, consistent with electron density seen in the published crystal structure of tPBP2^{H041} acylated by ceftriaxone.¹³⁴ In each conformation, R₁ is in close proximity to Y422 or Y544 (both yellow).

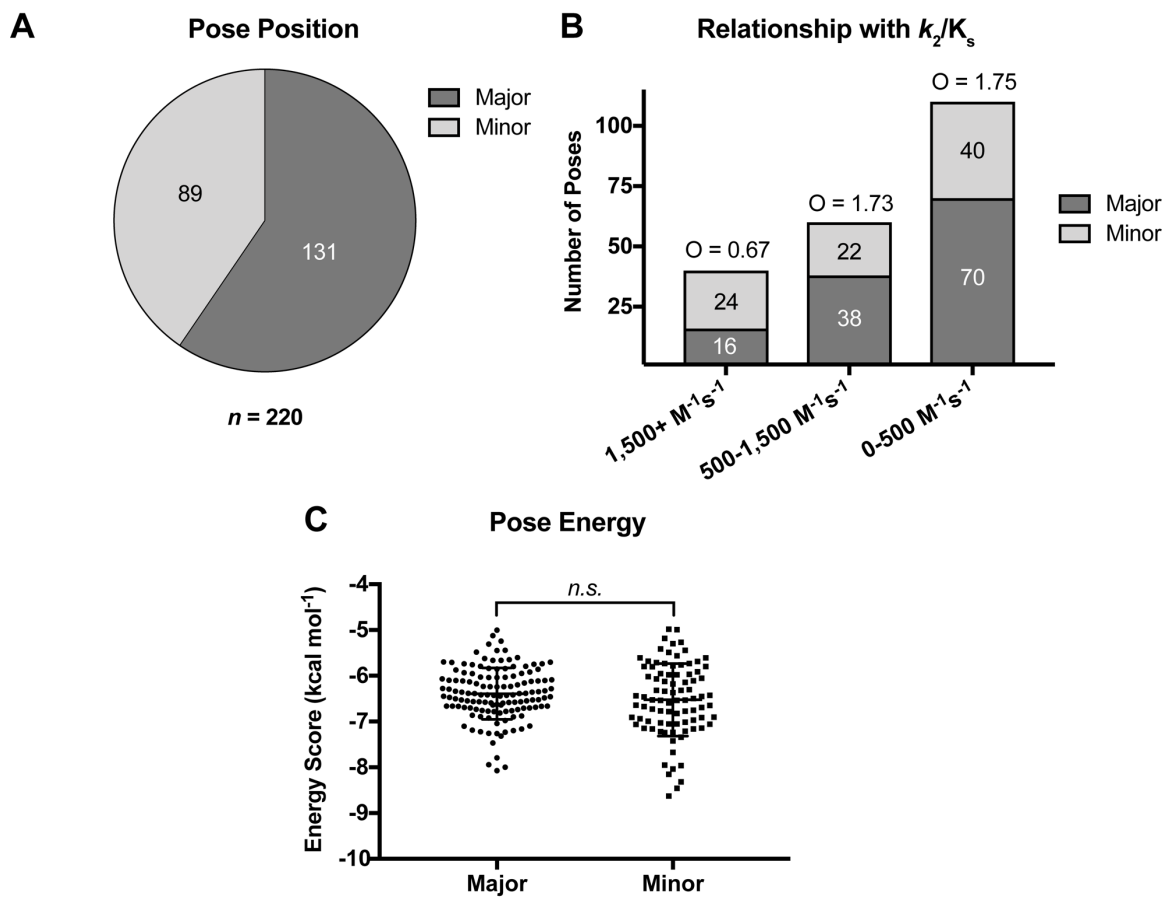


Figure 3.4: Statistical analysis of docked poses, showing two distinct predicted binding modes. **A.** Pie chart showing relative abundance of the two predicted binding modes. **B.** Predicted binding mode abundance stratified by second-order acylation rate constant. **C.** Pooled energy scores for poses in each of the two predicted binding modes. Error bars are standard deviation.

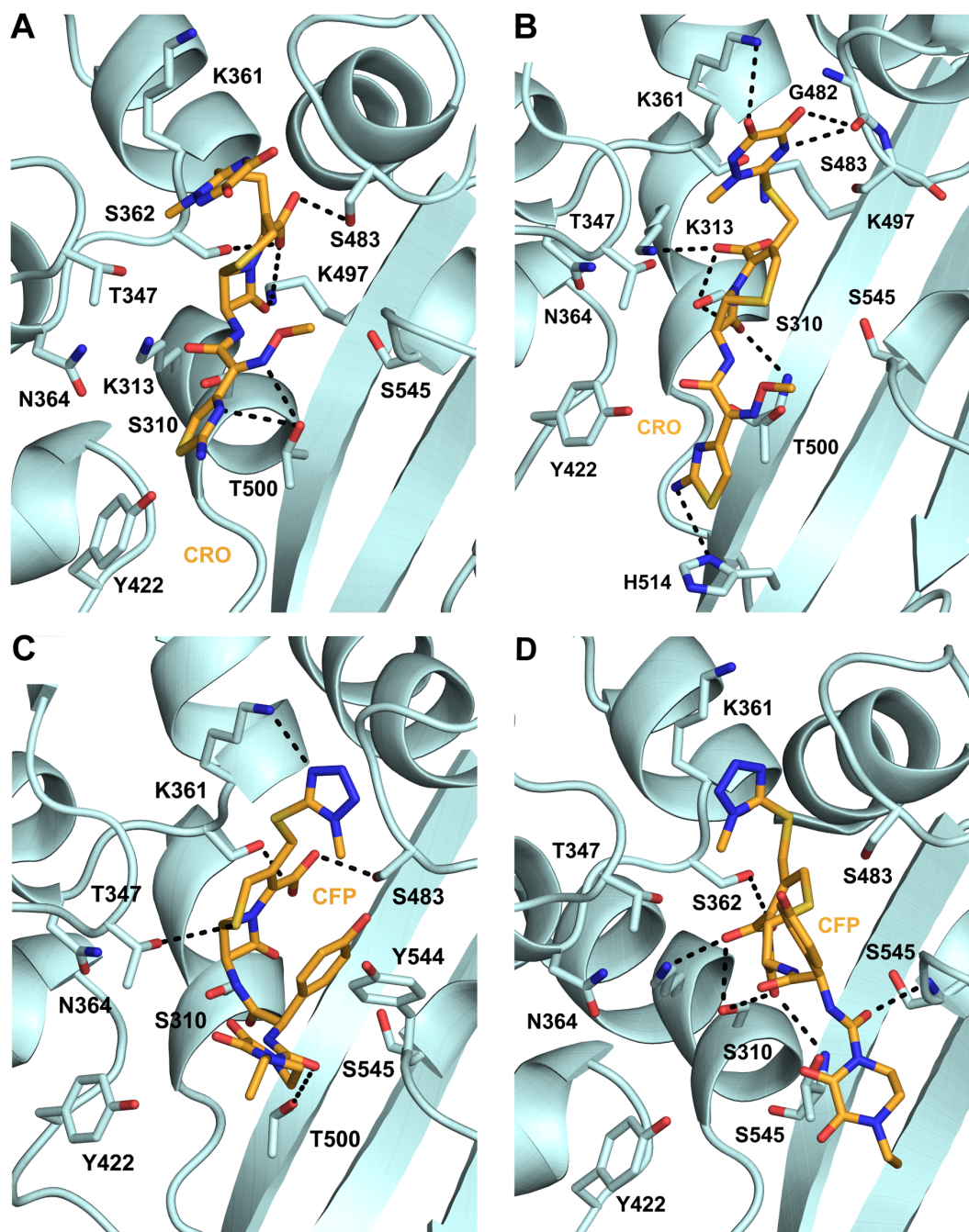


Figure 3.5: Representative poses of ceftriaxone and cefoperazone docked to $tPBP2^{H041}$. **A.** In the major pose predicted by the pharmacophore-constrained docking protocol, the C4 carboxylate of ceftriaxone interacts with S483, its R_2 side chain interacts with K361, and the β -lactam ring system is not optimally oriented for nucleophilic attack by S310. Ceftriaxone (CRO) is shown in orange, and potential hydrogen bonds made by the antibiotic are indicated by dashed lines. **B.** In the minor pose for CRO, the C4 carboxylate interacts with the side chains of K313 and S310, and the β -lactam ring is available for attack by S310. **C.** Cefoperazone (CFP) in the major pose. **D.** CFP in the minor pose.

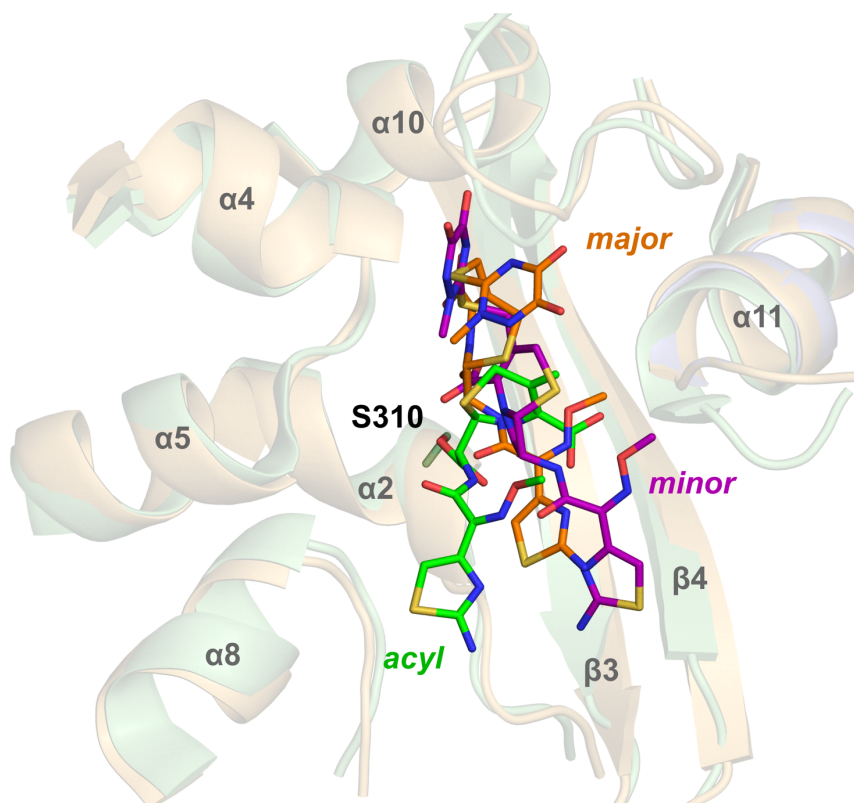


Figure 3.6: Overlay of docked ceftriaxone poses with $tBPB2^{H041}$ -CRO complex structure. Docked precovalent poses of ceftriaxone (major in orange, minor in purple) show marked differences from the acylated structure (green). In the minor pose, in which the β -lactam ring is well-positioned for attack by nucleophilic O_γ of S310, the aromatic thiazole ring has moved further from its final position near $\alpha 8$.

3.2.b. Pharmacophore-constrained docking of cephalosporins against $tBPB2^{WT}$

In order to draw more direct comparisons between $tBPB2^{H041}$ and $tBPB2^{WT}$, the panel of cephalosporins was docked to the active site of $tBPB2^{WT}$ using the same pharmacophore-constrained docking protocol as above. Because T498 rotation has been shown as critical for triggering the acylation reaction, the protocol was run for both *apo* and ceftriaxone-bound (T498-rotated) forms of $tBPB2^{WT}$. PLIF analysis for each ligand docked to *apo*- $tBPB2^{WT}$ is shown in **Figure 3.7**. In this system, the side chains of S310 and T500 contact the β -lactam carbonyl oxygen with side chain hydrogen bonding interactions, and T483 and S362 are predominantly involved in side chain hydrogen bonding interactions with the cephem C4 carboxylate group. In most poses, S1 of the

cephem dihydrothiazine ring participates in weak hydrogen bonding with the side chain hydroxyl group of T347. The common C7 acylamino moiety on R₁ of all cephalosporins forms a hydrogen bond with N364 in some poses, and some R₁ aromatic ring systems make contact with R502 and H514 of the β 3- β 4 loop. Large R₂ groups adopt two distinct conformations in the dataset: one in which electronegative elements make side chain and main chain polar contacts with K361 on α 4 and one in which they are rotated toward residues on α 11. A representative pose is shown in **Figure 3.9A**.

The picture is significantly different for the poses of cephalosporins docked to a structure of tPBP2^{WT} in which the T498 side chain is rotated toward the active site (**Figure 3.8**). First, the C4 carboxylate is in direct contact with the side chains of K497, T498, and T500 in a majority of poses, consistent with the post-covalent crystal structures of cefixime and ceftriaxone in complex with tPBP2^{WT} (**Figure 3.10**). In these poses, the β -lactam ring is in a more favorable position for attack by O_γ of Ser310. Similar to what is seen in docking against the *apo* structure, S1 of the dihydrothiazine ring participates in weak hydrogen bonding interactions with the side chain of T347. The R₁ adopts a position in which the C7 acylamino forms consistent hydrogen bonding interactions with the side chain of N364, and aromatic systems generally come in close enough proximity to Y422 to form H- π or π - π interactions with its side chain. While there is a small subset of poses in which R₂ groups interact with K361, a majority occupy the cleft between the α 10- β 3 loop and α 11, consistent with a crystal structure of tPBP2^{WT}-ceftriaxone in which the leaving group is trapped before departure. A representative pose for this analysis is shown in **Figure 3.9B**. Together, the results of our docking experiments suggest that the initial recognition of the C4 carboxylate is similar for tPBP2^{WT} and tPBP2^{H041}. Subsequent rotation of T498 in tPBP2^{WT} may result in a dramatic change in ligand position preparing it for acylation, a repositioning that does not occur in tPBP2^{H041} due to locking of T498 by a hydrogen bond with S545.

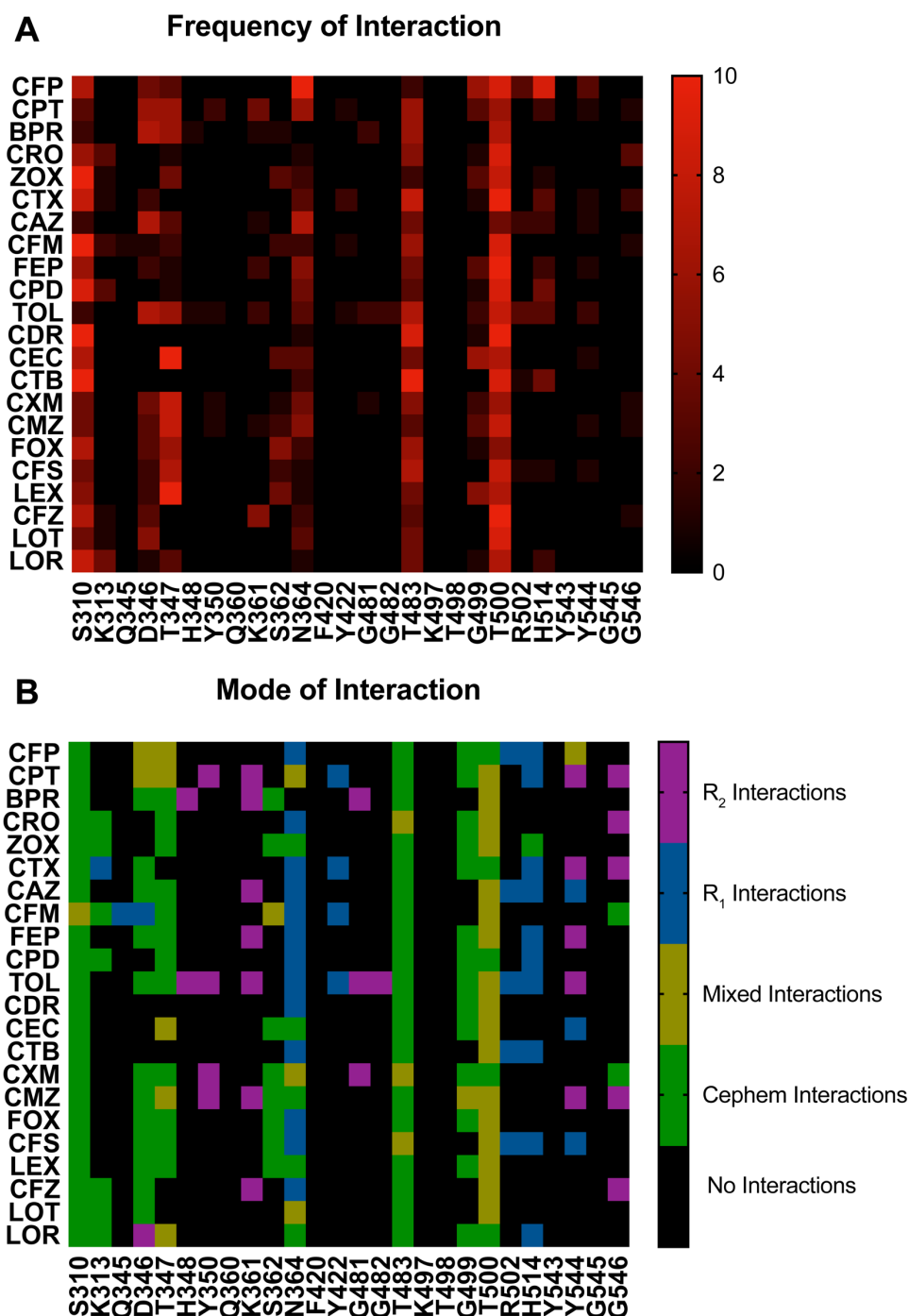


Figure 3.7: Protein-ligand interaction fingerprints (PLIFs) for pharmacophore-constrained induced-fit docking of cephalosporins to apo *tPBP2^{WT}*. **A.** Heat map of cephalosporin-*tPBP2^{WT}* interactions colored by number of poses interacting with a given residue. **B.** Heat map of cephalosporin-*tPBP2^{WT}* interactions, colored by the cephalosporin moiety interacting with a given residue. Key: cefoperazone (CFP), ceftaroline (CPT), ceftobiprole (BPR), ceftriaxone (CRO), ceftizoximine (ZOX), cefotaxime (CTX), ceftazidime (CAZ), cefixime (CFM), cefepime (FEP), cefpodoxime (CPD), ceftolozane (TOL), cefdinir (CDR), cefaclor (CEC), ceftibuten (CTB), cefuroxime (CXM), cefmetazole (CMZ), cefoxitin (FOX), cefsulodin (CFS), cephalixin (LEX), cefazolin (CFZ), cephalothin (LOT), cephaloridine (LOR)

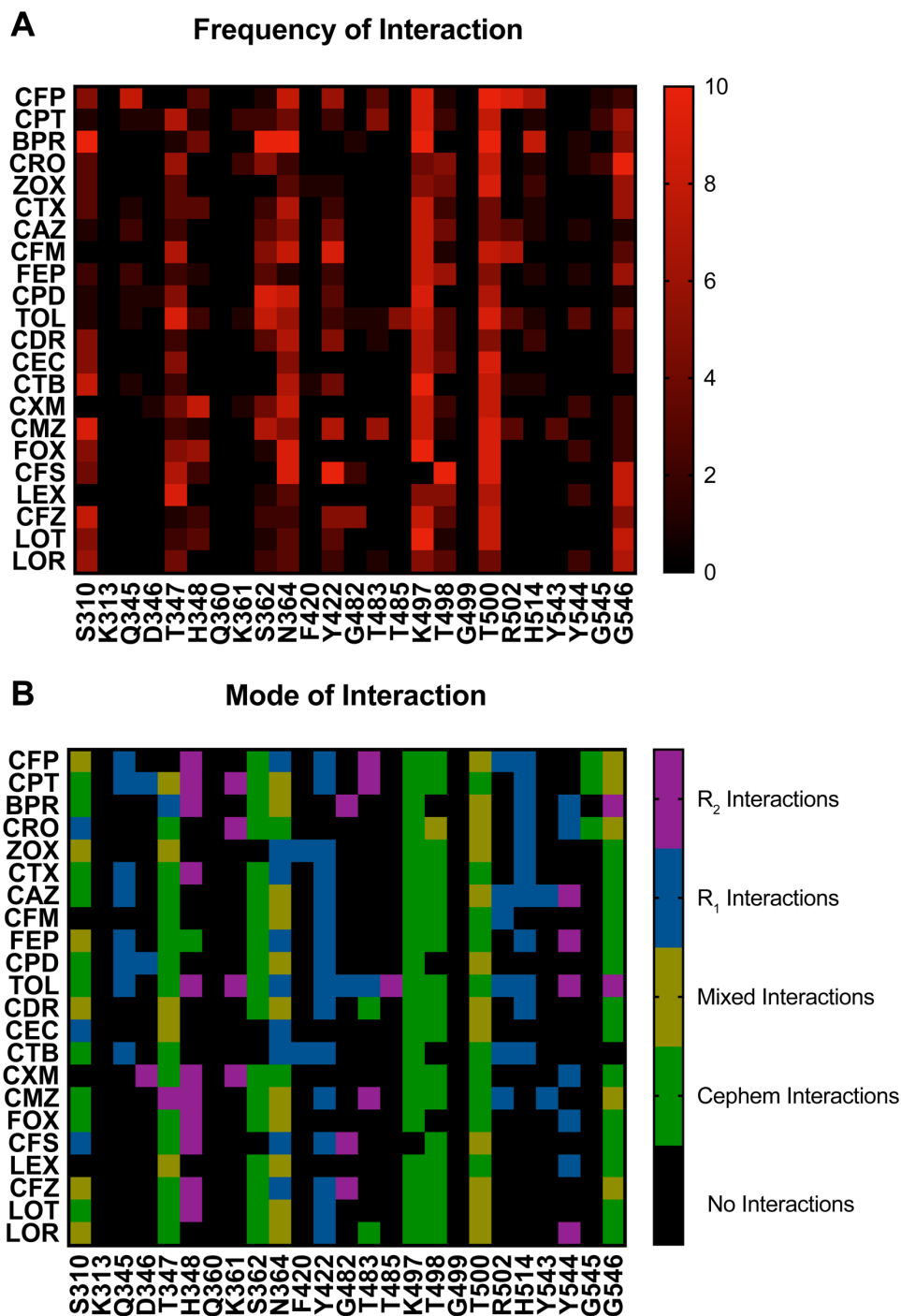


Figure 3.8: Protein-ligand interaction fingerprints (PLIFs) for pharmacophore-constrained induced-fit docking of cephalosporins to $tPBP2^{WT}$ with T498 rotated toward the active site, as is seen in the ceftriaxone-bound structure. **A.** Heat map of cephalosporin- $tPBP2^{WT}$ interactions colored by number of poses interacting with a given residue. **B.** Heat map of cephalosporin- $tPBP2^{WT}$ interactions, colored by the cephalosporin moiety interacting with a given residue. Key: cefoperazone (CFP), ceftaroline (CPT), ceftobiprole (BPR), ceftriaxone (CRO), ceftizoximine (ZOX), cefotaxime (CTX), ceftazidime (CAZ), cefixime (CFM), cefepime (FEP), cefpodoxime (CPD), ceftolozane (TOL), cefdinir (CDR), cefaclor (CEC), ceftibuten (CTB), cefuroxime (CXM), cefmetazole (CMZ), cefoxitin (FOX), cefsulodin (CFS), cephalixin (LEX), cefazolin (CFZ), cephalothin (LOT), cephaloridine (LOR)

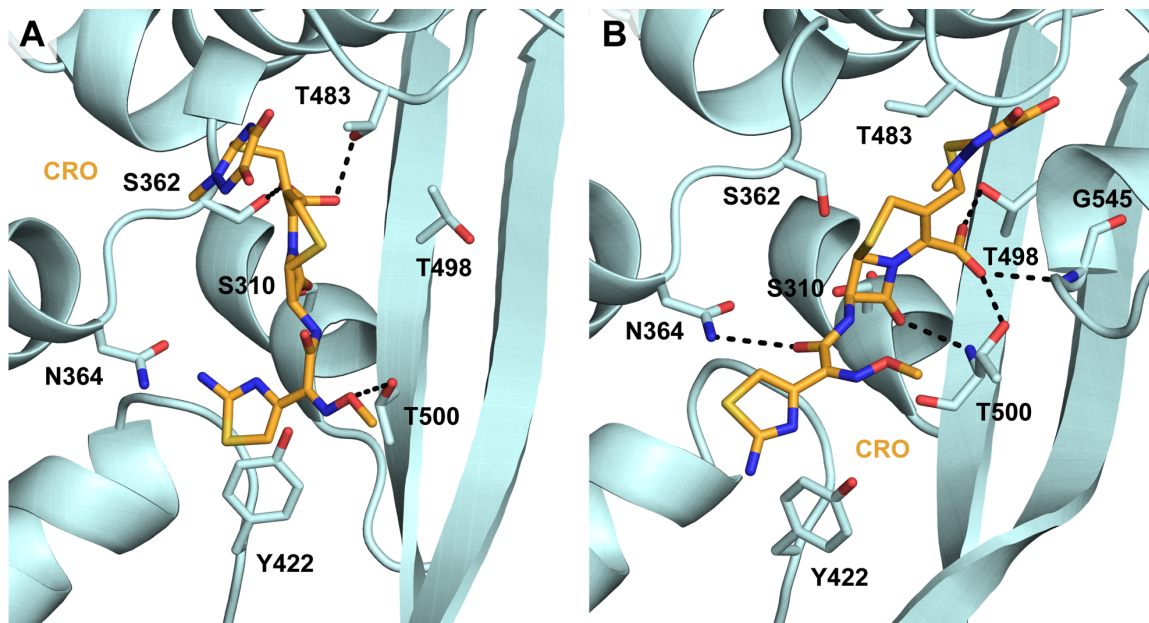


Figure 3.9: Representative poses of ceftriaxone docked to *tPBP2^{WT}*. **A.** When docked to *apo* *tPBP2*, the C4 carboxylate of ceftriaxone interacts with T483, and the β -lactam ring system is not optimally oriented for nucleophilic attack by S310. Ceftriaxone (CRO) is shown in orange, and potential hydrogen bonds made by the antibiotic are indicated by dashed lines. **B.** When docked to *tPBP2^{WT}* in which T498 is rotated toward the active site, the C4 carboxylate interacts with the side chains of T498 and T500, and the β -lactam ring is available for attack by S310.

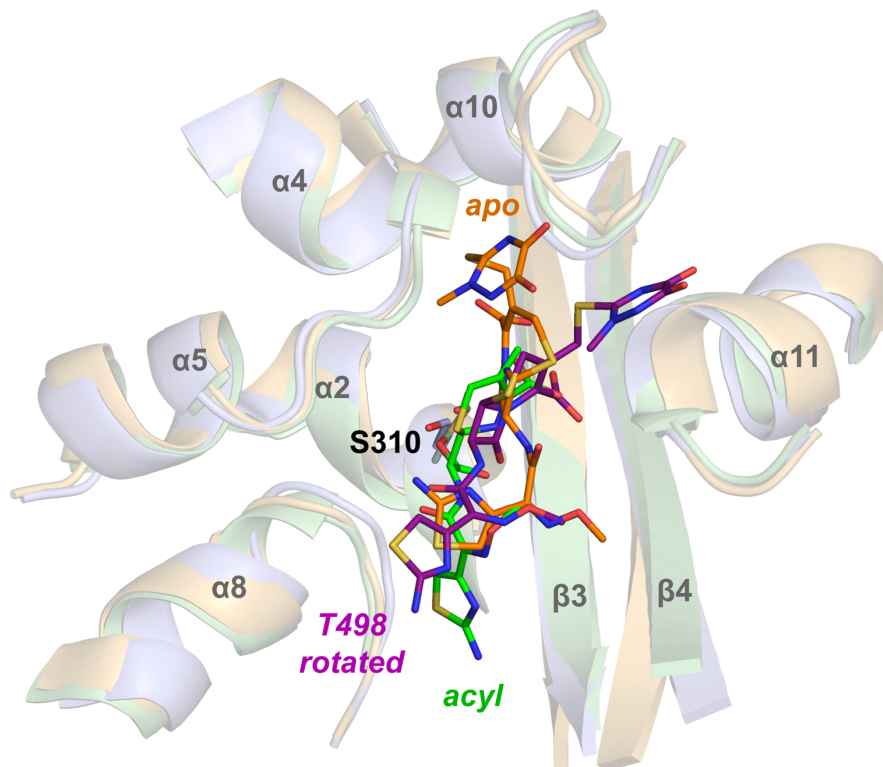


Figure 3.10: Overlay of docked ceftriaxone poses with $tPBP2^{WT}$ -CRO complex structure. Docked pre-covalent poses of ceftriaxone with apo $tPBP2^{WT}$ (orange) show marked differences from the acylated structure (green). When T498 is rotated toward the active site, however, the docked poses (purple) better resemble the post-covalent state.

3.3. Activity data for cephalosporins against *N. gonorrhoeae* strain H041 and its PBP2

3.3.a. Second-order acylation rate constants against $tPBP2^{H041}$

As a prerequisite to determining the second-order rates of acylation for the panel of cephalosporins against $tPBP2^{H041}$, we first measured the second-order acylation rate of Bocillin-FL against $tPBP2^{H041}$ using a time-dependent gel-based assay (**Figure 3.11**). The obtained value, $275 \pm 9 \text{ M}^{-1}\text{s}^{-1}$, is consistent with values previously reported for [^{14}C]penicillin G against PBP2 from H041.³⁸⁴ k_2/K_s was then determined for each cephalosporin with a gel-based competition assay using Bocillin-FL (untransformed inhibition data shown in **Appendix B**). The 22 cephalosporins exhibit a wide range of activities against $tPBP2^{H041}$ (**Table 3.1**), with acylation rates ranging from 0 to over 10,000

$M^{-1}s^{-1}$. Three of the cephalosporins exhibit 2-7 fold faster rates of acylation than third-generation ceftriaxone ($1,710 \pm 320 M^{-1}s^{-1}$). These are the third-generation agent cefoperazone ($11,800 \pm 1,300 M^{-1}s^{-1}$) and the fifth-generation agents ceftaroline ($10,900 \pm 1,700 M^{-1}s^{-1}$) and ceftobiprole ($3,230 \pm 190 M^{-1}s^{-1}$). Ceftizoxime (third-generation) exhibits activity comparable to that of ceftriaxone ($1,000 \pm 210 M^{-1}s^{-1}$), whereas several other third-generation cephalosporins exhibit slightly slower rates of acylation, including cefotaxime ($880 \pm 120 M^{-1}s^{-1}$), ceftazidime ($780 \pm 150 M^{-1}s^{-1}$), cefixime ($720 \pm 60 M^{-1}s^{-1}$), and cefpodoxime ($590 \pm 90 M^{-1}s^{-1}$). The remaining cephalosporins exhibit very slow acylation rates; in fact, for four of these, cephalixin, ceftazolin, cephalothin, and cephaloridine, rates could not be measured.

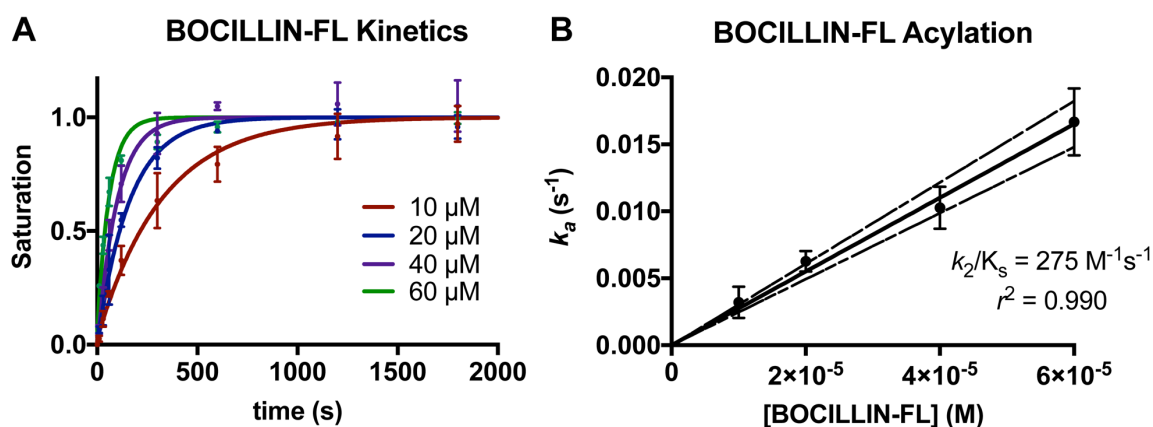
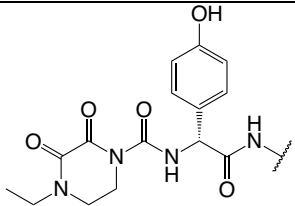
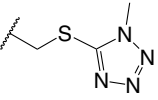
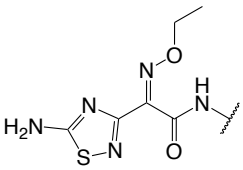
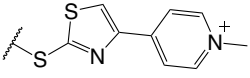
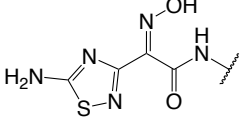
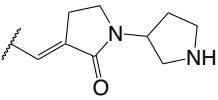
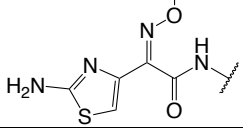
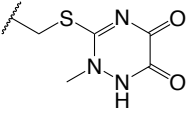
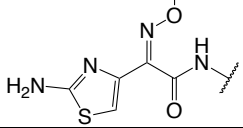
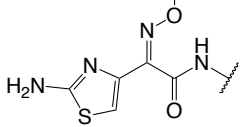
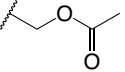
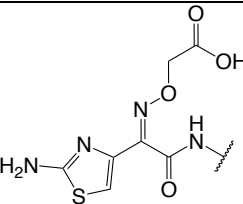
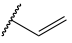
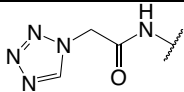
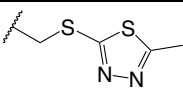
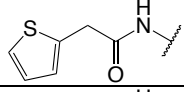
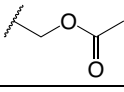
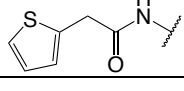
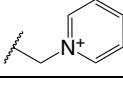


Figure 3.11: Second-order rate of acylation of Bocillin-FL against $tPBP2^{H041}$. **A.** Time-dependent acylation of $tPBP2^{H041}$ at various Bocillin-FL concentrations. Each curve was used to derive the pseudo first-order rate constant, k_a . **B.** Plot of k_a against the concentration of Bocillin-FL, where the slope is the second order acylation rate constant (k_2/K_s). A minimum of three kinetics experiments were completed for each concentration. Error bars are standard deviation.

Table 3.1: Second-order acylation rates and minimum inhibitory concentrations for the selected panel of cephalosporins. ^aThe acylation rate constant for each cephalosporin was derived from kinetic measurements of the formation of the acyl-enzyme complex, as described in Chapter 2. The rates were determined by a competition assay with Bocillin-FL. Values were derived from a minimum of three separate determinations. Error is expressed as standard deviation. ^bThe minimum inhibitory concentration (MIC) for each cephalosporin was determined using an agar dilution protocol, as described in Chapter 2. Values were derived from a minimum of two separate determinations. [†]Inhibition plot could not be fit due to lack of a plateau at the highest concentration used; however, approximately 50% inhibition was seen at 10 mM. [‡]Inhibition plot could not be fit due to minimal inhibition seen at the highest concentration used. *Cephamycin – possesses a C7-OMe group. All IC₅₀ curves are shown in **Appendix B**.

Ceph	R ₁	R ₂	k_2/K_s (M ⁻¹ s ⁻¹) ^a	median MIC (µg/mL) ^b [range]
CFP			11,800 ± 1,300	1 [1]
CPT			10,900 ± 1,700	2 [1-4]
BPR			3,230 ± 190	4 [2-4]
CRO			1,710 ± 320	2 [1-4]
ZOX		H	1,000 ± 210	6 [4-8]
CTX			880 ± 120	6 [4-8]
CFM			720 ± 60	6 [4-8]

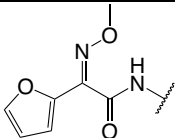
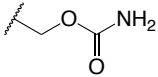
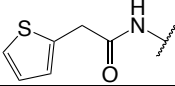
CAZ			790 ± 150	24 [16-32]
FEP			630 ± 50	32 [16-32]
CPD			590 ± 90	16 [16]
TOL			200 ± 20	>32
CDR			82 ± 7	1.5 [1-2]
CEC		Cl	29 ± 4	>32
CTB		H	19.1 ± 0.2	>32
CXM			6.8 ± 0.2	16 [16]
FOX*			3.3 ± 0.6	3 [2-4]
CMZ*			3.6 ± 0.1	32 [32]
CFS			0.8 ± 0.1	>32
LEX		CH ₃	$\sim 0.3^\dagger$	>32

CFZ			~ 0 [‡]	12 [8-16]
LOT			~ 0 [‡]	32 [32]
LOR			~ 0 [‡]	16 [16]

Examining the acylation data qualitatively, it appears that the R₁ side chain has a significant impact on tPBP2^{H041} acylation rate, as seen in pairwise comparisons of compounds with identical R₂ side chains (**Table 3.2**). These pairings exhibit up to 3,000-fold differences in activity (*e.g.*, cefoperazone versus cefmetazole). By contrast, the R₂ side chain has a much lower impact on acylation rate, as evidenced by the narrow range of values obtained for cephalosporins containing the 2-(2-aminothiazol-4yl)-2-(alkoxyimino)acetyl (ATAO) moiety at R₁.

Table 3.2: Pairwise comparisons of cephalosporins with identical R_2 . ^aSecond-order acylation rate constants taken from **Table 1**. ^bQuotient of second-order acylation rate constants for fast- versus slow-acylating cephalosporin. [†]Cephameycin – possesses C7-OMe group. [‡]Inhibition plot could not be fit due to minimal inhibition seen at the highest concentration used.

Ceph	R_1	R_2	k_2/K_s ($M^{-1}s^{-1}$) ^a	Fold-Change ^b
CFP			$11,800 \pm 1,300$	3,300
CMZ [†]			3.6 ± 0.1	
ZOX		H	$1,000 \pm 210$	52
CTB			19.1 ± 0.2	
CTX			880 ± 120	∞
LOT			$\sim 0^{\ddagger}$	
CAZ			790 ± 150	∞
LOR			$\sim 0^{\ddagger}$	
CFM			720 ± 60	8.8
CDR			82 ± 7	

CFM			6.8 ± 0.2	2.1
FOX [†]			3.3 ± 0.6	

3.3.b. Antimicrobial activity against *N. gonorrhoeae* H041

Minimum inhibitory concentrations (MICs) were determined for the panel of cephalosporins using agar dilution (**Table 3.1**). The tested compounds exhibit varying degrees of antimicrobial potency against H041, ranging from 1 to >32 $\mu\text{g/mL}$. Consistent with the acylation data, cefoperazone shows slightly more inhibition of bacterial growth than ceftriaxone (1 vs 2 $\mu\text{g/mL}$), albeit within the error of dilution. Despite their rapid target acylation rates against tPBP2^{H041}, the MICs for ceftaroline and ceftobiprole are similar or slightly higher compared to ceftriaxone. By contrast, cefdinir and cefoxitin, which both exhibit relatively low acylation rates against tPBP2^{H041}, inhibit the growth of H041 at concentrations comparable to ceftriaxone (MIC = 1.5 and 3 $\mu\text{g/mL}$, respectively). The anti-gonococcal activity of the remaining cephalosporins is generally weaker, falling in the range of 8 to 16 $\mu\text{g/mL}$. Cephalothin, ceftazidime, cefaclor, cefsulodin, and cephalexin are exceptionally poor antimicrobials, and cannot inhibit growth of the H041 strain except at concentrations of 32 $\mu\text{g/mL}$ or more. In general, antimicrobial potency correlates relatively poorly with acylation rate because MICs are also influenced by the degree of permeation through porins and efflux rates, in addition to reactivity with the PBP target.

3.4. Quantitative structure-activity relationship for cephalosporins against *N. gonorrhoeae* strain H041 and its PBP2

3.4.a. Partial least squares QSAR for second-order acylation rate constant against tPBP2^{H041}

Correlation of acylation data for the 18 cephalosporins with measurable acylation rates with their molecular descriptors yielded a partial least squares model with an r^2 of 0.995 and a cross-validated r^2 of 0.957 (**Fig. 3.12A**). In addition to its high degree of predictability within the training set, the model successfully predicts near-zero activity for four cephalosporins not in the training set that have unmeasurable acylation rates against tPBP2^{H041} (**Table 3.3**). To assess the probability of chance correlation, y -randomization was performed, in which activity values were randomly assigned to a structure. This yielded an r^2 of 0.937 and a cross-validated r^2 of 0.067 (**Figure 3.12B**), indicating that correlations seen in the model are not random. Definitions of descriptors used in QSAR models can be found in **Appendix C**.

From the PLS model, it can be seen that the second-order acylation rate of tPBP2^{H041} by cephalosporins is greatly affected by the van der Waals surface area and lipophilicity of the R₁ substituent, with large, modestly lipophilic groups being favored. Other features of the R₁ substituent were also found to correlate with high activity, including overall shape, connectivity, and topology. The contributions of these variables indicate that active molecules possess a high degree of unsaturation and cyclicity, with modest heteroatom counts and branching. The R₂ side chain makes relatively less contribution to acylation compared to R₁ but does have some effect. R₂ groups containing a large number of hydrogen bond acceptors appear to confer higher acylation rates. The model also points to partial positive charge and hydrophobicity of R₂ as being favorable, the former of which may be an indirect result of inductive effects by electronegative atoms in R₂ of highly active compounds.

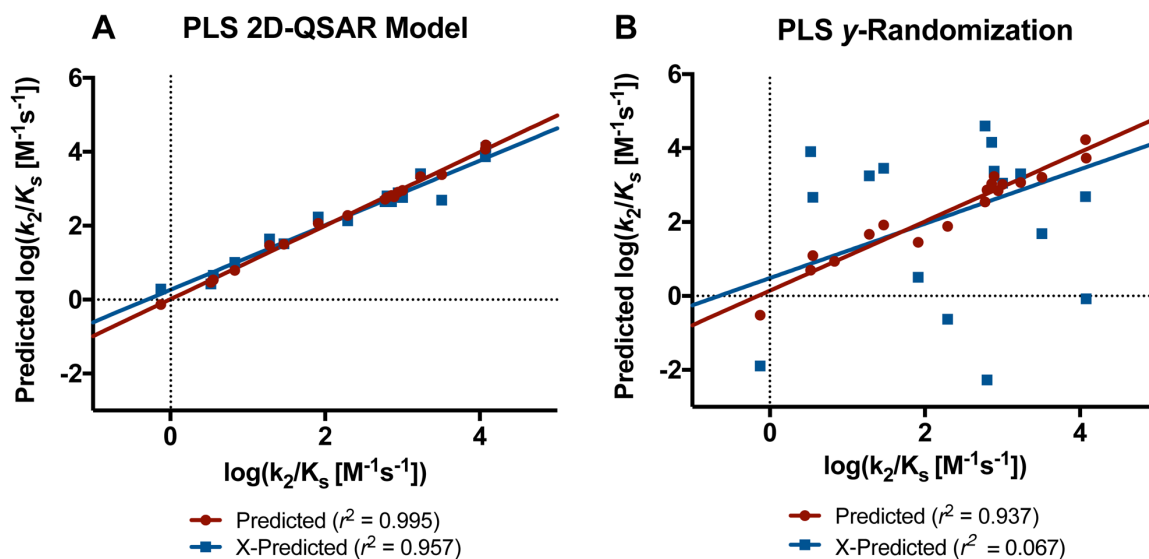


Figure 3.12: Partial least squares quantitative structure activity relationship of cephalosporins against $tPBP2^{H041}$. **A.** PLS QSAR model of $tPBP2^{H041}$ acylation rate constant data, generated using the physicochemical and structural descriptors shown in **Table 3.3**. The model exhibits high internal validity by direct application to the training set ($r^2 = 0.995$) and by leave-one-out cross validation ($X-r^2 = 0.957$). **B.** QSAR validation by y-randomization. Random assignment of second-order acylation rate constants to physicochemical and structural descriptors shown in **Table 3.3** yields a poor PLS model of $tPBP2^{H041}$ -inhibitory activity ($X-r^2 = 0.067$).

Table 3.3: Partial least squares QSAR model of $tPBP2^{H041}$ acylation rate constant data. ^aDescriptor definitions can be found in **Appendix C**.

Descriptor ^a	Moiety	Coefficient	Importance
<i>vdw_area</i>	R ₁	+ 4.8926	1
<i>Kier1</i>	R ₁	- 4.5005	0.9198
<i>zagreb</i>	R ₁	- 0.8829	0.1804
<i>KierA2</i>	R ₁	+ 0.6690	0.1367
<i>chi0v</i>	R ₁	+ 0.5917	0.1209
<i>BCUT_SLOGP_0</i>	R ₁	- 0.5145	0.1052
<i>BCUT_SLOGP_1</i>	R ₁	- 0.3783	0.0773
<i>a_ICM</i>	R ₁	+ 0.3723	0.0761
<i>SlogP_VSA7</i>	R ₂	+ 0.3679	0.0752
<i>BCUT_SLOGP_3</i>	R ₁	- 0.3626	0.0741
<i>BCUT_SMR_3</i>	R ₁	- 0.1991	0.0407
<i>a_acc</i>	R ₂	+ 0.1939	0.0396
<i>BCUT_PEOE_3</i>	R ₁	- 0.1797	0.0367
<i>GCUT_PEOE_2</i>	R ₂	+ 0.1737	0.0355
<i>BCUT_PEOE_0</i>	R ₁	+ 0.1693	0.0346
<i>PEOE_VSA_FPNEG</i>	R ₁	+ 0.1104	0.0226
<i>Q_RPC+</i>	R ₂	+ 0.0854	0.0175

Table 3.4: Application of PLS QSAR to a test set of null cephalosporins. ^aSecond-order acylation rates for tPBP2^{H041}, as reported in **Table 3.1**. ^bSecond-order acylation rates computed using the model reported in **Table 3.3** and **Figure 3.12**. Test set computations exhibit an overall root mean square error of 12.4 M⁻¹s⁻¹ compared to true acylation rate.

Cephalosporin	k_2/K_s (M ⁻¹ s ⁻¹) ^a	Predicted k_2/K_s (M ⁻¹ s ⁻¹) ^b
cephalexin (LEX)	~ 0.3 [†]	2.6
cefazolin (CFZ)	~ 0 [‡]	0.1
cephalothin (LOT)	~ 0 [‡]	1.4
cephaloridine (LOR)	~ 0 [‡]	24.6

3.4.b. Classification QSAR for antimicrobial activity against *Neisseria gonorrhoeae* H041

Since MIC values obtained were in discrete, two-fold increments, classification QSAR was used to examine the relationship between MIC and the cephalosporin molecular descriptors rather than PLS QSAR. Using a median MIC cut-off of ≤ 4 $\mu\text{g/mL}$, we defined 5 cephalosporins as active and 16 as inactive. The resulting model has an overall predictive accuracy of 100% ($p = 0.0005$) and cross-predictive accuracy of 100% ($p = 0.0005$) (**Figure 3.13A**). As for the acylation-based QSAR, the validity of the model was checked by y -randomization to assess the probability of chance correlation (**Figure 3.13B**). While the structural features driving acylation rate are largely the lipophilicity and topology of R₁, antimicrobial activity is enhanced by overall hydrophilicity of the molecule. Features shown to contribute to greater activity include more hydrogen bonding elements, increased water solubility, and formal charge. Similar to acylation, the model also indicates that antimicrobial activity is enhanced by specific cephalosporin shape and topology, consistent with this activity being dependent upon their inhibition of tPBP2^{H041}.

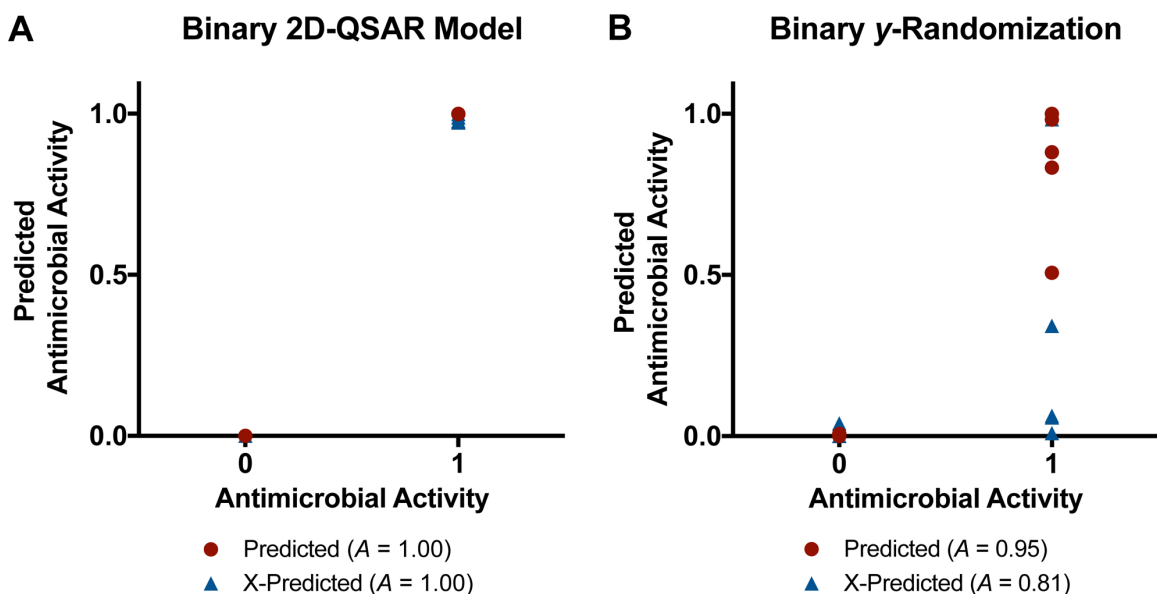


Figure 3.13: Classification quantitative structure activity relationship of cephalosporins against *N. gonorrhoeae* H041. **A.** Classification QSAR model of antimicrobial activity against *Neisseria gonorrhoeae* H041, generated using the descriptors shown in **Table 3.5**. The model exhibits high predictive power (100% accuracy upon direct application to the test set, as well as cross-validation). **B.** QSAR validation by y-randomization. Random assignment of MIC values to physicochemical and structural descriptors shown in **Table 3.5** yields a poor classification model of *N. gonorrhoeae* H041 antimicrobial activity (X-A = 0.81).

Table 3.5: Classification QSAR model of *Neisseria gonorrhoeae* H041 antimicrobial activity data. ^aDescriptor definitions can be found in **Appendix C**.

Descriptor ^a	Importance
PEOE_VSA+1	0.402125
SlogP_VSA0	0.390994
PEOE_VSA+0	0.376126
zagreb	0.368061
PEOE_VSA+4	0.363402
SlogP_VSA1	0.363401
PEOE_VSA-1	0.356382
PEOE_VSA+3	0.342549
PEOE_VSA+6	0.332761
PEOE_VSA-4	0.330928
SMR_VSA4	0.301794
SMR_VSA3	0.295544
PEOE_VSA-3	0.293242
SlogP_VSA4	0.287767
SlogP_VSA2	0.280906
a_donacc	0.250032
chi1v_C	0.249221
GCUT_PEOE_1	0.237011
h_logS	0.233228
KierFlex	0.225164
FCharge	0.219874

3.5. Importance of Lys361 to tPBP2^{H041}-cephalosporin complex formation

3.5.a. Homology modeling of class B PBPs and alignment with published crystal structures

As noted above, the docking data reveal a potential hydrogen bond between K361 of $\alpha 4$ in tPBP2^{H041} and polar R₂ side chains. Examination of crystal structures and homology models of class B PBPs from several species shows that a positively charged residue is highly conserved at this position in many Gram-negative pathogens (**Figure 3.14, Table 3.5**), including several belonging to the multi-drug resistant ESKAPE group, suggesting that it may be important for the transpeptidase activity of class B PBPs. By contrast, this residue is not conserved in class B PBPs of Gram-positive bacteria.

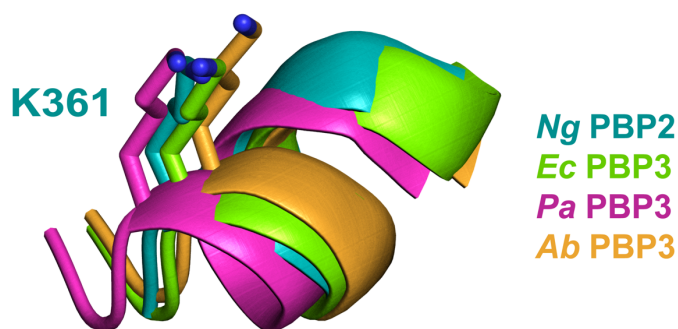


Figure 3.14: Alignment of $\alpha 4$ of class B PBPs showing conservation of a lysine residue in several important Gram negative pathogens. *N. gonorrhoeae* PBP2 shown in teal, *E. coli* PBP3 shown in chartreuse, *P. aeruginosa* PBP3 shown in magenta, and *A. baumannii* PBP3 shown in orange.

Table 3.6: Superimposition of class B PBPs. ^aResidues from rigid structural alignment that generate a receptor surface analogous to the shallow cleft containing K361 in PBP2 of *N. gonorrhoeae*. ^bPredominant formal charge of the cleft. *No structural data available – homology model constructed using SWISS-MODEL.

Morphology	Organism	Class B PBP	Residues ^a	Charge ^b
Gram negative	<i>N. gonorrhoeae</i>	PBP2 ^{H041}	H348, Y350, K361	++
	<i>N. gonorrhoeae</i>	PBP2 ^{WT} (3EQU)	H348, Y350, K361	++
	<i>N. meningitidis</i>	PBP2*	V382, H386, V397	+
	<i>P. aeruginosa</i>	PBP3 (3PBN)	S334, K348	+
	<i>P. aeruginosa</i>	PBP3a*	A329, R331, N342	+
	<i>E. coli</i>	PBP3 (4BJP)	A345, Y347, K358	+
	<i>A. baumannii</i>	PBP3 (3UE3)	H376, Y378, K389	+
	<i>H. influenzae</i>	PBP2*	W378, K379, H383, E394	++/-
	<i>H. influenzae</i>	PBP3*	A365, R367, N378	+
	<i>H. pylori</i>	PBP2 (5LP4)	W349, K350, H354, E365	+/-
	<i>H. pylori</i>	PBP3*	F367, Q381	∅
Gram positive	<i>S. aureus</i>	PBP2a (5M1A)	E447, S461	-
	<i>S. pneumoniae</i>	PBP2x (5OAU)	W374, D375, H394	+/-
	<i>S. pneumoniae</i>	PBP2x (1PYY)	D375, E378, H394	+/-
	<i>S. pneumoniae</i>	PBP2x (1QME)	W374, D375, H394	+/-
	<i>S. pneumoniae</i>	PBP2b (2WAE)	W424, Y425, Y442	∅
	<i>E. faecalis</i>	PBP4 (6BSQ)	K468, N481	+
	<i>E. faecium</i>	PBP5 (6MKA)	S466, Y479	∅
	<i>B. subtilis</i>	PBP2a*	D398, E402, Y413	--
	<i>B. subtilis</i>	PBP2b*	W352, R363, K493	++
	<i>B. subtilis</i>	PBP3*	E455, T468	-
Atypical	<i>M. tuberculosis</i>	PBPA (3LO7)	G263, K280	+
	<i>B. burgdorferi</i>	PBP2*	W347, K348, H352, H363	+++

Table 3.7: Homology model template-target matching parameters for class B PBPs. ^aData acquisition method and resolution for template molecule. ^bPrimary structure sequence identity between template and target molecules, reported as a percentage. ^cGlobal Mean Quality Estimate for the generated homology models.

Target	Template	Method ^a	Identity ^b	GMQE ^c
<i>B. subtilis</i> PBP2a (SIQ60944.1)	<i>S. aureus</i> PBP2 (2olv.1)	X-ray, 2.8 Å	32.6	0.59
<i>B. subtilis</i> PBP2b (ARW31327.1)	<i>S. thermophilus</i> PBP2x (5u47.1.A)	X-ray, 2.0 Å	33.5	0.64
<i>B. subtilis</i> PBP3 (KIU10857.1)	<i>E. faecium</i> PBP2' (5e31.1)	X-ray, 2.3 Å	38.7	0.70
<i>H. influenzae</i> PBP2 (KPH67935.1)	<i>H. pylori</i> PBP2/MreC (5lp5.1)	X-ray, 2.7 Å	31.1	0.58
<i>H. influenzae</i> PBP3 (BAF48352.1)	<i>P. aeruginosa</i> PBP3 (4kqr.1)	X-ray, 2.0 Å	41.4	0.63
<i>H. pylori</i> PBP3 (CAX30260.1)	<i>P. aeruginosa</i> PBP3 (4kqr.1)	X-ray, 2.0 Å	28.1	0.57
<i>P. aeruginosa</i> PBP3a (CAA64770.1)	<i>P. aeruginosa</i> PBP3 (4kqr.1)	X-ray, 2.0 Å	49.8	0.74
<i>N. meningitidis</i> PBP2 (RGB21187.1)	<i>H. pylori</i> PBP2/MreC (5lp5.1)	X-ray, 2.7 Å	32.9	0.56
<i>B. burdorferi</i> PBP2 (ARS33437.1)	<i>H. pylori</i> PBP2/MreC (5lp5.1)	X-ray, 2.7 Å	27.0	0.58

Table 3.8: Homology model quality measures for class B PBPs. ^aPercent of residues with geometries in favorable or acceptable regions of the Ramachandran plot. ^bPercent of residues with geometries in favorable or acceptable regions of χ_1 - χ_2 plot. ^cLog-odds score for overall homology model geometry.

Model	Ramachandran (%) ^a	χ_1 - χ_2 (%) ^b	G-factor ^c
<i>B. subtilis</i> PBP2a	96.8	98.8	-0.14
<i>B. subtilis</i> PBP2b	97.9	98.7	-0.15
<i>B. subtilis</i> PBP3	97.9	99.0	-0.12
<i>H. influenzae</i> PBP2	99.2	99.7	-0.16
<i>H. influenzae</i> PBP3	99.1	99.0	-0.09
<i>H. pylori</i> PBP3	98.4	98.9	-0.25
<i>P. aeruginosa</i> PBP3a	99.5	98.9	-0.11
<i>N. meningitidis</i> PBP2	99.0	98.8	-0.17
<i>B. burdorferi</i> PBP2	97.5	98.6	-0.23

3.5.b. Second-order acylation rate constants of select cephalosporins against a tPBP2^{H041}-K361E mutant

To determine its influence on cephalosporin binding to tPBP2^{H041}, Lys361 was mutated to Glu, and the acylation rates of several cephalosporins with representative electronegative or electropositive R₂ side chains were determined. The second-order acylation rate of Bocillin-FL against tPBP2^{H041}-K361E is $57 \pm 1 \text{ M}^{-1}\text{s}^{-1}$, a 5-fold decrease compared to the native enzyme (**Figure 3.15**). The second-order acylation rates of ceftriaxone ($290 \pm 70 \text{ M}^{-1}\text{s}^{-1}$) and cefoperazone ($370 \pm 60 \text{ M}^{-1}\text{s}^{-1}$) are both markedly lower against the K361E mutant, with reductions of 83% and 97%, respectively (**Table 3.8**). Ceftazidime ($560 \pm 180 \text{ M}^{-1}\text{s}^{-1}$) and cefepime ($410 \pm 130 \text{ M}^{-1}\text{s}^{-1}$) also exhibit lower acylation rates, although less pronounced. These data indicate that in tPBP2^{H041}, the R₂ side chain binds the shallow cleft between the β 2c- β 2d loop and the α 10- β 3 loop containing K361 in the pre-covalent state.

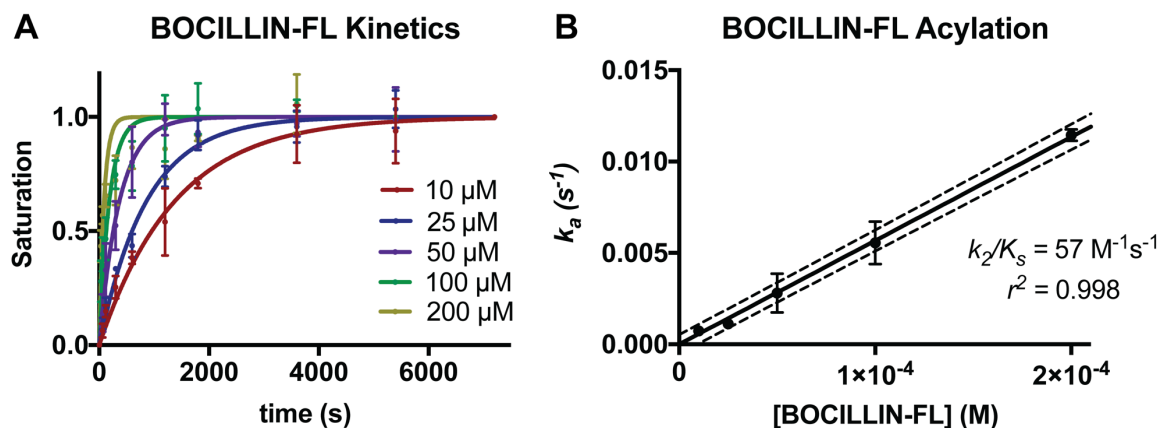
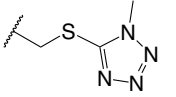
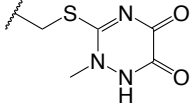
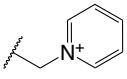
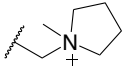


Figure 3.15: Second-order rate of acylation of Bocillin-FL against tPBP2^{H041}-K361E. **A.** Acylation of tPBP2^{H041}-K361E by Bocillin-FL was detected under pseudo-first order conditions using various ligand concentrations to determine rate constant k_a . **B.** The pseudo-first-order rates of acylation (k_a) were plotted against the concentration of Bocillin-FL to yield a plot whose slope is the second order acylation rate constant (k_2/K_s). A minimum of three kinetics experiments were completed for each concentration. Error bars are standard deviation.

Table 3.9: Second-order acylation rates for select cephalosporins against tPBP2^{H041}-K361E. ^aSecond order acylation rate constants against native tPBP2^{H041}, as reported in **Table 3.1**. ^bThe acylation rate constant for each cephalosporin was derived from kinetic measurements of the formation of the acyl-enzyme complex, as described in Chapter 2. The rates were determined by a competition assay with Bocillin-FL. Values were derived from a minimum of three separate determinations. Error is expressed as standard deviation. ^cThe fractional acylation rate compared to that with native tPBP2^{H041}.

Ceph	R ₂	k_2/K_s (M ⁻¹ s ⁻¹) ^a	K361E k_2/K_s (M ⁻¹ s ⁻¹) ^b	Fractional Activity ^c
CFP		11,800 ± 1,300	370 ± 60	0.03
CRO		1,710 ± 320	290 ± 70	0.17
CAZ		790 ± 150	560 ± 180	0.70
FEP		630 ± 50	410 ± 130	0.64

3.5.c. Docking of select cephalosporins to a tPBP2^{H041}-K361E mutant

When this mutation is modeled *in silico* and the above docking protocol repeated, the generated poses for ceftazidime and cefepime position R₂ toward the mutated residue due to electrostatic attraction, whereas the R₂ side chains of ceftriaxone and cefoperazone become oriented away from this region (**Figure 3.16**). The repulsion of electronegative R₂ by E361 seen in these models may be the basis for differential effects of the mutant on cefoperazone and ceftriaxone versus ceftazidime and cefepime.

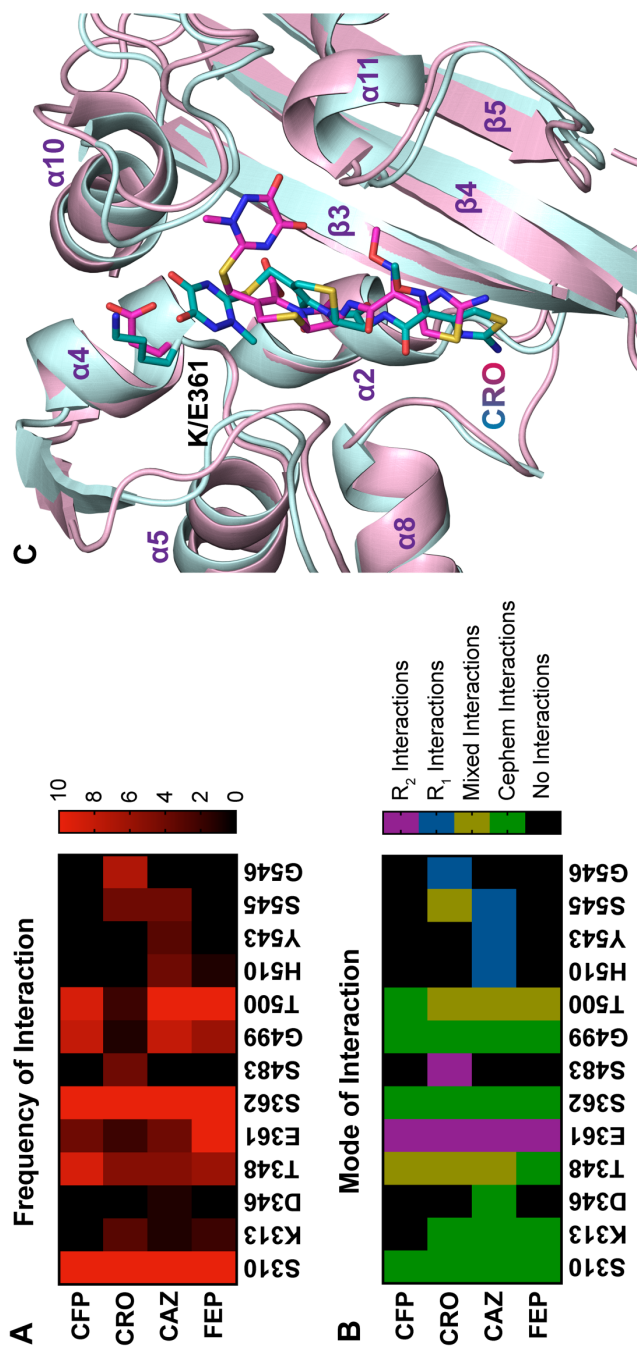


Figure 3.16: Pharmacophore-constrained induced fit docking of select cephalosporins to *tPBP2^{H041-K361E}*. Docking of the selected panel of cephalosporins against the K361E mutant lends insight into changes in the compounds' potential pre-covalent binding modes caused by the mutation. While interactions with S310 and T500 are conserved, interactions with residue 361 are seen more frequently for cephalosporins possessing positive formal charge at R₂ ($OR_{CAZ,CFP} = 21, p = 0.0002$). **A.** Heat map of cephalosporin-*tPBP2^{H041-K361E}* interactions colored by number of poses interacting with a given residue. Key: cefoperazone (CFP), ceftriaxone (CRO), ceftazidime (CAZ), cefepime (FEP). **B.** Heat map of cephalosporin-*tPBP2^{H041-K361E}* interactions, colored by the cephalosporin moiety interacting with a given residue. **C.** A representative pose of ceftriaxone shows the R₂ group occupying a different position. The native *tPBP2^{H041}* pose is shown in teal, and the *tPBP2^{H041-K361E}* pose is shown in magenta.

3.6. Further evaluation of cefoperazone as a potential antigonococcal agent

3.6.a. Crystallographic analysis of a tPBP2^{H041}-CFP complex structure

The rapid acylation of tPBP2^{H041} by cefoperazone compared to ceftriaxone, as well as its more favorable energetics of binding in the docked models, suggests it may bind more favorably in the transpeptidase active site compared to other cephalosporins. To examine this, the crystal structure of tPBP2^{H041} acylated by cefoperazone was determined at 2.2 Å resolution, obtained by soaking crystals of tPBP2^{H041} with antibiotic (**Table 3.9**).

Overall, the structure is very similar to the reported tPBP2^{H041}-CRO structure (C_{α} rmsd = 0.123 Å), including the “outbent” conformation of the β 3- β 4 loop (**Figure 3.17**). The unbiased |Fo|-|Fc| difference electron density map shows cefoperazone covalently bound to Ser310 (**Figure 3.18**). Electron density is observed for a majority of the cefoperazone molecule, with the exception of C3 of the dihydrothiazine ring, C6 of the 2,3-dioxopiperazine ring, and the *p*-phenol substituent on R₁. The lack of density at dihydrothiazine C3 and 2,3-dioxopiperazine C6 is consistent with the presence of a mixture of conformational states for these flexible ring systems. Cefoperazone forms a number of polar contacts with active site residues of tPBP2^{H041} (**Figure 3.18**). These include hydrogen bonds between the acyl carbonyl oxygen and the oxyanion hole comprising the main chain amides of Ser310 and Thr500, and between the C7 acylamino carbonyl oxygen and the side chain of Asn364 from the SxN motif. The C4 carboxylate forms hydrogen bonds with the main chain of Ser545 and the side chain of Thr500. The hydrophobic 2,3-dioxopiperazine ring system is positioned over the Y422 side chain, and the *p*-phenol system is solvent exposed. The tPBP2^{H041}-CFP structure does not show a great deal of overlap with either the major or minor pose of cefoperazone from our docking models (**Figure 3.19**).

Table 3.10: X-ray diffraction data and model refinement statistics for a preliminary crystal structure of *tPBP2^{H041}* in complex with cefoperazone.

Data collection:	
Space group	P2 ₁ 2 ₁ 2 ₁
Cell dimensions:	
<i>a</i> , <i>b</i> , <i>c</i> (Å)	50.2, 60.6, 109.1
α , β , γ (°)	90.0, 90.0, 90.0
Resolution range (Å)	40.56 - 2.17
R _{merge} * (%)	23.6 (60.9)
Completeness (%)	100 (99.8)
Redundancy	13.6 (13.9)
$\langle I \rangle / \langle \sigma \rangle$	22.4 (6.1)
No. of unique reflections	17,766 (1,688)
Refinement:	
Resolution (Å)	40.56 - 2.17
No. of non-hydrogen protein atoms	2,457
No. of antibiotic atoms	37
No. of water oxygen atoms	108
R _{cryst} /R _{free} (%)	0.179/0.225
RMS deviations from ideal stereochemistry	
bond lengths (Å)	0.003
bond angles (°)	0.8
<i>B</i> factors:	
Mean <i>B</i> factor (main chain) (Å ²)	23.4
RMS. deviation in main chain <i>B</i> factors (Å ²)	1.0
Mean <i>B</i> factor (side chains & waters) (Å ²)	28.3
RMS deviation in side chain <i>B</i> factors (Å ²)	1.8
Ramachandran plot:	
Residues in most favored region (%)	93.4
Residues is generously allowed region (%)	6.6
Residues in additional allowed region	0.0
Residues in disallowed region	0.0

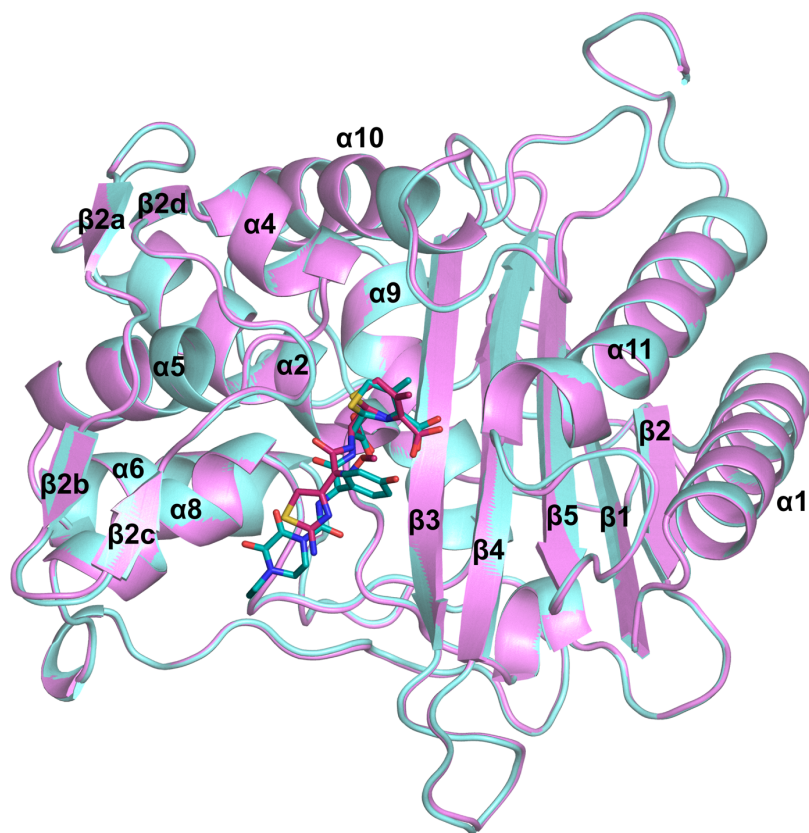


Figure 3.17: *Overlay of ceftriaxone- and cefoperazone-acylated structures of tPBP2^{H041}. Superimposition of tPBP2^{H041} in complex with ceftriaxone (aqua) and cefoperazone (pink) shows that the structures are nearly identical. Ceftriaxone and cefoperazone are shown as teal and magenta sticks, respectively. Note the “outbent” conformation of the β 3- β 4 loop in both complexes.*

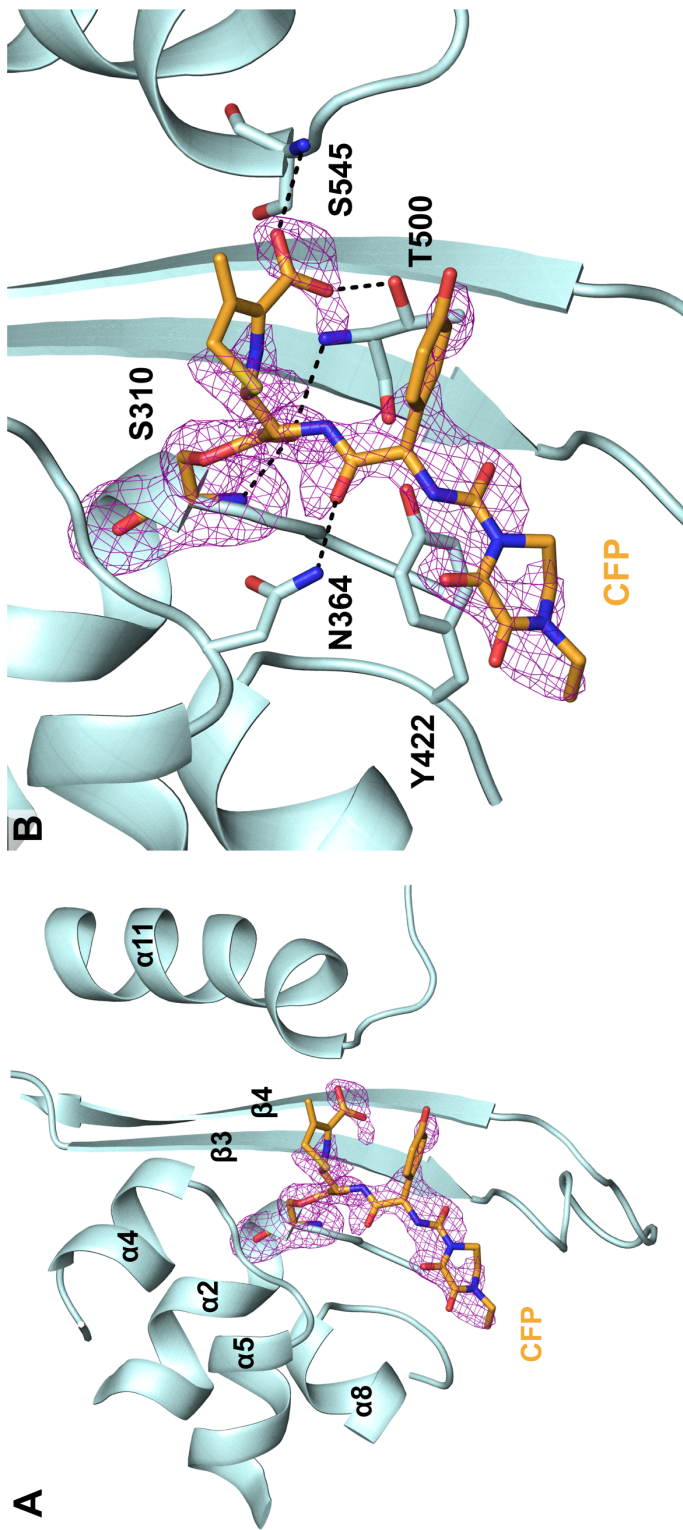


Figure 3.18: Crystal structure of cefoperazone in complex with *tPBP2^{H041}*. **A.** Unbiased $|F_o| - |F_c|$ difference electron density contoured at 2.3σ showing cefoperazone covalently bound to S310. **B.** Zoomed in view showing polar contacts between cefoperazone and active site residues. Cefoperazone shown as orange sticks. Hydrogen bonds shown as dashed lines.

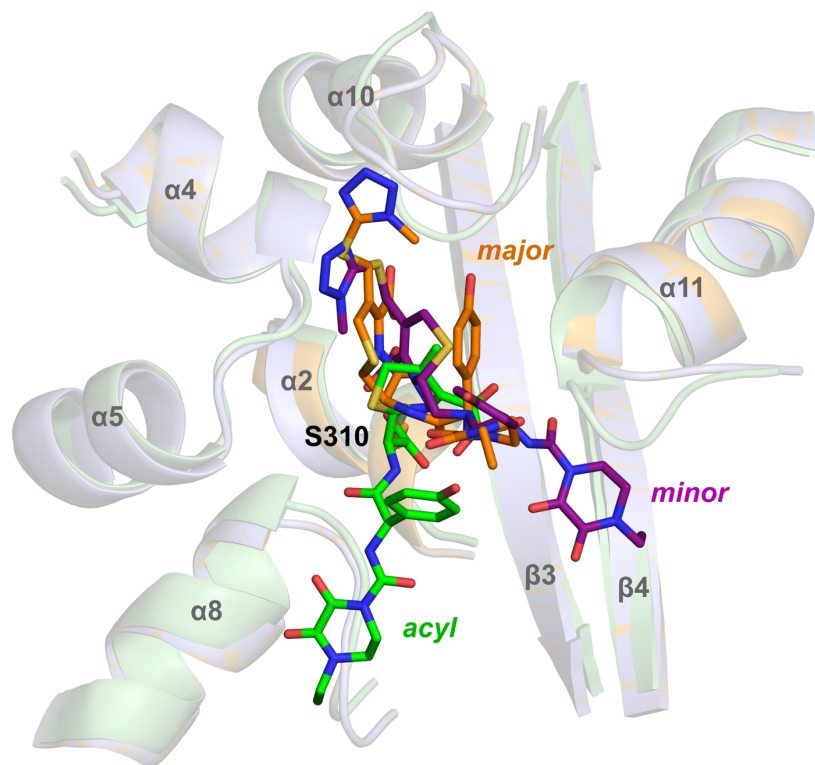


Figure 3.19: *Overlay of docked cefoperazone poses with tPBP2^{H041}-CFP complex structure.* Docked precovalent poses of cefoperazone (major in orange, minor in purple) show marked differences from the acylated structure (green sticks). In the minor pose, in which the β -lactam ring is well-positioned for attack by nucleophilic O γ of S310, the hydrophobic 2,3-dioxopiperazine ring has moved quite far from its final position near α 8.

3.6.b. *In vivo* testing of cefoperazone in a gonococcal model of infection

As noted above, cefoperazone exhibits an acylation rate against tPBP2^{H041} higher than ceftriaxone, suggesting it may have therapeutic potential to treat gonorrhea. To examine this, cefoperazone (60 or 120 mg/kg TID) was administered intraperitoneally to two groups of BALB/c mice infected with *N. gonorrhoeae* H041 (**Figure 3.20**). A 120 mg/kg TID dosing regimen results in 100% culture negativity by day 3, with a mean time-to-clearance of 2.1 days ($n = 9$), and shows equivalent efficacy to an identical regimen of ceftriaxone ($n = 10$, mean time-to-clearance 1.6 days, *log-rank* $p = 0.15$). By contrast, a gentamicin control regimen results in 100% culture negativity by day 4, with a mean time-to-clearance of 3.1 days ($n = 8$, *log-rank* $p = 0.02$ versus CFP, *log-rank* $p = 0.0004$ versus CRO). Quantitative differences in colonization load are seen beginning at 1 day for cefoperazone- and ceftriaxone-treated groups compared to vehicle control (two-way RM ANOVA $p < 0.01$), while no such differences are seen until day 2 for the gentamicin-treated group (two-way RM ANOVA $p < 0.01$). While a general trend toward decreased colonization load is seen with administration of 60 mg/kg cefoperazone TID or 60 mg/kg ceftriaxone TID, neither regimen is able to attain full infection clearance by day 8.

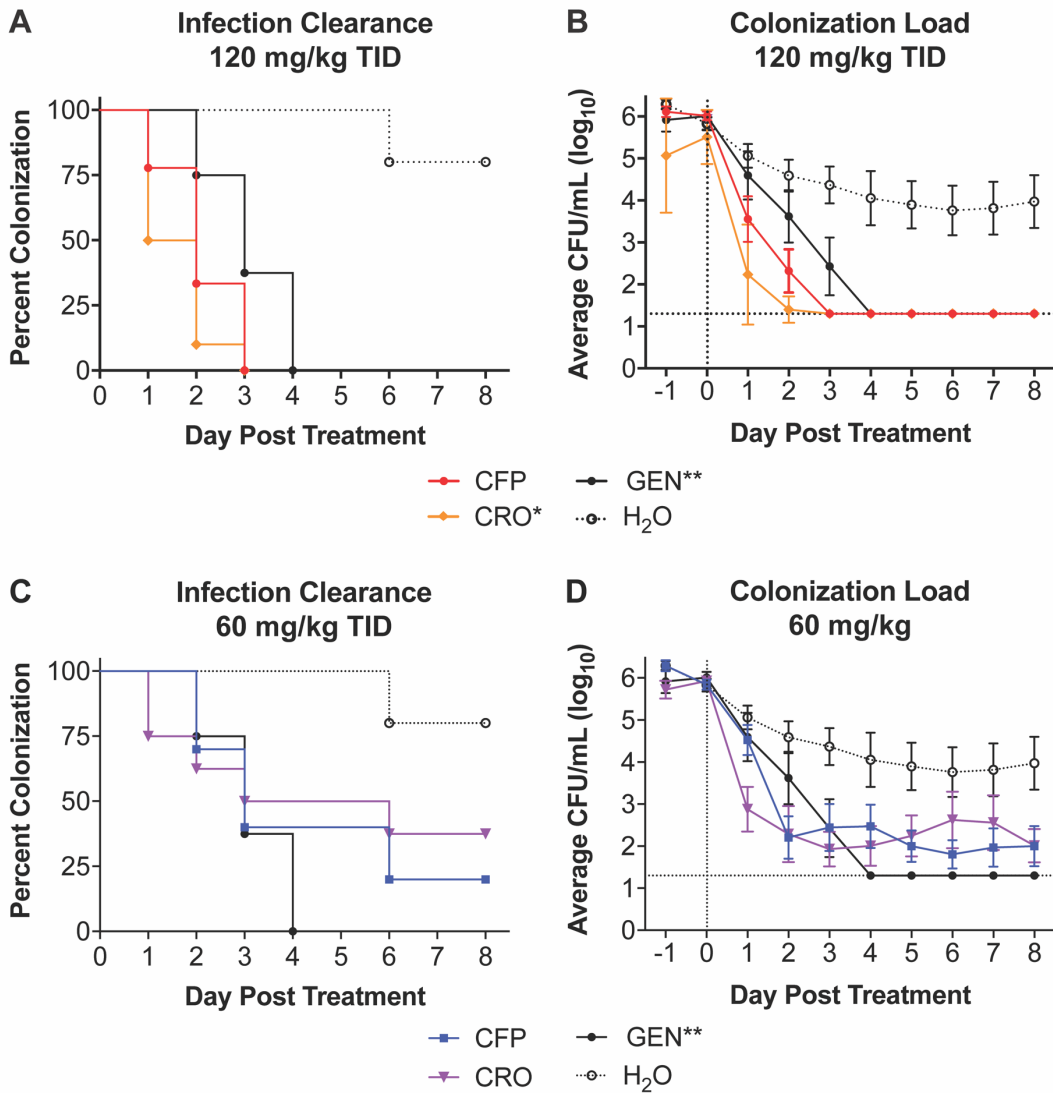


Figure 3.20: Evaluation of cefoperazone in a murine model of gonococcal infection. **A.** Kaplan-Meier curve for culture positivity in mice treated with 120 mg/kg intraperitoneal (IP) cefoperazone or ceftriaxone three times daily (TID). *Historical data from the Jerse laboratory. **Positive control group was given 48mg/kg gentamicin IP once daily (QD). **B.** Colonization load by day for groups treated with 120 mg/kg IP cefoperazone or ceftriaxone TID. **C.** Kaplan-Meier curve for culture positivity in mice treated with 60 mg/kg IP cefoperazone or ceftriaxone TID. **D.** Colonization load by day for groups treated with 60 mg/kg IP cefoperazone or ceftriaxone TID.

3.7. Discussion

The goal of the current work is to elucidate which features of the cephalosporin class of β -lactam antibiotics are important for antimicrobial activity against cephalosporin-resistant *Neisseria gonorrhoeae* H041 through inhibition of PBP2. We find that the structure of the R₁ (C7 acylamino) side chain of cephalosporins has a profound effect on the second-order rate of tPBP2^{H041} acylation, while the R₂ (C3) side chain plays a subtler role. Through molecular docking simulations of the precovalent ligand-receptor complex, we show that aromatic and hydrophobic groups on R₁ extend toward a hydrophobic patch of the tPBP2^{H041} active site, and electronegative elements of R₂ interact with K361. We also show that antimicrobial activity correlates somewhat with tPBP2^{H041} inhibition, but is complicated by a need to evade additional resistance mechanisms present in the organism. Finally, we observe that cefoperazone acylates tPBP2^{H041} at a rate 7-fold faster than ceftriaxone, and it exhibits comparable activity to ceftriaxone against *N. gonorrhoeae* H041 both *in vitro* and *in vivo*.

3.7.a. Contributions of R₁ to tPBP2^{H041}-cephalosporin complex formation.

In this study, we found evidence of a key role for R₁ structure and properties in the second-order rate of acylation of tPBP2^{H041}. The unfavorable contributions of several atomic lipophilicity descriptors indicate that the R₁-binding region of the PBP2^{H041} active site is not tolerant of highly hydrophobic moieties. However, the atomic molar refractivity descriptors show that this region cannot be extremely polar either. It therefore appears that while there may be areas where hydrogen bonding is advantageous (*e.g.*, interaction of the acylamino moiety in mimicry of the peptide substrate), the R₁ side chain should contain groups of modest hydrophobicity, such as aromatic- and heteroaromatic ring-containing systems. In addition, the total van der Waals surface area of the R₁ group contributes positively to acylation rate, suggesting a critical role for size of the cephalosporin in tPBP2^{H041} acylation. Hence, while the ATAO side chains (van der Waals

volume $V \sim 200 \text{ \AA}^3$, distribution coefficient $\log D_{7.4} = -0.7$) seen in many third-generation cephalosporins, as well as the chemically similar thiadiazolyl variants possessed by fifth-generation agents, generally confer some activity, the larger ($V > 400 \text{ \AA}^3$) and more lipophilic ($\log D_{7.4} = 0.6$) 2,3-dioxopiperazinyl moiety of cefoperazone dramatically increases acylation rate.

Shape and topology also play critical roles, with high degrees of unsaturation and cyclicality being associated with higher rates of acylation. Illustrating this trend is the vast difference in acylation rates between cefmetazole, which has a negligible acylation rate and is the only cephalosporin in our study lacking a ring system on R_1 , and cefoperazone, which has two ring systems and exhibits the highest rate among the cephalosporins tested. Also apparent in the R_1 topological parameters is a preference for modest numbers of heteroatoms, as well as a moderate degree of branching. The former is illustrated by the low activity conferred by the tetrazolyl R_1 of cefazolin, and the latter is apparent from differences in acylation rates between compounds with 2-unsubstituted acylamino groups (e.g., cephalothin and cephaloridine) and those with a single branch point at this position (e.g., ceftriaxone and cefoperazone). The exception is that several compounds with 2-substituted acylamino groups have very poor activity, including cephaloridine, cephalexin, and cefaclor. These, however, are suboptimal for tPBP2^{H041} acylation because they possess a small R_1 with sulfonic acid or primary amine moieties. Energy score analysis of docking data for R_2 -paired compounds suggests that these R_1 groups impact pre-covalent Michaelis complex formation by altering affinity for tPBP2^{H041} rather than acylation (**Figure 3.21**). With the exception of ceftizoxime and ceftibuten, the faster acylating compound of each pair shows a more favorable binding energy with the tPBP2^{H041} active site.

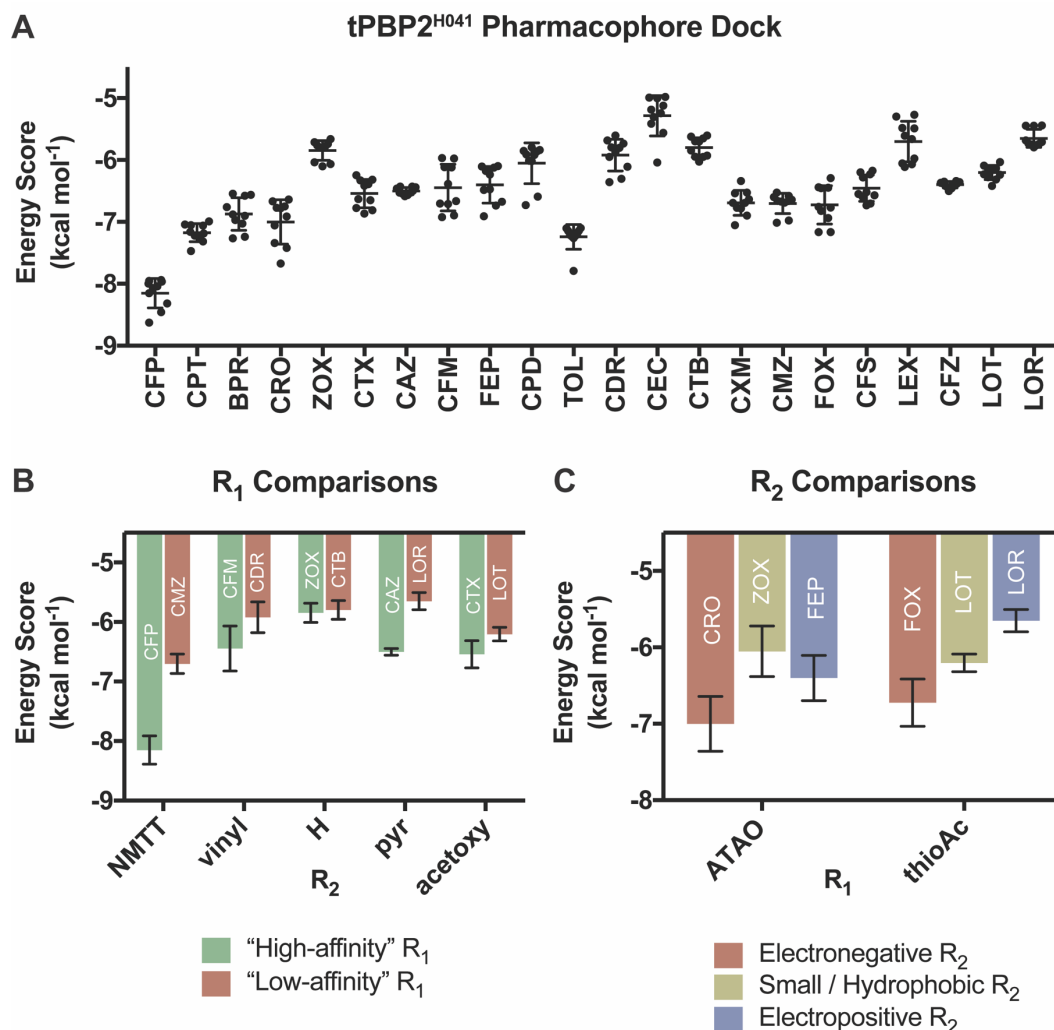


Figure 3.21: Energy score analyses for docking of cephalosporins against $tPBP2^{H041}$. **A.** Overall energy scores for the cephalosporins tested, rank ordered by second-order acylation rate ($n = 10$ poses), show a correlation of computational affinity with activity. **B.** Comparisons of energy scores for cephalosporins with different R_1 and identical R_2 . "High-affinity" indicates the molecule of the pair exhibiting more rapid acylation (e.g., cefoperazone). "Low-affinity" indicates the molecule of the pair exhibiting slower acylation (e.g., cefmetazole). *N*-methyltetrazole (NMTT), pyridyl (pyr). **C.** Comparisons of energy scores for cephalosporins with similar R_1 and different R_2 show a preference for negative electrostatics. 2-(2-aminothiazol-4-yl)-2-(alkoxyimino)acetyl (ATAO), thiophen-2-ylacetyl (thioAc).

Previous studies have also indicated that the R₁ side chain may be an important driver of affinity against PBPs. In a qualitative structure-activity relationship of penicillin analogues against *E. faecium* PBP5, it was found that azlocillin ($k_2/K_s = 15 \text{ M}^{-1}\text{s}^{-1}$) exhibits much more rapid acylation of the target than piperacillin ($k_2/K_s = 2.2 \text{ M}^{-1}\text{s}^{-1}$), ampicillin ($k_2/K_s = 1.8 \text{ M}^{-1}\text{s}^{-1}$), or Bocillin-FL ($k_2/K_s = 1.1 \text{ M}^{-1}\text{s}^{-1}$).¹³⁵ In a separate study of *Streptomyces* R61 DD-peptidase, penicillin G ($k_2/K_s = 10,300 \text{ M}^{-1}\text{s}^{-1}$) was shown to be manifold more potent than penicillin V ($k_2/K_s = 1,500 \text{ M}^{-1}\text{s}^{-1}$), carbenicillin ($k_2/K_s = 830 \text{ M}^{-1}\text{s}^{-1}$), and ampicillin ($k_2/K_s = 107 \text{ M}^{-1}\text{s}^{-1}$).¹³⁶ Since the β -lactams examined in these experiments are all penicillin analogues, which possess geminal dimethyl groups at the R₂ position, one can conclude that differences in activity are imparted by R₁. This idea is further supported by the differing specificities of compounds with identical R₂ for various transpeptidases. For example, in membrane preparations of *E. coli*, cefoperazone exhibits very different apparent affinities for PBPs (PBP3 > PBP1b > PBP2 > PBP1a > PBP4) from cefmetazole (PBP4 > PBP1a = PBP1b > PBP3 > PBP2).^{651,652}

The strong influence of the R₁ group on the activities of cephalosporins is important to consider in light of recent new understanding of how PBP2 is acylated by ESCs. Structures of tPBP2^{WT} acylated by cefixime or ceftriaxone reveal significant movement of the β 3- β 4 loop toward the active site, where several residues form a cluster around the aminothiazole ring, and such interactions may contribute to the affinity of ESCs for PBP2.¹¹³ The situation is very different in tPBP2^{H041} because movement of the loop appears restricted by mutations conferring resistance to ESCs, resulting in fewer interactions involving the aminothiazole in the acylated complex.¹³⁴ Interestingly, the electron density obtained for tPBP2^{H041} in complex with ceftriaxone shows a potential dual conformation of R₁, which can also be seen in our docking data (**Figure 3.3**). Such a dual conformation indicates a lack of a preferred, high-affinity binding mode for ceftriaxone with tPBP2^{H041}. While the β 3- β 4 loop is still locked in an “outbent” conformation in the tPBP2^{H041}-CFP structure reported here,

the modeled R₁ assumes an unexpected position in the modeled binding mode that may help to explain part of the increase in cefoperazone's tPBP2^{H041} acylation rate. Instead of the aromatic *p*-phenol group participating in π - π interactions with Y422, the 2,3-dioxopiperazine moiety lies flat in the active site, making considerable van der Waals contacts with Y422 and the surrounding residues (**Figure 3.22**). Perhaps, then, the ideal cephalosporin for acylation of tPBP2^{H041} is one whose R₁ can either 1) induce the hinging in the β 3- β 4 loop to form more extensive contacts with the transpeptidase active site or 2) create sufficient contacts in the absence of such hinging.

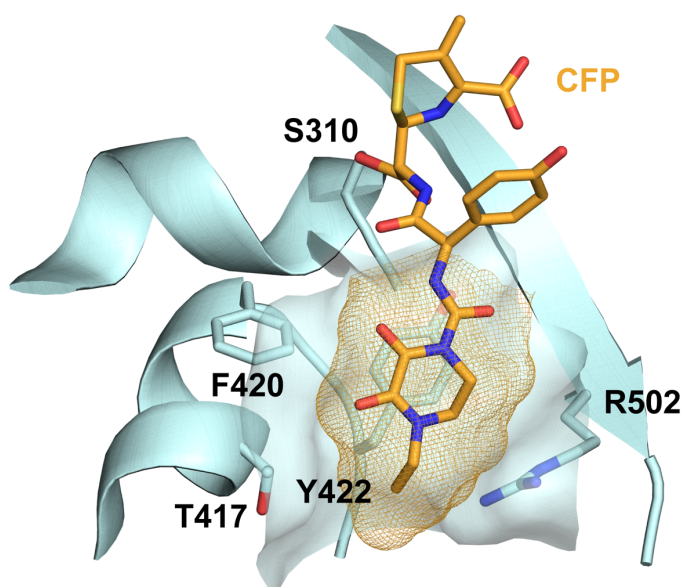


Figure 3.22: Contact of the 2,3-dioxopiperazine moiety of cefoperazone with tPBP2^{H041} in a preliminary complex crystal structure. While the 2,3-dioxopiperazine does not make any polar contacts with active site residues, it creates a large area of van der Waals contact with Y422 and surrounding residues. tPBP2^{H041} and its surface are shown in cyan, and cefoperazone and its surface mesh are shown in orange.

3.7.b. Contributions of R₂ to tPBP2^{H041}-cephalosporin complex formation.

We also found that structural variations in R₂ can have effects on tPBP2^{H041} acylation, albeit to a lesser extent than R₁. First, planar R₂ groups are correlated with faster acylation rates. In fact, the four fastest acylating compounds (*i.e.*, cefoperazone, ceftaroline, ceftobiprole, and ceftriaxone) all have planar R₂ groups with extended ring systems, conferring several-fold increases in acylation when compared with compounds of similar R₁ group (*e.g.*, ceftobiprole versus cefdinir). Second, the hydrogen bonding capacity of R₂ also appears to affect acylation, as exemplified by the thiotriazinone (TTN) moiety conferring a 1.5- to 3-fold enhancement over other ATA0-containing cephalosporins. Our docking data suggest that the electronegativity and hydrogen bonding capability of R₂ enhances affinity for the tPBP2^{H041} active site (**Figure 3.21**). In addition to influencing precovalent ligand-receptor complex formation, the R₂ group can also participate in long-range inductive effects through the conjugated cephem system.^{217,218} Thus, atoms in R₂ may also exert an electron-withdrawing inductive effect, thereby activating the β-lactam carbonyl for more rapid acylation. This is best illustrated by the differences in acylation rate between cefaclor ($29 \pm 4 \text{ M}^{-1}\text{s}^{-1}$) and cephalexin ($\sim 0.3 \text{ M}^{-1}\text{s}^{-1}$), which have identical R₁ groups but R₂ groups with opposite inductive effects.

Finally, we found no correlation between the presence or absence of a C3 leaving group on the dihydrothiazine ring of the cephalosporin and tPBP2^{H041} acylation. These C3 substituents are expelled by resonance upon acylation, and cephalosporins containing leaving groups are thought to form more stable acyl-enzyme complexes, thereby decreasing the rate of deacylation (k_3) and regeneration of the PBP in *apo* form.⁶⁵³ Our data are in keeping with the idea that departure of a C3 leaving group affects k_3 but not the rate of acylation. Nevertheless, given that tPBP2^{H041} has an enhanced rate of deacylation compared to tPBP2^{WT},¹³⁴ the leaving group should be taken into consideration when selecting or designing antigenococcal therapeutics.

In recent years, there have been several attempts to utilize the R₂ side chain of cephalosporins to reduce susceptibility to β-lactamases, and to enhance cell-wall permeability and PBP-binding affinity.⁶⁵⁴⁻⁶⁵⁶ As an example, the planar vinylpyrrolidinone side chain of ceftobiprole was designed to bind a narrow groove within the active site of *S. aureus* PBP2a.⁶⁵⁶ Although there have been no design efforts of this nature against *N. gonorrhoeae* PBP2 to date, our model can be used to make predictions about the structure of an R₂ side chain that would be expected to increase acylation rate. Generally, tetravalent nitrogen-containing leaving groups lead to poor acylation against tPBP2^{H041}, as in the case of ceftolozane, cefsulodin, and cephaloridine. This is consistent with previous studies showing that, although zwitterionic cephalosporins are distinguished by their superior transport through porins and decreased affinity for β-lactamases, they suffer from a loss of affinity for PBPs.²⁶⁶ By contrast, ceftaroline and ceftobiprole, which also contain nitrogen cations, acylate tPBP2^{H041} rapidly. Their formal positive charges are more distal to the bicyclic cephem core compared to others, suggesting a specific spatial discrimination against such a feature.

In the docked models, larger heterocyclic R₂ groups are shown to interact predominantly with K361 and surrounding residues, a finding corroborated by compromised acylation of a tPBP2^{H041}-K361E mutant by cefoperazone and ceftriaxone. By contrast, a crystal structure of tPBP2^{WT} acylated by ceftriaxone with the C3 leaving group intact shows R₂ interacting with residues immediately prior to α11, similar to the structure of *S. aureus* PBP2a in complex with ceftobiprole.⁶⁵⁷ Surprisingly, very few poses from our docking studies adopt this conformation. These differences may indicate a different binding mode between PBP2^{WT} and PBP2^{H041}, or they may suggest a shift in position that accompanies the acylation reaction.

3.7.c. Interactions of the C4 carboxylate with S483

In addition to providing structural insight into the trends above for R₁ and R₂, the docking data also model how the bicyclic cephem scaffold might fit into the active site during formation of the tPBP2^{H041}-cephalosporin precovalent complex. In the docking models, most of the cephalosporins interact directly with S483, which is mutated in PBP2^{H041} compared to PBP2^{WT} (from threonine) and contributes to cephalosporin resistance.³⁸⁴ Previously, Tomberg *et al.* postulated that S483 is important for recognition of the C4 carboxylate. In tPBP2^{H041}, a small pocket comprising S362, T/S483, and K497 binds the carboxylate (**Figure 3.23**), orienting the cephem in a position where the β-lactam carbonyl is inaccessible to the serine nucleophile (**Figure 3.5**). This binding mode differs significantly from what is seen in acylated structures of either tPBP2^{WT} or tPBP2^{H041}. In post-covalent crystal structures of tPBP2^{WT} acylated by cefixime or ceftriaxone, the C4 carboxylate interacts instead with the O_γ of T498, which has rotated to accommodate the ligand, bringing the β-lactam ring into optimal position for reaction with S310.¹¹³ In the acyl-enzyme structure of tPBP2^{H041} with ceftriaxone, the C4 carboxylate interacts with S545 in the post-covalent state to generate a binding mode distinct from that observed in tPBP2^{WT}.¹³⁴

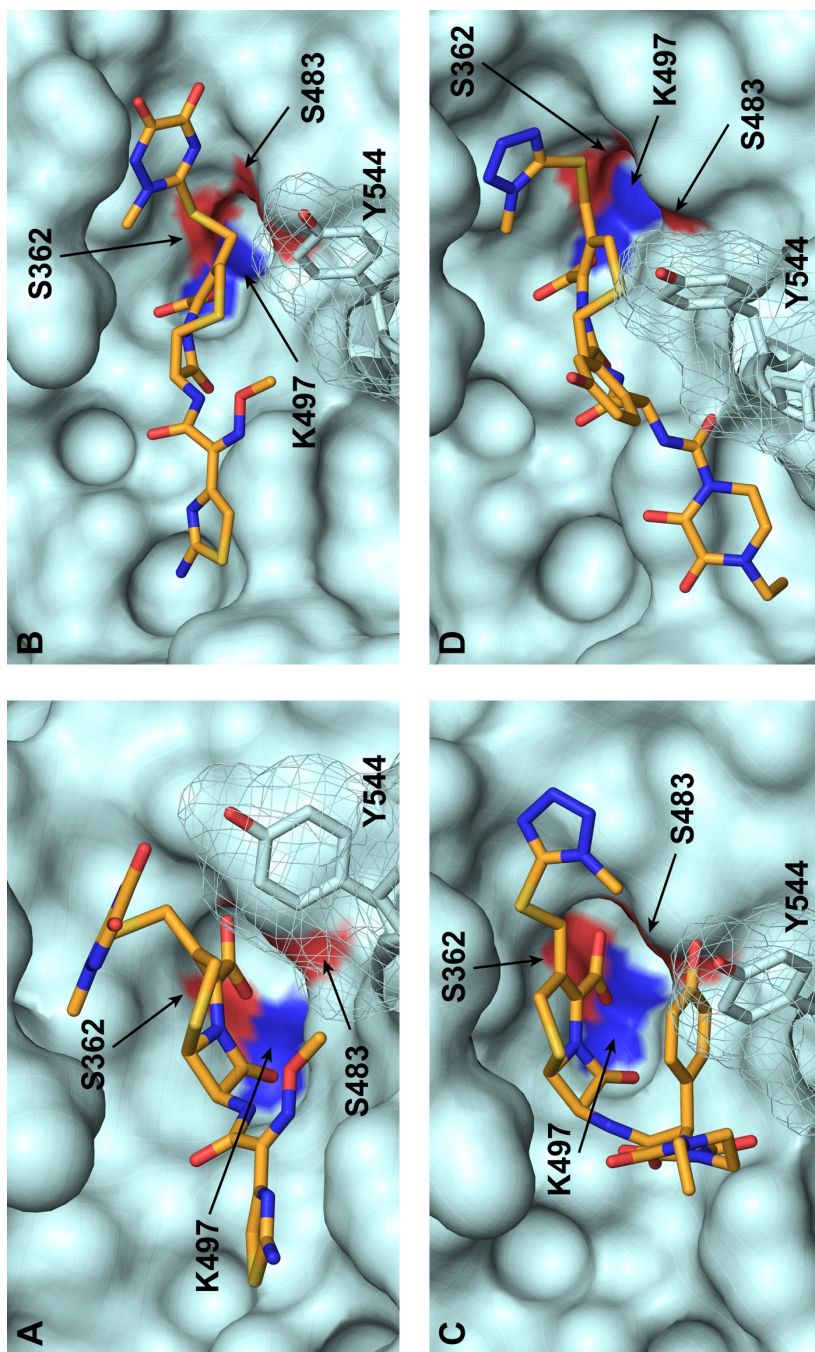


Figure 3.23: Surface views of ceftriaxone and cefoperazone docked to *tPBP2^{H041}*. **A.** In the major pose predicted by the pharmacophore-constrained docking protocol, the C4 carboxylate of ceftriaxone (orange) fits into a small pocket bordered by the side chains of S362, S483, and K497 (surface colored by atom type). **B.** In the minor pose, ceftriaxone is more extended, spanning the active site. **C.** Major pose for cefoperazone (orange). **D.** Minor pose for cefoperazone. Y544 is shown with a transparent mesh surface to visualize the binding pocket.

Repetition of the cephalosporin docking analyses with tPBP2^{WT} shows that the C4 carboxylate interacts with T483 in the *apo* form, occupying a very similar position to what is seen in the major pose of our tPBP2^{H041} docking data. This suggests a similar initial binding mode for both tPBP2^{WT} and tPBP2^{H041} in which T/S483 plays a critical role in carboxylate recognition (**Figure 3.24**). Additional experiments, in which the cephalosporins were docked against the T498-rotated form of tPBP2^{WT}, yield binding modes showing the carboxylate occupying a position closer to that seen in the acyl structure (**Figure 3.25**). However, in tPBP2^{H041}, the T498 side chain participates in a hydrogen bonding interaction with the S545 side chain, preventing its rotation to contact the β -lactam carboxylate during acylation.¹³⁴ As a result, it appears that the cephalosporin receives no enzymatic guidance toward a reactive position (represented in our dataset as the minor pose) when bound to tPBP2^{H041}, slowing the acylation rate. Our data do not explain the final position of the carboxylate in acylated structure of tPBP2^{H041}, however. Although this final position may be achieved during the course of the acylation reaction, more work is needed to confirm the importance residue 483 in initial carboxylate recognition.

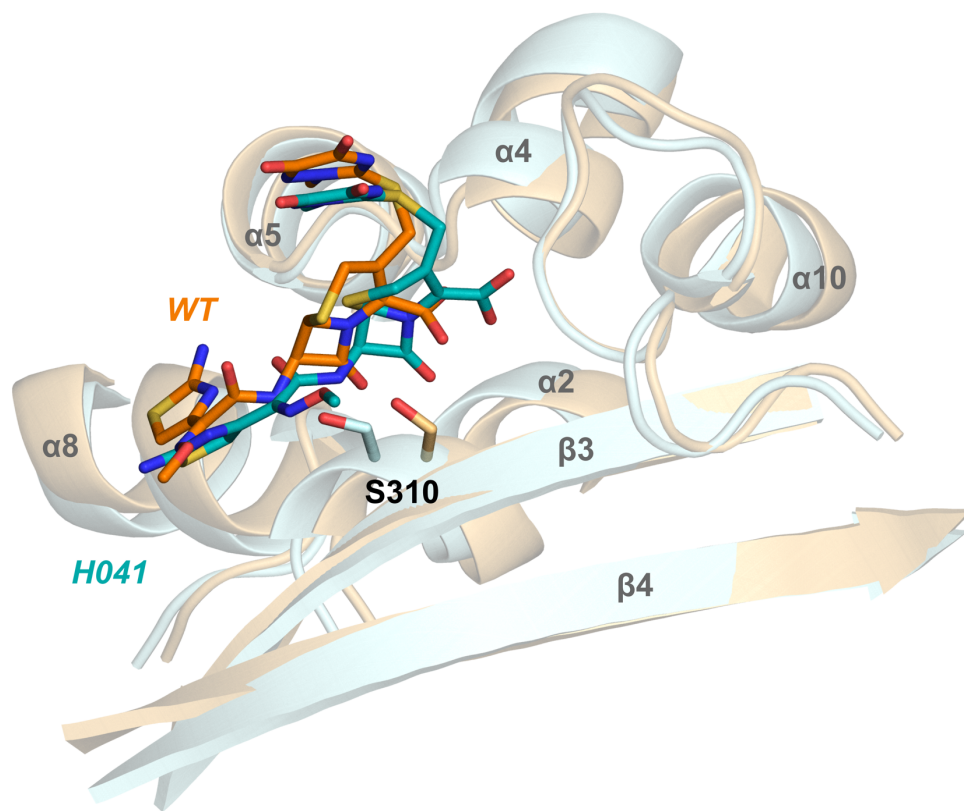


Figure 3.24: Overlay of ceftriaxone docked to apo $tPBP2^{WT}$ with the major pose of ceftriaxone docked to $tPBP2^{H041}$. Docked pre-covalent poses of ceftriaxone with apo $tPBP2^{WT}$ (orange) are very similar to the major pose reported from docking with $tPBP2^{H041}$ (teal).

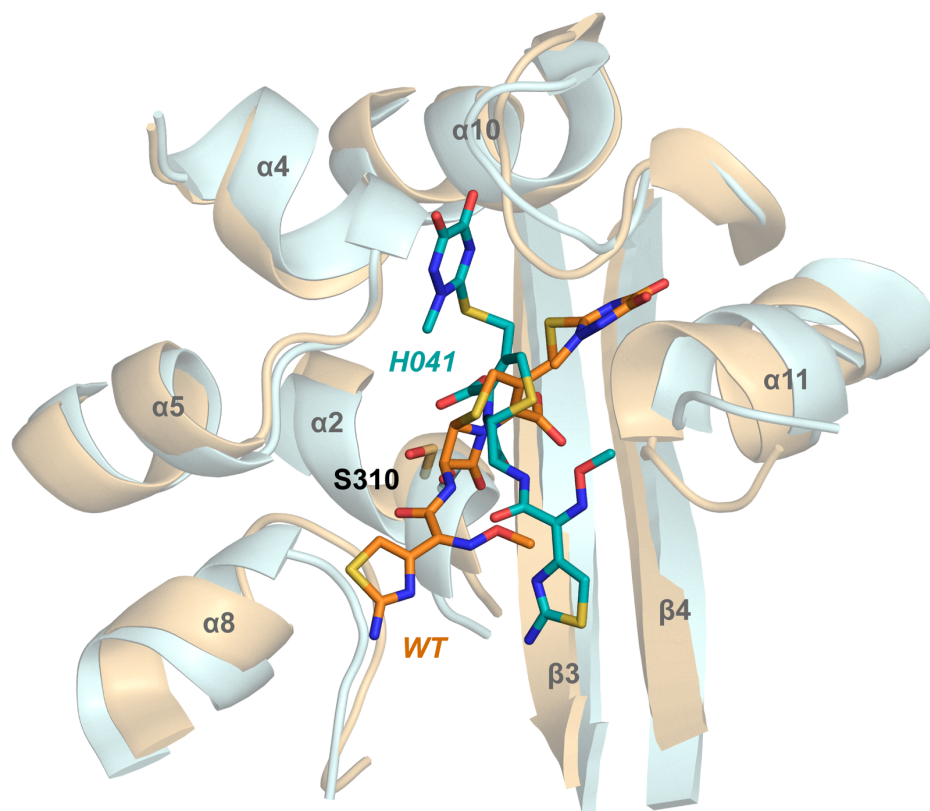


Figure 3.25: Overlay of ceftriaxone docked to T498-rotated $tPBP2^{WT}$ with the minor pose of ceftriaxone docked to $tPBP2^{H041}$. T498 rotation toward the active site in response to carboxylate binding orients the β -lactam ring in preparation for acylation, and also orients the aromatic thiazole toward its final position near $\alpha 8$ ($tPBP2^{WT}$ complex shown in orange). In the absence of this rotation, the ligand receives no enzymatic guidance toward a reactive position ($tPBP2^{H041}$ shown in teal).

3.7.d. Correlations between acylation rate and antimicrobial activity

There is some correlation between acylation rate and antimicrobial activity for the set of cephalosporins. For example, cefoperazone and ceftriaxone, which acylate tPBP2^{H041} rapidly, exhibit the most potent antimicrobial activity, while cefaclor, cefsulodin, cephalexin, and cephalothin, which do not acylate tPBP2^{H041}, exhibit the least. Some cephalosporins, however, deviate significantly from this trend. One reason for these discrepancies can be seen in the antimicrobial activity model, the descriptors of which reflect the ability of a molecule to access the periplasm by traversing the predominant porin in *N. gonorrhoeae* PorB1b, as well as their propensity to be substrates for efflux by the MtrCDE system. In fact, the same amphipathic features of cephalosporins that favor rapid acylation of tPBP2^{H041} (i.e., large, lipophilic R₁ and polar R₂) also result in decreased diffusion through porins and increased efflux.^{317,318} Examples of cephalosporins susceptible to such factors include ceftaroline and ceftobiprole, whose rapid acylation rates contrast with relatively weak antimicrobial potency. This is especially the case for ceftaroline, which is relatively hydrophobic compared to other cephalosporins ($\log D_{7.4} = 1.03$), and is relatively ineffective against H041 *in vitro*.⁴⁴⁴ The picture is less clear for ceftobiprole, whose relative hydrophilicity ($\log D_{7.4} = -2.33$) suggests it less likely to be removed from the gonococcal cell by efflux pumps. However, MtrCDE confers resistance to a number of cationic species and may also transport ceftobiprole.³¹² Strategic addition of anionic groups to cephalosporins exhibiting rapid tPBP2^{H041} acylation may therefore increase antimicrobial activity by increasing aqueous solvation and avoiding efflux mechanisms.

Another reason for the weak correlation between k_2/K_s and antimicrobial activity is that some cephalosporins may acylate PBP1 more rapidly than PBP2. For example, cefdinir and cefoxitin exhibit very slow acylation rates versus tPBP2^{H041}, but high antimicrobial activity (MICs are 1.5 and 3 $\mu\text{g/mL}$, respectively), consistent with them targeting PBP1 rather than PBP2. In fact, cefdinir and cefoxitin generally show preferential

binding to class A and class C PBPs from a number of bacterial species,⁶⁵⁸⁻⁶⁶⁵ and early studies of PBPs from *N. gonorrhoeae* show that cefoxitin acylates PBP1 more rapidly than PBP2 in penicillin-susceptible and -resistant strains.⁶⁶⁶

3.7.e. The potential of cefoperazone to treat ESC-resistant gonorrhea

This work has revealed the third-generation compound cefoperazone is nearly 7-fold more active against tPBP2^{H041} than ceftriaxone, is comparably potent against the H041 strain, and performs similarly in a mouse model of infection. This is consistent with previous studies of gonococcal PBPs that showed cefoperazone bound to PBP2 in membrane preparations at concentrations of less than 10^{-3} $\mu\text{g/mL}$.⁶⁶⁶ It is also consistent with the high activity of ureido penicillins and cephalosporins against class B PBPs from several Gram negative pathogens.^{589,651,667-669} To date, cefoperazone has been reported as being highly effective against infections by both penicillin-susceptible and -resistant gonococci.⁶⁷⁰⁻⁶⁷² Its activity against the H041 strain reported here suggests cefoperazone has potential to address ESC-resistant *N. gonorrhoeae* conferred by mosaic *penA* due to its higher acylation activity against PBP2 compared to ceftriaxone. Cefoperazone is FDA-approved and safe for use in most patients, with tolerated daily doses up to multiple grams and a similar side effect profile to other β -lactam antimicrobials.⁶⁷³ Cephalosporins with *N*-methyltetrazole (NMTT) leaving groups at R₂, such as cefoperazone, have been associated with an increase in prothrombin time (PT) via the inhibition of vitamin K dependent γ -carboxylases by NMTT and its symmetric disulfide oxidation product; however, the IC₅₀ is quite high for each species (~200 and 600 μM , respectively).⁶⁷⁴ Generally, this inhibition results in increases in PT without increases in clinically significant bleeding.⁶⁷⁵ One study shows increased risk with cefoperazone specifically, but cases and controls are poorly matched (*i.e.*, the exposed group had many more comorbidities associated with bleeding).⁶⁷⁶ While the pharmacokinetics of cefoperazone may be less favorable than ceftriaxone for treating urogenital infections, with a $t_{1/2}$ of 1-2 hours (versus

6-8 hours for CRO) and primarily biliary excretion (versus primarily renal for CRO),⁶⁷⁷ it may have utility in the treatment of mucosal infections due to its relative lipophilicity. In the murine model of gonococcal infection, 120 mg/kg cefoperazone administered TID exhibited similar efficacy to an identical regimen of ceftriaxone. With optimized dosing guided by pharmacokinetics, cefoperazone may offer another clinical option for highly resistant gonococcal infections in a relatively barren therapeutic landscape.

3.7.f. Significance

The overall picture emerging from our studies is that rapid tPBP2^{H041} acylation is promoted by a large R₁ (C7 acylamino side chain) with modestly lipophilic properties, and an electronegative R₂ (C3 side chain) with a planar structure. Unfortunately, these properties render cephalosporins less permeable to the Gram negative outer membrane and more prone to efflux, but strategic placement of anionic groups may help to overcome these barriers. Finally, we have shown that cefoperazone holds promise as an antigonococcal agent for strains harboring mosaic *penA* alleles.

CHAPTER 4: Discovery of Novel PBP-Inhibitory Chemotypes as Potential Antigonococcal Agents

4.1. Introduction

Due to their status as critical antibacterial targets, and given the rising number of bacteria resistant to existing β -lactams, the PBPs have become the subjects of numerous drug discovery ventures. Many efforts have centered on the modification of the β -lactam or lactivicin framework, adding novel side chains predicted to show enhanced interaction with the active site. Others have focused on tetrahedral intermediate mimicry via the reaction of phosphonates, boronates, and cyclobutanones with the serine nucleophile. However, if the mutations in PBP2 conferring cephalosporin resistance do so in part by decreasing reactivity to electrophiles, these strategies may prove fruitless.

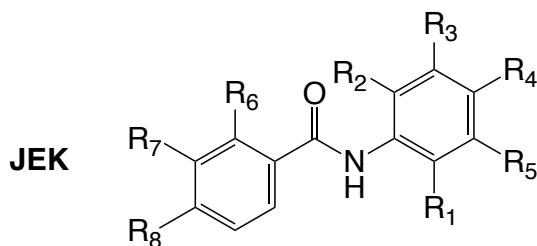
Another, perhaps more urgent, reason to explore non- β -lactam agents as PBP inhibitors is the emergence of highly efficient hydrolytic enzymes. Nearly 1,000 unique β -lactamases have been identified in clinical isolates across species, and extended-spectrum β -lactamases (ESBLs) have emerged in many Gram negative bacteria, including the highly resistant ESKAPE pathogens (*Enterococcus*, *Staphylococcus*, *Klebsiella*, *Acinetobacter*, *Pseudomonas*, and *Enterobacter*), necessitating the identification of alternatives to the current therapies.³⁴⁵ While strains of *Neisseria gonorrhoeae* capable of producing β -lactamases have been isolated, they are rarer than strains harboring chromosomal resistance determinants. Moreover, only penicillinases have been reported in the gonococcus to date.^{18,19,349} Recently, however, plasmids containing *bla*_{TEM-135} have been identified,³⁵⁰⁻³⁵² several of which possess an M182T mutation seen in many ESBL.³⁵¹ It is proposed that this mutation stabilizes the active site and may allow additional mutations to the encoded TEM-135 penicillinase that broaden its spectrum.

For these reasons, high throughput methods (*e.g.*, *in silico* and physical screening) have been employed with the goal of discovering novel chemotypes that inhibit PBPs noncovalently. Although several investigations have identified a number of chemical scaffolds as inhibitors of various class B PBPs, such molecules tend to lack potency and

require a great deal of optimization by medicinal chemistry. The identification of new PBP-inhibitory scaffolds should be continued, as it may increase the number of eventual successful molecules against the target by affording diverse candidates for development. While the specific QSAR models developed in Chapter 3 were constructed using activity data from cephalosporins, the general trends they reveal about features necessary for PBP2 inhibition can be applied to the identification of novel inhibitors. In this chapter, the discovery of two novel *N. gonorrhoeae* PBP2 inhibitors (**JEK-42** and **JMT-1**) possessing a common 1,1'-biphenyl moiety is described. These compounds are capable of inhibiting PBP2 of both β -lactam-susceptible (tPBP2^{WT}) and -resistant (tPBP2^{H041}) strains, and they show antimicrobial activity against *N. gonorrhoeae* FA19 and H041 in disc diffusion assays. Interestingly, they also show inhibition of *P. aeruginosa* PBP3. Through modeling of their PBP2 binding modes by docking and molecular dynamics, we show the potential for interaction with a number of residues conserved across class B PBPs, as well as possible β -lactam mimicry. Finally, we present a three-point pharmacophore model constructed from the structural similarities between these molecules and β -lactams to aid in the identification of additional scaffolds. Overall, our data reveal that **JEK-42** and **JMT-1** are attractive initial hits for medicinal chemical optimization.

4.2. Identification of 2-(biphenylamido)benzoic acids and isosteres as PBP2 inhibitors

4.2.a. Physical screen of (biphenylamido)benzoic acids against *tPBP2^{WT}*



16, 23-26, 29-24, 36-39, 41-46: R₁ = COOH

16:	R ₂ = H	R ₃ = H	R ₄ = H	R ₅ = H	R ₆ = H	R ₇ = H	R ₈ = Ph
23:	R ₂ = Me	R ₃ = H	R ₄ = H	R ₅ = H	R ₆ = H	R ₇ = H	R ₈ = Ph
24:	R ₂ = H	R ₃ = H	R ₄ = F	R ₅ = H	R ₆ = H	R ₇ = H	R ₈ = Ph
25:	R ₂ = F	R ₃ = H	R ₄ = H	R ₅ = H	R ₆ = H	R ₇ = H	R ₈ = Ph
26:	R ₂ = H	R ₃ = F	R ₄ = H	R ₅ = H	R ₆ = H	R ₇ = H	R ₈ = Ph
29:	R ₂ = H	R ₃ = H	R ₄ = F	R ₅ = H	R ₆ = H	R ₇ = Ph	R ₈ = H
30:	R ₂ = H	R ₃ = F	R ₄ = H	R ₅ = H	R ₆ = H	R ₇ = Ph	R ₈ = H
31:	R ₂ = H	R ₃ = H	R ₄ = H	R ₅ = H	R ₆ = Ph	R ₇ = H	R ₈ = H
32:	R ₂ = Me	R ₃ = H	R ₄ = H	R ₅ = H	R ₆ = Ph	R ₇ = H	R ₈ = H
33:	R ₂ = H	R ₃ = H	R ₄ = F	R ₅ = H	R ₆ = Ph	R ₇ = H	R ₈ = H
34:	R ₂ = F	R ₃ = H	R ₄ = H	R ₅ = H	R ₆ = Ph	R ₇ = H	R ₈ = H
36:	R ₂ = Me	R ₃ = H	R ₄ = H	R ₅ = H	R ₆ = 4-MePh	R ₇ = H	R ₈ = H
37:	R ₂ = H	R ₃ = H	R ₄ = H	R ₅ = H	R ₆ = 4-MeOPh	R ₇ = H	R ₈ = H
38:	R ₂ = Me	R ₃ = H	R ₄ = H	R ₅ = H	R ₆ = H	R ₇ = Ph	R ₈ = H
39:	R ₂ = F	R ₃ = H	R ₄ = H	R ₅ = H	R ₆ = H	R ₇ = Ph	R ₈ = H
41:	R ₂ = H	R ₃ = F	R ₄ = H	R ₅ = H	R ₆ = Ph	R ₇ = H	R ₈ = H
42:	R ₂ = H	R ₃ = H	R ₄ = F	R ₅ = H	R ₆ = H	R ₇ = H	R ₈ = 4-MePh
43:	R ₂ = H	R ₃ = H	R ₄ = F	R ₅ = H	R ₆ = 4-MePh	R ₇ = H	R ₈ = H
44:	R ₂ = Me	R ₃ = H	R ₄ = H	R ₅ = H	R ₆ = 2-MeOPh	R ₇ = H	R ₈ = H
45:	R ₂ = H	R ₃ = H	R ₄ = F	R ₅ = H	R ₆ = H	R ₇ = 4-MePh	R ₈ = H
46:	R ₂ = H	R ₃ = H	R ₄ = H	R ₅ = H	R ₆ = H	R ₇ = Ph	R ₈ = H

27, 28, 35: R₁ = H

27:	R ₂ = H	R ₃ = H	R ₄ = H	R ₅ = COOH	R ₆ = H	R ₇ = H	R ₈ = Ph
28:	R ₂ = H	R ₃ = H	R ₄ = COOH	R ₅ = H	R ₆ = H	R ₇ = H	R ₈ = Ph
35:	R ₂ = H	R ₃ = H	R ₄ = H	R ₅ = COOH	R ₆ = Ph	R ₇ = H	R ₈ = H

Figure 4.1: Structures of compounds reported by Kirkpatrick et al. (coded JEK-XX).

From the ligand binding data (*i.e.*, cephalosporin docking data and structure-activity relationships) described in Chapter 3, we found that large, somewhat lipophilic groups of high cyclicality are favored in the direction of the cephalosporin R₁ side chain. This information, in combination with the knowledge that active β -lactam antimicrobials require a specific spatial arrangement of their carboxylate and carbonyl groups for binding to PBPs,¹⁴² led to the selection of a group of (biphenylamido)benzoic acids as possible PBP2 binders (**Figure 4.1**), 24 of which were synthesized and provided by Joy Kirkpatrick. Testing of these compounds against tPBP2^{WT} revealed 2-(4'-methyl-[1,1'-biphenyl]-4-amido)-5-fluorobenzoic acid (**JEK-42**) and 2-(4'-methyl-[1,1'-biphenyl]-3-amido)-5-fluorobenzoic acid (**JEK-45**) as active in a competition assay with Bocillin-FL, exhibiting 89 \pm 5% and 86 \pm 4% inhibition at 100 μ M, respectively (**Figure 4.2A**). The beginnings of a structure-activity relationship can be seen from comparisons within this dataset (**Figure 4.2B**). First, a switch from anthranilic acid to its *meta*- or *para*-benzoic acid analogues results in little to no PBP2 inhibition. The substitution pattern of the anthranilic acid moiety also affects inhibition, with 3-substituted and fully unsubstituted systems showing greatly diminished activity compared to 4- and 5-substituted analogues. Next, a [1,1'-biphenyl]-4-amido or [1,1'-biphenyl]-3-amido structure is preferred, as [1,1'-biphenyl]-2-amido analogues of these compounds suffer a stark loss of potency. Finally, a 4'-methyl substitution appears to enhance inhibition considerably, as the only 4'-desmethyl analogue with any activity is the weak inhibitor **JEK-30** (27 \pm 10% inhibition). Due to its reasonable inhibition of tPBP2^{WT} at the concentration assayed, as well as the commercial availability of its building blocks, **JEK-42** was selected as a hit compound for further testing and derivatization.

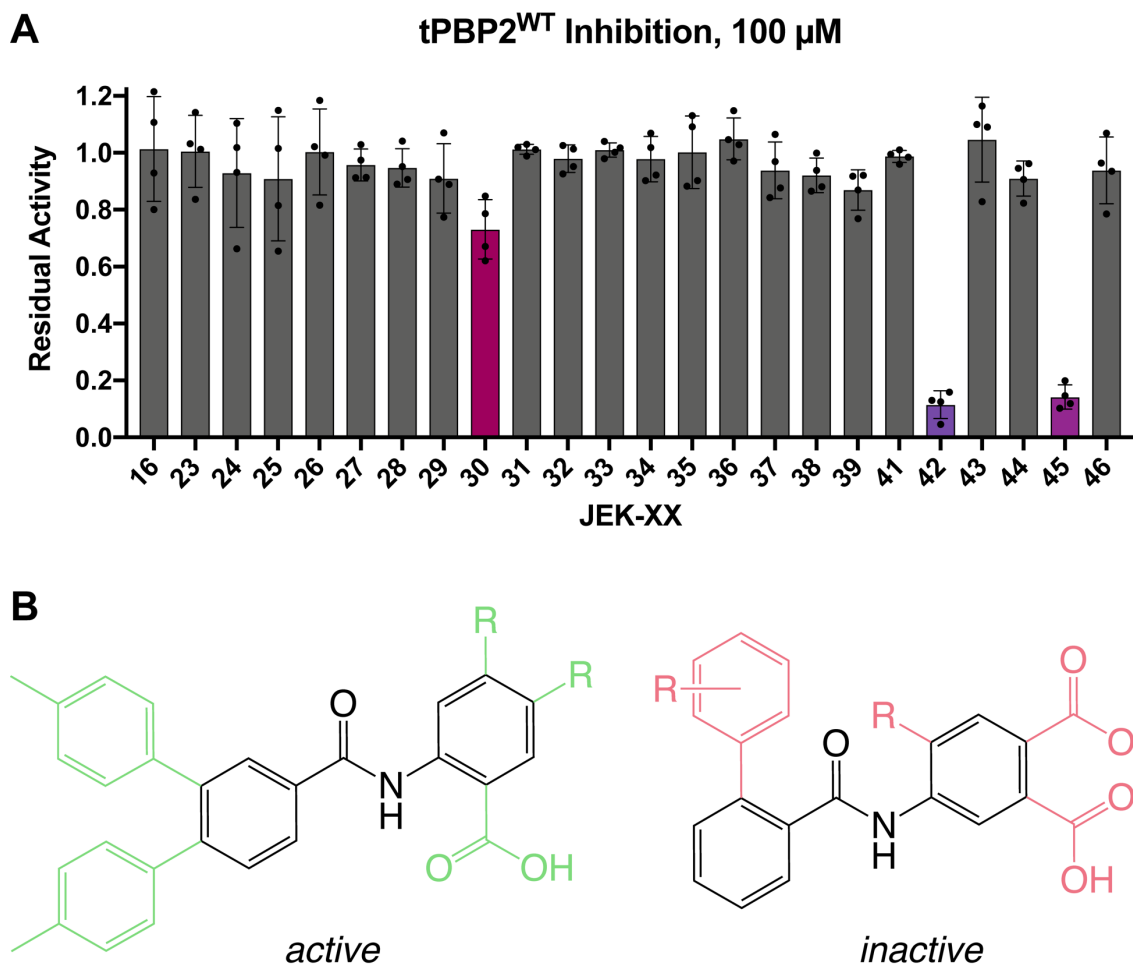
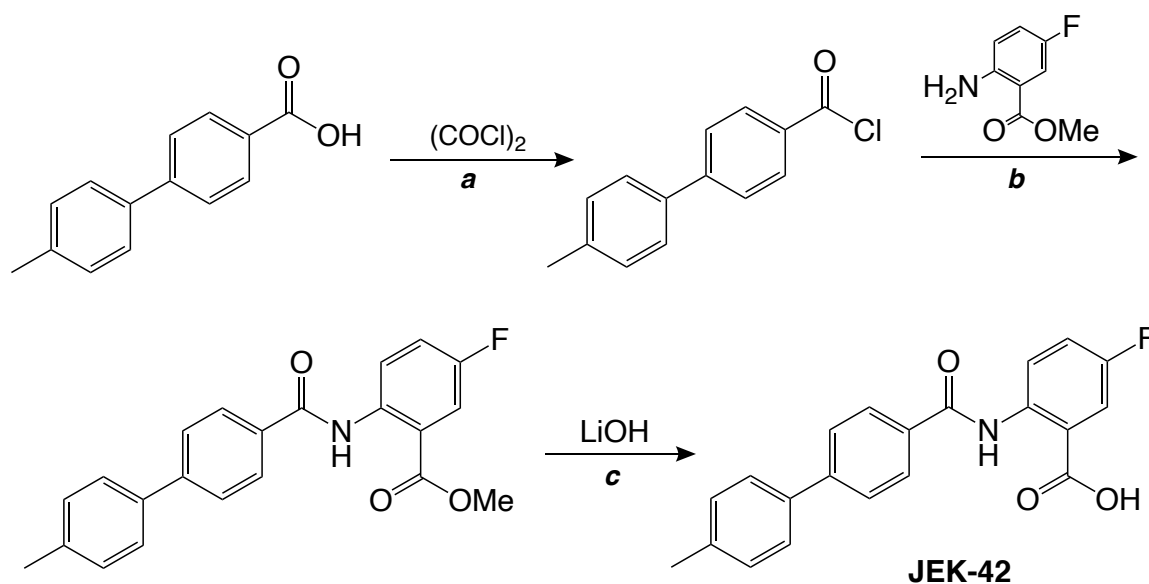


Figure 4.2: Inhibition data for JEK compounds against tPBP2^{WT}. **A.** Values were determined in a purified protein assay in which tPBP2^{WT} was preincubated with 100 μ M compound, followed by addition of 1 μ M Bocillin-FL. Data are presented as a fraction of DMSO control. Error bars are standard deviation. **B.** Structural features of PBP2-inhibitory (green) and -noninhibitory (red) compounds.

JEK-42 was resynthesized from 4'-methyl-[1,1'-biphenyl]-4-carboxylic acid and methyl 5-fluoroanthranilate using the method shown in **Scheme 4.1**. The compound was tested for inhibition of tPBP2^{H041} at 100 μ M and showed $99 \pm 1\%$ suppression of activity (**Figure 4.3A**). Further evaluation in a disc diffusion assay against *N. gonorrhoeae* FA19 and H041 revealed that **JEK-42** inhibits growth of these strains with 18.0 ± 0.9 mm and 15.3 ± 0.4 mm zones of inhibition, respectively (**Figure 4.3B**). This inhibition is comparable to a ceftriaxone control disc, which shows zones of inhibition measuring 19.3 ± 1.3 mm against FA19 and 14.6 ± 3.8 mm against H041. To assess the possibility for broad-spectrum activity, the compound was also assayed against *Pseudomonas aeruginosa* PBP3, against which it showed $74 \pm 1\%$ inhibition (**Figure 4.3A**).



Scheme 4.1: Synthesis of JEK-42 from 4'-methyl-[1,1'-biphenyl]-4-carboxylic acid. **a.** DMF, DCE, N_2 , RT, 12 h. **b.** pyridine, DCM, N_2 , RT, 8 h. **c.** 1:1 THF/ H_2O , RT, 12 h.

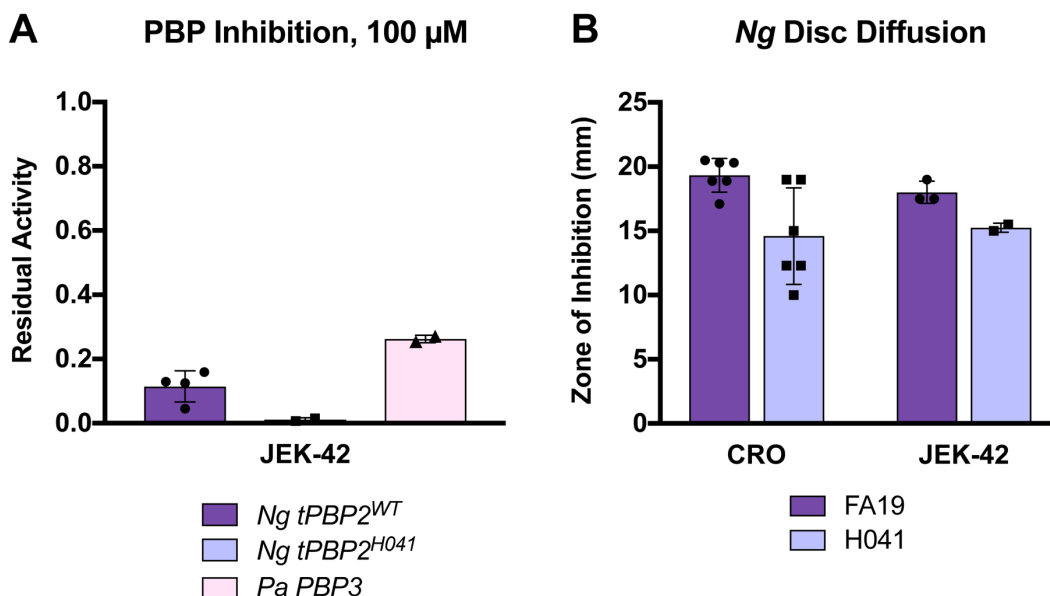
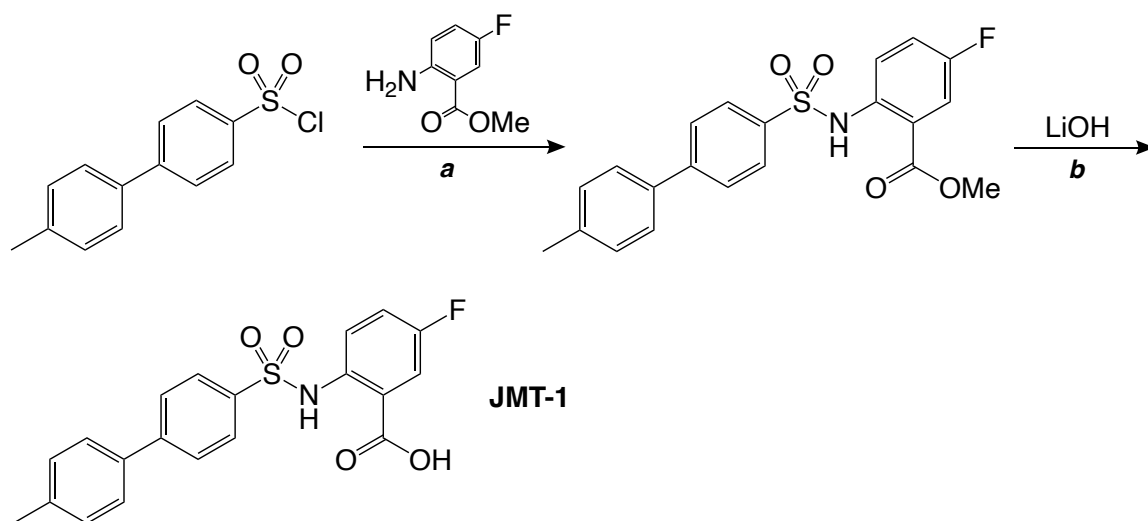


Figure 4.3: Activity data for JEK-42. **A.** PBP inhibition was determined in a purified protein assay in which a given PBP was preincubated with 100 μ M compound, followed by addition of 1 μ M Bocillin-FL. Data are presented as a fraction of DMSO control. **B.** Antimicrobial activity was determined in a disc diffusion assay against susceptible reference gonococcal strain FA19 and multi-drug resistant H041 at 10 μ g per disc. Data for a ceftriaxone control disc (CRO) are shown. Error bars are standard deviation.

4.2.b. Synthesis and testing of a sulfonamide derivative of JMT-1

To examine the effect of modifications to the carbonyl group of **JEK-42**, simple isosteric substitution of the amide with a sulfonamide was performed to give 5-fluoro-2-(4'-methyl-[1,1'-biphenyl]-4-sulfonamido)benzoic acid (**JMT-1**), obtained from 4'-methyl-[1,1'-biphenyl]-4-sulfonyl chloride and methyl 5-fluoroanthranilate using the synthetic method shown in **Scheme 4.2**. **JMT-1** was screened at 100 μ M against both tPBP2^{WT} and tPBP2^{H041}, against which it showed 93 \pm 7% and 84 \pm 2% inhibition, respectively (**Figure 4.4A**). The compound was found to have antimicrobial activity as well, albeit slightly less than that of **JEK-42**. In disc diffusion assays, **JMT-1** exhibits a 16.7 \pm 1.2 mm zone of inhibition against *N. gonorrhoeae* FA19 and a 10.8 \pm 0.4 mm zone of inhibition against *N. gonorrhoeae* H041 (**Figure 4.4B**). The compound is also active against *P. aeruginosa* PBP3, showing 70 \pm 2% inhibition at 100 μ M (**Figure 4.4A**).



Scheme 4.2: Synthesis of JMT-1 from 4'-methyl-[1,1'-biphenyl]-4-sulfonyl chloride. **a.** pyridine, DCM, N₂, RT, 12 h. **b.** 1:1 THF/H₂O, RT, 12 h.

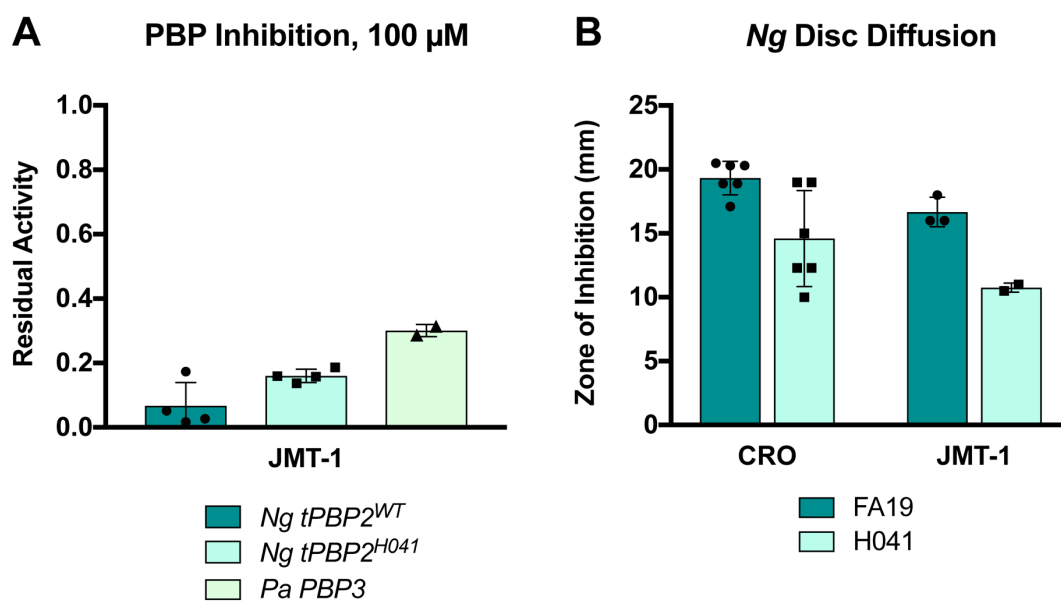


Figure 4.4: Activity data for sulfonamide derivative JMT-1. **A.** PBP inhibition was determined in a purified protein assay in which a given PBP was preincubated with 100 μ M compound, followed by addition of 1 μ M Bocillin-FL. Data are presented as a fraction of DMSO control. **B.** Antimicrobial activity was determined in a disc diffusion assay against susceptible reference gonococcal strain FA19 and multi-drug resistant H041 at 10 μ g per disc. Data for a ceftriaxone control disc (CRO) are shown. Error bars are standard deviation.

4.3. Prediction of the binding modes of JEK-42 and JMT-1

4.3.a. In tandem docking and molecular dynamics against *tPBP2^{WT}* and *tPBP2^{H041}*

Important for inhibition by the amides and sulfonamides is the presence of an anthranilic acid motif, and not its *meta*- or *para*-aminobenzoic acid analogues. This is perhaps due to the same constraints placed on β -lactam antimicrobials for their mimicry of the D-Ala-D-Ala substrate of peptidoglycan. Depending upon the C1-C2-N-C dihedral (or C1-C2-N-S in the case of sulfonamides), the distance between the carboxylate carbon and the amide oxygen in these molecules (analogous to the Cohen distance in β -lactams) ranges from 2.5 Å to 5.0 Å. Thus, in certain conformations, the reported scaffolds may be capable of mimicking β -lactams in their binding to PBPs. A comparison of the structural similarities among cepheids, **JEK-42**, and **JMT-1** is shown in **Figure 4.5**.

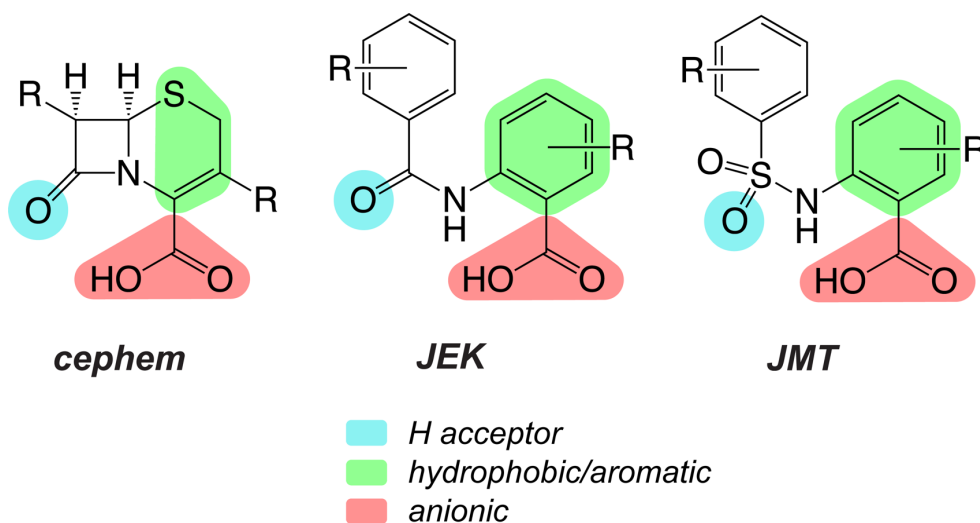


Figure 4.5: Structural similarities between cepheids and the base scaffolds of JEK-42 and JMT-1. The examined PBP2 inhibitors share a triad of features, including an acidic group, a hydrogen bond acceptor, and a hydrophobic/aromatic group.

Initial attempts to crystallize these compounds in complex with tPBP2 variants were unsuccessful, perhaps due to their limited affinity and aqueous solubility. For this reason, *in silico* tools were employed to model their potential binding modes. Using constraints informed by structures of PBP2 variants in complex with ceftriaxone, ligands **JEK-42** and **JMT-1** were flexibly docked into the active sites of tPBP2^{WT} and tPBP2^{H041}, followed by 5 ns molecular dynamics simulations to assess the stability of the generated poses. While substantial movement of the ligand anionic group is observed in the first 500 ps for simulations of **JEK-42** and **JMT-1** in complex with tPBP2^{WT} (**Figures 4.6** and **4.7**), the modeled complexes are stable for the remaining 4.5 ns according to measurements of ligand-tPBP2 interaction energy, ligand internal energy, and root mean square deviation (rmsd) of the ligand from its initial position (**Figures 4.6** and **4.9**). The tPBP2^{H041} complexes are stable for the entirety of the simulation by these same measures (**Figures 4.6**, **4.8**, and **4.10**). Overall, the consistency of energy scores and ligand positions indicate that the *in silico* analyses generated reasonable hypotheses for the ligands' true binding modes at equilibrium.

In the modeled poses, **JMT-1** shows a more favorable interaction energy with both tPBP2^{WT} and tPBP2^{H041} compared to **JEK-42**, due in large part to improved electrostatics (**Table 4.1**). However, while the sulfonamide may provide better contact with the active site, it appears to do so at the expense of ligand internal energy, as **JMT-1** must assume a higher energy conformation for binding to the transpeptidase active site. A majority of this energy comes from angle bending and intramolecular electrostatic repulsion. Interestingly, while **JMT-1** exhibits a significant reduction in interaction energy with tPBP2^{H041} compared to tPBP2^{WT}, there is no such reduction for **JEK-42**. This is a possible explanation for the relative activities of the compounds against tPBP2^{H041} in the *in vitro* competition assay with Bocillin-FL.

Table 4.1: Summary data for molecular dynamics simulations of JEK-42 and JMT-1 in complex with tPBP2. ^aAverage energy calculated from the state of the system in intervals of 500 ps ($n = 11$). ^bOverall variation in tPBP2 complex structure, as calculated by the alignment and superimposition of 11 states representing the system at 500 ps intervals. ^cTotal ligand displacement from its initial position.

	Receptor	tPBP2 ^{WT}		tPBP2 ^{H041}	
	Ligand	JEK-42	JMT-1	JEK-42	JMT-1
Ligand-Receptor Interaction Energies (kcal mol ⁻¹) ^a	Overall	-155.3 ± 11.8	-234.7 ± 9.8	-123.2 ± 4.9	-158.4 ± 12.6
	van der Waals	-26.1 ± 4.3	-26.4 ± 4.6	-29.1 ± 3.7	-32.2 ± 3.7
	Electrostatics	-129.0 ± 16.4	-208.5 ± 16.2	-123.2 ± 4.9	-125.9 ± 13.8
Ligand Internal Energy (kcal mol ⁻¹) ^a	Overall	60.5 ± 7.2	131.9 ± 6.4	56.0 ± 8.2	152.4 ± 4.7
	Strain	8.1 ± 3.7	10.1 ± 4.5	9.1 ± 4.3	9.9 ± 4.5
	Angle Bend	21.6 ± 4.3	37.8 ± 5.3	19.5 ± 3.7	41.3 ± 3.3
	Out of Plane	3.7 ± 1.8	2.8 ± 1.5	4.2 ± 1.6	5.0 ± 1.9
	Torsion	29.2 ± 4.0	21.9 ± 3.9	23.4 ± 3.8	27.0 ± 4.3
	van der Waals	11.0 ± 2.1	11.6 ± 2.2	13.4 ± 2.5	9.1 ± 1.3
	Electrostatics	-16.1 ± 4.0	47.4 ± 4.7	-15.0 ± 6.4	57.7 ± 3.4
Complex rmsd (Å) ^b		0.920	1.114	0.554	1.013
Ligand rmsd (Å) ^c		2.4	1.5	1.3	1.9

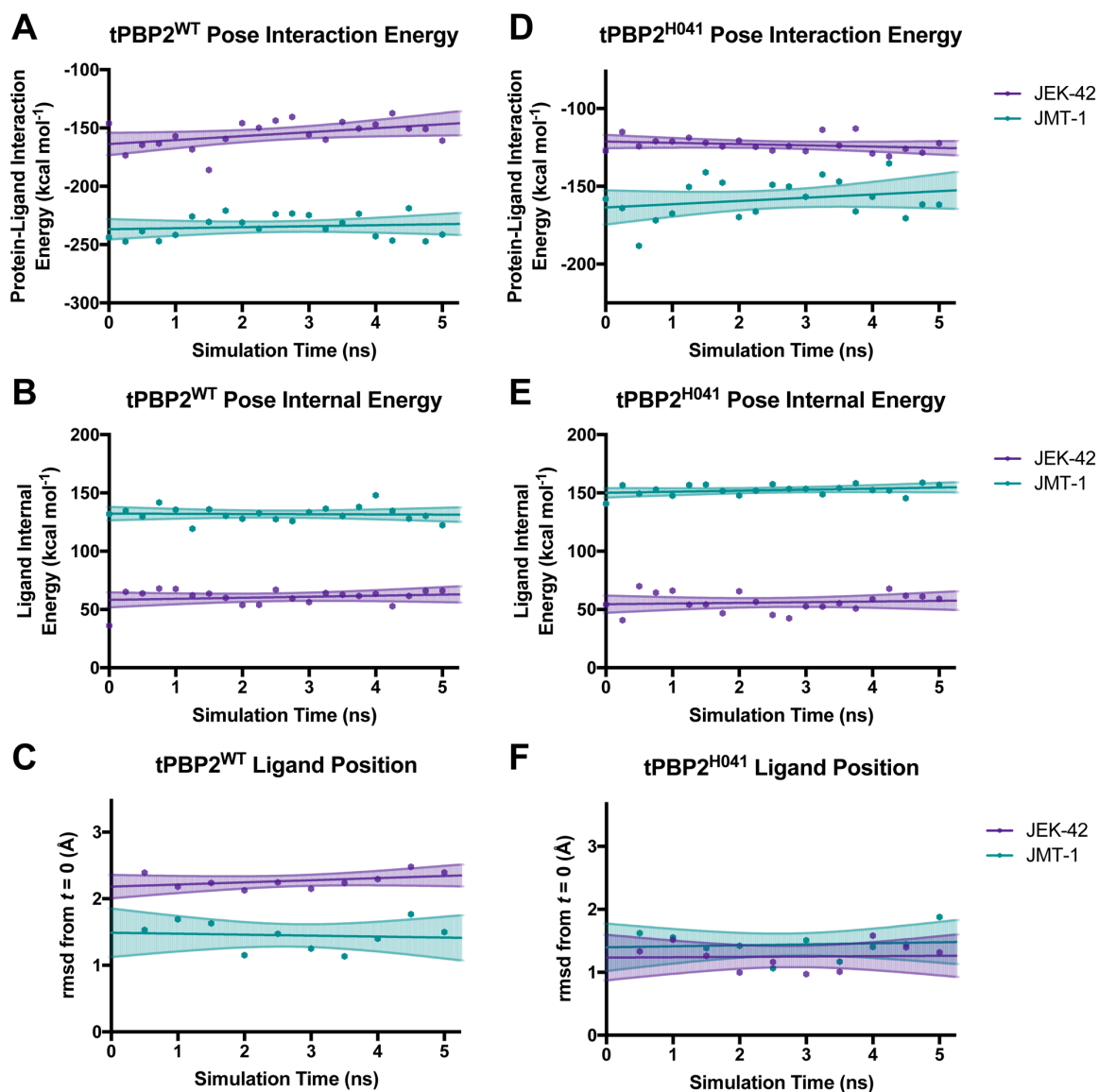


Figure 4.6: Energy and position analyses for molecular dynamics simulations of JEK-42 and JMT-1 in complex with $tPBP2^{WT}$ and $tPBP2^{H041}$. **A.** Potential energy of interaction was calculated for the $tPBP2^{WT}$ -JMT complexes at intervals of 250 ps. Data beyond 500 ps were fit to linear regressions to determine change in attractive/repulsive forces in the active site over time. All slopes are statistically insignificant. **B.** Ligand potential energy was calculated for poses in complex with $tPBP2^{WT}$ at intervals of 250 ps. Data beyond 500 ps were fit to linear regressions to determine change in pose energetic favorability over time. All slopes are statistically insignificant. **C.** Ligand displacement from its initial pose was calculated at intervals of 500 ps. Data beyond 500 ps were fit to linear regressions to determine ligand movement over time. All slopes are statistically insignificant. **D.** Potential energy of interaction analysis for $tPBP2^{H041}$ -JMT complexes. All slopes are statistically insignificant. **E.** Ligand potential energy analysis for $tPBP2^{H041}$ -JMT complexes. All slopes are statistically insignificant. **F.** Ligand displacement analysis for $tPBP2^{H041}$ -JMT complexes.

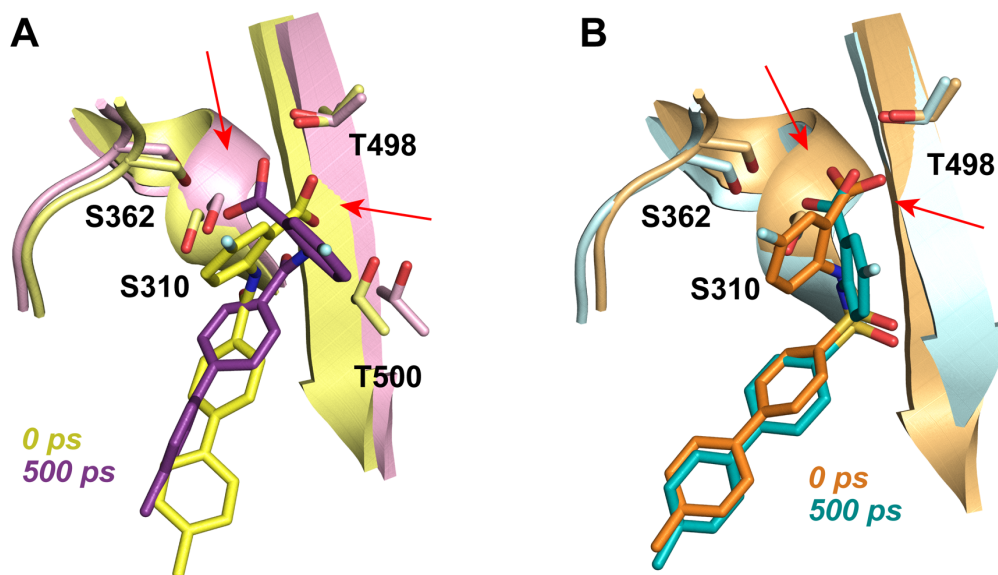


Figure 4.7: Change in positions of JEK-42 (**A**) and JMT-1 (**B**) in the active site of *tPBP2^{WT}* over the first 500 ps of molecular dynamics simulations. **A.** In the first 500 ps of the molecular dynamics simulation, JEK-42 moves to an rmsd of 2.4 Å, much of which is accounted for by the flipping of the anthranilic acid moiety. At the start of the simulation (ligand and receptor shown in yellow), the carboxylic acid faces T498, and the aromatic ring is angled such that it faces S310. At the end of the initial phase of the simulation (ligand shown in purple, receptor shown in pink), it has rotated approximately 90° such that the carboxylic acid now faces S310 and S362. **B.** JMT-1 moves to an rmsd of 1.5 Å in the first phase of the simulation. Like JEK-42, its carboxylic acid faces T498 at the start of the simulation (shown in orange), and by 500 ps (ligand shown in teal, receptor shown in cyan), the aromatic ring has rotated approximately 60° such that the carboxylic acid faces S310 and S362.

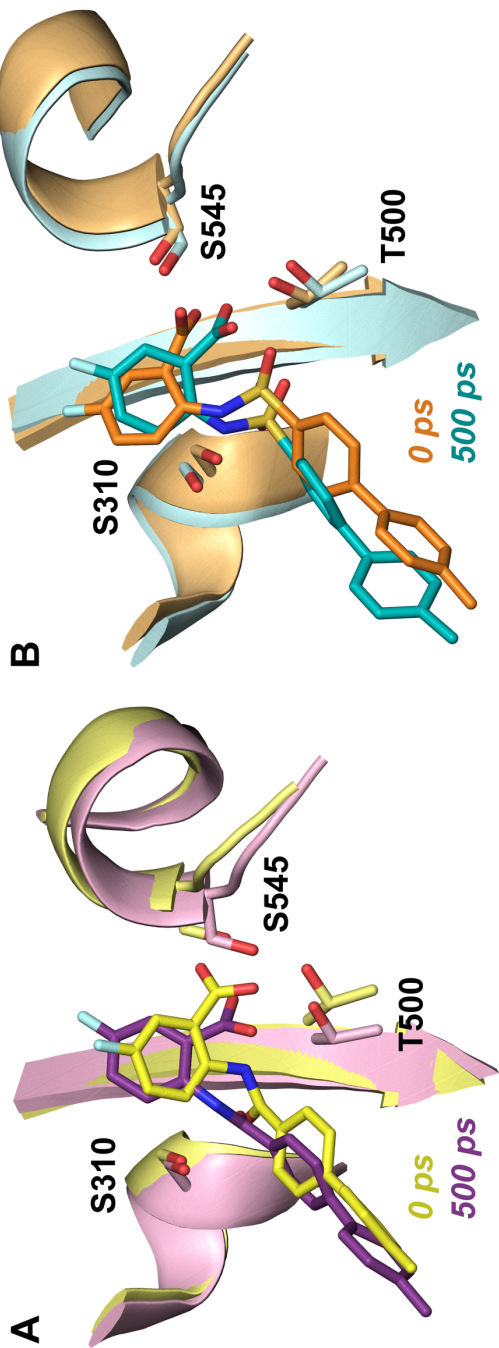


Figure 4.8: Change in positions of JEK-42 (A) and JMT-1 (B) in the active site of *tPBP2^{H041}* over the first 500 ps of molecular dynamics simulations. A. In the first 500 ps of the molecular dynamics simulation, JEK-42 does not experience much movement (rmsd of 1.3 Å). The carboxylic acid faces S545 both at the beginning (shown in yellow) and at the end of this period (ligand shown in purple, receptor shown in pink). B. JMT-1 also shows very little positional change over the initial phase of the simulation, moving to an rmsd of 1.6 Å. Like JEK-42, its carboxylic acid faces S545 both at the start (shown in orange), and at 500 ps (ligand shown in teal, receptor shown in cyan).

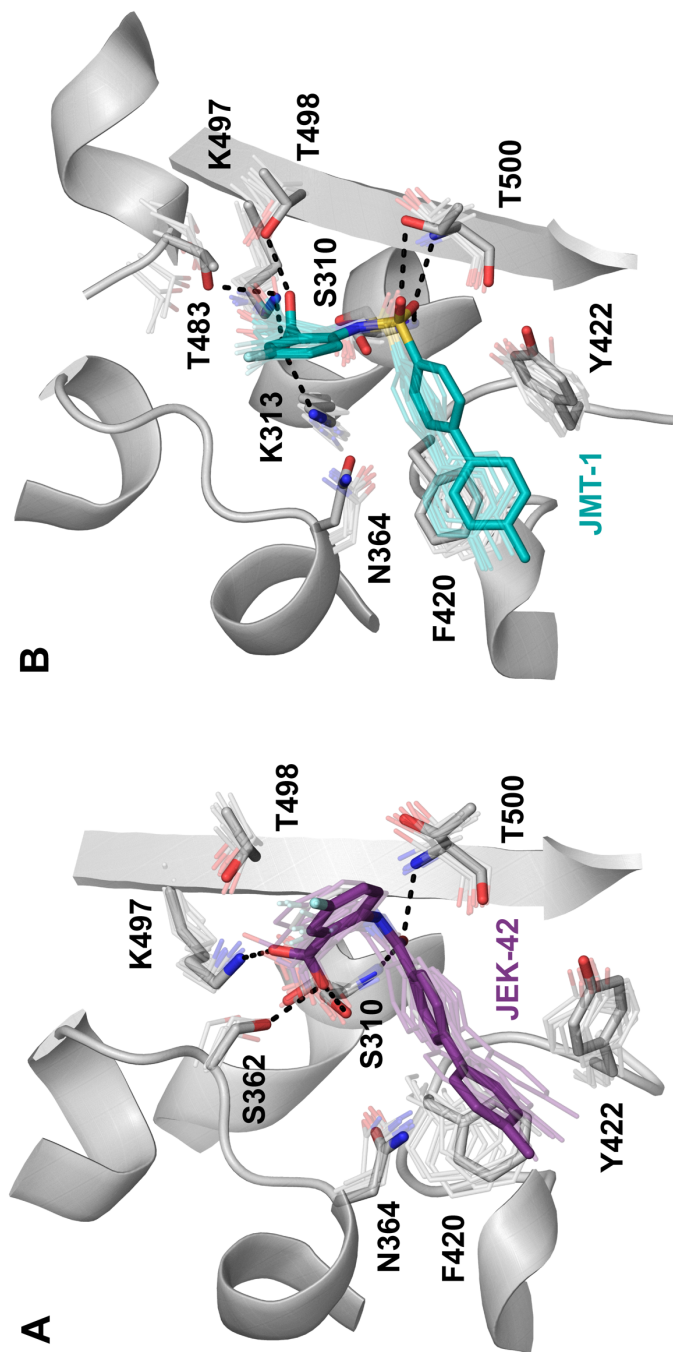


Figure 4.9: Molecular dynamics simulations of JEK-42 (A) and JMT-1 (B) in complex with tPBP2^{WT}. A. In the later stages of the molecular dynamics simulation, JEK-42 (purple) does not experience significant movement in the active site of tPBP2^{WT}. States isolated at 500-ps intervals are indicated by transparent sticks. In its final position (solid sticks), the carboxylic acid interacts with the side chains of S310, S362, and K497, and the amide carbonyl oxygen projects into the oxyanion hole created by S310 and T500. B. JMT-1 (teal) also shows very little positional change in the later stages of the simulation (timepoints represented as transparent sticks, final position represented as solid sticks). In its final position, the carboxylic acid interacts with the side chains of K313, T483, K497, and T498, and one sulfonyl oxygen projects into the oxyanion hole.

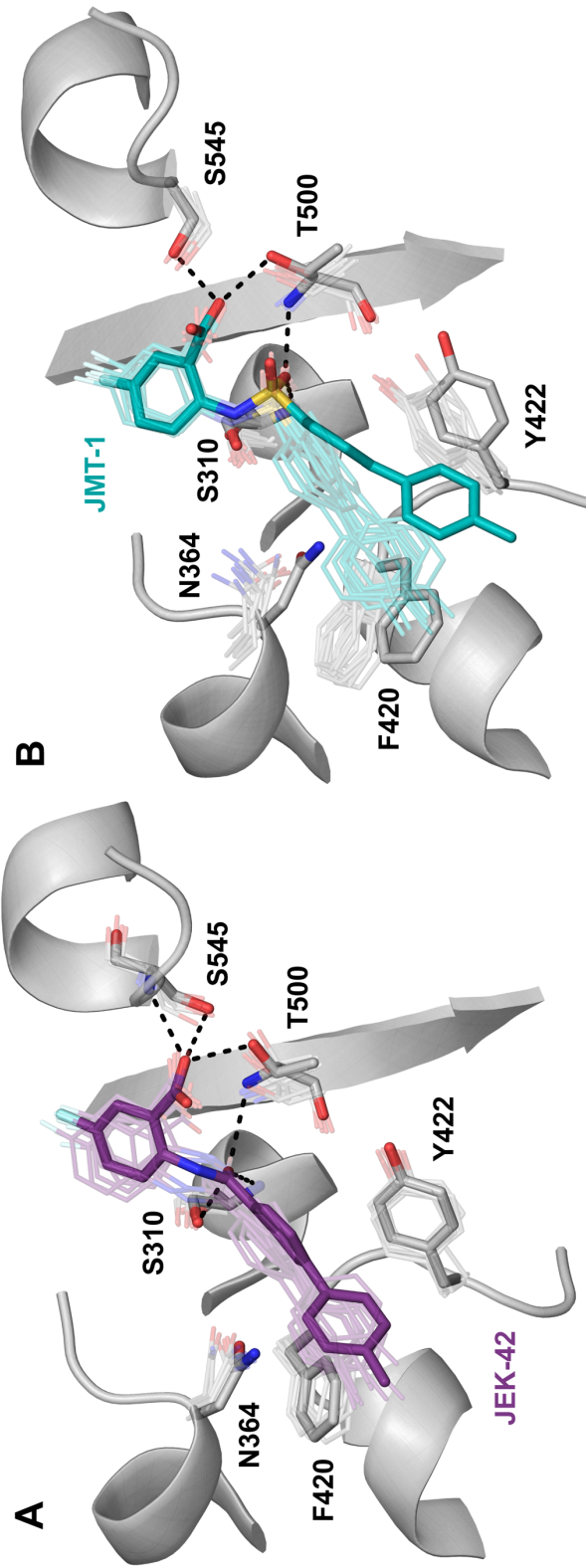


Figure 4.10: Molecular dynamics simulations of JEK-42 (A) and JMT-1 (B) in complex with tPBP2^{H041}. A. In the later stages of the molecular dynamics simulation, JEK-42 (purple) does not experience significant movement in the active site of tPBP2^{H041}. States isolated at 500-ps intervals are indicated by transparent sticks. In its final position (solid sticks), the carboxylic acid interacts with the side chains of T500 and S545, and the amide carbonyl oxygen projects into the oxyanion hole created by S310 and T500. B. JMT-1 (teal) also shows very little positional change in the later stages of the simulation (timepoints represented as transparent sticks, final position represented as solid sticks). In its final position, the carboxylic acid interacts with the side chains of T500 and S545, and one sulfonyl oxygen projects into the oxyanion hole.

For all complexes examined, a carbonyl or sulfonyl oxygen is positioned within the oxyanion hole created by the main chain nitrogens of Ser310 and Thr500, a position that is well-maintained throughout all molecular dynamics simulations (**Figure 4.11A**). An additional hydrogen bond is observed between the second sulfonyl oxygen of **JMT-1** and the side chain of Thr500. Also consistent across models is the position of the 1,1'-biphenyl system, which projects into a hydrophobic patch comprising Phe420 and Tyr422 (**Figure 4.11B**). In the distribution of states seen over the course of the simulations, these 1,1'-biphenyl systems assume two predominant positions related by rotation: one in which the secondary aromatic ring forms H- π interactions with Asn364, and one in which it participates in π -stacking with Phe420. There is another less abundant state in which the ring participates in π -stacking with Tyr422.

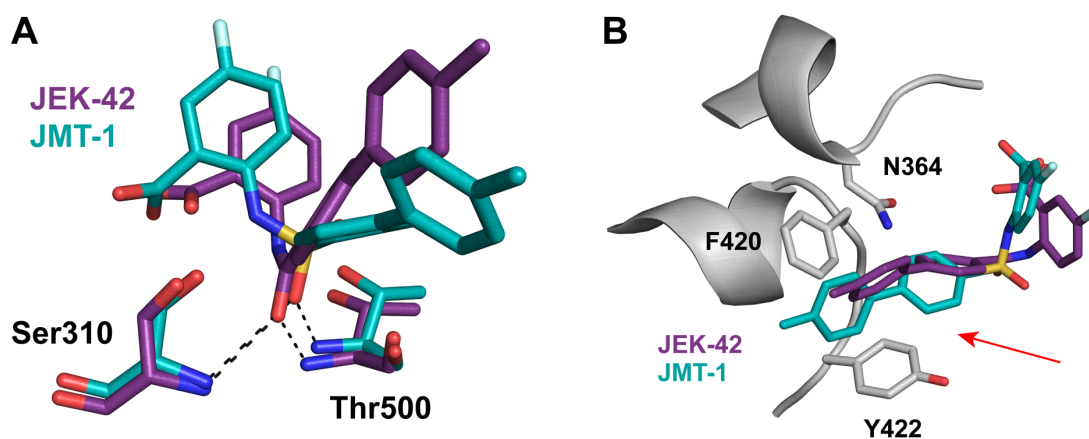


Figure 4.11: Common interactions of JEK-42 and JMT-1 with tPBP2. **A.** The carbonyl or sulfonyl oxygens of the ligands fits into the oxyanion hole created by the main chain nitrogens of S310 and T500 over the course of the molecular dynamics simulations. Polar contacts with the main chain are shown as black dashed lines. **B.** The biphenyl moieties of all three ligands sit in a hydrophobic patch of tPBP2 surface created by the side chains of F420 and T422 and can participate in either π - π interactions with these residues, or in H- π interactions with the N364 side chain.

Differences among the modeled complexes are apparent in the positioning of the acidic moieties of the ligands. For models of **JEK-42** and **JMT-1** in complex with tPBP2^{WT}, the anthranilic acid moieties adopt different orientations, perhaps due to differences in the geometries of their carbonyl (sp^2) and sulfonyl (sp^3) functional groups (**Figure 4.9**). **JEK-42** is positioned such that the anthranilic acid ring is angled toward $\beta 3$ and $\alpha 11$, with its carboxylate contacting the side chains of Ser310, Ser362, and Lys497. In the **JMT-1** complex, the anthranilic acid moiety occupies a more central position in the active site, and its carboxylate makes contacts with the side chains of Lys313, Thr483, Lys497, and Thr498. By contrast, in tPBP2^{H041}-bound poses, the anthranilic acid moieties of **JEK-42** and **JMT-1** are nearly identical (**Figure 4.10**). In the absence of Thr498 rotation toward a bound acidic group, the carboxylate participates in hydrogen bonding with Ser545 and Thr500, and the aromatic ring lies flat along the floor of the active site.

4.3.b. Homology modeling and rigid alignment of class B PBPs

As noted above, the docking and molecular dynamics data reveal potential interactions of the 1,1'-biphenyl systems of **JEK-42** and **JMT-1** with N364 and F420 of PBP2. As part of the SxN motif, N364 is highly conserved in bacterial transpeptidases. Examination of crystal structures and homology models of class B PBPs (model statistics for which are shown in **Chapter 3**) reveals that F420 is also highly conserved, with an aromatic residue being present at this position in many Gram-negative and Gram-positive pathogens (**Figure 4.12, Table 4.2**). If the proposed binding modes for **JEK-42** and **JMT-1** are correct, conservation of both N364 and F420 indicates promise for inhibition of a variety of class B PBPs and, thus, potential for broad spectrum antimicrobial activity.

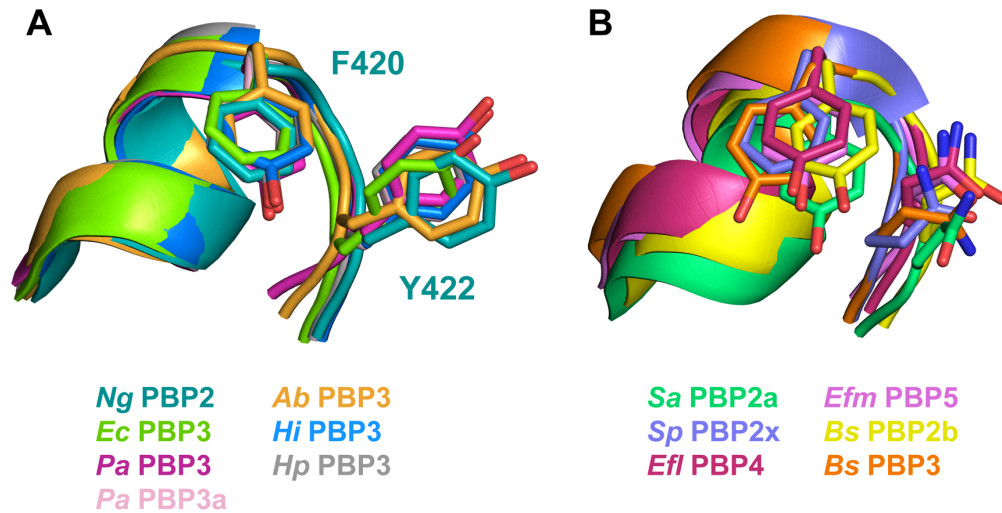


Figure 4.12: Alignment of $\alpha 8$ of class B PBPs showing conservation of an aromatic residue in several important Gram negative and Gram positive pathogens. **A.** In Gram negative pathogens, aromatic residues are conserved at the positions of F420 and Y422, creating an aro-x-aro motif. *N. gonorrhoeae* PBP2 (teal), *E. coli* PBP3 (chartreuse), *P. aeruginosa* PBP3 (magenta), *P. aeruginosa* PBP3a (pink), *A. baumannii* PBP3 (light orange), *H. influenzae* PBP3 (blue), *H. pylori* PBP3 (grey). **B.** In Gram positive pathogens, an aromatic residue at the position of F420 is frequently conserved, but there is generally a glutamine at the position of Y422. *S. aureus* PBP2a (green), *S. pneumoniae* PBP2x (purple), *E. faecalis* PBP4 (maroon), *E. faecium* PBP5 (pink), *B. subtilis* PBP2b (yellow), *B. subtilis* PBP3 (orange).

Table 4.2: Superimposition of class B PBPs. ^aResidues from rigid structural alignment that occupy the same position as F420 in PBP2 of *N. gonorrhoeae*. ^bResidue type. *No structural data available – homology model constructed using SWISS-MODEL.

Morphology	Organism	Class B PBP	F420^a	Type^b
Gram negative	<i>N. gonorrhoeae</i>	PBP2-H041	F420	aromatic
	<i>N. gonorrhoeae</i>	PBP2-WT (3EQU)	F420	aromatic
	<i>N. meningitidis</i>	PBP2*	I462	hydrophobic
	<i>P. aeruginosa</i>	PBP3 (3PBN)	Y407	aromatic
	<i>P. aeruginosa</i>	PBP3a*	F401	aromatic
	<i>E. coli</i>	PBP3 (4BJP)	F417	aromatic
	<i>A. baumannii</i>	PBP3 (3UE3)	Y448	aromatic
	<i>H. influenzae</i>	PBP2*	I461	hydrophobic
	<i>H. influenzae</i>	PBP3*	Y438	aromatic
	<i>H. pylori</i>	PBP2 (5LP4)	I432	hydrophobic
	<i>H. pylori</i>	PBP3*	Y441	aromatic
Gram positive	<i>S. aureus</i>	PBP2a (5M1A)	Y519	aromatic
	<i>S. pneumoniae</i>	PBP2x (5OAU)	F450	aromatic
	<i>S. pneumoniae</i>	PBP2x (1PYY)	F450	aromatic
	<i>S. pneumoniae</i>	PBP2x (1QME)	F450	aromatic
	<i>S. pneumoniae</i>	PBP2b (2WAE)	F450	aromatic
	<i>E. faecalis</i>	PBP4 (6BSQ)	Y540	aromatic
	<i>E. faecium</i>	PBP5 (6MKA)	Y538	aromatic
	<i>B. subtilis</i>	PBP2a*	I523	hydrophobic
	<i>B. subtilis</i>	PBP2b*	Y420	aromatic
<i>B. subtilis</i>	PBP3*	Y526	aromatic	
Atypical	<i>M. tuberculosis</i>	PBPA (3LO7)	I337	hydrophobic
	<i>B. burgdorferi</i>	PBP2*	I431	hydrophobic

4.4. Virtual screen of a molecular fragment library for putative PBP2 inhibitors.

The design of compounds applying the 4'-methyl-[1,1'-biphenyl] system to other C-terminal peptidomimetic functionalities may yield additional, more potent inhibitors of *N. gonorrhoeae* PBP2. To this end, a three-point pharmacophore comprising the common characteristics of bicyclic β -lactams (*i.e.*, penams, carbapenems, and cephalosporins) together with **JEK-42** and **JMT-1** was generated from a flexible alignment of the scaffolds using a stochastic conformational search (**Figure 4.13**). This pharmacophore was then employed to search an ~800,000-ligand fragment-like subset of the ZINC virtual database for putative inhibitors of *N. gonorrhoeae* PBP2, yielding 139,444 matching conformers (**Figure 4.14**).

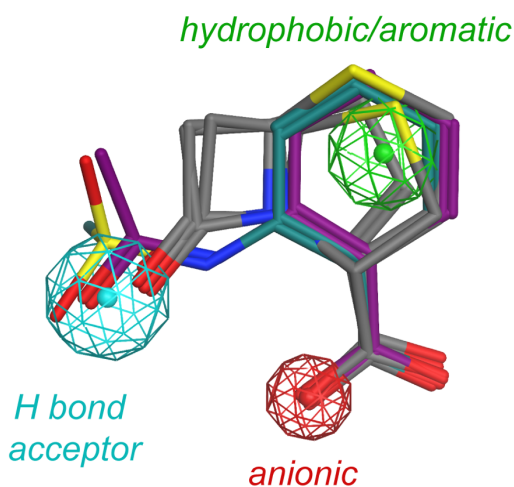


Figure 4.13: Pharmacophore model developed from the flexible alignment of JEK-42 and JMT-1 with bicyclic β -lactam scaffolds. Common features were identified using a threshold of 100% and a tolerance of 1.0 Å. The resulting model consists of three features: anionic (red mesh, radius = 0.7 Å), hydrophobic/aromatic (green mesh, radius = 0.9 Å), hydrogen bond acceptor (cyan mesh, radius = 1.0 Å). JEK-42 is shown in purple, JMT-1 is shown in teal, and β -lactams are shown in grey.

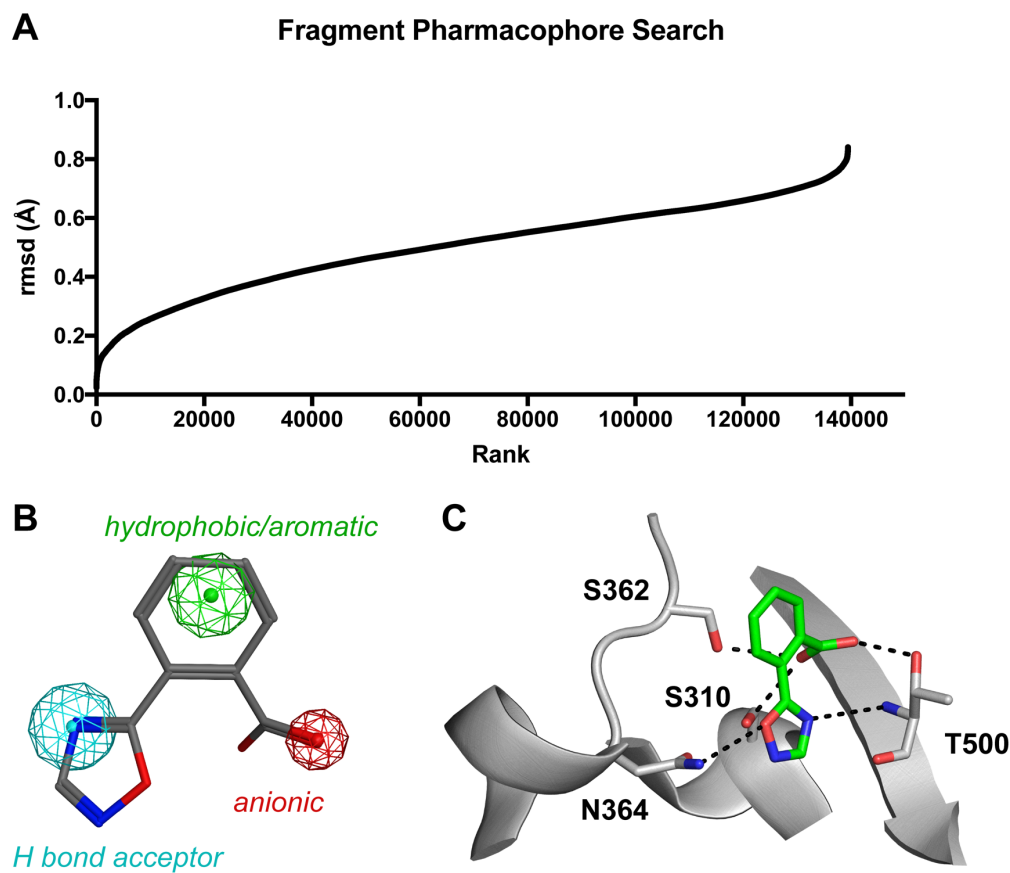


Figure 4.14: Pharmacophore search of a virtualized library of molecular fragments. **A.** A three-point pharmacophore consisting of one anionic feature (radius = 0.7 Å), one hydrophobic/aromatic feature (radius = 0.9 Å), and one hydrogen bond accepting feature (radius = 1.0 Å) was used to search a virtual library of molecular fragment structures, yielding 139,444 matching conformations. **B.** Example 2-(1,2,4-oxadiazol-5-yl)benzoic acid fragment shown in a pharmacophore-matching conformation (rmsd = 0.1 Å). **C.** Example 2-(1,2,4-oxadiazol-5-yl)benzoic acid (green) fragment modeled into the active site of tPBP2^{WT}. Polar contacts are indicated by black dashed lines.

Predictably, while the screen revealed a few structures that diverge significantly from known inhibitors, it predominantly yielded matches that represent simple derivatives of the above scaffolds. A majority of the putative hits can be divided into four structural categories. The first grouping is the most β -lactam-like, consisting of polycyclic carbonyl-containing structures substituted at the β -position with a carboxylic acid (**Figure 4.15**). The carbonyl groups are varied and include lactams, lactones, and acyclic amides. Because β -lactams generally form low-affinity Michaelis complexes with PBPs, fragments *i* through *iv* are likely not the best starting points for the design of potent inhibitors. More

interesting are the bridged structures **v** through **viii**, which can be used to investigate the effects of bulk and volume of the hydrophobic feature, in comparison to monocyclic systems that are flat, flexible, or both. The second grouping (**ix-xi**) consists of saturated carbocyclic carboxylic acids substituted at the 2-position with an amide, similar to **JEK-42** but with more conformational flexibility at the position of the hydrophobic feature (**Figure 4.16**). The third grouping contains benzoic acid analogues substituted at the 2-position with various amide isosteres, including esters (**xii**, acetyl salicylic acid), ketones (**xiii**), ureas (**xiv** and **xv**), and 5-membered heterocycles (*i.e.*, 1,3,4-oxadiazole **xvi**, 1,2,4-oxadiazole **xvii**, thiazoles **xviii** and **xix**, imidazole **xx**, and 1,3,4-triazole **xxi**) (**Figure 4.17**). Incorporation of these types of functional groups in place of the amide seen in **JEK-42** or the sulfonamide seen in **JMT-1** would help to explore specific requirements of shape and conformational flexibility at the hydrogen bond accepting feature. The fourth grouping (**xxii-xxvi**) contains fragments that combine the structural modifications of the first three (**Figure 4.18**). In all, the results from this experiment provide multiple avenues for the discovery of additional PBP-inhibitory molecules.

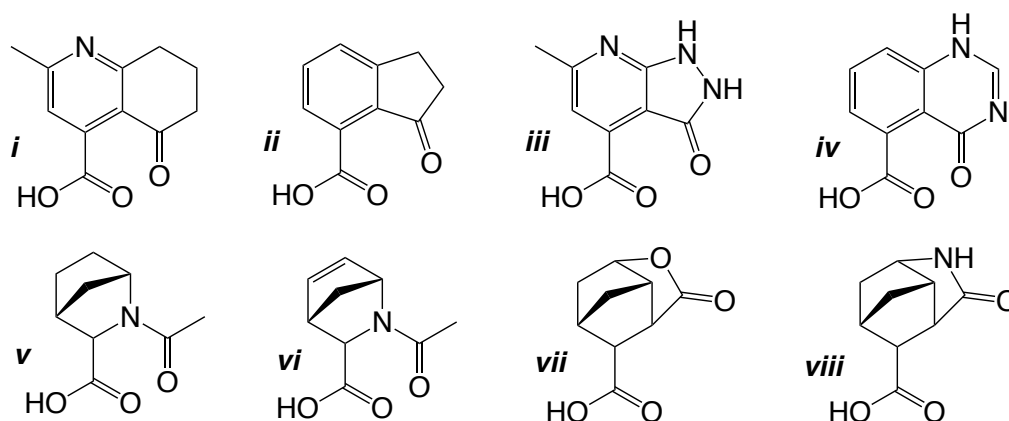


Figure 4.15: Structures of polycyclic fragments resembling β -lactams.

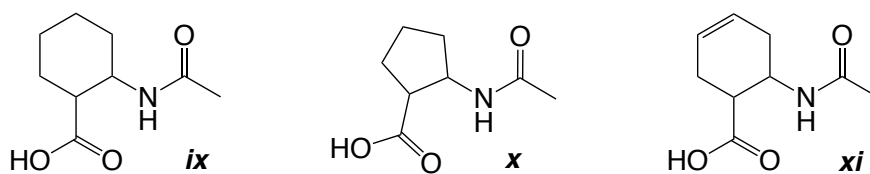


Figure 4.16: Structures of unsaturated carbocyclic fragments.

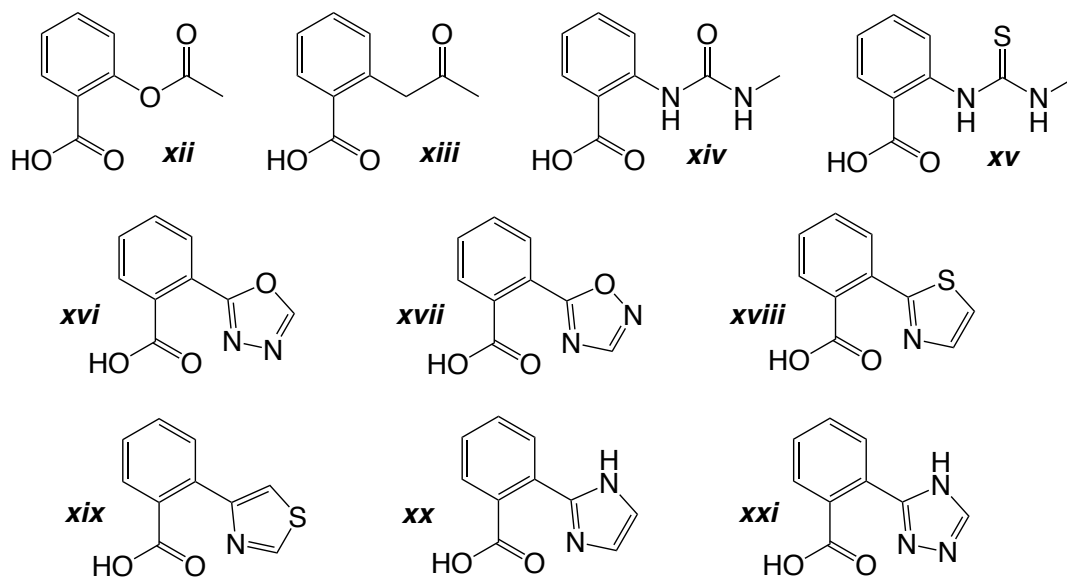


Figure 4.17: Structures of fragments possessing amide bioisosteres.

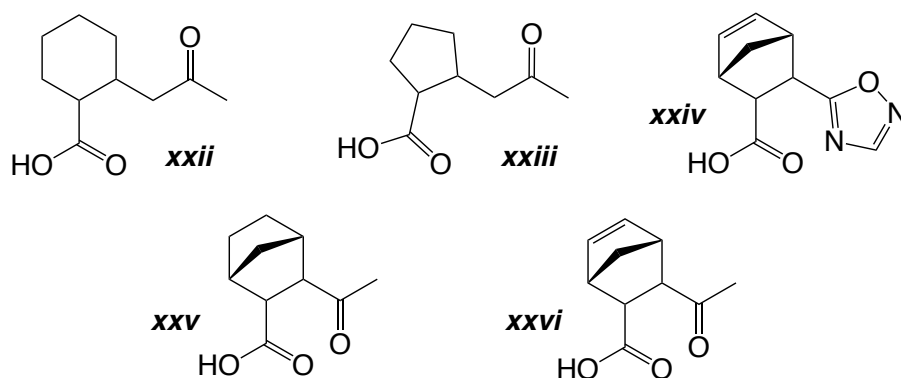


Figure 4.18: Structures of fragments possessing combinations of attributes from sets in **Figures 4.15-4.17.**

4.5. Discussion

In this work, we report the discovery of prototype PBP2 inhibitors and the creation of models for the identification or design of others. First, we show that **JEK-42** and its isosteric derivative **JMT-1** are PBP2-inhibitory scaffolds with antimicrobial activity against *N. gonorrhoeae* FA19 and H041. We also show that they are capable of inhibiting PBP3 from ESKAPE pathogen *P. aeruginosa*. With this cross-inhibition in mind, we present models for the binding of these compounds in which they resemble β -lactam antimicrobials, presumably mimicking the C-terminal D-Ala-D-Ala motif of peptidoglycan in a similar manner. Finally, we present a pharmacophore model used in the identification of putative PBP2 inhibitors through screening of a fragment library, putative hits from which serve as a source of guidance for future analogue design.

4.5.a. Arylamides and arylsulfonamides

To date, two studies have reported inhibition of PBPs by arylamides: a small physical screen followed by a structural similarity search for inhibitors of *S. aureus* PBP2a and *S. pneumoniae* PBP2x,⁶²⁷ and subsequent combinatorial chemistry to explore the scaffold, conducted in the Gobec laboratory.⁶²⁸ Their best hit was 5-bromo-2-(3-propoxybenzamido)benzoic acid, with an IC₅₀ of 230 μ M against PBP2a and 155 μ M against PBP2x (**Figure 4.19**). They also observed that only amides of anthranilic acids (*i.e.*, *o*-aminobenzoic acids) exhibit significant inhibition of either PBP2a or PBP2x, consistent with the results of our initial screen. The structures explored previously were limited to substituted phenyl systems, so the 1,1'-biphenyl system reported in **JEK-42** represents a departure into novel chemical space for PBP inhibition. In the same publications from the Gobec laboratory, arylsulfonamides derived from anthranilic acid were also shown to possess PBP-inhibitory activity.^{627,628} Around the same time, in a high-throughput physical screen conducted by Fedarovich *et al.*, additional arylsulfonamides were identified as inhibitors of *N. gonorrhoeae* PBP2.⁶²¹ The best hits from those studies

were 5-bromo-2-(naphthalene-2-sulfonamido)benzoic acid ($IC_{50} = 80 \mu\text{M}$ against *Sau*PBP2a) and *N*-(4-hydroxynaphthalen-1-yl)naphthalene-1-sulfonamide ($IC_{50} = 50 \mu\text{M}$ against *Ng*PBP2), respectively (**Figure 4.19**). Notably, this scaffold, unlike its carboxamide isostere, does not seem to require a carboxylic acid for inhibition. However, the active compounds lacking a carboxylic acid do possess an ionizable phenolic OH situated *para* to the sulfonamide. The chemical space examined in previous studies was limited largely to naphthyl moieties, so again, the 1,1'-biphenyl system reported in **JMT-1** is novel.

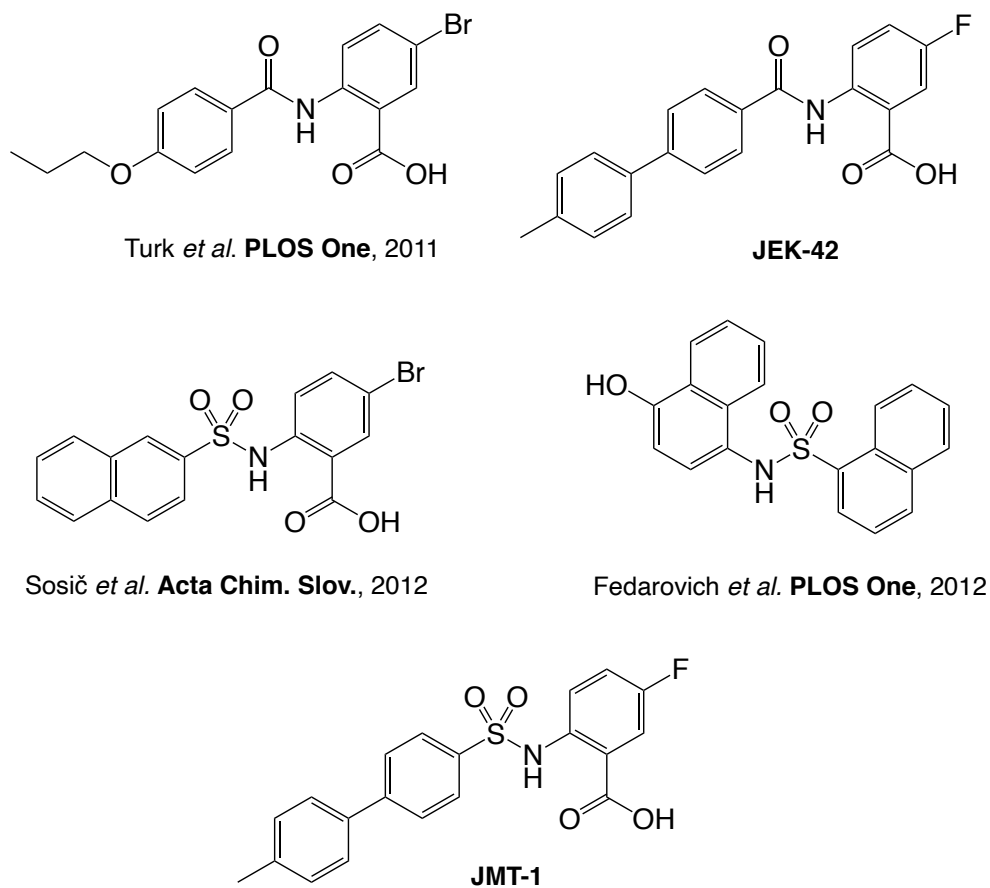
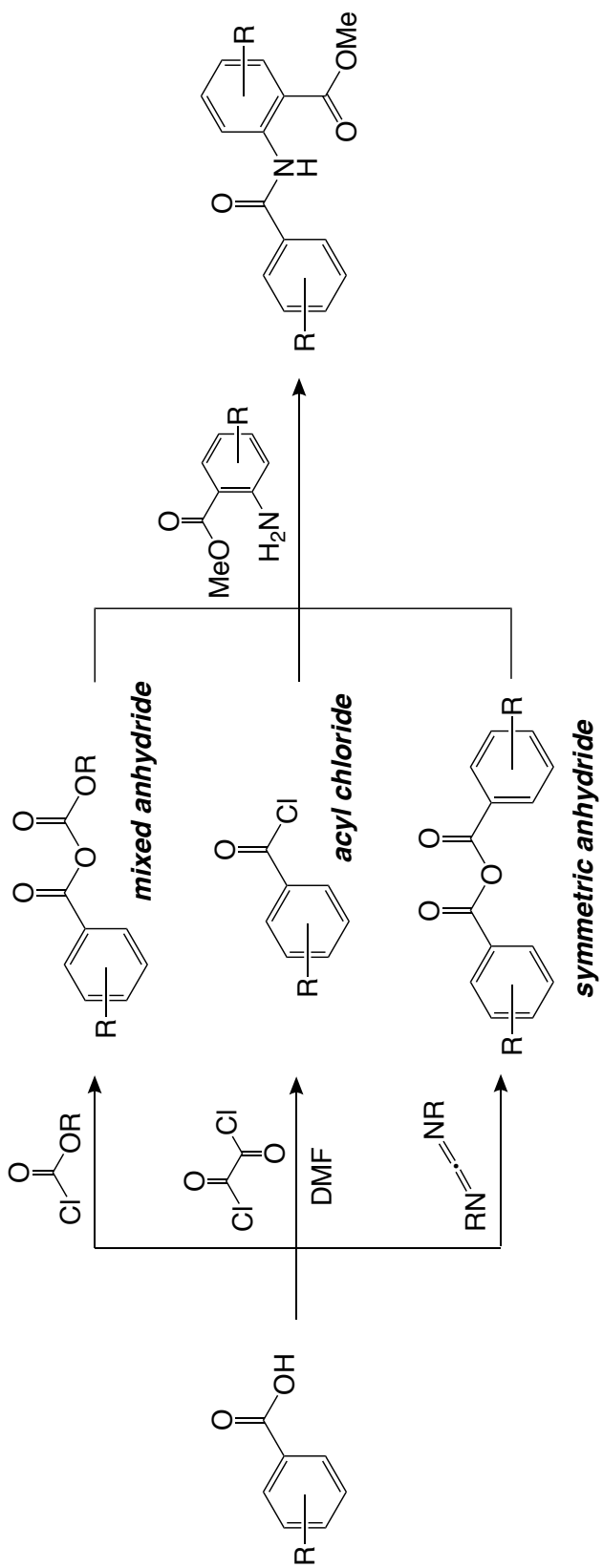
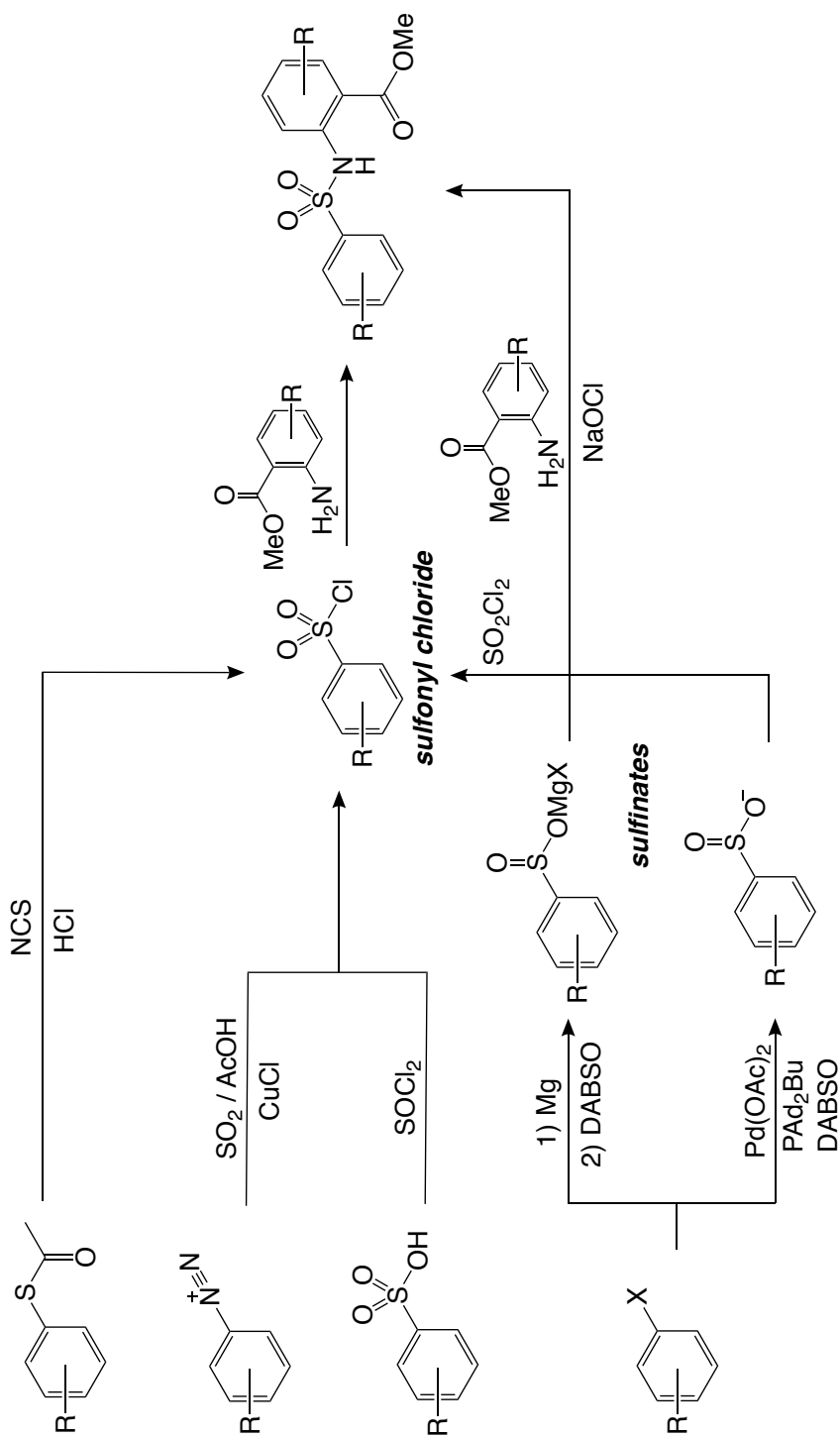


Figure 4.19: Structures of reported arylamide and arylsulfonamide PBP inhibitors.

While there are many available compounds belonging to these chemotypes for testing, future studies focusing on synthetic and medicinal chemistry may prove more useful. Amide synthesis from acyl chlorides is generally facile, and its broad functional group tolerance allows access to molecules with a variety of topologic and electronic structures. Most simple derivatives can be attained from their corresponding carboxylic acids and amines in two steps in excellent yield, as shown in **Scheme 4.3**. Fortunately, similar to the amides, the synthesis of sulfonamides from their corresponding sulfonyl chlorides and anthranilic acids can also be achieved in few steps in the presence of a variety of functional groups. In cases of derivatives for which the sulfonyl chloride is unavailable, other methods employing dediazotization or organometallic agents provide access to this functional group, as shown in **Scheme 4.4**.



Scheme 4.3: Synthetic routes to arylamides.



Scheme 4.4: Synthetic routes to arylsulfonamides.

4.5.b. Molecular dynamics and cross-inhibition of other class B PBPs – evidence for broad specificity

Due to key structural similarities between cephalosporins and the described scaffolds, we propose that **JEK-42** and **JMT-1** may bind the transpeptidase active site in a manner similar to cephalosporins, where the 1,1'-biphenyl system corresponds to R₁ and the anthranilic acid substitution corresponds to R₂. Docking and molecular dynamics of **JEK-42** and **JMT-1** yield poses similar to acylenzyme complexes of ceftriaxone with tPBP2^{WT} and tPBP2^{H041} 113,134 (**Figure 4.20**). In poses of both ligands in both receptors, the carbonyl or sulfonyl oxygen occupies the same position as the acyl oxygen of ceftriaxone within the oxyanion hole. While the positions of anionic groups are variable due to the different geometric constraints of each scaffold, they are generally in the same region of the active site in comparisons of the same tPBP2 variant. Moreover, the 1,1'-biphenyl system projects in the same direction as the 2-aminothiazol-4-yl group of ceftriaxone. There is better overlap with the tPBP2^{H041}-ceftriaxone structure, with the aromatic rings fitting into the hydrophobic area of PBP2 surface created by F420 and Y422. The basis for inhibition of both tPBP2^{WT} and tPBP2^{H041} by **JEK-42** and **JMT-1** may, therefore, be that they 1) mimic the peptide C-terminus in a manner similar to β -lactams, and 2) avoid the requirement for β 3- β 4 hinging proposed to enhance contacts of the cephalosporin thiazole with the tPBP2^{WT} active site. This, in combination with their predicted interactions with highly conserved residues, suggests that **JEK-42** and **JMT-1** may be capable of inhibiting a variety of class B PBPs. This hypothesis is further strengthened by the compounds' abilities to inhibit *P. aeruginosa* PBP3, another class B PBP with only 40% sequence identity.

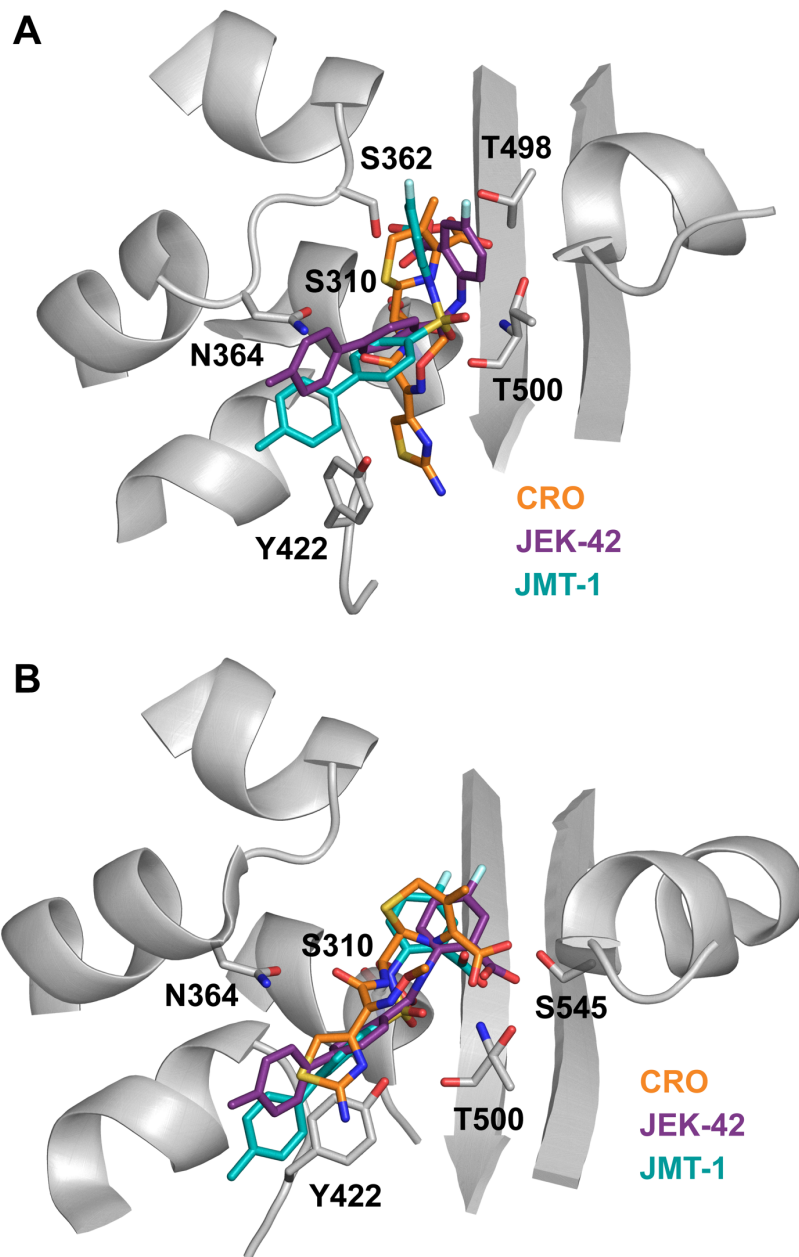
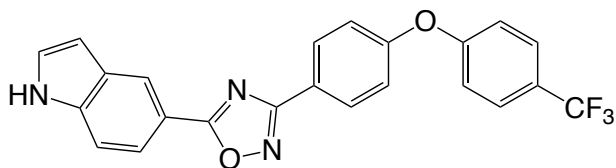


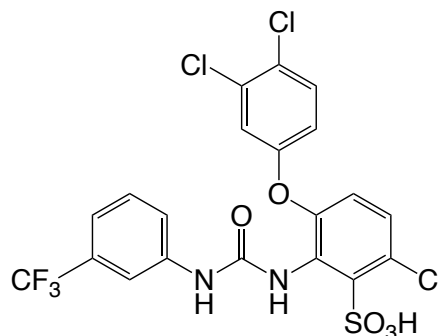
Figure 4.20: Overlay of ceftriaxone (CRO) acyl structures with JEK-42 and JMT-1. **A.** Published tPBP2^{WT}-CRO complex superimposed on final positions of ligands from molecular dynamics simulations with tPBP2^{WT} (receptor shown in grey, CRO shown as orange sticks, JEK-42 shown as purple sticks, JMT-1 shown as teal sticks). **B.** Published tPBP2^{H041}-CRO complex superimposed on final positions of ligands from molecular dynamics simulations with tPBP2^{H041} (same color scheme as above).

4.5.d. Guidance for further derivatization

The three-point pharmacophore screen of fragments proposes a number of changes that can be made to the anthranilic acid moiety, including replacement of the aromatic system with bridged polycyclic or flexible saturated carbocycles. The more interesting aspect of the fragment screen, however, is perhaps the variety of amide isosteres that emerged, including the 1,2,4-oxadiazoles. Many 1,2,4-oxadiazoles have now been reported with activity against *S. aureus* PBP2a,⁶³³⁻⁶³⁶ and the class is discussed in detail in Chapter 1. Briefly, shown in **Figure 4.21** is the current lead compound from this series, exhibiting an MIC of 4 µg/mL against MRSA, low *in vitro* cytotoxicity, favorable murine pharmacokinetics, and efficacy in a murine model of staphylococcal peritonitis.⁶³⁵ Another amide isostere emerging from the pharmacophore screen with precedent in the literature is urea. The 2-ureidobenzenesulfonic acids, also discussed in Chapter 1, were reported as inhibitors of *S. pneumoniae* PBP2x.⁶³⁰ The reported IC₅₀ for the ureido compound shown in **Figure 4.21** against PBP2x is 71 µM. Application of these isosteres, and others from the screen results, to our system will provide important information about the steric and electronic requirements of the PBP2 active site at the location occupied by the amide and sulfonamide of **JEK-42** and **JMT-1**, respectively.



Spink *et al.* **J. Med. Chem.**, 2015



Miguet *et al.* **J. Med. Chem.**, 2009

Figure 4.21: 1,2,4-oxadiazole and 2-ureidobenzenesulfonic acid PBP inhibitors.

4.5.e. Significance

Here we report the identification and initial characterization of two novel inhibitors of PBP2 from *N. gonorrhoeae*: 2-(arylamido)benzoic acid **JEK-42** and 2-(arylsulfonamido)benzoic acid **JMT-1**. The overall picture emerging from studies of these compounds is that they are not susceptible to the PBP2 modifications that result in cephalosporin resistance, and that they may be capable of inhibiting a number of other class B PBPs due to 1) their structural resemblance to β -lactams and 2) predicted interactions with highly conserved residues.

CHAPTER 5: Derivatization of Identified PBP-Inhibitory Chemotypes

5.1 Introduction

Chapter 4 outlines the discovery of novel PBP2-inhibitory chemotypes proposed to mimic the binding of β -lactams and, thus, the bacterial peptidoglycan D-Ala- D-Ala motif. The next phase of our investigation is the derivatization of these molecules, with the goal of enhancing *in vitro* potency against *N. gonorrhoeae* PBP2 and against the pathogen itself. In this chapter, the synthesis of 127 analogues of **JMT-1**, as well as their PBP2-inhibitory and antigonococcal activity, is described.

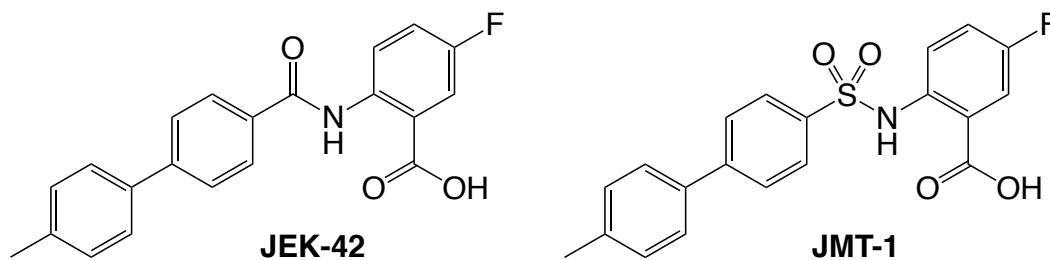
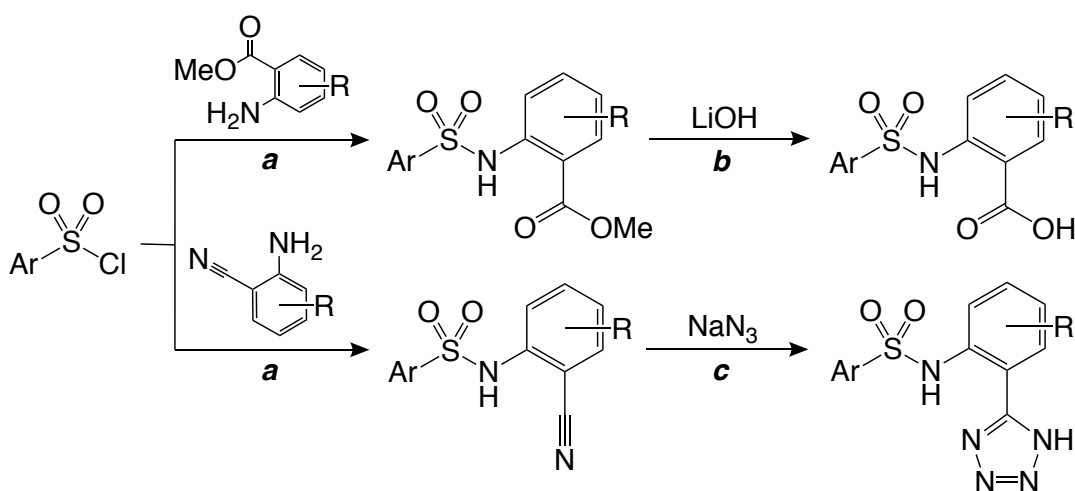


Figure 5.1: Structures of prototype compounds JEK-42 and JMT-1.

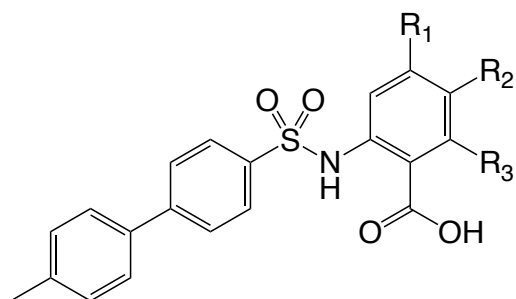
5.2. Derivatization of JMT-1 sulfonamides

Sulfonamide synthesis is achievable in two simple steps from commercially available sulfonyl chloride starting materials, shown in **Scheme 5.1**. The first step is substitution of the sulfonyl chloride (**a**) with either a methyl anthranilate or 2-aminobenzonitrile. The methyl benzoate products are treated with lithium hydroxide (**b**) to afford the corresponding carboxylic acid, and benzonitrile products undergo a 1,3-dipolar cycloaddition with sodium azide under copper (II) sulfate catalysis (**c**) to generate the corresponding tetrazole. All **JMT-1** derivatives reported herein were prepared using this route.



Scheme 5.1: Synthesis of JMT-1 derivatives. **a.** pyridine, DCM, N₂, RT, 12 h. **b.** 1:1 THF/H₂O, RT, 8 h. **c.** CuSO₄·5H₂O, DMSO, 150°C, 1 h.

5.2.a. Modifications to the anthranilic acid moiety I: Substitution at positions 4 through 6



2: R ₁ = H	R ₂ = H	R ₃ = H	9: R ₁ = Me	R ₂ = H	R ₃ = H
3: R ₁ = F	R ₂ = H	R ₃ = H	10: R ₁ = H	R ₂ = Me	R ₃ = H
4: R ₁ = F	R ₂ = F	R ₃ = H	11: R ₁ = H	R ₂ = H	R ₃ = Me
5: R ₁ = Cl	R ₂ = H	R ₃ = H	12: R ₁ = CF ₃	R ₂ = H	R ₃ = H
6: R ₁ = H	R ₂ = Cl	R ₃ = H	13: R ₁ = H	R ₂ = CF ₃	R ₃ = H
7: R ₁ = Br	R ₂ = H	R ₃ = H	14: R ₁ = OMe	R ₂ = H	R ₃ = H
8: R ₁ = H	R ₂ = Br	R ₃ = H	15: R ₁ = H	R ₂ = OMe	R ₃ = H

Figure 5.2: Structures of compounds **JMT-2** through **JMT-15**, which possess substitutions on the anthranilic acid moiety of **JMT-1**.

To begin, we surveyed each position on the anthranilic acid moiety of **JMT-1** to determine functional groups and substitution patterns that increase inhibition of PBP2. For all compounds synthesized, inhibition of tPBP2^{WT} and tPBP2^{H041} was determined at 100 μ M using the previously described competition assay with Bocillin-FL. Compounds showing >80% inhibition of both variants at 100 μ M were tested at 10 μ M. Data for this initial series are shown in **Figure 5.3** and **Figure 5.4**. Examining the compound set from Kirkpatrick *et al.* screened earlier (as described in Chapter 4), substitution at the 3-position was already found to abolish activity of carboxamido compounds related to **JEK-42**, so under the assumption that **JEK-42** and its sulfonamide isostere **JMT-1** bind similarly to PBP2, this position was not examined. The data show that the fully unsubstituted version (**JMT-2**) is less active at 100 μ M than **JMT-1**, with $71 \pm 4\%$ inhibition of tPBP2^{WT} compared to $93 \pm 7\%$ for **JMT-1**. A switch of the 5-fluoro moiety to the 4-position (**JMT-3**) did not change activity significantly; however, the 4,5-difluoro compound **JMT-4** exhibits a sharp

increase in potency, inhibiting tPBP2^{WT} and tPBP2^{H041} fully at 100 μ M and showing 87 \pm 6% inhibition against tPBP2^{H041} at 10 μ M. Note the 6-fluoro product was not obtained in sufficient yield and purity for testing.

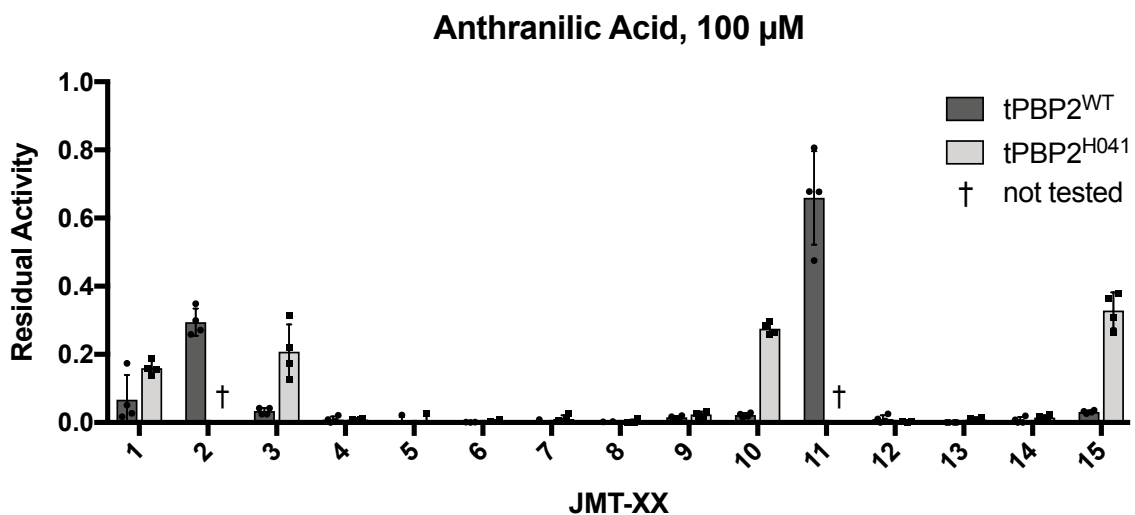


Figure 5.3: Inhibition data for JMT-2 through JMT-15 against tPBP2^{WT} and tPBP2^{H041} at 100 μ M. Values were determined in a purified protein assay in which tPBP2 was preincubated with 100 μ M compound, followed by addition of 1 μ M Bocillin-FL. Data are presented as a fraction of activity of the DMSO control. Error bars are standard deviation.

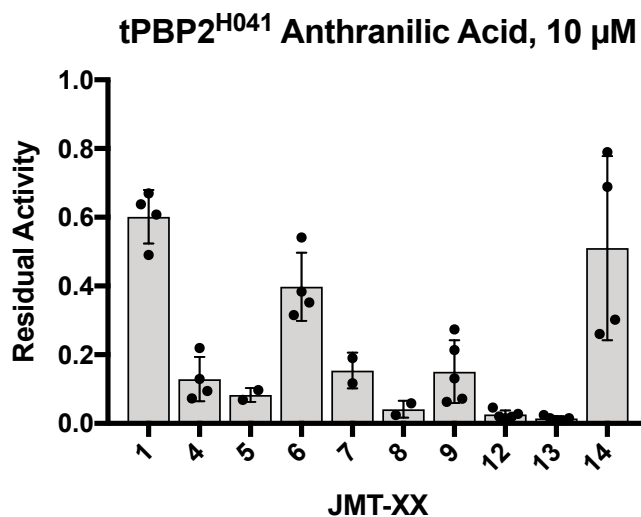


Figure 5.4: Inhibition data for selected anthranilic acid-substituted derivatives of JMT-1 against tPBP2^{H041} at 10 μ M. Compounds exhibiting greater than 80% inhibition of both tPBP2^{WT} and tPBP2^{H041} activity at 100 μ M (Figure 5.3) were tested. Values were determined in a purified protein assay in which tPBP2^{H041} was preincubated with 10 μ M compound, followed by addition of 1 μ M Bocillin-FL. Data are presented as a fraction of activity of the DMSO control. Error bars are standard deviation.

To examine the effects of increasing atomic radius at the 4- and 5-positions, analogues with additional halogens were synthesized. Analogues chlorinated (**JMT-5** & **JMT-6**) or brominated (**JMT-7** & **JMT-8**) at 4- and 5-positions are active at 100 μM , with the 5-bromo compound **JMT-8** exhibiting $96 \pm 2\%$ inhibition of tPBP2^{H041} at 10 μM . The 5-iodo product could not be synthesized in sufficient yield for testing. Further increases in bulk were explored with a series of methyl substitutions at the 4- and 5-positions, revealing the 4-methyl analogue **JMT-9** to be the more active. Interestingly, while **JMT-9** exhibits $85 \pm 9\%$ inhibition of tPBP2^{H041} at 10 μM , the 5-methyl analogue **JMT-10** fails to inhibit tPBP2^{H041} fully at 100 μM . The 6-position was also surveyed by testing 6-methyl analogue **JMT-11**, whose relatively weak inhibition indicates that substitution at this position is not favored.

Given the lesser activity of methyl compounds compared to their halogenated analogues, it can be inferred that either activity is dependent upon a very specific van der Waals radius of substituents to the anthranilic acid, or upon the polarizability of these substituents. To answer this question, analogues possessing a trifluoromethyl group at the 4- (**JMT-12**) or 5-position (**JMT-13**) were synthesized and potently inhibited both tPBP2^{WT} and tPBP2^{H041}. The relative potencies of compounds **JMT-12** and **JMT-13** ($97 \pm 1\%$ and $99 \pm 1\%$ inhibition, respectively, of tPBP2^{H041} at 10 μM) suggest that both van der Waals radius and polarizability of substituents correlate positively with PBP2 inhibition.

All generated compounds discussed to this point possess anthranilic acid moieties substituted with hydrophobic functional groups. In order to assess the effects of polarity, 4- (**JMT-14**) and 5-methoxy (**JMT-15**) compounds were generated. **JMT-14** is more active than **JMT-15** against tPBP2^{H041} but not more than the prototype **JMT-1**, indicating tolerance of modestly polar groups at this position rather than any preference for them. To explore polarity further, synthesis of a 5-nitro analogue was also attempted, but the desired product was not found on mass spectrometric analysis of the crude reaction

mixture. In all, the pattern emerging from these initial derivatization studies suggests the following in terms of tPBP2 inhibition:



Compounds exhibiting >75% inhibition of tPBP2^{H041} at 10 μM were tested in disc diffusion assays against *N. gonorrhoeae* FA19 and H041 (**Figure 5.5**). Consistent with their enzymatic inhibition, compounds **JMT-12**, and **JMT-13** exhibit the most potent antimicrobial activity against both strains. **JMT-12**, a 4-trifluoromethyl analogue of prototype **JMT-1**, inhibits growth of *N. gonorrhoeae* FA19 and H041 up to 20.5 ± 0.7 mm and 15.5 ± 1.8 mm, respectively, from the edge of a disc impregnated with 10 μg compound. **JMT-13**, the 5-trifluoromethyl analogue, shows a 19.0 ± 1.0 mm zone of inhibition against FA19 and a 16.3 ± 1.1 mm zone of inhibition against H041. **JMT-5** also shows good antimicrobial activity against both strains, in contrast with **JMT-8**, which shows a stark reduction in potency against H041.

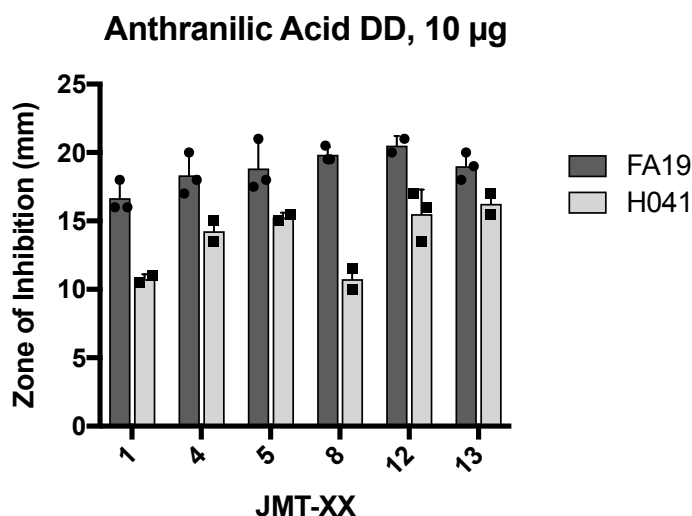
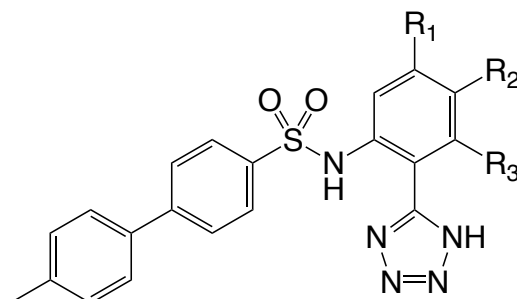


Figure 5.5: Disc diffusion data for potent anthranilic acid-substituted derivatives of JMT-1 against *N. gonorrhoeae* FA19 and H041. Compounds exhibiting greater than 75% inhibition of tPBP2^{H041} activity at 10 μM were tested against susceptible reference gonococcal strain FA19 and multi-drug resistant H041 at 10 μg per disc.

5.2.b. Modifications to the anthranilic acid moiety II: Isosteric replacement of the carboxylic acid for a 1H-tetrazol-5-yl moiety



16: R ₁ = F	R ₂ = H	R ₃ = H	21: R ₁ = H	R ₂ = Me	R ₃ = H
17: R ₁ = H	R ₂ = F	R ₃ = H	22: R ₁ = CF ₃	R ₂ = H	R ₃ = H
18: R ₁ = H	R ₂ = Cl	R ₃ = H	23: R ₁ = H	R ₂ = CF ₃	R ₃ = H
19: R ₁ = H	R ₂ = Br	R ₃ = H	24: R ₁ = OMe	R ₂ = H	R ₃ = H
20: R ₁ = Me	R ₂ = H	R ₃ = H	25: R ₁ = H	R ₂ = OMe	R ₃ = H

Figure 5.6: Structures of compounds JMT-16 through JMT-25, which possess a 1H-tetrazol-5-yl moiety at C1 in place of the carboxylic acid seen in JMT-1.

Next, we examined the effect of isosteric replacement of the carboxylic acid group of the anthranilic acid moiety on PBP2 inhibition. The 1H-tetrazol-5-yl system was chosen for these derivatives, as it confers favorable drug-like properties (e.g., improved membrane permeability and resistance to some forms of xenobiotic metabolism) and is easily accessed from nitriles using a copper(II)-catalyzed 1,3-dipolar cycloaddition. Inhibition data for this initial set of phenyltetrazoles against tPBP2 are shown in **Figure 5.7** and **Figure 5.8**. The generated tetrazoles **JMT-16** through **JMT-25** generally show similar activity to their carboxylic acid analogues against tPBP2^{WT} and tPBP2^{H041}. Modest improvements in tPBP2 inhibition are seen in several cases of 5-substitution, including 5-fluoro (**JMT-17**), 5-chloro (**JMT-18**), 5-methyl (**JMT-21**), and 5-methoxy (**JMT-25**) compounds. Consistent with results for the anthranilic acid compounds, substitution with a trifluoromethyl group yields excellent tPBP2 inhibition, with 4- (**JMT-22**) and 5-substituted (**JMT-23**) molecules showing $89 \pm 4\%$ and $83 \pm 12\%$ inhibition, respectively, of tPBP2^{H041} at 10 μM .

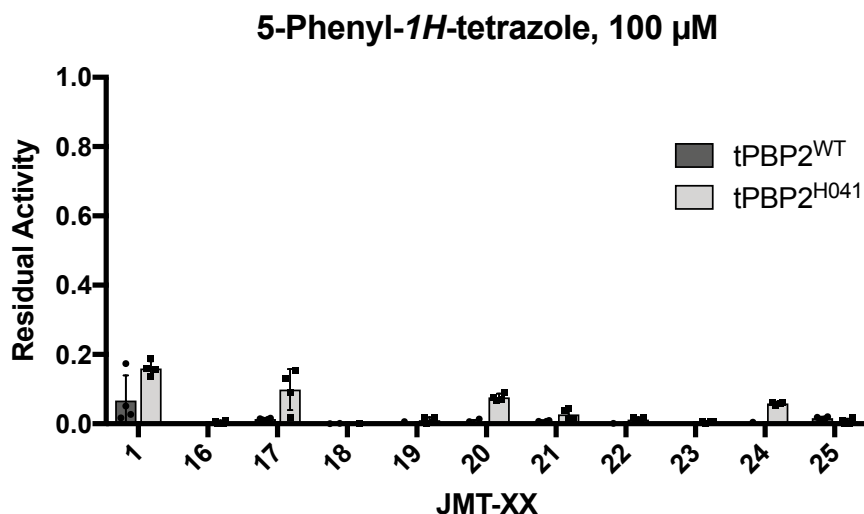


Figure 5.7: Inhibition data for JMT-16 through JMT-25 against tPBP2^{WT} and tPBP2^{H041} at 100 μ M. Values were determined in a purified protein assay in which tPBP2 was preincubated with 100 μ M compound, followed by addition of 1 μ M Bocillin-FL. Data are presented as a fraction of activity of the DMSO control. Error bars are standard deviation.

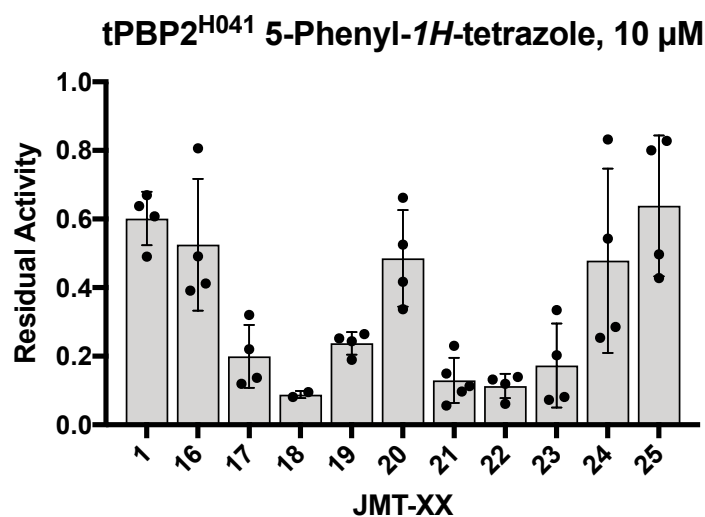


Figure 5.8: Inhibition data for 1H-tetrazol-5-yl derivatives of JMT-1 against tPBP2^{H041} at 10 μ M. Compounds exhibiting greater than 80% inhibition of both tPBP2^{WT} and tPBP2^{H041} activity at 100 μ M (Figure 5.7) were tested against tPBP2^{H041} at 10 μ M. Values were determined in a purified protein assay in which tPBP2 was preincubated with 10 μ M compound, followed by addition of 1 μ M Bocillin-FL. Data are presented as a fraction of activity of the DMSO control. Error bars are standard deviation.

As for the anthranilic acid compounds, the antimicrobial activity of the tetrazoles was tested against *N. gonorrhoeae* strains FA19 and H041. Overall, antimicrobial activity is weaker than for the carboxylic acid parent compounds (**Figure 5.9**). Trifluoromethyl compounds **JMT-22** and **JMT-23** inhibit growth of *N. gonorrhoeae* within less than 15 mm of the disc. Interestingly, whereas the 5-bromo carboxylic acid **JMT-8** exhibits excellent activity against FA19 but only modest activity against H041, its tetrazole analogue **JMT-19** seems to show very little difference between strains. **JMT-19** is the most potent of this series, exhibiting 17.3 ± 1.8 mm and 16.0 ± 1.4 mm zones of inhibition against FA19 and H041, respectively.

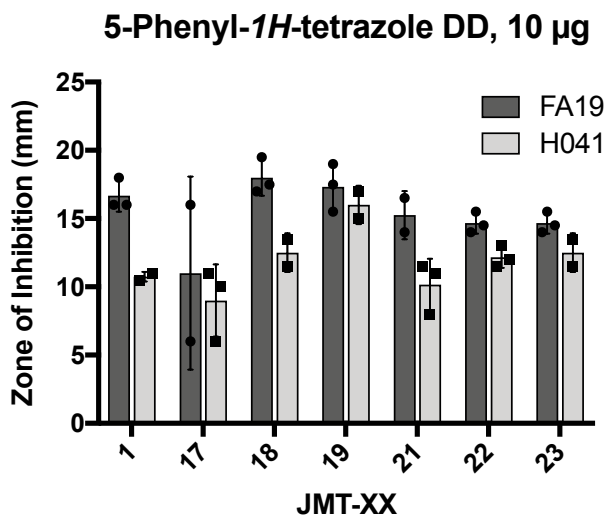
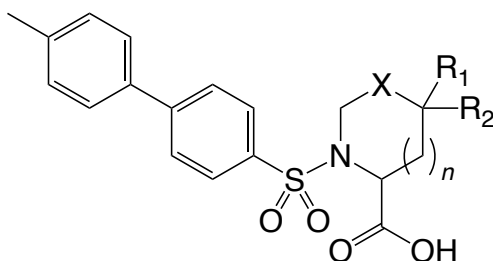


Figure 5.9: Disc diffusion data for potent 1H-tetrazol-5-yl derivatives of JMT-1 against *N. gonorrhoeae* FA19 and H041. Compounds exhibiting greater than 75% inhibition of tBPB2^{H041} activity at 10 µM were tested against susceptible reference gonococcal strain FA19 and multi-drug resistant H041 at 10 µg per disc.

5.2.c. Modifications to the anthranilic acid moiety III: Replacement of aromatic ring with heterocyclic carboxylic acids



26:	R ₁ = H	R ₂ = H	X = CH ₂	n = 0
27:	R ₁ = H	R ₂ = H	X = S	n = 0
28:	R ₁ = Me	R ₂ = Me	X = S	n = 0
29:	R ₁ = H	R ₂ = H	X = CH ₂	n = 1
30:	R ₁ = Me	R ₂ = H	X = S	n = 1

Figure 5.10: Structures of compounds JMT-26 through JMT-30, which possess nitrogen-containing heterocyclic carboxylic acids in place of the anthranilic acid seen in JMT-1.

A series of sulfonamides synthesized from nitrogen-containing heterocycles were attempted to create scaffolds more closely resembling β -lactam antimicrobials. Inhibition data for this series against tPBP2 are shown in **Figure 5.11**. Pyrrolidine (**JMT-26**) and thiazolidine (**JMT-27**) compounds inhibit tPBP2^{WT} only weakly at 100 μ M. Next, the 5,5-dimethylthiazolidine analogue **JMT-28** was tested. Although this has a structure very similar to most penams, it fails to show any inhibition at 100 μ M. Cephem-like 6-membered ring systems were also examined, but the incorporation of neither piperidine (**JMT-29**) nor tetrahydro-1,3-thiazine (**30**) improves activity.

To determine if loss of the anthranilic acid moiety abolishes PBP2 binding fully, the compounds were also tested at 1 mM. At this concentration, compounds **JMT-26** through **JMT-30** all inhibit tPBP2^{WT}, indicating a severe reduction in affinity, but not a complete loss. Because of their low inhibition, none of these analogues was tested against *N. gonorrhoeae*.

Heterocyclic Carboxylic Acid, 100 μ M

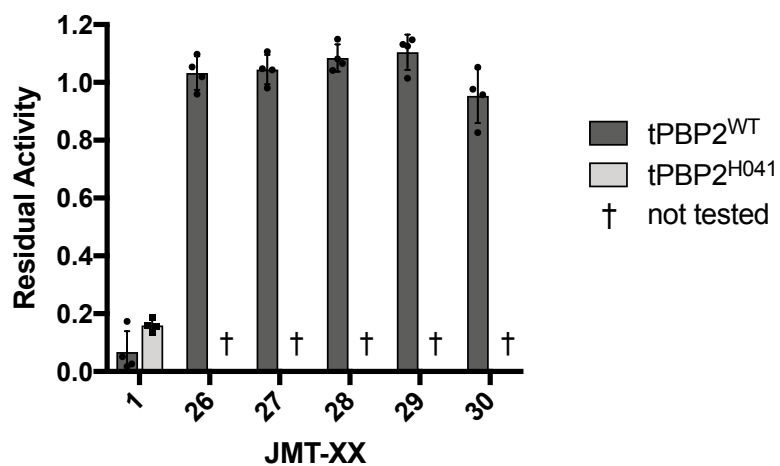
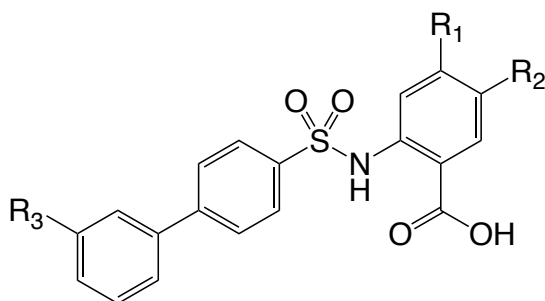


Figure 5.11: Inhibition data for JMT-26 through JMT-30 against tPBP2^{WT} and tPBP2^{H041} at 100 μ M. Values were determined in a purified protein assay in which tPBP2 was preincubated with 100 μ M compound, followed by addition of 1 μ M Bocillin-FL. Data are presented as a fraction of activity of the DMSO control. Error bars are standard deviation.

5.2.d. Modifications to the biphenyl ring system I: Replacement of the 4'-methyl group



31: R ₁ = H R ₂ = H R ₃ = H	36: R ₁ = F R ₂ = H R ₃ = Me
32: R ₁ = F R ₂ = H R ₃ = H	37: R ₁ = H R ₂ = F R ₃ = Me
33: R ₁ = H R ₂ = F R ₃ = H	38: R ₁ = H R ₂ = Br R ₃ = Me
34: R ₁ = H R ₂ = Me R ₃ = H	39: R ₁ = H R ₂ = Me R ₃ = Me
35: R ₁ = H R ₂ = Br R ₃ = H	

Figure 5.12: Structures of compounds JMT-31 through JMT-39, which lack the biphenyl 4'-methyl group seen in JMT-1.

To determine the importance of the 4'-substituent to PBP2 inhibition, a series of 4'-desmethyl analogues (**JMT-31** through **JMT-39**) were synthesized. Inhibition data for this series against tPBP2 are shown in **Figure 5.13** and **Figure 5.14**. The first of these, **JMT-31** through **JMT-35**, possess entirely unsubstituted biphenyl secondary aromatic systems. These compounds are generally much less active than their 4'-methylated counterparts, showing minimal inhibition of tPBP2^{WT} at 100 μ M. However, the 5-bromo analogue **JMT-35** inhibits both tPBP2^{WT} and tPBP2^{H041} fully at this concentration, and it retains some activity against tPBP2^{H041} upon dose reduction to 10 μ M (66 \pm 17% inhibition). Its relative potency among compounds of this series supports the assertion that a large, polarizable, hydrophobic group at C5 enhances inhibition.

To survey other positions on the biphenyl secondary aromatic ring, a small number of 3'-methyl analogues (**JMT-36** through **JMT-39**) were generated, which are marginally less active than their 4'-methyl parent compounds. The most active of those synthesized and tested is the 5-bromo analogue **JMT-38**, which exhibits 71 \pm 8% inhibition of tPBP2^{H041}

at 10 μM , again supporting the requirement for a large, polarizable group at C5. Overall, the lesser activity of 4'-desmethyl compounds indicates that substitution at the 4'-position enhances PBP2-inhibitory potency.

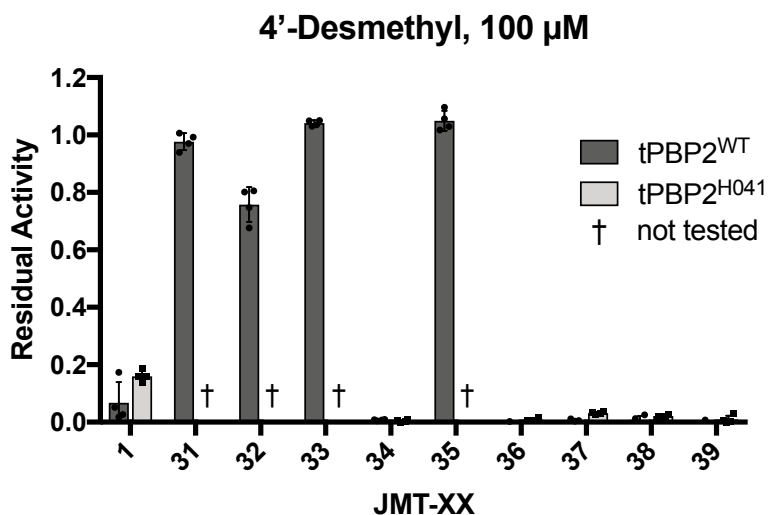


Figure 5.13: Inhibition data for JMT-31 through JMT-39 against tPBP2^{WT} and tPBP2^{H041} at 100 μM . Values were determined in a purified protein assay in which tPBP2 was preincubated with 100 μM compound, followed by addition of 1 μM Bocillin-FL. Data are presented as a fraction of activity of the DMSO control. Error bars are standard deviation.

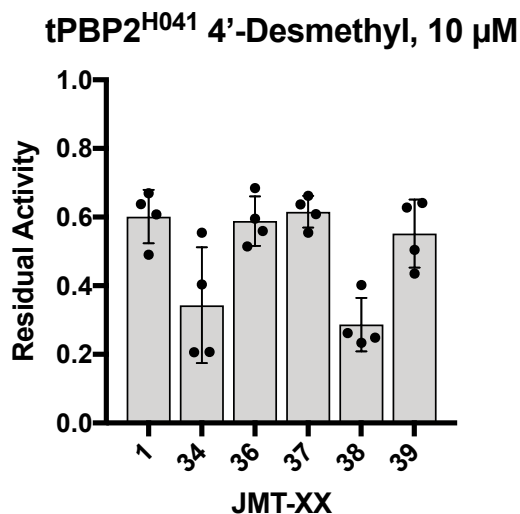
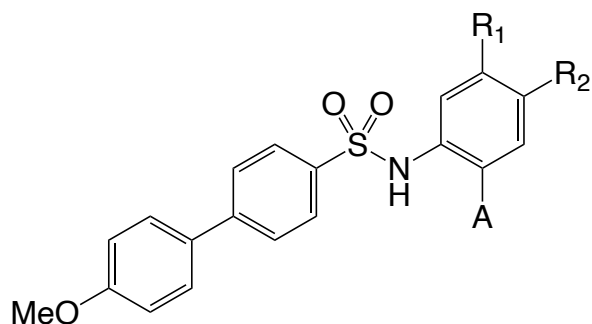


Figure 5.14: Inhibition data for 4'-desmethyl derivatives of JMT-1 against tPBP2^{H041} at 10 μM . Compounds exhibiting greater than 80% inhibition of both tPBP2^{WT} and tPBP2^{H041} activity at 100 μM (Figure 5.13) were tested against tPBP2^{H041} at 10 μM . Values were determined in a purified protein assay in which tPBP2 was preincubated with 10 μM compound, followed by addition of 1 μM Bocillin-FL. Data are presented as a fraction of activity of the DMSO control. Error bars are standard deviation.



40:	R ₁ = F	R ₂ = H	A = COOH	50:	R ₁ = F	R ₂ = H	A = TTZ
41:	R ₁ = H	R ₂ = F	A = COOH	51:	R ₁ = H	R ₂ = F	A = TTZ
42:	R ₁ = F	R ₂ = F	A = COOH	52:	R ₁ = H	R ₂ = Br	A = TTZ
43:	R ₁ = H	R ₂ = Br	A = COOH	53:	R ₁ = Me	R ₂ = H	A = TTZ
44:	R ₁ = Me	R ₂ = H	A = COOH	54:	R ₁ = H	R ₂ = Me	A = TTZ
45:	R ₁ = H	R ₂ = Me	A = COOH	55:	R ₁ = CF ₃	R ₂ = H	A = TTZ
46:	R ₁ = CF ₃	R ₂ = H	A = COOH	56:	R ₁ = H	R ₂ = CF ₃	A = TTZ
47:	R ₁ = H	R ₂ = CF ₃	A = COOH	57:	R ₁ = OMe	R ₂ = H	A = TTZ
48:	R ₁ = OMe	R ₂ = H	A = COOH	58:	R ₁ = H	R ₂ = OMe	A = TTZ
49:	R ₁ = H	R ₂ = OMe	A = COOH				

Figure 5.15: Structures of compounds *JMT-40* through *JMT-58*, which possess a 4'-methoxy in place of the 4'-methyl group seen in *JMT-1*. TTZ: 1*H*-tetrazol-5-yl

Since the 4'-substituent appears to be important for inhibition of PBP2, compounds with various 4'-substituents were synthesized to explore physicochemical requirements at this position. First, the influence of polarity was assessed by incorporation of a 4'-methoxy group (**JMT-40** through **JMT-58**). Inhibition data for this series against tPBP2 are shown in **Figure 5.16** and **Figure 5.17**. In general, this change yields less active compounds by direct comparison with 4'-methyl analogues, indicating that a polar group at this position is not favored. However, there are a few in the series that inhibit PBP2 relatively well. For example, 4- (**JMT-46**, **JMT-55**) and 5-trifluoromethyl (**JMT-47**, **JMT-56**) compounds are active, as well as 5-bromophenyl tetrazole **JMT-52**. In fact, **JMT-46** and **JMT-56** exhibit $94 \pm 0\%$ and $91 \pm 2\%$ inhibition of tPBP2^{H041}, respectively, at 10 μ M. Again, the activity conferred by these hydrophobic, polarizable 4- and 5-substitutions to the anthranilic acid or phenyltetrazole moiety further emphasizes the benefit of such groups at these positions.

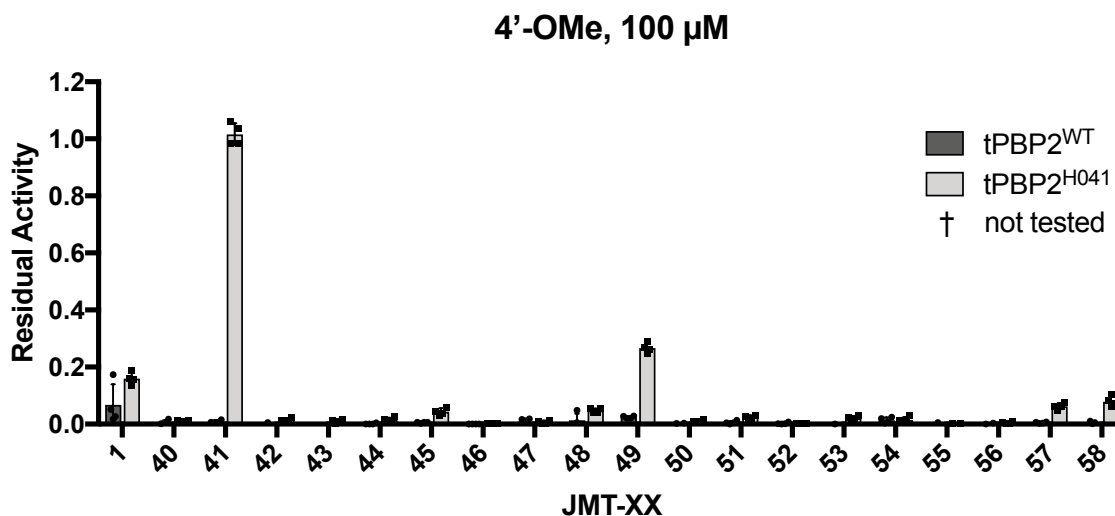


Figure 5.16: Inhibition data for JMT-40 through JMT-58 against tPBP2^{WT} and tPBP2^{H041} at 100 μ M. Values were determined in a purified protein assay in which tPBP2 was preincubated with 100 μ M compound, followed by addition of 1 μ M Bocillin-FL. Data are presented as a fraction of activity of the DMSO control. Error bars are standard deviation.

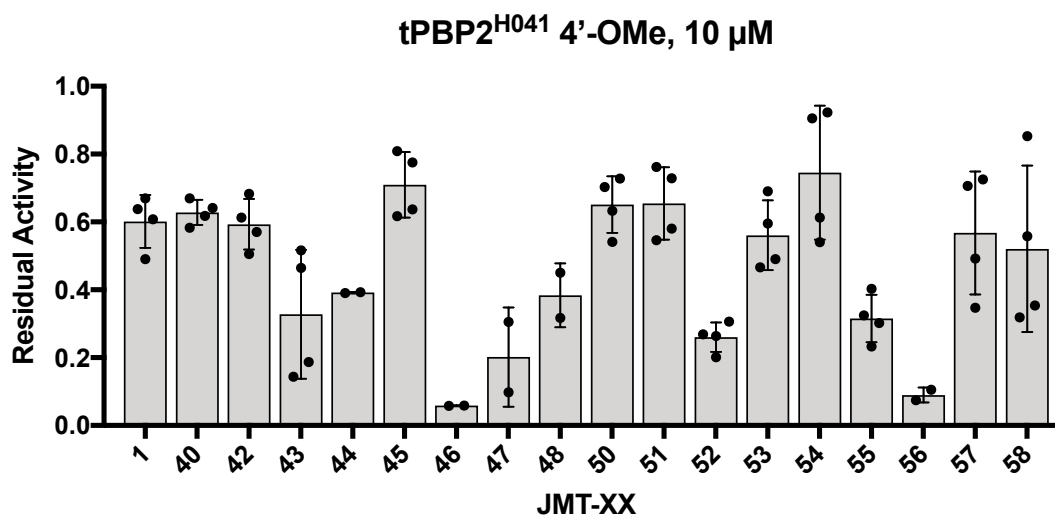
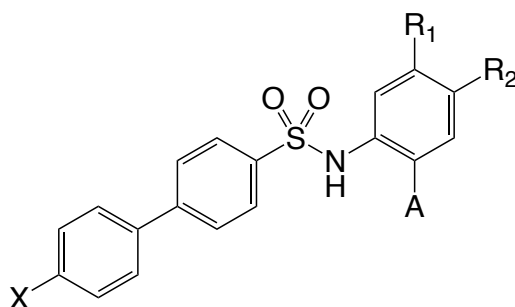


Figure 5.17: Inhibition data for 4'-methoxy derivatives of JMT-1 against tPBP2^{H041} at 10 μ M. Compounds exhibiting greater than 80% inhibition of both tPBP2^{WT} and tPBP2^{H041} activity at 100 μ M (**Figure 5.16**) were tested against tPBP2^{H041} at 10 μ M. Values were determined in a purified protein assay in which tPBP2 was preincubated with 10 μ M compound, followed by addition of 1 μ M Bocillin-FL. Data are presented as a fraction of activity of the DMSO control. Error bars are standard deviation.



59: R ₁ = F	R ₂ = H	A = COOH	X = F	72: R ₁ = Me	R ₂ = H	A = COOH	X = Cl
60: R ₁ = H	R ₂ = F	A = COOH	X = F	73: R ₁ = H	R ₂ = Me	A = COOH	X = Cl
61: R ₁ = F	R ₂ = F	A = COOH	X = F	74: R ₁ = CF ₃	R ₂ = H	A = COOH	X = Cl
62: R ₁ = H	R ₂ = Br	A = COOH	X = F	75: R ₁ = H	R ₂ = CF ₃	A = COOH	X = Cl
63: R ₁ = Me	R ₂ = H	A = COOH	X = F	76: R ₁ = OMe	R ₂ = H	A = COOH	X = Cl
64: R ₁ = H	R ₂ = Me	A = COOH	X = F	77: R ₁ = H	R ₂ = OMe	A = COOH	X = Cl
65: R ₁ = H	R ₂ = OMe	A = COOH	X = F	78: R ₁ = F	R ₂ = H	A = TTZ	X = Cl
66: R ₁ = H	R ₂ = F	A = TTZ	X = F	79: R ₁ = H	R ₂ = F	A = TTZ	X = Cl
67: R ₁ = H	R ₂ = Me	A = TTZ	X = F	80: R ₁ = Me	R ₂ = H	A = TTZ	X = Cl
68: R ₁ = F	R ₂ = H	A = COOH	X = Cl	81: R ₁ = H	R ₂ = Me	A = TTZ	X = Cl
69: R ₁ = H	R ₂ = F	A = COOH	X = Cl	82: R ₁ = OMe	R ₂ = H	A = TTZ	X = Cl
70: R ₁ = F	R ₂ = F	A = COOH	X = Cl	83: R ₁ = H	R ₂ = OMe	A = TTZ	X = Cl
71: R ₁ = H	R ₂ = Br	A = COOH	X = Cl				

Figure 5.18: Structures of compounds JMT-59 through JMT-83, which possess a halogen in place of the 4'-methyl group seen in JMT-1. TTZ: 1H-tetrazol-5-yl

The next parameter to be examined was a change in van der Waals radius at the 4'-position. To this end, a series of 4'-halogenated molecules was synthesized, and inhibition data are shown in **Figure 5.19** and **Figure 5.20**. While the 4'-fluoro (**JMT-59** through **JMT-67**) analogues are among the least active compounds reported in these studies, large hydrophobic substitutions on the anthranilic acid moiety again enhance PBP2-inhibitory activity. The 5-bromoanthranilic acid and 4-methylantranilic acid analogues **JMT-62** and **JMT-63** are the only compounds of this group to fully inhibit both tPBP2^{WT} and tPBP2^{H041} at 100 μ M. They exhibit 45 \pm 14% and 54 \pm 18% inhibition of tPBP2^{H041}, respectively, at 10 μ M. In all cases, the 4'-chloro compounds (**JMT-68** through **JMT-83**) are more potent than their 4'-fluoro analogues. However, the 4'-chloro substitution still appears to confer less activity than the 4'-methyl parent structure. Taken together, these data suggest that increasing van der Waals radius at the 4'-position is associated with increased inhibition, but potential effects of 4'-substituent polarizability

cannot be dismissed. Consistent with data from other series, the 4- (**JMT-74**) and 5-trifluoromethylantranilic acid (**JMT-75**) compounds are still quite active, inhibiting tPBP2^{H041} 89 ± 4% and 86 ± 6%, respectively, at 10 µM.

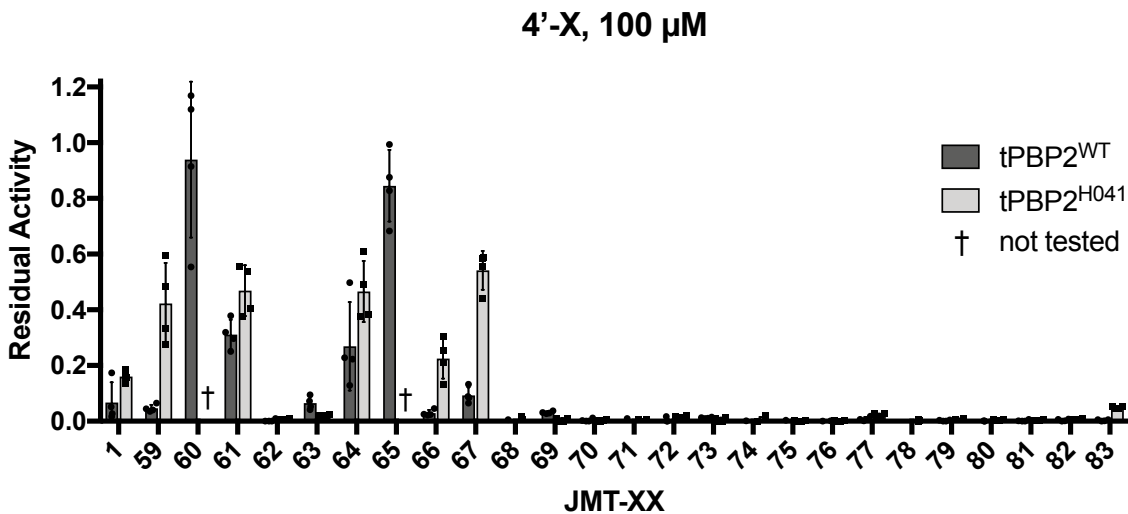


Figure 5.19: Inhibition data for JMT-59 through JMT-83 against tPBP2^{WT} and tPBP2^{H041} at 100 µM. Values were determined in a purified protein assay in which tPBP2 was preincubated with 100 µM compound, followed by addition of 1 µM Bocillin-FL. Data are presented as a fraction of activity of the DMSO control. Error bars are standard deviation.

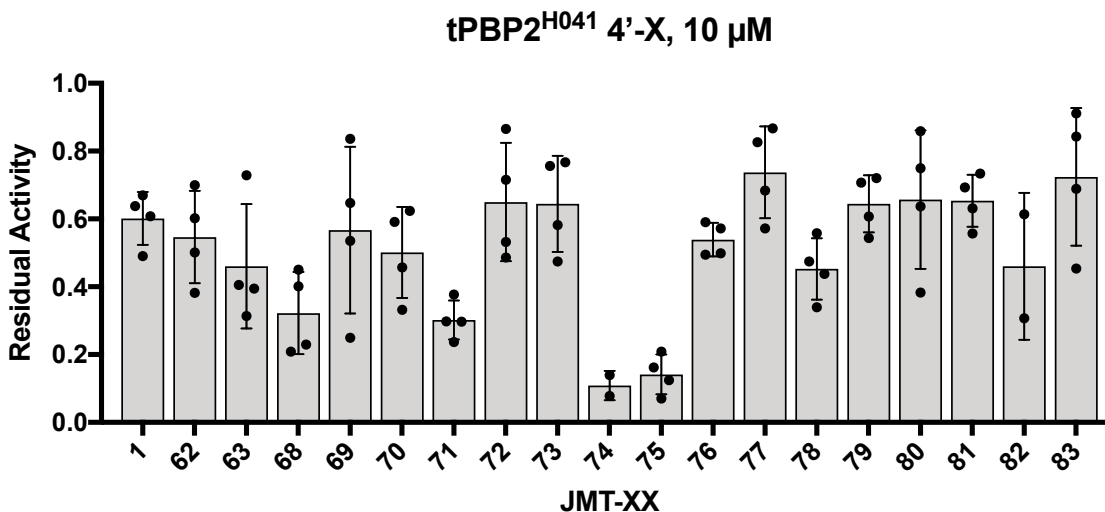
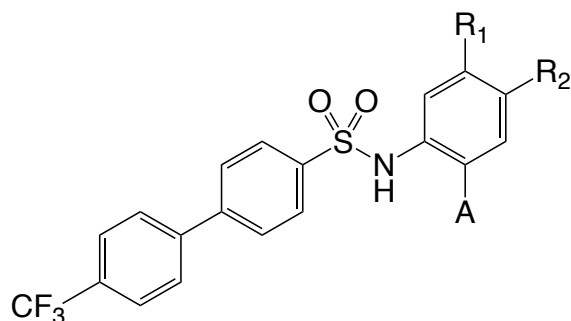


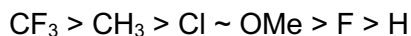
Figure 5.20: Inhibition data for 4-fluoro and 4-chloro derivatives of JMT-1 against tPBP2^{H041} at 10 µM. Compounds exhibiting greater than 80% inhibition of both tPBP2^{WT} and tPBP2^{H041} activity at 100 µM (**Figure 5.19**) were tested against tPBP2^{H041} at 10 µM. Values were determined in a purified protein assay in which tPBP2 was preincubated with 10 µM compound, followed by addition of 1 µM Bocillin-FL. Data are presented as a fraction of activity of the DMSO control. Error bars are standard deviation.



84:	R ₁ = F	R ₂ = H	A = COOH	93:	R ₁ = H	R ₂ = OMe	A = COOH
85:	R ₁ = H	R ₂ = F	A = COOH	94:	R ₁ = F	R ₂ = H	A = TTZ
86:	R ₁ = F	R ₂ = F	A = COOH	95:	R ₁ = H	R ₂ = F	A = TTZ
87:	R ₁ = H	R ₂ = Br	A = COOH	96:	R ₁ = H	R ₂ = Br	A = TTZ
88:	R ₁ = Me	R ₂ = H	A = COOH	97:	R ₁ = Me	R ₂ = H	A = TTZ
89:	R ₁ = H	R ₂ = Me	A = COOH	98:	R ₁ = H	R ₂ = Me	A = TTZ
90:	R ₁ = CF ₃	R ₂ = H	A = COOH	99:	R ₁ = OMe	R ₂ = H	A = TTZ
91:	R ₁ = H	R ₂ = CF ₃	A = COOH	100:	R ₁ = H	R ₂ = OMe	A = TTZ
92:	R ₁ = OMe	R ₂ = H	A = COOH				

Figure 5.21: Structures of compounds JMT-84 through JMT-100, which possess a 4'-trifluoromethyl group in place of the 4'-methyl group seen in JMT-1. TTZ: 1H-tetrazol-5-yl

To examine the effects of polarizability at the 4'-position further, a series of 4'-trifluoromethyl analogues was synthesized. Inhibition data for this series against tPBP2 are shown in **Figure 5.22** and **Figure 5.23**. Analogues **JMT-84** through **JMT-100** are the most active series of compounds from the collection of biphenyl 4'-position modifications, with nearly all exhibiting full inhibition of both tPBP2^{WT} and tPBP2^{H041} at 100 μ M. Their potent activity in the context of a variety of 4- and 5-substituted anthranilic acid and phenyltetrazole moieties suggests a role for both van der Waals radius and polarizability at the 4'-position. From the combined data on compounds derivatized at the 4'-position, the following pattern has emerged with respect to tPBP2 inhibition:



As in other series, the most active compounds from the 4'-trifluoromethyl series are the 4- and 5-trifluoromethylantranilic acid analogues **JMT-90** and **JMT-91**, which exhibit full inhibition of tPBP2^{H041} at 10 μ M. By contrast with other series, however, there are several other promising molecules among the 4'-trifluoromethyl analogues. For example, **JMT-86**

(4,5-difluoroanthranilic acid), **JMT-87** (5-bromoanthranilic acid), **JMT-88** (4-methylantranilic acid), **JMT95** ((5-fluorophenyl)tetrazole), and **JMT-98** ((5-methylphenyl)tetrazole) all show greater than 90% inhibition of tPBP2^{H041} at 10 μ M.

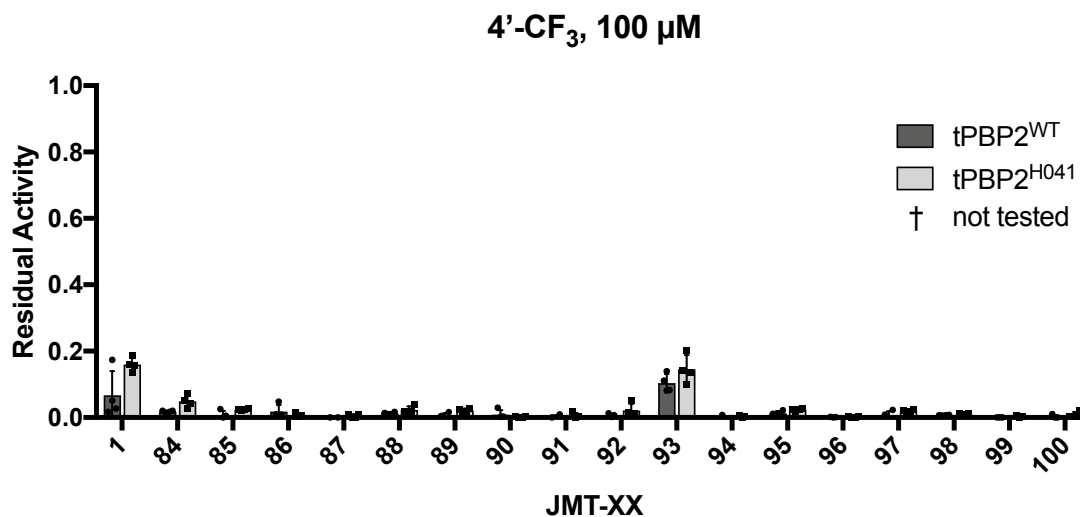


Figure 5.22: Inhibition data for JMT-84 through JMT-100 against tPBP2^{WT} and tPBP2^{H041} at 100 μ M. Values were determined in a purified protein assay in which tPBP2 was preincubated with 100 μ M compound, followed by addition of 1 μ M Bocillin-FL. Data are presented as a fraction of activity of the DMSO control. Error bars are standard deviation.

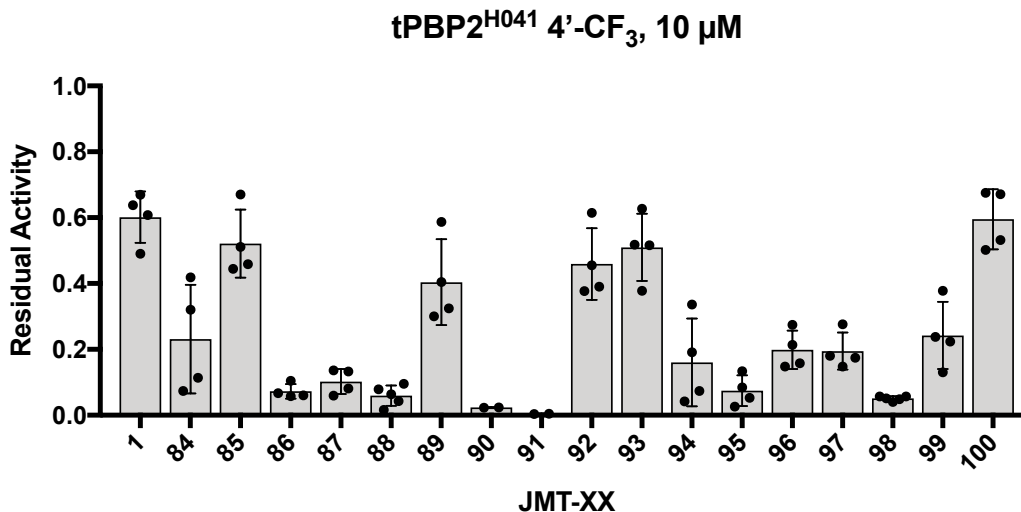


Figure 5.23: Inhibition data for 4'-trifluoromethyl derivatives of JMT-1 against tPBP2^{H041} at 10 μ M. Compounds exhibiting greater than 80% inhibition of both tPBP2^{WT} and tPBP2^{H041} activity at 100 μ M (Figure 5.22) were tested against tPBP2^{H041} at 10 μ M. Values were determined in a purified protein assay in which tPBP2 was preincubated with 10 μ M compound, followed by addition of 1 μ M Bocillin-FL. Data are presented as a fraction of activity of the DMSO control. Error bars are standard deviation.

Several of the most active compounds from the 4'-derivatized collection, defined as exhibiting greater than 75% inhibition against tPBP2^{H041} at 10 μ M, were tested against *N. gonorrhoeae* FA19 and H041 in disc diffusion assays (**Figure 5.24**). The most potent antigonococcal yet, **JMT-84**, is seen in this group. This anthranilic acid analogue with 4-fluoro and 4'-trifluoromethyl substitutions inhibits the growth of *N. gonorrhoeae* FA19 and H041 up to 21.2 ± 1.9 mm and 17.5 ± 0 mm, respectively, from discs imbued with 10 μ g compound. Consistent with what was seen for the initial derivatives, phenyltetrazole compounds appear to perform worse than their anthranilic acid analogues in measures of antimicrobial potency. Data for **JMT-47**, **JMT-56**, **JMT-74**, **JMT-90**, **JMT-91**, and **JMT-96** are pending.

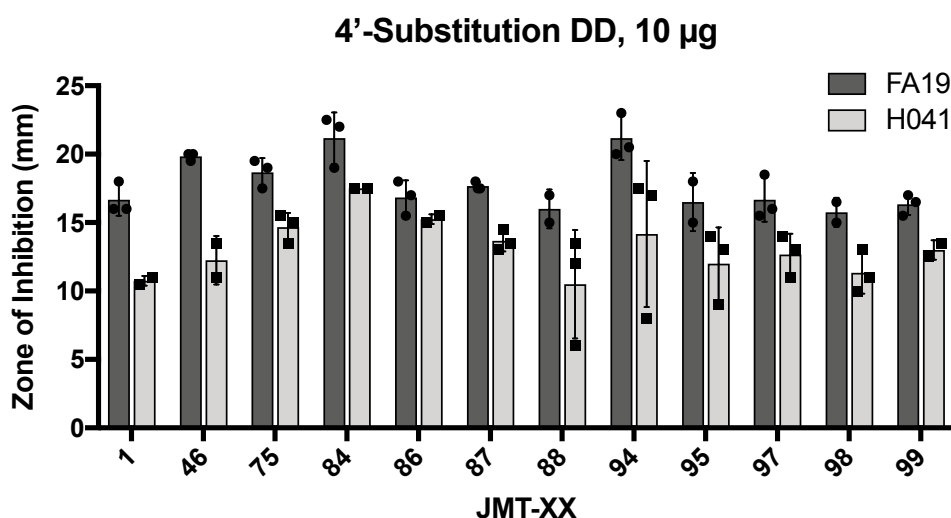
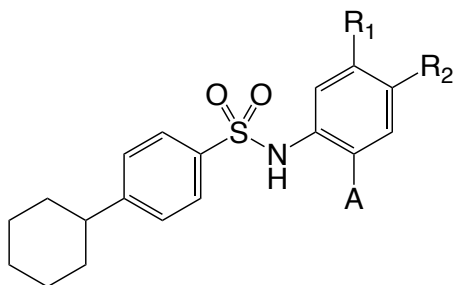


Figure 5.24: Disc diffusion data for potent 4'-substituted derivatives of JMT-1 against *N. gonorrhoeae* FA19 and H041. Compounds exhibiting greater than 75% inhibition of tPBP2^{H041} activity at 10 μ M were tested against susceptible reference gonococcal strain FA19 and multi-drug resistant H041 at 10 μ g per disc.

5.2.e. Modifications to the biphenyl ring system II: Changes to the secondary aromatic system



101:	R ₁ = F	R ₂ = H	A = COOH	110:	R ₁ = H	R ₂ = OMe	A = COOH
102:	R ₁ = H	R ₂ = F	A = COOH	111:	R ₁ = F	R ₂ = H	A = TTZ
103:	R ₁ = F	R ₂ = F	A = COOH	112:	R ₁ = H	R ₂ = F	A = TTZ
104:	R ₁ = H	R ₂ = Br	A = COOH	113:	R ₁ = H	R ₂ = Br	A = TTZ
105:	R ₁ = Me	R ₂ = H	A = COOH	114:	R ₁ = Me	R ₂ = H	A = TTZ
106:	R ₁ = H	R ₂ = Me	A = COOH	115:	R ₁ = H	R ₂ = Me	A = TTZ
107:	R ₁ = CF ₃	R ₂ = H	A = COOH	116:	R ₁ = H	R ₂ = CF ₃	A = TTZ
108:	R ₁ = H	R ₂ = CF ₃	A = COOH	117:	R ₁ = OMe	R ₂ = H	A = TTZ
109:	R ₁ = OMe	R ₂ = H	A = COOH	118:	R ₁ = H	R ₂ = OMe	A = TTZ

Figure 5.25: Structures of compounds **JMT-101** through **JMT-118**, which possess a 4-cyclohexylphenyl group in place of the 1,1'-biphenyl system seen in **JMT-1**. TTZ: 1H-tetrazol-5-yl

Next, we wanted to observe the effect of increased flexibility at the distal ring system on PBP2-inhibitory activity. Inhibition data for this series against tPBP2 are shown in **Figure 5.26** and **Figure 5.27**. Somewhat surprisingly, replacement of the secondary biphenyl aromatic ring with a cyclohexyl group (**JMT-101** through **JMT-118**) yields active compounds despite the absence of a 4'-substituent. This indicates that flexibility at this position may allow a conformation that involves more or better contacts with the PBP2 active site. The most active compound of the cyclohexylphenyl series is the 5-trifluoromethylantranilic acid **JMT-108**, which inhibits tPBP2^{H041} fully at 10 μ M. Other potent inhibitors include 4,5-difluoroantranilic acid **JMT-103**, (5-fluorophenyl)tetrazole **JMT-112**, and (5-methylphenyl)tetrazole **JMT-115**, all of which exhibit greater than 90% inhibition of tPBP2^{H041} at 10 μ M.

Cyclohexylphenyl, 100 μ M

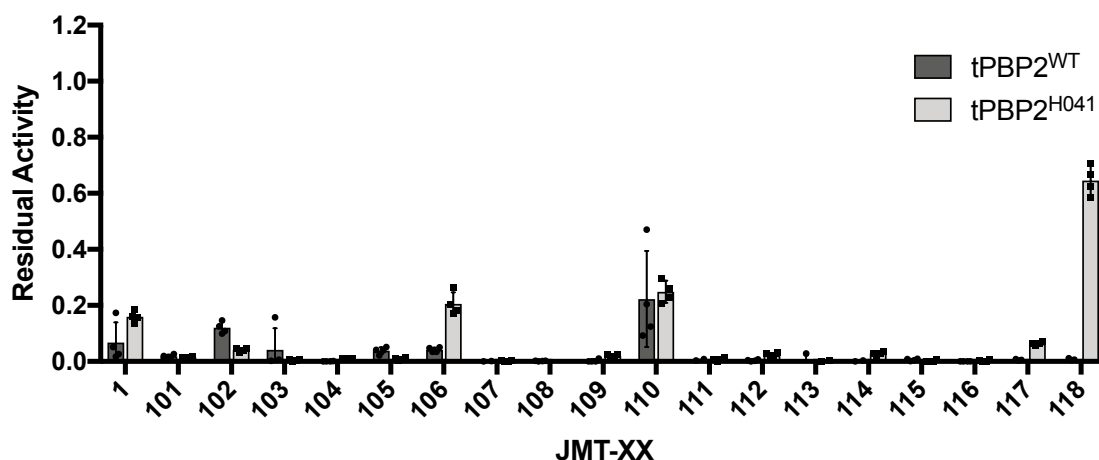


Figure 5.26: Inhibition data for JMT-101 through JMT-118 against tPBP2^{WT} and tPBP2^{H041} at 100 μ M. Values were determined in a purified protein assay in which tPBP2 was preincubated with 100 μ M compound, followed by addition of 1 μ M Bocillin-FL. Data are presented as a fraction of activity of the DMSO control. Error bars are standard deviation.

tPBP2^{H041} Cyclohexylphenyl, 10 μ M

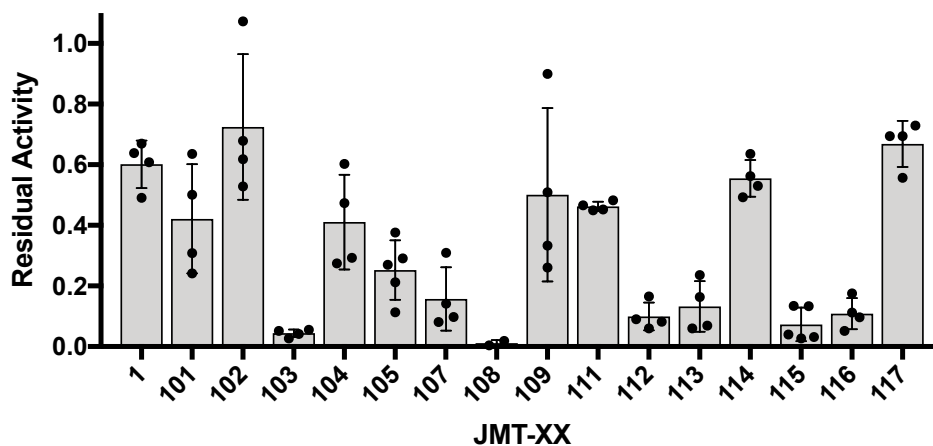
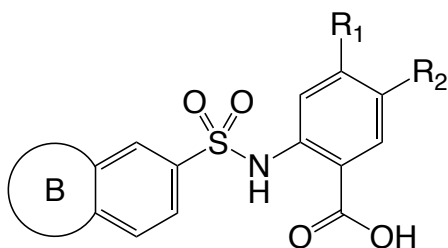


Figure 5.27: Inhibition data for 4-cyclohexylphenyl derivatives of JMT-1 against tPBP2^{H041} at 10 μ M. Compounds exhibiting greater than 80% inhibition of both tPBP2^{WT} and tPBP2^{H041} activity at 100 μ M (Figure 5.26) were tested against tPBP2^{H041} at 10 μ M. Values were determined in a purified protein assay in which tPBP2 was preincubated with 10 μ M compound, followed by addition of 1 μ M Bocillin-FL. Data are presented as a fraction of activity of the DMSO control. Error bars are standard deviation.



119:	R ₁ = F	R ₂ = H	B = CH=CHCH=CH
120:	R ₁ = H	R ₂ = F	B = CH=CHCH=CH
121:	R ₁ = H	R ₂ = Me	B = CH=CHCH=CH
122:	R ₁ = F	R ₂ = H	B = CH ₂ CH ₂ CH ₂ CH ₂
123:	R ₁ = H	R ₂ = F	B = CH ₂ CH ₂ CH ₂ CH ₂
124:	R ₁ = H	R ₂ = Me	B = CH ₂ CH ₂ CH ₂ CH ₂
125:	R ₁ = H	R ₂ = H	B = OCH ₂ CH ₂ O
126:	R ₁ = F	R ₂ = H	B = OCH ₂ CH ₂ O
127:	R ₁ = H	R ₂ = F	B = OCH ₂ CH ₂ O
128:	R ₁ = H	R ₂ = Me	B = OCH ₂ CH ₂ O

Figure 5.28: Structures of compounds *JMT-119* through *JMT-128*, which possess a bicyclo[4.4.0] ring system in place of the 1,1'-biphenyl system seen in *JMT-1*.

Less conservative changes were also made to the 1,1'-biphenyl system, including fusion to naphth-2-yl (**JMT-119** through **JMT-121**), 5,6,7,8-tetrahydronaphth-2-yl (**JMT-122** through **JMT-124**), and 1,4-benzodioxan-6-yl (**JMT-125** through **JMT-128**) systems. Inhibition data for this series against tPBP2 are shown in **Figure 5.29** and **Figure 5.30**. Each of these changes substantially decreases inhibition. The most active among this series of bicyclo[4.4.0] compounds are the 5,6,7,8-tetrahydronaphth-2-yl analogues, with 4-fluoro compound **JMT-122** exhibiting $97 \pm 1\%$ and $84 \pm 2\%$ inhibition of tPBP2^{WT} and tPBP2^{H041}, respectively, at 100 μM . **JMT-122** was further tested against tPBP2^{H041} at 10 μM but showed minimal inhibition at this concentration.

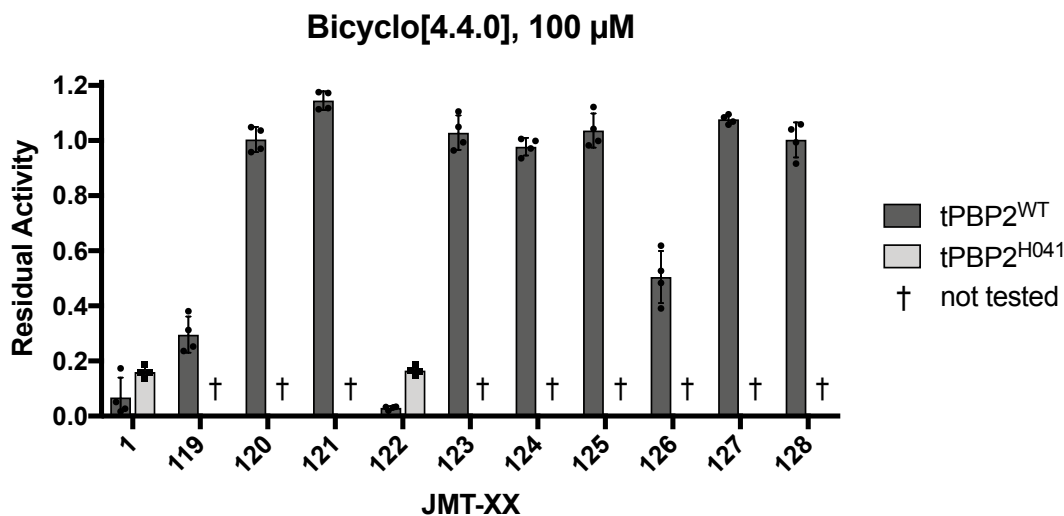


Figure 5.29: Inhibition data for JMT-119 through JMT-128 against tPBP2^{WT} and tPBP2^{H041} at 100 μ M. Values were determined in a purified protein assay in which tPBP2 was preincubated with 100 μ M compound, followed by addition of 1 μ M Bocillin-FL. Data are presented as a fraction of activity of the DMSO control. Error bars are standard deviation.

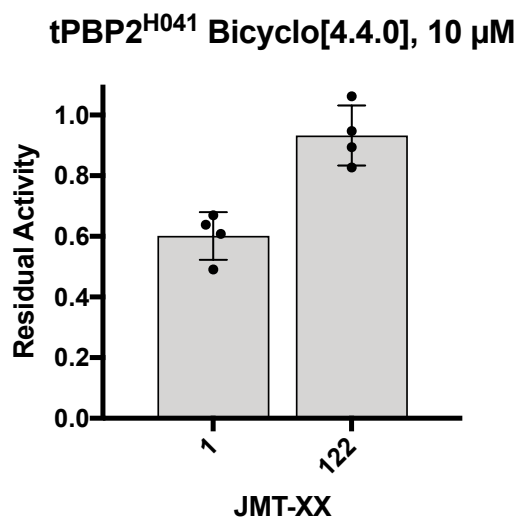


Figure 5.30: Inhibition data for bicyclo[4.4.0] derivatives of JMT-1 against tPBP2^{H041} at 10 μ M. Compounds exhibiting greater than 80% inhibition of both tPBP2^{WT} and tPBP2^{H041} activity at 100 μ M were tested against tPBP2^{H041} at 10 μ M. Values were determined in a purified protein assay in which tPBP2 was preincubated with 10 μ M compound, followed by addition of 1 μ M Bocillin-FL. Data are presented as a fraction of activity of the DMSO control. Error bars are standard deviation.

Potent PBP2 inhibitors from the final set of biphenyl modifications were tested against *N. gonorrhoeae* FA19 and H041 in disc diffusion assays, revealing the second most potent antigonococcal to emerge from these studies (**Figure 5.31**). **JMT-108**, a 5-trifluoromethylantranilic acid analogue from the cyclohexylphenyl series, exhibits large zones of inhibition against both FA19 (20.0 ± 0 mm) and H041 (16.0 ± 0.7 mm). Other compounds showing good antimicrobial activity include **JMT-103**, **JMT-107**, and **JMT-113**, all of which show zones of inhibition greater than 15 mm against both strains. No bicyclo[4.4.0] compounds were tested due to their poor performance in PBP2 inhibition assays.

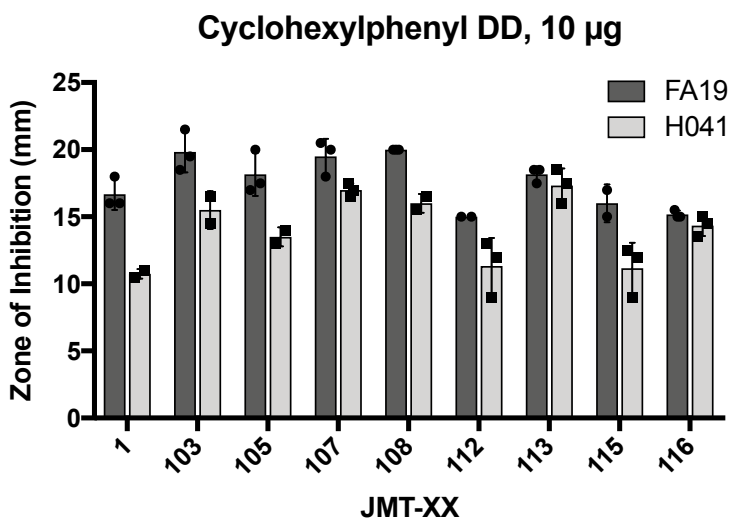


Figure 5.31: Disc diffusion data for potent cyclohexylphenyl derivatives of JMT-1 against *N. gonorrhoeae* FA19 and H041. Compounds exhibiting greater than 75% inhibition of tPBP2^{H041} activity at 10 μ M were tested against susceptible reference gonococcal strain FA19 and multi-drug resistant H041 at 10 μ g per disc.

5.3. Prediction of the binding modes of the most potent JMT-1 derivatives

The most potent PBP2 inhibitors (**JMT-13** and **JMT-108**) and the most potent antigonococcal (**JMT-84**) were docked to the active sites of tPBP2^{WT} and tPBP2^{H041} with guidance from the molecular dynamics simulations of **JEK-42** and **JMT-1** reported in Chapter 4. In the modeled complexes, a sulfonyl oxygen is positioned within the oxyanion hole created by the main chain nitrogens of Ser310 and Thr500, and the 1,1'-biphenyl system extends toward N364 and F420 (**Figure 5.32**). In the tPBP2^{WT} complexes, the carboxylic acid forms hydrogen bonds with the side chains of S362, S483, K497 and T498, and in the tPBP2^{H041} complexes, it forms hydrogen bonds with the side chain of T500 and S545. Because the changes to **JMT-1** represented in these molecules do not add opportunities for strong hydrogen bonding, the resulting increases in potency likely have to do with enhanced van der Waals interactions with the active site. Computationally, this appears to be the case. On the anthranilic acid moiety of the molecule, the 5-trifluoromethyl groups of **JMT-13** and **JMT-108** contribute 2-fold more van der Waals interaction energy to ligand-receptor complex formation than the 5-fluoro group of **JMT-1** ($-0.7 \text{ kcal}\cdot\text{mol}^{-1}$ v $-1.7 \text{ kcal}\cdot\text{mol}^{-1}$) (**Figures 5.33 & 5.34**), while the 4-fluoro group of **JMT-86** augments interaction only marginally ($-0.9 \text{ kcal}\cdot\text{mol}^{-1}$). With respect to the secondary ring of the 1,1'-biphenyl system, the cyclohexyl system seen in **JMT-108** show similar receptor interactions to the methylphenyl group of **JMT-1** and **JMT-13** ($-8.8 \text{ kcal}\cdot\text{mol}^{-1}$ v $-8.6 \text{ kcal}\cdot\text{mol}^{-1}$). However, the trifluoromethylphenyl system of **JMT-84** makes more extensive contact with the active site surface ($-10.5 \text{ kcal}\cdot\text{mol}^{-1}$).

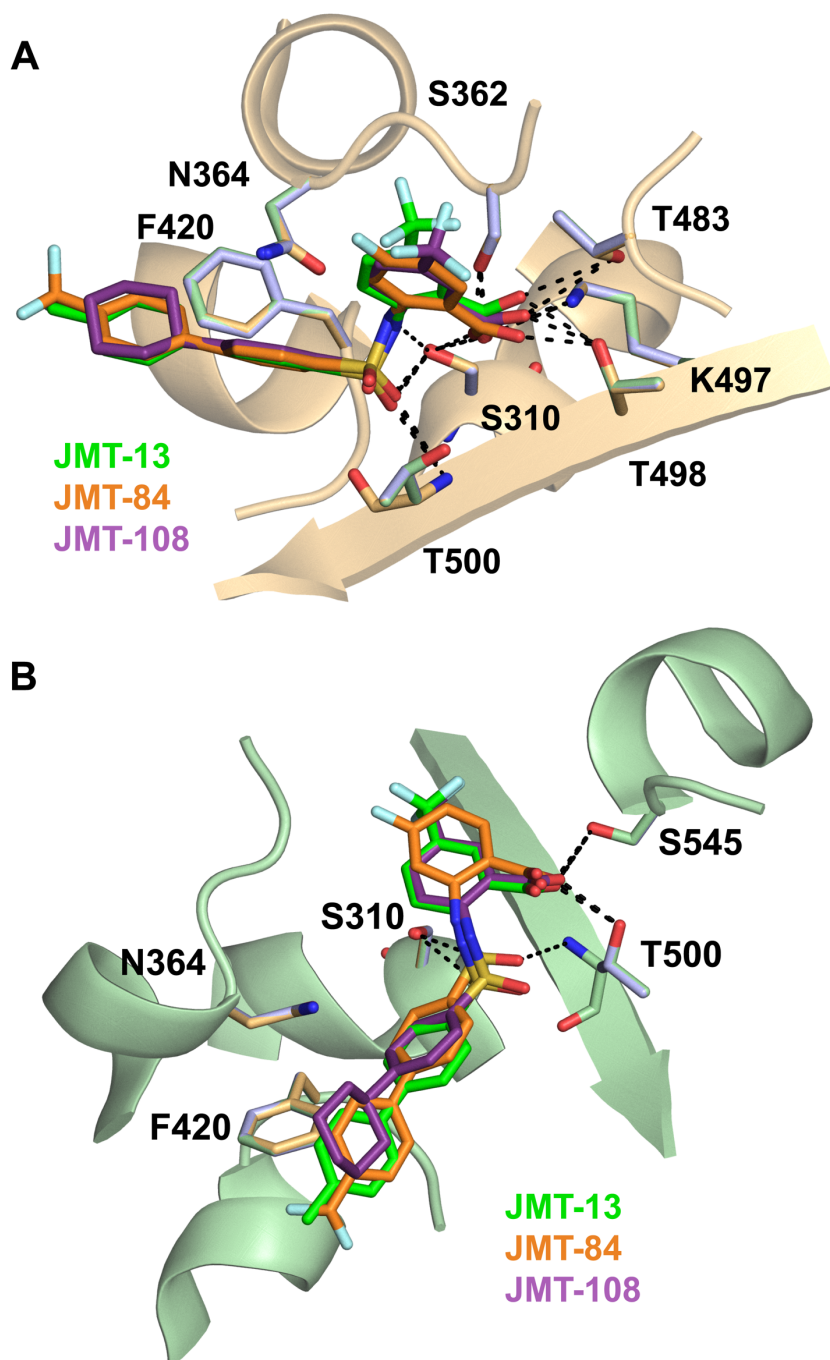


Figure 5.32: Docked poses of compounds showing potent tPBP2 inhibition and anticonococcal activity. **A.** When docked to tPBP2^{WT} with guidance from the predicted JMT-1 binding mode, potent compounds show similar interactions with the transpeptidase active site. The docked structure of JMT-13 is shown in green, JMT-84 is shown in orange, and JMT-108 is shown in purple. Predicted hydrogen bonds are shown as dashed lines. **B.** Potent compounds docked to tPBP2^{H041} with guidance from the predicted JMT-1 binding mode show similar interactions with the transpeptidase active site. The docked structure of JMT-13 is shown in green, JMT-84 is shown in orange, and JMT-108 is shown in purple. Predicted hydrogen bonds are shown as dashed lines.

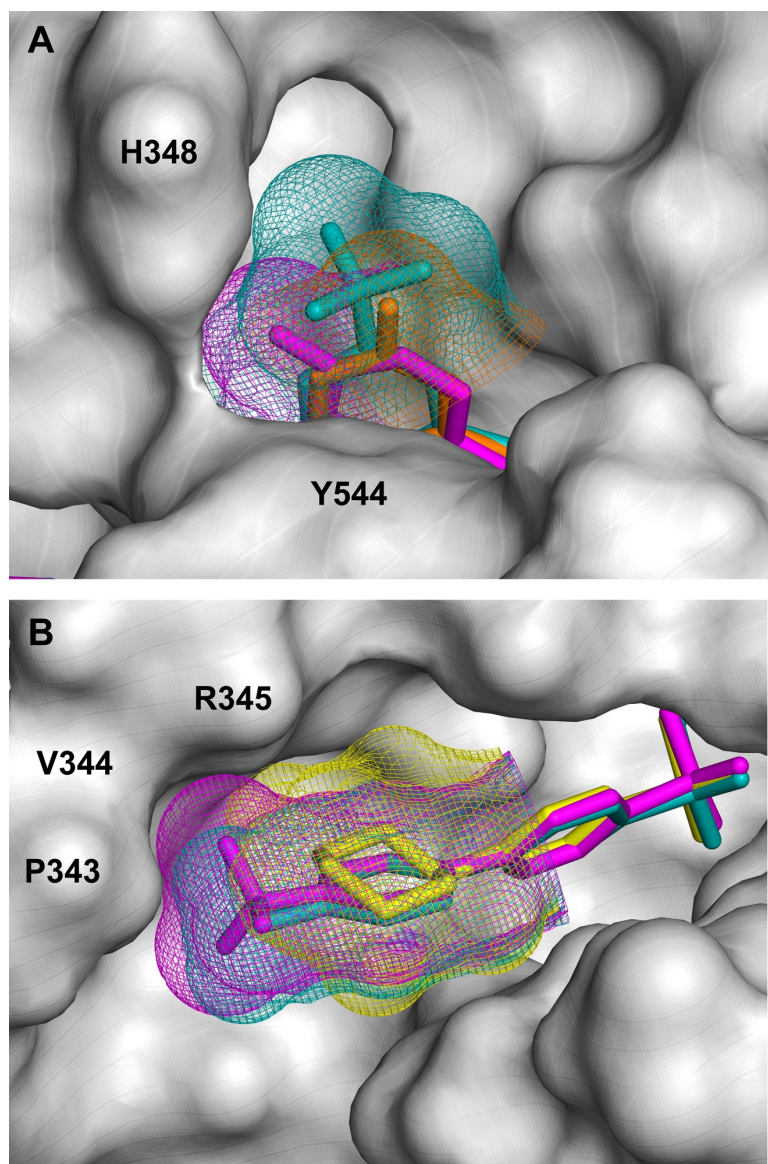


Figure 5.33: Surface rendering of modeled JMT-1 derivatives in complex with tPBP2^{WT}. **A.** The trifluoromethyl group seen on the anthranilic acid moiety of JMT-13 and JMT-108 (ligand shown as teal sticks, surface shown as teal mesh) and the 4-fluoro group of JMT-84 (ligand shown as magenta sticks, surface shown as magenta mesh) create more surface contact with the active site of tPBP2^{WT} than the 5-fluoro group of JMT-1 (ligand shown as orange sticks, surface shown as orange mesh). **B.** The trifluoromethylphenyl group of JMT-84 (ligand shown as magenta sticks, surface shown as magenta mesh) exhibits a closer contour to the tPBP2^{WT} surface (shown in grey) than the methylphenyl group of JMT-1 and JMT-13 (ligand shown as teal sticks, surface shown as teal mesh), while the cyclohexyl group of JMT-108 (ligand shown as yellow sticks, surface shown as yellow mesh) shows only marginally increased contact with the active site surface.

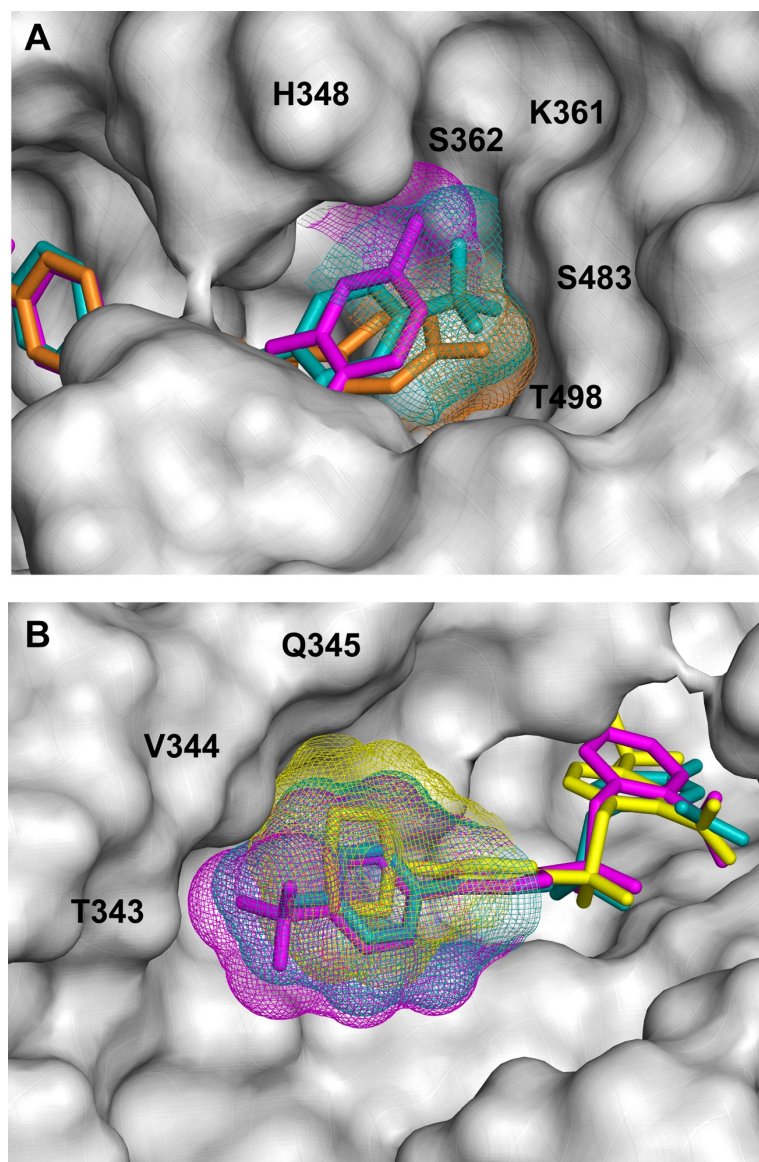


Figure 5.34: Surface rendering of modeled JMT-1 derivatives in complex with $tPBP2^{H041}$. **A.** As in $tPBP2^{WT}$, the trifluoromethyl group seen on the anthranilic acid moiety of JMT-13 and JMT-108 (ligand shown as teal sticks, surface shown as teal mesh) and the 4-fluoro group of JMT-84 (ligand shown as magenta sticks, surface shown as magenta mesh) create more surface contact with the active site of $tPBP2^{H041}$ than the 5-fluoro group of JMT-1 (ligand shown as orange sticks, surface shown as orange mesh). **B.** The trifluoromethylphenyl group of JMT-84 (ligand shown as magenta sticks, surface shown as magenta mesh) exhibits a closer contour to the $tPBP2^{H041}$ surface (shown in grey) than the methylphenyl group of JMT-1 and JMT-13 (ligand shown as teal sticks, surface shown as teal mesh), while the cyclohexyl group of JMT-108 (ligand shown as yellow sticks, surface shown as yellow mesh) shows only marginally increased contact with the active site surface.

5.4. Discussion

In this work, we present the derivatization of the prototype *N. gonorrhoeae* PBP2 inhibitor **JMT-1** with the goal of identifying modifications that enhance or diminish *in vitro* activity against both PBP2 and gonococci. First, we show that substitution of the **JMT-1** anthranilic acid moiety with hydrophobic groups at C4 or C5 is preferred for PBP2 inhibition, and that isosteric replacement of the C1 carboxylic acid with a *1H*-tetrazol-5-yl group results in compounds with similar activity. Next, we show that 4'-substitution of the 1,1'-biphenyl system is required for potent inhibition, but that this requirement is eliminated if the structure is changed to a more flexible 4-cyclohexylphenyl system. Modeling of the most potent compounds suggest the modifications to **JMT-1** responsible for increasing tPBP2 inhibition do so through augmented van der Waals interactions with the transpeptidase active site.

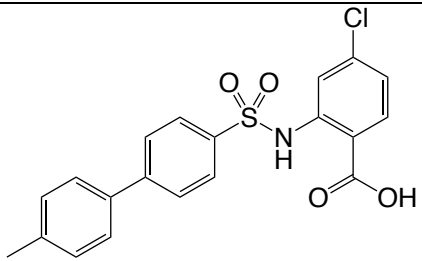
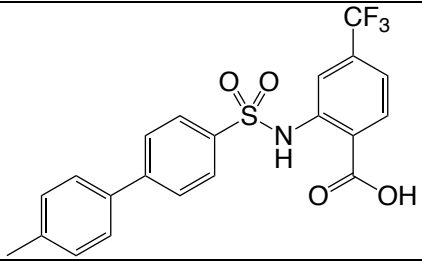
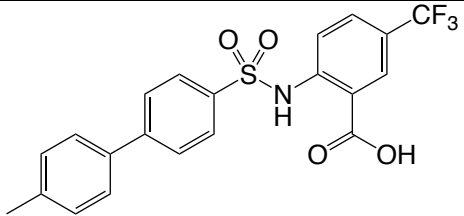
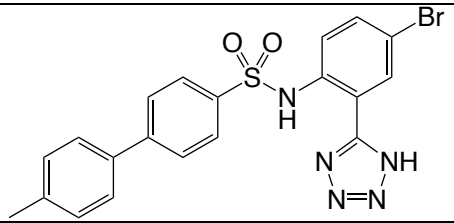
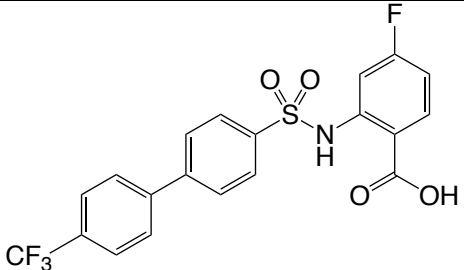
5.4.a. Summary of potent antigonococcal compounds and structure-activity relationships

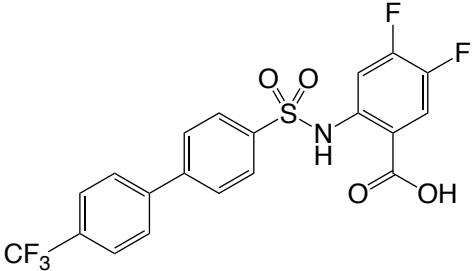
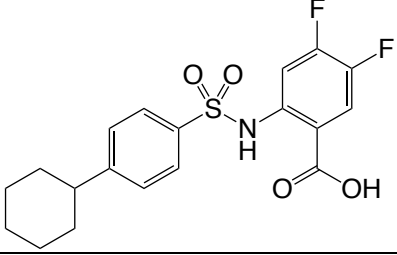
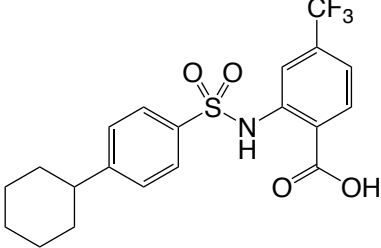
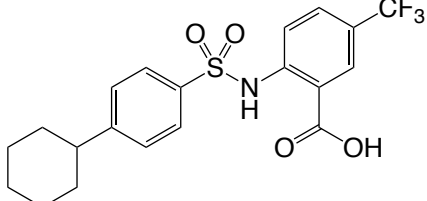
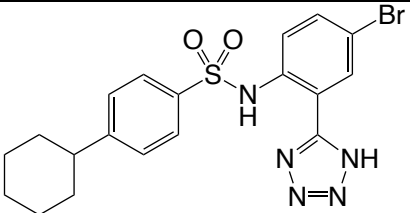
Compounds showing potent tPBP2 inhibition and antigonococcal activity are shown in **Table 5.1**. Overall, the most potent **JMT-1** derivatives possess lipophilic polarizable groups at the 4- and 5-positions of an anthranilic acid moiety. Increasing van der Waals radius at C4 or C5 appears to be correlated with greater activity as well, with six of the ten best compounds possessing a trifluoromethyl or bromo substituent. High activity is also observed in compounds 4,5-disubstituted with fluorine atoms, suggesting that there is a preference for a somewhat large area of hydrophobic surface at these positions. Phenyltetrazoles are generally less active against gonococci, and especially against H041, than their anthranilic acid analogues despite similar inhibition of tPBP2. This is perhaps due to the relative lipophilicity of the tetrazole-containing molecules (5-methyl-*1H*-tetrazole $\log D_{7.4} = -2.2$) compared to corresponding carboxylic acids (acetic acid $\log D_{7.4} = -3.0$). In both FA19 and H041, compounds must traverse the outer membrane

through porins that select for highly solvated, hydrophilic molecules. In H041, not only are these porins mutated to restrict entry,³⁰⁶ but there is also an overexpressed MtrCDE efflux system with the ability to extrude hydrophobic xenobiotics.^{317.318} Exceptions to this trend are the 5-bromophenyltetrazoles, which show improved antigonococcal activity compared to their 5-bromoanthranilic acid analogues and have a very narrow difference in activities between FA19 and H041.

Modifications to the 1,1'-biphenyl end of the **JMT-1** scaffold also result in some improvements in activity. Overall, compounds with larger hydrophobic groups at the 4'-position (*i.e.*, 4'-methyl and 4'-trifluoromethyl) tend to have better activity compared to smaller or more hydrophilic derivatives. Interestingly, while elimination of the 4'-substituent greatly diminishes activity of 1,1'-biphenyl compounds, incorporation of a 4'-unsubstituted cyclohexyl group causes no such decrease in activity and in fact, yields some of the most potent antigonococcal compounds resulting from these studies.

Table 5.1: Summary data for the JMT-1 derivatives showing the most potent antigonococcal activity. ^aPurified protein assay in which PBP2 is pre-incubated with compound or DMSO for 1 hour, followed by the addition of 1 μ M Bocillin-FL. Value reported is percent inhibition. ^bDisc diffusion assay performed with 10 μ g compound per disc. Value reported is zone of inhibition. Errors are standard deviation.

Compound	Structure	tPBP2 ^{H041} 10 μ M ^a	FA19 ^b (mm)	H041 ^b (mm)
JMT-5		92 \pm 8%	18.8 \pm 1.9	15.3 \pm 0.4
JMT-12		97 \pm 1%	20.5 \pm 0.7	15.5 \pm 1.8
JMT-13		99 \pm 1%	19.0 \pm 1.0	16.3 \pm 1.1
JMT-19		76 \pm 3%	17.3 \pm 1.8	16.0 \pm 1.4
JMT-84		77 \pm 16%	21.2 \pm 1.9	17.5 \pm 0

JMT-86		$93 \pm 2\%$	16.8 ± 1.3	15.3 ± 0.4
JMT-103		$96 \pm 1\%$	19.8 ± 1.5	15.5 ± 1.4
JMT-107		$84 \pm 10\%$	19.5 ± 1.3	17.0 ± 0.5
JMT-108		$99 \pm 1\%$	20.0 ± 0	16.0 ± 0.7
JMT-113		$87 \pm 8\%$	18.2 ± 0.6	17.3 ± 1.3

The most active compounds identified in the course of these studies were flexibly aligned using a stochastic conformational search, yielding an eight-point pharmacophore shown in **Figure 5.35**. This pharmacophore is generally supported by previous data on the inhibition of *S. aureus* PBP2a and *S. pneumoniae* by similar compounds,^{627,628} with the unique addition of the 1,1'-biphenyl system. Representation of the 1,1'-biphenyl system with two hydrophobic features, where only one is required to be aromatic, increases design capabilities by allowing the incorporation of a variety of 4-substituted phenyl systems like in the 4-cyclohexylphenyl series.

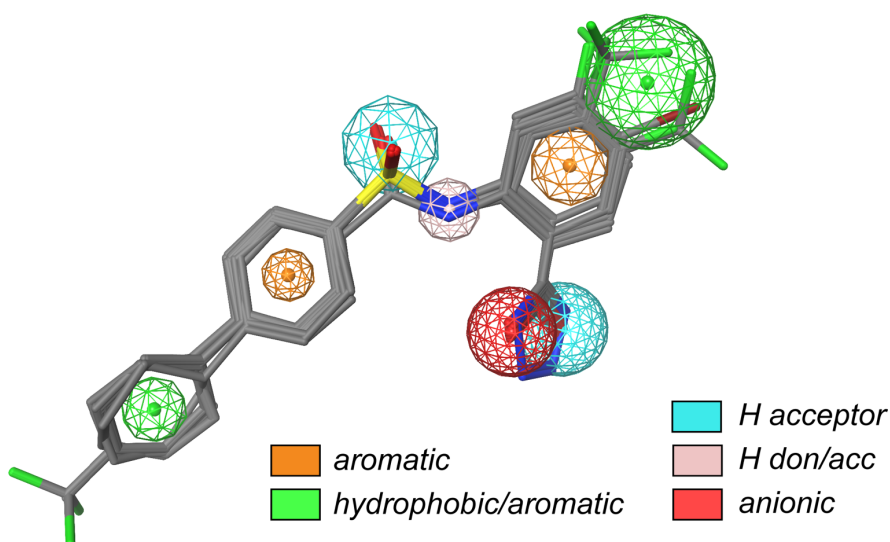


Figure 5.35: Flexible alignment and consensus pharmacophore based on the JMT-1 derivatives with the most potent antigonococcal activity.

Experiments published by other laboratories have determined zones of inhibition by several FDA-approved antimicrobials against *N. gonorrhoeae* strains with varied susceptibility profiles^{63,678} (**Table 5.2**). For example, with 0.5 μg penicillin G, the susceptible reference strain WHO F is inhibited with a 13.2 mm zone of inhibition, while neither penicillin-resistant strain (WHO K and H041) is inhibited at all. Similarly, a 0.5 μg

ceftriaxone disc inhibits the growth of WHO F with a 14.2 mm zone of inhibition, while it displays a decrease in potency against WHO K (6.7 mm) and fails to inhibit H041. By contrast, the reported **JMT-1** derivatives inhibit both FA19 and H041 to similar degrees. It should be noted that the masses of compound used in each disc is slightly different in the assays reported, as each takes into account the pharmacokinetic and pharmacodynamic factors determining efficacy, as well as epidemiologic values for susceptibility versus resistance. Since the reported **JMT-1** analogues represent a novel, experimental class, no such data exists. Thus, the 10 µg quantity used in these studies is not calibrated for direct comparisons of potency. Nonetheless, the large zones of inhibition seen against both reference strain FA19 and multidrug resistant H041 indicate real antimicrobial activity that is quite promising for the early development of a new class of compounds.

Table 5.2: Calibrated dichotomous sensitivity disc diffusion literature values for FDA-approved antimicrobials against *N. gonorrhoeae* with varied susceptibility profiles. †Taken from Mal *et al.*, 2016.⁶⁷⁸ ‡Taken from Ohnishi *et al.*, 2011.⁶³

Compound (mass, µg)	WHO F [†] (Pen ^S Ceph ^S)	WHO K [†] (Pen ^R Ceph ^{DS})	H041 [‡] (Pen ^R Ceph ^R)
penicillin G (0.5)	13.2 mm	0 mm	0 mm
ceftriaxone (0.5)	14.2 mm	6.7 mm	1 mm
ciprofloxacin (1)	15 mm	0 mm	1 mm
spectinomycin (100)	11 mm	16 mm	9 mm

5.4.b. Future testing of potent antigonococcal compounds

We have only just begun the hit-to-lead optimization and overall development processes for the reported scaffolds, and much more foundational work needs to be completed toward their biochemical and biological characterization. This includes more precise measures of potency against both the target (*i.e.*, IC₅₀ determinations against tPBP2^{WT} and tPBP2^{H041}) and pathogen (*i.e.*, MIC determinations against *N. gonorrhoeae* strains), as well as measures of selectivity (*i.e.*, cytotoxicity experiments against hepatic and renal lines). Additional experiments are needed to ensure the antigonococcal activity

results from transpeptidase inhibition. Such experiments include macromolecular synthesis assays measuring the incorporation of [¹⁴C]-diaminopimelate, microscopy for the observation of filament formation, and peptidoglycan cross-link formation assays measuring D-Ala release. If compounds are identified that show potent, on-target, selective antigonococcal activity, these compounds can be tested in the murine infection model described in Chapter 3.

Despite their lesser antigonococcal activity *in vitro*, tetrazole-containing derivatives should not yet be abandoned due to their potentially favorable properties *in vivo*. Xenobiotic carboxylic acids are commonly conjugated by phase II metabolic enzymes to acyl glucuronides and acyl coenzyme A thioesters.^{679,680} These modifications mask the acidic group critical to PBP2 inhibition, and the resulting acyl metabolites are reactive species implicated in hepatotoxicity. Tetrazoles, by contrast, are resistant to coenzyme A conjugation and form nonreactive *N*-glucuronide conjugates.^{681,682} Moreover, as mentioned above, tetrazole compounds are more lipophilic (5-methyl-1*H*-tetrazole logD_{7.4} = -2.2) than analogous carboxylic acids (acetic acid logD_{7.4} = -3.0), potentially improving their lipid bilayer permeability and bodily distribution.⁶⁸³ This property may be advantageous in the treatment of gonococcal cervicitis and pharyngitis by increasing accumulation at the site of infection. Taking into account the modest losses in activity seen in **JMT-1** analogues upon replacement of the carboxylic acid with a tetrazole, the potential for improved pharmacokinetics could ultimately outweigh such losses.

5.4.c. Future design strategies

In addition to biological characterization of the most potent compounds from these experiments, another immediate goal is further derivatization of the scaffolds, especially since the anthranilic acid moiety of **JMT-1** provides ample opportunity to explore additional chemical space. First, there is a need for data on the 6-fluoroanthranilic acid compound. While the 6-methyl analogue exhibited poor activity, substitution with a smaller fluorine

may better approximate the shape of the post-covalent cephalosporin complex after elimination of the C3 leaving group (**Figure 5.36**). Thus, the potency of such an analogue will provide insight into whether these compounds adopt a binding mode similar to the β -lactams after acylation. There is also a need for the investigation of less conservative substitutions on the anthranilic acid moiety, as the current dataset does not contain a great deal of structural diversity. Some modifications that can be incorporated to develop more comprehensive structure-activity relationships are the following: 1) polar hydrogen bonding substituents, including hydroxy and amino functionalities; 2) extended and branched aliphatics, such as ethyl and isopropyl groups; 3) bulkier 4,5-disubstitutions, including methylenedioxy and fused cyclopentyl groups; and 4) additional carboxylic acid isosteres, including those shown in **Figure 5.37**.⁶⁸⁴

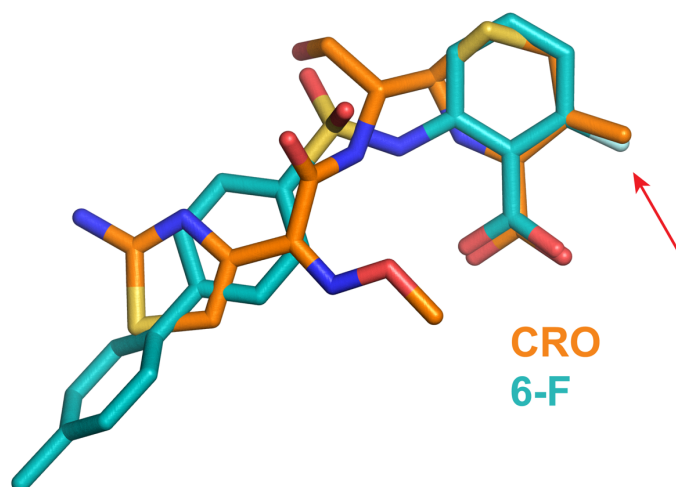


Figure 5.36: Overlay of ceftriaxone after leaving group departure and 2-(4'-methyl-[1,1'-biphenyl]-4-amido)-6-fluorobenzoic acid.

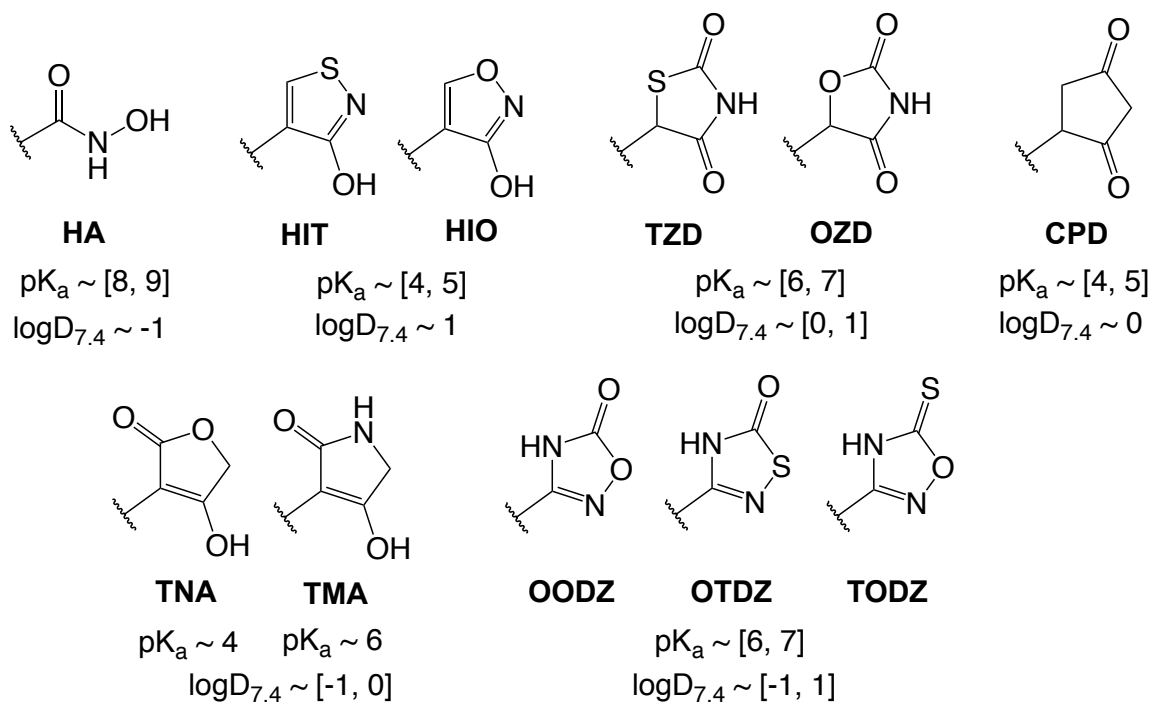
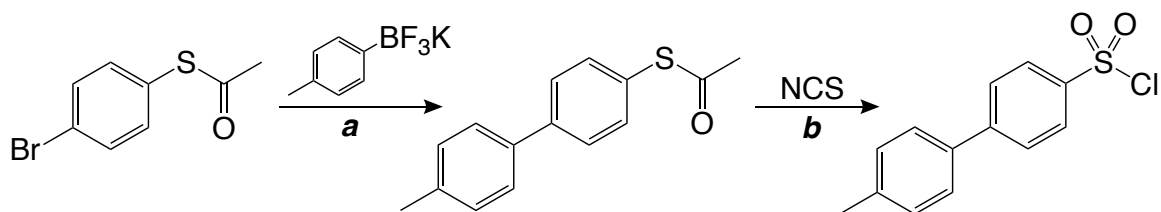


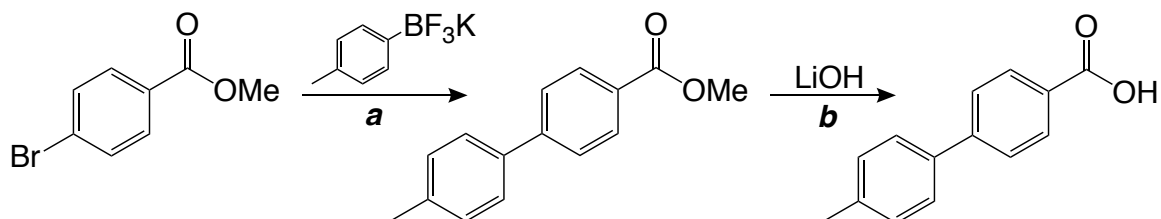
Figure 5.37: Carboxylic acid bioisosteres. HA: hydroxamic acid, HIT: 3-hydroxyisothiazole, HIO: 3-hydroxyisoxazole, TZD: thiazolidinedione, OZD: oxazolidinedione, CPD: 1,3-cyclopentanedione, TNA: tetronic acid, TMA: tetramic acid, OODZ: 5-oxo-1,2,4-oxadiazole, OTDZ: 5-oxo-1,2,4-thiadiazole, TODZ: 5-thioxo-1,2,4-oxadiazole, TTDZ: 5-thioxo-1,2,4-thiadiazole.

There is also opportunity to explore the 1,1'-biphenyl moiety of **JMT-1**. In our dataset, it was observed that incorporation of a methyl or trifluoromethyl group at the 4'-position enhances PBP2-inhibitory activity compared to substituents with smaller van de Waals radii (*i.e.*, H, F, and Cl). In this vein, the effects of shape and bulk should be assessed further by the incorporation of larger, more diverse groups, including branched aliphatics (*e.g.*, isopropyl and *t*-butyl) and small carbocycles (*e.g.*, cyclopropyl and cyclobutyl). The effect of 2'-substitution, as well as disubstitution, should also be examined. Finally, replacement of one or both rings with various aromatic or saturated heterocycles and carbocycles should be attempted. Sulfonyl chloride starting materials can be obtained through Suzuki cross-coupling reactions with thioacetate compounds, followed by oxidation with *N*-chlorosuccinimide^{685,686} (**Scheme 5.2**).



Scheme 5.2: Proposed synthesis of 4'-methyl[1,1'-biphenyl]-4-sulfonyl chloride from *S*-acetyl 4-bromothiophenol. **a.** Pd(dppf)₂Cl₂·CH₂Cl₂, Cs₂CO₃, 10:1 THF/H₂O, 100°C. **b.** 1:5 2 M HCl / MeCN, RT.

Amide analogues similar to **JEK-42** should be made for the most active **JMT-1** derivatives as well. Fortunately, benzoic acid starting materials can be obtained from similar syntheses using Suzuki cross-coupling reactions with methyl esters, followed by alkaline hydrolysis (**Scheme 5.3**). For a discussion of other possible changes to the sulfonamide functionality, see Chapter 4.



Scheme 5.3: Proposed synthesis of 4'-methyl[1,1'-biphenyl]-4-carboxylic acid from methyl 4-bromobenzoate. **a.** Pd(dppf)₂Cl₂·CH₂Cl₂, Cs₂CO₃, 10:1 THF/H₂O, 100°C. **b.** 1:1 THF/H₂O, RT.

5.4.d. Significance

Here we describe the synthesis 127 novel structures and their testing for inhibition of *N. gonorrhoeae* PBP2. We found that larger hydrophobic substitutions at C4 and C5 of the anthranilic acid moiety (*e.g.*, bromo, trifluoromethyl) improve PBP2 inhibition, as does a trifluoromethyl substitution at C4' of the 1,1'-biphenyl system. Interestingly, we also found that while lack of substitution at the C4' position results in decreased inhibition, modification of the secondary aromatic ring to a conformationally flexible cyclohexyl group

yields strong inhibition. Docked models predict the increased potency imparted by these substitutions is due to more favorable van der Waals interactions with the PBP2 active site compared to prototype **JMT-1**. Overall, the activity data coming from these early hit-to-lead optimization studies show the promise of this scaffold. It is capable of inhibiting PBP2 variants derived from both β -lactam-susceptible and -resistant strains and shows anticonococcal activity against both reference strain FA19 and multidrug resistant H041.

CHAPTER 6: Conclusion

6.1. Summary

Over the last several decades, *N. gonorrhoeae* has developed resistance to sulfonamides, penicillin, spectinomycin, tetracyclines, macrolides, fluoroquinolones, and now cephalosporins. With this proclivity for resistance development in mind, the CDC began recommending dual antimicrobial regimens of ceftriaxone with azithromycin or doxycycline, but patterns of increasing resistance to these agents globally have raised concerns of a future in which gonorrhea is untreatable. Therefore, continued efforts to identify antigonococcal compounds using all avenues of drug discovery are necessary to keep pace with the development of resistance. The body of work coming out of our laboratory has focused for several years on the structural biology of the penicillin-binding proteins, and more recently on the mechanisms of β -lactam resistance conferred by mutations in PBP2 of *N. gonorrhoeae*. In this project, emphasis was placed on ligand structure, specifically on the identification of features enhancing PBP2 inhibition, with the ultimate goal of designing novel antigonococcal agents. We report three studies to this end.

In Chapter 3, we outlined structure-activity relationships (SAR) for the cephalosporin class of β -lactams against cephalosporin-resistant *Neisseria gonorrhoeae* H041. We found that structural features of the C7 acylamino side chain (R_1) correlate highly with the second-order rate of tPBP2^{H041} acylation, with larger groups of modest lipophilicity containing multiple ring systems (e.g., the 2,3-dioxopiperazine side chain of cefoperazone) conferring greater activity. While the data suggest that the C3 side chain (R_2) plays a less obvious role, a combination of electronegative elements and planarity (e.g., the pyridylthiazole side chain of ceftaroline) can enhance tPBP2^{H041} acylation considerably.

Through molecular docking simulations of the precovalent ligand-receptor complex, we gained insight into how these features may enhance inhibition. In the docked

models, aromatic and hydrophobic groups on R_1 are shown extending toward a hydrophobic patch of the tPBP2^{H041} active site, and in a preliminary crystal structure of cefoperazone in complex with tPBP2^{H041}, the 2,3-dioxopiperazine moiety lies flat in this hydrophobic patch against the side chain of Y422. The models also show electronegative elements of R_2 interacting with K361. The importance of this residue for cephalosporin binding is supported by a stark reduction in the rate of acylation by ceftriaxone upon its mutation to a glutamate. We also found that many of the features enhancing target inhibition (*e.g.*, lipophilicity, aromaticity, *etc.*) diminish antimicrobial activity against the H041 strain, perhaps due to decreased accumulation in the periplasm. Finally, we observed that cefoperazone acylates tPBP2^{H041} much more rapidly than most other cephalosporins, and it exhibits comparable activity to ceftriaxone against *N. gonorrhoeae* H041 both *in vitro* and *in vivo*.

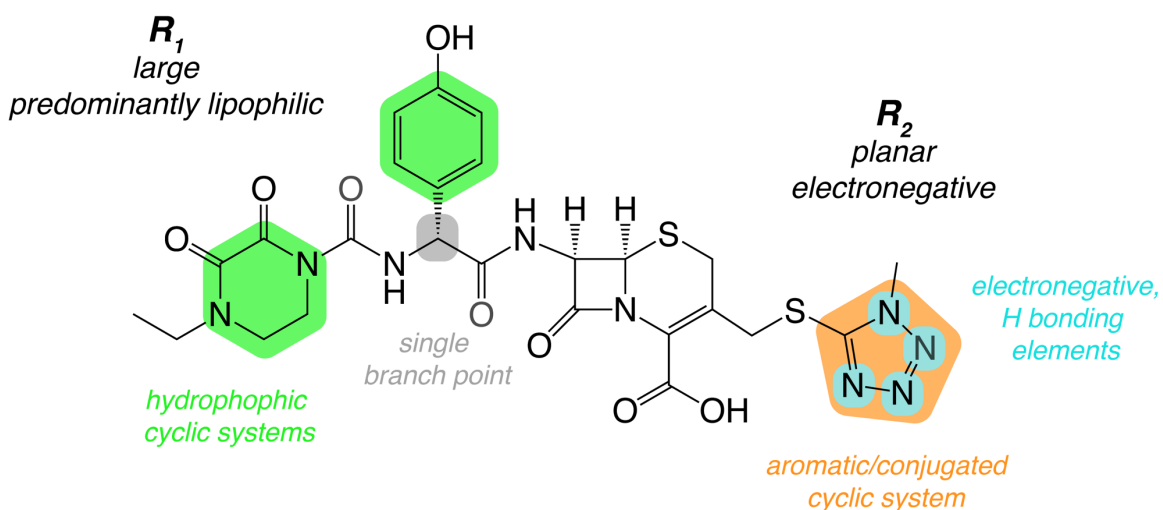


Figure 6.1: Features of cephalosporins enhancing the second-order rate of tPBP2^{H041} acylation, illustrated by cefoperazone.

In Chapter 4, we applied qualitative trends emerging from the cephalosporin SAR to identify novel noncovalent PBP2 inhibitors possessing a 1,1'-biphenyl system. **JEK-42** and its isosteric derivative **JMT-1** inhibit both tPBP2^{WT} and tPBP2^{H041}, and are capable of inhibiting growth of both β -lactam-susceptible (FA19) and -resistant (H041) gonococcal strains. Their cross-inhibition of *P. aeruginosa* PBP3 provides evidence of their potential for broader activity against class B PBPs. Models of their binding modes show that these molecules may bind in a way that mimics the precovalent complex formed by β -lactam antimicrobials. These models also show the 1,1'-biphenyl system interacting with highly conserved residues N364 and F420. Using the structural similarities between **JEK-42**, **JMT-1**, and bicyclic β -lactam scaffolds (*i.e.*, penam, carbapenem, and cephem), a three-point pharmacophore was generated that was then used to screen a virtual library of molecular fragments, yielding many structures for testing against PBP2 and *N. gonorrhoeae* as potential inhibitors.

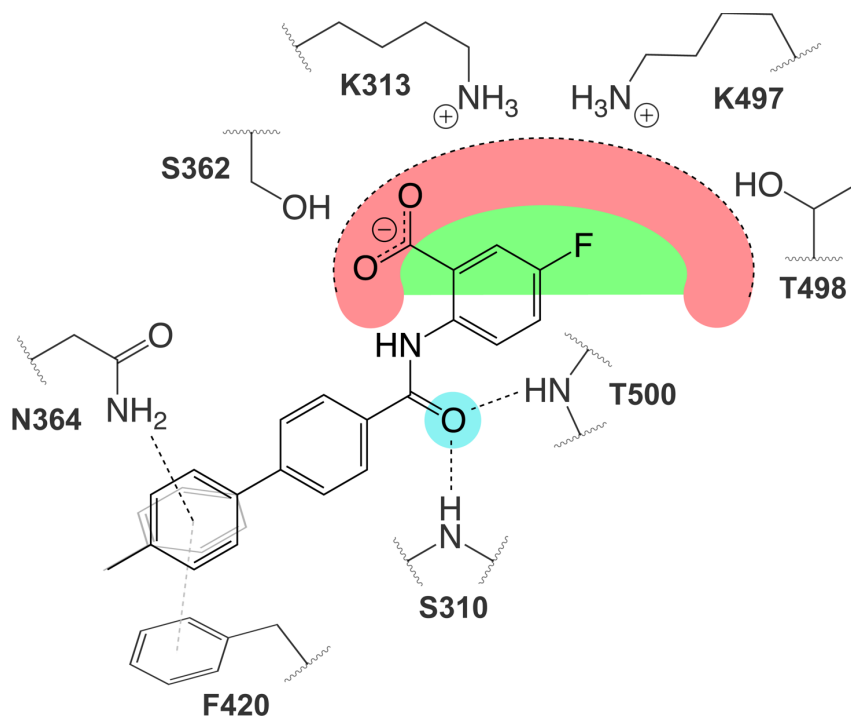


Figure 6.2: Predicted tBPB2 binding mode of antigenococcal prototypes. JEK-42 is shown in its predicted binding mode with tBPB2^{WT}. Areas of interaction for the shared acidic (red), hydrophobic (green) and hydrogen bond accepting (cyan) features of JEK-42 and JMT-1 are shown.

In Chapter 5, we began the process of hit-to-lead optimization by exploring the chemical space surrounding the prototype molecules to determine the effects of specific substitutions on PBP2 inhibition and antigonococcal activity. In all, 127 derivatives of **JMT-1** were synthesized and tested. First, PBP2 inhibition by the **JMT-1** sulfonamide scaffold is improved by the presence of hydrophobic, polarizable groups (*e.g.*, bromo, trifluoromethyl) at C4 or C5 of the anthranilic acid moiety. Second, replacement of the C1 carboxylic acid with a bioisosteric *1H*-tetrazol-5-yl group results in compounds with similar target inhibition but lesser antimicrobial activity. Third, a substitution at the 4'-position of the 1,1'-biphenyl system promotes potent inhibition, but is not required when the secondary aromatic ring is modified to a more flexible cyclohexyl group. In all, 10 molecules show promise as antigonococcal agents from *in vitro* measures of target inhibition and antimicrobial activity and will be tested further. These structures will also serve as the basis for future inhibitor design.

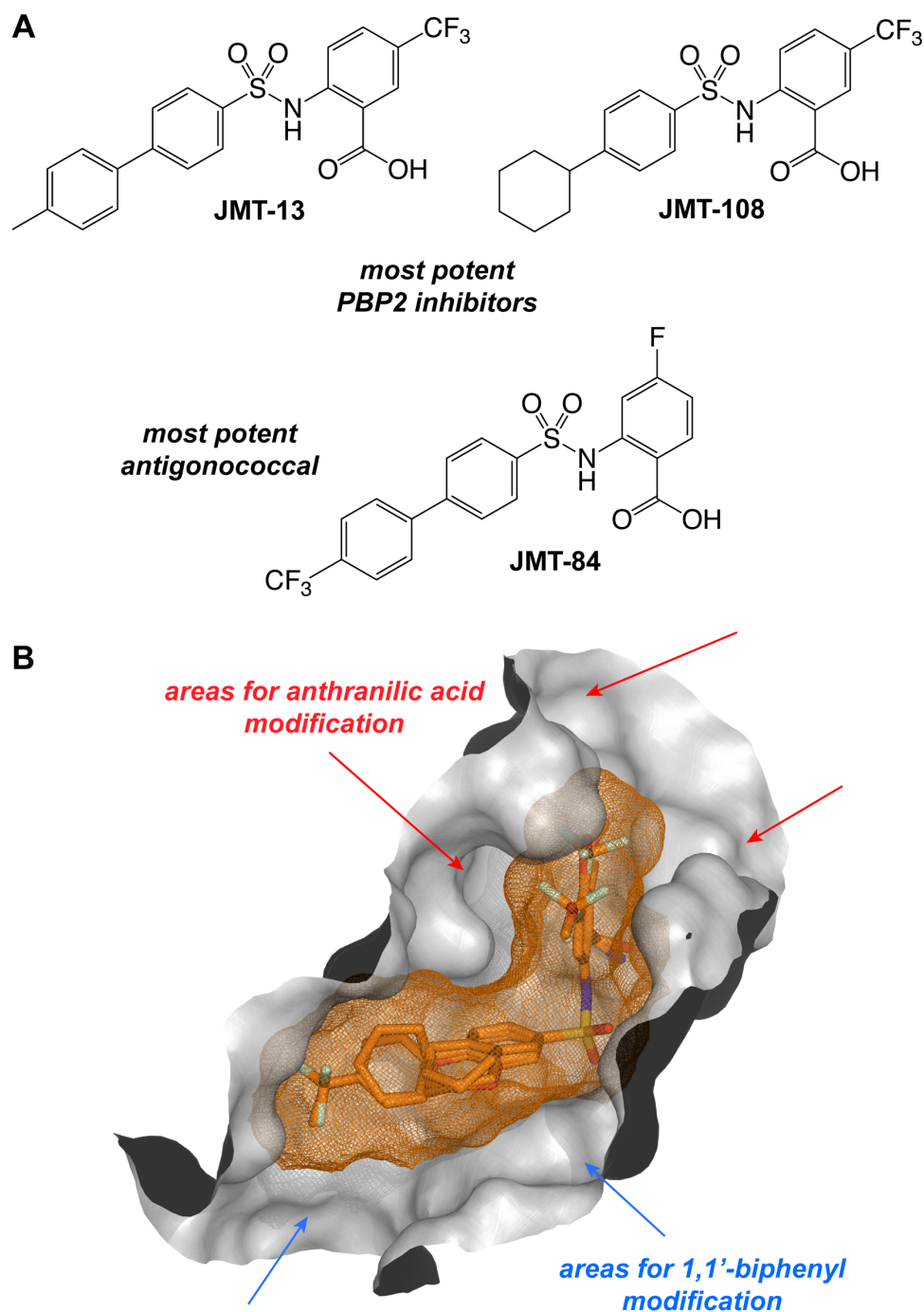


Figure 6.3: Structures of JMT-1 derivatives. **A.** JMT-13 and JMT-108 are the most potent inhibitors of *N. gonorrhoeae* PBP2. Both show $99 \pm 1\%$ inhibition of tPBP2^{H041} at $10 \mu\text{M}$. JMT-84 shows slightly lesser target inhibition but is the most potent antigonococcal agent, yielding 21.2 ± 1.9 mm and 17.5 ± 0 mm zones of inhibition against *N. gonorrhoeae* FA19 and H041, respectively. **B.** There is additional space in the tPBP2 active site that can be explored by derivatization of the JMT series. Composite surface for superimposed inhibitors shown in orange mesh. Receptor surface of tPBP2^{WT} shown in grey.

6.2. Common features among published PBP-inhibitory compounds

Returning to the literature with additional insight and sharper focus provided by these studies, pervasive trends become apparent in reported inhibitors of diverse PBPs from a variety of bacterial species. Many inhibitors are structurally similar to the **JMT** series (**Figure 6.4**). In combination with the inhibition of *P. aeruginosa* PBP3 reported for **JMT-1** and **JMT-2** in Chapter 4, these similarities suggest that **JMT** compounds may be capable of inhibiting the growth of a variety of pathogens. What is novel about the molecules reported in this work is the incorporation of the 1,1'-biphenyl system, whose secondary aromatic ring is uniquely capable of interacting with highly conserved N364 (of the SxN motif) and F420 of *N. gonorrhoeae* PBP2 according to the modeling data presented in Chapters 4 and 5. The predicted interactions with highly conserved residues provide further support for the hypothesis that these compounds may exhibit broad spectrum activity beyond *N. gonorrhoeae*.

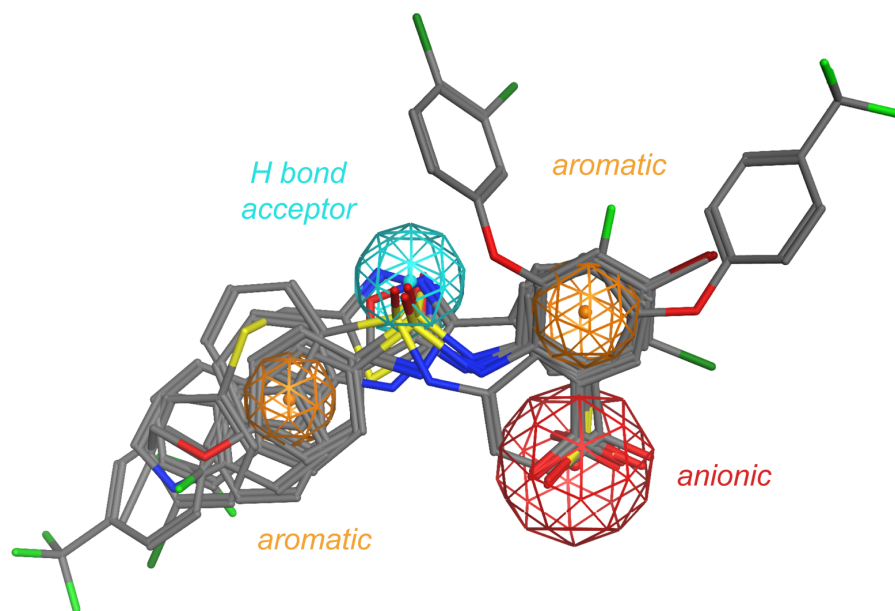
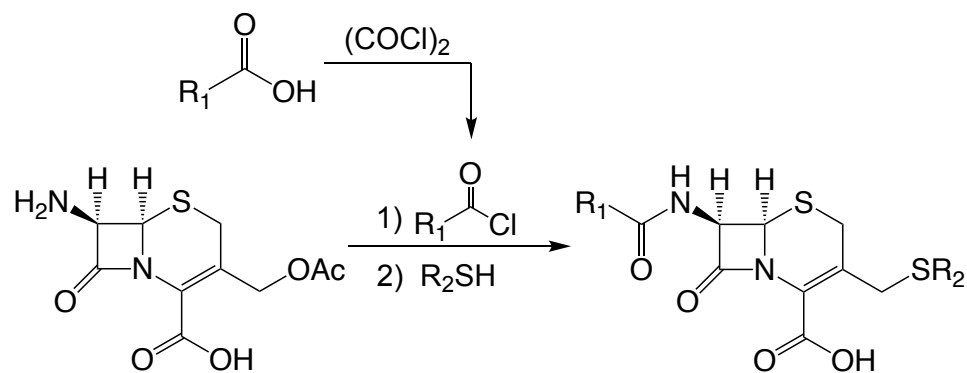


Figure 6.4: Flexible alignment of JMT-84 with published noncovalent PBP inhibitors. Commonalities among the compounds examined include acidic (red), aromatic (orange) and hydrogen bond accepting (cyan) features.

6.3. Future Directions

The data presented on cephalosporin activity against *N. gonorrhoeae* H041 and its PBP2 provide a means of identifying cephalosporins with high activity against ESC^R strains harboring mosaic *penA* alleles. First, cefoperazone should be investigated further for its application to gonococcal infections through the determination of murine pharmacokinetic parameters and subsequent dose optimization. Second, the generated QSAR models can also be applied to additional cephalosporins reported in the literature, including experimental compounds that were never developed, as well as those currently used solely in veterinary medicine. Finally, because the QSAR has been constructed using features of R₁ and R₂ separately, it can be used to computationally evaluate a series of carboxylic acids (R₁) and sulfur nucleophiles (R₂) for attachment to 7-aminocephalosporanic acid according to **Scheme 6.1**.



Scheme 6.1: Proposed synthesis of novel cephalosporins from 7-aminocephalosporanic acid.

Hit-to-lead optimization for **JEK-42** and **JMT-1** is underway, and many additional substitutions have been proposed for the scaffolds in Chapter 5, including less conservative modifications of the anthranilic acid and 1,1'-biphenyl moieties. Importantly, more biochemical and biological characterization is needed for the most potent molecules, including the determination of half-maximal inhibitory concentrations (IC_{50}) against PBP2, minimum inhibitory concentrations (MIC) against *N. gonorrhoeae* strains, and half-maximal eukaryotic cytotoxic doses (TD_{50}). Macromolecular synthesis assays, microscopic observation of gonococcal morphology, or peptidoglycan cross-linking assays should also be conducted to confirm the compounds are on-target. If potent, on-target, selective antigonococcal compounds emerge, these compounds can be tested in the murine infection model described in Chapter 3. Potent antigonococcal compounds should also be tested for inhibition of additional class B PBPs, as well as for antimicrobial activity against a variety of pathogens.

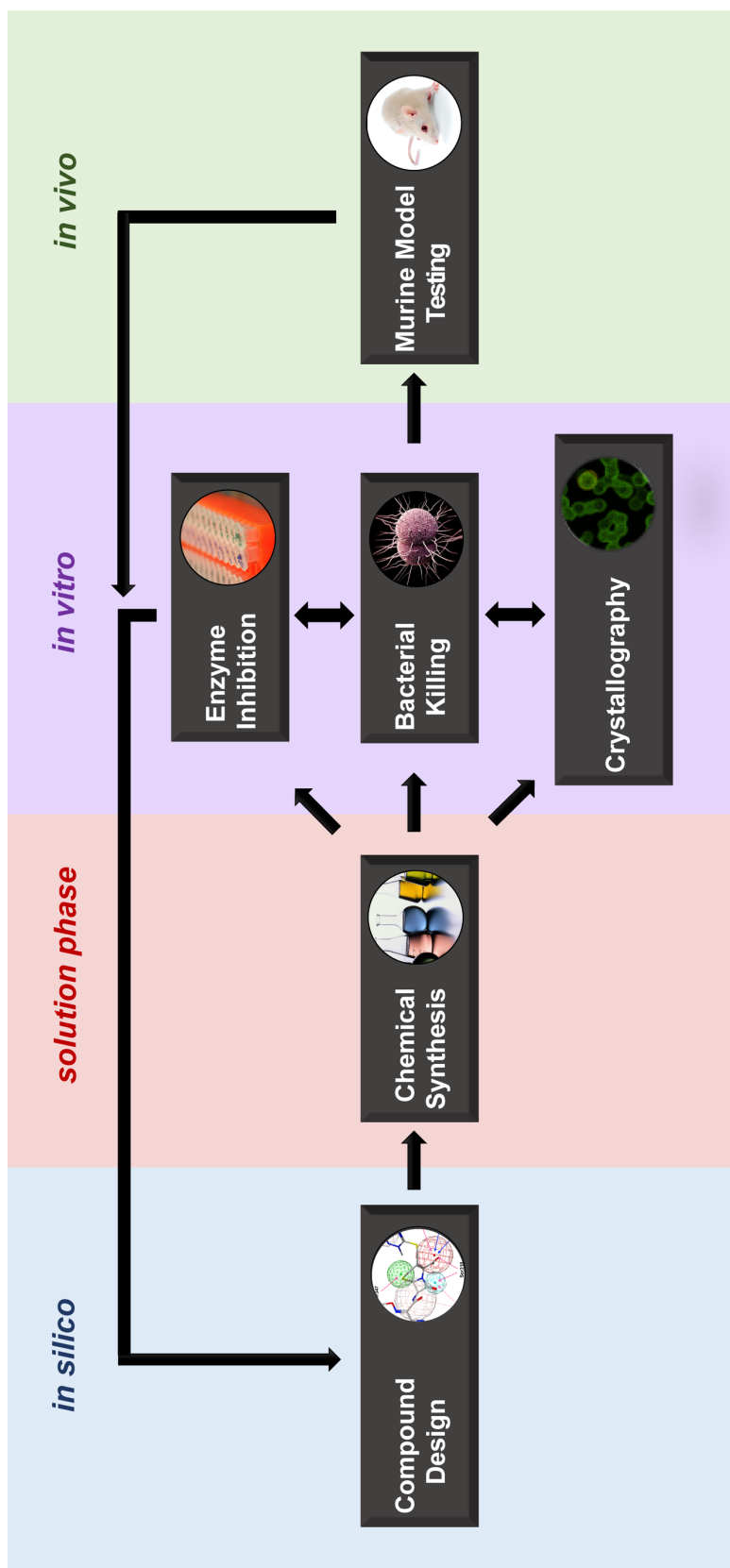


Figure 6.5: Model for early antimicrobial discovery

6.4. Overall impact

Together, these studies lay the groundwork for an antimicrobial discovery program targeted against the PBPs, with possibilities ranging from β -lactams to derivatives of the **JMT** series to entirely new, as yet unidentified chemotypes. The structure-activity relationships for cephalosporins against *N. gonorrhoeae* H041 provide mathematical models for *in silico* prediction of cephalosporin potency that can be employed in selecting semisynthetic cephalosporins from the literature, or in the design of entirely novel structures. In the latter case, such a model helps to reduce attrition by guiding the synthesis of molecules that are likely to be active in both enzymatic assays against tPBP2^{H041} and antimicrobial assays against *N. gonorrhoeae* H041. The synthesis and testing of **JEK-42** and **JMT-1** marks the discovery of two novel antimicrobial scaffolds that act through the inhibition of PBPs. These scaffolds are likely not susceptible to β -lactamases, and based on preliminary data, it appears they are not vulnerable to the same PBP2 modifications that result in resistance to cephalosporins. Finally, the creation of pharmacophore models from structural similarities in PBP inhibitors allows the *in silico* discovery of yet other scaffolds to pursue, opening the possibilities for chemically diverse leads and, thus, greater odds of generating a successful drug candidate.

REFERENCES CITED

1. Centers for Disease Control and Prevention. *Sexually transmitted disease surveillance, 2018*.
2. World Health Organization. *Report on global sexually transmitted infection surveillance, 2018*.
3. Florez-Pollack, S and MM Mauskar. (2019). Disseminated gonococcal infection. *N Engl J Med*, 380(16): 1565.
4. Rice, PA. (2005). Gonococcal arthritis (disseminated gonococcal infection). *Infect Dis Clin North Am*, 19(4): 853-861.
5. Ross, JD. (1996). Systemic gonococcal infection. *Genitourin Med*, 72(6): 404-407.
6. Schaefer, RA *et al.* (1992). Acute gonococcal flexor tenosynovitis in an adolescent male with pharyngitis: A case report and literature review. *Clin Orthop Relat Res*, 281: 212-215.
7. de Campos, FP *et al.* (2016). Gonococcal endocarditis: An ever-present threat. *Autops Case Rep*, 6(2): 19-25.
8. Cash, JM and SC Erzurum. (1988). Gonococcal meningitis: Case report and review of the literature. *S D J Med*, 41(11): 5-7.
9. Cohen, MS *et al.* (1997). Reduction of concentration of HIV-1 in semen after treatment of urethritis: Implications for prevention of sexual transmission of HIV-1. AIDSCAP Malawi Research Group. *Lancet*, 349(9069): 1868-1873.
10. Ghys, PD, *et al.* (1997). The associations between cervicovaginal HIV shedding, sexually transmitted diseases and immunosuppression in female sex workers in Abidjan, Côte d'Ivoire. *AIDS*, 11(12): F85-93.
11. Van Slyke, CJ, RC Arnold, and M Buchholtz. (1943). Penicillin therapy in sulfonamide-resistant gonorrhoea in men. *Am J Public Health Nations Health*, 33(12): 1392-1394.
12. Goodale, WT and L Schwab. (1944). Factors in the resistance of gonorrhoea to sulfonamides. *J Clin Invest*, 23(2): 217-223.
13. Sternberg, TH and TB Turner. (1944). The treatment of sulfonamide resistant gonorrhoea with penicillin sodium: Results in 1,686 cases. *Journal of the American Medical Association*, 126(3): 157-161.
14. Amies, CR. (1967). Development of resistance of gonococci to penicillin: An eight-year study. *Can Med Assoc J*, 96(1): 33-35.
15. Martin, JE, Jr. *et al.* (1970). Comparative study of gonococcal susceptibility to penicillin in the United States, 1955-1969. *J Infect Dis*, 122(5): 459-461.

16. Faruki, H *et al.* (1985). A community-based outbreak of infection with penicillin-resistant *Neisseria gonorrhoeae* not producing penicillinase (chromosomally mediated resistance). *N Engl J Med*, 313(10): 607-611.
17. Ashford, WA, RG Golash, and VG Hemming. (1976). Penicillinase-producing *Neisseria gonorrhoeae*. *Lancet*, 2(7987): 657-658.
18. Percival, A *et al.* (1976). Penicillinase-producing gonococci in Liverpool. *Lancet*, 2(8000): 1379-1382.
19. Phillips, I. (1976). Beta-lactamase-producing, penicillin-resistant gonococcus. *Lancet*, 2(7987): 656-657.
20. Phillips, CW, RD Aller, and SN Cohen. (1976). Penicillinase-producing *Neisseria gonorrhoeae*. *Lancet*, 2(7992): 960.
21. Ashford, WA *et al.* (1981). Spectinomycin-resistant penicillinase-producing *Neisseria gonorrhoeae*. *Lancet*, 2(8254): 1035-1037.
22. Boslego, JW *et al.* (1987). Effect of spectinomycin use on the prevalence of spectinomycin-resistant and of penicillinase-producing *Neisseria gonorrhoeae*. *N Engl J Med*, 317(5): 272-278.
23. Ison, CA *et al.* (1983). Spectinomycin resistant gonococci. *Br Med J (Clin Res Ed)*, 287(6408): 1827-1829.
24. Galimand, M, G Gerbaud, and P Courvalin. (2000). Spectinomycin resistance in *Neisseria spp.* due to mutations in 16S rRNA. *Antimicrob Agents Chemother*, 44(5): 1365-1366.
25. Ilina, EN *et al.* (2013). Mutation in ribosomal protein S5 leads to spectinomycin resistance in *Neisseria gonorrhoeae*. *Front Microbiol*, 4: 186.
26. Morse, SA *et al.* (1986). High-level tetracycline resistance in *Neisseria gonorrhoeae* is result of acquisition of streptococcal *tetM* determinant. *Antimicrob Agents Chemother*, 30(5): 664-670.
27. Roberts, MC *et al.* (1988). *tetM*- and β -lactamase-containing *Neisseria gonorrhoeae* (tetracycline resistant and penicillinase producing) in The Netherlands. *Antimicrob Agents Chemother*, 32(1): 158.
28. Knapp, JS *et al.* (1988). High-level tetracycline resistance resulting from TetM in strains of *Neisseria spp.*, *Kingella denitrificans*, and *Eikenella corrodens*. *Antimicrob Agents Chemother*, 32(5): 765-767.
29. Marquez, CM *et al.* (2002). Detection of a novel TetM determinant in tetracycline-resistant *Neisseria gonorrhoeae* from Uruguay, 1996-1999. *Sex Transm Dis*, 29(12): 792-797.

30. Hu, M *et al.* (2005). High-level chromosomally mediated tetracycline resistance in *Neisseria gonorrhoeae* results from a point mutation in the *rpsJ* gene encoding ribosomal protein S10 in combination with the *mtrR* and *penB* resistance determinants. *Antimicrob Agents Chemother*, 49(10): 4327-4334.
31. Gransden, WR *et al.* (1990). Decreased susceptibility of *Neisseria gonorrhoeae* to ciprofloxacin. *Lancet*, 335(8680): 51.
32. Patrick, D, C Shaw, and ML Rekart. (1995). *Neisseria gonorrhoeae* with decreased susceptibility to ciprofloxacin in British Columbia: An imported phenomenon. *Can Commun Dis Rep*, 21(15): 137-139.
33. Belland, RJ *et al.* (1994). *Neisseria gonorrhoeae* acquires mutations in analogous regions of *gyrA* and *parC* in fluoroquinolone-resistant isolates. *Mol Microbiol*, 14(2): 371-380.
34. Tanaka, M *et al.* (2000) Antimicrobial resistance of *Neisseria gonorrhoeae* and high prevalence of ciprofloxacin-resistant isolates in Japan, 1993 to 1998. *J Clin Microbiol*, 38(2): 521-525.
35. Su, X and I Lind. (2001). Molecular basis of high-level ciprofloxacin resistance in *Neisseria gonorrhoeae* strains isolated in Denmark from 1995 to 1998. *Antimicrob Agents Chemother*, 45(1): 117-123.
36. Iverson, CJ *et al.* (2004). Fluoroquinolone resistance among *Neisseria gonorrhoeae* isolates in Hawaii, 1990-2000: Role of foreign importation and increasing endemic spread. *Sex Transm Dis*, 31(12): 702-708.
37. Tanaka, M *et al.* (2004). Antimicrobial resistance of *Neisseria gonorrhoeae* in Japan, 1993-2002: Continuous increasing of ciprofloxacin-resistant isolates. *Int J Antimicrob Agents*, 24 Suppl 1: S15-S22.
38. Increases in fluoroquinolone-resistant *Neisseria gonorrhoeae* among men who have sex with men - United States, 2003, and revised recommendations for gonorrhea treatment, 2004. *MMWR Morb Mortal Wkly Rep*, 2004. 53(16): 335-338.
39. Centers for Disease Control and Prevention. Update to CDC's sexually transmitted diseases treatment guidelines, 2006: Fluoroquinolones no longer recommended for treatment of gonococcal infections. *MMWR Morb Mortal Wkly Rep*, 2007. 56(14): 332-336.
40. Centers for Disease Control and Prevention. Sexually transmitted diseases treatment guidelines, 2006. *MMWR Recomm Rep*, 2006. 55(Rr-11): 1-94.
41. Unemo, M *et al.* (2010). Two cases of verified clinical failures using internationally recommended first-line cefixime for gonorrhoea treatment, Norway, 2010. *Euro Surveill*, 15(47): 19721.
42. Barry, PM and JD Klausner. (2009). The use of cephalosporins for gonorrhea: The impending problem of resistance. *Expert Opin Pharmacother*, 10(4): 555-577.

43. Yokoi, S. *et al.* (2007). Threat to cefixime treatment for gonorrhoea. *Emerg Infect Dis*, 13(8): 1275-1277.
44. Chisholm, SA *et al.* (2010). Cephalosporin MIC creep among gonococci: Time for a pharmacodynamic rethink? *J Antimicrob Chemother*, 65(10): 2141-2148.
45. Ito, M *et al.* (2005). Emergence and spread of *Neisseria gonorrhoeae* clinical isolates harboring mosaic-like structure of penicillin-binding protein 2 in Central Japan. *Antimicrob Agents Chemother*, 49(1): 137-143.
46. Ameyama, S *et al.* (2002). Mosaic-like structure of penicillin-binding protein 2 gene (*penA*) in clinical isolates of *Neisseria gonorrhoeae* with reduced susceptibility to cefixime. *Antimicrob Agents Chemother*, 46(12): p. 3744-3749.
47. Centers for Disease Control and Prevention. Cephalosporin susceptibility among *Neisseria gonorrhoeae* isolates--United States, 2000-2010. *MMWR Morb Mortal Wkly Rep*, 2011. 60(26): 873-877.
48. Ison, CA *et al.* (2011). Gonorrhoea treatment failures to cefixime and azithromycin in England, 2010. *Euro Surveill*, 16(14).
49. Chisholm, SA *et al.* (2011). Emergence of a *Neisseria gonorrhoeae* clone showing decreased susceptibility to cefixime in England and Wales. *J Antimicrob Chemother*, 66(11): 2509-2512.
50. Unemo, M, D Golparian, and A Hestner. (2011). Ceftriaxone treatment failure of pharyngeal gonorrhoea verified by international recommendations, Sweden, July 2010. *Euro Surveill*, 16(6).
51. Unemo, M *et al.* (2011). First *Neisseria gonorrhoeae* strain with resistance to cefixime causing gonorrhoea treatment failure in Austria, 2011. *Euro Surveill*, 16(43).
52. Unemo, M *et al.* (2012). Treatment failure of pharyngeal gonorrhoea with internationally recommended first-line ceftriaxone verified in Slovenia, September 2011. *Euro Surveill*, 17(25).
53. Tanaka, M *et al.* (2002). A remarkable reduction in the susceptibility of *Neisseria gonorrhoeae* isolates to cepheims and the selection of antibiotic regimens for the single-dose treatment of gonococcal infection in Japan. *J Infect Chemother*, 8(1): 81-86.
54. Allen, VG *et al.* (2013). *Neisseria gonorrhoeae* treatment failure and susceptibility to cefixime in Toronto, Canada. *JAMA*, 309(2): 163-170.
55. Lewis, DA *et al.* (2013). Phenotypic and genetic characterization of the first two cases of extended-spectrum-cephalosporin-resistant *Neisseria gonorrhoeae* infection in South Africa and association with cefixime treatment failure. *J Antimicrob Chemother*, 68(6): 1267-1270.

56. Chen, MY *et al.* (2013). Failure of 500 mg of ceftriaxone to eradicate pharyngeal gonorrhoea, Australia. *J Antimicrob Chemother*, 68(6): 1445-1447.
57. Martin, I *et al.* (2013). Antimicrobial susceptibilities and distribution of sequence types of *Neisseria gonorrhoeae* isolates in Canada: 2010. *Can J Microbiol*, 59(10): 671-678.
58. Read, PJ *et al.* (2013). One confirmed and one suspected case of pharyngeal gonorrhoea treatment failure following 500mg ceftriaxone in Sydney, Australia. *Sex Health*, 10(5): 460-462.
59. Ison, CA *et al.* (2013). Decreased susceptibility to cephalosporins among gonococci: Data from the Gonococcal Resistance to Antimicrobials Surveillance Programme (GRASP) in England and Wales, 2007-2011. *Lancet Infect Dis*, 13(9): 762-768.
60. Centers for Disease Control and Prevention. Update to CDC's Sexually transmitted diseases treatment guidelines, 2010: Oral cephalosporins no longer a recommended treatment for gonococcal infections. *MMWR Morb Mortal Wkly Rep*, 2012. 61(31): 590-594.
61. Bignell, C and M Unemo. (2013). 2012 European guidelines on the diagnosis and treatment of gonorrhoea in adults. *Int J STD AIDS*, 24(2): 85-92.
62. Ohnishi, M *et al.* (2011). Ceftriaxone-resistant *Neisseria gonorrhoeae*, Japan. *Emerg Infect Dis*, 17(1): 148-149.
63. Ohnishi, M *et al.* (2011). Is *Neisseria gonorrhoeae* initiating a future era of untreatable gonorrhea? Detailed characterization of the first strain with high-level resistance to ceftriaxone. *Antimicrob Agents Chemother*, 55(7): 3538-3545.
64. Camara, J *et al.* (2012). Molecular characterization of two high-level ceftriaxone-resistant *Neisseria gonorrhoeae* isolates detected in Catalonia, Spain. *J Antimicrob Chemother*, 67(8): 1858-1860.
65. Deguchi, T *et al.* (2016). New clinical strain of *Neisseria gonorrhoeae* with decreased susceptibility to ceftriaxone, Japan. *Emerg Infect Dis*, 22(1): 142-144.
66. Nakayama, S *et al.* (2016). New ceftriaxone- and multidrug-resistant *Neisseria gonorrhoeae* strain with a novel mosaic *penA* gene isolated in Japan. *Antimicrob Agents Chemother*, 60(7): 4339-4341.
67. Lefebvre, B *et al.* (2018). Ceftriaxone-resistant *Neisseria gonorrhoeae*, Canada, 2017. *Emerg Infect Dis*, 24(2): 381-383.
68. Terkelsen, D *et al.* (2017). Multidrug-resistant *Neisseria gonorrhoeae* infection with ceftriaxone resistance and intermediate resistance to azithromycin, Denmark, 2017. *Euro Surveill*, 22(42).
69. Gianecini, R *et al.* (2016). *Neisseria gonorrhoeae* resistant to ceftriaxone and cefixime, Argentina. *Emerg Infect Dis*, 22(6): 1139-1141.

70. Unemo, M *et al.* (2012). High-level cefixime- and ceftriaxone-resistant *Neisseria gonorrhoeae* in France: novel *penA* mosaic allele in a successful international clone causes treatment failure. *Antimicrob Agents Chemother*, 56(3): 1273-1280.
71. Berenger, BM *et al.* (2019). Genetic characterization and enhanced surveillance of ceftriaxone-resistant *Neisseria gonorrhoeae* strain, Alberta, Canada, 2018. *Emerg Infect Dis*, 25(9): 1660-1667.
72. Lahra, MM, N Ryder, and DM Whiley. (2014). A new multidrug-resistant strain of *Neisseria gonorrhoeae* in Australia. *N Engl J Med*, 371(19): 1850-1851.
73. Xiu, L *et al.* (2020). Emergence of ceftriaxone-resistant *Neisseria gonorrhoeae* strains harbouring a novel mosaic *penA* gene in China. *J Antimicrob Chemother*, 75(4): 907-910.
74. Lahra, MM *et al.* (2018). Cooperative recognition of internationally disseminated ceftriaxone-resistant *Neisseria gonorrhoeae* strain. *Emerg Infect Dis*, 24(4): 735-740.
75. Chen, SC *et al.* (2019). Identification of internationally disseminated ceftriaxone-resistant *Neisseria gonorrhoeae* strain FC428, China. *Emerg Infect Dis*, 25(7): 1427-1429.
76. Eyre, DW *et al.* (2019). Detection in the United Kingdom of the *Neisseria gonorrhoeae* FC428 clone, with ceftriaxone resistance and intermediate resistance to azithromycin, October to December 2018. *Euro Surveill*, 24(10).
77. Golparian, D *et al.* (2018). Multidrug-resistant *Neisseria gonorrhoeae* isolate, belonging to the internationally spreading Japanese FC428 clone, with ceftriaxone resistance and intermediate resistance to azithromycin, Ireland, August 2018. *Euro Surveill*, 23(47).
78. Yuan, Q *et al.* (2019). Identification of multidrug-resistant *Neisseria gonorrhoeae* isolates with combined resistance to both ceftriaxone and azithromycin, China, 2017-2018. *Emerg Microbes Infect*, 8(1): 1546-1549.
79. Eyre, DW *et al.* (2018). Gonorrhoea treatment failure caused by a *Neisseria gonorrhoeae* strain with combined ceftriaxone and high-level azithromycin resistance, England, February 2018. *Euro Surveill*, 23(27).
80. Whiley, DM *et al.* (2018). Genetic characterisation of *Neisseria gonorrhoeae* resistant to both ceftriaxone and azithromycin. *Lancet Infect Dis*, 18(7): 717-718.
81. Poncin, T *et al.* (2018). Multidrug-resistant *Neisseria gonorrhoeae* failing treatment with ceftriaxone and doxycycline in France, November 2017. *Euro Surveill*, 23(21).
82. Yahara, K *et al.* (2018). Genomic surveillance of *Neisseria gonorrhoeae* to investigate the distribution and evolution of antimicrobial-resistance determinants and lineages. *Microbial genomics*, 4(8): e000205.

83. Lee, K *et al.* (2019). Clonal expansion and spread of the ceftriaxone-resistant *Neisseria gonorrhoeae* strain FC428, identified in Japan in 2015, and closely related isolates. *J Antimicrob Chemother*, 74(7): 1812-1819.
84. Katz, AR. (2018). Ceftriaxone-resistant *Neisseria gonorrhoeae*, Canada, 2017. *Emerg Infect Dis*, 24(3): 608.
85. Scharbaai-Vázquez, R, AL González-Caraballo, and LJ Torres-Bauzá. (2015). Ceftriaxone-resistant *Neisseria gonorrhoeae*, Puerto Rico. *Sex Transm Infect*, 91(2): 99.
86. Yang, F *et al.* (2019). Detection and analysis of two cases of the internationally spreading ceftriaxone-resistant *Neisseria gonorrhoeae* FC428 clone in China. *J Antimicrob Chemother*, 74(12): 3635-3636.
87. Ko, K *et al.* (2019). First case of ceftriaxone-resistant multidrug-resistant *Neisseria gonorrhoeae* in Singapore. *Antimicrob Agents Chemother*, 63(5).
88. Katz, AR *et al.* (2012). *Neisseria gonorrhoeae* with high-level resistance to azithromycin: Case report of the first isolate identified in the United States. *Clin Infect Dis*, 54(6): 841-843.
89. Unemo, M, D Golparian, and B Hellmark. (2014). First three *Neisseria gonorrhoeae* isolates with high-level resistance to azithromycin in Sweden: A threat to currently available dual-antimicrobial regimens for treatment of gonorrhea? *Antimicrob Agents Chemother*, 58(1): 624-625.
90. Fifer, H *et al.* (2018). Sustained transmission of high-level azithromycin-resistant *Neisseria gonorrhoeae* in England: An observational study. *Lancet Infect Dis*, 18(5): 573-581.
91. Young, H, A Moyes, and A McMillan. (1997). Azithromycin and erythromycin resistant *Neisseria gonorrhoeae* following treatment with azithromycin. *Int J STD AIDS*, 8(5): 299-302.
92. Palmer, HM *et al.* (2008). Emergence and spread of azithromycin-resistant *Neisseria gonorrhoeae* in Scotland. *J Antimicrob Chemother*, 62(3): 490-494.
93. Starnino, S and P Stefanelli. (2009). Azithromycin-resistant *Neisseria gonorrhoeae* strains recently isolated in Italy. *J Antimicrob Chemother*, 63(6): 1200-1204.
94. Day, MJ *et al.* (2018). Stably high azithromycin resistance and decreasing ceftriaxone susceptibility in *Neisseria gonorrhoeae* in 25 European countries, 2016. *BMC Infect Dis*, 18(1): 609.
95. Starnino, S *et al.* (2012). Retrospective analysis of antimicrobial susceptibility trends (2000-2009) in *Neisseria gonorrhoeae* isolates from countries in Latin America and the Caribbean shows evolving resistance to ciprofloxacin, azithromycin and decreased susceptibility to ceftriaxone. *Sex Transm Dis*, 39(10): 813-821.

96. Lewis, DA. (2010). *The gonococcus fights back: Is this time a knock out?* *Sex Transm Infect*, 86(6): 415-421.
97. Whiley, DM *et al.* (2012). The ticking time bomb: escalating antibiotic resistance in *Neisseria gonorrhoeae* is a public health disaster in waiting. *J Antimicrob Chemother*, 67(9): 2059-2061.
98. Lewis, DA. (2014). Global resistance of *Neisseria gonorrhoeae*: When theory becomes reality. *Curr Opin Infect Dis*, 27(1): 62-67.
99. Owusu-Edusei, K, Jr. *et al.* (2013). The estimated direct medical cost of selected sexually transmitted infections in the United States, 2008. *Sex Transm Dis*, 40(3): 197-201.
100. Chan, CH, CJ McCabe, and DN Fisman. (2012). Core groups, antimicrobial resistance and rebound in gonorrhoea in North America. *Sex Transm Infect*, 88(3): 200-204.
101. Macheboeuf, P *et al.* (2006). Penicillin binding proteins: Key players in bacterial cell cycle and drug resistance processes. *FEMS Microbiol Rev*, 30(5): 673-691.
102. Sauvage, E *et al.* (2008). The penicillin-binding proteins: Structure and role in peptidoglycan biosynthesis. *FEMS Microbiol Rev*, 32(2): 234-258.
103. Goffin, C and JM Ghuysen (1998). Multimodular penicillin-binding proteins: An enigmatic family of orthologs and paralogs. *Microbiol Mol Biol Rev*, 62(4): 1079-1093.
104. Vollmer, W, D Blanot, and MA de Pedro. (2008). Peptidoglycan structure and architecture. *FEMS Microbiol Rev*, 32(2): 149-167.
105. Hebel, BH and FE Young. (1975). Autolysis of *Neisseria gonorrhoeae*. *J Bacteriol*, 122(2): 385-392.
106. Bobba, S and WG Gutheil. (2011). Multivariate geometrical analysis of catalytic residues in the penicillin-binding proteins. *Int J Biochem Cell Biol*, 43(10): 1490-1499.
107. Kumarasiri, M *et al.* (2014). Protonation states of active-site lysines of penicillin-binding protein 6 from *Escherichia coli* and the mechanistic implications. *Proteins*, 82(7): 1348-1358.
108. Zhang, W *et al.* (2007). Catalytic mechanism of penicillin-binding protein 5 of *Escherichia coli*. *Biochemistry*, 46(35): 10113-10121.
109. Smith, JD *et al.* (2013). Structural analysis of the role of *Pseudomonas aeruginosa* penicillin-binding protein 5 in β -lactam resistance. *Antimicrob Agents Chemother*, 57(7): 3137-3146.

110. Shi, Q *et al.* (2008) Investigation of the mechanism of the cell wall DD-carboxypeptidase reaction of penicillin-binding protein 5 of *Escherichia coli* by quantum mechanics / molecular mechanics calculations. *Journal of the American Chemical Society*, 130(29): 9293-9303.
111. Stefanova, ME *et al.* (2003). *Neisseria gonorrhoeae* penicillin-binding protein 3 exhibits exceptionally high carboxypeptidase and β -lactam binding activities. *Biochemistry*, 42(49): 14614-14625.
112. Hargis, JC *et al.* (2014). Can molecular dynamics and QM/MM solve the penicillin-binding protein protonation puzzle? *J Chem Inf Model*, 54(5): 1412-1424.
113. Singh, A *et al.* (2019). Recognition of the β -lactam carboxylate triggers acylation of *Neisseria gonorrhoeae* penicillin-binding protein 2. *J Biol Chem*, 294(38): 14020-14032.
114. Macheboeuf, P. *et al.* (2008). Trapping of an acyl-enzyme intermediate in a penicillin-binding protein (PBP)-catalyzed reaction. *J Mol Biol*, 376(2): 405-413.
115. McDonough, MA *et al.* (2002). Structures of two kinetic intermediates reveal species specificity of penicillin-binding proteins. *J Mol Biol*, 322(1): 111-122.
116. Lee, W *et al.* (2001). A 1.2-Å snapshot of the final step of bacterial cell wall biosynthesis. *Proc Natl Acad Sci USA*, 98(4): 1427-1431.
117. Nicola, G *et al.* (2005). Crystal structure of *Escherichia coli* penicillin-binding protein 5 bound to a tripeptide boronic acid inhibitor: A role for Ser-110 in deacylation. *Biochemistry*, 44(23): 8207-8217.
118. Wise, EM, Jr. and JT Park (1965). Penicillin: Its basic site of action as an inhibitor of a peptide cross-linking reaction in cell wall mucopeptide synthesis. *Proc Natl Acad Sci USA*, 54(1): 75-81.
119. Izaki, K, M Matsushashi, and JL Strominger. (1966). Glycopeptide transpeptidase and D-alanine carboxypeptidase: Penicillin-sensitive enzymatic reactions. *Proc Natl Acad Sci USA*, 55(3): 656-663
120. Tipper, DJ and JL Strominger. (1968). Biosynthesis of the peptidoglycan of bacterial cell walls XII. Inhibition of cross-linking by penicillins and cephalosporins: Studies in *Staphylococcus aureus in vivo*. *J Biol Chem*, 243(11): 3169-3179.
121. Strominger, JL *et al.* (1967). Peptidoglycan transpeptidase and D-alanine carboxypeptidase: Penicillin-sensitive enzymatic reactions. *Fed Proc*, 26(1): 9-22.
122. Izaki, K, M Matsushashi, and JL Strominger. (1968). Biosynthesis of the peptidoglycan of bacterial cell walls 8. Peptidoglycan transpeptidase and D-alanine carboxypeptidase: Penicillin-sensitive enzymatic reaction in strains of *Escherichia coli*. *J Biol Chem*, 243(11): 3180-3192.

123. Tipper, DJ and JL Strominger. (1965). Mechanism of action of penicillins: A proposal based on their structural similarity to acyl- D-alanyl-D-alanine. *Proc Natl Acad Sci USA*, 54(4): 1133-1141.
124. Lee, B. (1971). Conformation of penicillin as a transition-state analog of the substrate of peptidoglycan transpeptidase. *J Mol Biol*, 61(2): 463-469.
125. Yocum, RR, JR Rasmussen, and JL Strominger. (1980). The mechanism of action of penicillin. Penicillin acylates the active site of *Bacillus stearothermophilus* D-alanine carboxypeptidase. *J Biol Chem*, 255(9): 3977-3986.
126. Yocum, RR *et al.* (1979). Mechanism of penicillin action: Penicillin and substrate bind covalently to the same active site serine in two bacterial D-alanine carboxypeptidases. *Proc Natl Acad Sci USA*, 76(6): 2730-2734.
127. Waxman, DJ, RR Yocum, and JL Strominger. (1980). Penicillins and cephalosporins are active site-directed acylating agents: Evidence in support of the substrate analogue hypothesis. *Philos Trans R Soc Lond B Biol Sci*, 289(1036): 257-271.
128. Tomberg, J *et al.* (2010). Molecular and structural analysis of mosaic variants of penicillin-binding protein 2 conferring decreased susceptibility to expanded-spectrum cephalosporins in *Neisseria gonorrhoeae*: Role of epistatic mutations. *Biochemistry*, 49(37): 8062-8070.
129. Lu, WP *et al.* (2001). Kinetics of β -lactam interactions with penicillin-susceptible and -resistant penicillin-binding protein 2x proteins from *Streptococcus pneumoniae*. Involvement of acylation and deacylation in β -lactam resistance. *J Biol Chem*, 276(34): 31494-31501.
130. Chambers, HF, MJ Sachdeva, and CJ Hackbarth. (1994). Kinetics of penicillin binding to penicillin-binding proteins of *Staphylococcus aureus*. *Biochem J*, 301: 139-144.
131. Nicola, G *et al.* (2010). Crystal structures of covalent complexes of β -lactam antibiotics with *Escherichia coli* penicillin-binding protein 5: Toward an understanding of antibiotic specificity. *Biochemistry*, 49(37): 8094-8104.
132. Chesnel, L *et al.* (2002). Increase of the deacylation rate of PBP2x from *Streptococcus pneumoniae* by single point mutations mimicking the class A β -lactamases. *Eur J Biochem*, 269(6): 1678-1683.
133. Barbour, AG. (1981). Properties of penicillin-binding proteins in *Neisseria gonorrhoeae*. *Antimicrob Agents Chemother*, 19(2): 316-322.
134. Singh, A. *et al.* (2020). Mutations in penicillin-binding protein 2 from cephalosporin-resistant *Neisseria gonorrhoeae* hinder ceftriaxone acylation by restricting protein dynamics. *J Biol Chem*.

135. Hujer, AM *et al.* (2005). Structure-activity relationships of different β -lactam antibiotics against a soluble form of *Enterococcus faecium* PBP5, a type II bacterial transpeptidase. *Antimicrob Agents Chemother*, 49(2): 612-618.
136. Frère, JM, JM Ghuysen, and M Iwatsubo. (1975). Kinetics of interaction between the exocellular DD-carboxypeptidase-transpeptidase from *Streptomyces* R61 and β -lactam antibiotics. A choice of models. *Eur J Biochem*, 57(2): 343-351.
137. Jeong, JH, HJ Cha, and YG Kim. (2018). Crystal structures of penicillin-binding protein D2 from *Listeria monocytogenes* and structural basis for antibiotic specificity. *Antimicrob Agents Chemother*, 62(9).
138. Graves-Woodward, K and RF Pratt. (1998). Reaction of soluble penicillin-binding protein 2a of methicillin-resistant *Staphylococcus aureus* with β -lactams and acyclic substrates: Kinetics in homogeneous solution. *Biochem J*, 332: 755-761.
139. Knox, R. (1961). A survey of new penicillins. *Nature*, 192: 492-496.
140. Josephine, HR, I Kumar, and RF Pratt. (2004). The perfect penicillin? Inhibition of a bacterial DD-peptidase by peptidoglycan-mimetic β -lactams. *J Am Chem Soc*, 126(26): 8122-8123.
141. Silvaggi, NR *et al.* (2005). Crystal structures of complexes between the R61 DD -peptidase and peptidoglycan-mimetic β -lactams: A non-covalent complex with a "perfect penicillin". *J Mol Biol*, 345(3): 521-533.
142. Cohen, NC. (1983). β -lactam antibiotics: Geometrical requirements for antibacterial activities. *J Med Chem*, 26(2): 259-264.
143. Van Heyningen, E and LK Ahern. (1968). The chemistry of cephalosporins XII. Configuration of the carboxyl group in Δ^2 -cephalosporins. *J Med Chem*, 11(5): 933-936.
144. Hunkapiller, MW *et al.* (1973). Ionization behavior of the histidine residue in the catalytic triad of serine proteases. Mechanistic implications. *J Biol Chem*, 248(23): 8306-8308.
145. Blow, DM, JJ Birktoft, and BS Hartley. (1969). Role of a buried acid group in the mechanism of action of chymotrypsin. *Nature*, 221(5178): 337-340.
146. Cruickshank, WH and H Kaplan. (1972). Properties of the active center histidine of α -chymotrypsin. *Biochem Biophys Res Commun*, 46(6): 2134-2140.
147. Fersht, AR and J Sperling. (1973). The charge relay system in chymotrypsin and chymotrypsinogen. *J Mol Biol*, 74(2): 137-149.
148. Pace, CN, GR Grimsley, and JM Scholtz. (2009). Protein ionizable groups: pK values and their contribution to protein stability and solubility. *J Biol Chem*, 284(20): 13285-13289.

149. Harris, TK and GJ Turner. (2002). Structural basis of perturbed pKa values of catalytic groups in enzyme active sites. *IUBMB Life*, 53(2): 85-98.
150. Laurents, DV *et al.* (2003). Charge-charge interactions are key determinants of the pK values of ionizable groups in ribonuclease Sa (pI=3.5) and a basic variant (pI=10.2). *J Mol Biol*, 325(5): 1077-1092.
151. Shokri, A *et al.* (2012). Effect of hydrogen bonds on pKa values: Importance of networking. *J Am Chem Soc*, 134(25): 10646-10650.
152. Isom, DG *et al.* (2011). Large shifts in pKa values of lysine residues buried inside a protein. *Proc Natl Acad Sci USA*, 108(13): 5260-5265.
153. van der Linden, MP *et al.* (1994). Site-directed mutagenesis of proposed active-site residues of penicillin-binding protein 5 from *Escherichia coli*. *Biochem J*, 303: 357-362.
154. Robinson, FA. (1949). *The Chemistry of Penicillin*. Edited by Hans T. Clarke, John R Johnson, and Sir Robert Robinson. Princeton University Press, New Jersey
155. Sweet, RM and LF Dahl. (1970). Molecular architecture of the cephalosporins. Insights into biological activity based on structural investigations. *J Am Chem Soc*, 92(18): 5489-5507.
156. Pfaendler, HR *et al.* (1981). Structure, reactivity, and biological activity of strained bicyclic β -lactams. *Journal of the American Chemical Society*, 103(15): 4526-4531.
157. Green, GF, JE Page, and SE Staniforth. (1965). Cephalosporanic acids I: Infrared absorption and proton magnetic resonance spectra of cephalosporin and penicillin analogues. *J Chem Soc*, 65: 1595-605.
158. Boyd, DB *et al.* (1980). Electronic structures of cephalosporins and penicillins 11. Parabolic relationships between antibacterial activity of cephalosporins and β -lactam reactivity predicted from molecular orbital calculations. *Journal of the American Chemical Society*, 102(6): 1812-1814.
159. Morin, RB *et al.* (1969). Chemistry of cephalosporin antibiotics XV. Transformations of penicillin sulfoxide. A synthesis of cephalosporin compounds. *J Am Chem Soc*, 91(6): 1401-1407.
160. Ernest, I *et al.* (1978). The penems, a new class of β -lactam antibiotics: 6-acylaminopenem-3-carboxylic acids. *Journal of the American Chemical Society*, 100(26): 8214-8222.
161. Lang, M *et al.* (1979). The penems, a new class of β -lactam antibiotics 2. Total synthesis of racemic 6-unsubstituted representatives. *Journal of the American Chemical Society*, 101(21): 6296-6301.
162. Woodward, RB. (1980). Penems and related substances. *Philos Trans R Soc Lond B Biol Sci*, 289(1036): 239-250.

163. Asai, M *et al.* (1981). Sulfazecin, a novel β -lactam antibiotic of bacterial origin. Isolation and chemical characterization. *J Antibiot (Tokyo)*, 34(6): 621-627.
164. Imada, A *et al.* (1981). Sulfazecin and isosulfazecin, novel β -lactam antibiotics of bacterial origin. *Nature*, 289(5798): 590-591.
165. Sykes, RB *et al.* (1981). Monocyclic β -lactam antibiotics produced by bacteria. *Nature*, 291(5815): 489-491.
166. Neu, HC. (1986). β -lactam antibiotics: Structural relationships affecting *in vitro* activity and pharmacologic properties. *Reviews of Infectious Diseases*, 8: S237-S259.
167. Georgopapadakou, NH, SA Smith, and RB Sykes. (1982). Mode of action of azthreonam. *Antimicrob Agents Chemother*, 21(6): 950-956.
168. Rittenbury, MS. (1990). How and why aztreonam works. *Surg Gynecol Obstet*, 171 Suppl: 19-23.
169. Cunha, BA. (1993). Aztreonam. *Urology*, 41(3): 249-258.
170. Sykes, RB *et al.* (1982). Azthreonam (SQ 26,776), a synthetic monobactam specifically active against aerobic Gram-negative bacteria. *Antimicrob Agents Chemother*, 21(1): 85-92.
171. Balsamo, A, P Domiano, and B Macchia. (1980). Is the conformation of the thiazolidine ring of penicillins of any importance for their antibacterial activity? *European Journal of Medicinal Chemistry*, 15: 559-562.
172. Boles, MO, RJ Girven, and PAC Gane. (1978). The structure of amoxicillin trihydrate and a comparison with the structures of ampicillin. *Acta Crystallographica Section B*, 34(2): 461-466.
173. Yoshimoto, M *et al.* (1972). Studies on β -lactam antibiotics I. Skeletal conversion of cephalosporin to penicillin. *Tetrahedron Letters*, 13(29): 2923-2926.
174. Dexter, DD and JM van der Veen. (1978). Conformations of penicillin G: Crystal structure of procaine penicillin G monohydrate and a refinement of the structure of potassium penicillin G. *J Chem Soc Perkin 1*, 3: 185-190.
175. Kukolja, S *et al.* (1975). Azetidinone antibiotics XIII. Structure and stereochemistry of isomeric penam and cepham derivatives. *The Journal of Organic Chemistry*, 40(16): 2388-2391.
176. Cox, PJ, RJ McClure, and GA Sim. (1974). Crystal structure of 6 β -trimethylammonioopenicillanate hemihydriodide. *Journal of the Chemical Society, Perkin Transactions 2*, 4: 360-363.
177. Abrahamsson, S, DC Hodgkin, and EN Maslen. (1963). The crystal structure of phenoxymethylpenicillin. *Biochem J*, 86(3): 514-535.

178. Csoregh, I and TB Palm. (1977). The crystal and molecular structure of benzylpenicillin 1'-diethyl carbonate ester. *Acta Crystallographica Section B*, 33(7): 2169-2175.
179. Blanpain, P and F Durant. (1976). 3-(2-chlorophenyl)-5-methyl-4-isoxazolylpenicillin sulfoxide (cloxacillin sulfoxide) dioxane monohydrate, C₁₉H₁₈ClO₆N₃S·C₄H₈O₂·H₂O. *Crystal Structure Communications*, 5: 89-94.
180. Blanpain, P and F Durant. (1976). 3-(2-chlorophenyl)-5-methyl-4-isoxazolylpenicillin methyl ester (cloxacillin methyl ester): C₂₀H₂₀C₁N₃O₅S. *Crystal Structure Communications*, 5: 83-88.
181. Cameron, AF *et al.* (1979). Methyl 6 α -ethoxyformamido-6 β -phenoxyacetamidopenicillanate. *Acta Crystallographica Section B*, 35(5): 1263-1266.
182. Dauter, Z *et al.* (1981). The structure of 2,2-dimethyl-3-ureido-6-phenoxyacetamidopenam. *Acta Crystallographica Section B*, 37(12): p. 2179-2183.
183. Boles, MO and RJ Girven. (1976). The structures of ampicillin: a comparison of the anhydrate and trihydrate forms. *Acta Crystallographica Section B*, 32(8): 2279-2284.
184. Palm, TB and I Csoregh. (1978). The crystal and molecular structure of (S)-1'-ethoxycarbonyloxyethyl-6 β -[(hexahydro-1H-azepin-1-yl)methyleneamino]penicillanate hydrochloride (bacmecillinam hydrochloride). *Acta Crystallographica Section B*, 34(1): 138-143.
185. Lovell FM and NA Perkinson. (1978). Piperacillin hydrate. *Crystal Structure Communications*, 7: 7.
186. James, MN, D Hall, and DC Hodgkin. (1968). Crystalline modifications of ampicillin I: The trihydrate. *Nature*, 220(5163): 168-70.
187. Blanpain, P, M Melebeck, and F Durant. (1977). (2,6-dimethoxyphenyl)penicillin methyl ester (methicillin methyl ester). *Acta Crystallographica Section B: Structural Science*, 33: 580-582.
188. Fleming, A. (1929). On the antibacterial action of cultures of a penicillium, with special reference to their use in the isolation of *B. influenzae*. *Br J Exp Path*, 79(8): 780-90.
189. Libby, RL and NL Holmberg. (1945). The activity of penicillins G and X *in vitro*. *Science*, 102(2647): 303-304.
190. Eagle, H. (1946). The relative activity of penicillins F, G, K, and X against spirochetes and streptococci *in vitro*. *J Bacteriol*, 52: 81-88.
191. Nell, EE and JH Hill. (1947). Comparison of the *in vitro* antigonococcal actions of penicillins G, F, K, and X. *Am J Syph Gonorrhea Vener Dis*, 31(1): 14-19.

192. Eagle, H. (1947). The therapeutic activity of penicillins F, G, K, and X in experimental infections with pneumococcus type I and *Streptococcus pyogenes*. *J Exp Med*, 85(2): 175-186.
193. Thomsen, VF and SO Larsen. (1962). *In vitro* activity of penicillin. Comparative studies on benzylpenicillin, phenoxymethylpenicillin, phenoxyethylpenicillin and dimethoxyphenylpenicillin. *Nord Med*, 67: 111-119. [Original article in Danish]
194. Barber, M and PM Waterworth. (1964). Penicillinase-resistant penicillins and cephalosporins. *Br Med J*, 2(5405): 344-349.
195. Klein, JO and M Finland. (1963). The new penicillins. *N Engl J Med*, 269: 1019-1025.
196. Klein, JO and M Finland. (1963). Nafcillin. Antibacterial action *in vitro* and absorption and excretion in normal young men. *Am J Med Sci*, 246: 10-26.
197. Gourevitch, A *et al.* (1961). Microbiological evaluation of 5-methyl-3-phenyl-4-isoxazolyl penicillin. *Antibiot Chemother (Northfield)*, 11: 780-789.
198. Knudsen, ET, DM Brown, and GN Rolinson. (1962). A new orally effective penicillinase-stable penicillin - BRL1621. *Lancet*, 2(7257): 632-634.
199. Naumann, P and B Kempf. (1965). Dicloxacillin, a new, acid-stable and penicillinase-resistant oral penicillin. *Arzneimittelforschung*, 15: 139-145. [Original article in German]
200. Doyle, FP *et al.* (1961). New penicillins stable towards both acid and penicillinase. *Nature*, 192: 1183-1184.
201. Gourevitch, A *et al.* (1961). Activity of α -phenoxyalkyl penicillins against sensitive and resistant staphylococci. *Proc Soc Exp Biol Med*, 107: 455-458.
202. Richards, HC, JR Housley, and DF Spooner. (1963). Quinacillin: A new penicillin with unusual properties. *Nature*, 199: 354-356.
203. Rolinson, GN *et al.* (1960). Bacteriological studies on a new penicillin - BRL1241. *Lancet*, 2(7150): 564-567.
204. Smith, JT, JM Hamilton-Miller, and R Knox. (1962). Isoxazolyl penicillins and penicillinase. *Nature*, 195: 1300-1301.
205. Bodey, GP and J Nance. (1972). Amoxicillin: *in vitro* and pharmacological studies. *Antimicrob Agents Chemother*, 1(4): 358-362.
206. Acred, P *et al.* (1962). Pharmacology and chemotherapy of ampicillin - a new broad-spectrum penicillin. *Br J Pharmacol Chemother*, 18(2): 356-369.
207. Ekstroem, B *et al.* (1965). Semisynthetic penicillins 3. Aminopenicillins via azidopenicillins. *Acta Chem Scand*, 19: 281-299.

208. Fass, RJ. (1983). Statistical comparison of the antibacterial activities of broad-spectrum penicillins against Gram-negative bacilli. *Antimicrob Agents Chemother*, 24(2): 156-162.
209. Basker, MJ, RA Edmondson, and R Sutherland. (1979). Comparative antibacterial activity of azlocillin, mezlocillin, carbenicillin and ticarcillin and relative stability to β -lactamases of *Pseudomonas aeruginosa* and *Klebsiella aerogenes*. *Infection*, 7(2): 67-73.
210. Chanal, M *et al.* (1983). *In vitro* study of the bacteriostatic and bactericidal activity of temocillin (BRL17421). *Pathol Biol (Paris)*, 31(6): 467-470. [Original article in French]
211. Chattopadhyay, B, I Hall, and SR Curnow. (1983). Comparative *in vitro* activity of ticarcillin, piperacillin, azlocillin and mezlocillin. *Curr Med Res Opin*, 8(8): 577-581.
212. Rolinson, GN and R Sutherland. (1967). Carbenicillin, a new semisynthetic penicillin active against *Pseudomonas aeruginosa*. *Antimicrob Agents Chemother (Bethesda)*, 7: 609-613.
213. Machka, K, H Dickert, and I Braveny. (1980). *In vitro* activity of piperacillin compared with that of ampicillin, ticarcillin, azlocillin, and mezlocillin. *Arzneimittelforschung*, 30(2): 304-307.
214. Verbist, L. (1979). Comparison of the activities of the new ureidopenicillins piperacillin, mezlocillin, azlocillin, and Bay K 4999 against Gram-negative organisms. *Antimicrob Agents Chemother*, 16(2): 115-119.
215. Buckwell, S, MI Page, and JL Longridge. (1986). Equilibria between enamine and α,β -unsaturated imine in cephalosporin hydrolysis. *Journal of the Chemical Society, Chemical Communications*, 13: 1039-1040.
216. Faraci, WS and RF Pratt. (1986). Interactions of cephalosporins with the *Streptomyces* R61 DD-transpeptidase/carboxypeptidase. Influence of the 3'-substituent. *Biochem J*, 238(1): 309-312.
217. Boyd, DB. (1984). Electronic structures of cephalosporins and penicillins 15. Inductive effect of the 3-position side chain in cephalosporins. *J Med Chem*, 27(1): 63-66.
218. Boyd, DB *et al.* (1975). Electronic structures of cephalosporins and penicillins 4. Modeling acylation by the β -lactam ring. *J Med Chem*, 18(4): 408-417.
219. Brotzu, G., *Ricerche su di un nuovo antibiotico*. Lavori dell'Istituto d'Igiene di Cagliari, 1948 1-11. [Original article in Italian]
220. Jago, M and NG Heatley. (1961). Some biological properties of cephalosporin C and a derivative. *Br J Pharmacol Chemother*, 16(2): 170-179.
221. Newton, GG and EP Abraham. (1955). Cephalosporin C, a new antibiotic containing sulphur and D- α -amino adipic acid. *Nature*, 175(4456): 548.

222. Newton, GG and EP Abraham. (1956). Isolation of cephalosporin C, a penicillin-like antibiotic containing D- α -aminoadipic acid. *Biochem J*, 62(4): 651-658.
223. Abraham, EP and GG Newton. (1961). The structure of cephalosporin C. *The Biochemical Journal*, 79(2): 377-393.
224. Crawford, K *et al.* (1952). Antibiotic production by a species of *Cephalosporium*. *J Gen Microbiol*, 6(1-2): 47-59.
225. Hodgkin, DC and EN Maslen. (1961). The x-ray analysis of the structure of cephalosporin C. *Biochem J*, 79(2): 393-402.
226. Spencer, JL *et al.* (1966). Chemistry of cephalosporin antibiotics VII. Synthesis of cephaloglycin and some homologs. *J Med Chem*, 9(5): 746-750.
227. Spencer, JL *et al.* (1966). Chemistry of cephalosporin antibiotics VIII. Synthesis and structure-activity relationships of cephaloridine analogues. *Antimicrob Agents Chemother (Bethesda)*, 6: 573-580.
228. Chauvette, RR *et al.* (1962). Chemistry of cephalosporin antibiotics. II. Preparation of a new class of antibiotics and the relation of structure to activity. *Journal of the American Chemical Society*, 84(17): 3401-3402.
229. Spencer, JL *et al.* (1967). Chemistry of cephalosporin antibiotics IX. Synthesis of cephaloridine. *The Journal of Organic Chemistry*, 32(2): 500-501.
230. Godzeski, CW, G Brier, and DE Pavey. (1963). Cephalothin, a new cephalosporin with a broad antibacterial spectrum. I. *In vitro* studies employing the gradient plate technique. *Appl Microbiol*, 11(2): 122-127.
231. Ryan, CW, RL Simon, and EM Van Heyningen. (1969). Chemistry of cephalosporin antibiotics 13. Desacetoxycephalosporins. The synthesis of cephalixin and some analogs. *J Med Chem*, 12(2): 310-313.
232. Hsieh, WC and SW Ho. (1975). Evaluation of antibacterial activities of cephalosporin antibiotics: cefazolin, cephaloridine, cephalothin, and cephalixin. *Zhonghua Min Guo Wei Sheng Wu Xue Za Zhi*, 8(1): 1-11.
233. Eykyn, S *et al.* (1973). Antibacterial activity of cefamandole, a new cephalosporin antibiotic, compared with that of cephaloridine, cephalothin, and cephalixin. *Antimicrob Agents Chemother*, 3(6): 657-661.
234. Neu, HC. (1974). Cefoxitin, a semisynthetic cephamycin antibiotic: Antibacterial spectrum and resistance to hydrolysis by Gram-negative β -lactamases. *Antimicrob Agents Chemother*, 6(2): 170-176.
235. Neu, HC. (1974). Cefamandole, a cephalosporin antibiotic with an unusually wide spectrum of activity. *Antimicrob Agents Chemother*, 6(2): 177-182.

236. Hamilton-Miller, JM, DW Kerry, and W Brumfitt. (1974). An *in vivo* comparison of cefoxitin, a semi-synthetic cephamycin, with cephalothin. *J Antibiot (Tokyo)*, 27(1): 42-48.
237. Wallick, H and D Hendlin. (1974). Cefoxitin, a semisynthetic cephamycin antibiotic: susceptibility studies. *Antimicrob Agents Chemother*, 5(1): 25-32.
238. Kosmidis, J *et al.* (1973). Cefoxitin, a new semi-synthetic cephamycin: an *in vitro* and *in vivo* comparison with cephalothin. *Br Med J*, 4(5893): 653-655.
239. Nomura, H *et al.* (1974). Semisynthetic β -lactam antibiotics 6. Sulfocephalosporins and their antipseudomonal activities. *J Med Chem*, 17(12): 1312-1315.
240. Tsuchiya, K, M Kondo, and H Nagatomo. (1978). SCE-129, antipseudomonal cephalosporin: *in vitro* and *in vivo* antibacterial activities. *Antimicrob Agents Chemother*, 13(2): 137-145.
241. O'Callaghan, CH *et al.* (1976). Cefuroxime - a new cephalosporin antibiotic. *J Antibiot (Tokyo)*, 29(1): 29-37.
242. O'Callaghan, CH *et al.* (1976). Cefuroxime, a new cephalosporin antibiotic: Activity *in vitro*. *Antimicrob Agents Chemother*, 9(3): 511-519.
243. Ryan, DM, C O'Callaghan, and PW Muggleton. (1976). Cefuroxime, a new cephalosporin antibiotic: Activity *in vivo*. *Antimicrob Agents Chemother*, 9(3): 520-525.
244. Reiner, R *et al.* (1980). Ro 13-9904/001, a novel potent and long-acting parenteral cephalosporin. *J Antibiot (Tokyo)*, 33(7): 783-786.
245. Shannon, K *et al.* (1980). *In vitro* antibacterial activity and susceptibility of the cephalosporin Ro 13-9904 to β -lactamases. *Antimicrob Agents Chemother*, 18(2): 292-298.
246. Neu, HC, NJ Meropol, and KP Fu. (1981). Antibacterial activity of ceftriaxone (Ro 13-9904), a β -lactamase-stable cephalosporin. *Antimicrob Agents Chemother*, 19(3): 414-423.
247. Kojo, H *et al.* (1979). Antibacterial activity of ceftizoxime (FK 749), a new cephalosporin, against cephalosporin-resistant bacteria, and its stability to β -lactamase. *Antimicrob Agents Chemother*, 16(5): 549-553.
248. Matsubara, N *et al.* (1979). *In vitro* antibacterial activity of cefoperazone (T-1551), a new semisynthetic cephalosporin. *Antimicrob Agents Chemother*, 16(6): 731-735.
249. Sosna, JP, PR Murray, and G Medoff. (1978). Comparison of the *in vitro* activities of HR756 with cephalothin, cefoxitin, and cefamandole. *Antimicrob Agents Chemother*, 14(6): 876-879.

250. Wise, R, JM Andrews, and KA Bedford (1980). Comparison of *in vitro* activity of GR 20263, a novel cephalosporin derivative, with activities of other β -lactam compounds. *Antimicrob Agents Chemother*, 17(5): 884-889.
251. Verbist, L and J Verhaegen. (1980). GR-20263: a new aminothiazolyl cephalosporin with high activity against *Pseudomonas* and *Enterobacteriaceae*. *Antimicrob Agents Chemother*, 17(5): 807-812.
252. O'Callaghan, CH *et al.* (1980). GR 20263, a new broad-spectrum cephalosporin with anti-pseudomonal activity. *Antimicrob Agents Chemother*, 17(5): 876-883.
253. Kamimura, T *et al.* (1984). *In vitro* and *in vivo* antibacterial properties of FK 027, a new orally active cephem antibiotic. *Antimicrob Agents Chemother*, 25(1): 98-104.
254. Neu, HC, NX Chin, and P Labthavikul (1984). Comparative *in vitro* activity and β -lactamase stability of FR17027, a new orally active cephalosporin. *Antimicrob Agents Chemother*, 26(2): 174-180.
255. Inamoto, Y *et al.* (1988). FK482, a new orally active cephalosporin synthesis and biological properties. *J Antibiot (Tokyo)*, 41(6): 828-830.
256. Neu, HC, G Saha, and NX Chin. (1989). Comparative *in vitro* activity and β -lactamase stability of FK482, a new oral cephalosporin. *Antimicrob Agents Chemother*, 33(10): 1795-800.
257. Inamoto, Y *et al.* (1990). Studies on FK482. II. Synthesis and structure-activity relationships of 7 β -[(Z)-2-(2-aminothiazol-4-yl)-2-substituted acetamido]-3-vinyl-3-cephem-4-carboxylic acid derivatives. *Yakugaku Zasshi*, 110(4): 246-257. [Original article in Japanese]
258. Inamoto, Y *et al.* (1990). Studies on FK482 (Cefdinir). III. Synthesis and structure-activity relationships of 7 β -[(Z)-2-aryl-2-hydroxyiminoacetamido]-3-vinyl-3-cephem-4-carboxylic acid derivatives. *Yakugaku Zasshi*, 110(9): 658-664. [Original article in Japanese]
259. Yokoo, C *et al.* (1991). Studies on cephalosporin antibiotics. IV. Synthesis, antibacterial activity and oral absorption of new 3-(2-substituted-vinylthio)-7 β -[(Z)-2-(2-aminothiazol-4-yl)-2-(carboxymethoxyimino)acetamido]cephalosporins. *J Antibiot (Tokyo)*, 44(12): 1422-1431.
260. Khan, NJ *et al.* (1984). Antimicrobial activities of BMY-28142, cefbuperazone, and cefpiramide compared with those of other cephalosporins. *Antimicrob Agents Chemother*, 26(4): 585-590.
261. Kessler, RE *et al.* (1985). Comparison of a new cephalosporin, BMY 28142, with other broad-spectrum β -lactam antibiotics. *Antimicrob Agents Chemother*, 1985. 27(2): 207-16.
262. Seibert, G *et al.* (1983). HR 810, a new parenteral cephalosporin with a broad antibacterial spectrum. *Arzneimittelforschung*, 33(8): 1084-1086.

263. Machka, K and I Braveny. (1983). *In vitro* activity of HR 810, a new broad-spectrum cephalosporin. *Eur J Clin Microbiol*, 2(4): 345-349.
264. Limbert, M *et al.* (1991). Antibacterial activities *in vitro* and *in vivo* and pharmacokinetics of cefquinome (HR 111V), a new broad-spectrum cephalosporin. *Antimicrob Agents Chemother*, 35(1): 14-19.
265. Chin, NX *et al.* (1992). *In vitro* activity of cefquinome, a new cephalosporin, compared with other cephalosporin antibiotics. *Diagn Microbiol Infect Dis*, 15(4): 331-337.
266. Hancock, RE and F Bellido. (1992). Factors involved in the enhanced efficacy against Gram-negative bacteria of fourth generation cephalosporins. *J Antimicrob Chemother*, 29 Suppl A: 1-6.
267. Entenza, JM *et al.* (2002). BAL9141, a novel extended-spectrum cephalosporin active against methicillin-resistant *Staphylococcus aureus* in treatment of experimental endocarditis. *Antimicrob Agents Chemother*, 46(1): 171-177.
268. Zbinden, R, V Pünter, and A von Graevenitz. (2002). *In vitro* activities of BAL9141, a novel broad-spectrum pyrrolidinone cephalosporin, against Gram-negative nonfermenters. *Antimicrob Agents Chemother*, 46(3): 871-874.
269. Wootton, M *et al.* (2002). BAL 9141, a new broad-spectrum pyrrolidinone cephalosporin: Activity against clinically significant anaerobes in comparison with 10 other antimicrobials. *J Antimicrob Chemother*, 49(3): 535-539.
270. Issa, NC *et al.* (2004). *In vitro* activity of BAL9141 against clinical isolates of Gram-negative bacteria. *Diagn Microbiol Infect Dis*, 48(1): 73-75.
271. Takeda, S *et al.* (2007). *In vitro* and *in vivo* activities of a new cephalosporin, FR264205, against *Pseudomonas aeruginosa*. *Antimicrob Agents Chemother*, 51(3): 826-830.
272. Takeda, S *et al.* (2007). Stability of FR264205 against AmpC β -lactamase of *Pseudomonas aeruginosa*. *Int J Antimicrob Agents*, 30(5): 443-445.
273. Toda, A *et al.* (2008). Synthesis and SAR of novel parenteral anti-pseudomonal cephalosporins: discovery of FR264205. *Bioorg Med Chem Lett*, 18(17): 4849-4852.
274. Ishikawa, T *et al.* (2003). TAK-599, a novel *N*-phosphono type prodrug of anti-MRSA cephalosporin T-91825: Synthesis, physicochemical and pharmacological properties. *Bioorg Med Chem*, 11(11): 2427-2437.
275. Iizawa, Y *et al.* (2004). *In vitro* antimicrobial activity of T-91825, a novel anti-MRSA cephalosporin, and *in vivo* anti-MRSA activity of its prodrug, TAK-599. *J Infect Chemother*, 10(3): 146-156.

276. Sader, HS *et al.* (2005). Antimicrobial activity and spectrum of PPI-0903M (T-91825), a novel cephalosporin, tested against a worldwide collection of clinical strains. *Antimicrob Agents Chemother*, 49(8): 3501-3512.
277. Kohira, N. *et al.* (2016). *In Vitro* Antimicrobial Activity of a Siderophore Cephalosporin, S-649266, against *Enterobacteriaceae* Clinical Isolates, Including Carbapenem-Resistant Strains. *Antimicrob Agents Chemother*, 60(2): 729-734.
278. Ito, A. *et al.* (2016). Siderophore Cephalosporin Cefiderocol Utilizes Ferric Iron Transporter Systems for Antibacterial Activity against *Pseudomonas aeruginosa*. *Antimicrob Agents Chemother*, 60(12): 7396-7401.
279. Dobias, J *et al.* (2017). Activity of the novel siderophore cephalosporin cefiderocol against multidrug-resistant Gram-negative pathogens. *Eur J Clin Microbiol Infect Dis*, 36(12): 2319-2327.
280. Aoki, T *et al.* (2018). Cefiderocol (S-649266), A new siderophore cephalosporin exhibiting potent activities against *Pseudomonas aeruginosa* and other Gram-negative pathogens including multi-drug resistant bacteria: Structure activity relationship. *Eur J Med Chem*, 155: 847-868.
281. Kahan, JS *et al.* (1979). Thienamycin, a new β -lactam antibiotic I. Discovery, taxonomy, isolation and physical properties. *J Antibiot (Tokyo)*, 32(1): 1-12.
282. Tally, FP, NV Jacobus, and SL Gorbach. (1978). *In vitro* activity of thienamycin. *Antimicrob Agents Chemother*, 14(3): 436-438.
283. Kesado, T, T Hashizume, and Y Asahi. (1980). Antibacterial activities of a new stabilized thienamycin, *N*-formimidoyl thienamycin, in comparison with other antibiotics. *Antimicrob Agents Chemother*, 17(6): 912-917.
284. Iso, Y *et al.* (1996). A novel 1 β -methylcarbapenem antibiotic, S-4661. Synthesis and structure-activity relationships of 2-(5-substituted pyrrolidin-3-ylthio)-1 β -methylcarbapenems. *J Antibiot (Tokyo)*, 49(2): 199-209.
285. Edwards, JR *et al.* (1989). *In vitro* antibacterial activity of SM-7338, a carbapenem antibiotic with stability to dehydropeptidase I. *Antimicrob Agents Chemother*, 33(2): 215-222.
286. Fuchs, PC, AL Barry, and SD Brown. (1999). *In-vitro* antimicrobial activity of a carbapenem, MK-0826 (L-749,345) and provisional interpretive criteria for disc tests. *J Antimicrob Chemother*, 43(5): 703-706.
287. Taibi, P and S Mobashery. (1995). Mechanism of turnover of imipenem by the TEM β -lactamase revisited. *Journal of the American Chemical Society*, 117(29): 7600-7605.
288. Miyashita, K. (1996). Quantification of the extent of attenuation of the rate of turnover chemistry of the TEM-1 β -lactamase by the α -1R-hydroxyethyl group in substrates. *Bioorg. Med. Chem. Lett.*, 6: 319-322.

289. Basker, MJ, RJ Boon, and PA Hunter. (1980). Comparative antibacterial properties *in vitro* of seven olivanic acid derivatives: MM 4550, MM 13902, MM 17880, MM 22380, MM 22381, MM 22382 and MM 22383. *J Antibiot (Tokyo)*, 33(8): 878-884.
290. Methicillin-resistant *Staphylococcus aureus*. *Nat Rev Dis Primers*, 2018. 4: 18034.
291. Ahmed, MO and KE Baptiste. (2018). Vancomycin-Resistant *Enterococci*: A Review of Antimicrobial Resistance Mechanisms and Perspectives of Human and Animal Health. *Microb Drug Resist*, 24(5): 590-606.
292. Pang, Z *et al.* (2019). Antibiotic resistance in *Pseudomonas aeruginosa*: mechanisms and alternative therapeutic strategies. *Biotechnol Adv*, 37(1): 177-192.
293. Lee, CR *et al.* (2017). Antimicrobial resistance of hypervirulent *Klebsiella pneumoniae*: Epidemiology, hypervirulence-associated determinants, and resistance mechanisms. *Front Cell Infect Microbiol*, 7: 483.
294. Santajit, S and N Indrawattana. (2016). Mechanisms of antimicrobial resistance in ESKAPE pathogens. *Biomed Res Int*, 2016: 2475067.
295. Unemo, M *et al.* (2019). *Gonorrhoea*. *Nat Rev Dis Primers*, 5(1): 79.
296. Tien, V, C Punjabi, and MK Holubar. (2020). Antimicrobial resistance in sexually transmitted infections. *J Travel Med*, 27(1).
297. World Health Organization. *Antimicrobial resistance: global report on surveillance*. 2014.
298. Pagès, JM, CE James, and M Winterhalter (2008). The porin and the permeating antibiotic: a selective diffusion barrier in Gram-negative bacteria. *Nat Rev Microbiol*, 6(12): 893-903.
299. Goldstein, FW *et al.* (1983). *In vivo* and *in vitro* emergence of simultaneous resistance to both β -lactam and aminoglycoside antibiotics in a strain of *Serratia marcescens*. *Ann Microbiol (Paris)*, 134a(3): 329-337.
300. Medeiros, AA *et al.* (1987). Loss of OmpC porin in a strain of *Salmonella typhimurium* causes increased resistance to cephalosporins during therapy. *J Infect Dis*, 156(5): 751-757.
301. Burns, JL and AL Smith. (1987). A major outer-membrane protein functions as a porin in *Haemophilus influenzae*. *J Gen Microbiol*, 133(5): 1273-1277.
302. Quinn, JP *et al.* (1986). Emergence of resistance to imipenem during therapy for *Pseudomonas aeruginosa* infections. *J Infect Dis*, 154(2): 289-294.
303. Doménech-Sánchez, A *et al.* (2003). Role of *Klebsiella pneumoniae* OmpK35 porin in antimicrobial resistance. *Antimicrob Agents Chemother*, 47(10): 3332-3335.

304. Olesky, M, M Hobbs, and RA Nicholas. (2002). Identification and analysis of amino acid mutations in porin IB that mediate intermediate-level resistance to penicillin and tetracycline in *Neisseria gonorrhoeae*. *Antimicrob Agents Chemother*, 46(9): 2811-2820.
305. Gill, MJ *et al.* (1998). Gonococcal resistance to β -lactams and tetracycline involves mutation in loop 3 of the porin encoded at the *penB* locus. *Antimicrob Agents Chemother*, 42(11): 2799-2803.
306. Olesky, M *et al.* (2006). Porin-mediated antibiotic resistance in *Neisseria gonorrhoeae*: Ion, solute, and antibiotic permeation through PIB proteins with *penB* mutations. *J Bacteriol*, 188(7): 2300-2308.
307. Zhao, S *et al.* (2005). The *penC* mutation conferring antibiotic resistance in *Neisseria gonorrhoeae* arises from a mutation in the PilQ secretin that interferes with multimer stability. *Mol Microbiol*, 57(5): 1238-1251.
308. Nikaido, H. (2003). Molecular basis of bacterial outer membrane permeability revisited. *Microbiol Mol Biol Rev*, 67(4): 593-656.
309. Piddock, LJ. (2006). Clinically relevant chromosomally encoded multidrug resistance efflux pumps in bacteria. *Clin Microbiol Rev*, 19(2): 382-402.
310. Du, D *et al.* (2018). Multidrug efflux pumps: Structure, function and regulation. *Nat Rev Microbiol*, 16(9): 523-539.
311. Poole, K. (2005). Efflux-mediated antimicrobial resistance. *J Antimicrob Chemother*, 56(1): 20-51.
312. Shafer, WM *et al.* (1998). Modulation of *Neisseria gonorrhoeae* susceptibility to vertebrate antibacterial peptides due to a member of the resistance/nodulation/division efflux pump family. *Proc Natl Acad Sci USA*, 95(4): 1829-1833.
313. Janganan, TK *et al.* (2011). Evidence for the assembly of a bacterial tripartite multidrug pump with a stoichiometry of 3:6:3. *J Biol Chem*, 286(30): 26900-26912.
314. Bolla, JR *et al.* (2014). Crystal structure of the *Neisseria gonorrhoeae* MtrD inner membrane multidrug efflux pump. *PLoS One*, 9(6): e97903.
315. Edwards, MJ *et al.* (2012). Analysis of structural MtrC models based on homology with the crystal structure of MtrF. *Biochem Soc Trans*, 40(6): 1181-1185.
316. Lei, HT *et al.* (2014). Crystal structure of the open state of the *Neisseria gonorrhoeae* MtrE outer membrane channel. *PLoS One*, 9(6): e97475.
317. Hagman, KE *et al.* (1995). Resistance of *Neisseria gonorrhoeae* to antimicrobial hydrophobic agents is modulated by the mtrRCDE efflux system. *Microbiology*, 141 (Pt 3): 611-622.

318. Hagman, KE *et al.* (1997). The MtrD protein of *Neisseria gonorrhoeae* is a member of the resistance/nodulation/division protein family constituting part of an efflux system. *Microbiology*, 143 (Pt 7): 2117-2125.
319. Rouquette, C, JB Harmon, and WM. Shafer. (1999). Induction of the *mtrCDE*-encoded efflux pump system of *Neisseria gonorrhoeae* requires MtrA, an AraC-like protein. *Mol Microbiol*, 33(3): 651-658.
320. Hagman, KE and WM Shafer. (1995). Transcriptional control of the *mtr* efflux system of *Neisseria gonorrhoeae*. *Journal of Bacteriology*, 177(14): 4162-4165.
321. Pan, W and BG Spratt. (1994). Regulation of the permeability of the gonococcal cell envelope by the *mtr* system. *Mol Microbiol*, 11(4): 769-775.
322. Lucas, CE *et al.* (1997). The MtrR repressor binds the DNA sequence between the *mtrR* and *mtrC* genes of *Neisseria gonorrhoeae*. *J Bacteriol*, 179(13): 4123-4128.
323. Wang, DM *et al.* (2004). Multiple resistance of *Neisseria gonorrhoeae* and mutations in the inverted sequence within the *mtrR* promoter region. *Zhong Nan Da Xue Xue Bao Yi Xue Ban*, 29(5): 544-547. [Original article in Chinese]
324. Zarantonelli, L *et al.* (1999). Decreased azithromycin susceptibility of *Neisseria gonorrhoeae* due to *mtrR* mutations. *Antimicrob Agents Chemother*, 43(10): 2468-2472.
325. Veal, WL, RA Nicholas, and WM Shafer. (2002). Overexpression of the MtrC-MtrD-MtrE efflux pump due to an *mtrR* mutation is required for chromosomally mediated penicillin resistance in *Neisseria gonorrhoeae*. *J Bacteriol*, 184(20): 5619-5624.
326. Warner, DM, WM Shafer, and AE Jerse. (2008). Clinically relevant mutations that cause derepression of the *Neisseria gonorrhoeae* MtrC-MtrD-MtrE Efflux pump system confer different levels of antimicrobial resistance and *in vivo* fitness. *Mol Microbiol*, 70(2): 462-478.
327. Shafer, WM *et al.* (1995). Missense mutations that alter the DNA-binding domain of the MtrR protein occur frequently in rectal isolates of *Neisseria gonorrhoeae* that are resistant to faecal lipids. *Microbiology*, 141 (Pt 4): 907-911.
328. Ciofu, O and T Tolker-Nielsen. (2019). Tolerance and resistance of *Pseudomonas aeruginosa* biofilms to antimicrobial agents - How *P. aeruginosa* can escape antibiotics. *Front Microbiol*, 10: 913.
329. Wang, LC *et al.* (2018). *Neisseria gonorrhoeae* aggregation reduces its ceftriaxone susceptibility. *Antibiotics (Basel)*, 7(2): 48
330. Stewart, PS. (2015). Antimicrobial tolerance in biofilms. *Microbiol Spectr*, 3(3).
331. Lewis, K. (2007). Persister cells, dormancy and infectious disease. *Nat Rev Microbiol*, 5(1): 48-56.

332. Zöllner, R *et al.* (2017). Phase and antigenic variation govern competition dynamics through positioning in bacterial colonies. *Sci Rep*, 7(1): 12151.
333. Stein, DC *et al.* (2015). Expression of opacity proteins interferes with the transmigration of *Neisseria gonorrhoeae* across polarized epithelial cells. *PLoS One*, 10(8): e0134342.
334. LeVan, A *et al.* (2012). Construction and characterization of a derivative of *Neisseria gonorrhoeae* strain MS11 devoid of all *opa* genes. *J Bacteriol*, 194(23): 6468-6478.
335. Greiner, LL *et al.* (2005). Biofilm formation by *Neisseria gonorrhoeae*. *Infect Immun*, 73(4): 1964-1970.
336. Steichen, CT *et al.* (2008) Gonococcal cervicitis: A role for biofilm in pathogenesis. *J Infect Dis*, 198(12): 1856-1861.
337. Wright, GD. (2005). Bacterial resistance to antibiotics: Enzymatic degradation and modification. *Adv Drug Deliv Rev*, 57(10): 1451-1470.
338. Ramirez, MS and ME Tolmasky. (2010). Aminoglycoside modifying enzymes. *Drug Resist Updat*, 13(6): 151-171.
339. Shaw, WV. (1983). Chloramphenicol acetyltransferase: Enzymology and molecular biology. *CRC Crit Rev Biochem*, 14(1): 1-46.
340. Allignet, J *et al.* (1993). Sequence of a staphylococcal gene, *vat*, encoding an acetyltransferase inactivating the A-type compounds of virginiamycin-like antibiotics. *Gene*, 130(1): 91-98.
341. Lombardini, JB and M Cheng-Chu. (1980). Properties of gentamicin adenyl transferase obtained from R-factor-resistant *Escherichia coli*. *Int J Biochem*, 12(3): 427-431.
342. Leclercq, R *et al.* (1985). Plasmid-mediated resistance to lincomycin by inactivation in *Staphylococcus haemolyticus*. *Antimicrob Agents Chemother*, 28(3): 421-424.
343. Schwarz, S *et al.* (2004). Molecular basis of bacterial resistance to chloramphenicol and florfenicol. *FEMS Microbiol Rev*, 28(5): 519-542.
344. Abraham, EP and E Chain. (1988). An enzyme from bacteria able to destroy penicillin 1940. *Rev Infect Dis*, 10(4): 677-678.
345. Bush, K. (2018). Past and Present Perspectives on β -Lactamases. *Antimicrob Agents Chemother*, 62(10): e01076-18.
346. Ghafourian, S *et al.* (2015). Extended Spectrum β -lactamases: Definition, Classification and Epidemiology. *Curr Issues Mol Biol*, 17: 11-21.

347. Bush, K. (2013). Proliferation and significance of clinically relevant β -lactamases. *Ann N Y Acad Sci*, 1277: 84-90.
348. Paterson, DL and RA Bonomo. (2005). Extended-spectrum β -lactamases: A clinical update. *Clin Microbiol Rev*, 18(4): 657-686.
349. Williams, RA. (1981). Penicillinase-producing *Neisseria gonorrhoeae*. *Am Fam Physician*, 24(6): 117-119.
350. Chen, SC *et al.* (2013). Prevalence and molecular epidemiological typing of penicillinase-producing *Neisseria gonorrhoeae* and their bla_{TEM-135} gene variants in Nanjing, China. *Sex Transm Dis*, 40(11): 872-876.
351. Nakayama, S *et al.* (2012). Molecular analyses of TEM genes and their corresponding penicillinase-producing *Neisseria gonorrhoeae* isolates in Bangkok, Thailand. *Antimicrob Agents Chemother*, 56(2): 916-920.
352. Ohnishi, M *et al.* (2010). Identification of TEM-135 β -lactamase in penicillinase-producing *Neisseria gonorrhoeae* strains in Japan. *Antimicrob Agents Chemother*, 54(7): 3021-3023.
353. Vincent, LR *et al.* (2018). *In Vivo* Selected compensatory mutations restore the fitness cost of mosaic *penA* alleles that confer ceftriaxone resistance in *Neisseria gonorrhoeae*. *mBio*, 9(2): e01905-17.
354. Li, H *et al.* (2019). Comprehensive proteomic and metabolomic profiling of *mcr-1*-mediated colistin resistance in *Escherichia coli*. *Int J Antimicrob Agents*, 53(6): 795-804.
355. Sun, L *et al.* (2019). Mutations of *Mycobacterium tuberculosis* induced by anti-tuberculosis treatment result in metabolism changes and elevation of ethambutol resistance. *Infect Genet Evol*, 72: 151-158.
356. Sieradzki, K and A Tomasz. (2003). Alterations of cell wall structure and metabolism accompany reduced susceptibility to vancomycin in an isogenic series of clinical isolates of *Staphylococcus aureus*. *J Bacteriol*, 185(24): 7103-7110.
357. Tran, TT *et al.* (2013). Whole-genome analysis of a daptomycin-susceptible *Enterococcus faecium* strain and its daptomycin-resistant variant arising during therapy. *Antimicrob Agents Chemother*, 57(1): 261-268.
358. Zhao, S *et al.* (2009). Genetics of chromosomally mediated intermediate resistance to ceftriaxone and cefixime in *Neisseria gonorrhoeae*. *Antimicrob Agents Chemother*, 53(9): 3744-3751.
359. Lambert, PA. (2005). Bacterial resistance to antibiotics: Modified target sites. *Adv Drug Deliv Rev*, 57(10): 1471-1485.
360. Maravić, G. (2004). Macrolide resistance based on the Erm-mediated rRNA methylation. *Curr Drug Targets Infect Disord*, 4(3): 193-202.

361. Weisblum, B. (1995). Erythromycin resistance by ribosome modification. *Antimicrob Agents Chemother*, 39(3): 577-585.
362. Martínez-Martínez, L, A Pascual, and GA Jacoby. (1998). Quinolone resistance from a transferable plasmid. *Lancet*, 351(9105): 797-799.
363. Aldred, KJ, RJ Kerns, and N Osheroff. (2014). Mechanism of quinolone action and resistance. *Biochemistry*, 53(10): 1565-1574.
364. Lakhundi, S and K Zhang. (2018). Methicillin-resistant *Staphylococcus aureus*: molecular characterization, evolution, and epidemiology. *Clin Microbiol Rev*, 31(4): e00020-18.
365. Ubukata, K *et al.* (1989). Expression and inducibility in *Staphylococcus aureus* of the *mecA* gene, which encodes a methicillin-resistant *S. aureus*-specific penicillin-binding protein. *J Bacteriol*, 171(5): 2882-2885.
366. Lim, D and NC Strynadka. (2002). Structural basis for the β -lactam resistance of PBP2a from methicillin-resistant *Staphylococcus aureus*. *Nat Struct Biol*, 9(11): p. 870-876.
367. Laible, G *et al.* (1989) Nucleotide sequences of the *pbpX* genes encoding the penicillin-binding proteins 2x from *Streptococcus pneumoniae* R6 and a cefotaxime-resistant mutant, C506. *Mol Microbiol*, 3(10): 1337-1348.
368. Laible, G, BG Spratt, and R Hakenbeck. (1991). Interspecies recombinational events during the evolution of altered PBP2x genes in penicillin-resistant clinical isolates of *Streptococcus pneumoniae*. *Mol Microbiol*, 15(8): 1993-2002.
369. Hakenbeck, R *et al.* (1991). Penicillin-binding proteins in *Streptococcus pneumoniae*: Alterations during development of intrinsic penicillin resistance. *J Chemother*, 3(2): 86-90.
370. Muñoz, R *et al.* (1992). Genetics of resistance to third-generation cephalosporins in clinical isolates of *Streptococcus pneumoniae*. *Mol Microbiol*, 6(17): 2461-2465.
371. Hakenbeck, R, M Tarpay, and A Tomasz. (1980). Multiple changes of penicillin-binding proteins in penicillin-resistant clinical isolates of *Streptococcus pneumoniae*. *Antimicrob Agents Chemother*, 17(3): 364-371.
372. Dowson, CG *et al.* (1989). Horizontal transfer of penicillin-binding protein genes in penicillin-resistant clinical isolates of *Streptococcus pneumoniae*. *Proc Natl Acad Sci USA*, 86(22): 8842-8846.
373. Hakenbeck, R *et al.* (1998). Acquisition of five high-Mr penicillin-binding protein variants during transfer of high-level β -lactam resistance from *Streptococcus mitis* to *Streptococcus pneumoniae*. *J Bacteriol*, 180(7): 1831-1840.
374. Dahesh, S *et al.* (2008). Point mutation in the group B streptococcal *pbp2x* gene conferring decreased susceptibility to β -lactam antibiotics. *Antimicrob Agents Chemother*, 52(8): 2915-2918.

375. Fontana, R *et al.* (1983). Identification of a streptococcal penicillin-binding protein that reacts very slowly with penicillin. *J Bacteriol*, 155(3): 1343-1350.
376. Ligozzi, M, F Pittaluga, and R Fontana. (1996). Modification of penicillin-binding protein 5 associated with high-level ampicillin resistance in *Enterococcus faecium*. *Antimicrob Agents Chemother*, 40(2): 354-357.
377. Fontana, R *et al.* (1994). Overproduction of a low-affinity penicillin-binding protein and high-level ampicillin resistance in *Enterococcus faecium*. *Antimicrob Agents Chemother*, 38(9): 1980-1983.
378. Matic, V *et al.* (2003). Contribution of β -lactamase and PBP amino acid substitutions to amoxicillin/clavulanate resistance in β -lactamase-positive, amoxicillin/clavulanate-resistant *Haemophilus influenzae*. *J Antimicrob Chemother*, 52(6): 1018-1021.
379. Clark, C *et al.* (2004). *In vitro* selection of resistance in *Haemophilus influenzae* by 4 quinolones and 5 beta-lactams. *Diagn Microbiol Infect Dis*, 49(1): 31-36.
380. Bozdogan, B, S Tristram, and PC Appelbaum. (2006). Combination of altered PBPs and expression of cloned extended-spectrum β -lactamases confers cefotaxime resistance in *Haemophilus influenzae*. *J Antimicrob Chemother*, 57(4): 747-749.
381. Ubukata, K *et al.* (2001). Association of amino acid substitutions in penicillin-binding protein 3 with β -lactam resistance in β -lactamase-negative ampicillin-resistant *Haemophilus influenzae*. *Antimicrob Agents Chemother*, 45(6): 1693-1699.
382. Park, M and F Rafii. (2017). Exposure to β -lactams results in the alteration of penicillin-binding proteins in *Clostridium perfringens*. *Anaerobe*, 45: 78-85.
383. Williamson, R. (1983). Resistance of *Clostridium perfringens* to β -lactam antibiotics mediated by a decreased affinity of a single essential penicillin-binding protein. *J Gen Microbiol*, 129(8): 2339-2342.
384. Tomberg, J *et al.* (2013). Identification of amino acids conferring high-level resistance to expanded-spectrum cephalosporins in the *penA* gene from *Neisseria gonorrhoeae* strain H041. *Antimicrob Agents Chemother*, 57(7): 3029-3036.
385. Dougherty, TJ, AE Koller, and A Tomasz. (1980). Penicillin-binding proteins of penicillin-susceptible and intrinsically resistant *Neisseria gonorrhoeae*. *Antimicrob Agents Chemother*, 18(5): 730-737.
386. Dougherty, TJ. (1986). Genetic analysis and penicillin-binding protein alterations in *Neisseria gonorrhoeae* with chromosomally mediated resistance. *Antimicrob Agents Chemother*, 30(5): 649-652.

387. Powell, AJ *et al.* (2009). Crystal structures of penicillin-binding protein 2 from penicillin-susceptible and -resistant strains of *Neisseria gonorrhoeae* reveal an unexpectedly subtle mechanism for antibiotic resistance. *J Biol Chem*, 284(2): 1202-1212.
388. Tomberg, J *et al.* (2012). A highly conserved interaction involving the middle residue of the SXN active-site motif is crucial for function of class B penicillin-binding proteins: mutational and computational analysis of PBP 2 from *N. gonorrhoeae*. *Biochemistry*, 51(13): 2775-2784.
389. Fedarovich, A *et al.* (2014). Structural effect of the Asp345a insertion in penicillin-binding protein 2 from penicillin-resistant strains of *Neisseria gonorrhoeae*. *Biochemistry*, 53(48): 7596-7603.
390. Ochiai, S *et al.* (2007). Decreased affinity of mosaic-structure recombinant penicillin-binding protein 2 for oral cephalosporins in *Neisseria gonorrhoeae*. *J Antimicrob Chemother*, 60(1): 54-60.
391. Wainwright, M and HT Swan. (1986). C.G. Paine and the earliest surviving clinical records of penicillin therapy. *Medical History*, 30(1): 42-56.
392. (1945). Outpatient penicillin therapy of sulfonamide resistant gonorrhoea. *Cal West Med*, 63(3): 153.
393. (1944). Penicillin used for sulphonamide-resistant gonorrhoea. *Br J Vener Dis*, 20(1): 44.
394. (1945). Ambulatory penicillin treatment of sulphonamide-resistant gonorrhoea. *Br J Vener Dis*, 21(4): 173.
395. Irmisch, GW. (1946). Penicillin therapy for sulfonamide resistant gonorrhoea. *J Urol*, 55: 306-308.
396. Lees, R. (1946). Penicillin for sulphonamide-resistant gonorrhoea. *Br Med J*, 1(4450): 605-606.
397. Lees, R. (1946). Treatment of sulphonamide-resistant gonorrhoea by penicillin. *Br Med J*, 1: 605.
398. Willcox, RR. (1958). All-purpose penicillin in the treatment of gonorrhoea: Increasing failure rates with repository penicillins. *Antibiot Annu*, 6: 125-133.
399. Dallas, NL. (1958). Penicillin treatment failures in male gonorrhoea. *Br J Vener Dis*, 34(3): 194-195.
400. Epstein, E. (1959). Failure of penicillin in treatment of acute gonorrhoea in American troops in Korea. *J Am Med Assoc*, 169(10): 1055-1059.
401. Gjessing, HC. (1959). Increasing failure rate after using the same preparation and dosage of penicillin in the treatment of gonorrhoea. *Br J Vener Dis*, 35(4): 256-257.

402. King, AJ and CS Nicol. (1961). The problem of gonorrhoea in England and Wales. *Bull World Health Organ*, 24(3): 373-384.
403. Aepinus, M. (1965). The current decrease of effect of penicillin treatment of gonorrhoea. *Z Haut Geschlechtskr*, 39(1): 11-13. [Original article in German]
404. Martin, JE, Jr. *et al.* (1965). *In vitro* antimicrobial susceptibility of *Neisseria gonorrhoeae* from penicillin treatment failures. *Antimicrob Agents Chemother (Bethesda)*, 5: 366-368.
405. Willcox, RR. (1970). A survey of problems in the antibiotic treatment of gonorrhoea. With special reference to South-East Asia. *Br J Vener Dis*, 46(3): 217-242.
406. Elwell, LP *et al.* (1977). Plasmid-mediated β -lactamase production in *Neisseria gonorrhoeae*. *Antimicrob Agents Chemother*, 11(3): 528-533.
407. Biswas, G, S Comer, and PF Sparling. (1976). Chromosomal location of antibiotic resistance genes in *Neisseria gonorrhoeae*. *J Bacteriol*, 125(3): 1207-1210.
408. Hook, EW, 3rd *et al.* (1987). Auxotype/serovar diversity and antimicrobial resistance of *Neisseria gonorrhoeae* in two mid-sized American cities. *Sex Transm Dis*, 14(3): 141-146.
409. Rice, RJ *et al.* (1986). Chromosomally mediated resistance in *Neisseria gonorrhoeae* in the United States: Results of surveillance and reporting, 1983-1984. *J Infect Dis*, 153(2): 340-345.
410. Centers for Disease Control and Prevention. (1984). Changing trends in gonococcal antibiotic resistance in the United States, 1983-1984. *MMWR CDC Surveill Summ*, 33(4): 11ss-15ss.
411. Centers for Disease Control and Prevention. (1983). Penicillin-resistant gonorrhoea - North Carolina. *MMWR Morb Mortal Wkly Rep*, 32(21): 273-275.
412. Centers for Disease Control and Prevention (1984). Chromosomally mediated resistant *Neisseria gonorrhoeae*--United States. *MMWR Morb Mortal Wkly Rep*, 33(28): 408-410.
413. Spratt, BG. (1988). Hybrid penicillin-binding proteins in penicillin-resistant strains of *Neisseria gonorrhoeae*. *Nature*, 332(6160): 173-176.
414. Spratt, BG *et al.* (1992). Role of interspecies transfer of chromosomal genes in the evolution of penicillin resistance in pathogenic and commensal *Neisseria species*. *J Mol Evol*, 34(2): 115-125.
415. Dowson, CG *et al.* (1989). Penicillin-binding protein 2 genes of non- β -lactamase-producing, penicillin-resistant strains of *Neisseria gonorrhoeae*. *Mol Microbiol*, 3(1): 35-41.

416. Brannigan, JA *et al.* (1990). Insertion of an extra amino acid is the main cause of the low affinity of penicillin-binding protein 2 in penicillin-resistant strains of *Neisseria gonorrhoeae*. *Mol Microbiol*, 4(6): 913-919.
417. Lindberg, R *et al.* (2007). *Neisseria gonorrhoeae* isolates with reduced susceptibility to cefixime and ceftriaxone: Association with genetic polymorphisms in *penA*, *mtrR*, *porB1b*, and *ponA*. *Antimicrob Agents Chemother*, 51(6): 2117-2122.
418. Osaka, K, *et al.* (2008). Analysis of amino acid sequences of penicillin-binding protein 2 in clinical isolates of *Neisseria gonorrhoeae* with reduced susceptibility to cefixime and ceftriaxone. *J Infect Chemother*, 14(3): 195-203.
419. Igawa, G, *et al.* (2018). *Neisseria cinerea* with high ceftriaxone MIC is a source of ceftriaxone and cefixime resistance-mediating *penA* sequences in *Neisseria gonorrhoeae*. *Antimicrob Agents Chemother*, 62(3): e02069-17.
420. Furuya, R. *et al.* (2007). Antimicrobial resistance in clinical isolates of *Neisseria subflava* from the oral cavities of a Japanese population. *J Infect Chemother*, 13(5): 302-304.
421. Saika, T *et al.* (2001). Comparison of *Neisseria gonorrhoeae* isolates from the genital tract and pharynx of two gonorrhea patients. *J Infect Chemother*, 7(3): 175-179.
422. Takahata, S *et al.* (2006). Amino acid substitutions in mosaic penicillin-binding protein 2 associated with reduced susceptibility to cefixime in clinical isolates of *Neisseria gonorrhoeae*. *Antimicrob Agents Chemother*, 50(11): 3638-3645.
423. Centers for Disease Control and Prevention (2013). *Antibiotic resistance threats in the United States, 2013*.
424. Whiley, DM *et al.* (2007). Diversity of *penA* alterations and subtypes in *Neisseria gonorrhoeae* strains from Sydney, Australia, that are less susceptible to ceftriaxone. *Antimicrob Agents Chemother*, 51(9): 3111-3116.
425. Lee, SG *et al.* (2010). Various *penA* mutations together with *mtrR*, *porB* and *ponA* mutations in *Neisseria gonorrhoeae* isolates with reduced susceptibility to cefixime or ceftriaxone. *J Antimicrob Chemother*, 65(4): 669-675.
426. Pandori, M *et al.* (2009). Mosaic penicillin-binding protein 2 in *Neisseria gonorrhoeae* isolates collected in 2008 in San Francisco, California. *Antimicrob Agents Chemother*, 53(9): 4032-4034.
427. Bharat, A *et al.* (2015). Effect of variants of penicillin-binding protein 2 on cephalosporin and carbapenem susceptibilities in *Neisseria gonorrhoeae*. *Antimicrob Agents Chemother*, 59(8): 5003-5006.
428. Tomberg, J *et al.* (2017). Alanine 501 mutations in penicillin-binding protein 2 from *Neisseria gonorrhoeae*: Structure, mechanism, and effects on cephalosporin resistance and biological fitness. *Biochemistry*, 56(8): 1140-1150.

429. Whiley, DM *et al.* (2010). Reduced susceptibility to ceftriaxone in *Neisseria gonorrhoeae* is associated with mutations G542S, P551S and P551L in the gonococcal penicillin-binding protein 2. *J Antimicrob Chemother*, 65(8): 1615-1618.
430. Ropp, PA *et al.* (2002). Mutations in *ponA*, the gene encoding penicillin-binding protein 1, and a novel locus, *penC*, are required for high-level chromosomally mediated penicillin resistance in *Neisseria gonorrhoeae*. *Antimicrob Agents Chemother*, 46(3): 769-77.
431. Kirkcaldy, RD *et al.* (2014). The efficacy and safety of gentamicin plus azithromycin and gemifloxacin plus azithromycin as treatment of uncomplicated gonorrhea. *Clin Infect Dis*, 59(8): 1083-1091.
432. Dowell, D and RD Kirkcaldy. (2013). Effectiveness of gentamicin for gonorrhoea treatment: systematic review and meta-analysis. *Postgrad Med J*, 89(1049): 142-147.
433. Dowell, D and RD Kirkcaldy. (2012). Effectiveness of gentamicin for gonorrhoea treatment: systematic review and meta-analysis. *Sex Transm Infect*, 88(8): 589-594.
434. Yang, J, S Dhital, and T Naderer. (2019). Efficacy and safety of injectable and oral antibiotics in treating gonorrhea: A systematic review and network meta-analysis. *J Clin Med*, 8(12): 2182.
435. Hathorn, E *et al.* (2014). The effectiveness of gentamicin in the treatment of *Neisseria gonorrhoeae*: A systematic review. *Syst Rev*, 3: 104.
436. Wersäll, J, PG Lundquist, and B Björkroth. (1969). Ototoxicity of gentamicin. *J Infect Dis*, 119(4): 410-416.
437. Falco, FG, HM Smith, and GM Arcieri. (1969). Nephrotoxicity of aminoglycosides and gentamicin. *J Infect Dis*, 119(4): 406-409.
438. Ross, JDC *et al.* (2019). Gentamicin compared with ceftriaxone for the treatment of gonorrhoea (G-ToG): A randomised non-inferiority trial. *Lancet*, 393(10190): 2511-2520.
439. Ross, JDC *et al.* (2019). Gentamicin as an alternative to ceftriaxone in the treatment of gonorrhoea: The G-TOG non-inferiority RCT. *Health Technol Assess*, 23(20): 1-104.
440. Hauser, C *et al.* (2015). *In vitro* activity of fosfomycin alone and in combination with ceftriaxone or azithromycin against clinical *Neisseria gonorrhoeae* isolates. *Antimicrob Agents Chemother*, 59(3): 1605-1611.
441. Dickgiesser, N and P Kuntz. (1984). The activity of rosoxacin, fosfomycin, cefotiam, and spectinomycin on β -lactamase producing *Neisseria gonorrhoeae*. *Br J Vener Dis*, 60(3): 154-156.

442. Barbee, LA *et al.* (2014). *In vitro* synergy testing of novel antimicrobial combination therapies against *Neisseria gonorrhoeae*. *J Antimicrob Chemother*, 69(6): 1572-1578.
443. Wind, CM, HJ de Vries, and AP van Dam. (2015). Determination of *in vitro* synergy for dual antimicrobial therapy against resistant *Neisseria gonorrhoeae* using Etest and agar dilution. *Int J Antimicrob Agents*, 45(3): 305-308.
444. Lagacé-Wiens, PRS *et al.* (2017). Antimicrobial susceptibility of clinical isolates of *Neisseria gonorrhoeae* to alternative antimicrobials with therapeutic potential. *J Antimicrob Chemother*, 72(8): 2273-2277.
445. Rodríguez, A *et al.* (1977). Bacteriological evaluation of fosfomycin in clinical studies. *Chemotherapy*, 23 Suppl 1: 247-58.
446. López-Gracia, J. (1977). Treatment of acute and subacute gonococcal urethritis with fosfomycin. *Chemotherapy*, 23 Suppl 1: 293-300.
447. Nilsson, AI *et al.* (2003). Biological costs and mechanisms of fosfomycin resistance in *Escherichia coli*. *Antimicrob Agents Chemother*, 47(9): 2850-2858.
448. Yuan, Z *et al.* (2016). Randomized controlled clinical trial on the efficacy of fosfomycin trometamol for uncomplicated gonococcal urethritis in men. *Clin Microbiol Infect*, 22(6): 507-512.
449. Lee, H. *et al.* (2017). *In vitro* activity of tigecycline alone and antimicrobial combinations against clinical *Neisseria gonorrhoeae* isolates. *Diagn Microbiol Infect Dis*, 87(2): 160-162.
450. Deshpande, LM, AC Gales, and RN Jones. (2001). GAR-936 (9-t-butylglycylamido-minocycline) susceptibility test development for streptococci, *Haemophilus influenzae* and *Neisseria gonorrhoeae*: preliminary guidelines and interpretive criteria. *Int J Antimicrob Agents*, 18(1): 29-35.
451. Stein, GE and WA Craig. (2006). Tigecycline: A critical analysis. *Clin Infect Dis*, 43(4): 518-524.
452. Unemo, M *et al.* (2012). *In vitro* activity of ertapenem versus ceftriaxone against *Neisseria gonorrhoeae* isolates with highly diverse ceftriaxone MIC values and effects of ceftriaxone resistance determinants: ertapenem for treatment of gonorrhea? *Antimicrob Agents Chemother*, 56(7): 3603-3609.
453. Quaye, N, MJ Cole, and CA Ison. (2014). Evaluation of the activity of ertapenem against gonococcal isolates exhibiting a range of susceptibilities to cefixime. *J Antimicrob Chemother*, 69(6): 1568-1571.
454. Nilius, AM *et al.* (2003). *In vitro* antibacterial potency and spectrum of ABT-492, a new fluoroquinolone. *Antimicrob Agents Chemother*, 47(10): 3260-3269.
455. Harnett, SJ *et al.* (2004). Comparative study of the *in vitro* activity of a new fluoroquinolone, ABT-492. *J Antimicrob Chemother*, 53(5): 783-792.

456. Soge, OO *et al.* (2016). *In vitro* activity of delafloxacin against clinical *Neisseria gonorrhoeae* isolates and selection of gonococcal delafloxacin resistance. *Antimicrob Agents Chemother*, 60(5): 3106-3111.
457. Hook, EW, 3rd *et al.* (2019). Efficacy and safety of single-dose oral delafloxacin compared with intramuscular ceftriaxone for uncomplicated gonorrhea treatment: an open-label, noninferiority, Phase 3, multicenter, randomized study. *Sex Transm Dis*, 46(5): 279-286.
458. Bala, M *et al.* (2016). Gentamicin *in vitro* activity and tentative gentamicin interpretation criteria for the CLSI and calibrated dichotomous sensitivity disc diffusion methods for *Neisseria gonorrhoeae*. *J Antimicrob Chemother*, 71(7): 1856-1859.
459. Furuya, R *et al.* (2013). *In vitro* activities of antimicrobial combinations against clinical isolates of *Neisseria gonorrhoeae*. *J Infect Chemother*, 19(6): 1218-1220.
460. Pettus, K, S Sharpe, and JR Papp. (2015). *In vitro* assessment of dual drug combinations to inhibit growth of *Neisseria gonorrhoeae*. *Antimicrob Agents Chemother*, 59(4): 2443-2445.
461. Rob, F *et al.* (2020). Gentamicin 240 mg plus azithromycin 2 g vs. ceftriaxone 500 mg plus azithromycin 2 g for treatment of rectal and pharyngeal gonorrhoea: A randomized controlled trial. *Clin Microbiol Infect*, 26(2): 207-212.
462. Southern, P.M., Jr. *et al.* (1969). Acute gonococcal urethritis: Failure of response to phosphonomycin therapy. *Antimicrob Agents Chemother (Bethesda)*, 9: 343-345.
463. Loza, E *et al.* (2003). Comparative *in vitro* activity of ertapenem against aerobic and anaerobic bacteria. *Rev Esp Quimioter*, 16(2): 209-215. [Original article in Spanish]
464. Livermore, DM *et al.* (2004). Activity of ertapenem against *Neisseria gonorrhoeae*. *J Antimicrob Chemother*, 54(1): 280-281.
465. Petraitis, V *et al.* (2018). Pharmacokinetics and comprehensive analysis of the tissue distribution of eravacycline in rabbits. *Antimicrob Agents Chemother*, 62(9): e00275-18.
466. Hamasuna, R *et al.* (2018). *In vitro* activity of sitafloxacin and additional newer generation fluoroquinolones against ciprofloxacin-resistant *Neisseria gonorrhoeae* isolates. *Microb Drug Resist*, 24(1): 30-34.
467. Jönsson, A *et al.* (2018). *In vitro* activity and time-kill curve analysis of sitafloxacin against a global panel of antimicrobial-resistant and multidrug-resistant *Neisseria gonorrhoeae* isolates. *APMIS*, 126(1): 29-37.

468. Biedenbach, DJ *et al.* (2012). Activity of JNJ-Q2, a novel fluoroquinolone, tested against *Neisseria gonorrhoeae*, including ciprofloxacin-resistant strains. *Diagn Microbiol Infect Dis*, 74(2): 204-206.
469. Jacobsson, S *et al.* (2015). *In vitro* activities of the novel bicycclides modithromycin (EDP-420, EP-013420, S-013420) and EDP-322 against MDR clinical *Neisseria gonorrhoeae* isolates and international reference strains. *J Antimicrob Chemother*, 70(1): 173-177.
470. Fujimoto, K *et al.* (2013). Novel carbapenem antibiotics for parenteral and oral applications: *in vitro* and *in vivo* activities of 2-aryl carbapenems and their pharmacokinetics in laboratory animals. *Antimicrob Agents Chemother*, 57(2): 697-707.
471. Savage, VJ *et al.* (2016). Efficacy of a novel tricyclic topoisomerase inhibitor in a murine model of *Neisseria gonorrhoeae* infection. *Antimicrob Agents Chemother*, 60(9): 5592-5594.
472. Chen, MY *et al.* (2019). Solithromycin versus ceftriaxone plus azithromycin for the treatment of uncomplicated genital gonorrhoea (SOLITAIRE-U): A randomised phase 3 non-inferiority trial. *Lancet Infect Dis*, 19(8): 833-842.
473. Taylor, SN *et al.* (2018). Single-dose zoliflodacin (ETX0914) for treatment of urogenital gonorrhoea. *N Engl J Med*, 379(19): 1835-1845.
474. Escaich, S *et al.* (2011). The MUT056399 inhibitor of FabI is a new antistaphylococcal compound. *Antimicrob Agents Chemother*, 55(10): 4692-4697.
475. Swanson, S *et al.* LpxC inhibitors as novel therapeutics for treatment of antibiotic-resistant *Neisseria gonorrhoeae*. *18th International Pathogenic Neisseria Conference*, September 2012. Abstract O-33.
476. Paukner, S, A Gruss, and JS Jensen. (2018). *In vitro* activity of lefamulin against sexually transmitted bacterial pathogens. *Antimicrob Agents Chemother*, 62(5) e02380-17.
477. Jacobsson, S *et al.* (2017). *In vitro* activity of the novel pleuromutilin lefamulin (BC-3781) and effect of efflux pump inactivation on multidrug-resistant and extensively drug-resistant *Neisseria gonorrhoeae*. *Antimicrob Agents Chemother*, 61(11): e01497-17.
478. Golparian, D *et al.* (2012). *In vitro* activity of the new fluoroketolide solithromycin (CEM-101) against a large collection of clinical *Neisseria gonorrhoeae* isolates and international reference strains, including those with high-level antimicrobial resistance: Potential treatment option for gonorrhoea? *Antimicrob Agents Chemother*, 56(5): 2739-2742.
479. Bouchillon, SK *et al.* *In vitro* activities of AN3365: A novel boron containing protein synthesis inhibitor, and other antimicrobial agents against anaerobes and *Neisseria gonorrhoeae*. *50th Interscience Conference on Antimicrobial Agents and Chemotherapy*, September 2010. Abstract F1-1640.

480. Jeverica, S *et al.* (2014). High *in vitro* activity of a novel dual bacterial topoisomerase inhibitor of the ATPase activities of GyrB and ParE (VT12-008911) against *Neisseria gonorrhoeae* isolates with various high-level antimicrobial resistance and multidrug resistance. *J Antimicrob Chemother*, 69(7): 1866-1872.
481. Jacobsson, S *et al.* (2014). High *in vitro* activity of the novel spiropyrimidinetrione AZD0914, a DNA gyrase inhibitor, against multidrug-resistant *Neisseria gonorrhoeae* isolates suggests a new effective option for oral treatment of gonorrhea. *Antimicrob Agents Chemother*, 58(9): 5585-5588.
482. Huband, MD *et al.* (2015). *In vitro* antibacterial activity of AZD0914, a new spiropyrimidinetrione DNA gyrase/topoisomerase inhibitor with potent activity against Gram-positive, fastidious Gram-Negative, and atypical bacteria. *Antimicrob Agents Chemother*, 59(1): 467-74.
483. Unemo, M *et al.* (2015). High *in vitro* susceptibility to the novel spiropyrimidinetrione ETX0914 (AZD0914) among 873 contemporary clinical *Neisseria gonorrhoeae* isolates from 21 European countries from 2012 to 2014. *Antimicrob Agents Chemother*, 59(9): 5220-5225.
484. Savage, VJ *et al.* (2016). Biological profiling of novel tricyclic inhibitors of bacterial DNA gyrase and topoisomerase IV. *J Antimicrob Chemother*, 71(7): 1905-1913.
485. Farrell, DJ *et al.* (2017). *In Vitro* Activity of Gepotidacin (GSK2140944) against *Neisseria gonorrhoeae*. *Antimicrob Agents Chemother*, 61(3): e02047-16.
486. Smoum, R *et al.* (2012). Boron containing compounds as protease inhibitors. *Chem Rev*, 112(7): 4156-4220.
487. Kiener, PA and SG Waley (1978). Reversible inhibitors of penicillinases. *Biochem J*, 169(1): 197-204.
488. Beesley, T *et al.* (1983). The inhibition of class C β -lactamases by boronic acids. *Biochem J*, 209(1): 229-33.
489. Crompton, IE *et al.* (1988). β -lactamase inhibitors. The inhibition of serine β -lactamases by specific boronic acids. *Biochem J*, 251(2): 453-459.
490. Pechenov, A *et al.* (2003). Potential transition state analogue inhibitors for the penicillin-binding proteins. *Biochemistry*, 42(2): 579-588.
491. Dzhekieva, L *et al.* (2010). Crystal structure of a complex between the *Actinomadura* R39 DD-peptidase and a peptidoglycan-mimetic boronate inhibitor: Interpretation of a transition state analogue in terms of catalytic mechanism. *Biochemistry*, 49(30): 6411-6419.
492. Contreras-Martel, C *et al.* (2011). Structure-guided design of cell wall biosynthesis inhibitors that overcome β -lactam resistance in *Staphylococcus aureus* (MRSA). *ACS Chem Biol*, 6(9): 943-951.

493. Woon, EC *et al.* (2011). Structure guided development of potent reversibly binding penicillin binding protein inhibitors. *ACS Med Chem Lett*, 2(3): 219-223.
494. Zervosen, A *et al.* (2012). Synthesis and evaluation of boronic acids as inhibitors of penicillin binding proteins of classes A, B and C. *Bioorg Med Chem*, 20(12): p. 3915-3924.
495. Zervosen, A *et al.* (2011). Unexpected tricovalent binding mode of boronic acids within the active site of a penicillin-binding protein. *J Am Chem Soc*, 133(28): 10839-10848.
496. Inglis, SR *et al.* (2009). Synthesis and evaluation of 3-(dihydroxyboryl)benzoic acids as DD-carboxypeptidase R39 inhibitors. *J Med Chem*, 52(19): 6097-6106.
497. Brem, J *et al.* (2016). Structural basis of metallo- β -lactamase, serine- β -lactamase and penicillin-binding protein inhibition by cyclic boronates. *Nat Commun*, 7: 12406.
498. Dzhekieva, L *et al.* (2013). Inhibition of DD-peptidases by a specific trifluoroketone: crystal structure of a complex with the *Actinomadura* R39 DD-peptidase. *Biochemistry*, 52(12): 2128-2138.
499. Gordon, EM, J Plušćec, and MA Ondetti. (1981). Carbacyclic isosteres of penicillanic and carbapenemic acids. Synthesis of bicyclo[3.2.0]heptan-6-ones as potential enzyme inhibitors. *Tetrahedron Letters*, 22(20): 1871-1874.
500. Cocuzza, A.J and GA Boswell. (1985). Cyclobutanone analogs of β -lactam antibiotics: Sythesis of *N*-acetyldeazathienamycin. *Tetrahedron Letters*, 26(44): 5363-5366.
501. Lowe, G and S Swain. (1985). Synthesis of a cyclobutanone analogue of a β -lactam antibiotic. *Journal of the Chemical Society, Perkin Transactions 1*, 0: 391-398.
502. Lange, G *et al.* (1985). Synthesis of 4-carboxy-2-thiabicyclo [3.2.0]heptan-6-ones via 3-carboxy-2,3-dihydrothiophenes: Potential β -lactamase inhibitors. *Tetrahedron Letters*, 26(15): 1791-1794.
503. Kelly, JA *et al.* (1985). 2.8 Å structure of penicillin-sensitive D-alanyl carboxypeptidase-transpeptidase from *Streptomyces* R61 and complexes with β -lactams. *J Biol Chem*, 260(10): 6449-6458.
504. Johnson, JW *et al.* (2008). Cyclobutanone mimics of penicillins: Effects of substitution on conformation and hemiketal stability. *J Org Chem*, 73(18): 6970-6982.
505. Johnson, JW *et al.* (2010). Cyclobutanone analogues of β -lactams revisited: Insights into conformational requirements for inhibition of serine- and metallo- β -lactamases. *J Am Chem Soc*, 132(8): 2558-2560.

506. Pratt, RF. (1989). Inhibition of a class C β -lactamase by a specific phosphonate monoester. *Science*, 246(4932): 917-919.
507. Adediran, SA *et al.* (2010). Substituted aryl malonamates as new serine β -lactamase substrates: Structure-activity studies. *Bioorg Med Chem*, 18(1): 282-291.
508. Rahil, J and RF Pratt. (1991). Phosphonate monoester inhibitors of class A β -lactamases. *Biochem J*, 275 (Pt 3): 793-795.
509. Rahil, J and RF Pratt. (1992) Mechanism of inhibition of the class C β -lactamase of *Enterobacter cloacae* P99 by phosphonate monoesters. *Biochemistry*, 31(25): 5869-5878.
510. Rahil, J and RF Pratt. (1993). Kinetics and mechanism of β -lactamase inhibition by phosphonamidates: the quest for a proton. *Biochemistry*, 32(40): 10763-10772.
511. Rahil, J and RF Pratt. (1993). Structure-activity relationships in the inhibition of serine β -lactamases by phosphonic acid derivatives. *Biochem J*, 296(Pt 2): 389-393.
512. Payne, DJ *et al.* (1996) Phosphoramidate analogues of dipeptides with carboxypeptidase A and β -lactamase-inhibitory activity: Elucidation of the mechanism of β -lactamase inhibition by electrospray mass spectrometry. *Biochem J*, 314 (Pt 2): 457-461.
513. Chen, CC *et al.* (1993). Structure of a phosphonate-inhibited β -lactamase. An analog of the tetrahedral transition state/intermediate of β -lactam hydrolysis. *J Mol Biol*, 234(1): 165-178.
514. Lobkovsky, E *et al.* (1994). Crystallographic structure of a phosphonate derivative of the *Enterobacter cloacae* P99 cephalosporinase: mechanistic interpretation of a β -lactamase transition-state analog. *Biochemistry*, 33(22): 6762-6772.
515. Maveyraud, L, RF Pratt, and JP Samama. (1998). Crystal structure of an acylation transition-state analog of the TEM-1 β -lactamase. Mechanistic implications for class A β -lactamases. *Biochemistry*, 37(8): 2622-8.
516. Li, N *et al.* (1997). Structure-activity studies of the inhibition of serine β -lactamases by phosphonate monoesters. *Bioorg Med Chem*, 5(9): 1783-1788.
517. Pratt, RF and NJ Hammar. (1998). Salicyloyl cyclic phosphate, a "penicillin-like" inhibitor of β -lactamases. *Journal of the American Chemical Society*, 120(13): 3004-3006.
518. Kaur, K, MJ Lan, and RF Pratt. (2001). Mechanism of inhibition of the class C β -lactamase of *Enterobacter cloacae* P99 by cyclic acyl phosph(on)ates: Rescue by return. *J Am Chem Soc*, 123(43): 10436-10443.
519. Kaur, K *et al.* (2003). Inhibition of β -lactamases by monocyclic acyl phosph(on)ates. *Biochemistry*, 42(6): 1529-1536.

520. Silvaggi, NR *et al.* (2004). Toward better antibiotics: Crystallographic studies of a novel class of DD-peptidase/ β -lactamase inhibitors. *Biochemistry*, 43(22): 7046-7053.
521. Li, N and RF Pratt. (1998). Inhibition of serine β -lactamases by acyl phosph(on)ates: A new source of inert acyl [and phosphyl] enzymes. *Journal of the American Chemical Society*, 120(18): 4264-4268.
522. Majumdar, S *et al.* (2005). Inhibition of class D β -lactamases by diaroyl phosphates. *Biochemistry*, 44(49): 16121-16129.
523. Adediran, SA *et al.* (2005). Inhibition of class D β -lactamases by acyl phosphates and phosphonates. *Antimicrob Agents Chemother*, 49(10): 4410-4412.
524. Majumdar, S and RF Pratt. (2009). Inhibition of class A and C β -lactamases by diaroyl phosphates. *Biochemistry*, 48(35): 8285-8292.
525. Moural, TW *et al.* (2019). Crystal structure of phosphoserine BlaC from *Mycobacterium tuberculosis* inactivated by bis(benzoyl) phosphate. *Int J Mol Sci*, 2019. 20(13): 3247.
526. Majumdar, S and RF Pratt. (2009). Intramolecular cooperativity in the reaction of diacyl phosphates with serine β -lactamases. *Biochemistry*, 48(35): 8293-8298.
527. Kaur, K and RF Pratt. (2001). Mechanism of reaction of acyl phosph(on)ates with the β -lactamase of *Enterobacter cloacae* P99. *Biochemistry*, 40(15): 4610-4621.
528. Morrison, MJ, N Li, and RF Pratt. (2001). Inverse acyl phosph(on)ates: Substrates or inhibitors of beta-lactam-recognizing enzymes? *Bioorg Chem*, 29(5): 271-81.
529. Lassaux, P *et al.* (2010) Mercaptophosphonate compounds as broad-spectrum inhibitors of the metallo- β -lactamases. *J Med Chem*, 2010. **53**(13): p. 4862-76.
530. Skagseth, S *et al.* (2017). Metallo- β -lactamase inhibitors by bioisosteric replacement: Preparation, activity and binding. *Eur J Med Chem*, 135: 159-173.
531. Tan, Q *et al.* (2011). Thiophenyl oxime-derived phosphonates as nano-molar class C β -lactamase inhibitors reducing MIC of imipenem against *Pseudomonas aeruginosa* and *Acinetobacter baumannii*. *Bioorg Med Chem Lett*, 2011. **21**(14): p. 4363-5.
532. Perumal, SK and RF Pratt. (2006). Synthesis and evaluation of ketophosph(on)ates as β -lactamase inhibitors. *J Org Chem*, 71(13): 4778-4785.
533. Perumal, SK, SA Adediran, and RF Pratt. (2008). β -ketophosphonates as β -lactamase inhibitors: Intramolecular cooperativity between the hydrophobic subsites of a class D β -lactamase. *Bioorg Med Chem*, 16(14): 6987-6994.
534. Beck, J *et al.* (2008). 2-Aminopropane-1,2,3-tricarboxylic acid: Synthesis and cocrystallization with the class A β -lactamase BS3 of *Bacillus licheniformis*. *Bioorg Med Chem Lett*, 18(13): 3764-3768.

535. Beck, J *et al.* (2009). Discovery of novel lipophilic inhibitors of OXA-10 enzyme (class D β -lactamase) by screening amino analogs and homologs of citrate and isocitrate. *Bioorg Med Chem Lett*, 19(13): 3593-3597.
536. Fonzé, E *et al.* (2002). Crystal structures of the *Bacillus licheniformis* BS3 class A β -lactamase and of the acyl-enzyme adduct formed with cefoxitin. *Biochemistry*, 41(6): 1877-1885.
537. Na, JH, YJ An, and SS Cha. (2017). GMP and IMP are competitive inhibitors of CMY-10, an extended-spectrum class C β -lactamase. *Antimicrob Agents Chemother*, 61(5): e00098-17.
538. Pemberton, OA *et al.* (2019). Heteroaryl phosphonates as noncovalent inhibitors of both serine- and metallo-carbapenemases. *J Med Chem*, 62(18): 8480-8496.
539. Hinchliffe, P *et al.* (2018). Structural and kinetic studies of the potent inhibition of metallo- β -lactamases by 6-phosphonomethylpyridine-2-carboxylates. *Biochemistry*, 57(12): 880-1892.
540. Du Vineaud, V and F Carpenter. (1949). The γ -lactam of benzylhomopenicilloic acid and related compounds. *The Chemistry of Penicillin*, 1004-1017.
541. Wasserman, HH, FM Precopio, and TC Liu. (1952). Studies on the mucohalic acids. II. The synthesis of fused α -lactam-thiazolidines related to penicillin. *Journal of the American Chemical Society*, 74(16): 4093-4095.
542. Wasserman, H *et al.* (1956). The synthesis of a new homologue of (+/-)-penicillin. *Chem Ind*, 38: 1022.
543. Baldwin, JE. (1983). γ -Lactam analogues of penicillanic and carbapenicillanic acids. *Journal of the Chemical Society, Chemical Communications*, (5): 250-252.
544. Baldwin, JE *et al.* (1984). γ -Lactam analogues of penicillanic and carbapenicillanic acids. *Tetrahedron*, 40(21): 4513-4525.
545. Crossley, MJ *et al.* (1987). γ -lactam analogues of monocyclic β -lactam antibiotics. *Tetrahedron Letters*, 28(25): 2883-2886.
546. Baldwin, JE, RT Freeman, and C Schofield. (1989). Synthesis of a novel bicyclic γ -lactam analogue of the 1-oxapenams. *Tetrahedron Letters*, 30(30): 4019-4020.
547. Baldwin, JE *et al.* (1985). γ -Lactam analogues of carbapenicillanic acids. *Journal of the Chemical Society, Chemical Communications*, (4): 194-196.
548. Baldwin, JE *et al.* (1986). γ -Lactam analogues of carbapenicillanic acids. *Tetrahedron*, 42(17): 4879-4888.
549. Heck, JV. (1982). 3-Amino-6-substituted thio-1-azabicyclo[3.2.0]hept-6-en-2-one-7-carboxylic acids. US Patent US4428960A

550. Baldwin, JE *et al.* (1986). A γ -lactam analogue of penems possessing antibacterial activity. *Tetrahedron Letters*, 27(30): 3461-3464.
551. Boyd, DB, *et al.* (1986). γ -lactam analogues of the penems. *Tetrahedron Letters*, 27(30): 3453-3456.
552. Baldwin, JE and E Lee. (1986). Synthesis of bicyclic γ -lactams via oxazolidinones. *Tetrahedron*, 42(23): 6551-6554.
553. Baldwin, JE *et al.* (1989). A γ -lactam analogue of the penems possessing antibacterial activity. *Tetrahedron*, 45(14): 4537-4550.
554. Allen, NE *et al.* (1989). Molecular modeling of γ -lactam analogues of β -lactam antibacterial agents: synthesis and biological evaluation of selected penem and carbapenem analogues. *Tetrahedron*, 45(7): 1905-1928.
555. Hashiguchi, S, H Natsugari, and M Ochiai. (1988). Synthesis of γ -Lactam Analogues of Carbapenems with Substituted-thio Groups at the C-3 Position. *Journal of the Chemical Society, Perkin Transactions 1*, 8: 2345-2352.
556. Taylor, EC, HM Davies, and JS Hinkle. (1986). Synthesis and reactions of some 1, 2-disubstituted 1, 2-diazetid-3-ones: an intramolecular aldol approach to bicyclic systems. *The Journal of Organic Chemistry*, 51(9): 1530-1536.
557. Taylor, EC and HM Davies. (1986). Synthesis of fused 1, 2-diazetid-3-ones via an intramolecular Horner-Emmons reaction. *The Journal of Organic Chemistry*, 51(9): 1537-1540.
558. Jungheim, LN, SK Sigmund, and JW Fisher. (1987). Bicyclic pyrazolidinones, a new class of antibacterial agent based on the β -lactam model. *Tetrahedron Letters*, 28(3): 285-288.
559. Jungheim, LN *et al.* (1987). Bicyclic pyrazolidinones, steric and electronic effects on antibacterial activity. *Tetrahedron Letters*, 28(3): 289-292.
560. Jungheim, LN and SK Sigmund. (1987). 1,3-Dipolar cycloaddition reactions of pyrazolidinium ylides with acetylenes. Synthesis of a new class of antibacterial agents. *The Journal of Organic Chemistry*, 52(18): 4007-4013.
561. Jungheim, LN and R Holmes (1986). 4-Substituted diazolidinones. Eur. Pat. Appl. EP0202795A1
562. Jungheim, LN *et al.* (1986). 7-Substituted bicyclic pyrazolidinones, their preparation, and their use as antibacterials. Eur. Pat. Appl. EP0202046B1
563. Jungheim, LN *et al.* (1988). 1,3-Dipolar cycloaddition reactions of pyrazolidinium ylides with vinyl sulfones. A regioselective synthesis of bicyclic pyrazolidinone antibacterial agents. *Tetrahedron*, 44(11): 3119-3126.

564. Ternansky, RJ and SE Draheim. (1990). [3.3.0]Pyrazolidinones: An efficient synthesis of a new class of synthetic antibacterial agents. *Tetrahedron Letters*, 31(20): 2805-2808.
565. Boyd, DB. (1993). Application of the hypersurface iterative projection method to bicyclic pyrazolidinone antibacterial agents. *Journal of Medicinal Chemistry*, 36(10): 1443-1449.
566. Ternansky, RJ *et al.* (1993). Structure-activity relationship within a series of pyrazolidinone antibacterial agents. 2. Effect of side-chain modification on *in vitro* activity and pharmacokinetic parameters. *Journal of Medicinal Chemistry*, 36(22): 3224-3229.
567. Allen, N *et al.* (1990). Antibacterial properties of the bicyclic pyrazolidinones. *The Journal of Antibiotics*, 43(1): 92-99.
568. Indelicato, JM and CE Pasini (1988). The acylating potential of γ -lactam antibacterials: Base hydrolysis of bicyclic pyrazolidinones. *Journal of Medicinal Chemistry*, 31(6): 1227-1230.
569. Jungheim, LN *et al.* (1991). Synthesis, hydrolysis rates, supercomputer modeling, and antibacterial activity of bicyclic tetrahydropyridazinones. *Journal of Medicinal Chemistry*, 34(5): 1732-1739.
570. Jungheim, LN. (1989). Bicyclic pyrazolidinone antibacterial agents. Synthesis of side chain analogues of carbapenems PS-5 and thienamycin. *Tetrahedron Letters*, 30(15): 1889-1892.
571. Ternansky, RJ and SE. Draheim (1988). [4.3.0] pyrazolidinones as potential antibacterial agents. *Tetrahedron Letters*, 29(50): 6569-6572.
572. Panfil I *et al.* (2002). Synthesis of pyrazolidinone analogs of β -lactam antibiotics. *Tetrahedron*, 58(6): 1199-1212.
573. Jungheim, LN and SK Sigmund. (1990). Bicyclic pyrazolidinones, compositions and use. US Patent US4902707A
574. Couloigner, E, D Cartier, and R Labie. (1999). Synthesis of pyrazolidinone antibacterial agents. *Bioorganic & Medicinal Chemistry Letters*, 9(15): 2205-2206.
575. Davies, GM *et al.* (1996). Synthesis of reactive γ -lactams related to penicillins and cephalosporins. *Tetrahedron Letters*, 37(31): 5601-5604.
576. Aszodi, J *et al.* (2004). Design and synthesis of bridged γ -lactams as analogues of β -lactam antibiotics. *Bioorg Med Chem Lett*, 14(10): 2489-2492.
577. Imming, P, B Klar, and D Dix. (2000). Hydrolytic stability versus ring size in lactams: Implications for the development of lactam antibiotics and other serine protease inhibitors. *J Med Chem*, 43(22): 4328-4331.

578. Todd, D and S Teich. (1953). The Synthesis of Analogs of Penicillin. *Journal of the American Chemical Society*, 75(8): 1895-1900.
579. Nozaki, Y *et al.* (1989). Lactivicin, a naturally occurring non- β -lactam antibiotic having β -lactam-like action: Biological activities and mode of action. *J Antibiot (Tokyo)*, 42(1): 84-93.
580. Natsugari, H *et al.* (1987). Synthesis of lactivicin and its derivatives. *Journal of the Chemical Society, Chemical Communications*, (2): 62-63.
581. Tamura, N *et al.* (1990). Synthesis and antibacterial activity of lactivicin derivatives. *Chem Pharm Bull (Tokyo)*, 38(1): 116-22.
582. Macheboeuf, P *et al.* (2007). Structural and mechanistic basis of penicillin-binding protein inhibition by lactivicins. *Nat Chem Biol*, 3(9): 565-569.
583. Starr, J *et al.* (2014). Siderophore receptor-mediated uptake of lactivicin analogues in Gram-negative bacteria. *J Med Chem*, 57(9): 3845-55.
584. Calvopiña, K *et al.* (2016). Sideromimic modification of lactivicin dramatically increases potency against extensively drug-resistant *Stenotrophomonas maltophilia* clinical isolates. *Antimicrob Agents Chemother*, 60(7): 4170-4175.
585. Macheboeuf, P *et al.* (2005). Active site restructuring regulates ligand recognition in class A penicillin-binding proteins. *Proc Natl Acad Sci U S A*, 102(3): 577-582.
586. Panfil, I, Z Urbańczyk-Lipkowska, and M Chmielewski. (1998). Isoxazolidin-5-one analogs of β -lactam antibiotics. *Carbohydrate Research*, 306(4): 505-515.
587. Cao, X *et al.* (2003). 3-alkoxy-5-isoxazolidinones mimic β -lactams. *Biochem Biophys Res Commun*, 311(2): 267-271.
588. Bonnefoy, A *et al.* (2004). *In vitro* activity of AVE1330A, an innovative broad-spectrum non- β -lactam β -lactamase inhibitor. *J Antimicrob Chemother*, 54(2): 410-417.
589. Stachyra, T *et al.* (2010). Mechanistic studies of the inactivation of TEM-1 and P99 by NXL104, a novel non- β -lactam β -lactamase inhibitor. *Antimicrobial Agents and Chemotherapy*, 54(12): 5132-5138.
590. Xu, H, S Hazra, and JS Blanchard. (2012). NXL104 irreversibly inhibits the β -lactamase from *Mycobacterium tuberculosis*. *Biochemistry*, 51(22): 4551-4557.
591. Ehmman, DE *et al.* (2012). Avibactam is a covalent, reversible, non- β -lactam β -lactamase inhibitor. *Proc Natl Acad Sci U S A*, 109(29): 11663-11668.
592. Lahiri, SD *et al.* (2013). Structural insight into potent broad-spectrum inhibition with reversible recyclization mechanism: Avibactam in complex with CTX-M-15 and *Pseudomonas aeruginosa* AmpC β -lactamases. *Antimicrob Agents Chemother*, 57(6): 2496-2505.

593. Lahiri, SD *et al.* (2015). Molecular basis of selective inhibition and slow reversibility of avibactam against class D carbapenemases: A structure-guided study of OXA-24 and OXA-48. *ACS Chem Biol*, 10(2): 591-600.
594. King, DT *et al.* (2015). Molecular mechanism of avibactam-mediated β -lactamase inhibition. *ACS Infect Dis*, 1(4): 175-184.
595. Lagacé-Wiens, PR *et al.* (2011). Activity of NXL104 in combination with β -lactams against genetically characterized *Escherichia coli* and *Klebsiella pneumoniae* isolates producing class A extended-spectrum β -lactamases and class C beta-lactamases. *Antimicrob Agents Chemother*, 55(5): 2434-2437.
596. Berkhout, J *et al.* (2015). *In vitro* activity of ceftazidime-avibactam combination in *in vitro* checkerboard assays. *Antimicrob Agents Chemother*, 59(2): 1138-1144.
597. Asli, A *et al.* (2016). Distinctive binding of avibactam to penicillin-binding proteins of Gram-negative and Gram-positive bacteria. *Antimicrob Agents Chemother*, 60(2): 752-756.
598. Sutaria, DS *et al.* (2018). First penicillin-binding protein occupancy patterns of β -lactams and β -lactamase inhibitors in *Klebsiella pneumoniae*. *Antimicrob Agents Chemother*, 62(6): e00282-18
599. Blizzard, TA *et al.* (2014). Discovery of MK-7655, a β -lactamase inhibitor for combination with Primaxin. *Bioorg Med Chem Lett*, 24(3): 780-785.
600. Hirsch, EB *et al.* (2012). *In vitro* activity of MK-7655, a novel β -lactamase inhibitor, in combination with imipenem against carbapenem-resistant Gram-negative bacteria. *Antimicrob Agents Chemother*, 56(7): 3753-3757.
601. Kaushik, A., *et al.* (2019). *In Vitro* Activity of the New β -Lactamase Inhibitors Relebactam and Vaborbactam in Combination with β -Lactams against *Mycobacterium abscessus* Complex Clinical Isolates. *Antimicrob Agents Chemother*, 63(3): e02623-18.
602. Karlowsky, JA *et al.* (2020). *In-vitro* activity of imipenem/relebactam and key β -lactam agents against Gram-negative bacilli isolated from lower respiratory tract infection samples of intensive care unit patients - SMART Surveillance United States 2015-2017. *Int J Antimicrob Agents*, 55(1): 105841.
603. Lapuebla, A *et al.* (2015). Activity of Imipenem with Relebactam against Gram-Negative Pathogens from New York City. *Antimicrob Agents Chemother*, 59(8): 5029-5031.
604. Goldstein, EJC *et al.* (2018). Comparative *In Vitro* Activities of Relebactam, Imipenem, the Combination of the Two, and Six Comparator Antimicrobial Agents against 432 Strains of Anaerobic Organisms, Including Imipenem-Resistant Strains. *Antimicrob Agents Chemother*, 62(2): e01992-17.

605. Morinaka, A *et al.* (2015). OP0595, a new diazabicyclooctane: mode of action as a serine β -lactamase inhibitor, antibiotic and β -lactam 'enhancer'. *J Antimicrob Chemother*, 70(10): 2779-2786.
606. King, AM *et al.* (2016). Structural and Kinetic Characterization of Diazabicyclooctanes as Dual Inhibitors of Both Serine- β -Lactamases and Penicillin-Binding Proteins. *ACS Chem Biol*, 11(4): 864-868.
607. King, DT *et al.* (2017). Structural Insights into Inhibition of *Escherichia coli* Penicillin-binding Protein 1B. *J Biol Chem*, 292(3): 979-993.
608. Moya, B *et al.* (2017). WCK 5107 (Zidebactam) and WCK 5153 Are Novel Inhibitors of PBP2 Showing Potent " β -Lactam Enhancer" Activity against *Pseudomonas aeruginosa*, Including Multidrug-Resistant Metallo- β -Lactamase-Producing High-Risk Clones. *Antimicrob Agents Chemother*, 61(6): e02529-16.
609. Moya, B *et al.* (2017). Potent β -Lactam Enhancer Activity of Zidebactam and WCK 5153 against *Acinetobacter baumannii*, Including Carbapenemase-Producing Clinical Isolates. *Antimicrob Agents Chemother*, 61(11): e01238-17.
610. Moya, B *et al.* (2019). *In Vitro* and *In Vivo* Activities of β -Lactams in Combination with the Novel β -Lactam Enhancers Zidebactam and WCK 5153 against Multidrug-Resistant Metallo- β -Lactamase-Producing *Klebsiella pneumoniae*. *Antimicrob Agents Chemother*, 63(5): e00128-19
611. Livermore, DM *et al.* (2017). *In vitro* activity of cefepime/zidebactam (WCK 5222) against Gram-negative bacteria. *J Antimicrob Chemother*, 72(5): 1373-1385.
612. Durand-Réville, TF *et al.* (2017). ETX2514 is a broad-spectrum β -lactamase inhibitor for the treatment of drug-resistant Gram-negative bacteria including *Acinetobacter baumannii*. *Nat Microbiol*, 2: 17104.
613. Barnes, MD *et al.* (2019). Targeting Multidrug-Resistant *Acinetobacter spp.*: Sulbactam and the Diazabicyclooctenone β -Lactamase Inhibitor ETX2514 as a Novel Therapeutic Agent. *mBio*, 10(2): e00159-19
614. Levy, N *et al.* (2019). Structural Basis for *E. coli* Penicillin Binding Protein (PBP) 2 Inhibition, a Platform for Drug Design. *J Med Chem*, 62(9): 4742-4754.
615. Ranjitkar, S *et al.* (2019). Identification of Mutations in the *mrdA* Gene Encoding PBP2 That Reduce Carbapenem and Diazabicyclooctane Susceptibility of *Escherichia coli* Clinical Isolates with Mutations in *ftsI* (PBP3) and Which Carry *bla*_{NDM-1}. *mSphere*, 4(4): e00074-19
616. Lampilas, M *et al.* (2011). Nitrogenous heterocyclic compounds, preparation thereof and use thereof as antibacterial medicaments. US Patent US20080595120.
617. Aszodi, J *et al.* (2007). Heterocyclic compounds, method for preparing same and use thereof as medicines, in particular as antibacterial agents. US Patent US7288549B2

618. Levasseur, P *et al.* (2010). Novel combinations of nitrogenated heterocyclic antibacterial compounds with other antibacterial compounds and the use of same as drugs. US Patent US2010092443.
619. Miller, AA *et al.* (2020). *In Vitro* Characterization of ETX1317, a Broad-Spectrum β -Lactamase Inhibitor That Restores and Enhances β -Lactam Activity against Multi-Drug-Resistant *Enterobacteriales*, Including Carbapenem-Resistant Strains. *ACS Infect Dis*, Online ahead of print.
620. Zervosen, A *et al.* (2004). Interactions between penicillin-binding proteins (PBPs) and two novel classes of PBP inhibitors, arylalkylidene rhodanines and arylalkylidene iminothiazolidin-4-ones. *Antimicrob Agents Chemother*, 48(3): 961-969.
621. Fedarovich, A *et al.* (2012). High-throughput screening for novel inhibitors of *Neisseria gonorrhoeae* penicillin-binding protein 2. *PLoS One*, 7(9): e44918.
622. Powers, JP *et al.* (2006). SAR and mode of action of novel non-nucleoside inhibitors of hepatitis C NS5b RNA polymerase. *J Med Chem*, 49(3): 1034-1046.
623. Tomasić, T and LP Masic (2009). Rhodanine as a privileged scaffold in drug discovery. *Curr Med Chem*, 16(13): 1596-1629.
624. Toney, JH. *et al.* (1998). Soluble penicillin-binding protein 2a: β -lactam binding and inhibition by non- β -lactams using a 96-well format. *Anal Biochem*, 255(1): 113-119.
625. Yribarren, AS *et al.* (2003). Selection of peptides inhibiting a β -lactamase-like activity. *Eur J Biochem*, 270(13): 2789-2795.
626. Phichith, D *et al.* (2010). Novel peptide inhibiting both TEM-1 β -lactamase and penicillin-binding proteins. *FEBS J*, 277(23): 4965-4972.
627. Turk, S *et al.* (2011). New noncovalent inhibitors of penicillin-binding proteins from penicillin-resistant bacteria. *PLoS One*, 6(5): e19418.
628. Sosič, I *et al.* (2012). Exploration of the chemical space of novel naphthalene-sulfonamide and anthranilic acid-based inhibitors of penicillin-binding proteins. *Acta Chim Slov*, 59(2): 280-388.
629. Qiao, Y *et al.* (2018). Aspermerodione, a novel fungal metabolite with an unusual 2,6-dioxabicyclo[2.2.1]heptane skeleton, as an inhibitor of penicillin-binding protein 2a. *Sci Rep*, 8(1): 5454.
630. Miguet, L *et al.* (2009). Discovery of new inhibitors of resistant *Streptococcus pneumoniae* penicillin binding protein (PBP) 2x by structure-based virtual screening. *J Med Chem*, 52(19): 5926-36.
631. Shilabin, AG *et al.* (2012). 4-quinolones as noncovalent inhibitors of high molecular mass penicillin-binding proteins. *ACS Med Chem Lett*, 3(7): p. 592-5.

632. O'Daniel, PI *et al.* (2014). Discovery of a new class of non- β -lactam inhibitors of penicillin-binding proteins with Gram-positive antibacterial activity. *J Am Chem Soc*, 136(9): 3664-3672.
633. Ding, D *et al.* (2015). Exploration of the structure-activity relationship of 1,2,4-oxadiazole antibiotics. *Bioorg Med Chem Lett*, 25(21): 4854-4857.
634. Janardhanan, J, M Chang, and S Mobashery. (2016). The oxadiazole antibacterials. *Curr Opin Microbiol*, 33: 13-17.
635. Spink, E *et al.* (2015) Structure-activity relationship for the oxadiazole class of antibiotics. *J Med Chem*, 58(3): 1380-1389.
636. Ceballos, S *et al.* (2018). Activities of Oxadiazole Antibacterials against *Staphylococcus aureus* and Other Gram-Positive Bacteria. *Antimicrob Agents Chemother*, 62(8).
637. Leemans, E *et al.* (2016). Three-dimensional QSAR analysis and design of new 1,2,4-oxadiazole antibacterials. *Bioorg Med Chem Lett*, 26(3): 1011-1015.
638. Zhao, G *et al.* (1999). BOCILLIN FL, a sensitive and commercially available reagent for detection of penicillin-binding proteins. *Antimicrob Agents Chemother*, 43(5): 1124-1128.
639. Schneider, CA, WS Rasband, and KW Eliceiri (2012). NIH Image to ImageJ: 25 years of image analysis. *Nature Methods*, 9(7): 671-675.
640. Otwinowski, Z and W Minor. (1997). Processing of X-ray diffraction data collected in oscillation mode. *Methods in Enzymology*. Academic Press. 307-326.
641. Jones, TA *et al.* (1991). Improved methods for building protein structures in electron-density maps and the location of errors in these models. *Acta Cryst.*, A47: 110-119.
642. Emsley, P *et al.* (2010). Features and development of Coot. *Acta Crystallogr D Biol Crystallogr*, 66(pt 4): 486-501.
643. Murshudov, GN, AA Vagin, and EJ Dodson. (1997). Refinement of macromolecular structures by the maximum-likelihood method. *Acta Cryst.* D53: 240-255.
644. Laskowski, R *et al.* (1993). PROCHECK: A program to check the stereochemical quality of protein structures. *Journal of Applied Crystallography*, 26: 283-291.
645. Case, D *et al.* (2012). AMBER 12. *University of California, San Francisco*. Vol. 79. 926-935.
646. Sturgeon, JB and BB Laird. (2000). Symplectic algorithm for constant-pressure molecular dynamics using a Nosé–Poincaré thermostat. *The Journal of Chemical Physics*, 112(8): 3474-3482.

647. Waterhouse, A *et al.* (2018). SWISS-MODEL: Homology modelling of protein structures and complexes. *Nucleic Acids Res*, 46(W1): W296-W303.
648. Mysinger, MM *et al.* (2012). Directory of useful decoys, enhanced (DUD-E): Better ligands and decoys for better benchmarking. *J Med Chem*, 55(14): 6582-6594.
649. Moustakas, DT *et al.* (2006). Development and validation of a modular, extensible docking program: DOCK 5. *J Comput Aided Mol Des*, 20(10-11): 601-619.
650. Sterling, T and JJ Irwin. (2015). ZINC 15 - *Ligand Discovery for Everyone*. *Journal of Chemical Information and Modeling*, 55(11): 2324-2337.
651. Matsubara, N *et al.* (1980). Affinity of cefoperazone for penicillin-binding proteins. *Antimicrob Agents Chemother*, 18(1): 195-199.
652. Ohya, S *et al.* (1982). Penem derivatives: β -lactamase stability and affinity for penicillin-binding proteins in *Escherichia coli*. *Antimicrobial Agents and Chemotherapy*, 21(3): 492-497.
653. Faraci, WS and RF Pratt. (1986). Interactions of cephalosporins with the *Streptomyces* R61 DD-transpeptidase/carboxypeptidase. Influence of the 3'-substituent. *Biochemical Journal*, 238(1): 309-312.
654. Laws, A and M Page. (1996). The chemistry and structure-activity relationships of C3-quaternary ammonium cephem antibiotics. *J Chemother*, 8 Suppl 2: 7-22.
655. Zhanel, GG *et al.* (2014). Ceftolozane/tazobactam: a novel cephalosporin/ β -lactamase inhibitor combination with activity against multidrug-resistant Gram-negative bacilli. *Drugs*, 74(1): 31-51.
656. Goo, KS and TS Sim. (2011). Designing new β -lactams: Implications from their targets, resistance factors and synthesizing enzymes. *Curr Comput Aided Drug Des*, 7(1): 53-80.
657. Lovering, AL *et al.* (2012). Structural insights into the anti-methicillin-resistant *Staphylococcus aureus* (MRSA) activity of ceftobiprole. *J Biol Chem*, 287(38): 32096-32102.
658. Fukuoka, T *et al.* (1997). *In vitro* and *in vivo* antibacterial activities of CS-834, a novel oral carbapenem. *Antimicrob Agents Chemother*, 41(12): 2652-2663.
659. Inui, T *et al.* (1999). Potent bacteriolytic activity of ritipenem associated with a characteristic profile of affinities for penicillin-binding proteins of *Haemophilus influenzae*. *Antimicrobial agents and chemotherapy*, 43(10): 2534-2537.
660. Watanabe, Y *et al.* (1999). *In vitro* antibacterial activity of FK041, a new orally active cephalosporin. *J Antibiot (Tokyo)*, 52(7): 649-59.
661. Sakagawa, E *et al.* (1998). *In vitro* and *in vivo* antibacterial activities of CS-834, a new oral carbapenem. *J Antimicrob Chemother*, 42(4): 427-437.

662. Sharifzadeh, S *et al.* (2020). Harnessing β -lactam antibiotics for illumination of the activity of penicillin-binding proteins in *Bacillus subtilis*. *ACS Chem Biol*, 15(5): 1242-1251.
663. Chambers, HF and M Sachdeva. (1990). Binding of β -lactam antibiotics to penicillin-binding proteins in methicillin-resistant *Staphylococcus aureus*. *J Infect Dis*, 161(6): 1170-1176.
664. Matsushashi, M and S Tamaki. (1978). Enzymatic studies on the mechanism of action of cefoxitin. Correlation between the affinities of cefoxitin to penicillin-binding proteins and its rates of inhibition of the respective penicillin-sensitive reactions in *E. coli*. *J Antibiot (Tokyo)*, 31(12): 1292-1295.
665. Ohya, S *et al.* (1978). New cephamycin antibiotic, CS-1170: Binding affinity to penicillin-binding proteins and inhibition of peptidoglycan cross-linking reactions in *Escherichia coli*. *Antimicrob Agents Chemother*, 14(5): 780-785.
666. Dougherty, TJ, AE Koller, and A Tomasz. (1981). Competition of β -lactam antibiotics for the penicillin-binding proteins of *Neisseria gonorrhoeae*. *Antimicrob Agents Chemother*, 20(1): 109-114.
667. Curtis, NA *et al.* (1979). Affinities of penicillins and cephalosporins for the penicillin-binding proteins of *Escherichia coli* K-12 and their antibacterial activity. *Antimicrobial Agents and Chemotherapy*, 16(5): 533-539.
668. Lei, Y and JT Li. (1989). Affinity of penicillin-binding proteins of *Escherichia coli* K-12 for furbenicillin and other β -lactam antibiotics. *Zhongguo Yao Li Xue Bao*, 10(2): 177-180. [Original article in Chinese]
669. Yotsuji, A *et al.* (1988). Mechanism of action of cephalosporins and resistance caused by decreased affinity for penicillin-binding proteins in *Bacteroides fragilis*. *Antimicrobial Agents and Chemotherapy*, 32(12): 1848-1853.
670. Kim, JH, YT Kim, and DH Hwang. (1984). Cefoperazone for urethritis due to penicillinase-producing *Neisseria gonorrhoeae*. *Clin Ther*, 6(2): 193-197.
671. Hook, EW, 3rd *et al.* (1986). Comparative study of cefoperazone and spectinomycin for treatment of uncomplicated gonorrhea in men. *Antimicrob Agents Chemother*, 30(4): 619-21.
672. Kim, JH, YS Ro, and YT Kim. (1984). Cefoperazone (Cefobid) for treating men with gonorrhoea caused by penicillinase producing *Neisseria gonorrhoeae*. *Br J Vener Dis*, 60(4): 238-240.
673. Gerber, AU and WA Craig. (1981). Worldwide clinical experience with cefoperazone. *Drugs*, 22 Suppl 1: 108-118.
674. Lipsky, JJ. (1984). Mechanism of the inhibition of the γ -carboxylation of glutamic acid by *N*-methylthiotetrazole-containing antibiotics. *Proc Natl Acad Sci USA*, 81(9): 2893-2897.

675. Strom, BL *et al.* (1999). Risk of bleeding and hypoprothrombinaemia associated with NMTT side chain antibiotics: using cefoperazone as a test case. *Pharmacoepidemiol Drug Saf*, 8(2): 81-94.
676. Chen, LJ *et al.* (2016). Use of Hypoprothrombinemia-Inducing Cephalosporins and the Risk of Hemorrhagic Events: A Nationwide Nested Case-Control Study. *PLoS One*, 11(7): p. e0158407.
677. Craig, WA and AU Gerber. (1981). Pharmacokinetics of cefoperazone: a review. *Drugs*, 22 Suppl 1: 35-45.
678. Mal, PB *et al.* (2016). Antimicrobial susceptibility testing of *Neisseria gonorrhoeae* isolates in Pakistan by Etest compared to Calibrated Dichotomous Sensitivity and Clinical Laboratory Standards Institute disc diffusion techniques. *BMC Microbiol*, 16(1): 236.
679. Boelsterli, UA. (2002). Xenobiotic acyl glucuronides and acyl CoA thioesters as protein-reactive metabolites with the potential to cause idiosyncratic drug reactions. *Curr Drug Metab*, 3(4): 439-450.
680. Darnell, M and L Weidolf. (2013). Metabolism of xenobiotic carboxylic acids: Focus on coenzyme A conjugation, reactivity, and interference with lipid metabolism. *Chem Res Toxicol*, 26(8): 1139-1155.
681. Huskey, SE, RR Miller, and SH Chiu. (1993). *N*-glucuronidation reactions. I. Tetrazole *N*-glucuronidation of selected angiotensin II receptor antagonists in hepatic microsomes from rats, dogs, monkeys, and humans. *Drug Metab Dispos*, 21(5): 792-799.
682. Jeong, ES *et al.* (2015). Glucuronidation of fimasartan, a new angiotensin receptor antagonist, is mainly mediated by UGT1A3. *Xenobiotica*, 45(1): 10-18.
683. Hansch, C, A Leo, and D Hoekman. (1995). *Exploring QSAR: fundamentals and applications in chemistry and biology*. Vol. 557. American Chemical Society, Washington, DC.
684. Ballatore, C, DM Huryn, and AB Smith, 3rd, (2013). Carboxylic acid (bio)isosteres in drug design. *ChemMedChem*, 8(3): 385-395.
685. Molander, GA and B Biolatto. (2003). Palladium-catalyzed Suzuki–Miyaura cross-coupling reactions of potassium aryl- and heteroaryltrifluoroborates. *The Journal of Organic Chemistry*, 68(11): 4302-4314.
686. Nishiguchi, A, K Maeda, and S Miki. (2006). Sulfonyl chloride formation from thiol derivatives by *N*-chlorosuccinimide mediated oxidation. *Synthesis*, 24: 4131-4134.

APPENDIX MATERIALS

Appendix A. Pharmacophore-constrained cephalosporin docking parameters

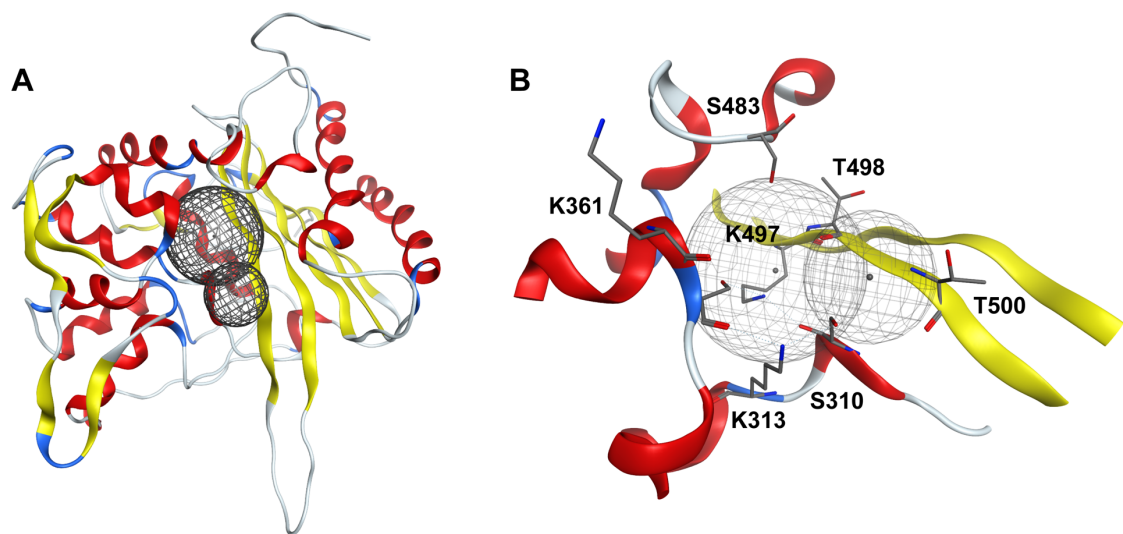


Figure A.1: Placement constraints for docking of cephalosporins to *tPBP2^{H041}*. Criteria for placement in the docking protocol include: 1) a carboxylate centroid near proposed electrostatic anchor K497 and 2) a lactam ring adjacent S310 and projecting toward the oxyanion hole defined by S310 and T500. **A.** Full receptor view. **B.** Detailed view.

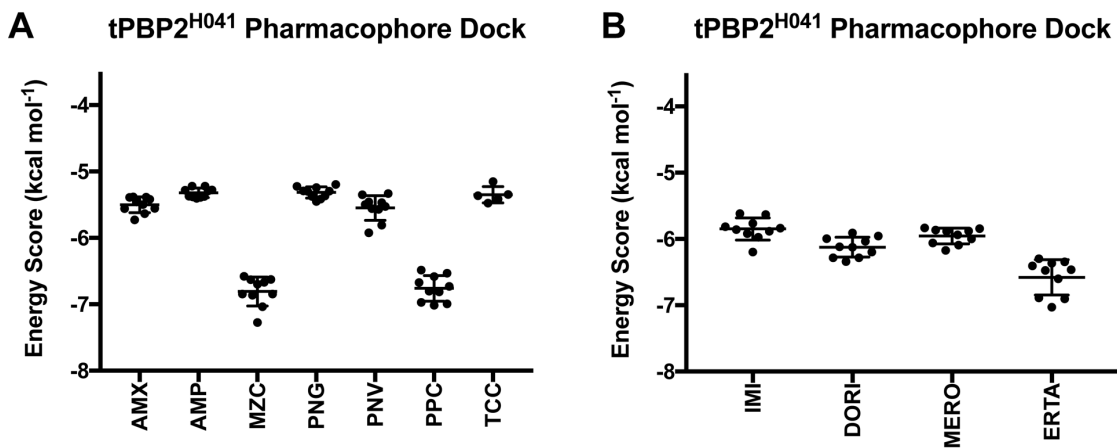


Figure A.2: Energy scores for pharmacophore-constrained docking of penams (**A**) and carbapenems (**B**). AMX: amoxicillin, AMP: ampicillin, MZC: mezlocillin, PNG: penicillin G, PNV: penicillin V, PPC: piperacillin, TCC: ticarcillin, IMI: imipenem, DORI: doripenem, MERO: meropenem, ERTA: ertapenem.

Appendix B. Untransformed activity data (IC_{50}) for cephalosporins against $tPBP2^{H041}$

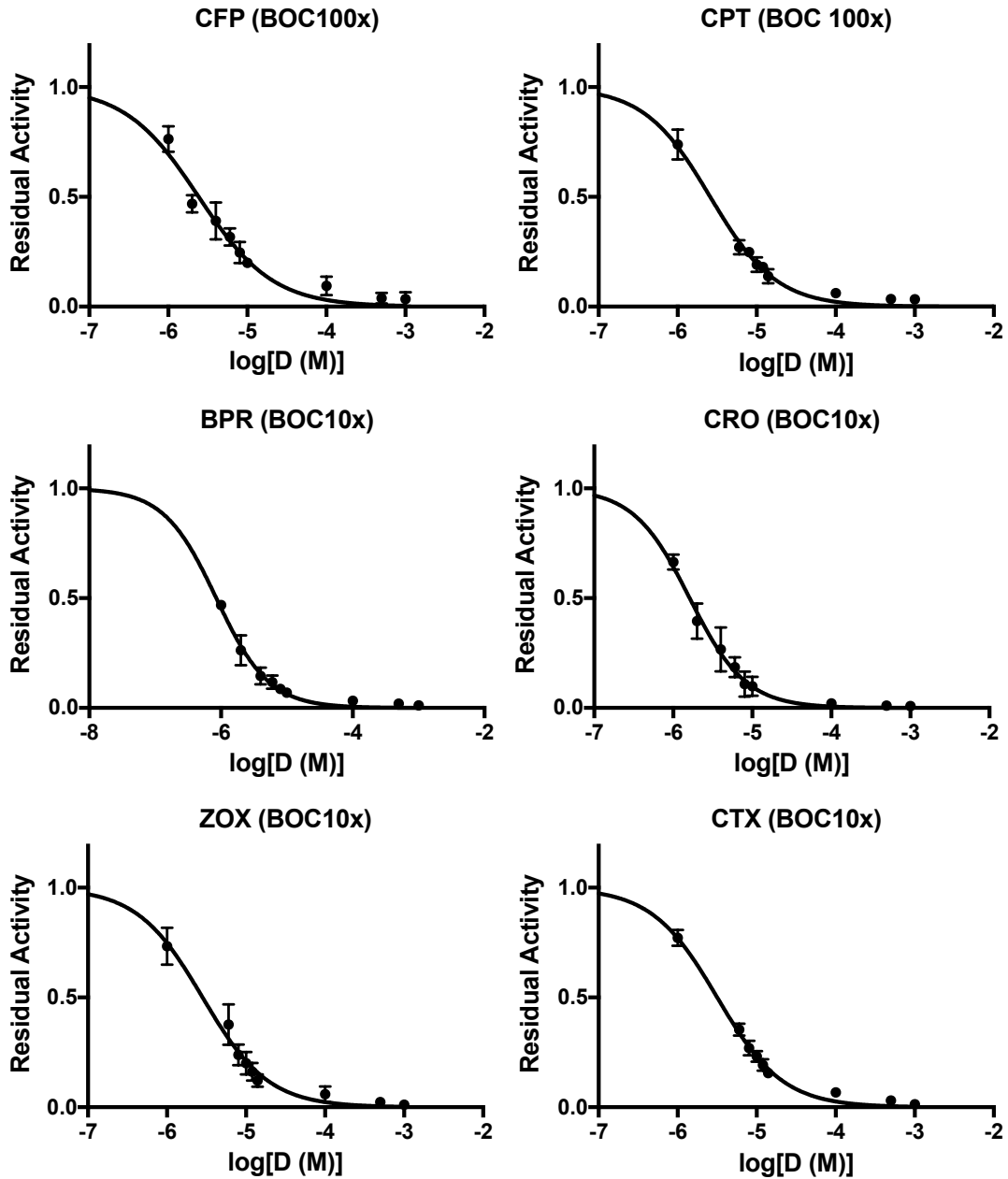


Figure B.1: $tPBP2^{H041}$ IC_{50} curves for cephalosporins reported in Chapter 3. CFP: cefoperazone ($2.5 \pm 0.3 \mu\text{M}$, $r^2 = 0.966$), CPT: ceftaroline ($2.6 \pm 0.4 \mu\text{M}$, $r^2 = 0.987$), BPR: ceftobiprole ($0.9 \pm 0.1 \mu\text{M}$, $r^2 = 0.990$), CRO: ceftriaxone ($1.8 \pm 0.3 \mu\text{M}$, $r^2 = 0.977$), ZOX: ceftizoxime ($2.9 \pm 0.8 \mu\text{M}$, $r^2 = 0.974$), CTX: ceftotaxime ($3.0 \pm 0.5 \mu\text{M}$, $r^2 = 0.993$). BOC10x: co-incubation with $10 \mu\text{M}$ Bocillin-FL, BOC-100x: co-incubation with $100 \mu\text{M}$ Bocillin-FL. $n \geq 3$ determinations for each. Error bars are standard deviation.

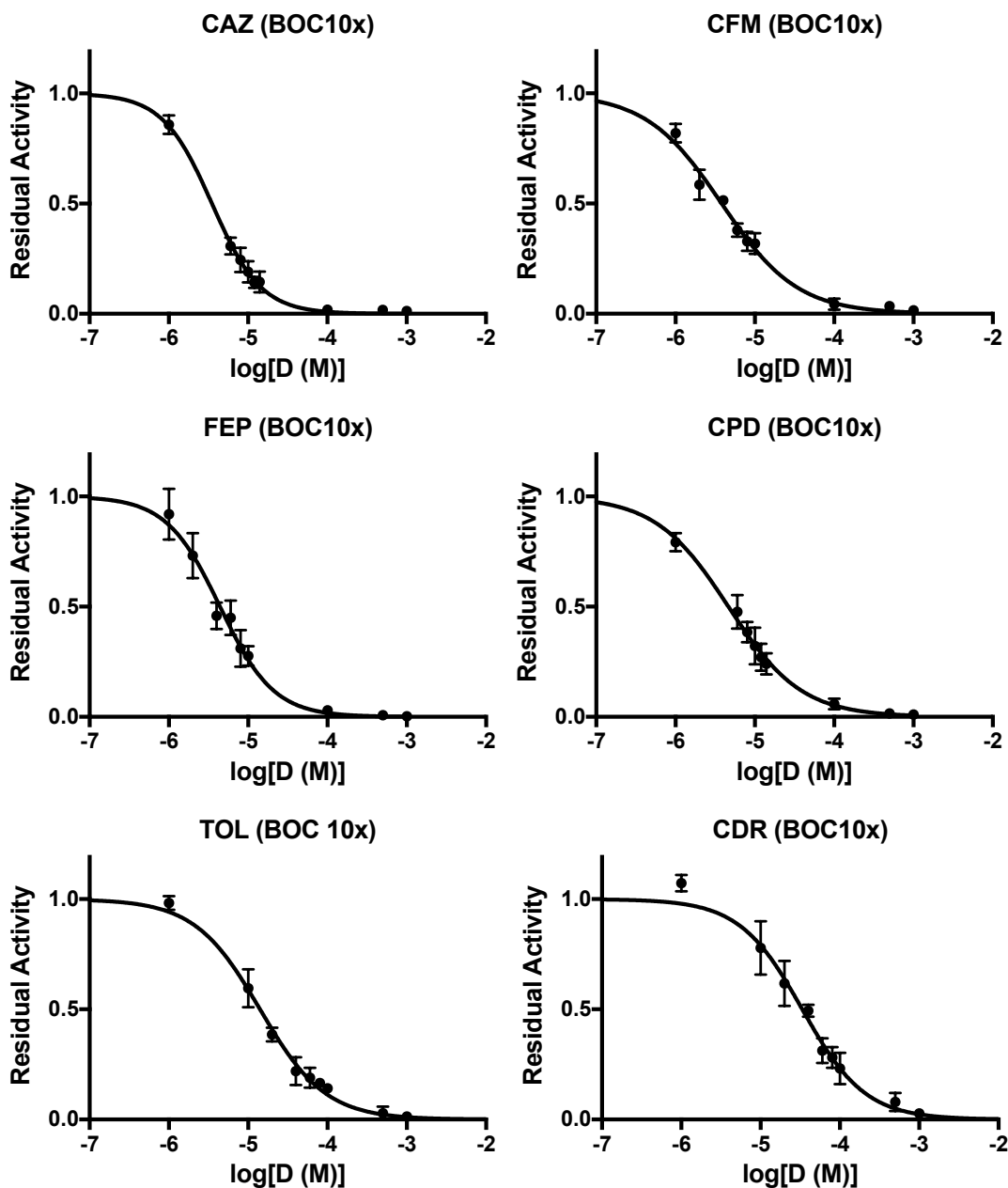


Figure B.2: *tPBP2^{H041}* IC_{50} curves for cephalosporins reported in Chapter 3, continued. CAZ: ceftazidime ($3.6 \pm 0.6 \mu\text{M}$, $r^2 = 0.991$), CFM: cefixime ($3.8 \pm 0.4 \mu\text{M}$, $r^2 = 0.983$), FEP: cefepime ($4.4 \pm 0.4 \mu\text{M}$, $r^2 = 0.966$), CPD: cefpodoxime ($4.7 \pm 1.0 \mu\text{M}$, $r^2 = 0.979$), TOL: ceftolozane ($14.7 \pm 1.8 \mu\text{M}$, $r^2 = 0.985$), CDR: cefdinir ($33.8 \pm 2.9 \mu\text{M}$, $r^2 = 0.968$). BOC10x: co-incubation with $10 \mu\text{M}$ Bocillin-FL. $n \geq 3$ determinations for each. Error bars are standard deviation.

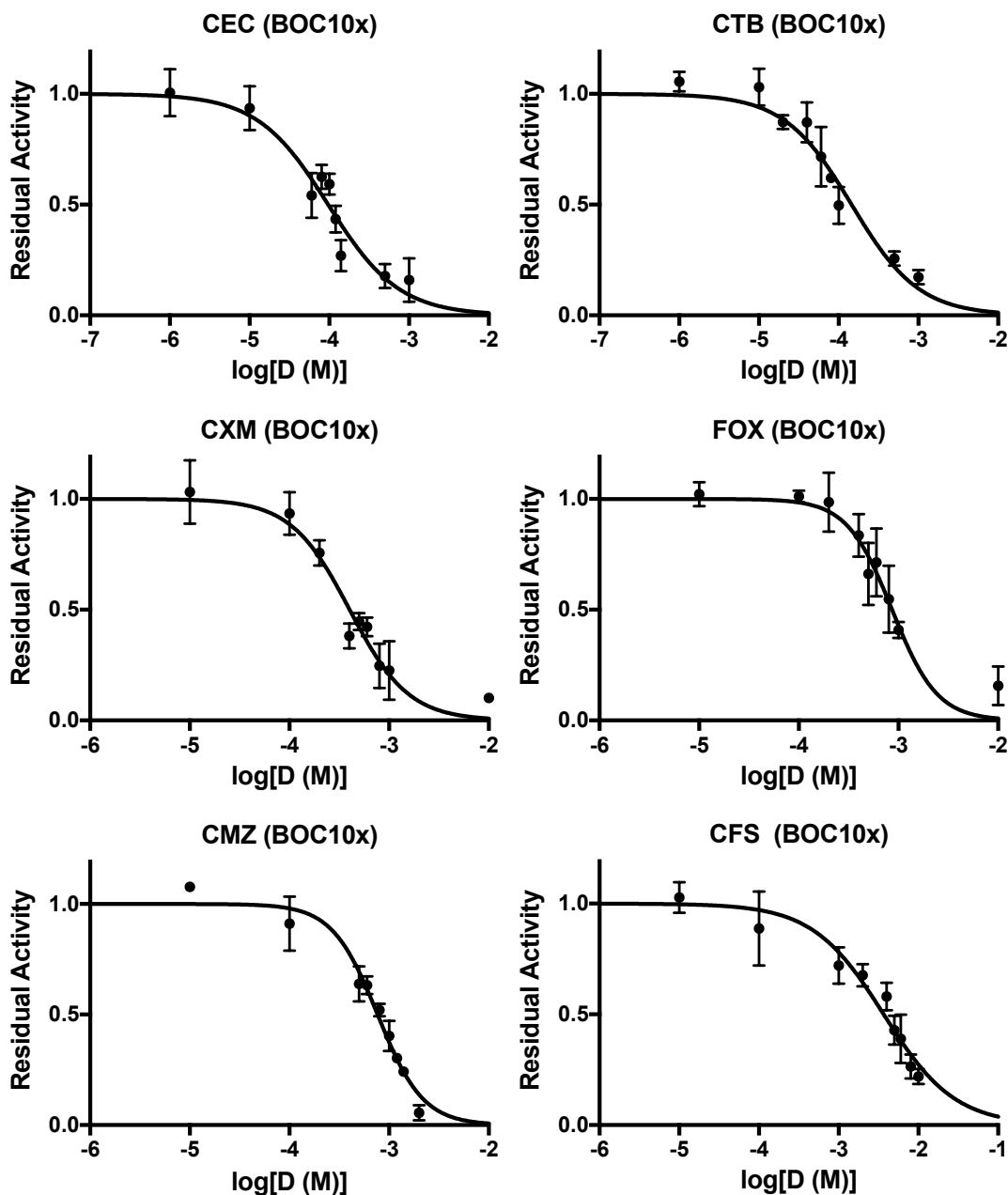


Figure B.3: *tPBP2^{H041}* IC_{50} curves for cephalosporins reported in Chapter 3, continued. CEC: cefaclor ($97.0 \pm 16.5 \mu\text{M}$, $r^2 = 0.908$), CTB: ceftibuten ($144 \pm 1 \mu\text{M}$, $r^2 = 0.932$), CXM: cefuroxime ($400 \pm 10 \mu\text{M}$, $r^2 = 0.931$), FOX: cefoxitin ($840 \pm 130 \mu\text{M}$, $r^2 = 0.878$), CMZ: cefmetazole ($770 \pm 10 \mu\text{M}$, $r^2 = 0.959$), CFS: cefsulodin ($3.7 \pm 0.5 \text{ mM}$, $r^2 = 0.911$). BOC10x: co-incubation with $10 \mu\text{M}$ Bocillin-FL. $n \geq 3$ determinations for each. Error bars are standard deviation.

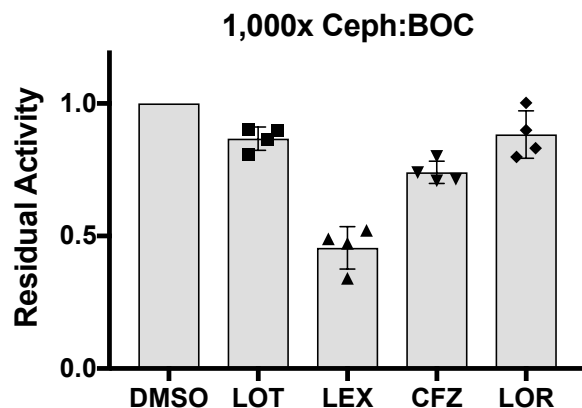


Figure B.4: *tPBP2^{H041}* inhibition data for cephalosporins classified in Chapter 3 as inactive. LOT: cefelothin ($13 \pm 4\%$ inhibition), LEX: cephalixin ($54 \pm 8\%$ inhibition), CFZ: cefazolin ($26 \pm 4\%$ inhibition), LOR: cephaloridine ($12 \pm 9\%$ inhibition). 1,000x Ceph:BOC: co-incubation of 10 mM cephalosporin with 10 μ M Bocillin-FL. Error bars are standard deviation.

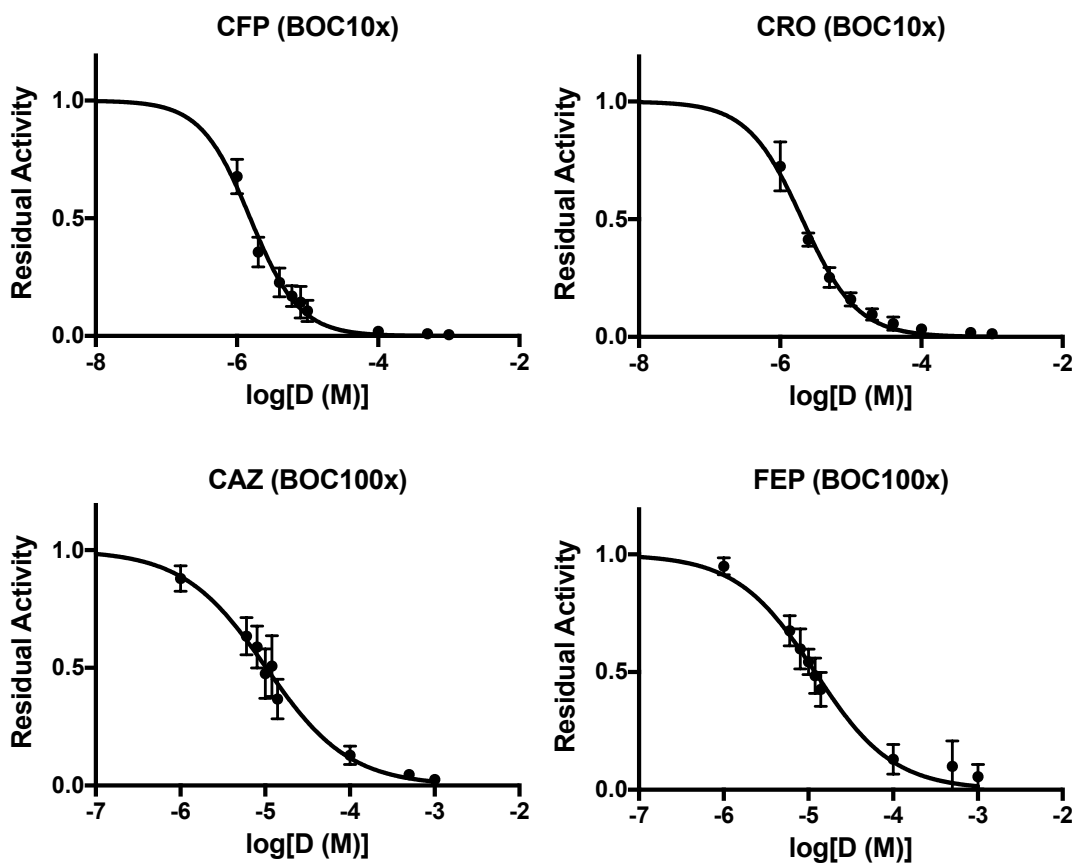


Figure B.5: *tPBP2^{H041}-K361E* IC_{50} curves for cephalosporins reported in Chapter 3. CFP: cefoperazone ($1.6 \pm 0.2 \mu$ M, $r^2 = 0.975$), CRO: ceftriaxone ($2.0 \pm 0.5 \mu$ M, $r^2 = 0.984$), CAZ: ceftazidime ($11.1 \pm 3.6 \mu$ M, $r^2 = 0.950$), FEP: cefepime ($13.4 \pm 5.1 \mu$ M, $r^2 = 0.955$). BOC10x: co-incubation with 10 μ M Bocillin-FL, BOC-100x: co-incubation with 100 μ M Bocillin-FL. $n \geq 3$ determinations for each. Error bars are standard deviation.

Appendix C. Quantitative structure-activity relationship descriptors

Table C.1: Definitions of physicochemical descriptors using the quantitative structure-activity relationships developed in Chapter 3.

Descriptor	Definition
<i>a_acc</i>	Number of hydrogen bond acceptor atoms (excluding acidic atoms, but including atoms that function as both hydrogen bond donors and acceptors)
<i>a_donacc</i>	Number of hydrogen bond donor atoms plus number of hydrogen bond acceptors atoms
<i>a_ICM</i>	Mean atom information content / entropy of element distribution. Sum of $p_i \log p_i$ for all i , where $p_i = n_i/n$, n_i is the number of occurrences of atomic number i in the molecule, and n is the total number of atoms.
<i>BCUT_PEOE_0</i>	Smallest eigenvalue of a modified adjacency matrix in which each ij entry takes the value $1/\sqrt{b_{ij}}$, where b_{ij} is the formal bond order between bonded atoms i and j . The diagonal takes the value of PEOE partial charges.
<i>BCUT_PEOE_3</i>	Largest eigenvalue of a modified adjacency matrix in which each ij entry takes the value $1/\sqrt{b_{ij}}$, where b_{ij} is the formal bond order between bonded atoms i and j . The diagonal takes the value of PEOE partial charges.
<i>BCUT_SLOGP_0</i>	Smallest eigenvalue of a modified adjacency matrix in which each ij entry takes the value $1/\sqrt{b_{ij}}$, where b_{ij} is the formal bond order between bonded atoms i and j . The diagonal takes the value of atomic contribution to $\log P(o/w)$.
<i>BCUT_SLOGP_1</i>	Second eigenvalue of a modified adjacency matrix in which each ij entry takes the value $1/\sqrt{b_{ij}}$, where b_{ij} is the formal bond order between bonded atoms i and j . The diagonal takes the value of atomic contribution to $\log P(o/w)$.
<i>BCUT_SLOGP_3</i>	Largest eigenvalue of a modified adjacency matrix in which each ij entry takes the value $1/\sqrt{b_{ij}}$, where b_{ij} is the formal bond order between bonded atoms i and j . The diagonal takes the value of atomic contribution to $\log P(o/w)$.
<i>BCUT_SMR_3</i>	Largest eigenvalue of a modified adjacency matrix in which each ij entry takes the value $1/\sqrt{b_{ij}}$, where b_{ij} is the formal bond order between bonded atoms i and j . The

	diagonal takes the value of atomic contribution to molar refractivity.
<i>chi0v</i>	Atomic valence connectivity index (order 0) from Hall, calculated as the sum of $1/\sqrt{v_i}$ over all heavy atoms i with $v_i > 0$. For heavy atom i , let $v_i = (p_i - h_i)/(Z_i - p_i - 1)$ where p_i is the number of s and p valence electrons.
<i>chi1v_C</i>	Carbon valence connectivity index (order 1), calculated as the sum of $1/\sqrt{v_i v_j}$ over all bonds between carbon atoms i and j where $i < j$. For heavy atom i , let $v_i = (p_i - h_i)/(Z_i - p_i - 1)$ where p_i is the number of s and p valence electrons.
<i>FCharge</i>	Total formal charge.
<i>GCUT_PEOE_1</i>	Second eigenvalue of a modified distance adjacency matrix in which each ij entry takes the value $1/\sqrt{d_{ij}}$, where d_{ij} is the graph distance between atoms i and j . The diagonal takes the value of PEOE partial charges.
<i>GCUT_PEOE_2</i>	Third eigenvalue of a modified distance adjacency matrix in which each ij entry takes the value $1/\sqrt{d_{ij}}$, where d_{ij} is the graph distance between atoms i and j . The diagonal takes the value of PEOE partial charges.
<i>h_logS</i>	log of aqueous solubility (mol/L) using a 7-parameter model based on Hueckel Theory with $r^2 = 0.83$, RMSE 0.85 on 1,708 molecules.
<i>Kier1</i>	First kappa shape index: $(n-1)^2/m^2$, where n is the number of atoms in a hydrogen-suppressed molecular graph and m is the number of bonds.
<i>KierA2</i>	Second alpha modified shape index: $s(s-1)^2/m^2$ where $s = n+a$, where a is a correction factor derived from the covalent radii of bonded atoms.
<i>KierFlex</i>	Kier molecular flexibility index: $(KierA1)(KierA2)/n$.
<i>PEOE_VSA_FPNEG</i>	Fractional negative polar van der Waals surface area: sum of approximate van der Waals surface area v_i (\AA^2) for each atom i with partial charge $q_i < -0.2$, divided by the total van der Waals surface area.
<i>PEOE_VSA-1</i>	Sum of approximate van der Waals surface area v_i (\AA^2) for each atom i whose contribution to PEOE q_i is in the range $[-0.1, 0.05]$.

<i>PEOE_VSA-3</i>	Sum of approximate van der Waals surface area v_i (\AA^2) for each atom i whose contribution to <i>PEOE</i> q_i is in the range [-0.2, -0.15].
<i>PEOE_VSA-4</i>	Sum of approximate van der Waals surface area v_i (\AA^2) for each atom i whose contribution to <i>PEOE</i> q_i is in the range [-0.25, -0.2].
<i>PEOE_VSA+0</i>	Sum of approximate van der Waals surface area v_i (\AA^2) for each atom i whose contribution to <i>PEOE</i> q_i is in the range [0, 0.05].
<i>PEOE_VSA+1</i>	Sum of approximate van der Waals surface area v_i (\AA^2) for each atom i whose contribution to <i>PEOE</i> q_i is in the range [0.05, 0.1].
<i>PEOE_VSA+3</i>	Sum of approximate van der Waals surface area v_i (\AA^2) for each atom i whose contribution to <i>PEOE</i> q_i is in the range [0.15, 0.2].
<i>PEOE_VSA+4</i>	Sum of approximate van der Waals surface area v_i (\AA^2) for each atom i whose contribution to <i>PEOE</i> q_i is in the range [0.2, 0.25].
<i>PEOE_VSA+6</i>	Sum of approximate van der Waals surface area v_i (\AA^2) for each atom i whose contribution to <i>PEOE</i> $q_i > 0.3$.
<i>Q_RPC+</i>	Relative positive partial charge: the largest positive q_i divided by the sum of positive q_i .
<i>SlogP_VSA0</i>	Sum of approximate van der Waals surface area v_i (\AA^2) for each atom i whose contribution to <i>logP(o/w)</i> $L_i \leq -0.4$.
<i>SlogP_VSA1</i>	Sum of approximate van der Waals surface area v_i (\AA^2) for each atom i whose contribution to <i>logP(o/w)</i> L_i is in the range (-0.4, 0.2].
<i>SlogP_VSA2</i>	Sum of approximate van der Waals surface area v_i (\AA^2) for each atom i whose contribution to <i>logP(o/w)</i> L_i is in the range (-0.2, 0].
<i>SlogP_VSA4</i>	Sum of approximate van der Waals surface area v_i (\AA^2) for each atom i whose contribution to <i>logP(o/w)</i> L_i is in the range (0.1, 0.15].
<i>SlogP_VSA7</i>	Sum of approximate van der Waals surface area v_i (\AA^2) for each atom i whose contribution to <i>logP(o/w)</i> L_i is in the range (0.25, 0.30].
<i>SMR_VSA3</i>	Sum of approximate van der Waals surface area v_i (\AA^2) for each atom i whose contribution to molar refractivity R_i is in the range (0.35, 0.39].

<i>SMR_VSA4</i>	Sum of approximate van der Waals surface area v_i (\AA^2) for each atom i whose contribution to molar refractivity R_i is in the range (0.4, 0.44].
<i>vdw_area</i>	area of van der Waals surface (\AA^2) calculated using connection table approximation.
<i>zagreb</i>	Zagreb index: the sum of squares of heavy atom degree d_i over all heavy atoms i .

Appendix D. Characterization of synthesized compounds by ESI-MS and ¹H NMR

5-fluoro-2-(4'-methyl-[1,1'-biphenyl]-4-carboxamido)benzoic acid (JEK-42). The reaction of 4'-methyl-[1,1'-biphenyl]-4-carboxylic acid afforded JEK-42 as a white powder. ¹H NMR (600 MHz, D₃COCD₃): δ = 12.19 (s, 1H), 9.00 (dd, *J* = 5.2, 9.3 Hz, 1H), 8.09 (d, *J* = 8.4 Hz, 2H), 7.84 (d, *J* = 8.5 Hz, 2H), 7.86 (m, 1H), 7.64 (d, *J* = 8.2 Hz, 2H), 7.50 (dq, *J* = 3.2, 9.3 Hz, 1H), 7.32 (d, *J* = 7.9 Hz, 2H), 3.08 (s, 3H). ESI-MS for C₂₁H₁₆FNO₃: [M-H]⁻ calculated 348.1, found 348.2

5-fluoro-2-(4'-methyl-[1,1'-biphenyl]-4-sulfonamido)benzoic acid (JMT-1). The reaction of 4'-methyl-[1,1'-biphenyl]-4-sulfonyl chloride according to General Procedure I afforded JMT-1 as a beige powder. ¹H NMR (600 MHz, D₃COCD₃): δ = 10.73 (s, 1H), 7.87 (d, *J* = 8.5 Hz, 2H), 7.80 (m, 1H), 7.79 (d, *J* = 8.6 Hz, 2H), 7.67 (dd, *J* = 3.1, 9.1 Hz, 1H), 7.57 (d, *J* = 8.1 Hz, 2H), 7.43 (dq, *J* = 3.0, 10.3 Hz, 1H), 7.29 (d, *J* = 8.0 Hz, 2H), 2.35 (s, 3H). ESI-MS for C₂₀H₁₆FNO₄S: [M-H]⁻ calculated 384.1, found 384.2

2-(4'-methyl-[1,1'-biphenyl]-4-sulfonamido)benzoic acid (JMT-2). The reaction of 4'-methyl-[1,1'-biphenyl]-4-sulfonyl chloride according to General Procedure I afforded JMT-2 as a white powder. ESI-MS for C₂₀H₁₇NO₄S: [M-H]⁻ calculated 366.1, found 366.2

4-fluoro-2-(4'-methyl-[1,1'-biphenyl]-4-sulfonamido)benzoic acid (JMT-3). The reaction of 4'-methyl-[1,1'-biphenyl]-4-sulfonyl chloride according to General Procedure I afforded JMT-2 as a beige powder. ESI-MS for C₂₀H₁₆FNO₄S: [M-H]⁻ calculated 384.1, found 384.2

4,5-difluoro-2-(4'-methyl-[1,1'-biphenyl]-4-sulfonamido)benzoic acid (JMT-4). The reaction of 4'-methyl-[1,1'-biphenyl]-4-sulfonyl chloride according to General Procedure I afforded JMT-4 as a beige powder. ESI-MS for C₂₀H₁₅F₂NO₄S: [M-H]⁻ calculated 402.1, found 402.2

4-chloro-2-(4'-methyl-[1,1'-biphenyl]-4-sulfonamido)benzoic acid (JMT-5). The reaction of 4'-methyl-[1,1'-biphenyl]-4-sulfonyl chloride according to General Procedure I afforded JMT-5 as a white powder. ¹H NMR (600 MHz, D₃COCD₃): δ = 11.27 (s, 1H), 8.02 (d, *J* = 8.5 Hz, 1H), 7.96 (d, *J* = 8.6 Hz, 2H), 7.84 (d, *J* = 8.5 Hz, 2H), 7.74 (d, *J* = 2.0 Hz, 1H), 7.58 (d, *J* = 8.2 Hz, 2H), 7.29 (d, *J* = 8.0 Hz, 2H), 7.26 (dd, *J* = 2.0, 8.5 Hz, 1H), 2.35 (s, 3H). ESI-MS for C₂₀H₁₆ClNO₄S: [M-H]⁻ calculated 400.0, found 400.2, 402.2

5-chloro-2-(4'-methyl-[1,1'-biphenyl]-4-sulfonamido)benzoic acid (JMT-6). The reaction of 4'-methyl-[1,1'-biphenyl]-4-sulfonyl chloride according to General Procedure I afforded JMT-6 as a white powder. ESI-MS for C₂₀H₁₆ClNO₄S: [M-H]⁻ calculated 400.0, found 400.2, 402.2

4-bromo-2-(4'-methyl-[1,1'-biphenyl]-4-sulfonamido)benzoic acid (JMT-7). The reaction of 4'-methyl-[1,1'-biphenyl]-4-sulfonyl chloride according to General Procedure I afforded JMT-7 as a white powder. ESI-MS for C₂₀H₁₆BrNO₄S: [M-H]⁻ calculated 444.0, found 444.1, 446.1

5-bromo-2-(4'-methyl-[1,1'-biphenyl]-4-sulfonamido)benzoic acid (JMT-8). The reaction of 4'-methyl-[1,1'-biphenyl]-4-sulfonyl chloride according to General Procedure I afforded JMT-8 as a white powder. ESI-MS for C₂₀H₁₆BrNO₄S: [M-H]⁻ calculated 444.0, found 444.2, 446.1

4-methyl-2-(4'-methyl-[1,1'-biphenyl]-4-sulfonamido)benzoic acid (JMT-9). The reaction of 4'-methyl-[1,1'-biphenyl]-4-sulfonyl chloride according to General Procedure I afforded JMT-9 as a white powder. ESI-MS for C₂₁H₁₉NO₄S: [M-H]⁻ calculated 380.1, found 380.2

5-methyl-2-(4'-methyl-[1,1'-biphenyl]-4-sulfonamido)benzoic acid (JMT-10). The reaction of 4'-methyl-[1,1'-biphenyl]-4-sulfonyl chloride according to General Procedure I afforded JMT-10 as a white powder. ESI-MS for C₂₁H₁₉NO₄S: [M-H]⁻ calculated 380.1, found 380.2

6-methyl-2-(4'-methyl-[1,1'-biphenyl]-4-sulfonamido)benzoic acid (JMT-11). The reaction of 4'-methyl-[1,1'-biphenyl]-4-sulfonyl chloride according to General Procedure I afforded JMT-11 as a white powder. ESI-MS for C₂₁H₁₉NO₄S: [M-H]⁻ calculated 380.1, found 380.3

4-(trifluoromethyl)-2-(4'-methyl-[1,1'-biphenyl]-4-sulfonamido)benzoic acid (JMT-12). The reaction of 4'-methyl-[1,1'-biphenyl]-4-sulfonyl chloride according to General Procedure I afforded JMT-12 as a white powder. ¹H NMR (600 MHz, D₃COCD₃): δ = 11.29 (s, 1H), 8.23 (d, *J* = 8.2 Hz, 1H), 8.02 (d, *J* = 0.6 Hz, 1H), 7.95 (d, *J* = 8.6 Hz, 2H), 7.84 (d, *J* = 8.7 Hz, 2H), 7.58 (d, *J* = 8.2 Hz, 2H), 7.46 (dd, *J* = 1.1, 8.2 Hz, 1H), 7.29 (d, *J* = 7.8 Hz, 2H), 2.35 (s, 3H). ESI-MS for C₂₁H₁₆F₃NO₄S: [M-H]⁻ calculated 434.1, found 434.2

5-(trifluoromethyl)-2-(4'-methyl-[1,1'-biphenyl]-4-sulfonamido)benzoic acid (JMT-13). The reaction of 4'-methyl-[1,1'-biphenyl]-4-sulfonyl chloride according to General Procedure I afforded JMT-13 as a white powder. ¹H NMR (600 MHz, D₃COCD₃): δ = 11.39 (s, 1H), 8.29 (s, 1H), 8.02 (d, *J* = 8.5 Hz, 1H), 7.91 (m, 2H), 7.84 (d, *J* = 8.3 Hz, 2H), 7.58 (d, *J* = 7.9 Hz, 2H), 7.29 (d, *J* = 8.0 Hz, 2H), 2.35 (s, 3H). ESI-MS for C₂₁H₁₆F₃NO₄S: [M-H]⁻ calculated 434.1, found 434.2

4-methoxy-2-(4'-methyl-[1,1'-biphenyl]-4-sulfonamido)benzoic acid (JMT-14). The reaction of 4'-methyl-[1,1'-biphenyl]-4-sulfonyl chloride according to General Procedure I afforded JMT-14 as an off-white powder. ESI-MS for C₂₁H₁₉NO₅S: [M-H]⁻ calculated 396.1, found 396.2

5-methoxy-2-(4'-methyl-[1,1'-biphenyl]-4-sulfonamido)benzoic acid (JMT-15). The reaction of 4'-methyl-[1,1'-biphenyl]-4-sulfonyl chloride according to General Procedure I afforded JMT-15 as an off-white powder. ESI-MS for C₂₁H₁₉NO₅S: [M-H]⁻ calculated 396.1, found 396.3

N-(2-(1H-tetrazol-5-yl)-5-fluorophenyl)-4'-methyl-[1,1'-biphenyl]-4-sulfonamide (JMT-16). The reaction of 4'-methyl-[1,1'-biphenyl]-4-sulfonyl chloride according to General Procedure II afforded JMT-16 as a white powder. ESI-MS for C₂₀H₁₆FN₅O₂S: [M-H]⁻ calculated 408.1, found 408.3

N-(2-(1H-tetrazol-5-yl)-4-fluorophenyl)-4'-methyl-[1,1'-biphenyl]-4-sulfonamide (JMT-17). The reaction of 4'-methyl-[1,1'-biphenyl]-4-sulfonyl chloride according to General Procedure II afforded JMT-17 as a white powder. ESI-MS for C₂₀H₁₆FN₅O₂S: [M-H]⁻ calculated 408.1, found 408.2

N-(2-(1H-tetrazol-5-yl)-4-chlorophenyl)-4'-methyl-[1,1'-biphenyl]-4-sulfonamide (JMT-18). The reaction of 4'-methyl-[1,1'-biphenyl]-4-sulfonyl chloride according to General Procedure II afforded JMT-18 as a white powder. ESI-MS for C₂₀H₁₆ClN₅O₂S: [M-H]⁻ calculated 424.1, found 424.2, 426.3

N-(2-(1*H*-tetrazol-5-yl)-4-bromophenyl)-4'-methyl-[1,1'-biphenyl]-4-sulfonamide (**JMT-19**). The reaction of 4'-methyl-[1,1'-biphenyl]-4-sulfonyl chloride according to General Procedure II afforded JMT-19 as a white powder. ¹H NMR (600 MHz, D₃COCD₃): δ = 10.70 (s, 1H), 8.15 (d, *J* = 2.3, 1H), 8.03 (d, *J* = 8.6 Hz, 1H), 7.79 (m, 1H), 7.73 (dd, *J* = 2.3, 8.9 Hz, 1H), 7.53 (d, *J* = 8.2 Hz, 2H), 7.27 (d, *J* = 7.9 Hz, 2H), 7.03 (d, *J* = 8.6 Hz, 2H) 2.35 (s, 3H). ESI-MS for C₂₀H₁₆BrN₅O₂S: [M-H]⁻ calculated 468.0, found 468.2, 470.2

N-(2-(1*H*-tetrazol-5-yl)-5-methylphenyl)-4'-methyl-[1,1'-biphenyl]-4-sulfonamide (**JMT-20**). The reaction of 4'-methyl-[1,1'-biphenyl]-4-sulfonyl chloride according to General Procedure II afforded JMT-20 as a white powder. ESI-MS for C₂₁H₁₉N₅O₂S: [M-H]⁻ calculated 404.1, found 404.3

N-(2-(1*H*-tetrazol-5-yl)-4-methylphenyl)-4'-methyl-[1,1'-biphenyl]-4-sulfonamide (**JMT-21**). The reaction of 4'-methyl-[1,1'-biphenyl]-4-sulfonyl chloride according to General Procedure II afforded JMT-21 as a white powder. ESI-MS for C₂₁H₁₉N₅O₂S: [M-H]⁻ calculated 404.1, found 404.3

N-(2-(1*H*-tetrazol-5-yl)-5-(trifluoromethyl)phenyl)-4'-methyl-[1,1'-biphenyl]-4-sulfonamide (**JMT-22**). The reaction of 4'-methyl-[1,1'-biphenyl]-4-sulfonyl chloride according to General Procedure II afforded JMT-22 as a white powder. ESI-MS for C₂₁H₁₆F₃N₅O₂S: [M-H]⁻ calculated 458.1, found 458.2

N-(2-(1*H*-tetrazol-5-yl)-4-(trifluoromethyl)phenyl)-4'-methyl-[1,1'-biphenyl]-4-sulfonamide (**JMT-23**). The reaction of 4'-methyl-[1,1'-biphenyl]-4-sulfonyl chloride according to General Procedure II afforded JMT-23 as a white powder. ESI-MS for C₂₁H₁₆F₃N₅O₂S: [M-H]⁻ calculated 458.1, found 458.2

N-(2-(1*H*-tetrazol-5-yl)-5-methoxyphenyl)-4'-methyl-[1,1'-biphenyl]-4-sulfonamide (**JMT-24**). The reaction of 4'-methyl-[1,1'-biphenyl]-4-sulfonyl chloride according to General Procedure II afforded JMT-24 as a beige powder. ESI-MS for C₂₁H₁₉N₅O₃S: [M-H]⁻ calculated 420.1, found 420.3

N-(2-(1*H*-tetrazol-5-yl)-4-methoxyphenyl)-4'-methyl-[1,1'-biphenyl]-4-sulfonamide (**JMT-25**). The reaction of 4'-methyl-[1,1'-biphenyl]-4-sulfonyl chloride according to General Procedure II afforded JMT-25 as an off-white powder. ESI-MS for C₂₁H₁₉N₅O₃S: [M-H]⁻ calculated 420.1, found 420.3

((4'-methyl-[1,1'-biphenyl]-4-yl)sulfonyl)proline (**JMT-26**). The reaction of 4'-methyl-[1,1'-biphenyl]-4-sulfonyl chloride according to General Procedure I afforded JMT-26 as a white powder. ESI-MS for C₁₈H₁₉NO₄S: [M-H]⁻ calculated 344.1, found 344.2

3-((4'-methyl-[1,1'-biphenyl]-4-yl)sulfonyl)thiazolidine-4-carboxylic acid (**JMT-27**). The reaction of 4'-methyl-[1,1'-biphenyl]-4-sulfonyl chloride according to General Procedure I afforded JMT-27 as a white powder. ESI-MS for C₁₇H₁₇NO₄S₂: [M-H]⁻ calculated 362.1, found 362.2

5,5-dimethyl-3-((4'-methyl-[1,1'-biphenyl]-4-yl)sulfonyl)thiazolidine-4-carboxylic acid (**JMT-28**). The reaction of 4'-methyl-[1,1'-biphenyl]-4-sulfonyl chloride according to General Procedure I afforded JMT-28 as a white powder. ESI-MS for C₁₉H₂₁NO₄S₂: calculated 390.1, found 390.2

1-((4'-methyl-[1,1'-biphenyl]-4-yl)sulfonyl)piperidine-2-carboxylic acid (JMT-29). The reaction of 4'-methyl-[1,1'-biphenyl]-4-sulfonyl chloride according to General Procedure I afforded JMT-29 as a white powder. ESI-MS for $C_{19}H_{21}NO_4S$: $[M-H]^-$ calculated 358.1, found 358.3

3-((4'-methyl-[1,1'-biphenyl]-4-yl)sulfonyl)-1,3-thiazinane-4-carboxylic acid (JMT-30). The reaction of 4'-methyl-[1,1'-biphenyl]-4-sulfonyl chloride according to General Procedure I afforded JMT-30 as a white powder. ESI-MS for $C_{18}H_{19}NO_4S_2$: $[M-H]^-$ calculated 376.1, found 376.2

2-([1,1'-biphenyl]-4-sulfonamido)benzoic acid (JMT-31). The reaction of [1,1'-biphenyl]-4-sulfonyl chloride according to General Procedure I afforded JMT-31 as a white powder. ESI-MS for $C_{19}H_{15}NO_4S$: $[M-H]^-$ calculated 352.1, found 352.2

4-fluoro-2-([1,1'-biphenyl]-4-sulfonamido)benzoic acid (JMT-32). The reaction of [1,1'-biphenyl]-4-sulfonyl chloride according to General Procedure I afforded JMT-32 as a beige powder. ESI-MS for $C_{19}H_{14}FNO_4S$: $[M-H]^-$ calculated 370.1, found 370.2

5-fluoro-2-([1,1'-biphenyl]-4-sulfonamido)benzoic acid (JMT-33). The reaction of [1,1'-biphenyl]-4-sulfonyl chloride according to General Procedure I afforded JMT-33 as an off-white powder. ESI-MS for $C_{19}H_{14}FNO_4S$: $[M-H]^-$ calculated 370.1, found 370.2

5-bromo-2-([1,1'-biphenyl]-4-sulfonamido)benzoic acid (JMT-34). The reaction of [1,1'-biphenyl]-4-sulfonyl chloride according to General Procedure I afforded JMT-34 as a white powder. ESI-MS for $C_{19}H_{14}BrNO_4S$: $[M-H]^-$ calculated 430.0, found 430.0, 432.1

5-methyl-2-([1,1'-biphenyl]-4-sulfonamido)benzoic acid (JMT-35). The reaction of [1,1'-biphenyl]-4-sulfonyl chloride according to General Procedure I afforded JMT-35 as a white powder. ESI-MS for $C_{20}H_{17}NO_4S$: $[M-H]^-$ calculated 366.1, found 366.2

4-fluoro-2-(3'-methyl-[1,1'-biphenyl]-4-sulfonamido)benzoic acid (JMT-36). The reaction of 3'-methyl-[1,1'-biphenyl]-4-sulfonyl chloride according to General Procedure I afforded JMT-36 as an off-white powder. ESI-MS for $C_{20}H_{16}FNO_4S$: $[M-H]^-$ calculated 384.1, found 384.2

5-fluoro-2-(3'-methyl-[1,1'-biphenyl]-4-sulfonamido)benzoic acid (JMT-37). The reaction of 3'-methyl-[1,1'-biphenyl]-4-sulfonyl chloride according to General Procedure I afforded JMT-37 as an off-white powder. ESI-MS for $C_{20}H_{16}FNO_4S$: $[M-H]^-$ calculated 384.1, found 384.2

5-bromo-2-(3'-methyl-[1,1'-biphenyl]-4-sulfonamido)benzoic acid (JMT-38). The reaction of 3'-methyl-[1,1'-biphenyl]-4-sulfonyl chloride according to General Procedure I afforded JMT-38 as a white powder. ESI-MS for $C_{20}H_{16}BrNO_4S$: $[M-H]^-$ calculated 444.0, found 444.1, 446.2

5-methyl-2-(3'-methyl-[1,1'-biphenyl]-4-sulfonamido)benzoic acid (JMT-39). The reaction of 3'-methyl-[1,1'-biphenyl]-4-sulfonyl chloride according to General Procedure I afforded JMT-39 as a white powder. ESI-MS for $C_{21}H_{19}NO_4S$: $[M-H]^-$ calculated 380.1, found 380.3

4-fluoro-2-(4'-methoxy-[1,1'-biphenyl]-4-sulfonamido)benzoic acid (JMT-40). The reaction of 4'-methoxy-[1,1'-biphenyl]-4-sulfonyl chloride according to General Procedure I afforded JMT-40 as a beige powder. ESI-MS for $C_{20}H_{16}FNO_5S$: [M-H]⁻ calculated 400.1, found 400.2

5-fluoro-2-(4'-methoxy-[1,1'-biphenyl]-4-sulfonamido)benzoic acid (JMT-41). The reaction of 4'-methoxy-[1,1'-biphenyl]-4-sulfonyl chloride according to General Procedure I afforded JMT-41 as an off-white powder. ESI-MS for $C_{20}H_{16}FNO_5S$: [M-H]⁻ calculated 400.1, found 400.3

4,5-difluoro-2-(4'-methoxy-[1,1'-biphenyl]-4-sulfonamido)benzoic acid (JMT-42). The reaction of 4'-methoxy-[1,1'-biphenyl]-4-sulfonyl chloride according to General Procedure I afforded JMT-42 as a beige powder. ESI-MS for $C_{20}H_{15}F_2NO_5S$: [M-H]⁻ calculated 418.1, found 418.2

5-bromo-2-(4'-methoxy-[1,1'-biphenyl]-4-sulfonamido)benzoic acid (JMT-43). The reaction of 4'-methoxy-[1,1'-biphenyl]-4-sulfonyl chloride according to General Procedure I afforded JMT-43 as a beige powder. ESI-MS for $C_{20}H_{16}BrNO_5S$: [M-H]⁻ calculated 460.0, found 460.0, 462.1

4-methyl-2-(4'-methoxy-[1,1'-biphenyl]-4-sulfonamido)benzoic acid (JMT-44). The reaction of 4'-methoxy-[1,1'-biphenyl]-4-sulfonyl chloride according to General Procedure I afforded JMT-44 as an off-white powder. ESI-MS for $C_{21}H_{19}NO_5S$: [M-H]⁻ calculated 396.1, found 396.3

5-methyl-2-(4'-methoxy-[1,1'-biphenyl]-4-sulfonamido)benzoic acid (JMT-45). The reaction of 4'-methoxy-[1,1'-biphenyl]-4-sulfonyl chloride according to General Procedure I afforded JMT-45 as a white powder. ESI-MS for $C_{21}H_{19}NO_5S$: [M-H]⁻ calculated 396.1, found 396.3

4-(trifluoromethyl)-2-(4'-methoxy-[1,1'-biphenyl]-4-sulfonamido)benzoic acid (JMT-46). The reaction of 4'-methoxy-[1,1'-biphenyl]-4-sulfonyl chloride according to General Procedure I afforded JMT-46 as a white powder. ESI-MS for $C_{21}H_{16}F_3NO_5S$: [M-H]⁻ calculated 450.1, found 450.2

5-(trifluoromethyl)-2-(4'-methoxy-[1,1'-biphenyl]-4-sulfonamido)benzoic acid (JMT-47). The reaction of 4'-methoxy-[1,1'-biphenyl]-4-sulfonyl chloride according to General Procedure I afforded JMT-47 as a white powder. ESI-MS for $C_{21}H_{16}F_3NO_5S$: [M-H]⁻ calculated 450.1, found 450.1

4-methoxy-2-(4'-methoxy-[1,1'-biphenyl]-4-sulfonamido)benzoic acid (JMT-48). The reaction of 4'-methoxy-[1,1'-biphenyl]-4-sulfonyl chloride according to General Procedure I afforded JMT-48 as a beige powder. ESI-MS for $C_{21}H_{19}NO_6S$: [M-H]⁻ calculated 412.1, found 412.3

5-methoxy-2-(4'-methoxy-[1,1'-biphenyl]-4-sulfonamido)benzoic acid (JMT-49). The reaction of 4'-methoxy-[1,1'-biphenyl]-4-sulfonyl chloride according to General Procedure I afforded JMT-49 as an off-white powder. ESI-MS for $C_{21}H_{19}NO_6S$: [M-H]⁻ calculated 412.1, found 412.3

N-(2-(1*H*-tetrazol-5-yl)-5-fluorophenyl)-4'-methoxy-[1,1'-biphenyl]-4-sulfonamide (**JMT-50**). The reaction of 4'-methoxy-[1,1'-biphenyl]-4-sulfonyl chloride according to General Procedure II afforded JMT-50 as a white powder. ESI-MS for C₂₀H₁₆FN₅O₃S: [M-H]⁻ calculated 424.1, found 424.3

N-(2-(1*H*-tetrazol-5-yl)-4-fluorophenyl)-4'-methoxy-[1,1'-biphenyl]-4-sulfonamide (**JMT-51**). The reaction of 4'-methoxy-[1,1'-biphenyl]-4-sulfonyl chloride according to General Procedure II afforded JMT-51 as a white powder. ESI-MS for C₂₀H₁₆FN₅O₃S: [M-H]⁻ calculated 424.1, found 424.2

N-(2-(1*H*-tetrazol-5-yl)-4-bromophenyl)-4'-methoxy-[1,1'-biphenyl]-4-sulfonamide (**JMT-52**). The reaction of 4'-methoxy-[1,1'-biphenyl]-4-sulfonyl chloride according to General Procedure II afforded JMT-52 as a white powder. ESI-MS for C₂₀H₁₆BrN₅O₃S: [M-H]⁻ calculated 484.0, found 484.2, 486.2

N-(2-(1*H*-tetrazol-5-yl)-5-methylphenyl)-4'-methoxy-[1,1'-biphenyl]-4-sulfonamide (**JMT-53**). The reaction of 4'-methoxy-[1,1'-biphenyl]-4-sulfonyl chloride according to General Procedure II afforded JMT-53 as a white powder. ESI-MS for C₂₁H₁₉N₅O₃S: [M-H]⁻ calculated 420.1, found 420.3

N-(2-(1*H*-tetrazol-5-yl)-4-methylphenyl)-4'-methoxy-[1,1'-biphenyl]-4-sulfonamide (**JMT-54**). The reaction of 4'-methoxy-[1,1'-biphenyl]-4-sulfonyl chloride according to General Procedure II afforded JMT-54 as a white powder. ESI-MS for C₂₁H₁₉N₅O₃S: [M-H]⁻ calculated 420.1, found 420.3

N-(2-(1*H*-tetrazol-5-yl)-5-(trifluoromethyl)phenyl)-4'-methoxy-[1,1'-biphenyl]-4-sulfonamide (**JMT-55**). The reaction of 4'-methoxy-[1,1'-biphenyl]-4-sulfonyl chloride according to General Procedure II afforded JMT-55 as a white powder. ESI-MS for C₂₁H₁₆F₃N₅O₃S: [M-H]⁻ calculated 474.1, found 474.3

N-(2-(1*H*-tetrazol-5-yl)-4-(trifluoromethyl)phenyl)-4'-methoxy-[1,1'-biphenyl]-4-sulfonamide (**JMT-56**). The reaction of 4'-methoxy-[1,1'-biphenyl]-4-sulfonyl chloride according to General Procedure II afforded JMT-56 as a white powder. ESI-MS for C₂₁H₁₆F₃N₅O₃S: [M-H]⁻ calculated 474.1, found 474.3

N-(2-(1*H*-tetrazol-5-yl)-5-methoxyphenyl)-4'-methoxy-[1,1'-biphenyl]-4-sulfonamide (**JMT-57**). The reaction of 4'-methoxy-[1,1'-biphenyl]-4-sulfonyl chloride according to General Procedure II afforded JMT-57 as an off-white powder. ESI-MS for C₂₁H₁₉N₅O₄S: [M-H]⁻ calculated 436.1, found 436.2

N-(2-(1*H*-tetrazol-5-yl)-4-methoxyphenyl)-4'-methoxy-[1,1'-biphenyl]-4-sulfonamide (**JMT-58**). The reaction of 4'-methoxy-[1,1'-biphenyl]-4-sulfonyl chloride according to General Procedure II afforded JMT-58 as an off-white powder. ESI-MS for C₂₁H₁₉N₅O₄S: [M-H]⁻ calculated 436.1, found 436.3

4-fluoro-2-(4'-fluoro-[1,1'-biphenyl]-4-sulfonamido)benzoic acid (**JMT-59**). The reaction of 4'-fluoro-[1,1'-biphenyl]-4-sulfonyl chloride according to General Procedure I afforded JMT-59 as a beige powder. ESI-MS for C₁₉H₁₃F₂NO₄S: [M-H]⁻ calculated 388.1, found 388.2

5-fluoro-2-(4'-fluoro-[1,1'-biphenyl]-4-sulfonamido)benzoic acid (JMT-60). The reaction of 4'-fluoro-[1,1'-biphenyl]-4-sulfonyl chloride according to General Procedure I afforded JMT-60 as a beige powder. ESI-MS for C₁₉H₁₃F₂NO₄S: [M-H]⁻ calculated 388.1, found 388.1

4,5-difluoro-2-(4'-fluoro-[1,1'-biphenyl]-4-sulfonamido)benzoic acid (JMT-61). The reaction of 4'-fluoro-[1,1'-biphenyl]-4-sulfonyl chloride according to General Procedure I afforded JMT-61 as a beige powder. ESI-MS for C₁₉H₁₂F₃NO₄S: [M-H]⁻ calculated 406.0, found 406.2

5-bromo-2-(4'-fluoro-[1,1'-biphenyl]-4-sulfonamido)benzoic acid (JMT-62). The reaction of 4'-fluoro-[1,1'-biphenyl]-4-sulfonyl chloride according to General Procedure I afforded JMT-62 as a white powder. ESI-MS for C₁₉H₁₃FBrNO₄S: [M-H]⁻ calculated 448.0, found 448.0, 450.0

4-methyl-2-(4'-fluoro-[1,1'-biphenyl]-4-sulfonamido)benzoic acid (JMT-63). The reaction of 4'-fluoro-[1,1'-biphenyl]-4-sulfonyl chloride according to General Procedure I afforded JMT-63 as an off-white powder. ESI-MS for C₂₀H₁₆FNO₄S: [M-H]⁻ calculated 384.1, found 384.2

5-methyl-2-(4'-fluoro-[1,1'-biphenyl]-4-sulfonamido)benzoic acid (JMT-64). The reaction of 4'-fluoro-[1,1'-biphenyl]-4-sulfonyl chloride according to General Procedure I afforded JMT-64 as an off-white powder. ESI-MS for C₂₀H₁₆FNO₄S: [M-H]⁻ calculated 384.1, found 384.2

5-methoxy-2-(4'-fluoro-[1,1'-biphenyl]-4-sulfonamido)benzoic acid (JMT-65). The reaction of 4'-fluoro-[1,1'-biphenyl]-4-sulfonyl chloride according to General Procedure I afforded JMT-65 as an off-white powder. ESI-MS for C₂₀H₁₆FNO₅S: [M-H]⁻ calculated 400.1, found 400.2

N-(2-(1H-tetrazol-5-yl)-4-fluorophenyl)-4'-fluoro-[1,1'-biphenyl]-4-sulfonamide (JMT-66). The reaction of 4'-fluoro-[1,1'-biphenyl]-4-sulfonyl chloride according to General Procedure II afforded JMT-66 as a white powder. ESI-MS for C₁₉H₁₃F₂N₅O₂S: [M-H]⁻ calculated 412.1, found 412.2

N-(2-(1H-tetrazol-5-yl)-4-methylphenyl)-4'-fluoro-[1,1'-biphenyl]-4-sulfonamide (JMT-67). The reaction of 4'-fluoro-[1,1'-biphenyl]-4-sulfonyl chloride according to General Procedure II afforded JMT-67 as a white powder. ESI-MS for C₂₀H₁₆FN₅O₂S: [M-H]⁻ calculated 408.1, found 408.3

4-fluoro-2-(4'-chloro-[1,1'-biphenyl]-4-sulfonamido)benzoic acid (JMT-68). The reaction of 4'-chloro-[1,1'-biphenyl]-4-sulfonyl chloride according to General Procedure I afforded JMT-68 as an off-white powder. ESI-MS for C₁₉H₁₃ClFNO₄S: [M-H]⁻ calculated 404.0, found 404.1, 406.1

5-fluoro-2-(4'-chloro-[1,1'-biphenyl]-4-sulfonamido)benzoic acid (JMT-69). The reaction of 4'-chloro-[1,1'-biphenyl]-4-sulfonyl chloride according to General Procedure I afforded JMT-69 as a white powder. ESI-MS for C₁₉H₁₃ClFNO₄S: [M-H]⁻ calculated 404.0, found 404.1, 406.1

4,5-difluoro-2-(4'-chloro-[1,1'-biphenyl]-4-sulfonamido)benzoic acid (JMT-70). The reaction of 4'-chloro-[1,1'-biphenyl]-4-sulfonyl chloride according to General Procedure I afforded JMT-70 as an off-white powder. ESI-MS for $C_{19}H_{12}ClF_2NO_4S$: $[M-H]^-$ calculated 422.0, found 422.2, 424.1

5-bromo-2-(4'-chloro-[1,1'-biphenyl]-4-sulfonamido)benzoic acid (JMT-71). The reaction of 4'-chloro-[1,1'-biphenyl]-4-sulfonyl chloride according to General Procedure I afforded JMT-71 as a white powder. ESI-MS for $C_{19}H_{13}BrClNO_4S$: $[M-H]^-$ calculated 463.9, found 464.1, 466.1

4-methyl-2-(4'-chloro-[1,1'-biphenyl]-4-sulfonamido)benzoic acid (JMT-72). The reaction of 4'-chloro-[1,1'-biphenyl]-4-sulfonyl chloride according to General Procedure I afforded JMT-72 as a white powder. ESI-MS for $C_{20}H_{16}ClNO_4S$: $[M-H]^-$ calculated 400.0, found 400.2, 402.1

5-methyl-2-(4'-chloro-[1,1'-biphenyl]-4-sulfonamido)benzoic acid (JMT-73). The reaction of 4'-chloro-[1,1'-biphenyl]-4-sulfonyl chloride according to General Procedure I afforded JMT-73 as a white powder. ESI-MS for $C_{20}H_{16}ClNO_4S$: $[M-H]^-$ calculated 400.1, found 400.1, 402.2

4-(trifluoromethyl)-2-(4'-chloro-[1,1'-biphenyl]-4-sulfonamido)benzoic acid (JMT-74). The reaction of 4'-chloro-[1,1'-biphenyl]-4-sulfonyl chloride according to General Procedure I afforded JMT-74 as a white powder. ESI-MS for $C_{20}H_{13}ClF_3NO_4S$: $[M-H]^-$ calculated 454.0, found 454.1

5-(trifluoromethyl)-2-(4'-chloro-[1,1'-biphenyl]-4-sulfonamido)benzoic acid (JMT-75). The reaction of 4'-chloro-[1,1'-biphenyl]-4-sulfonyl chloride according to General Procedure I afforded JMT-75 as a white powder. ESI-MS for $C_{20}H_{13}ClF_3NO_4S$: $[M-H]^-$ calculated 454.0, found 454.2, 456.0

4-methoxy-2-(4'-chloro-[1,1'-biphenyl]-4-sulfonamido)benzoic acid (JMT-76). The reaction of 4'-chloro-[1,1'-biphenyl]-4-sulfonyl chloride according to General Procedure I afforded JMT-76 as an off-white powder. ESI-MS for $C_{20}H_{16}ClNO_5S$: $[M-H]^-$ calculated 416.0, found 416.2, 418.2

5-methoxy-2-(4'-chloro-[1,1'-biphenyl]-4-sulfonamido)benzoic acid (JMT-77). The reaction of 4'-chloro-[1,1'-biphenyl]-4-sulfonyl chloride according to General Procedure I afforded JMT-77 as an off-white powder. ESI-MS for $C_{20}H_{16}ClNO_5S$: $[M-H]^-$ calculated 416.0, found 416.2, 418.2

N-(2-(1H-tetrazol-5-yl)-5-fluorophenyl)-4'-chloro-[1,1'-biphenyl]-4-sulfonamide (JMT-78). The reaction of 4'-chloro-[1,1'-biphenyl]-4-sulfonyl chloride according to General Procedure II afforded JMT-78 as a white powder. ESI-MS for $C_{19}H_{13}ClFN_5O_2S$: $[M-H]^-$ calculated 428.0, found 428.2, 430.3

N-(2-(1H-tetrazol-5-yl)-4-fluorophenyl)-4'-chloro-[1,1'-biphenyl]-4-sulfonamide (JMT-79). The reaction of 4'-chloro-[1,1'-biphenyl]-4-sulfonyl chloride according to General Procedure II afforded JMT-79 as a white powder. ESI-MS for $C_{19}H_{13}ClFN_5O_2S$: $[M-H]^-$ calculated 428.0, found 428.2, 430.2

N-(2-(1*H*-tetrazol-5-yl)-5-methylphenyl)-4'-chloro-[1,1'-biphenyl]-4-sulfonamide (**JMT-80**). The reaction of 4'-chloro-[1,1'-biphenyl]-4-sulfonyl chloride according to General Procedure II afforded JMT-80 as a white powder. ESI-MS for C₂₀H₁₆ClN₅O₂S: [M-H]⁻ calculated 424.1, found 424.3, 426.2

N-(2-(1*H*-tetrazol-5-yl)-4-methylphenyl)-4'-chloro-[1,1'-biphenyl]-4-sulfonamide (**JMT-81**). The reaction of 4'-chloro-[1,1'-biphenyl]-4-sulfonyl chloride according to General Procedure II afforded JMT-81 as a white powder. ESI-MS for C₂₀H₁₆ClN₅O₂S: [M-H]⁻ calculated 424.1, found 424.2, 426.2

N-(2-(1*H*-tetrazol-5-yl)-5-methoxyphenyl)-4'-chloro-[1,1'-biphenyl]-4-sulfonamide (**JMT-82**). The reaction of 4'-chloro-[1,1'-biphenyl]-4-sulfonyl chloride according to General Procedure II afforded JMT-82 as a beige powder. ESI-MS for C₂₀H₁₆ClN₅O₃S: [M-H]⁻ calculated 440.1, found 440.2, 442.2

N-(2-(1*H*-tetrazol-5-yl)-4-methoxyphenyl)-4'-chloro-[1,1'-biphenyl]-4-sulfonamide (**JMT-83**). The reaction of 4'-chloro-[1,1'-biphenyl]-4-sulfonyl chloride according to General Procedure II afforded JMT-83 as an off-white powder. ESI-MS for C₂₀H₁₆ClN₅O₃S: [M-H]⁻ calculated 440.1, found 440.2, 442.2

4-fluoro-2-(4'-(trifluoromethyl)-[1,1'-biphenyl]-4-sulfonamido)benzoic acid (**JMT-84**). The reaction of 4'-(trifluoromethyl)-[1,1'-biphenyl]-4-sulfonyl chloride according to General Procedure I afforded JMT-84 as a beige powder. ¹H NMR (600 MHz, D₃COCD₃): δ = 11.60 (s, 1H), 8.11 (dd, *J* = 6.5, 8.9 Hz, 1H), 8.06 (d, *J* = 8.5 Hz, 2H), 7.95 (d, *J* = 8.7 Hz, 2H), 7.93 (d, *J* = 8.5 Hz, 2H), 7.83 (d, *J* = 8.2 Hz, 2H), 7.47 (dd, *J* = 2.5, 11.1 Hz, 1H), 6.93 (dt, *J* = 2.5, 8.1 Hz, 1H). ESI-MS for C₂₀H₁₃F₄NO₄S: [M-H]⁻ calculated 438.0, found 438.2

5-fluoro-2-(4'-(trifluoromethyl)-[1,1'-biphenyl]-4-sulfonamido)benzoic acid (**JMT-85**). The reaction of 4'-(trifluoromethyl)-[1,1'-biphenyl]-4-sulfonyl chloride according to General Procedure I afforded JMT-85 as an off-white powder. ¹H ESI-MS for C₂₀H₁₃F₄NO₄S: [M-H]⁻ calculated 438.0, found 438.2

4,5-difluoro-2-(4'-(trifluoromethyl)-[1,1'-biphenyl]-4-sulfonamido)benzoic acid (**JMT-86**). The reaction of 4'-(trifluoromethyl)-[1,1'-biphenyl]-4-sulfonyl chloride according to General Procedure I afforded JMT-86 as a beige powder. ¹H NMR (600 MHz, D₃COCD₃): δ = 11.14 (s, 1H), 8.02 (d, *J* = 8.6 Hz, 2H), 7.93 (m, 5H), 7.83 (d, *J* = 8.3 Hz, 2H), 7.67 (dd, *J* = 7.1, 12.4 Hz, 1H). ESI-MS for C₂₀H₁₂F₅NO₄S: [M-H]⁻ calculated 456.0, found 456.2

5-bromo-2-(4'-(trifluoromethyl)-[1,1'-biphenyl]-4-sulfonamido)benzoic acid (**JMT-87**). The reaction of 4'-(trifluoromethyl)-[1,1'-biphenyl]-4-sulfonyl chloride according to General Procedure I afforded JMT-87 as a white powder. ESI-MS for C₂₀H₁₃BrF₃NO₄S: [M-H]⁻ calculated 498.0, found 498.1, 500.2

4-methyl-2-(4'-(trifluoromethyl)-[1,1'-biphenyl]-4-sulfonamido)benzoic acid (**JMT-88**). The reaction of 4'-(trifluoromethyl)-[1,1'-biphenyl]-4-sulfonyl chloride according to General Procedure I afforded JMT-88 as an off-white powder. ESI-MS for C₂₁H₁₆F₃NO₄S: [M-H]⁻ calculated 434.1, found 434.2

5-methyl-2-(4'-(trifluoromethyl)-[1,1'-biphenyl]-4-sulfonamido)benzoic acid (JMT-89). The reaction of 4'-(trifluoromethyl)-[1,1'-biphenyl]-4-sulfonyl chloride according to General Procedure I afforded JMT-89 as an off-white powder. ESI-MS for $C_{21}H_{16}F_3NO_4S$: $[M-H]^-$ calculated 434.1, found 434.2

4-(trifluoromethyl)-2-(4'-(trifluoromethyl)-[1,1'-biphenyl]-4-sulfonamido)benzoic acid (JMT-90). The reaction of 4'-(trifluoromethyl)-[1,1'-biphenyl]-4-sulfonyl chloride according to General Procedure I afforded JMT-90 as a white powder. ESI-MS for $C_{21}H_{13}F_6NO_4S$: $[M-H]^-$ calculated 488.0, found 488.2

5-(trifluoromethyl)-2-(4'-(trifluoromethyl)-[1,1'-biphenyl]-4-sulfonamido)benzoic acid (JMT-91). The reaction of 4'-(trifluoromethyl)-[1,1'-biphenyl]-4-sulfonyl chloride according to General Procedure I afforded JMT-91 as a white powder. ESI-MS for $C_{21}H_{13}F_6NO_4S$: $[M-H]^-$ calculated 488.0, found 488.2

4-methoxy-2-(4'-(trifluoromethyl)-[1,1'-biphenyl]-4-sulfonamido)benzoic acid (JMT-92). The reaction of 4'-(trifluoromethyl)-[1,1'-biphenyl]-4-sulfonyl chloride according to General Procedure I afforded JMT-92 as an off-white powder. ESI-MS for $C_{21}H_{16}F_3NO_5S$: $[M-H]^-$ calculated 450.1, found 450.2

5-methoxy-2-(4'-(trifluoromethyl)-[1,1'-biphenyl]-4-sulfonamido)benzoic acid (JMT-93). The reaction of 4'-(trifluoromethyl)-[1,1'-biphenyl]-4-sulfonyl chloride according to General Procedure I afforded JMT-93 as a white powder. ESI-MS for $C_{21}H_{16}F_3NO_5S$: $[M-H]^-$ calculated 450.1, found 450.2

N-(2-(1H-tetrazol-5-yl)-5-fluorophenyl)-4'-(trifluoromethyl)-[1,1'-biphenyl]-4-sulfonamide (JMT-94). The reaction of 4'-(trifluoromethyl)-[1,1'-biphenyl]-4-sulfonyl chloride according to General Procedure II afforded JMT-94 as a white powder. ESI-MS for $C_{20}H_{13}F_4N_5O_2S$: $[M-H]^-$ calculated 462.1, found 462.2

N-(2-(1H-tetrazol-5-yl)-4-fluorophenyl)-4'-(trifluoromethyl)-[1,1'-biphenyl]-4-sulfonamide (JMT-95). The reaction of 4'-(trifluoromethyl)-[1,1'-biphenyl]-4-sulfonyl chloride according to General Procedure II afforded JMT-95 as a white powder. ESI-MS for $C_{20}H_{13}F_4N_5O_2S$: $[M-H]^-$ calculated 462.1, found 462.2

N-(2-(1H-tetrazol-5-yl)-4-bromophenyl)-4'-(trifluoromethyl)-[1,1'-biphenyl]-4-sulfonamide (JMT-96). The reaction of 4'-(trifluoromethyl)-[1,1'-biphenyl]-4-sulfonyl chloride according to General Procedure II afforded JMT-96 as a white powder. ESI-MS for $C_{20}H_{13}BrF_3N_5O_2S$: $[M-H]^-$ calculated 522.0, found 522.1, 524.2

N-(2-(1H-tetrazol-5-yl)-5-methylphenyl)-4'-(trifluoromethyl)-[1,1'-biphenyl]-4-sulfonamide (JMT-97). The reaction of 4'-(trifluoromethyl)-[1,1'-biphenyl]-4-sulfonyl chloride according to General Procedure II afforded JMT-97 as an off-white powder. ESI-MS for $C_{21}H_{16}F_3N_5O_2S$: $[M-H]^-$ calculated 458.1, found 458.2

N-(2-(1H-tetrazol-5-yl)-4-methylphenyl)-4'-(trifluoromethyl)-[1,1'-biphenyl]-4-sulfonamide (JMT-98). The reaction of 4'-(trifluoromethyl)-[1,1'-biphenyl]-4-sulfonyl chloride according to General Procedure II afforded JMT-98 as a white powder. ESI-MS for $C_{21}H_{16}F_3N_5O_2S$: $[M-H]^-$ calculated 458.1, found 458.2

N-(2-(1*H*-tetrazol-5-yl)-5-methoxyphenyl)-4'-(trifluoromethyl)-[1,1'-biphenyl]-4-sulfonamide (**JMT-99**). The reaction of 4'-(trifluoromethyl)-[1,1'-biphenyl]-4-sulfonyl chloride according to General Procedure II afforded JMT-99 as a beige powder. ESI-MS for C₂₁H₁₆F₃N₅O₃S: [M-H]⁻ calculated 474.1, found 474.3

N-(2-(1*H*-tetrazol-5-yl)-4-methoxyphenyl)-4'-(trifluoromethyl)-[1,1'-biphenyl]-4-sulfonamide (**JMT-100**). The reaction of 4'-(trifluoromethyl)-[1,1'-biphenyl]-4-sulfonyl chloride according to General Procedure II afforded JMT-100 as a white powder. ESI-MS for C₂₁H₁₆F₃N₅O₃S: [M-H]⁻ calculated 474.1, found 474.3

2-((4-cyclohexylphenyl)sulfonamido)-4-fluorobenzoic acid (**JMT-101**). The reaction of 4-cyclohexylbenzenesulfonyl chloride according to General Procedure I afforded JMT-101 as a beige powder. ESI-MS for C₁₉H₂₀FNO₄S: [M-H]⁻ calculated 376.1, found 376.2

2-((4-cyclohexylphenyl)sulfonamido)-5-fluorobenzoic acid (**JMT-102**). The reaction of 4-cyclohexylbenzenesulfonyl chloride according to General Procedure I afforded JMT-102 as an off-white powder. ESI-MS for C₁₉H₂₀FNO₄S: [M-H]⁻ calculated 376.1, found 376.2

2-((4-cyclohexylphenyl)sulfonamido)-4,5-difluorobenzoic acid (**JMT-103**). The reaction of 4-cyclohexylbenzenesulfonyl chloride according to General Procedure I afforded JMT-103 as a beige powder. ESI-MS for C₁₉H₁₉F₂NO₄S: [M-H]⁻ calculated 394.1, found 394.2

2-((4-cyclohexylphenyl)sulfonamido)-5-bromobenzoic acid (**JMT-104**). The reaction of 4-cyclohexylbenzenesulfonyl chloride according to General Procedure I afforded JMT-104 as a white powder. ESI-MS for C₁₉H₂₀BrNO₄S: [M-H]⁻ calculated 436.0, found 436.1, 438.1

2-((4-cyclohexylphenyl)sulfonamido)-4-methylbenzoic acid (**JMT-105**). The reaction of 4-cyclohexylbenzenesulfonyl chloride according to General Procedure I afforded JMT-105 as a white powder. ESI-MS for C₂₀H₂₃NO₄S: [M-H]⁻ calculated 372.1, found 372.3

2-((4-cyclohexylphenyl)sulfonamido)-5-methylbenzoic acid (**JMT-106**). The reaction of 4-cyclohexylbenzenesulfonyl chloride according to General Procedure I afforded JMT-106 as a white powder. ESI-MS for C₂₀H₂₃NO₄S: [M-H]⁻ calculated 372.1, found 372.3

2-((4-cyclohexylphenyl)sulfonamido)-4-(trifluoromethyl)benzoic acid (**JMT-107**). The reaction of 4-cyclohexylbenzenesulfonyl chloride according to General Procedure I afforded JMT-107 as a white powder. ESI-MS for C₂₀H₂₀F₃NO₄S: [M-H]⁻ calculated 426.1, found 426.2

2-((4-cyclohexylphenyl)sulfonamido)-5-(trifluoromethyl)benzoic acid (**JMT-108**). The reaction of 4-cyclohexylbenzenesulfonyl chloride according to General Procedure I afforded JMT-108 as a white powder. ¹H NMR (600 MHz, D₃COCD₃): δ = 11.27 (s, 1H), 8.28 (s, 1H), 7.87 (m, 4H), 2.60 (tt, *J* = 2.8, 11.5 Hz, 1H), 1.79 (dt, *J* = 2.8, 12.2 Hz, 4H), 1.70 (dt, *J* = 1.5, 3.0, 12.9 Hz, 1H), 1.40 (ddt, *J* = 1.7, 12.7, 24.0 Hz, 4H), 1.25 (ddt, *J* = 3.1, 12.7, 23.9 Hz, 1H). ESI-MS for C₂₀H₂₀F₃NO₄S: [M-H]⁻ calculated 426.1, found 426.3

2-((4-cyclohexylphenyl)sulfonamido)-4-methoxybenzoic acid (**JMT-109**). The reaction of 4-cyclohexylbenzenesulfonyl chloride according to General Procedure I afforded JMT-109 as an off-white powder. ESI-MS for C₂₀H₂₃NO₅S: [M-H]⁻ calculated 388.1, found 388.3

2-((4-cyclohexylphenyl)sulfonamido)-5-methoxybenzoic acid (JMT-110). The reaction of 4-cyclohexylbenzenesulfonyl chloride according to General Procedure I afforded JMT-110 as an off-white powder. ESI-MS for $C_{20}H_{23}NO_5S$: [M-H]⁻ calculated 388.1, found 388.3

N-(2-(1H-tetrazol-5-yl)-5-fluorophenyl)-4-cyclohexylbenzenesulfonamide (JMT-111). The reaction of 4-cyclohexylbenzenesulfonyl chloride according to General Procedure II afforded JMT-111 as a white powder. ESI-MS for $C_{19}H_{20}FN_5O_2S$: [M-H]⁻ calculated 400.1, found 400.3

N-(2-(1H-tetrazol-5-yl)-4-fluorophenyl)-4-cyclohexylbenzenesulfonamide (JMT-112). The reaction of 4-cyclohexylbenzenesulfonyl chloride according to General Procedure II afforded JMT-112 as a white powder. ESI-MS for $C_{19}H_{20}FN_5O_2S$: [M-H]⁻ calculated 400.1, found 400.2

N-(2-(1H-tetrazol-5-yl)-4-bromophenyl)-4-cyclohexylbenzenesulfonamide (JMT-113). The reaction of 4-cyclohexylbenzenesulfonyl chloride according to General Procedure II afforded JMT-113 as a white powder. ¹H NMR (600 MHz, D₃COCD₃): δ = 10.63 (s, 1H), 8.14 (d, *J* = 2.2, 1H), 7.75 (d, *J* = 8.9, 1H), 7.71 (m, 1H), 7.67 (d, *J* = 8.4 Hz, 2H), 7.31 (d, *J* = 8.3 Hz, 2H), 2.53 (d, *J* = 8.3 Hz, 2H), 2.53 (tt, *J* = 2.9, 11.6 Hz, 1H), 1.76 (dt, *J* = 4.2, 22.3 Hz, 4H), 1.69 (dtt, *J* = 1.5, 2.9, 12.8 Hz, 4H), 1.36 (ddt, *J* = 2.0, 12.8, 23.0 Hz, 1H) 1.24 (ddt, *J* = 3.5, 12.7, 22.9 Hz, 1H). ESI-MS for $C_{19}H_{20}BrN_5O_2S$: [M-H]⁻ calculated 460.0, found 460.2, 462.2

N-(2-(1H-tetrazol-5-yl)-5-methylphenyl)-4-cyclohexylbenzenesulfonamide (JMT-114). The reaction of 4-cyclohexylbenzenesulfonyl chloride according to General Procedure II afforded JMT-114 as a white powder. ESI-MS for $C_{20}H_{23}N_5O_2S$: [M-H]⁻ calculated 396.2, found 396.3

N-(2-(1H-tetrazol-5-yl)-4-methylphenyl)-4-cyclohexylbenzenesulfonamide (JMT-115). The reaction of 4-cyclohexylbenzenesulfonyl chloride according to General Procedure II afforded JMT-115 as a white powder. ESI-MS for $C_{20}H_{23}N_5O_2S$: [M-H]⁻ calculated 396.2, found 396.3

N-(2-(1H-tetrazol-5-yl)-5-(trifluoromethyl)phenyl)-4-cyclohexylbenzenesulfonamide (JMT-116). The reaction of 4-cyclohexylbenzenesulfonyl chloride according to General Procedure II afforded JMT-116 as a white powder. ESI-MS for $C_{20}H_{20}F_3N_5O_2S$: [M-H]⁻ calculated 450.1, found 450.2

N-(2-(1H-tetrazol-5-yl)-5-methoxyphenyl)-4-cyclohexylbenzenesulfonamide (JMT-117). The reaction of 4-cyclohexylbenzenesulfonyl chloride according to General Procedure II afforded JMT-117 as an off-white powder. ESI-MS for $C_{20}H_{23}N_5O_3S$: [M-H]⁻ calculated 412.1, found 412.3

N-(2-(1H-tetrazol-5-yl)-4-methoxyphenyl)-4-cyclohexylbenzenesulfonamide (JMT-118). The reaction of 4-cyclohexylbenzenesulfonyl chloride according to General Procedure II afforded JMT-118 as a white powder. ESI-MS for $C_{20}H_{23}N_5O_3S$: [M-H]⁻ calculated 412.1, found 412.3

4-fluoro-2-(naphthalene-2-sulfonamido)benzoic acid (JMT-119). The reaction of naphthalene-2-sulfonyl chloride according to General Procedure I afforded JMT-119 as a beige powder. ESI-MS for $C_{17}H_{12}FNO_4S$: [M-H]⁻ calculated 344.0, found 344.2

5-fluoro-2-(naphthalene-2-sulfonamido)benzoic acid (JMT-120). The reaction of naphthalene-2-sulfonyl chloride according to General Procedure I afforded JMT-120 as an off-white powder. ESI-MS for C₁₇H₁₂FNO₄S: [M-H]⁻ calculated 344.0, found 344.1

5-methyl-2-(naphthalene-2-sulfonamido)benzoic acid (JMT-121). The reaction of naphthalene-2-sulfonyl chloride according to General Procedure I afforded JMT-121 as an off-white powder. ESI-MS for C₁₈H₁₅NO₄S: [M-H]⁻ calculated 340.1, found 340.2

4-fluoro-2-((5,6,7,8-tetrahydronaphthalene)-2-sulfonamido)benzoic acid (JMT-122). The reaction of 5,6,7,8-tetrahydronaphthalene-2-sulfonyl chloride according to General Procedure I afforded JMT-122 as a beige powder. ESI-MS for C₁₇H₁₆FNO₄S: [M-H]⁻ calculated 348.1, found 348.2

5-fluoro-2-((5,6,7,8-tetrahydronaphthalene)-2-sulfonamido)benzoic acid (JMT-123). The reaction of 5,6,7,8-tetrahydronaphthalene-2-sulfonyl chloride according to General Procedure I afforded JMT-123 as an off-white powder. ESI-MS for C₁₇H₁₆FNO₄S: [M-H]⁻ calculated 348.1, found 348.2

5-methyl-2-((5,6,7,8-tetrahydronaphthalene)-2-sulfonamido)benzoic acid (JMT-124). The reaction of 5,6,7,8-tetrahydronaphthalene-2-sulfonyl chloride according to General Procedure I afforded JMT-124 as an off-white powder. ESI-MS for C₁₈H₁₉NO₄S: [M-H]⁻ calculated 344.1, found 344.2

2-((2,3-dihydrobenzo[b][1,4]dioxine)-6-sulfonamido)benzoic acid (JMT-125). The reaction of 2,3-dihydrobenzo[b][1,4]dioxine-6-sulfonyl chloride according to General Procedure I afforded JMT-125 as an off-white powder. ESI-MS for C₁₅H₁₃NO₆S: [M-H]⁻ calculated 334.0, found 334.1

2-((2,3-dihydrobenzo[b][1,4]dioxine)-6-sulfonamido)-4-fluorobenzoic acid (JMT-126). The reaction of 2,3-dihydrobenzo[b][1,4]dioxine-6-sulfonyl chloride according to General Procedure I afforded JMT-126 as a beige powder. ESI-MS for C₁₅H₁₂FNO₆S: [M-H]⁻ calculated 352.0, found 352.1

2-((2,3-dihydrobenzo[b][1,4]dioxine)-6-sulfonamido)-5-fluorobenzoic acid (JMT-127). The reaction of 2,3-dihydrobenzo[b][1,4]dioxine-6-sulfonyl chloride according to General Procedure I afforded JMT-127 as an off-white powder. ESI-MS for C₁₅H₁₂FNO₆S: [M-H]⁻ calculated 352.0, found 352.1

2-((2,3-dihydrobenzo[b][1,4]dioxine)-6-sulfonamido)-5-methylbenzoic acid (JMT-128). The reaction of 2,3-dihydrobenzo[b][1,4]dioxine-6-sulfonyl chloride according to General Procedure I afforded JMT-128 as an off-white powder. ESI-MS for C₁₆H₁₅NO₆S: [M-H]⁻ calculated 348.1, found 348.2

Appendix E. Pharmacophore screening of FDA-approved therapies for putative PBP inhibitors

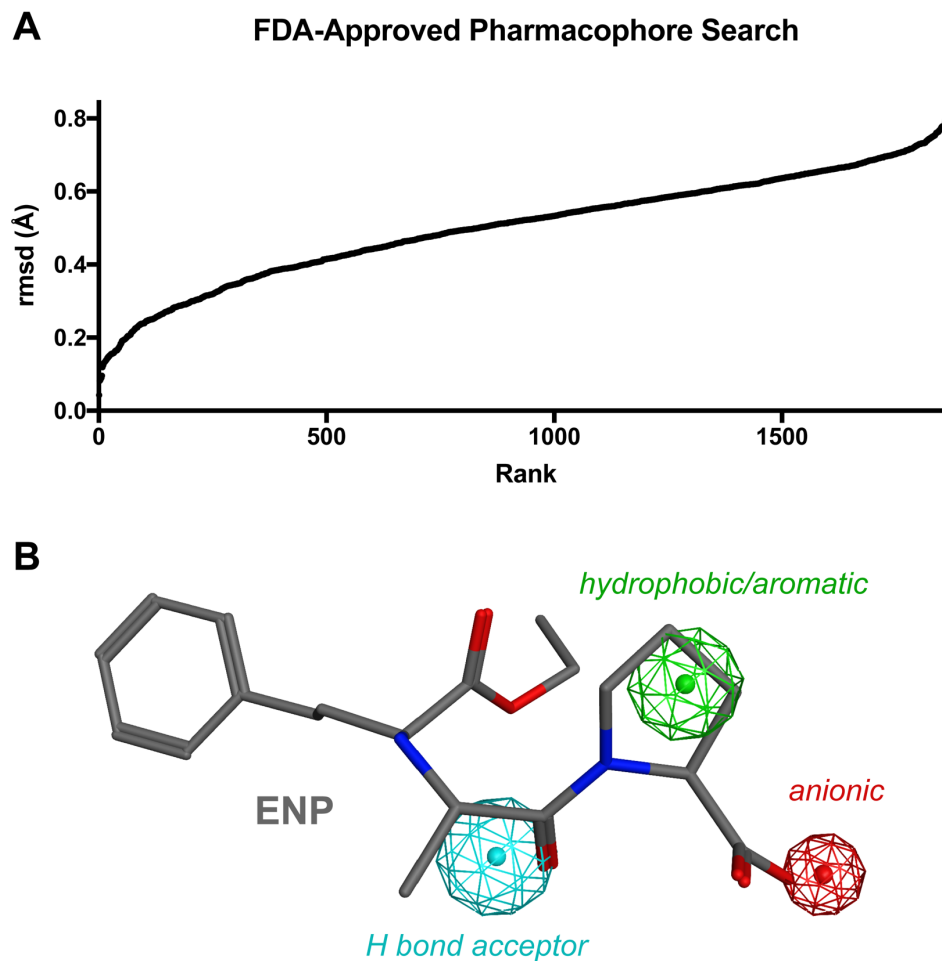


Figure E.1: Pharmacophore search of a virtualized library of FDA-approved drugs. **A.** A three-point pharmacophore consisting of one anionic feature (radius = 0.7 Å), one hydrophobic/aromatic feature (radius = 0.9 Å), and one hydrogen bond accepting feature (radius = 1.0 Å) was used to search a virtual library of FDA-approved drug structures, yielding 1,862 matching conformations. **B.** Enalapril shown in a pharmacophore-matching conformation (rmsd = 0.6 Å).

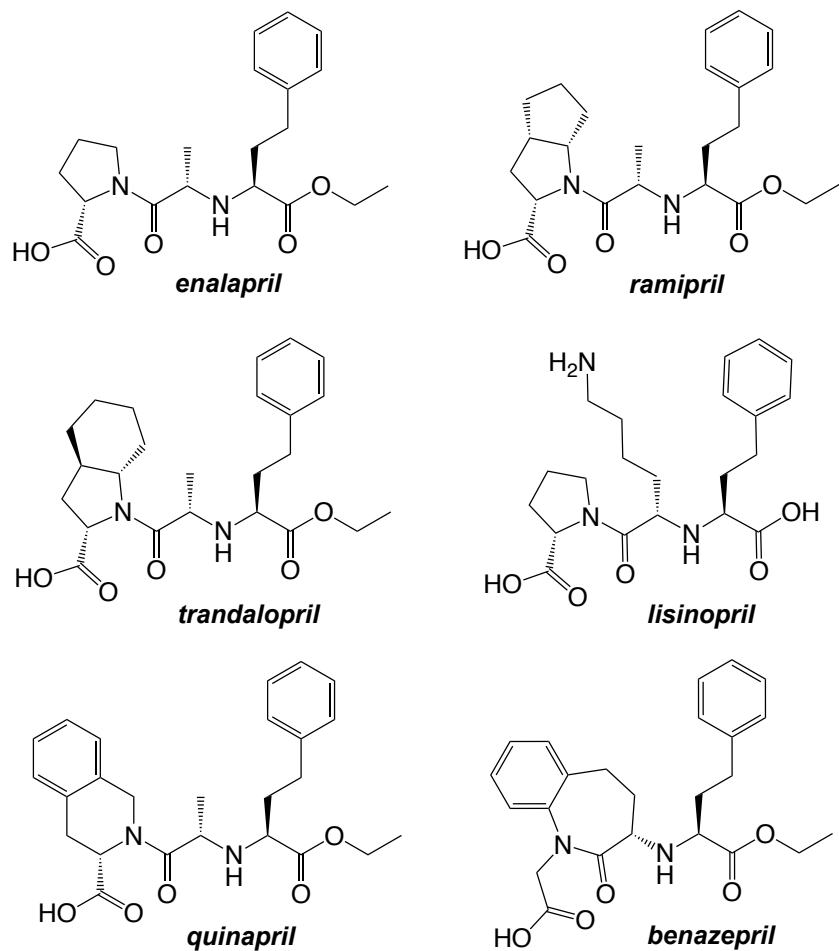


Figure E.2: Example structures of ACE inhibitors matching the three-point pharmacophore model.

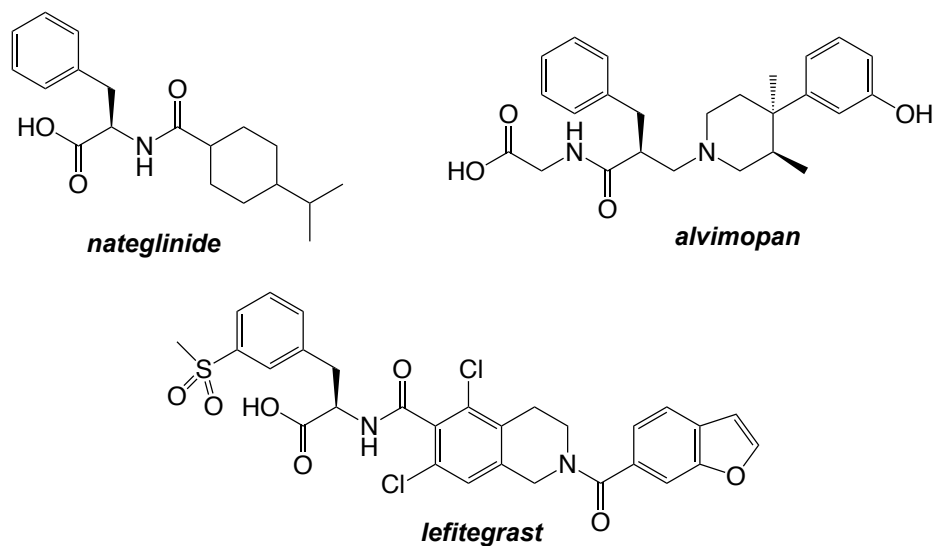


Figure E.3: Example structures of other C-terminal peptide and peptoid drugs matching the three-point pharmacophore model.

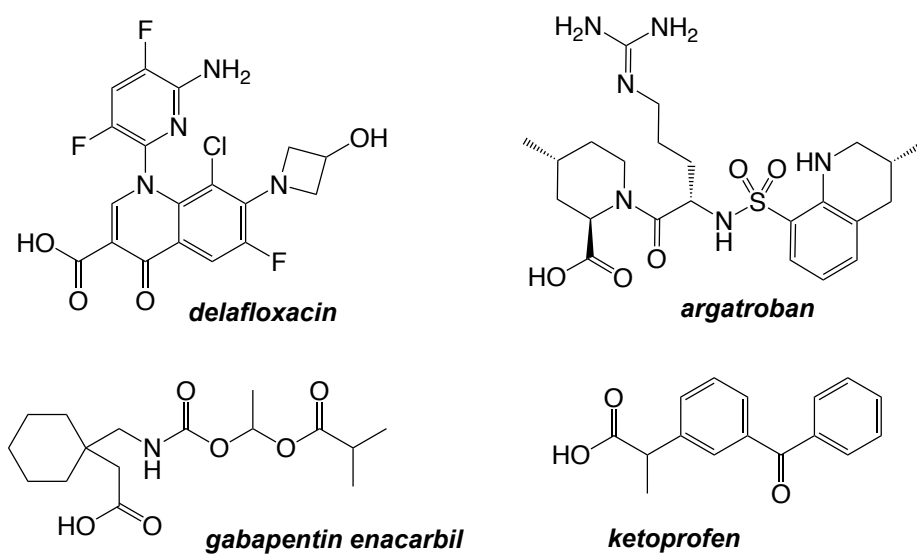


Figure E.4: Example structures of additional miscellaneous drugs matching the three-point pharmacophore model.

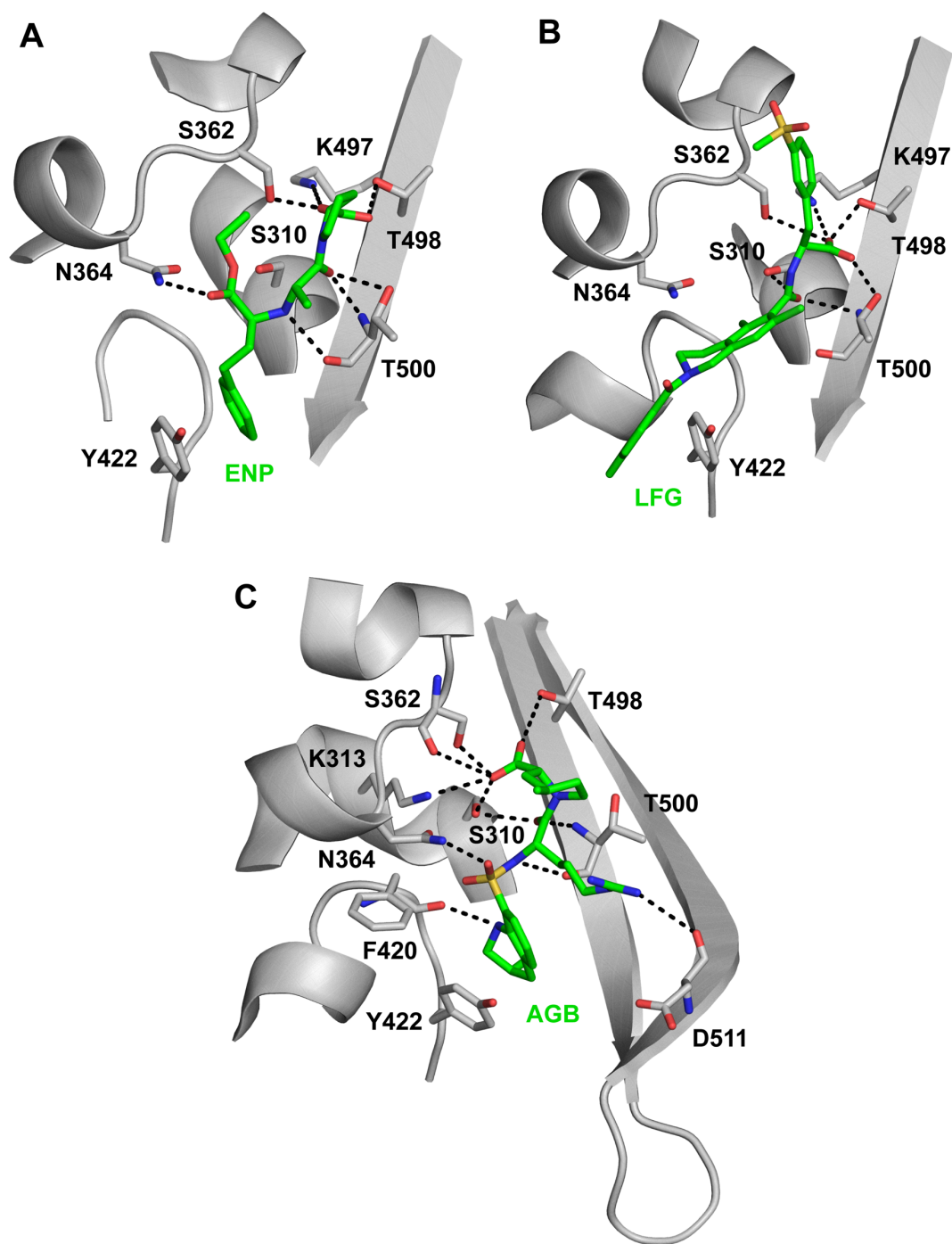


Figure E.5: Modeled binding modes of example FDA-approved pharmacophore matches with *tPBP2*^{WT}. **A.** Enalapril (ENP, green). **B.** Lifitegrast (LFG, green). **C.** Argatroban (AGB, green). Polar contacts are indicated by black dashed lines.

Appendix F: High-throughput virtual screen for inhibitors of *Pseudomonas aeruginosa* PBP3

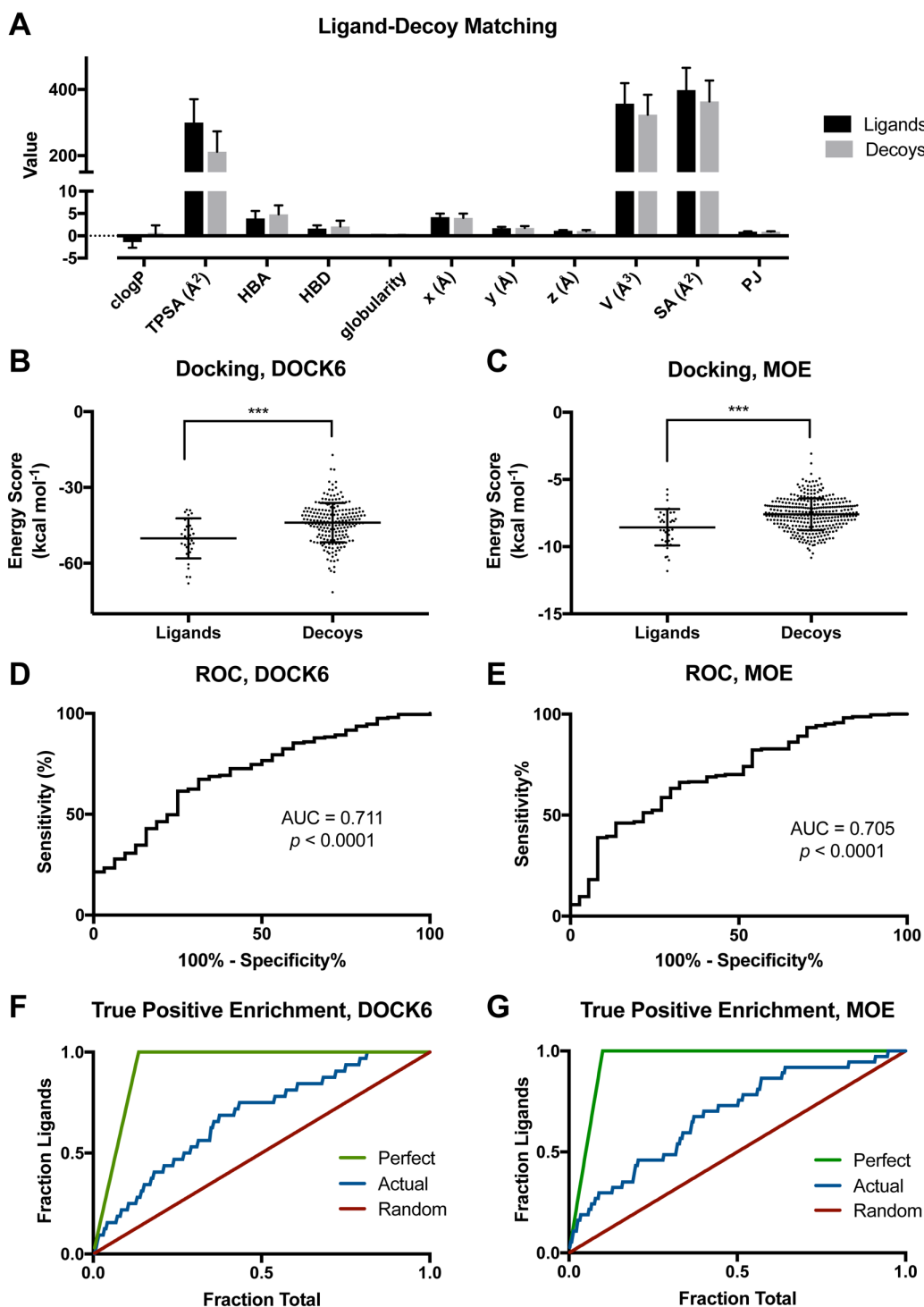


Figure F.1: *In silico* screen performance characteristics. **A.** Physicochemical properties of ligands (β -lactams) and matched decoys, **C.** Comparison of ligand and decoy energy scores ($***p < 0.001$). **D.** **E.** Receiver-operator curves for true ligand detection. **F.** **G.** Enrichment curves for true ligands versus the full rank-ordered dataset (AUC 0.682 and 0.684, respectively).

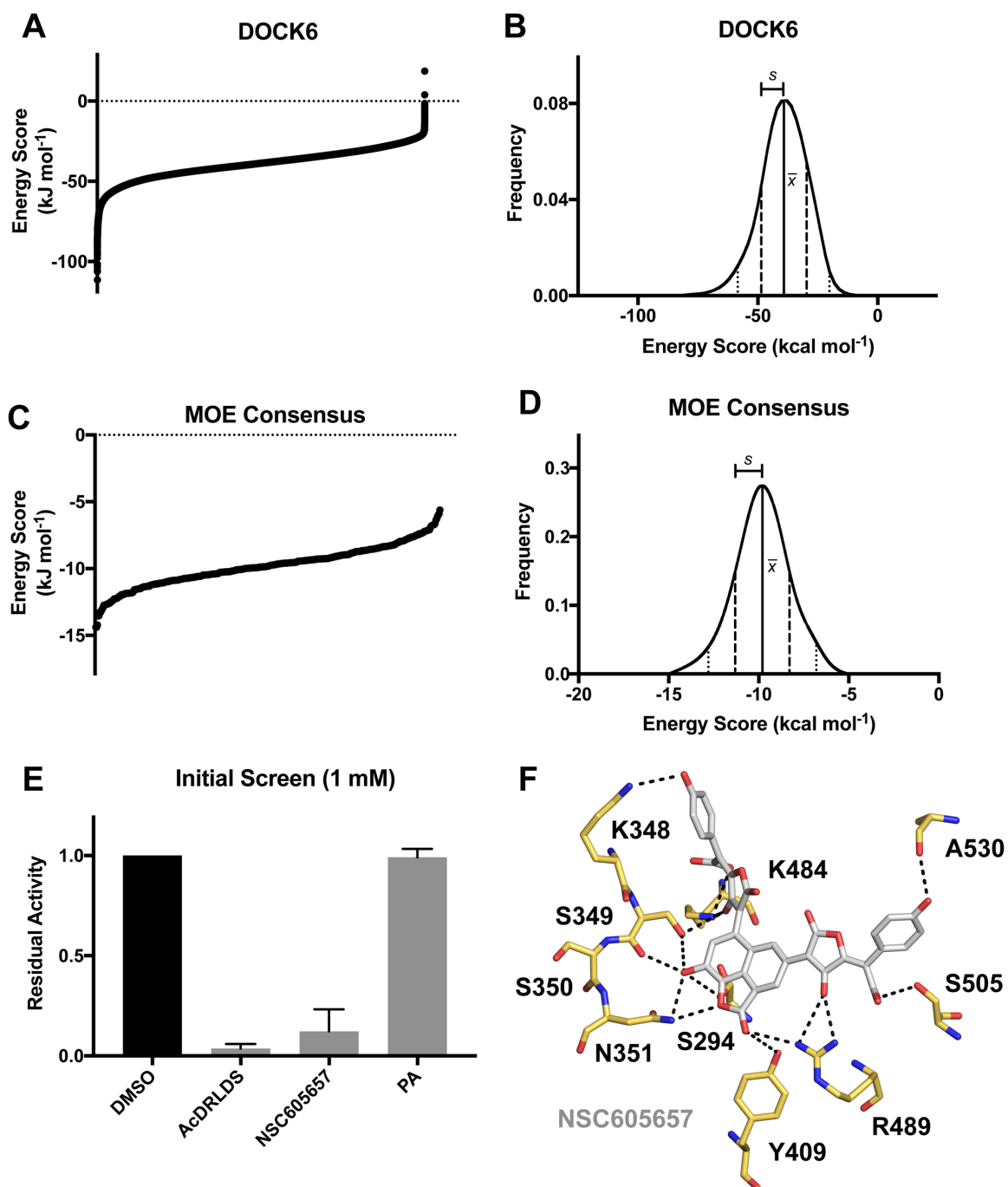


Figure F.2: High-throughput virtual screen against *P. aeruginosa* PBP3. **A.** Rigid-receptor dock rank-ordered energy scores. **B.** Rigid-receptor dock energy score distribution. **C.** Induced fit consensus dock rank-ordered energy scores. **D.** Induced fit consensus dock energy score distribution. **E.** Inhibition of *P. aeruginosa* PBP3 by 1 mM of purchased compounds exhibiting favorable scores from the high-throughput virtual screen. **F.** Least energy conformer for NSC605657, a mid-micromolar, dose-dependent inhibitor of PBP3 identified from the high-throughput virtual screen.

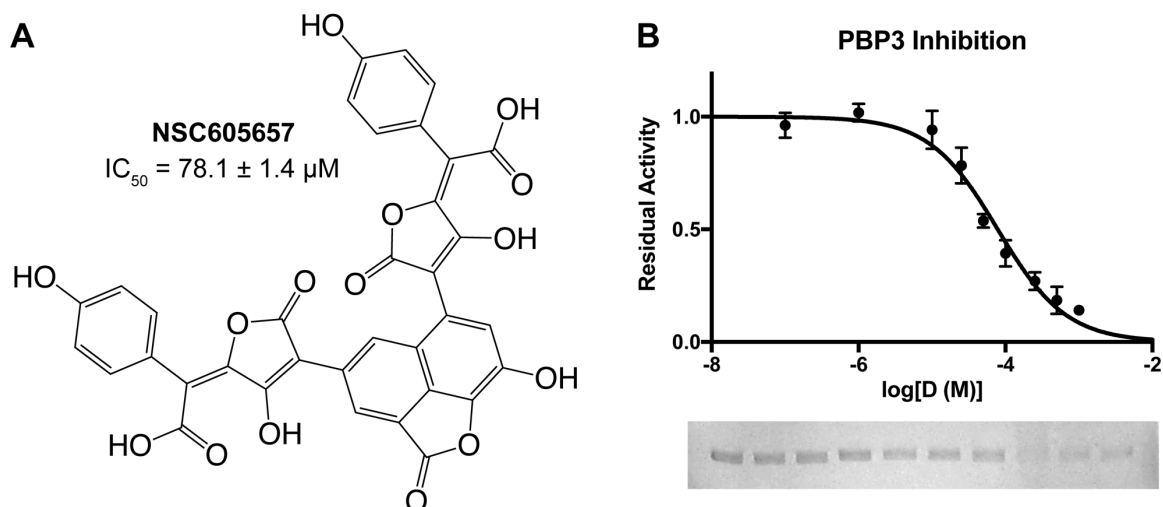


Figure F.3: NSC605657 (norbadiione A) inhibition of *P. aeruginosa* PBP3. **A.** NSC605657 is a 2-oxatricyclo[6.3.1.0^{4,12}]dodeca-1(11),4,6,8(12),9-pentaen-3-one comprising two pulvinic acid moieties. **B.** NSC605657 exhibits dose-dependent inhibition of PBP3 with half-maximal activity at $78.1 \pm 1.4 \mu\text{M}$ ($n = 3$ replicates per concentration, $r^2 = 0.967$).

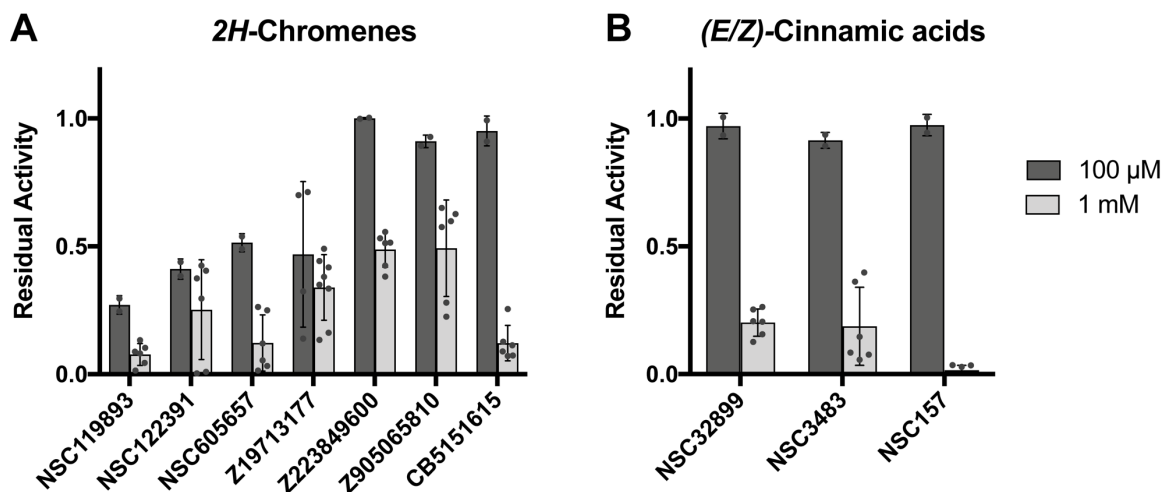


Figure F.4: Screening of 2H-chromene (**A**) and cinnamic acid (**B**) compounds against PBP3. Values were determined in a purified protein assay in which PBP3 was preincubated with compound, followed by addition of $1 \mu\text{M}$ Bocillin-FL. Data are presented as a fraction of DMSO control.

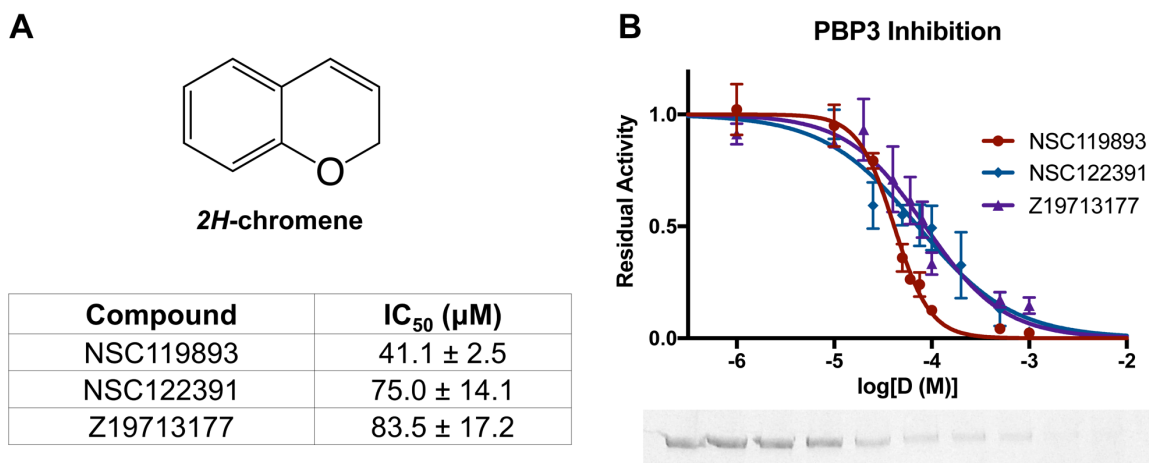


Figure F.5: *2H-chromene* inhibition of *P. aeruginosa* PBP3. **A.** NSC119893, NSC122391, and Z19713177 are *2H-chromenes* with carboxylate or phenolate moieties. **B.** NSC119893, NSC122391, and Z19713177 exhibit dose-dependent inhibition of PBP3 with half-maximal inhibitory activities at $41.1 \pm 2.5 \mu\text{M}$ ($n = 3$ replicates per concentration, $r^2 = 0.982$), $75.0 \pm 14.1 \mu\text{M}$ ($n = 4$ replicates per concentration, $r^2 = 0.924$), and $83.5 \pm 17.2 \mu\text{M}$ ($n = 3$ replicates per concentration, $r^2 = 0.910$), respectively.

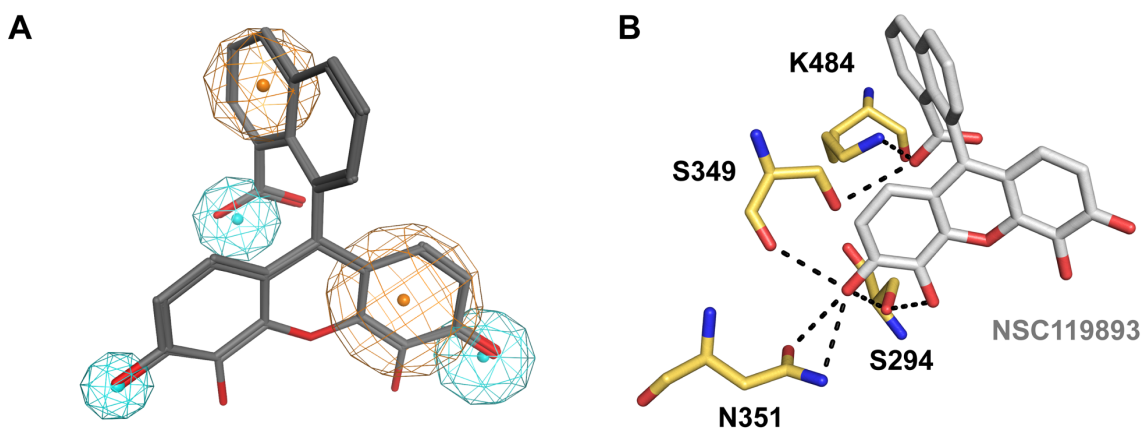


Figure F.6: Proposed mode of PBP3 inhibition by *2H-chromenes*. **A)** Flexible alignment to show common features of most potent inhibitors from the class (hydrogen bond donors, magenta; hydrogen bond acceptors, cyan; interchangeable donors/acceptors, rose; anionic atoms, red; aromatic centers, orange; hydrophobic atoms, green). **B)** Least energy conformer for *2H-chromene* NSC119893 docked against *P. aeruginosa* PBP3, polar contacts shown in black.

3-Hydroxy-1,5-dihydro-2H-pyrrol-2-ones

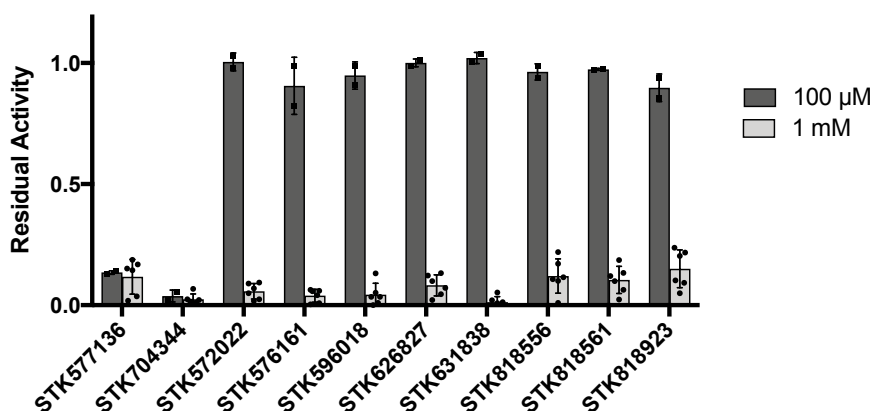
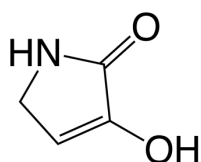


Figure F.7: Screening of 3-hydroxy-1,5-dihydro-2H-pyrrol-2-ones against PBP3. Values were determined in a purified protein assay in which PBP3 was preincubated with compound, followed by addition of 1 μM Bocillin-FL. Data are presented as a fraction of DMSO control.

A



3-hydroxy-1,5-dihydro-2H-pyrrol-2-one

Compound	IC ₅₀ (μM)
STK577136	25.8 \pm 1.9
STK704344	24.9 \pm 2.7

B

PBP3 Inhibition

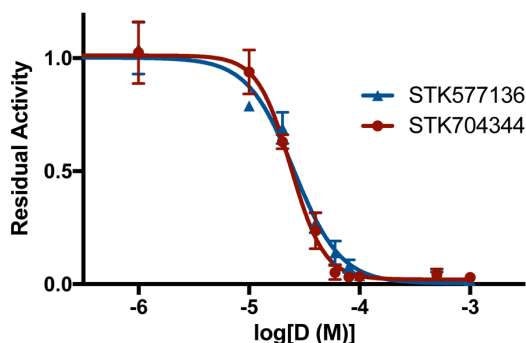


Figure F.8: STK577136 and STK704344 inhibition of *P. aeruginosa* PBP3. **A.** STK577136 and STK704344 are 3-hydroxy-1,5-dihydro-2H-pyrrol-2-ones with aromatic substitutions at their 1-, 4-, and 5-positions. **B.** STK577136 and STK704344 exhibit dose-dependent inhibition of PBP3 with half-maximal activities at 25.8 \pm 1.9 μM ($n = 3$ replicates per concentration, $r^2 = 0.980$) and 24.9 \pm 2.7 μM ($n = 3$ replicates per concentration, $r^2 = 0.983$), respectively.

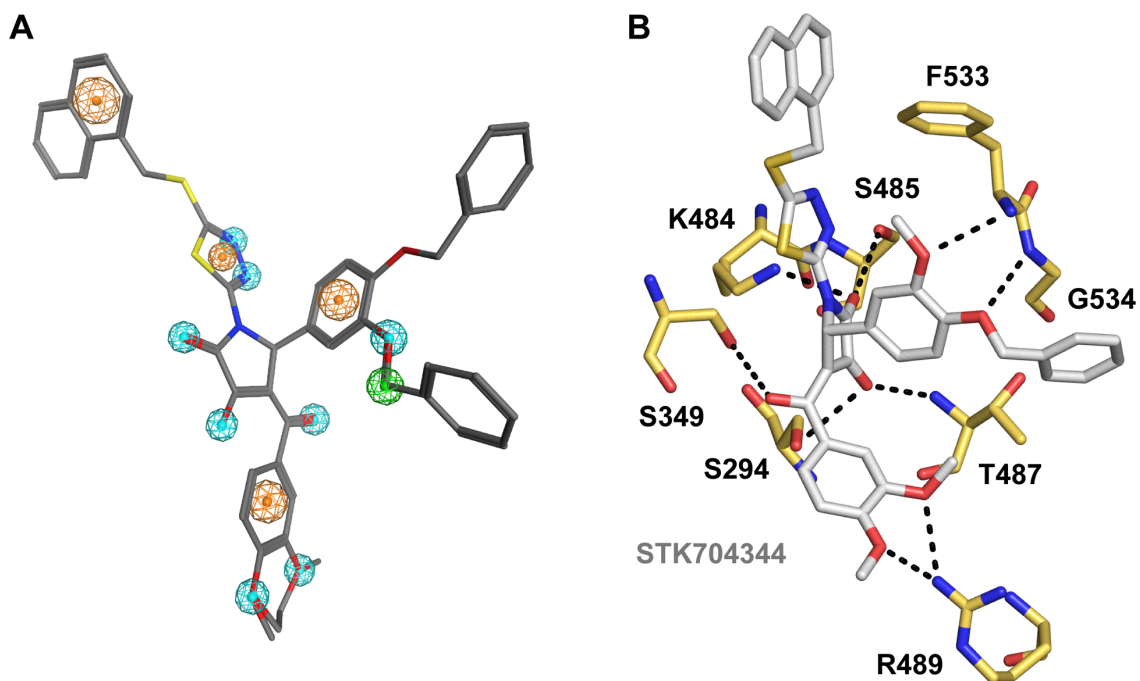


Figure F.9: Proposed mode of PBP3 inhibition by 3-hydroxy-1,5-dihydro-2H-pyrrol-2-ones. **A)** Flexible alignment to show common features of most potent inhibitors from the class (hydrogen bond donors, magenta; hydrogen bond acceptors, cyan; interchangeable donors/acceptors, rose; anionic atoms, red; aromatic centers, orange; hydrophobic atoms, green). **B)** Least energy conformer for 3-hydroxy-1,5-dihydro-2H-pyrrol-2-one STK704344 docked against *P. aeruginosa* PBP3, polar contacts shown in black.

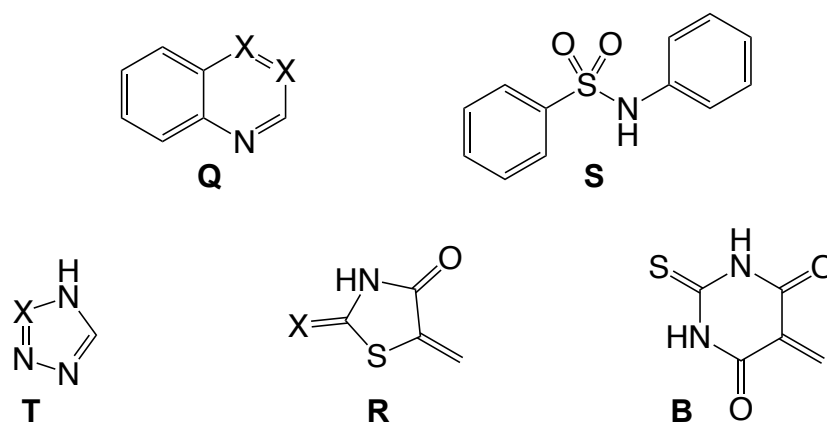


Figure F.10: Structures of additional PBP3-inhibitory chemotypes. Other non- β -lactam PBP inhibitors found in the course of this work include quinolines and quinoline analogues **Q**, arylsulfonamides **S**, triazoles and tetrazoles **T**, 4-thiazolidinones (rhodanines) **R**, and 2-thioxodihydropyrimidine-4,6(1*H*,5*H*)-diones (barbituric acids) **B**.

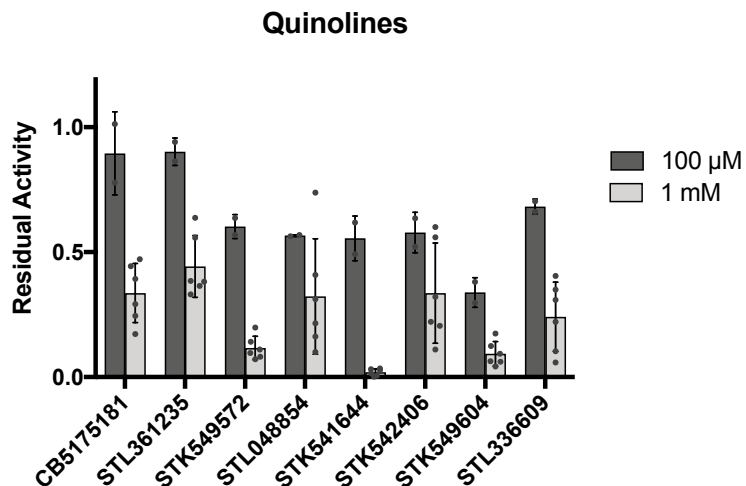


Figure A.11: Screening of quinolones, quinazolines, and quinoxalines **Q** against PBP3. Values were determined in a purified protein assay in which PBP3 was preincubated with compound, followed by addition of 1 μ M Bocillin-FL. Data are presented as a fraction of DMSO control.

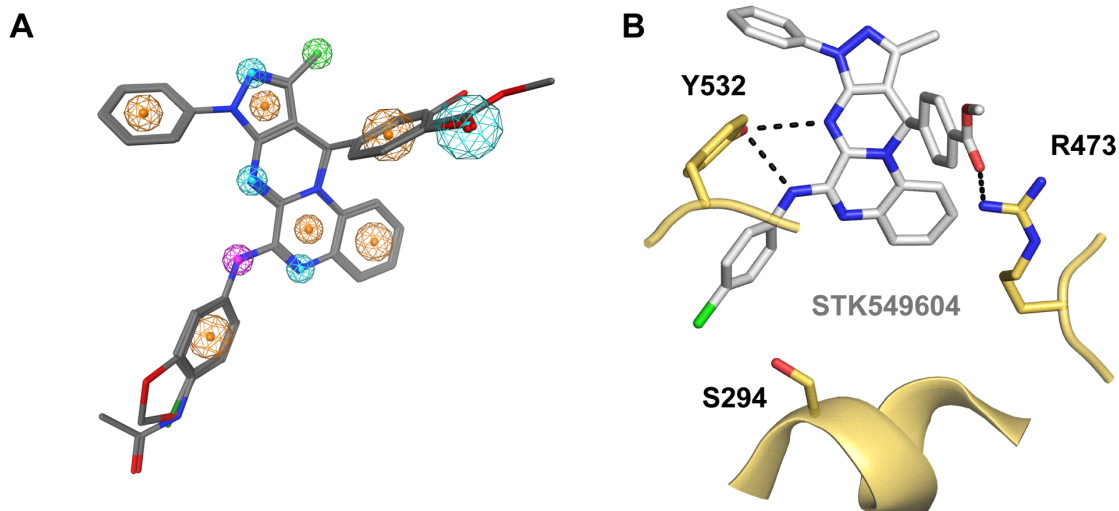


Figure F.12: Proposed mode of PBP3 inhibition by quinoxalines **Q**. **A.** Flexible alignment to show common features of most potent quinolines (hydrogen bond donors, magenta; hydrogen bond acceptors, cyan; interchangeable donors/acceptors, rose; anionic atoms, red; aromatic centers, orange; hydrophobic atoms, green). **B)** Least energy conformer for quinoxaline STK549604 docked against *P. aeruginosa* PBP3, polar contacts shown in black.

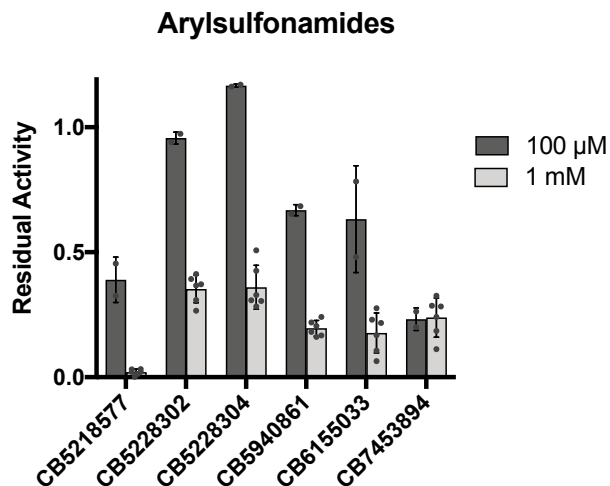


Figure F.13: Screening of sulfonamides **S** against PBP3. Values were determined in a purified protein assay in which PBP3 was preincubated with compound, followed by addition of 1 μ M Bocillin-FL. Data are presented as a fraction of DMSO control.

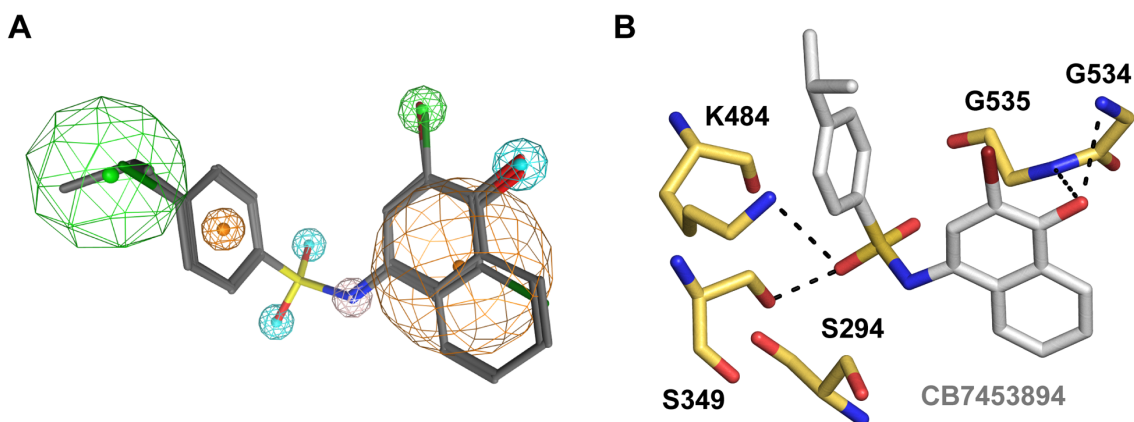


Figure F.14: Proposed mode of PBP3 inhibition by sulfonamides **S**. **A**. Flexible alignment to show common features of most potent arylsulfonamides (hydrogen bond donors, magenta; hydrogen bond acceptors, cyan; interchangeable donors/acceptors, rose; anionic atoms, red; aromatic centers, orange; hydrophobic atoms, green). **B**. Least energy conformer for arylsulfonamide CB7453894 docked against *P. aeruginosa* PBP3, polar contacts shown in black.

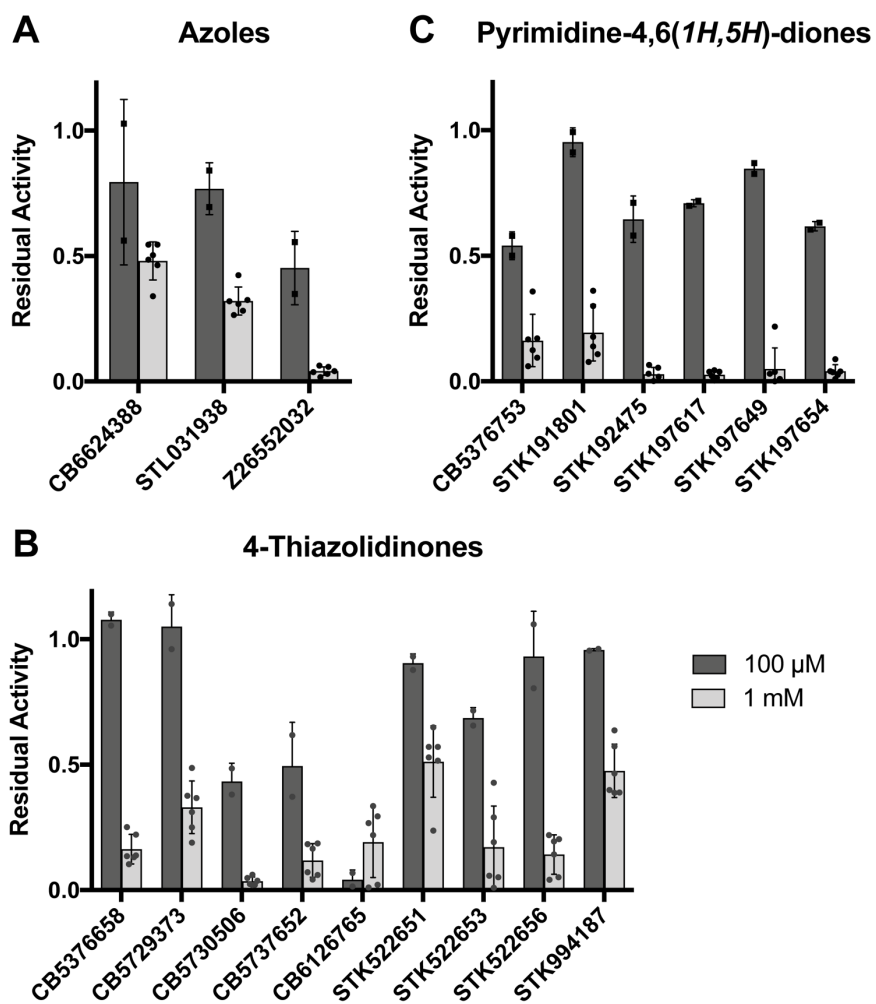


Figure F.15: Screening of azoles (A), 4-thiazolidinones (B), and pyrimidine-4,6(1H,5H)-diones (C) against PBP3. Values were determined in a purified protein assay in which PBP3 was preincubated with compound, followed by addition of 1 μM Bocillin-FL. Data are presented as a fraction of DMSO control.

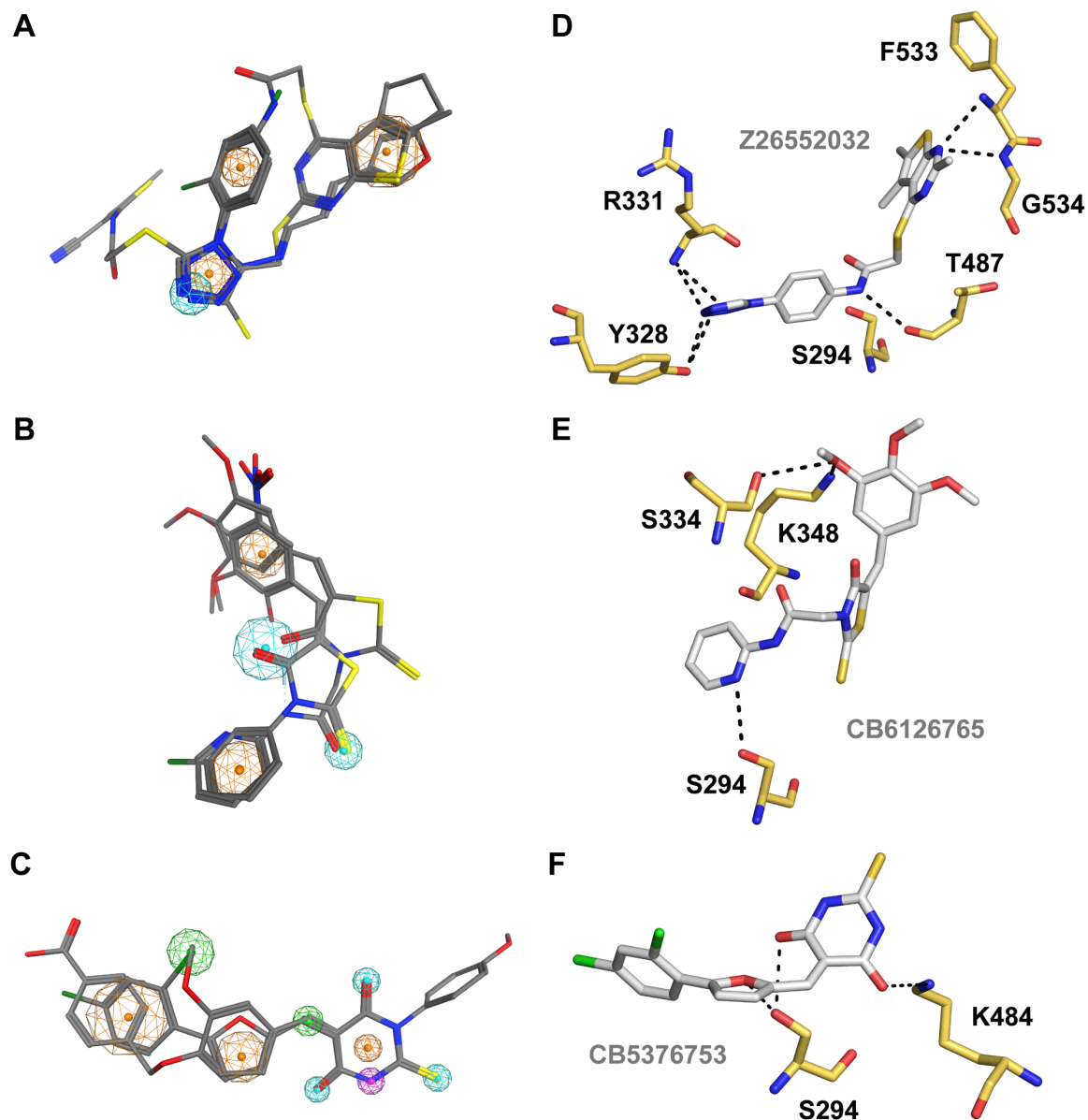


Figure F.16: Proposed modes of PBP3 inhibition by azoles, 4-thiazolidinones, and pyrimidine-4,6(1H,5H)-diones. **A-C.** Flexible alignment to show common features of most potent azoles (**A**), 4-thiazolidinones (**B**), and pyrimidine-4,6(1H,5H)-diones (**C**) (hydrogen bond donors, magenta; hydrogen bond acceptors, cyan; interchangeable donors/acceptors, rose; anionic atoms, red; aromatic centers, orange; hydrophobic atoms, green). **D-F.** Least energy conformers for aryltetrazole Z26552032 (**D**), 4-thiazolidinone CB6126765 (**E**), and pyrimidine-4,6(1H,5H)-dione CB5376753 (**F**) docked against *P. aeruginosa* PBP3, polar contacts shown in black.

Table F.1: PBP3 inhibition data for NSC605657 analogues identified through substructure and similarity searches of the PubChem database. Most potent hits (defined as >50% inhibition at 100 μ M) are highlighted in green.

Compound	Inhibition at 1 mM (%)	Inhibition at 100 μM (%)
NSC5897	13.7 \pm 6.8	ND
NSC167376	NS	ND
NSC311454	NS	ND
NSC338986	46.9 \pm 12.9	NS
NSC621468	57.5 \pm 17.5	NS
NSC81924	NS	ND
NSC631509	22.8 \pm 20.9	ND
NSC155504	28.1 \pm 5.8	ND
NSC32899	79.8 \pm 5.3	NS
NSC347512	NS	ND
NSC3483	81.3 \pm 15.8	8.5 \pm 3.1
NSC720435	NS	ND
NSC119893	92.3 \pm 4.3	72.9 \pm 3.6
NSC157	98.5 \pm 1.9	NS
NSC19027	NS	ND
NSC19801	38.1 \pm 29.7	ND
NSC101137	NS	ND
NSC155476	9.1 \pm 4.4	ND
NSC215568	11.0 \pm 9.9	ND
NSC720435	NS	ND
EN300-41020	NS	ND
Z90122589	NS	ND
Z1946684614	NS	ND
Z905065810	50.7 \pm 18.9	8.9 \pm 2.5
Z95232844	22.6 \pm 11.7	ND
Z223849600	51.3 \pm 6.8	NS
Z19713177	66.1 \pm 12.8	53.1 \pm 28.4
EN300-305263	10.0 \pm 2.7	ND
NSC122391	74.8 \pm 19.5	58.9 \pm 3.9
NSC622475	NS	ND
STL099530	NS	ND
STL099536	NS	ND
STK007398	26.2 \pm 10.6	ND
STK034285	47.3 \pm 17.6	ND
STK447520	13.9 \pm 6.5	ND
STK791461	NS	ND
STK837716	NS	ND
STK987640	NS	ND
STL058314	NS	ND
STL061985	NS	ND
STL295948	NS	ND

Table F.2: PBP3 inhibition data for compounds predicted to have activity from structure-activity relationships of noncovalent inhibitors against PBP3.

Compound	Inhibition at 1 mM (%)	Inhibition at 100 μM (%)
STK369807	95.2 \pm 2.4	21.5 \pm 7.1
STK888755	41.4 \pm 10.7	ND
STK270718	24.8 \pm 19.6	ND
STK522653	82.8 \pm 16.4	31.4 \pm 4.2
STK549572	88.4 \pm 4.7	39.8 \pm 4.8
STK522651	48.8 \pm 14.2	ND
STK522656	85.8 \pm 7.8	NS
STL048854	67.7 \pm 23.1	43.4 \pm 0.3
STK541644	98.1 \pm 1.4	44.5 \pm 8.9
STK328887	NS	ND
STK887542	NS	ND
STK994187	51.2 \pm 9.8	NS
STK191801	80.6 \pm 11.3	NS
STK718016	NS	ND
STK577136	88.3 \pm 7.2	86.5 \pm 0.7
STL031938	55.5 \pm 17.6	23.2 \pm 10.3
STK460513	NS	ND
CB6140541	NS	ND
CB6126765	80.9 \pm 14.1	95.8 \pm 3.8
CB6130015	44.3 \pm 8.1	ND
STL031936	39.0 \pm 27.9	ND
STK704344	97.5 \pm 2.2	96.2 \pm 2.4
STK818923	85.0 \pm 7.8	10.3 \pm 5.7
Z26552032	95.9 \pm 1.7	54.8 \pm 14.6
STK192475	97.2 \pm 2.8	35.4 \pm 9.3
STK197617	97.3 \pm 1.6	29.1 \pm 1.4
STK197649	95.1 \pm 8.4	15.3 \pm 3.0
STK197654	96.0 \pm 2.6	38.2 \pm 1.9
STK542406	66.3 \pm 20.1	42.2 \pm 8.0
STK549604	90.7 \pm 4.9	66.1 \pm 5.9
STL336609	75.9 \pm 13.9	31.7 \pm 3.0
STK059577	90.3 \pm 4.7	76.8 \pm 7.0
STK572022	94.3 \pm 3.2	NS
STK576161	96.1 \pm 2.7	NS
STK589175	NS	ND
STK596018	95.6 \pm 4.7	NS
STK626827	91.8 \pm 4.4	NS
STK631838	98.8 \pm 2.4	NS
STK818556	87.9 \pm 7.1	NS
STK818561	89.6 \pm 5.6	NS
STK819418	48.7 \pm 5.1	ND
STK098795	NS	ND
STL361235	55.7 \pm 12.4	9.8 \pm 5.5
STK095131	28.4 \pm 14.4	ND
STK052461	13.2 \pm 4.5	ND

STK129507	20.6 ± 15.0	ND
STK071540	8.6 ± 6.3	ND
STK634916	NS	ND
STK029374	NS	ND
STK871156	NS	ND
STK871000	NS	ND
STK202948	30.6 ± 2.7	ND
STK070625	NS	ND
STK084156	44.4 ± 23.3	ND
STK010482	NS	ND
STK057971	NS	ND
STL040105	NS	ND
STK041773	NS	ND
CB5477031	96.2 ± 2.4	68.5 ± 7.9
CB5530695	91.8 ± 6.1	NS
CB6624338	51.9 ± 7.6	NS
CB7647715	NS	ND
CB5151615	87.8 ± 6.9	NS
CB5730506	96.4 ± 1.7	56.7 ± 7.3
CB5729373	67.0 ± 10.5	NS
CB5737652	88.2 ± 6.7	50.5 ± 17.4
CB7630081	85.1 ± 3.6	66.8 ± 11.2
CB5214931	66.9 ± 7.0	43.2 ± 7.1
CB5218577	97.9 ± 1.2	61.0 ± 9.1
CB5247550	39.5 ± 21.8	ND
CB5238280	53.9 ± 28.0	ND
CB5376753	83.7 ± 10.5	46.0 ± 5.5
CB5376658	83.7 ± 5.9	NS
CB5175181	66.4 ± 11.8	NS
CB5228302	64.7 ± 5.5	4.3 ± 2.4
CB5228304	64.0 ± 8.8	NS
CB6155033	82.3 ± 8.0	36.8 ± 21.4
CB7453894	76.1 ± 7.8	76.8 ± 4.5
CB5940861	80.4 ± 3.2	33.1 ± 2.2